PROCEEDINGS OF THE NASA • INDUSTRY • UNIVERSITY GENERAL AVIATION DRAG REDUCTION WORKSHOP

Edited by: Jan Roskam

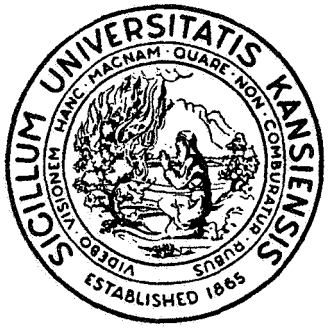

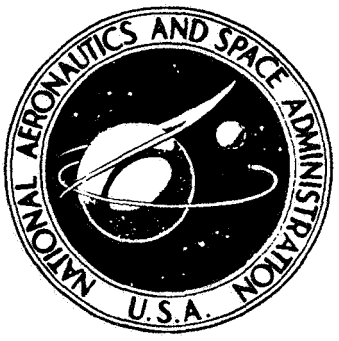

July 14-16, 1975

Space Technology Center
University of Kansas
Lawrence, Kansas 66045

TABLE OF CONTENTS

TABLE OF CONTENTS (Cont')

TABLE OF CONTENTS (Cont')

1. INTRODUCTION

Preceding Page Blank

1. INTRODUCTION

This document contains all papers presented at the "NASA/Industry/ University General Aviation Drag Reduction Workshop," held at the University of Kansas July 14-16, 1975. The conference was sponsored by NASA Langley Research Center under NASA Grant NSG 1175. The sequence of papers in this document is the same as that found on the Program Outline, Chapter 2. The actual papers are distributed over Chapters 3 through 8. A number of papers were received after the conference. Several of these were judged to be of sufficient interest to the subject of general aviation drag reduction to include them in this document in Chapter 9. In addition, a summary of all technical discussions which followed the papers is found in Chapter 10.

The purpose of the conference was to: (1) Identify the state-of-the art, and (2) Formulate a NASA/University R & D program aimed at achieving significant drag reductions in the near term future.

Chapter 11 contains a summary of recommendations for drag reduction research aimed at improving general aviation airplanes.

2. FINAL PROGRAM OUTLINE AND GENERAL OVERVIEW ON DRAG

2. FINAL PROGRAM OUTLINE AND GENERAL OVERVIEW ON DRAG

2.1 Final Program of the NASA/Industry/University General Aviation Drag Reduction Workshop

■ Monday, July 14, 1975

8:15 - 8:45 Registration, Lobby, Nichols Hall

8:45 - 9:00 Welcome and Introduction
J. Roskam, University of Kansas

9:00 - 9:45 General Overview of Drag
S. B. Anderson, NASA-Ames Research Center

★ Session I - Status of Drag Prediction Methods

9:45 - 10:30 Overview of Drag Prediction Methods
D. Ruhmel, Cessna Aircraft Company

10:30 - 10:45 Break

10:45 - 11:30 Brief Presentations by Industry, Universities and NASA

The following presentations are scheduled:

1. Prospects and Time Tables for Analytical Estimation of the Drag of Complete Aircraft Configurations
F. O. Smetana, North Carolina State University
2. Summary of Drag Cleanup Tests in the NASA Langley Full-Scale Tunnel
M. O. McKinney, NASA Langley Research Center
3. Simplified Theoretical Methods for Aerodynamic Design
J. Tulinius, NASA Langley Research Center

11:30 - 12:00 Open Discussions. Formulation of research and development work needed in the area of drag prediction methods.

12:00 - 2:00 Dutch Treat Luncheon - Centennial Room, Student Union Building

Speaker: O. W. Nicks, NASA Langley Research Center
Topic: Drag Reduction/Back to Basics

★ Session II - Fuselage Drag

2:00 - 2:30 Overview of Fuselage Drag
J. Roskam, University of Kansas

2:30 - 3:00 Brief Presentations by Industry, Universities and NASA

The following presentations are scheduled:

1. Propeller Blockage Research Needs
R. Tumlinson, Beech Aircraft Corporation
2. Preservation of Wing Leading Edge Suction at the Plane of Symmetry as a Factor in Wing-Fuselage Design
E. E. Larrabee, Massachusetts Institute of Technology

3. Asymptotic Analytic Methods in Fluid Mechanics Related to Drag Prediction
G. R. Inger, Virginia Polytechnic Institute

3:00 - 3:15 Break

3:15 - 4:30 Open Discussions. Formulation of research and development work needed in the area of fuselage drag.

4:30 - 5:30 Visit to KU Flight Research Laboratory Facilities

4:30 Flight Simulator Lab, Nichols Hall
5:00 Wind Tunnel & Tornado Lab, Learned Hall

6:00 - 7:00 Dutch Treat Social Hour, Ramada Inn

7:00 Dutch Treat Dinner, Ramada Inn

Speaker: R. D. Neal, Gates Learjet Corporation
Topic: The Economic Impact of Drag in General Aviation

Tuesday, July 15, 1975

Session III - Wing Drag

8:30 - 9:00 Methods for Reducing Wing Drag and Wing-Nacelle Interference
T. C. Kelly, NASA Langley Research Center

9:00 - 10:30 Brief Presentations by Industry, Universities and NASA

Scheduled are the following brief presentations:

1. Drag Reduction through Higher Wing Loading
D. L. Kohlman, University of Kansas
2. Use of a Pitot Static Probe for Determining Wing Section Drag in Flight
L. C. Montoya, P. S. Bikle and E. Saltzman, NASA Flight Research Center
3. Flight Test Results with an Ogee Wing Tip
J. Vogel, Beech Aircraft Corporation
4. Wing-Tip Vanes as Vortex Attenuation and Induced Drag Reduction Devices
W. H. Wentz, Jr., Wichita State University
5. Wing Tip Vortex Drag
V. U. Muirhead, University of Kansas

10:30 - 10:45 Break

10:45 - 12:00 Open Discussions. Formulation of research and development work needed in the area of wing drag.

12:00 - 2:00 Dutch Treat Luncheon - Centennial Room, Student Union

Speaker: R. Winblade, NASA Headquarters
Topic: NASA Light Aircraft Performance Research: Opportunities and Limitations
(Cancelled; S. Anderson showed and narrated a V/STOL movie instead.)

✱Session IV - External Nacelle Drag and Interference Drag

2:00 - 2:45 Overview of External Nacelle Drag and Interference Drag
R. D. Neal, Gates Learjet Corporation

2:45 - 3:45 Brief Presentations by Industry, Universities and NASA

1. Installation Drag Considerations Other than External Nacelle and Interference Drag as Related to Turboprop and Turbofan Engines
G. Burnett, Garrett AiResearch Manufacturing Co. of Arizona
2. Nacelle Drag Reduction: An Analytical Guided Experimental Program
F. Smetana, North Carolina State University
3. Cooling Drag Associated with General Aviation Propulsive Systems
E. J. Cross, Jr., Mississippi State University
4. Propellers of Minimum Induced Loss, and Water Tunnel Tests of Such a Propeller
E. E. Larrabee, Massachusetts Institute of Technology

3:45 - 4:00 Break

4:00 - 5:00 Open Discussions. Formulation of research and development work needed in the area of nacelle and interference drag.

6:00 - 7:00 Dutch Treat Social Hour

7:00 Dutch Treat Dinner, Ramada Inn

■Wednesday, July 16, 1975

✱Session V - Trim Drag

8:30 - 9:15 Overview of Trim Drag
J. Roskam, University of Kansas

9:15 - 10:15 Brief Presentations by Industry, Universities and NASA

Scheduled are the following brief presentations:

1. Trim Drag Research Results
H. Chevalier, Texas A & M University
2. Reduction of Trim Drag in General Aviation Airplanes
F. H. Lutz, Virginia Polytechnic Institute
3. Trim Drag in the Light of Munk's Stagger Theorem
E. E. Larrabee, Massachusetts Insitute of Technology

10:15 - 10:30 Break

10:30 - 11:30 Open Discussions. Formulation of research and development work needed in the area of trim drag.

11:30 - 1:00 Dutch Treat Luncheon - Centennial Room, Student Union
No Speaker Scheduled

✱Session VI - Drag of the Complete Configuration

1:00 - 1:30 Overview of Configuration Drag

Part I - Cost Considerations; R. Tumlinson, Beech Aircraft Corporation

Part II - Aerodynamic Considerations; J. Roskam, University of Kansas

1:30 - 2:30 Brief Presentations by Industry, Universities and NASA

Scheduled are the following brief presentations:

1. Learjet Model 25 Drag Analysis
   R. Ross and R. Neal, Gates Learjet Corporation
2. Problems in Propulsion System Integration
   W. Henderson and J. Runckel, NASA Langley Research Center
3. Propulsion/Airframe Integration
   D. Mikkelson, NASA Lewis Research Center
4. Determination of the Level Flight Performance of Propeller-Driven Aircraft
   E. J. Cross, Jr., Mississippi State University

2:30 - 3:15 Open Discussions. Formulation of research and development work needed in the area of complete configuration drag.

3:15 - 3:30 Closing Remarks

J. Stickle, NASA Research Center and
J. Roskam, University of Kansas

2.2 General Overview of Drag

S.A. Anderson
Ames Research Center

The importance of reducing drag for general aviation aircraft is increasingly evident for the reasons noted in Figure 1. This includes rising fuel costs and the demand for improved performance to meet foreign competition. Equally important is the impact of more stringent noise and pollution standards because these factors indirectly affect aerodynamic performance. Although the general principles of how to achieve drag reduction are known to aircraft designers, applications to general aviation aircraft are a significant challenge because this aircraft category is particularly sensitive to costs, maintenance, marketing, safety utility, and even stability and control.

How much do we really know about potential drag reductions for a typical high-performance business aircraft? A casual inspection of a current twin shows an abundance of brazier head rivets on all parts of the aircraft, several large external antennas, a lack of wing-fuselage filleting, lapped skin joints, many air inlets at obviously undesirable aerodynamic locations, and a single large-diameter exhaust pipe protruding at close to 90° to the airstream. On one twin turboprop aircraft, seven separate NACA flush inlets were located on each engine nacelle, some obviously of questionable value for pressure recovery. Although it is recognized that little systematic research on drag for current aircraft configurations has been conducted recently, many of the results of early NACA research can be usefully applied to current aircraft. Obviously, there is little similarity between the blunt, radial-engine transport aircraft of the late 1930's, for which most of the early research was conducted, to today's sleek business jet, so few would question the need for additional research.

As noted in the program for this workshop, it is timely to identify the state-of-the-art on aerodynamic drag reduction and develop a program plan for achieving meaningful results. There are, of course, many elements making up the total drag of an aircraft, including fuselage, wing, nacelles, trim, interference, tail, and cooling drag. The various topics to be covered in the next three days are shown on Figure 2. Note that although cooling drag can be a large percentage of total drag (as high as 25%), it has previously been covered in a NASA/University/Industry workshop and will not be considered explicitly at this workshop. As noted in Figure 3, the purpose of this paper is to review the relative drag contributions of these various elements,

pausing briefly to note what is known about each from past research, thereby identifying gaps in the knowledge for further consideration by speakers who will follow with detailed discussions.

Basic Sources of Drag

It is important to identify the basic sources of drag in order to gain a better understanding of how improvements in performance can be made. Shown on Figure 4 are the following: (1) skin friction due to the air molecules rubbing the surface, the magnitude being a function of the flow conditions (laminar or turbulent) and the amount of wetted area; (2) induced flow or vortex flow primarily a function of wing aspect ratio; and (3) pressure effects associated with the profile or form of various parts of the aircraft.

Shown on Figure 5 is the variation of flat plate drag coefficient based on wetted area with Reynolds number for fully turbulent and laminar flow conditions. Note that at large R_e numbers typical of flight cruise conditions, the drag associated with turbulent flow is ten times higher than for laminar flow. In another example of the effect of flow conditions, Figure 6 compares the equivalent drag of a laminar flow airfoil and a circular wire. If nothing else, this is an incentive to avoid using exposed landing wires.

Drag Prediction Techniques

Moving along to the first topic of our workshop, the various drag prediction techniques in use today are noted in Figure 7. The empirical approach takes advantage of semi-analytical methods in which wind-tunnel and flight-test results of similar type aircraft are factored in to establish a data base. Wind tunnel measurements of drag for a new design are usually made, particularly for high-performance aircraft. Extrapolation of small-scale (low R_e no.) data to flight conditions can be difficult when including power effects and the accuracy of how well the small-scale model represents the actual aircraft. Finally, theoretical estimates, although used extensively in the past, have become more popular because of the availability of large capacity digital computers. Solutions of 3-dimensional viscous flow effects appear to remain a challenge even with very large (and expensive) digital computers such as the ILLIAC IV based at the NASA Ames Research Center.

Relative Contributions to Drag

An example of results from drag prediction methods developed at NASA-Ames is shown in Figure 8. The aerodynamics subroutine calculates a series of factors which are used to establish drag values. Form factors are used for each component to represent drag increases above that of a flat plate to account for 3-D effects, interference, roughness, and excrescences. These calculations were made for the Learjet, Citation, Cessna 340, Piper Arrow, and Cessna 150. Note first, not unexpectedly, that the wing and fuselage are responsible for the largest source of drag. Of interest in the last column is the amount to be added to match flight values of drag. This item varies greatly, going from less than 2 percent for the Learjet to 37 percent for the Cessna 150. Improvements are needed to more accurately account for such factors as 3-D effects, cooling drag, landing gear, slipstream drag, etc.

Factors Influencing Fuselage Drag

In the next item of our workshop agenda, Figure 9 gives several factors which affect fuselage drag. The surface conditions are very important because of the large wetted area. Windshield shape can significantly affect total drag at the higher Mach numbers. Fuselage shape in terms of fineness ratio, nose shape and rear-end shape must be carefully considered. Shown in Figure 10 is the effect of afterbody contraction ratio on drag. The contraction ratio must be greater than 2.0 to avoid a drag increase. A similar consideration must be given in the vertical plane.

Factors Influencing Wing Drag

Figure 11 lists several factors which are considered in selecting a wing for a new aircraft design. A large background of data is available from NACA research on airfoil sections and newer types such as the GAW-1 airfoil to challenge the designer in selecting the correct airfoil section for his aircraft. The NASA has underway a program on airfoil development aimed primarily at optimizing airfoils for specific operating conditions. Thickness ratio effects are generally well-documented. Planform and aspect ratio effects are also important as influenced by structural considerations. Wing-tip effects on induced drag will be covered specifically in a Langley Research Center paper describing the trade-offs on using "Winglets."

Another reminder of the importance of surface conditions and thickness ratio on drag is given in Figure 12. These NACA data tend to exaggerate the effect of roughness because the lower curve represents a mirror-finish surface condition. The

trend today for the higher performance jets is to use thicker airfoil sections for structural and fuel volume considerations.

Factors Influencing Trim Drag

Of the various factors shown in Figure 13 which affect trim drag, tail location and static stability have recently been given increased attention. A tail location out of the slipstream ("T" tail designs) offer some drag decrease, and canard horizontal tail locations have appeared on experimental aircraft. In consideration of the small percentage of the tail surfaces to total drag indicated previously, one must be careful not to compromise stability and control in looking for performance imporvements. In this connection the control configured-vehicle (CCV) and relaxed static stability have received attention recently. An illustration of the effect of reducing static margin on the horizontal tail area required is shown in Figure 14. These curves indicate the variation of tail size with static margin to trim out the wing-fuselage pitching moment and the tail area needed for maneuvering. To achieve the minimum tail area and therefore the least amount of drag, the static margin must be slightly aft of the neutral point ($d\delta_e/dC_L = 0$) but ahead of the maneuver point ($dF_e/dA_z = 0$). Obviously, some for of stability augmentation must be provided to meet the FAR if minimum tail size is desired. At this point one would logically question the merits of reducing static margin for most General Aviation aircraft.

Considerations for Drag of Complete Aircraft

In the final analysis, drag of the complete configuration is the most difficult to rationalize. As noted in Figure 15, cost is a factor that must be considered in each aspect of aerodynamic drag reduction. Cost aspects will be discussed in a paper later in the workshop. In this regard use of composites may offer promise in that extremely smooth surfaces with attendant low drag can be achieved without high-cost manufacturing techniques. The second point, aerodynamic drag of the complete configuration, must take into account items such as wing nacelle and tail location, fuselage camber, wing and nacelle incidence, wing loading, cruise lift coefficient, etc. This area will be covered also on the last day of the workshop. The next item, propulsion system integration, is an important area, particularly for higher performance aircraft. Nacelle size and location can significantly affect high subsonic Mach number performance, as will be discussed by NASA Lewis Research Center. Fabrication details, the next item, must be considered in the light of cost and aircraft appearance. A

smooth-looking aircraft not only has the potential for higher performance, but also sales appeal. Finally, an important point to know is the relative magnitude of the various sources of drag because of the many trade-offs in aerodynamic drag reduction. This leads to the next point of discussion.

In Figure 16 the relative drag values are compared for a high performance aircraft. Leading the list is the friction drag, with induced drag a close second. Cross flow or 3-D effects can cause drag problems and are unfortunately the most difficult to predict. Induced drag primarily a function of wing aspect ratio can be reduced by wing-tip modifications, as will be covered by Langley Research Center.

Historical Survey of Drag

Figure 17 presents the variation of drag based on wetted area as a function of time. Starting with the Wright Brother's design as the highest drag vehicle--not too surprising if you recall how large a drag penalty wires can create. The lowest drag values correspond to fighter aircraft such as the Douglas A-4 and LTV F-8.

There is no question that improvements have been made with time, but how well are we doing in realizing the goals of drag previously noted. Shown in Figure 18 is a comparison of flight drag data with flat plate skin fraction curves for turbulent and laminar flow conditions. The data which are for typical general aviation aircraft fall short of even achieving the turbulent flow drag values. The lowest drag value quoted is for the black buzzard (coragyps atratus) which in some 150 million years of evolution has no doubt managed to achieve reasonably good flow conditions without having to contend with cooling drag and propeller slipstream effects. There are indications that these idealized goals can be approached by aircraft with good surface finishes, such as the point for the Learjet at 30 million R_e.

Concluding Remarks

In conclusion, three main points should be kept in mind during the next three days (see Figure 19). We need to more accurately clarify the sources of drag for general aviation-type aircraft so that new designs can benefit from more accurate prediction techniques. Next, by knowing more about the sources of drag it will be possible to bring out the greatest potential for drag reduction. Finally, we must use our expertise to identify gaps in knowledge and point out areas which should receive high priority R and D efforts.

In closing, I would like to mention my personal drag reduction program carried out on a Vultee BY-13 trainer aircraft. By using NACA drag information, the high speed of this aircraft was improved from 160 to 210 mph, representing a change in equivalent flatplate area from 16.1 to 7.2 square feet.

NEED FOR DRAG REDUCTION

- RISING FUEL COSTS
- INCREASED FOREIGN COMPETITION
- NOISE AND POLLUTION

Figure 1. General Overview of Drag

- STATUS OF DRAG PREDICTION METHODS
- FUSELAGE DRAG
- WING DRAG
- EXTERNAL NACELLE DRAG & INTERFERENCE DRAG
- TRIM DRAG
- DRAG OF COMPLETE CONFIGURATION

Figure 2. General Aviation Drag Reduction Workshop Sessions

- HIGHLIGHT CAUSES OF DRAG
- INDICATE DRAG STATUS OF CURRENT A/C
- IDENTIFY GAPS IN KNOWLEDGE

Figure 3. Purpose of Presentation

- SKIN FRICTION
- INDUCED FLOW
- PRESSURE EFFECTS

Figure 4. Basic Sources of Drag

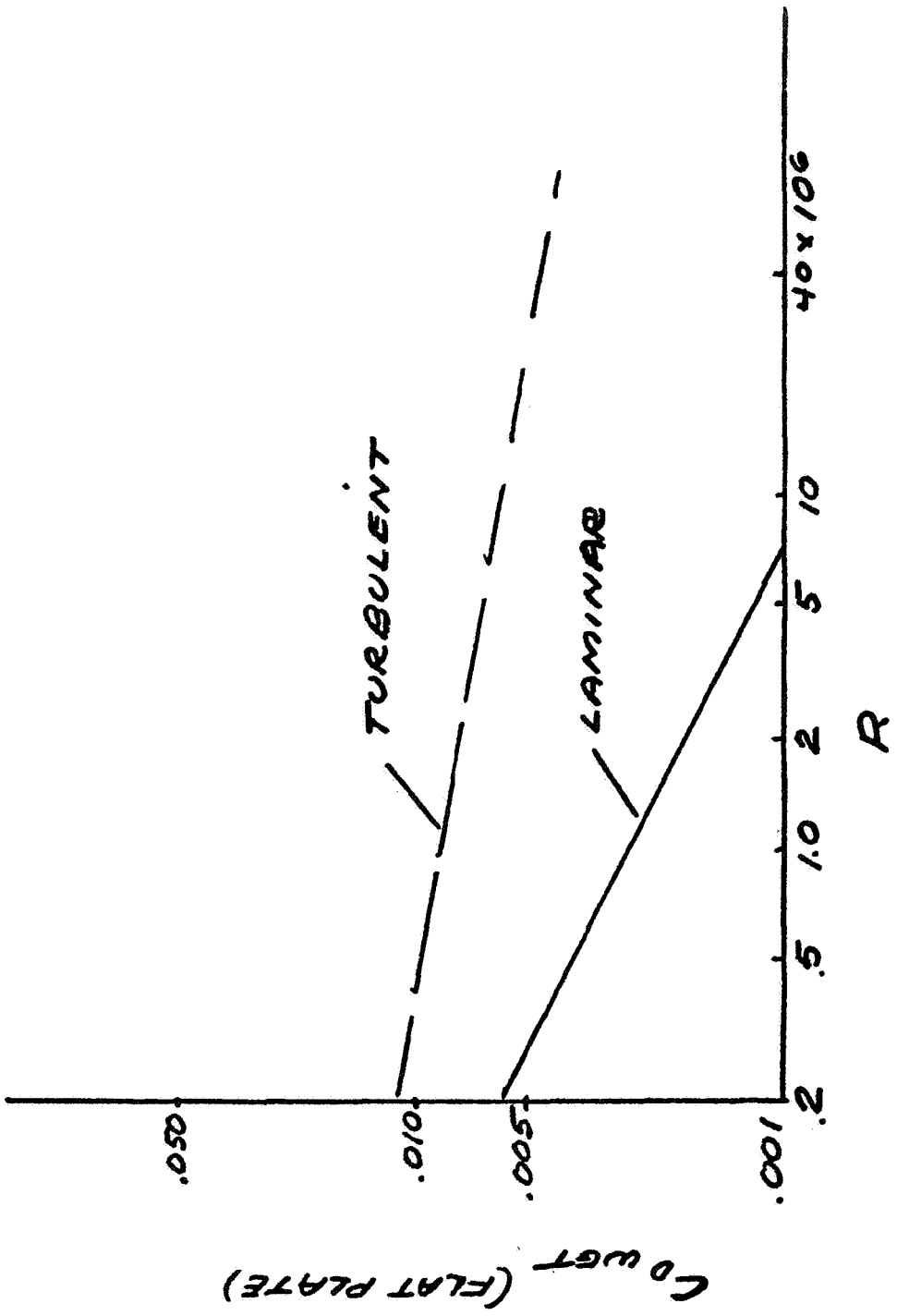

Figure 5. Effect of Flow Conditions on Flat Plate Drag

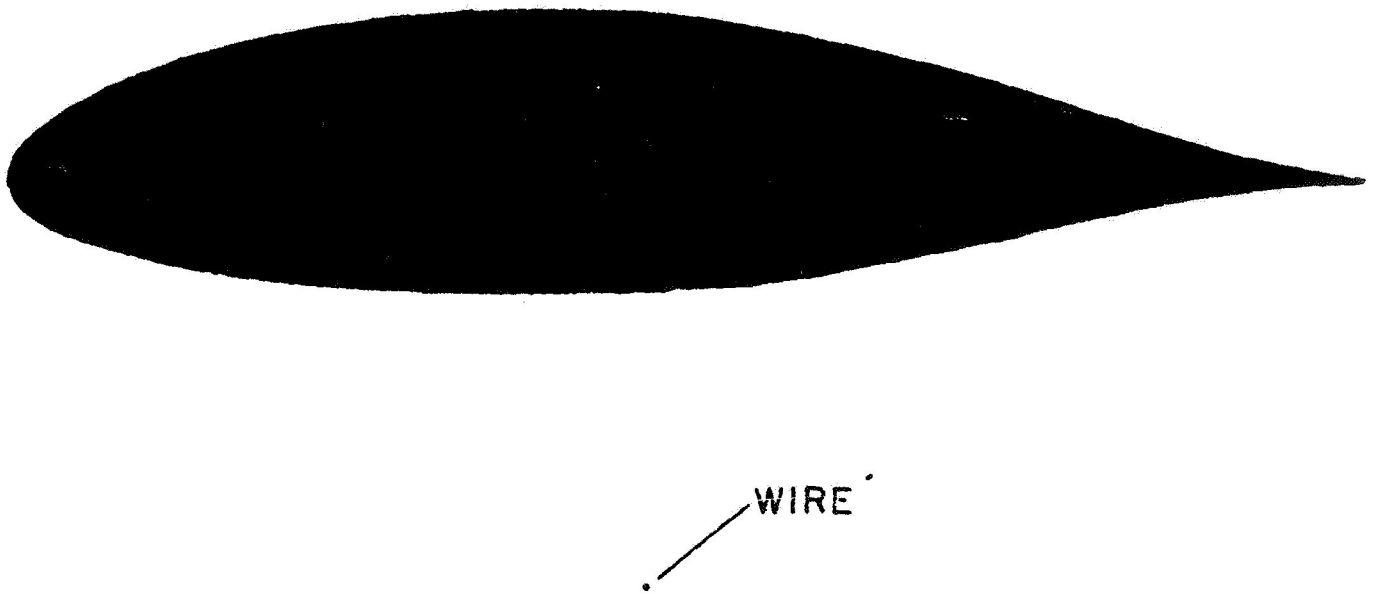

Figure 6. Airfoil Compared with Circular Wire Having Equal Drag

- EMPIRICAL METHODS
- WIND TUNNEL MEASUREMENTS
- THEORETICAL ESTIMATES

Figure 7. Drag Prediction Techniques

Figure 8. Relative Component Contribution to Drag

- SURFACE CONDITIONS
- FINENESS RATIO
- NOSE SHAPE
- WIND SHIELD ANGLE
- CONTRACTION RATIO

Figure 9. Factors Influencing Fuselage Drag

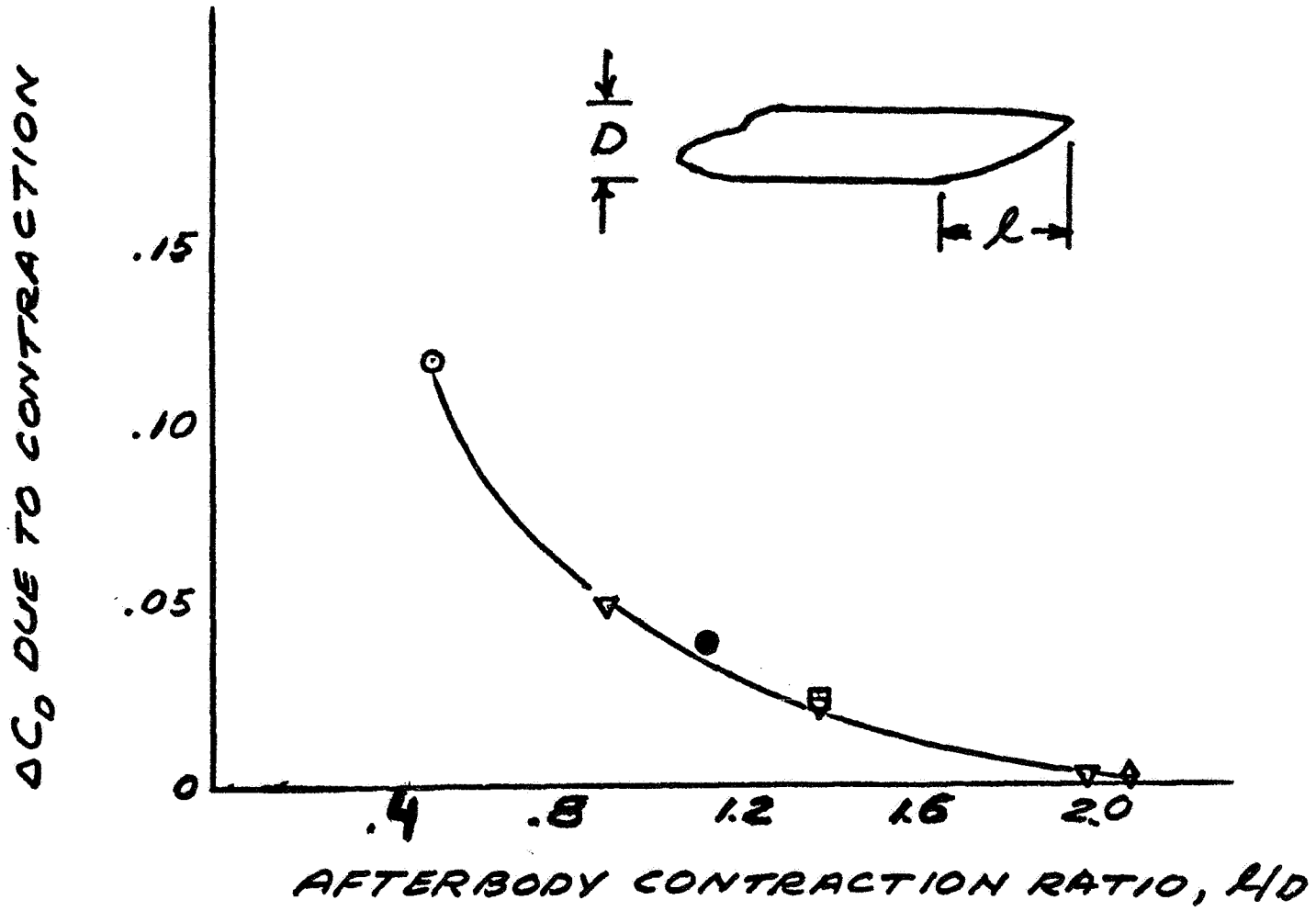

Figure 10. Effect of Afterbody Contraction Ratio on Drag

- AIRFOIL SECTION
- THICKNESS RATIO
- ASPECT RATIO
- PLAN FORM
- WING TIP
- SWEEP ANGLE
- SURFACE CONDITIONS

Figure 11. Factors Influencing Wing Drag

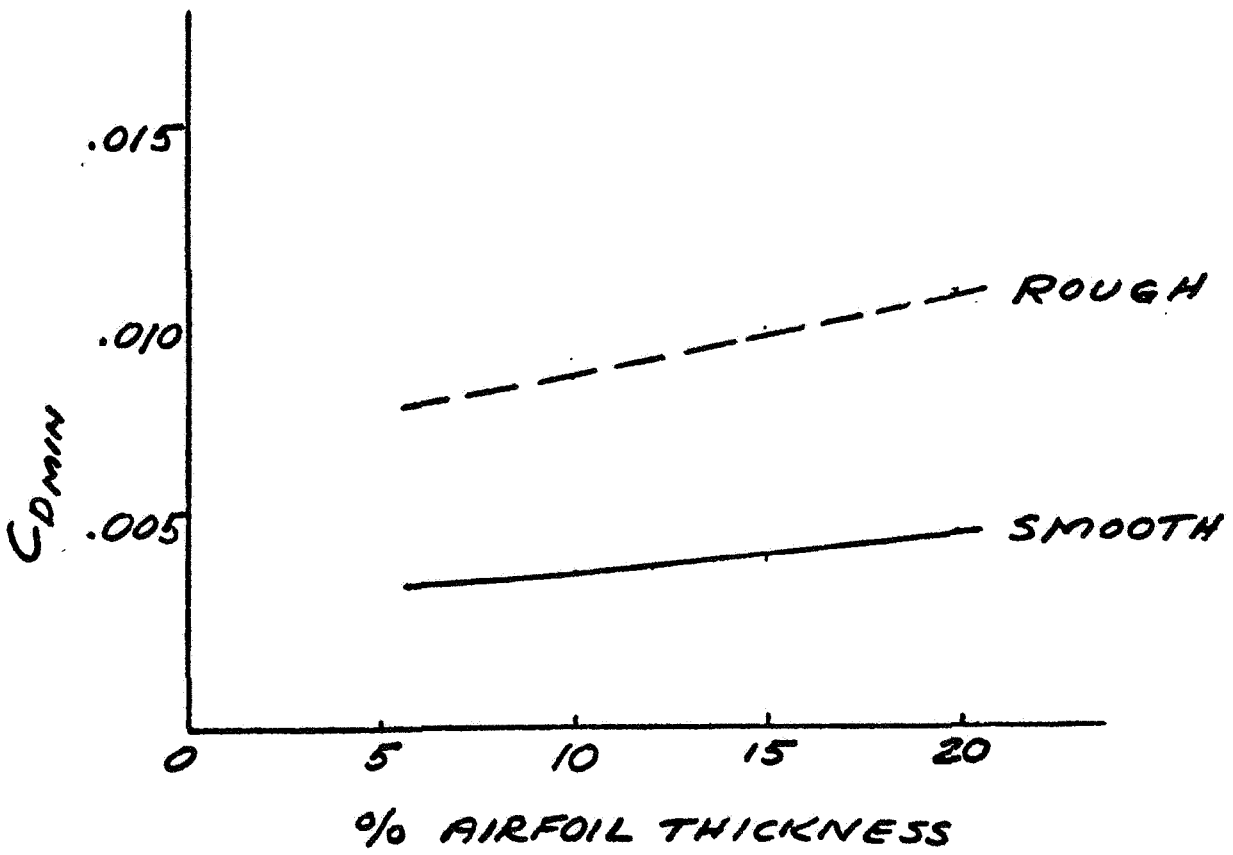

Figure 12. Effect of Roughness on Minimum Drag

- WING - FUSELAGE C_{M_o}
- TAIL LOCATION
- STATIC MARGIN

Figure 13. Factors Influencing Trim Drag

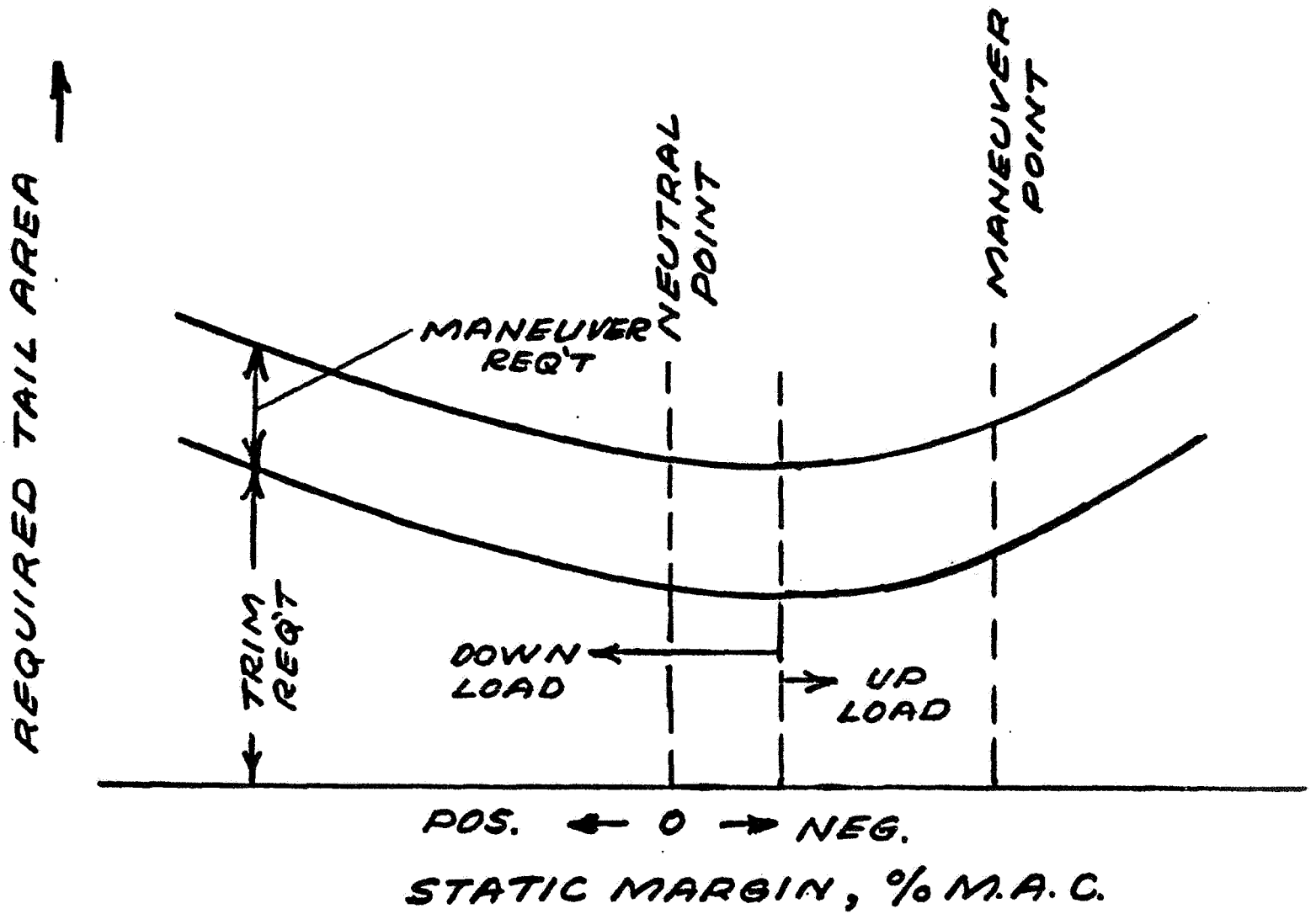

Figure 14. Typical Effect of Static Margin on Tail Size

- COST
- AERODYNAMIC DESIGN
- PROPULSION SYSTEM INTEGRATION
- FABRICATION DETAILS
- IDENTIFICATION OF SOURCES OF DRAG

Figure 15. Considerations for Drag of Complete Aircraft

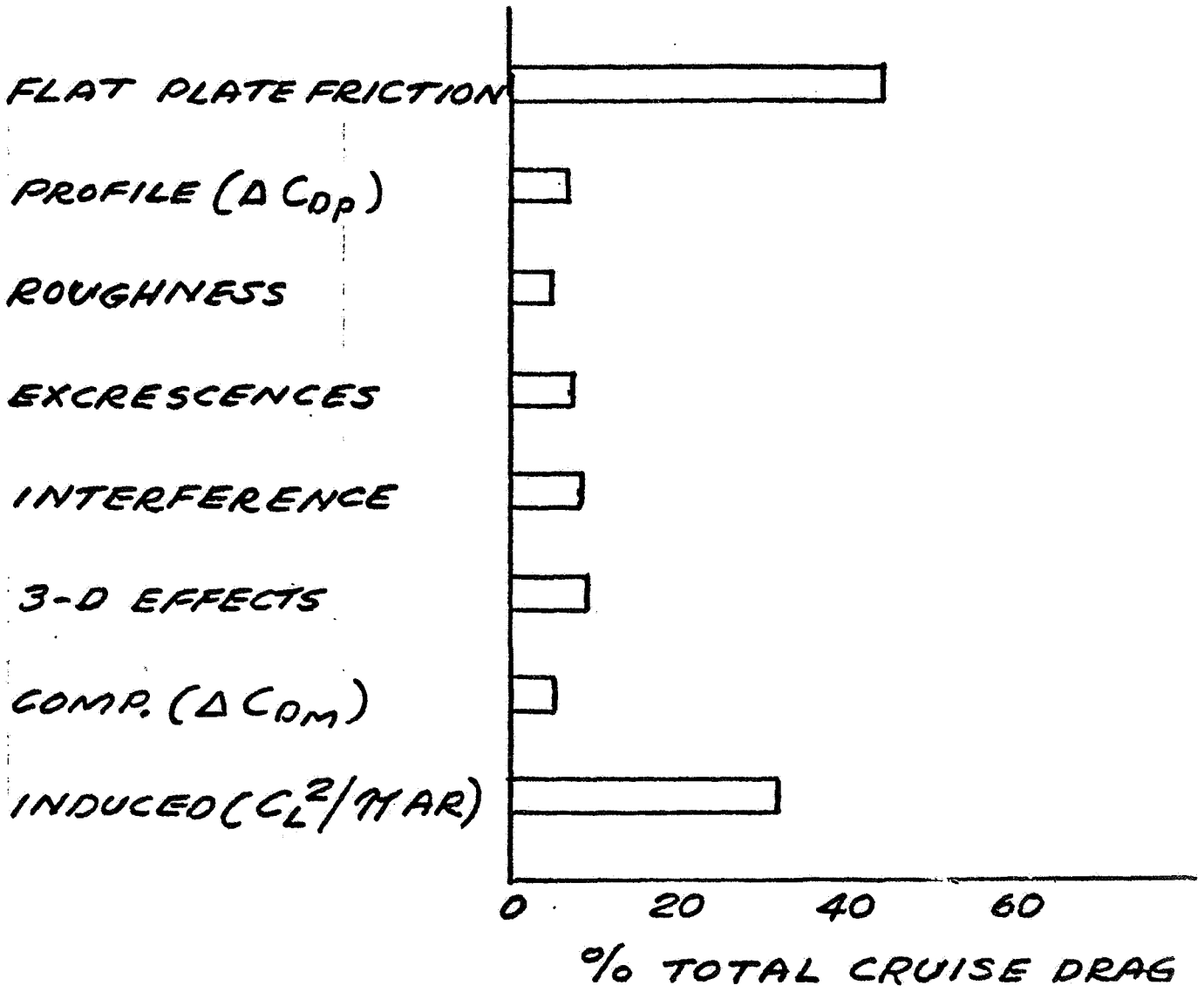

Figure 16. Typical Drag Buildup for Jet Transport

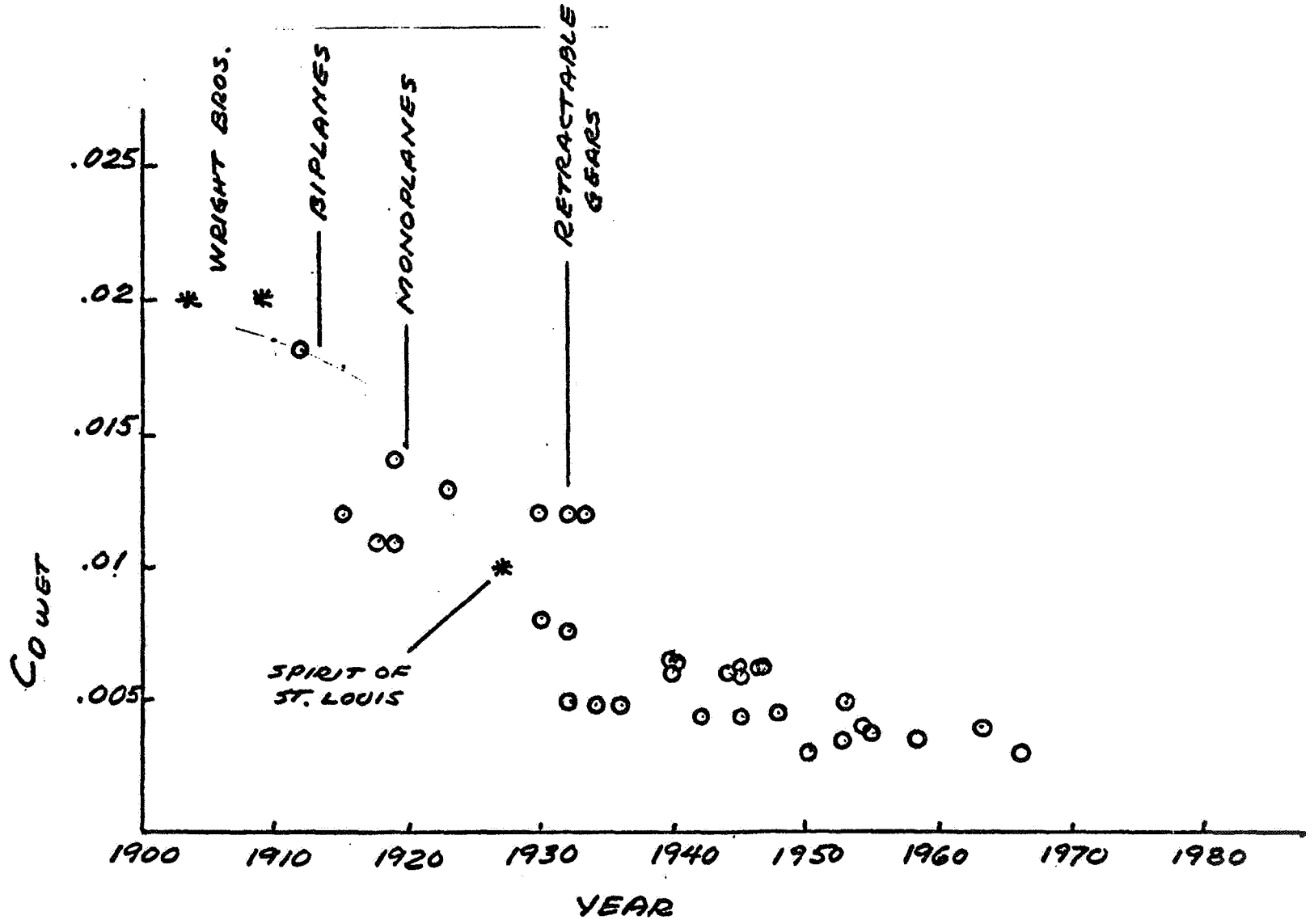

Figure 17. Historical Survey of Drag

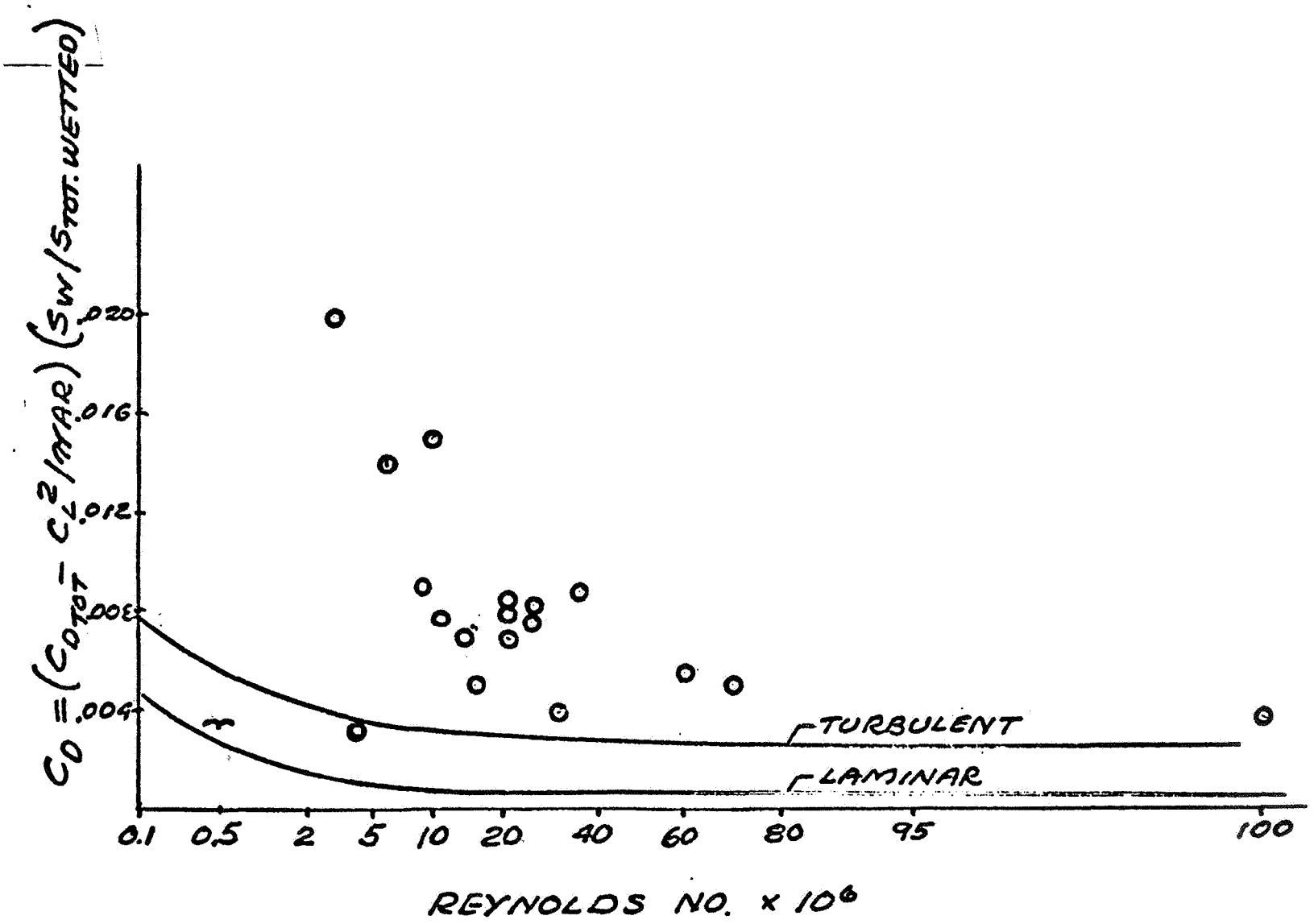

Figure 18. Comparison of Flight Data with Flat Plate Skin Friction

- NEED TO CLARIFY SOURCES OF DRAG FOR GENERAL AVIATION AIRCRAFT
- POINT OUT GREATEST POTENTIALS FOR DRAG REDUCTION
- IDENTIFY AREAS FOR R&D

Figure 19. Concluding Remarks

3. PAPERS OF SESSION I - STATUS OF DRAG PREDICTION METHODS

3.1 Overview of Drag Prediction Methods
D. Ruhmel, Cessna Aircraft Company

3.2 Prospects and Time Tables for Analytical Estimation of the Drag of Complete Aircraft Configurations
F. O. Smetana, North Carolina State University

3.3 Summary of Drag Cleanup Tests in the NASA Langley Full-Scale Tunnel
M. O. McKinney, NASA Langley Research Center

3.4 Simplified Theoretical Methods for Aerodynamic Design
J. Tulinius, NASA Langley Research Center

3.5 Drag Reduction/Back to Basics
O. W. Nicks, NASA Langley Research Center

3.1 Overview of Drag Prediction Methods

D. Ruhmel
Cessna Aircraft Company

This paper was not submitted for inclusion in these proceedings.

3.2 Prospects and Time Tables for Analytical Estimation of the Drag of Complete Aircraft Configurations

Frederick O. Smetana
North Carolina State University

The estimation of the aerodynamic drag of a proposed subsonic aircraft configuration is still largely an art practiced with more or less skill by those called upon to perform it. For bodies such as fuselages and nacelles, one usually employs a correlation of wind tunnel and flight test drag data against finess ratio and surface area for generally similar bodies at low angles of attack as a basis for estimation. Wing and empennage profile drag are usually estimated from the rather extensive collection of airfoil test data which is now available. The drag due to lift can be determined in what may be called a semi-empirical fashion, that is to say, an adequate theory is usually simple enough to apply with perhaps some biasing here and there to make it agree better with experimental results. Interference effects, power effects, cooling losses, and protuberance drag are almost always obtained by extrapolation from previous experience.

The reason for following the aforementioned procedure is quite simple: It's the only one, one could realistically conceive of undertaking--until recently at least. Now, however, the situation is beginning to change. Largely, because of the capacity of the digital computer to carry out literally millions of calculations inexpensively in a short period of time, it is now possible to

1. Determine in a rigorous fashion from fundamental principles the lift, drag, and pitching moment of airfoils without concave surfaces at moderate angles of attack with good accuracy.
2. Determine reliably the lift, drag (profile as well as induced), and pitching moment distributions on moderate-to-high aspect ratio unswept wings or, alternately, the lift, pitching moment, and induced drag only of wings of arbitrary sweep and aspect ratio.
3. Determine with a fair degree of confidence the drag of quasi-streamlined bodies having a plane of symmetry, if the body is aligned with the stream.
4. Determine in some instances the interference effects of nacelles and fuselages on wing lift, or alternately the inviscid pressure distributions on simple, complete configurations.

Any of these four calcualtions can be done today in less than 15 minutes at a cost of less than $80.00. A more significant expense is frequently the preparation of an input data set to the computation program. For a fuselage some 1800 coordinates accurately

representing the half-body and related so as to describe the body surface by quadrilaterals of nearly equal area are required.

The boundary layer routines used in these calculations are two-dimensional momentum integral types, although on simple axisymmetric bodies at zero angle of attack as well as airfoil problems, finite difference calculations are possible without exhorbitant additional cost or excessive computer storage requirements. The use of steady-flow, two-dimensional boundary layer model and its associated calculation techniques, however, make it difficult to locate the flow separation point accurately. Their use makes it almost impossible to determine the flow behavior in the separated wake (where the flow is almost invariably three-dimensional and unsteady). Flow models and calculation procedures to overcome these deficiencies are known but require computation times and computer storage two-to-three orders of magnitude larger than are presently practical for routine engineering analysis. As a result, completely analytical treatments of

1. the lift, drag, and pitching moment of bodies at angle of attack
2. the behavior of airfoils and wings near $C_{L_{max}}$ and beyond
3. flow separation due to interference
4. viscous flow over swept and low aspect ratio wings
5. turbulent onset flows containing a helical component and/or energetic streamwise component
6. disturbances produced by protuberances;

cannot be anticipated until the necessary computer hardware is available, estimated by Chapman (Ref. 1) to be about 1985.

There are, however, a number of developments known to be in progress which should reach fruition by the time the next generation of "number crunching" computers reaches the market, about 1977. Among these are

1. Improved singularity distribution techniques which permit the inviscid flow shield over bodies to be calculated with fewer but curved panels and which can give reliable results for bodies having concave surfaces.
2. Improvements on the Allen-Perkins method of estimating the forces on inclined bodies of revolution wherein the "inviscid" portion of the flow is to be calculated from a distribution of singularities.
3. Availability of three-dimensional boundary layer calculation routines for simple but non-axisymmetric bodies.
4. Availability of optimization algorithims linked to viscous flow field calculation schemes to permit one to specify the aerodynamic behavior

of bodies or wings desired and obtain the geometry which will provide it (Ref. 2). Later, this approach can be expanded to more complex configurations.

If progress in computer hardware continues as expected, then by about 1990 it should be possible to input a contemporary configuration, state some constraints as to performance, stability, and geometry, and the program will produce the geometric offsets for a modified configuration which will satisfy the stated constraints in an optimum fashion. Other programs could then be employed to produce the requisite structural configurations and to drive appropriate numerically-controlled manufacturing equipment. Whether these things come to pass will be dependent upon

1. The cost of developing the programs. Presumably this would be borne largely by the government.
2. The cost of running the programs. This is largely dependent upon the availability of hardware of the requisite speed and capacity.
3. The cost of engineering and technician labor to implement the programs or alternately, to do the computation task or parts of it manually.
4. The economic incentive to modify an existing aircraft or to build a new one for improved performance and stability with the same fuel consumption.

From this vantage point at least, one would estimate that a 10% increase in development cost could be tolerated if these procedures can yield a significant improvement (10%) in vehicle performance with the same power plant and with no degradation in handling qualities.

References

1. Chapman, Dean R., "Remarks presented at the NASA Conference on Aerodynamic Analysis," March 1975.
2. Hicks, R. M., and Vanderplaats, G. N., "Application of Numerical Optimization to Airfoil Design," NASA Conference on Aerodynamic Analysis. Also NASA TMX-3213, March 1975, 24 pp.

3.3 Summary of Drag Clean-Up Tests in NASA Langley Full-Scale Tunnel

Marion O. McKinney
NASA Langley Research Center

Introduction

Before I start to describe the drag clean-up work in the Langley full-scale tunnel, let me recognize the pre-eminent work in the drag field. The late Sighard F. Hoerner in his book Fluid-Dynamic Drag (Ref. 1) has done a wonderful job of pulling together, organizing, and summarizing the vast and fragmented knowledge of aerodynamic drag. His book is the Bible on the subject. The book is vastly detailed in its presentation and references, and is about all one would need to work the drag problem for general aviation airplanes other than those that are pushing the drag-rise Mach number. Such high-speed aircraft are particularly subject to compressibility and interference problems which will be addressed by Mr. Thomas C. Kelly in his paper for the wing-drag session of this workshop.

It should be noted that Hoerner's book is not a "how-to" book. It does not set forth a design procedure. Any sensible aerodynamicist knows that airplanes are not designed for low drag alone. They must be designed to do their job (accommodate people, etc.); they must be designed for practical, economical manufacture; and they must be designed with enough sex appeal to sell. So Hoerner's book, in effect, tells how to get to the ideal shape, and the drag price for departing from that ideal shape. Thus it gives the drag information needed for trades of performance versus other requirements.

Potential in Drag Clean-Up

Now to get to the specific subject of this paper--the drag clean-up work in the full-scale tunnel. This work was done between 1935 and 1945 on W. W. II fighters and light bombers; so there is reason to question how applicable it is to today's general aviation airplanes. If it is applicable at all, it is obviously most applicable to the propeller powered airplanes. Since I am not very well acquainted with general aviation airplanes, I started out by making a few calculations that would let me see in terms of size, shape, and drag how some of today's general aviation airplanes compare with the small military airplanes that were the subject of the drag clean-up work.

Figure 1 presents a tabulation which resulted from these calculations. Here are compared certain characteristics of early W. W. II fighters and today's light twin general aviation aircraft. The figures given in each column are averages for five aircraft. These aircraft did not differ from the mean by more than ±15 percent in any item. The W. W. II fighters selected were the cleaner of the 23 aircraft for which results are summarized in references 2 and 3. There are the P-40, P-41, P-51, P-63, and F4F. They are early models, if not prototypes, of these aircraft as can be inferred from the low gross weight. The light twins are those for which drag could be calculated from information given in a recent issue of Jane's All The World's Aircraft--that is, aircraft for which maximum speed was quoted at sea level or within the range of altitude for which supercharged engines were flat-rated. The calculated characteristics of the light twins are therefore no better than the information in "Jane's" or assumptions of 80 percent propulsive efficiency and 80 percent span efficiency factor with regard to drag due to lift.

Now let us trace through the figures and see what we can conclude. The two classes of airplanes have very nearly the same span and length. The light twins have 20 percent less wing area and 10 percent more wetted area, which factors would tend to cause their drag coefficient to be 30 percent higher than that of the fighters. On the other hand, they have only about one-half as much engine to cool which tends to offset one-third to one-half this difference. So, for equal aerodynamic cleanness we might expect the light twins to have 10 to 20 percent higher drag than the fighters. The figures show that the value of C_{D_o} (drag coefficient at zero lift) for the present light twins is indeed slightly higher than that of the fighters as received at the full-scale tunnel before the drag clean-up. Actually since the value of C_{D_o} for the light twins is only 10 percent higher than that of the fighters (as received), it would seem that they were slightly cleaner. (Before we go further, note that the measured values of C_{D_o} for the fighters have been corrected for Reynolds number effects from the 80 mph speed at which the tests were run to the 200 mph speed of the light twins.)

Let us continue by running down the rest of the drag figures for the fighters as received. The friction drag coefficient is that calculated on the basis of the wetted area, body and airfoil thickness, and a fully turbulent boundary layer. The cooling and parasite drag values are specifically those of the P-41 which will be discussed later. The figures for the cleaned up fighters show marked reductions in cooling and parasite drag. These reductions were achieved by reasonable changes which could be made on a practical operating airplane. The friction drag could not be reduced without impractical surface smoothing. But there was a substantial reduction in total C_{D_o}.

For the present light twins, the friction drag was calculated and was larger than that of the fighters because of the greater wetted area and because of the smaller wing area used as a reference. The cooling and parasite drag could not be separated. The last column indicates what the potential for drag clean-up might be. On the basis of the cleaned-up fighter data, the parasite drag might be similar to that of the fighter, the cooling power of the engines of only one-half the total power might be only one-half as great; and the total C_{D_o} might be reduced from 0.0255 to 0.0195. This is a 13 percent reduction which would result in a 4 percent increase in speed, or a 13 percent increase in range or reduction in fuel consumption at the same speed.

The foregoing figures are admittedly very rough, but they indicate enough potential for drag reduction to warrant pursuing the subject. Another conclusion that might be inferred from the drag figures for the light twin is that parasite drag can hardly be responsible for the high drag over and above friction drag; so there must be very substantial gains to be made in cooling drag.

Full-Scale Tunnel Tests

The remainder of this paper will examine some of the principal items in the W. W. II airplane drag clean-up work which accounted for considerable amounts of excess drag. And by the way, I have gone over general aviation aircraft in the NASA hangars, and at our local airport, and have found all of these items on current general aviation aircraft--not all on any one aircraft, of course. The total of all of them would make the value of C_{D_o} of the average light twin of Figure 1, 30 percent higher than that shown.

Drag Clean-Up Tests of a Representative Airplane

The procedure in the full-scale tunnel tests was to remove all the protuberances from the airplane, to seal all openings, and to fair obvious sources of drag such as a blunt sealed radial engine cowling. The drag of this sealed and faired airplane was measured and if there was any reason to suspect that it was unduly high, the trouble spots were sought with tufts, surface pressure data, and wake surveys and were then refaired to give a good basic shape. Such a sealed and faired condition for the XP-41 airplane is indicated in Figure 2.

As the seals and fairings associated with the powerplant installation were removed one-by-one, the drag of the following items was identified as show in Figure 3, the drag values being given in percent of the drag of the airplane in the sealed and faired condition:

Open engine cowling engine and exit to permit cooling air flow	18.6%
Unfaired carburetor airscoop	3.6%
Cooling airflow through accessory compartment	3.0%
Projecting exhause stacts and open hole through which they project	3.6%
Intercooler	6.6%
Oil cooler	10.2%

The total drag of these items associated with the power plant installation increased the drag 45.6 percent above that for the sealed and faired condition.

The drag for the additional features required to bring the airplane to service condition are shown in Figure 4 by the underlined numbers:

Removing seals from gaps in cowling flaps	5.4%
Opening case and link ejector chute	1.8%
Opening seals around landing gear doors	1.2%
Sanded walkway	4.2%
Radio aerials	4.8%
Guns and blast tubes	1.8%

The total drag of this group of protrusion, roughness, and leakage items equals 19.2 percent of the drag for the sealed and faired condition.

Look at what has happened to the clean airplane we started with! In order to make it useful we have increased its drag nearly 65 percent mostly by adding items that by themselves do not appear particularly large.

All of this drag, however, is not necessary. Additional tests and careful analysis showed that the drag of the power plant items could be reduced to 26.6 percent and the drag of the roughness and leakage items could be reduced to 2.5 percent, thus saving nearly 36 percent of the drag of the basic condition.

It is particularly important to note that in general those items have drags of only a few percent each. Yet, when taken altogether, they add up to an impressive total. We started with an airplane in Figure 1 that was exceptionally clean and in bringing it to a usable configuration unnecessary drag was added along with the drag associated with the necessary functions. The message here would seem to be that there is a lot to be gained from attention to details in aerodynamic design.

Design Features Contributing to Excessive Drag

The following selected examples illustrate some of the design features in which lack of attention to detail led to excessive drag.

Cooling drag - The first principles of reducing cooling drag are: do not take in too much air, keep the internal flow passages clean, and dump the air tangential to the surface in a streamwise direction. But look, in Figure 5, at what a difference details can make. An exhaust collect or ring, cowling-flap actuating linkage, and a sharp lip just inside the cowling flap outlet caused an increase in drag coefficient of 0.0007 which is 5 percent as great as the friction drag of the entire airplane.

Variable cowling outlet flaps are, of course, used to reduce cooling drag in high speed conditions; but look, in Figure 6, at what leakage through joints in the flaps can do if they are not sealed. High pressure air from inside the cowling squirts out normal to the stream causing an increase in drag of 4 percent of the airplane friction drag for this case. Such cowling leakage was a very common cause of excessive drag in the World War II airplane as received at the full-scale tunnel. It could probably be more properly classified as leakage drag than cooling drag, but in this paper I have chosen in most cases to relate leakage drag to the functional item with which it is associated.

Engine exhaust stacks - It would seem that exhaust stacks if properly recessed or faired and turned rearward would cause virtually no external drag, but improper treatment of exhaust stacks can result in large amounts of drag as shown in Figure 7. The installation shown at the top of the figure appears very similar to the treatment of the exhaust nozzles of turboprop engines in some of today's general aviation airplanes; and it caused an increase in drag corresponding to 16 percent of the friction drag of the entire airplane. The installation shown at the bottom of the figure does not protrude into the stream, but caused a drag increase of 8 percent of the friction drag because the exhaust gases and the cooling air coming out the hole around the exhaust stacks were ejected almost normal to the airstream.

It is also evident from such installations that designers sometimes fail to take advantage of the considerable thrust the exhaust gases can affort if directed rearward. I do not have data for today's general aviation engines, but based on the exhaust gas thrust per horsepower of World War II fighter engines, I would expect the thrust coefficient $(\frac{T}{qS})$ of the average light twin of Figure 1 to be 0.0026 at full power and a speed of 200 knots. This is enough thrust to offset 15 percent of the friction drag of the airplane.

Landing gears - Even retractable landing gears can have considerable drag if not properly treated. Figure 8 shows that the fully faired landing gear shown at the top of the figure had a drag of 7 percent of the friction drag when the seals over the joints were removed. This drag was caused by air leakage through the 1/8-inch cracks around the coverplate. Removal of the rear door to expose half the wheel resulted in

an additional small (2 percent C_{D_f}) increase in drag. This result, that failure to seal the landing gear doors caused considerable drag, was found repeatedly in the drag clean-up tests.

Control surface gaps - Figure 9 indicates that tail surface gaps can cause an increase in drag of about 5 percent of the friction drag--and it would seem that the ailerons could cause an additional 2- to 3-percent increase. Such control surface drag can result from several sources. Air can leak through unsealed gaps from the high pressure side of the surface to the low pressure side where it can exhaust normally to the stream as a jet spoiler. The base drag of the blunt rear of the fin or stabilizer can cause considerable drag, both directly as base drag and additionally, by pumping air through the airframe if there are lightening holes in the rear spar. Hoerner indicates that such base drag can be reduced markedly, in fact the drag of the entire tail can be reduced nearly 20 percent by reducing the thickness of the airfoil at the blunt base of the fixed surface about 10 percent so that it is thinner than the maximum thickness of the control surface.

Irregularities and leakage - Figure 10 shows the results of irregularities and leakage in one small area of a wing which had a fold joint and a number of access panels. Probably very few general aviation airplanes have features corresponding to the wing-fold joint, but the total number of doors and access panels might be even larger than for this case. In any event, most drag of this type can be eliminated by better fitting and by elimination of air leakage.

Walkways - Figure 11 shows the drag coefficient of a sanded walkway to be 0.0010, or 8 percent as great as the friction drag. This is an extreme case because the walkway protruded about 1/4-inch above the wing surface. But, even for more representative cases, the walkway drag was two-thirds this great.

Conclusions

It would seem that two general conclusions might be drawn from the foregoing analysis and examples.

1. There is probably considerable possibility for marked reductions in the cooling drag of general aviation airplanes with reciprocating engines.
2. Careful attention to detail design and fabrication can result in substantial reductions in drag.

References

1. Hoerner, Sighard F., Fluid Dynamic Drag, published by the author, 1958. Library of Congress Caralog Card No. 57-13009.

2. Dearborn, C. H., and Silverstein, Abe, Drag Analysis of Single-Engine Military Airplanes Tested in the NACA Full-Scale Wind Tunnel. NACA Wartime Report ACR, October 1940.

3. Lange, Roy H., A Summary of Drag Results from Recent Langley Full-Scale-Tunnel Tests of Army and Navy Airplanes. NACA ACR No. L5A30, 1945.

	EARLY WWII FIGHTER+		LIGHT TWIN+	
SPAN	37		39	
L.O.A.	31		32	
WING AREA	240		200	
WETTED AREA	950		1050	
HORSEPOWER	1100		560	
T.O. WEIGHT	7100		5700	
	AS RECEIVED	CLEANED UP	PRESENT	POTENTIAL
C_{D_o}	.0225*	.0175*	.0255	.0195
$C_{D_{friction}}$	.0130	.0130	.0170	.0170
$C_{D_{cooling}}$	.0070	.0040	.0085	.0020
$C_{D_{parasite}}$	.0025	.0005		.0005

+AVERAGE OF FIVE AIRCRAFT EACH.
MAX DEVIATION FROM MEAN = ±15%

*CORRECTED TO SAME SPEED AS LIGHT TWIN

Figure 1. Drag Comparison

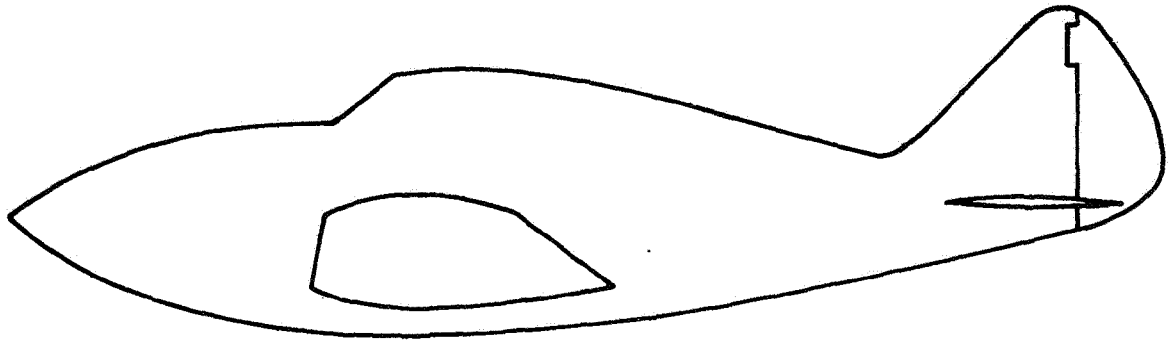

Figure 2. Airplane in the Faired and Sealed Condition

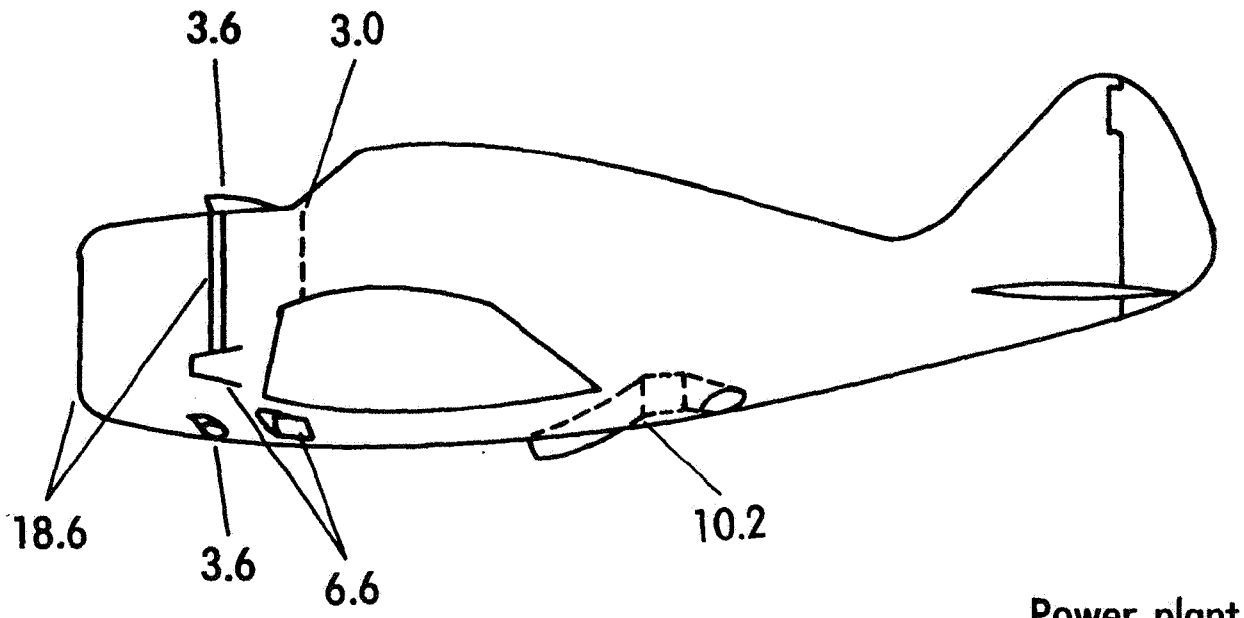

Note: Numbers indicate added drag

in percent sealed-and faired drag.

Figure 3. Airplane with Power-Plant-Installation Drag Items Added

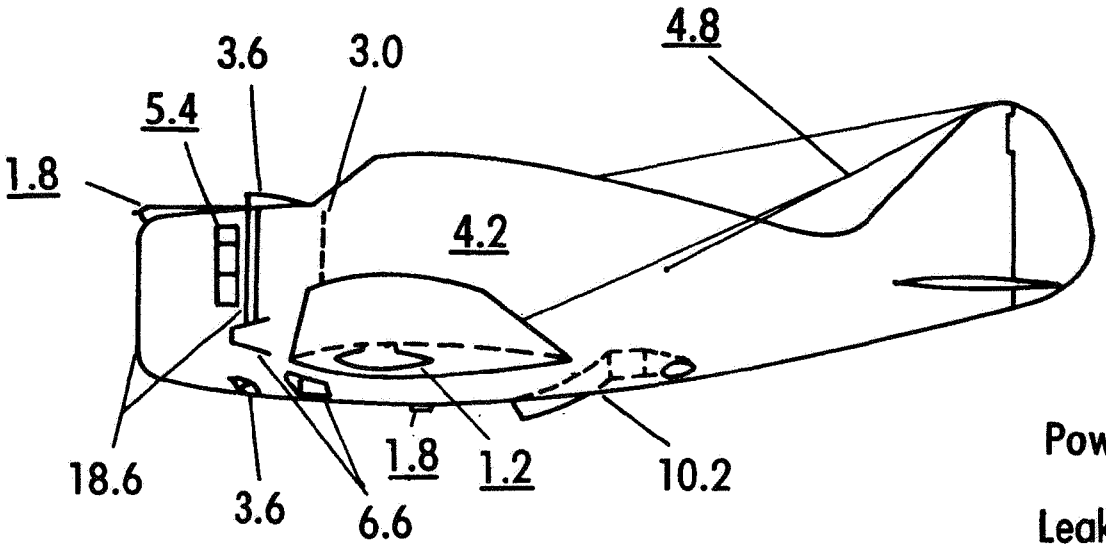

Power plant	45.6
Leakage and roughness	19.2
	64.8
Possible reduction	35.7

Note: Numbers indicate added drag in percent sealed-and-faired drag.

Figure 4. Airplane in the Service Condition

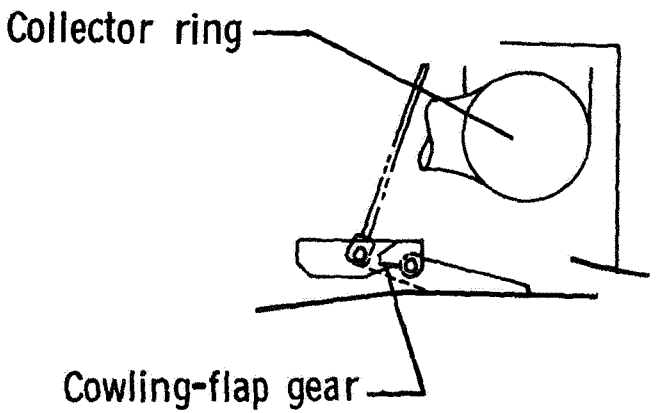

Section at original cowling inlet

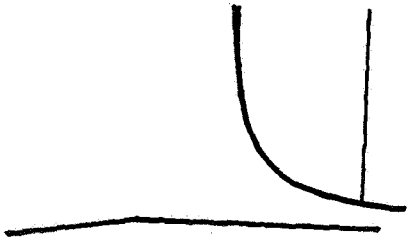

Section at smooth cowling outlet

$\Delta C_D = 0.0007$ or 5% C_{D_f}

Figure 5. Engine-Cowling Outlet

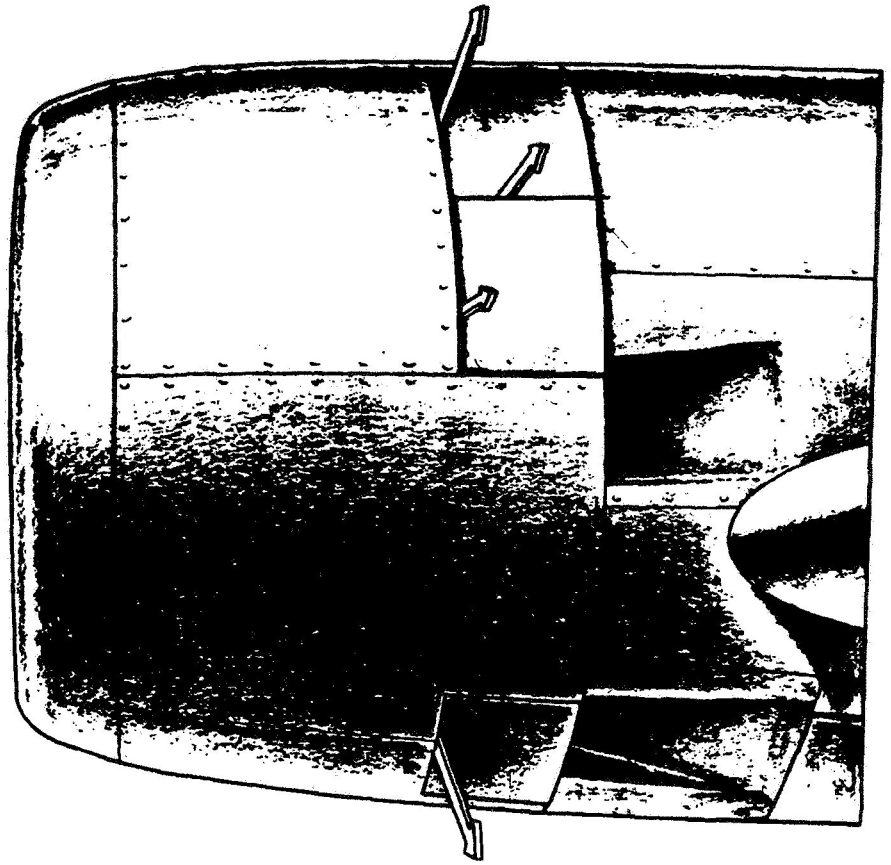

$$\Delta C_D = 0.0005 \text{ or } 4\% \ C_{D_f}$$

Figure 6. Cowling Flap Leakage

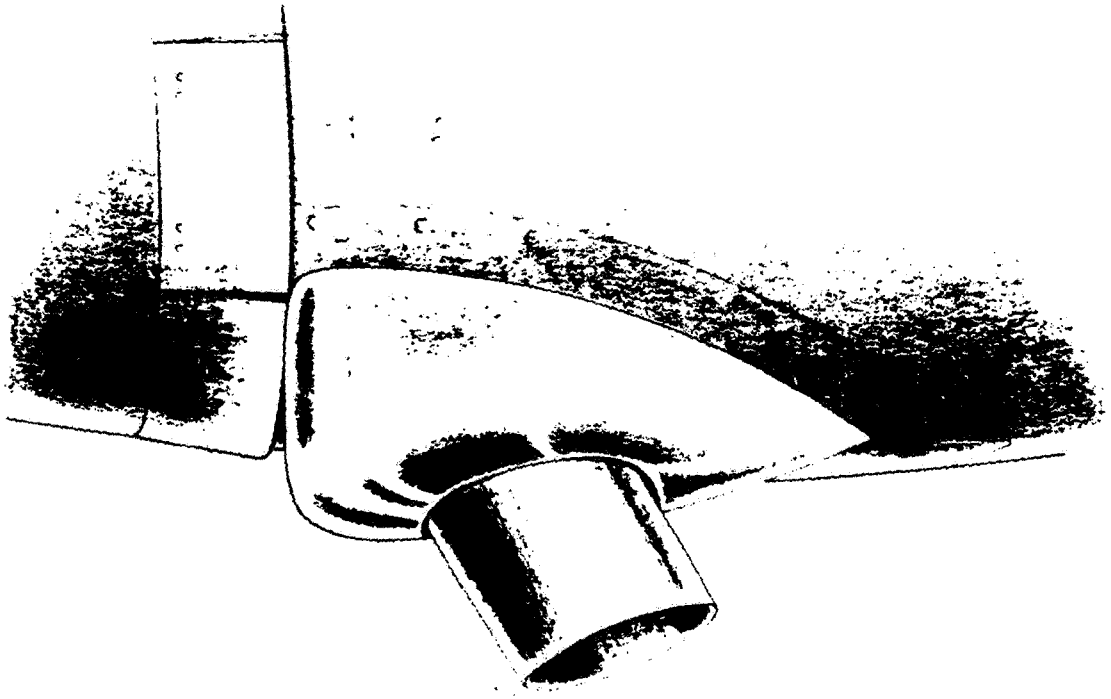

ΔC_D = 0.0021 or 16% C_{D_f}

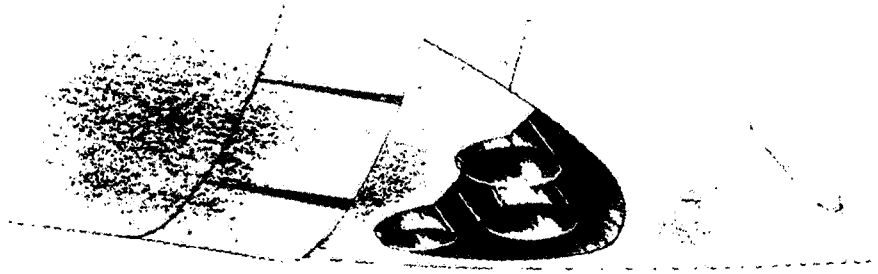

ΔC_D = 0.0010 or 8% C_{D_f}

Figure 7. Exhaust-Stack Drag

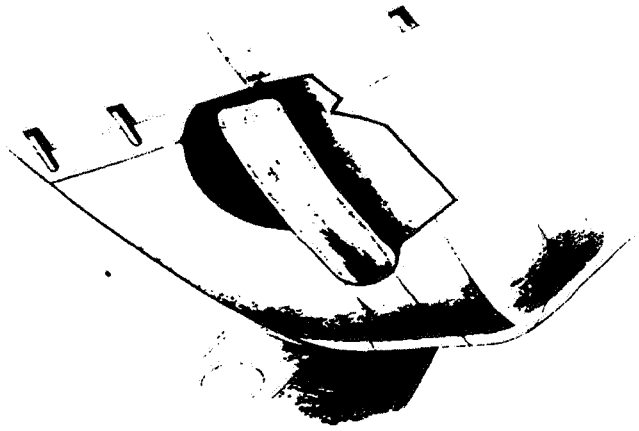

Full length fairing, not sealed

$\Delta C_D = 0.0009$ or 7% C_{D_f}

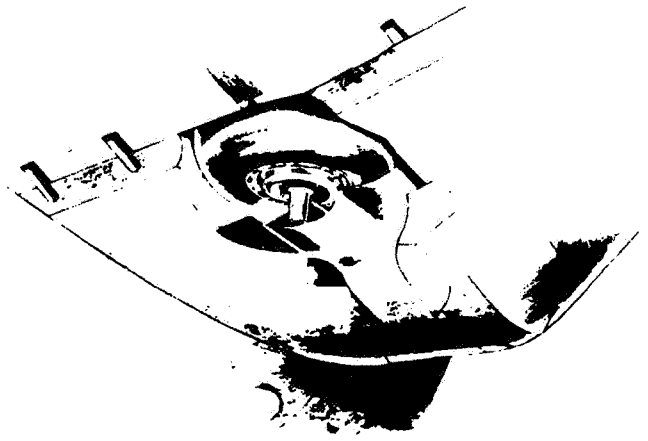

Short length fairing

$\Delta C_D = 0.0012$ or 9% C_{D_f}

Figure 8. Landing Gear Drag

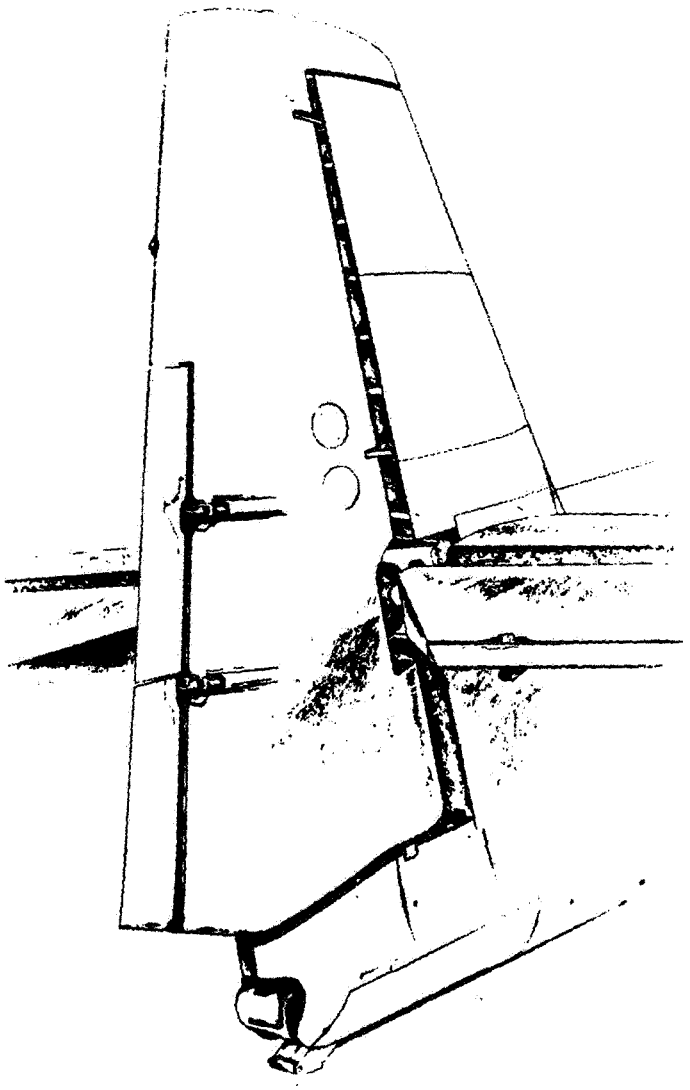

$\Delta C_D = 0.0007$ or 5% C_{Df}

Figure 9. Control Gap Drag

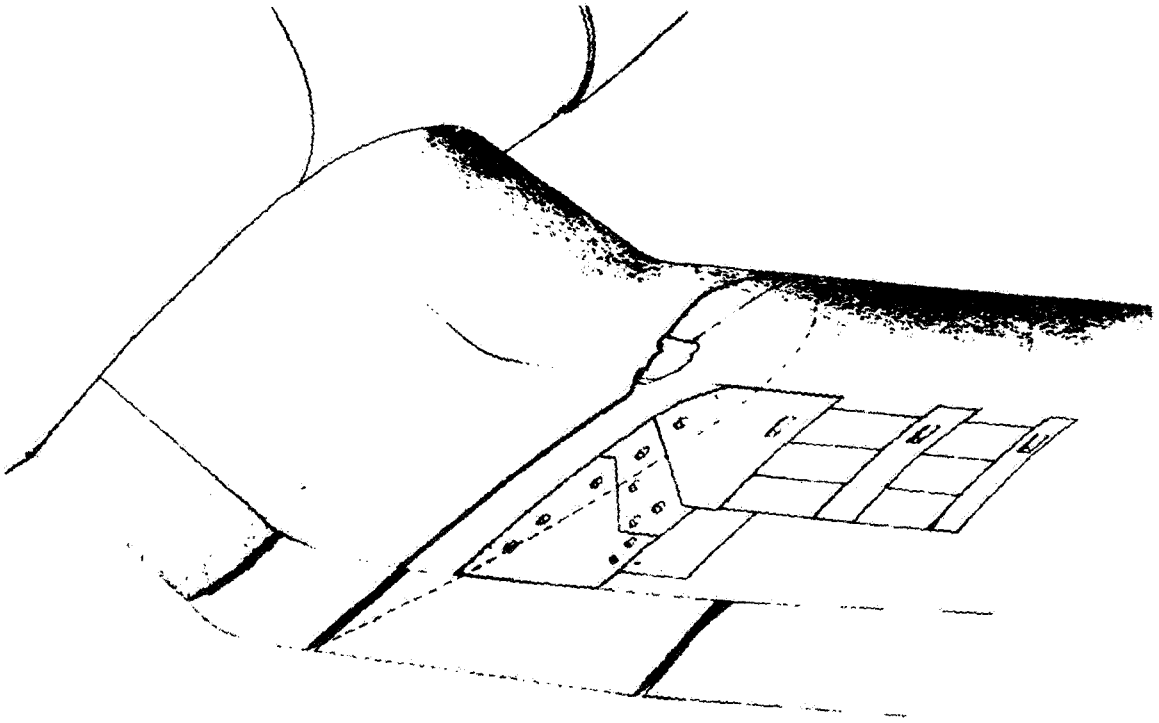

$$\Delta C_D = 0.0012 \text{ or } 9\% \, C_{D_f}$$

Figure 10. Irregularities and Leakage

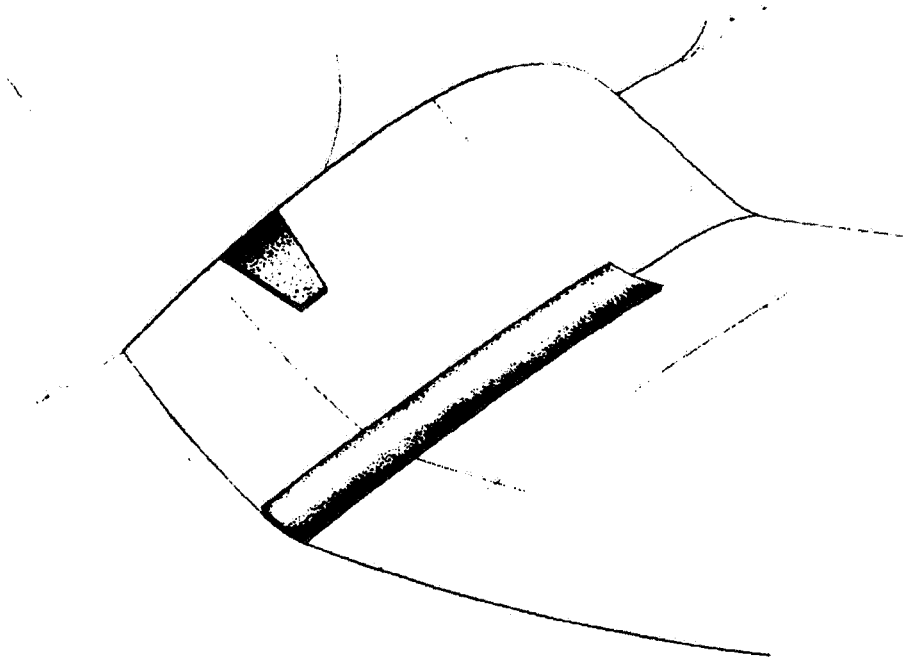

$$\Delta C_D = 0.0010 \text{ or } 8\% \ C_{D_f}$$

Figure 11. Sanded Walkway

3.4 Simplified Theoretical Methods for Aerodynamic Design

Jan R. Tulinius
NASA Langley Research Center

Introduction

The objective of this paper is to describe theoretical procedures which can be utilized by the general aviation industry for aerodynamic design. It is recognized that the general aviation industry has a requirement for a wide range of levels of sophistication in aerodynamic design. However, very simple procedures requiring minimum computer size and operational costs, coupled with minimum input effort and maximum numerical stability, are in general required.

This paper is organized to first discuss the design process and theoretical methods used to design a wing. Then theoretical methods for estimating the interference velocities due to the fuselage, or other bodies, and nacelles are discussed. It is assumed that the flow fields due to the different components can be superimposed, and then the pressure coefficients computed from the Bernoulli equation.

Methods to estimate the induced, viscous form, and compressible drags are also discussed.

In addition, a procedure for modifying the surface contours to reduce adverse pressure distributions induced by component interference is discussed.

Source/Vortex Lattice

In order to theoretically design a finite aspect ratio wing, it is necessary to have a thick-lifting-surface theory. If the boundary conditions are linearized, the flow fields induced by the wing can be divided into two parts: (1) the flow field due to lift; and (2) the flow field due to thickness. Also, due to the linearization, the perturbation velocity due to lift can be linearly related to the local angle of attack of the mean camber surface and the perturbation velocity due to thickness can be linearly related to the freestream component of the gradient of the thickness distribution.

The most simplified thick-lifting-surface theory is the source/vortex lattice shown in Figure 1. The vortex lattice is a system of lifting lines where one lifting line is placed on each quadrilateral panel of the wing. The source lattice is analogous to the lifting line, except that the velocities induced by a source line

are rotated 90° to that induced by a vortex line. Also, the vortex lines cannot end in space, and, therefore, there must be trailing legs going off to infinity. The vortex lines are usually placed at the quarter chord of each panel and the source lines at both the quarter and three-quarter chord points of each panel. The wing surface velocities are computed at the three-quarter-chord point. Derivations of the influence equations for the source/vortex lattice along with second order corrections for blunt leading edges, interference between thickness and lift, and compressibility are given in References 1 and 2.

The source/vortex lattice can be used to solve for the surface pressures for a given wing twist, camber, angle of attack, and thickness distribution, or it can be used to solve for the wing twist, camber, angle of attack, and thickness distribution for a desired set of surface pressures.

Figure 2 describes how the wing can be designed using the source/vortex lattice. If an airfoil has been designed with the desired section properties, the wing surface shape, which will produce the same upper and lower surface pressures as the two-dimensional airfoil, can be solved for using the approach shown on the left side of Figure 2.

If no two-dimensional design is available, with the desired section characteristics, the second approach shown on the right side of Figure 2 can be used. This approach is analogous to the two-dimensional "ideal angle of attack" design technique discussed in Reference 3. Essentially what this design procedure does is define a wing which has minimum induced drag at the design lift coefficient and a minimum adverse leading-edge pressure gradient, for low viscous form drag, at what is defined as $C_{L_{OPT.}}$ in Figure 2.

As shown in Figure 2, this design procedure gives the wing camber and twist such that the induced-drag polar is tangent to the locus of minimum induced drags at C_{L_D} and the zero percent suction polar is tangent to the induced-drag polar at $C_{L_{OPT.}}$. The data should fall somewhere between these two polars. The zero percent suction drag is defined as that for which there is no thrust at the leading edge of the section.

General Slender Body Theory

General slender body theory can be used to compute the flow fields due to arbitrary shaped fuselages or other bodies. The theory requires access to only a body of revolution and a two-dimensional airfoil theory. The arbitrary body flow fields are computed, as depicted in Figure 3, by superimposing the flow fields from

the equivalent body of revolution plus a correction for the noncircular cross-section, which is computed with a two-dimensional airfoil program.

The correction flow field due to the noncircular cross-section is obtained by subtracting the two-dimensional solution for the circular cross-section from that for the noncircular cross-section. These solutions are obtained using the full three-dimensional boundary conditions in the two-dimensional airfoil program. The difference between the usual two-dimensional boundary conditions, which would represent the effects due to angle of attack and sideslip, and the three-dimensional boundary conditions is the effect due to body growth in the longitudinal direction.

There are several possible variations to the solution of the general slender body problem. Langley Research Center is in the process of developing a version which will be coupled with a thick-lifting-surface theory. A derivation of the theory is given in Reference 4.

The application of this theory and its component parts are listed in Figure 4.

Induced-Drag Analysis and Design

The induced drag of an arbitrary lifting system can be computed by an equivalent lifting line in the Trefftz plane. Figure 5 depicts the equivalent lifting line as seen from an end view. The dots represent the trailing legs of the horse-shoe vortices pointing out of the paper. The bound vortex line segments between the dots have circulation strengths equal to Γ. The line can be bent to represent any arbitrary wake shape. Also, any number of wakes can be represented to account for multiple lifting surfaces such as horizontal tails, canards, fins, and vertical tails as well as the wing. End plates or winglets can also be represented by this method.

As listed in Figure 6, the theory can be used to solve for not only the drag of a given configuration, after the span loads have been computed by the source/vortex lattice theory, but due to the quadratic nature of the drag expression, the optimum span loads can also be computed for both trimmed and untrimmed conditions using the method of Lagrange multipliers.

A computer program has been developed at Langley Research Center by Blair Gloss and the author to compute the induced drag for given span loads or solve for optimum span loads utilizing the equation in Figure 5. This equation is derived in Reference 1.

Viscous Form Drag

The viscous form drag is due to the boundary layer giving the airfoil section an effective change in shape due to the displacement thickness. As listed in Figure 7, the viscous form drag can be estimated from two-dimensional experimental drag polars at each span station along the wing, utilizing the wing section lift coefficient, and then integrating. This approach is presently being developed by Professor Ralph Krenkel of the Polytechnic Institute of New York under a NASA grant from Langley Research Center.

The viscous form drag can also be computed using an infinite yawed wing boundary-layer program at a series of span stations and then integrating. This approach is being presently worked on at Langley utilizing a boundary-layer program developed by Frank Dvorak and Frank Woodward (Ref. 5). In this approach, equivalent airfoils are developed at each span station which produce the same pressure distributions in two-dimensional flow as is developed by the actual section on the finite wing in three-dimensional flow. These airfoils are then run through the infinite yawed wing boundary-layer program to determine the section viscous form drag.

A third procedure, which is most appropriate during preliminary design, is to utilize a percent suction versus C_L curve from a configuration with similar section properties. This curve, shown in Figure 8, is obtained by the following equation:

$$\% \text{ suction} = \frac{C_L^{2}/C_{L_\alpha} - \left(C_D - C_{D_o}\right)}{C_L^{2}/C_{L_\alpha} - C_L^{2}/\pi AR} \times 100$$

The two boundary curves defined by C_L^{2}/C_{L_α} and $C_L^{2}/\pi AR$ are the upper and lower bounds, respectively. The location of the data relative to these two curves is primarily a function of viscous effects due to the section shape. As can be seen in Figure 8, the GA(W)-1 section has good characteristics up to a $C_L = 1.2$. The theory shown on this figure is from a vortex-lattice program developed by the author.

Compressible Drag

The compressible drag for conventional airfoils can be estimated using the crest theory. The crest theory states that drag divergence will occur shortly after the crest of the airfoil becomes sonic. The crest is defined as that point on the airfoil where the free stream is tangent to the airfoil surface. The critical pressure

coefficient is defined on Figure 9. It should be noted that it is a function of both sweep and the free-stream Mach number.

Once the Mach number for drag divergence M_{DD} is known, then an incremental drag due to compressibility can be obtained from an empirical curve of ΔC_{D_C} versus M/M_{DD}. This increment is then added to the incompressible drag obtained from the sum of the skin friction drag, induced drag, and viscous form drag.

Contour Modifications due to Interference Effects

With the procedures discussed in the previous sections, the surface pressures and associated pressure drag and lift can be estimated for a complete aircraft. Since the wing alone was designed to have an optimum pressure distribution, the addition of the fuselage, tip tanks, and nacelles will deteriorate the wing-alone design. These interference effects can be minimized by modifying the component contours to relieve the unfavorable interference pressures.

The incremental pressures due to the interference can be converted to incremental velocities through the use of the Bernoulli equation. As much of this increment as possible should be relieved by judicious placement of the components. Then the remainder should be minimized by locally contouring adjacent components.

The change in wing shape to account for flow induced by another component can be solved for by means of the relationship between velocity and the slope of the surface given in Figure 1. If the induced velocity is primarily in the chord direction, the thickness can be modified by the process outlined in Figure 10.

The contour modification might have to be divided between the wing thickness and the adjacent component surface. If the adjacent component is a body, approximately twice as big a slope change must be made for the same change in velocity as is needed on the wing. This is due to the fact that the perturbation velocity produced by a two-dimensional contour is about twice as large as that produced by a body. This is only an approximate rule of thumb. However, for the case of a sphere and a cylinder, the difference is exactly twice.

If the induced flow is perpendicular to the chord, then a twist and camber modification will be needed. In this case, it is just necessary to change the mean camber surface angle of attack by an amount equal to the induced angle of attack.

Conclusions

There exist sufficient simplified theories applicable to the design of general aviation aircraft. However, most of these theories have not been programmed for general aviation design purposes, and in many cases, the computer programs and their application have not been published in the open literature.

Langley Research Center is supporting the development of programs, utilizing these theories, which will be sized for general aviation purposes. Some of these programs are being developed by center researchers and others under university grants. A significant portion of this capability will be available a year from now.

References

1. Tulinius, J., Clever, W., Niemann, A., Dunn, K., and Gaither, B., "Theoretical Prediction of Airplane Stability Derivatives at Subcritical Speeds," NASA CR-132681, 1975.
2. Tulinius, J., "Theoretical Prediction of Thick Wing and Pylon-Fuselage-Fanpod-Nacelle Aerodynamic Characteristics at Subcritical Speeds," NASA CR-137578, 1974.
3. Abbott, I., and von Doenhoff, A., Theory of Wing Sections, Dover Publications, Inc., 1959.
4. Ashley, H., and Landahl, M., Aerodynamics of Wings and Bodies, Addison-Wesley Publishing Co., Inc., 1965.
5. Dvorak, F., and Woodward, F., "A Viscous/Potential Flow Interaction Analysis Method for Multi-Element Infinite Swept Wings," NASA CR-2476, 1974.

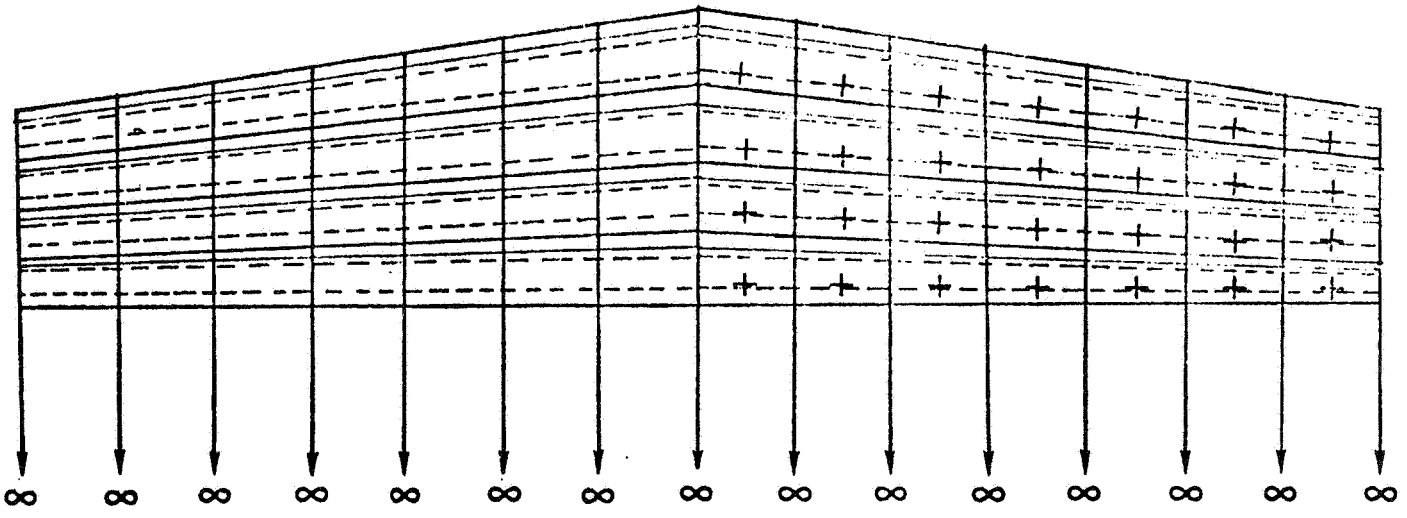

PANEL EDGES

SOURCE LINES

VORTEX LINES

\+ CONTROL POINTS

$$\left\{\frac{V_t}{V_\infty}\right\} = \left[S\right]\left\{\frac{dz_t}{dx}\right\}$$

$$\left\{\alpha\right\} = \left[A\right]\left\{\frac{V_\ell}{V_\infty}\right\}$$

Figure 1. Source/Vortex Lattice Analysis and Design Method

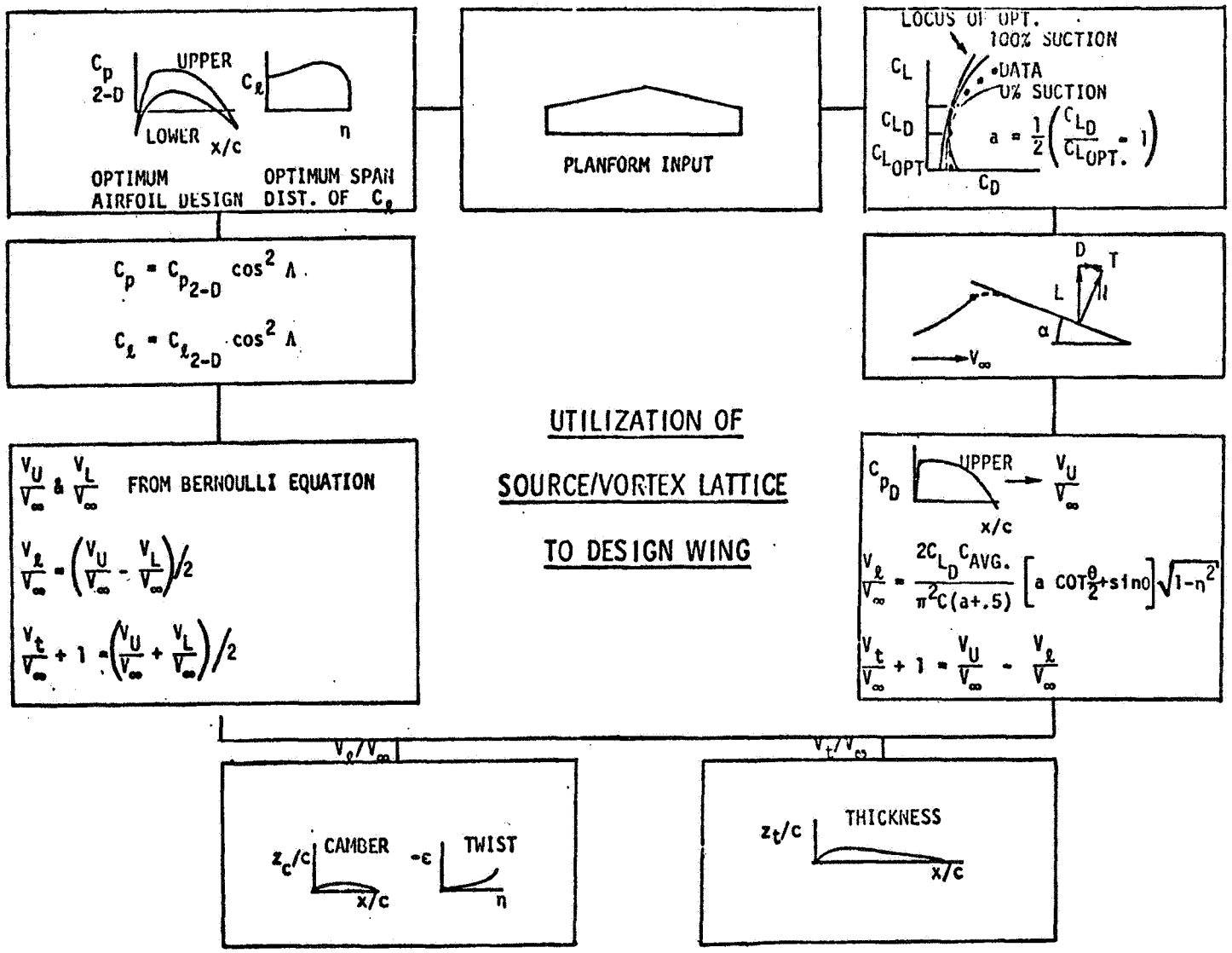

Figure 2. Utilization of Source/Vortex Lattice to Design Wing

FLOW FIELD AT ANY POINT DUE TO AN ARBITRARY BODY IS GIVEN BY SUPERPOSITION:

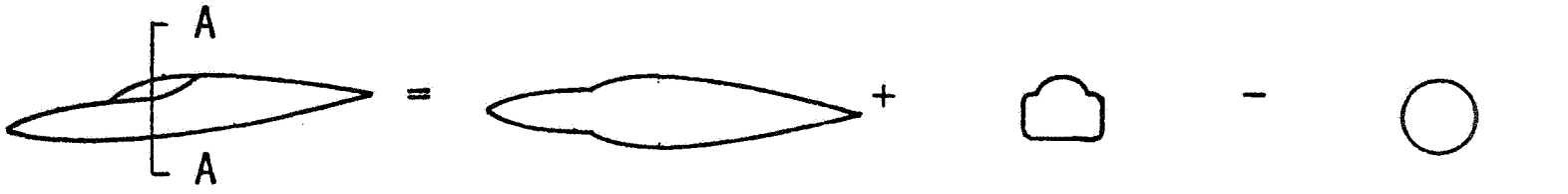

FLOW FIELD DUE TO ACTUAL BODY = SOLUTION FOR EQUIVALENT BODY OF REVOLUTION + 2-D SOLUTION FOR ACTUAL BODY CROSS-SECTION A-A - 2-D SOLUTION FOR EQUIVALENT CROSS-SECTION A-A

3-D BOUNDARY CONDITIONS ARE SATISFIED IN THESE 2-D SOLUTIONS

Figure 3. General Slender Body Theory

MAIN CAPABILITY

- COMBINE GENERAL SLENDER BODY THEORY WITH SOURCE/VORTEX LATTICE TO OBTAIN:
  - Velocities tangent to wing surface due to the fuselage and other bodies
  - Upwash on the wing due to the fuselage and other bodies

ADDITIONAL CAPABILITY

- USE BODY OF REVOLUTION PORTION OF SOLUTION TO OBTAIN VELOCITIES INDUCED BY NACELLES
- USE 2-D PORTION OF SOLUTION TO EVALUATE AIRFOIL DESIGNS

Figure 4. Utilization of General Slender Body Theory

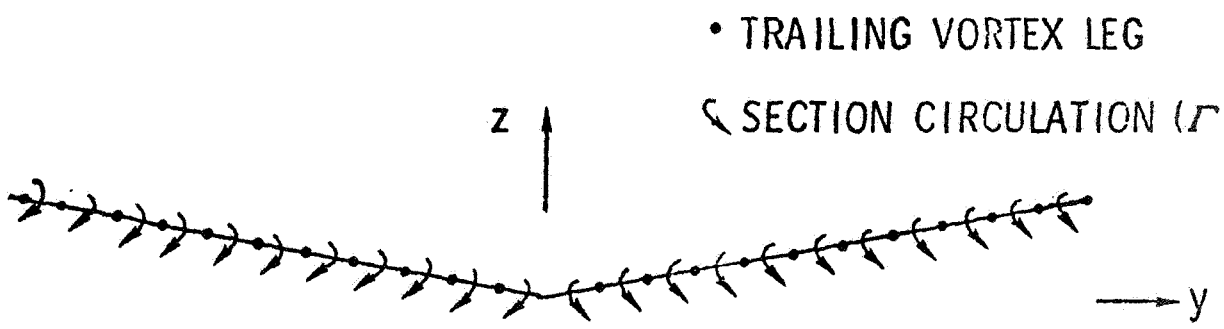

$$C_{D_i} = \frac{AR}{2\pi b^2} \sum_{j=1}^{n} \sum_{k=1}^{n} \left(\frac{\Gamma}{V_\infty}\right)_j \left(\frac{\Gamma}{V_\infty}\right)_k \left[\left(Ev_{jk}\, T_{y_k} + Ew_{jk}\, N_{y_k}\right) T_{z_j} - \left(Ev_{jk}\, T_{z_k} + Ew_{jk}\, N_{z_k}\right) T_{y_j}\right] \Delta S_j$$

$\vec{T}$ UNIT VECTOR TANGENT TO WAKE

$\vec{N}$ UNIT VECTOR NORMAL TO WAKE

ΔS_j INCREMENTAL SECTION WIDTH

E_v y COMPONENT OF INFLUENCE FUNCTION FOR PAIR OF TRAILING LEGS

E_w z COMPONENT OF INFLUENCE FUNCTION FOR PAIR OF TRAILING LEGS

Figure 5. Induced Drag Analysis and Design Method

- COMPUTE INDUCED DRAG
  - WING WITH ARBITRARY DISTRIBUTION OF DIHEDRAL
  - MULTIPLE LIFTING SURFACES
- COMPUTE OPTIMUM SPAN LOADS FOR TRIMMED CONDITIONS

Figure 6. Utilization of Induced Drag Trefftz Plane Method

- AIRFOIL DRAG POLAR DATA APPLIED ALONG STRIPS

- BOUNDARY-LAYER STRIP ANALYSIS
  - SOLVE FOR EQUIVALENT AIRFOIL TO SUPPORT 3-D POTENTIAL PRESSURE DISTRIBUTIONS
  - UTILIZE INFINITE YAWED BOUNDARY-LAYER PROCEDURE

- EMPIRICAL PERCENT SUCTION METHOD
  - UTILIZE PERCENT SUCTION VERSUS C_L CURVE FROM CONFIGURATION WITH SIMILAR SECTION CHARACTERISTICS

Figure 7. Viscous Form Drag Analysis

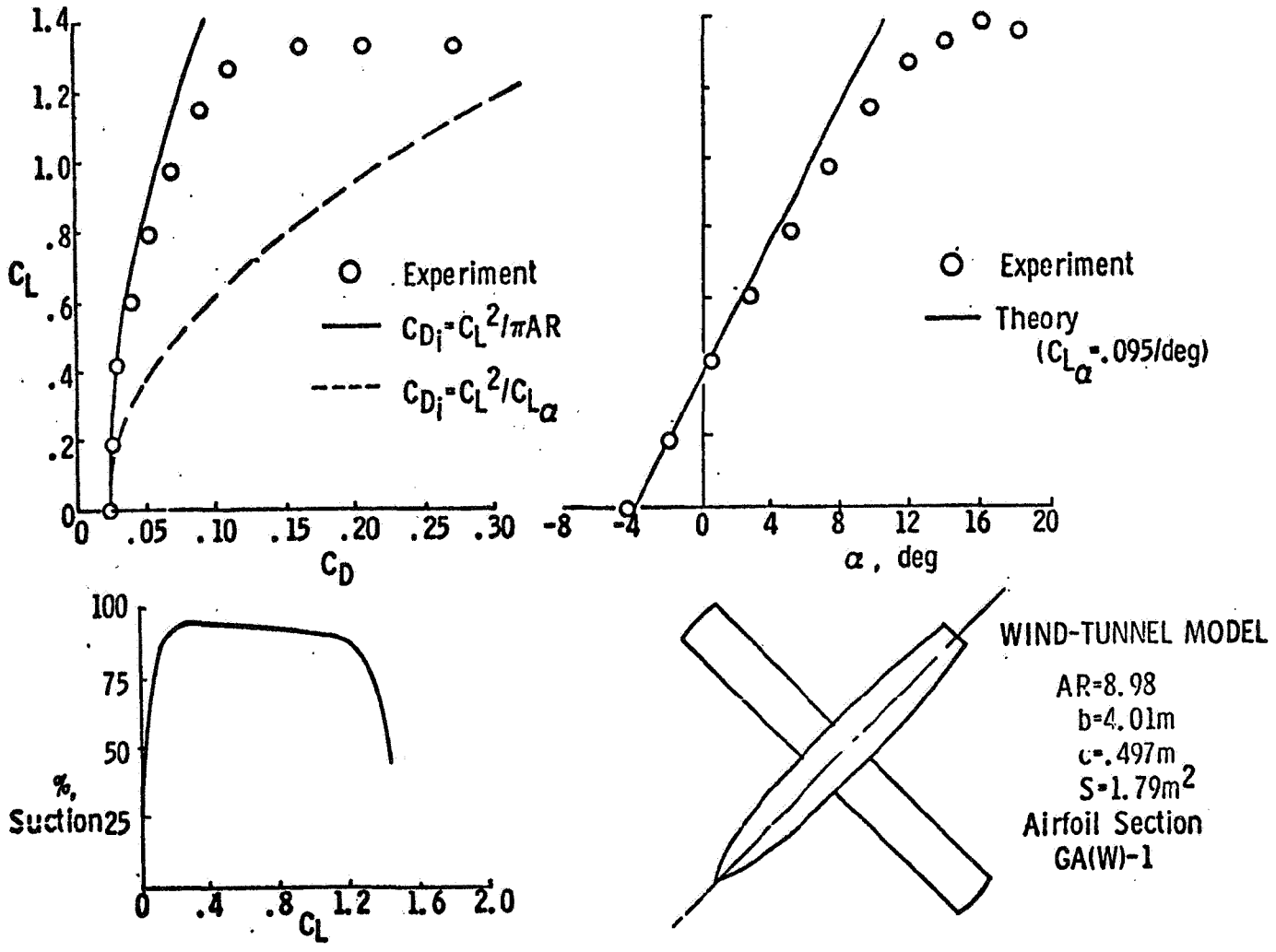

Figure 8. Aerodynamic Characteristics of General Aviation Model

- CALCULATE C_L AND MACH NUMBER AT WHICH THE PRESSURE COEFFICIENT AT THE CREST OF THE AIRFOIL BECOMES CRITICAL

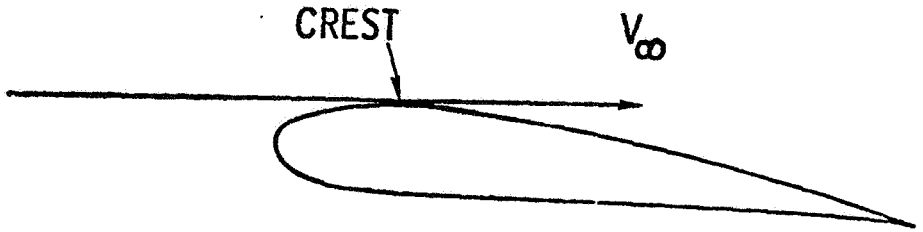

$$C_p^* = \frac{2}{\gamma M_\infty^2}\left[\left\{\frac{2}{\gamma+1}\left(1+\frac{\gamma-1}{2}M_\infty^2\cos^2\Lambda\right)\right\}^{\gamma/(\gamma-1)} - 1\right]$$

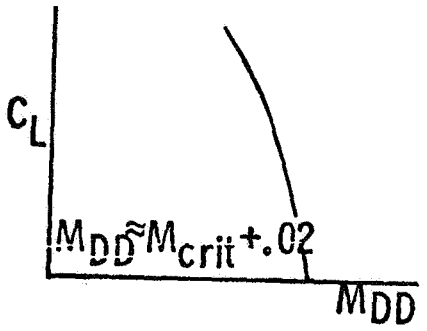

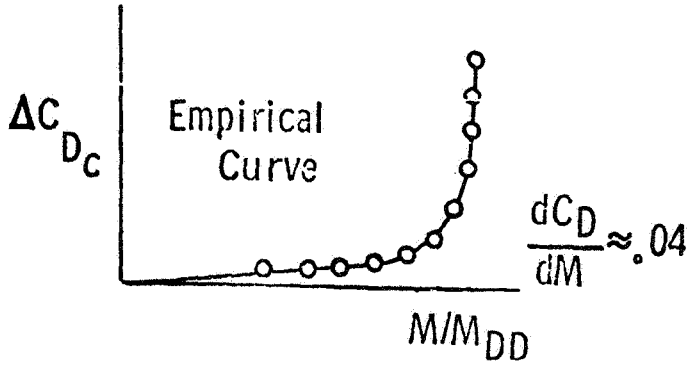

Figure 9. Compressible Drag

- UNFAVORABLE INDUCED WING SURFACE VELOCITIES
  - SOLVE FOR Δz_t UTILIZING

$$\left\{\frac{\Delta V_t}{V_\infty}\right\} = \left[S \right] \left\{\Delta \frac{dz_t}{dx}\right\}$$

  - APPLY NEGATIVE Δz_t TO WING CONTOUR
  - APPLY NEGATIVE $\approx 2\,\Delta z_t$ TO ADJACENT BODY CONTOUR

Figure 10. Contour Modification to Relieve Unfavorable Interference Effects

3.5 Drag Reduction - Back to Basics

Oran W. Nicks
NASA Langley Research Center

Introduction - Perspective

From the beginning of manned flight, the iteration of lift, weight, drag, and thrust have been the balancing factors involved in so-called aeronautical engineering. Lift greater than weight is needed to get up, thrust greater than drag is needed to go anywhere. These fundamentals are still as true as ever. The list of variables involved in successful aeronautical engineering has grown significantly to include speed, cost, comfort, aesthetics, pollution, noise, etc., with perhaps the most significant current interest in fuel economy. There will surely be other tradeoffs to be faced, but never will we be able to ignore lift, weight, drag, and thrust.

In this conference, we will deliberately focus attention on drag reduction. Drag is the basic parameter affecting the ability of aircraft to go somewhere efficiently. A hot gas balloon can get up and stay up reasonably well, with essentially no consideration for drag. It goes when the wind blows, at no more than the speed of wind. But as soon as you decide to make it go faster than the wind, or in another direction, its drag becomes very important.

In the early days, airplanes were a lot like the free balloon--getting up and staying up was difficult enough without worrying much about going somewhere efficiently. The structures guys were hard pressed to make lightweight structures, and the aerodynamicists struggled to develop the lift necessary to keep them up. As the aerodynamicists really got to working on the drag problem, the propulsion guys came along and helped solve the problem by providing better engines and propellers--that may be one reason we have some unanswered questions about the science of low speed flight today. I often wonder what a few more years of studying the birds might have produced, had the propeller not allowed an effective alternate to the aerodynamic-propulsion techniques still employed by the birds.

At any rate, these are the kind of questions I think we should consider during this Drag Reduction Conference, as we look back to basics.

Wing Lift-Drag Relationships

In addition to providing almost all the lift, the wing produces the biggest

percentage of the drag, about 50 to 60 percent during cruise for usual configurations. Since the wing is fundamental to lifting the weight, getting the required lift with the least drag has been the challenge for wing design through the years. If an airplane had some way of getting to cruise speed and altitude, the wing required for cruise might be roughly half the area of the wing required for acceptable takeoff, climb, and landing. Of course, under such ideal conditions, there would be little need for variable geometry. In this case, the wing designed only for cruise flight for a four-place airplane cruising at 200 miles per hour would contribute only about 30 percent of the drag.

To give the same airplane a good takeoff, climb, and landing capability with a plain wing of the same design, the wing would contribute about 70 percent of the total drag at 200 miles per hour. Of course, it is that situation which has led to the development of variable geometry high lift devices such as flaps and slats. With today's technologies, such devices reduce the wing drag penalty during cruise to about 50 percent of the total; however, there are several basic shortcomings of these devices which we might well consider.

First of all, the most common trailing edge flaps cause increased pitching moments which require increased down loads on the tail for trim. In a typical landing configuration, about ten percent of the lift of the wing is negated by the down load on the tail required for trim. In addition, high performance flaps which increase the wing area usually decrease the span efficiency with an associated penalty due to higher induced drag. It would be helpful if we had variable camber devices or variable span techniques to increase lift coefficient while keeping the center of pressure forward, and to minimize induced drag at high lift conditions. Birds use forward sweep, variable camber, variable aspect ratio and lifting tails every day. Such variable geometry features are tough to design and build; however, some of the newer technologies may make them more attractive possibilities than they have been in the past. The thicker wing section, for example, gives structural depth; new composite materials may simplify controlled bending of aerodynamic surfaces. While I am not proposing any particular solution to the problem, I do suggest that a thorough review of the basics which cause drag, and some imaginative consideration of techniques for reducing drag, may be productive.

Profile Drag

The resistance of an object moving through air is pretty clearly a function of the cross-sectional area, the wetted area, the shape of the object, and the friction caused by the scrubbing of the air over the object. Here again, the wing, although

streamlined in appearance, contributes 20-40 percent of the total airplane parasite drag. There is only so much that can be done about the cross-sectional area associated with the volume required for passengers or payload, but there are many other smaller factors which add up in the profile drag account.

Sometimes the quantity and types of protrusions on modern general aviation aircraft make me think it would be helpful if aerodynamicists were forced to re-do some simple experiments on streamlining conducted in the early days of aviation. My teen-age son recently conducted a science experiment in a small wind tunnel to show the effects of streamlining by comparing a circular flat plate, a sphere, and a streamlined shape with a fineness ratio of 3 1/2, all having the same diameter. The difference in drag for the plate and the streamlined body is a factor of about 30, in case you don't remember. My son's teacher could not believe the measurements when the much larger body produced the dramatic reduction, and I think many aerodynamicists would be impressed as well. (I guess I was, even though I knew Hoerner's data were to be trusted.)

Many airplanes flying today pay a large price in parasite drag for fixed landing gear, steps, antennae, windshields, and the usual joints, rivet heads, doors, and other discontinuities attributed to production. Hoerner has data on German tests of an actual ME-109 wing and on a section of a P-51 wing--both of course being real construction though quite different in detail. The data are not presented in a manner such that they can be compared over a range of conditions--they are single points--but they show the drag of the ME-109 wing to be 70 percent higher than that of the P-51 wing. According to Hoerner, the high drag of the 109 wing is due largely to manufacturing features: surface waviness, holes, cover plates, control gaps, ill-fitting slat, rivet heads, and bolt heads, whereas the P-51 wing was flush riveted, filled, sanded and painted. The desirability of achieving laminar flow was the motivation for the attention to smoothness on the P-51 wing, although it is doubtful that very much laminar flow existed. It is likely that the elimination of protuberances helped make most of the difference. Better fabrication techniques, or possibly surface coverings that might cover up production artifacts, may be worth more attention than they have been given in the production of many current airplanes. The possibility of applying a space age material coating over a standard production surface is being studied at Langley.

Propulsion Drag

Another form of drag many of us have gotten used to is that associated with

internal flows around engines and accessories. To be sure, the matter is an interdisciplinary problem involving interfaces with the engine, propeller, and airframe. Until the jet engine came along and caused more aerodynamicists to concern themselves with internal flows, the matter of engine-nacelle drag was largely an empirical or experimental matter. The NACA's experimental work on cowlings in the 20's and 30's provided data for use with radial and in-line engines used extensively during the 1940's. The advent of the horizonally opposed engine brought with it many opportunities for better streamlining and while there are many good examples flying, I am not aware of a systematic set of data on the subject relevant to aircraft and engines of today. Considering the fact that recent workshops have indicated that from 5 to 25 percent of the total aircraft drag may be caused by cooling air flows, and knowing that the velocity inside cowlings may be well above 100 miles an hour, it is clear that drag reduction possibilities exist for future designs if attention is paid to internal flows.

From the standpoint of basics, a subsonic ramjet can be made to produce internal thrust with efficient heat addition to air flow. Assuming that the external drag of a cowl is a part of the airplane drag, the fact that the engine is adding heat energy is significant. To take advantage of this, the internal flows and the cooling flow exhaust must be treated carefully to reduce losses and to recover the air momentum along the thrust axis. While first priority for cooling air is obviously to cool the engine, there is nothing which says the design should not capitalize on the heat addition. Efficient baffling designs which preclude dumping of air, high speed flows past structure, supports and other drag producing items, may help make the most of the cooling air situation. A simple calculation based on data from Hoerner indicates that for a flight speed of 200 MPH, a cooling air flow receiving a 300 degree temperature rise through a 2-sq. ft. cowl would produce an internal thrust of about 25 pounds. By contrast, a cold engine would produce about 50 pounds of drag. A classic example of turning such potential losses into a gain was the design of the P-51 Mustang glycol radiator, which reportedly produced a net thrust for the complete installation.

Propellers have evolved in the face of many compromises, but their efficiencies continue to suffer because of basic tradeoffs. The propellers developed by the Wright Brothers provided an ideal efficiency of 80 percent and actually delivered 66 percent of the power available to the airstream. This was achieved by careful attention to theory and the fact that they were large and rotated at relatively low speeds. As engines have become smaller, their speeds have become higher and the unfavorable gearing have led toward small diameter, high speed propellers. Propeller efficiency

is not only compromised somewhat, but the higher velocity scrubbing and outward flows around nacelles may contribute additional losses of a few percent.

Most of the general aviation jet aircraft benefit from the aft engine locations which tend to accelerate flows near the base of the airplane where wakes and boundary layers are pronounced. Rear mounted propellers have the same potential for flow improvements around the wing and fuselage, but of course, they are not as readily adapted to airplanes as the jet engine and have not found as much use.

Some Anomalies from the Past and Present

Since most of the ideas that occur to me have already been exercised in the past, I make it a practice to look back frequently to anomalies which may provide lessons for today. Many good ideas have failed to materialize into practice because of shortcomings in the technologies other than the disciplines being explored. What I am referring to is the fact that an aerodynamicist with a good idea may have been thwarted because of a structures or materials problem, for example, and advances in these other fields may have opened the door later without his knowing it. With this philosophy in mind, let me challenge your thinking a bit with some questions which arose out of looking back.

In the 1930's there was a lot of effort applied to the matter of drag reduction. This era produced airplanes like the Cessna Airmaster, the Lockheed Vega, and the Northrop Gamma. Larry Loftin, who has gathered data from many sources and done many calculations, provided estimates of the minimum drag coefficients for these examples which I averaged to be about 0.0270. Similar calculations for representative fixed gear monoplanes of today give an average of about 0.0370. I realize I am comparing the very best of the 30's with the average of today, but the question is, "What was it about those airplanes that made them appear to be better from a drag standpoint that might teach us something." You will have to decide, but let me mention a few things to stimulate your thinking.

First, the airplanes considered from the 30's were all tail draggers and the current examples considered all have nose wheels. Obviously, some penalty is being paid for nose gear; Hoerner gives numbers ranging from 6 to 12 percent, not including effects on propeller efficiency, but this alone does not account for the difference. Another characteristic of these airplanes of the 30's was a carefully cowled radial engine, whereas the examples of today all have horizontally opposed engines. The high performance airplanes of the 30's were also extremely smooth, usually employing many coats of dope over fabric or plywood and having few extrernal protuberances

(before transponders, ELTs and the like were required). Frontal areas were reduced to a minimum, and careful attention paid to cross-sectional areas, fuselage shapes, wing taper, wing tips, and fairings.

The story for retractables is somewhat different. Some of the current retractable gear configurations compare favorably with the best of World War II and it appears that when paying the price of retractable gear, aerodynamicists are also concerned about other forms of drag. However, I do not suggest that you immediately conclude that doing as well as World War II aircraft is acceptable for today--that is not a good assumption.

Some more recent anomalies which are of interest because of their concepts should be mentioned. Gus Raspet and his colleagues at Mississippi State University worked hard to reduce drag. Gus recognized the importance of skin friction and did many experiments on methods of reducing it. Some work at MSU in 1967, not long after his accident, involved several research aircraft with highly advanced technologies. The XV-11A developed for the U.S. Army had a variable camber fiberglas wing with boundary layer suction and a pusher shrouded propeller. While only 40 hours of flight tests were conducted, significant indications of improvements were achieved. For example, stall speed was decreased from about 75 knots to about 52 knots with no change in wing area.

All of us are familiar with the work of Jim Bede--I think it is fair to say that his primary aerodynamic emphasis is on drag reduction. Almost every basic principle we have discussed has been considered by Jim in his decisions.

Another drag reduction effort of the last few years that impressed me was the work of Wil Schuemann. Starting with a Libelle high performance fiberglas sailplane, with an advertised L/D of about 39 at 59 MPH, Wil substantially improved its high speed capabilities without compromise to its low speed performance. His efforts involved a combination of improving the flow over the airfoil by modest leading edge modifications and by employing the basics of Dr. Hoerner to fillets, air leaks, control surfaces, and laminar flow surface considerations. His tests show that the cruise lift drag ratio at 100 knots was improved by 30 percent to a value of about 20; the fact that this was possible starting with an extremely clean configuration illustrates the possibilities for drag reduction by applying basic principles.

While talking about sailplanes and anomalies, it seems appropriate to note that there are many high performance sailplanes regularly employing the advantages of significant runs of laminar flow. While practical means have not yet been demonstrated for achieving these benefits on higher speed aircraft, there is a lot of pay dirt for drag

reduction between fully turbulent and fully laminar flow. Considering the fact that friction drag accounts for 60-70 percent of the average airplane drag, work on compliant surfaces, boundary layer control, and other means of reducing skin friction are "musts" for research.

Summary

In a sweeping manner, and with some academic liberties, I have touched on many items that are on the agenda for this conference. Most of you are familiar with the basics, but you may not have had the opportunity to ponder them in one sitting for a long time. I am mindful that this country makes the best general aviation aircraft in the world--last year, about 15,000 of them. This is a fact for which we can be proud, and yet, we are gathered here to discuss the important matter of making them better.

I hope that while your meal was settling, our brief revisit to fundamentals has helped stimulate an open-minded consideration of old ideas with a new twist. Summed up, my comments were aimed at making two points: (1) We can enhance our fundamental knowledge if we carefully review and reconsider the basics unravelled by those who preceded us; and (2) With a good understanding of the basics, we must be as bold and innovative as the pioneers of the past in searching for means of applying new technologies.

4. PAPERS OF SESSION II - FUSELAGE DRAG

4.1 Some Comments on Fuselage Drag

Jan Roskam
University of Kansas

Introduction

This paper focuses on the following areas relating to fuselage drag:

1. Fuselage fineness - ratio and why and how this can be selected during preliminary design;
2. Windshield drag;
3. Skin roughness; and
4. Research needs in the area of fuselage drag.

Fuselage Fineness Ratio and How It Can Be Selected

Table 1 presents some data on fuselage fineness ratios for several current general aviation airplanes. It is interesting to note, that with one exception, all have values of around $\ell_B/d = 5$ to 6. In Reference 1, the fuselage (or body) drag is estimated from:

$$C_{D_{o_B}} = C_{f_B}\left[1 + \frac{60}{(\ell_B/d)^3} + .0025\left(\frac{\ell_B}{d}\right)\right]\frac{S_{wet_{body}}}{S_{wing}} \qquad (1)$$

This equation assumes zero base drag. Figure 1 shows how the [ ]-term in equation (1) is related to ℓ_B/d. Note that the [ ]-term no longer decreases significantly significantly after $\ell_B/d = 6.0$ is exceeded. This would indeed suggest that values of 5 to 6 for ℓ_B/d are about optimum. However, there are three other factors to contend with:

1. increasing ℓ_B/d will decrease C_{f_B};
2. increasing ℓ_B/d will increase $S_{wet_{body}}$; and
3. increasing ℓ_B/d will decrease tail wetted area requirements, for constant stability levels.

It appears that a more detailed examination of fuselage fineness ratio is therefore in order. The next section presents a method for minimizing the sum of fuselage and empennage friction drag, under a constant directional and longitudinal stability constraint.

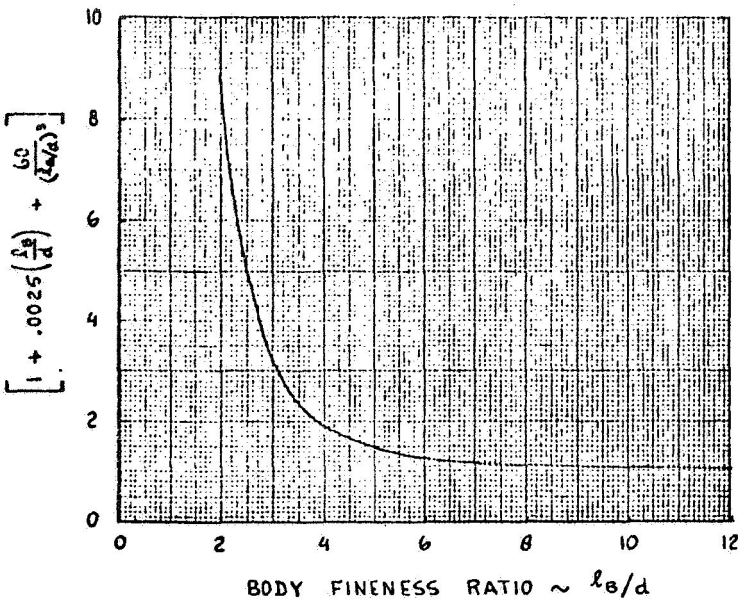

Figure 1. Body Zero-Lift Drag Factor as a Function of Body Fineness Ratio

Table 1. Examples of Fuselage Fineness Ratios and Wetted Areas for General Aviation Aircraft

Type	$\frac{\ell_B}{d}$	S_{wing}	$S_{wet\ body}$	$\frac{S_{wet\ body}}{S_{wing}}$
Cessna 210	5.02	175	319	1.82
Cessna 207	5.69	174	425	2.44
Beech Sierra	5.22	146	332	2.27
Cessna 185	5.15	176	292	1.68
Beech Bonanza ('58)	4.98	181	323	1.78
Beech Baron	5.69	199.2	362	1.82
Piper Navajo	5.97	229	502	2.19
Cessna 310	5.40	179	306	1.71
Piper Seneca	5.68	206.5	356	1.72
Beech Duke	5.59	212.9	586	2.28
Cessna 414	5.52	195.7	488	2.49
Beech King Air	6.06	294	652	2.22
Gates Learjet 24	8.8	232	502	2.16

A Method for Minimizing General Aviation Airplane Fuselage and Empennage Friction Drag

Fuselage Drag - The objective is to show how fuselage drag and empennage friction drag can be estimated under constant static stability constraints.

It is assumed that the fuselage from nose to passenger compartment is defined roughly as in Figure 2.

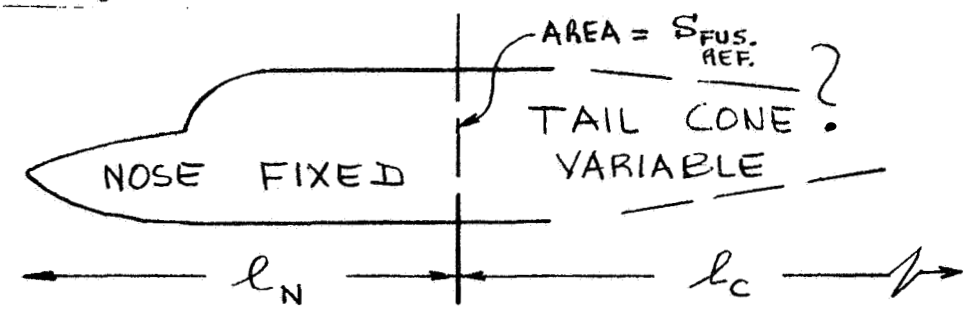

Figure 2. Definition of Fuselage in Two Parts

It is also assumed that the tail cone can be represented by a skewed cone as in Figure 3.

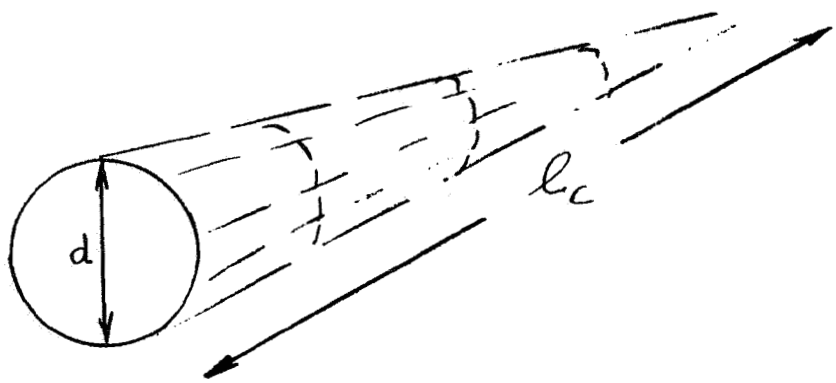

Figure 3. Modeling Aft Fuselage as a Skewed Cone

The equivalent fuselage diameter is defined such that:

$$\frac{\pi}{4}d^2 = S_{\substack{FUS. \\ REF.}} \Rightarrow d = \sqrt{\frac{4S_{\substack{FUS \\ REF}}}{\pi}} \qquad (2)$$

The wetted area of the fuselage can now be written as:

$$S_{\substack{WET \\ BODY}} = S_{\substack{WET \\ NOSE}} + S_{\substack{WET \\ CONE}} = S_{\substack{WET \\ NOSE}} + F \cdot \pi \cdot \frac{d}{2}\sqrt{\left(\frac{d}{2}\right)^2 + \ell_C^2} \qquad (3)$$

where F is a correction factor accounting for the fact that the rear fuselage is not a cone. F can be found by comparison to existing aircraft.

The Fuselage Drag coefficient (zero-lift) can be expressed as:

$$C_{D_{o_{FUS.}}} = C_{F_B}\left[1 + \frac{60}{\left[(\ell_N+\ell_c)/d\right]^3} + .0025\left(\frac{\ell_N+\ell_c}{d}\right)\right]\frac{S'_{WET_{BODY}}}{S_{wing}} R_{WB} \qquad (4)$$

All symbols are defined in Reference 1. Fuselage base drag is neglected. For given ℓ_c, $C_{D_{of_{US}}}$ can thus be computed as a function of ℓ_c.

Empennage Drag - The horizontal tail wetted area may be approximated by:

$$S'_{WET_{H.T.}} = S'_H\left(2 + \underbrace{f(t/c)}_{<<1.0}\right) - C_{R_H}^2\frac{d}{\ell_c} \qquad (5)$$

where the geometry is defined in Figure 4.

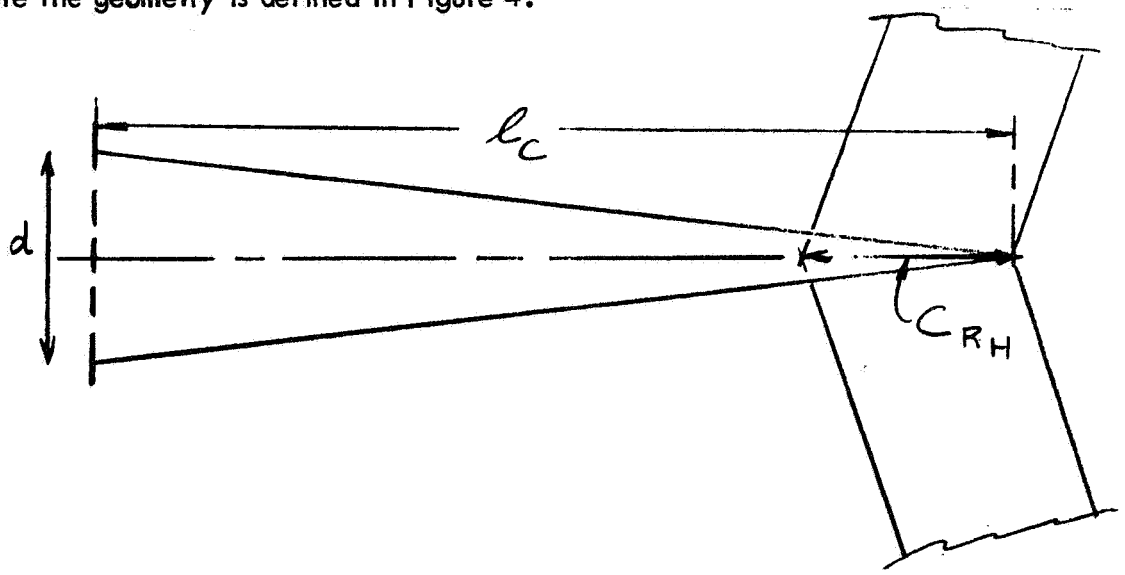

Figure 4. Horizontal Tail in Relation to Fuselage Cone

The horizontal tail drag coefficient can be written as:

$$C_{D_{o_{H.T.}}} = C_{F_H}\left[1 + L\left(\frac{t}{c}\right)_{H.T.} + 100\left(\frac{t}{c}\right)^4_{H.T.}\right] R_{L.S.}\frac{S'_{WET_{H.T.}}}{S_{WING}} \qquad (6)$$

where all symbols are defined in Reference 1.

The vertical tail wetted area may be approximated by:

$$S'_{WET_{V.T.}} = S'_V\left(2 + \underbrace{f(t/c)}_{<<1.0}\right) - \tfrac{1}{2}C_{R_V}^2\frac{d}{\ell_c} \qquad (7)$$

where the geometry is defined in Figure 5.

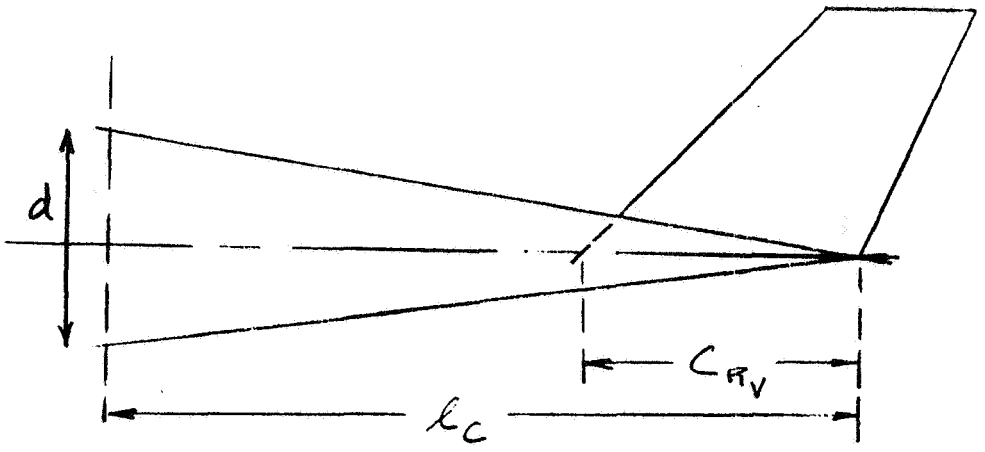

Figure 5. Vertical Tail in Relation to Fuselage Cone

The vertical tail drag coefficient can be written as:

$$C_{D_{o_{V.T.}}} = C_{f_V}\left[1 + L\left(\frac{t}{c}\right)_{V.T.} + 100\left(\frac{t}{c}\right)^4_{V.T.}\right] R_{l.s.} \frac{S_{WET_{V.T.}}}{S_{WING}} \qquad (8)$$

where all symbols are defined in Reference 1. Horizontal and vertical tail sizes are here assumed to be determined by minimum stability requirements, i.e.,:

$$C_{n_{\beta_{MIN.}}} \text{ and } C_{m_{\alpha_{MIN.}}}$$

Directional Stability - Neglecting the wing contribution, the directional stability of an airplane can be written as:

$$C_{n_\beta} = C_{n_{\beta_B}} + C_{n_{\beta_V}} \frac{S_{B_s}}{S_{WING}} \frac{(\ell_V + \ell_c)}{b} + C_{L_{\alpha_V}} \frac{S_V}{S_{WING}} \frac{\ell_V}{b} \qquad (9)$$
$$= -57.3 K_N K_{R_\ell}$$

where the symbols are defined in Reference 2. The geometry is defined in Figure 6.

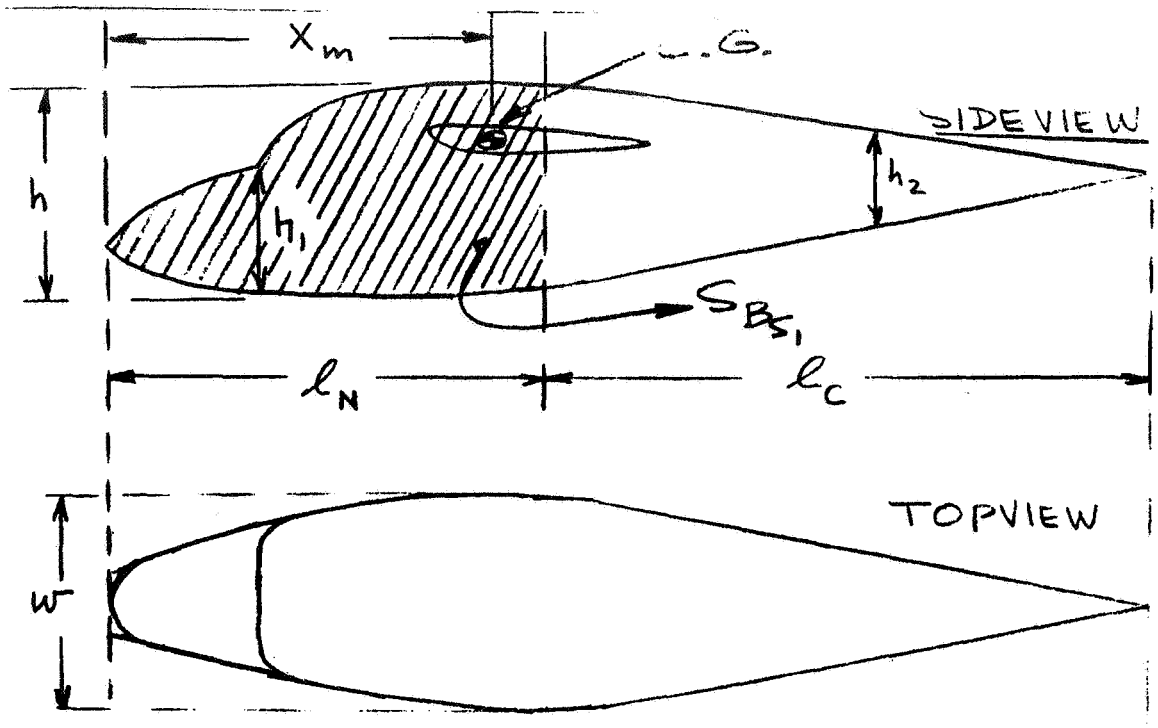

Figure 6. Fuselage Geometry for Estimating Directional Stability

Note than K_N and K_{R_ℓ} are functions of ℓ_c. Body side area, S_{B_S} can be expressed as:

$$S_{B_S} = S_{B_{S_1}} + \frac{1}{2} h \ell_C \times F \qquad (10)$$

where F is as in equation (3).

Note that:

$$C_{L_{\alpha_V}} = f(A_V, \lambda_V, \Lambda_V) \qquad (11)$$

and $\ell_V = f(\ell_C, \Lambda_{LE_V}, C_{R_V})$ as illustrated in Figure 7. (12)

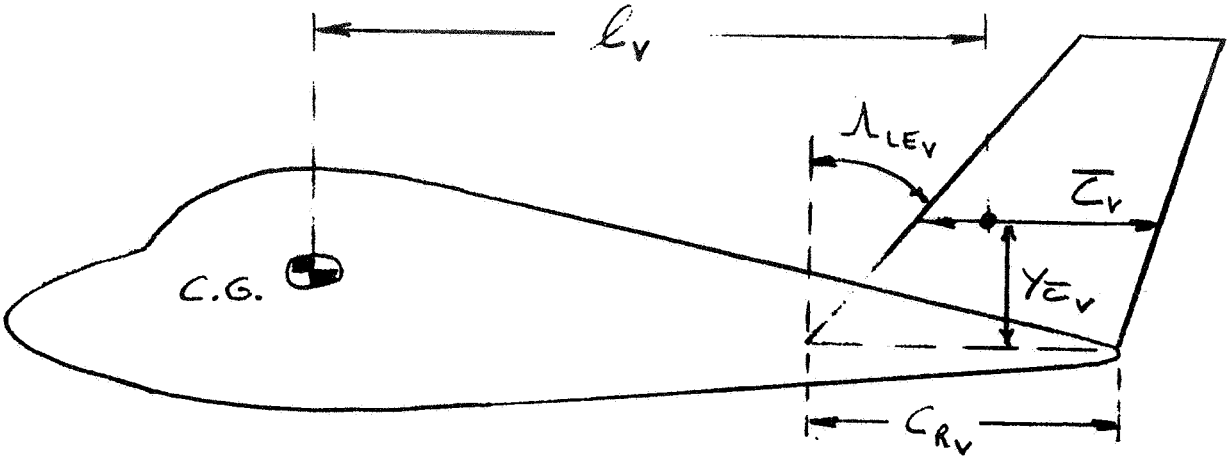

Figure 7. Definition of ℓ_v for Swept Vertical Tail

From the sketch the following equations may be deduced:

$$\ell_v = (\ell_N - X_m) + (\ell_c - c_{R_v}) + y_{\bar{c}_v} \tan \Lambda_{LE_v} + \frac{\bar{c}_v}{4} \tag{13}$$

$$y_{\bar{c}_v} = b_v \frac{1}{3}\left(\frac{1+2\lambda_v}{1+\lambda_v}\right) \tag{14}$$

$$b_v = \sqrt{S_v A_v} \tag{15}$$

$$c_{R_v} = \frac{2 S_v}{(1+\lambda_v)\sqrt{S_v A_v}} \tag{16}$$

$$\bar{c}_v = \frac{2}{3} c_{R_v}\left(\frac{1+\lambda_v+\lambda_v^2}{1+\lambda_v}\right) \tag{17}$$

Now, substitute equation (13) into (9) while using equations (14), (15), and (16):

$$C_{n_\beta} = -57.3 K_N K_{R_\ell}\left(\frac{S_{B_{S_1}} + \frac{1}{2} h \ell_c}{S_{wing}}\right)\left(\frac{\ell_N + \ell_c}{b}\right) + \text{GIVEN AS A DESIRED MINIMUM}$$

$$+ C_{L_{\alpha_v}}{}_{RAD} \frac{S_v}{S_{wing}} \frac{1}{b}\left\{(\ell_N - X_m) + \left(\ell_c - \frac{2 S_v}{(1+\lambda_v)\sqrt{S_v A_v}}\right) + \frac{1}{3}\sqrt{S_v A_v}\left(\frac{1+2\lambda_v}{1+\lambda_v}\right)\tan \Lambda_{LE_v} + \frac{\bar{c}_v}{4}\right\} \tag{18}$$

For preselected values of $S_{B_{S_1}}$, h, S_{wing}, b, ℓ_N, A_v, λ_v and Λ_{LE_v},

it is now possible to solve for S_v for any given value of ℓ_c.

Having done that, it is possible to compute $C_{D_{o_{v.T.}}}$ as a function of ℓ_c.

Longitudinal Stability - Longitudinal stability can be expressed by:

$$\frac{dC_m}{dC_L} = \bar{X}_{cg} - \bar{X}_{ac} \text{ , where :} \tag{19a}$$

$$\bar{X}_{ac_A} = \frac{\bar{X}_{ac_{WB}} + \frac{C_{L\alpha_H}}{C_{L\alpha_{WB}}} \frac{X_{ac_H}}{\bar{c}} \frac{S_H}{S_w}\left(1 - \frac{d\varepsilon}{d\alpha}\right)}{1 + \frac{C_{L\alpha_H}}{C_{L\alpha_W}} \frac{S_H}{S_w}\left(1 - \frac{d\varepsilon}{d\alpha}\right)} \tag{19b}$$

where all symbols are defined in Reference 3 and where:

$$X_{ac_H} = X_{ac_W} + \ell_H \tag{20}$$

as shown in Figure 8.

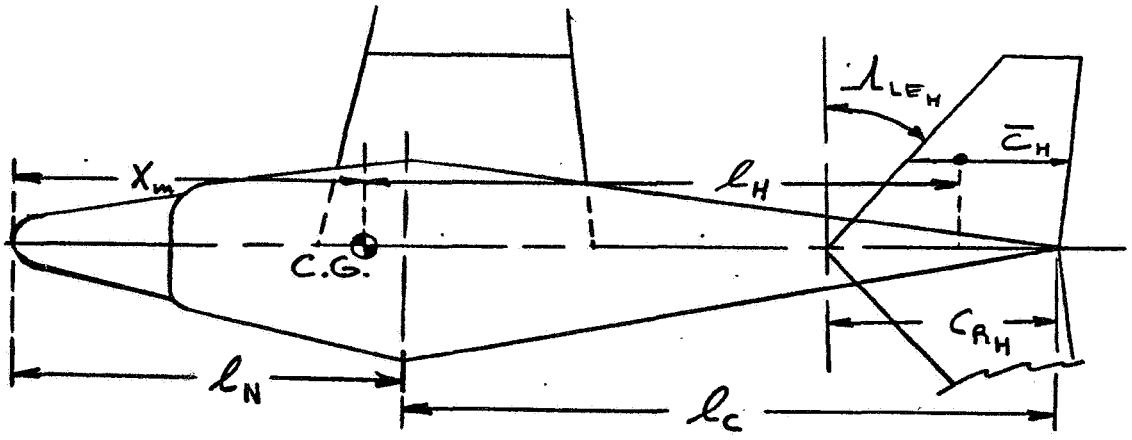

Figure 8. Definition of Horizontal Tail in Relation to Fuselage

It is assumed, that $\bar{X}_{ac_{WB}}$, $C_{L\alpha_{WB}}$, $\bar{c}$, $d\varepsilon/d\alpha$, $S_{w(ing)}$ and $\bar{X}_{ac_w}$ are known and fixed quantities.

The following expressions can be shown to hold:

$$\ell_H = (\ell_N - X_m) + (\ell_c - c_{R_H}) + \bar{y}_{c_H} \tan\Lambda_{LE_H} + \frac{\bar{c}_H}{4} \tag{21}$$

$$\bar{c}_H = \frac{2}{3} c_{R_H}\left(\frac{1 + \lambda_H + \lambda_H^2}{1 + \lambda_H}\right) \tag{22}$$

$$\bar{y}_{c_H} = \frac{1}{2} b_H \frac{2}{3}\left(\frac{1 + 2\lambda_H}{1 + \lambda_H}\right) \tag{23}$$

$$b_H = \sqrt{S_H A_H} \tag{24}$$

$$c_{R_H} = \frac{2 S_H}{(1 + \lambda_H)\sqrt{S_H A_H}} \tag{25}$$

Plugging equation (21) into equation (20) and using equations (22) through (25) it is found that:

$$X_{ac_H} = X_{ac_W} + (\ell_N - X_m) + \left(\ell_c - \frac{2S_H}{(1+\lambda_H)\sqrt{S_H A_H}}\right) \quad (26)$$
$$+ \frac{1}{3}\sqrt{S_H A_H}\left(\frac{1+2\lambda_H}{1+\lambda_H}\right)\tan\Lambda_{LE_H} + \frac{1}{6}\left(\frac{1+\lambda_H+\lambda_H^2}{1+\lambda_H}\right)\frac{2S_H}{(1+\lambda_H)\sqrt{S_H A_H}}$$

Now, setting dC_m/dC_L = some constant value and preselecting: A_H, λ_H and Λ_{LE_H}, it is possible to solve for S_H (using equation (19) for any given value of ℓ_c. Having done this, it is possible to compute $C_{D_{OHT}}$ as a function of ℓ_c).

Parametric Study - The methods of of the previous sections allow the computation of $C_{D_{ofus}}$, $C_{D_{oh.t.}}$ and $C_{D_{ov.t.}}$ for given values of $\Lambda_{LE(H,V)}$ and for given values of ℓ_c.

These contributions can be plotted against ℓ_c/d as shown in Figure 9.

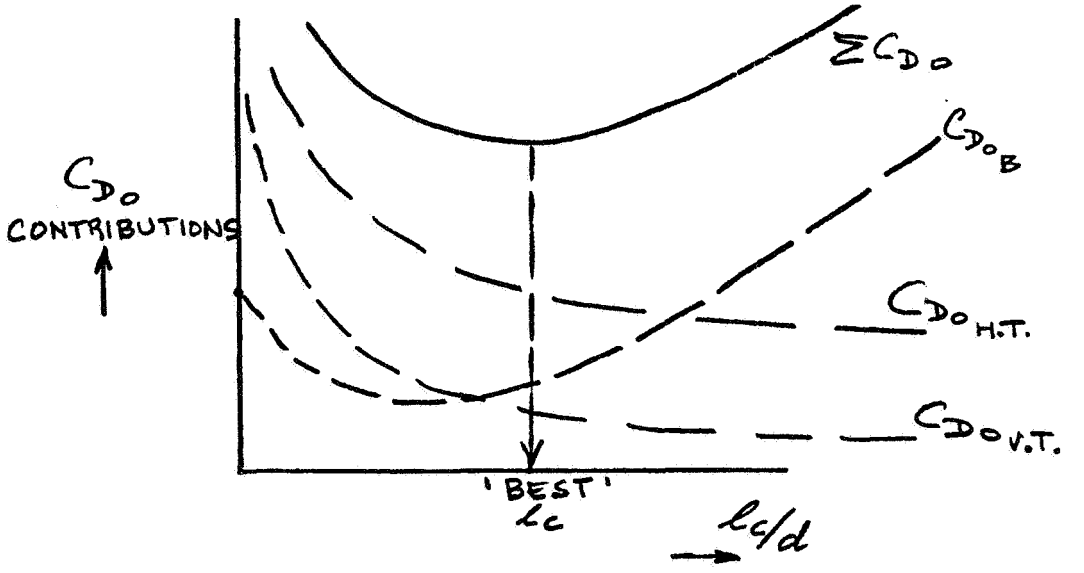

Figure 9. Plotted Results of Parametric Study

If need be this process can be repeated for a variety of empennage sweep angles. The rear fuselage length ℓ_c for minimum fuselage plus empennage drag can be readily found from Figure 9.

It would be of interest to include the effect of weight in this parametric study.

Figure 9a shows some results obtained from calculations using a Beech King Air as example. It is seen that the airplane fuselage plus empennage drag is indeed not optimum from this point of view. It would be of interest to extend this analysis to other airplanes.

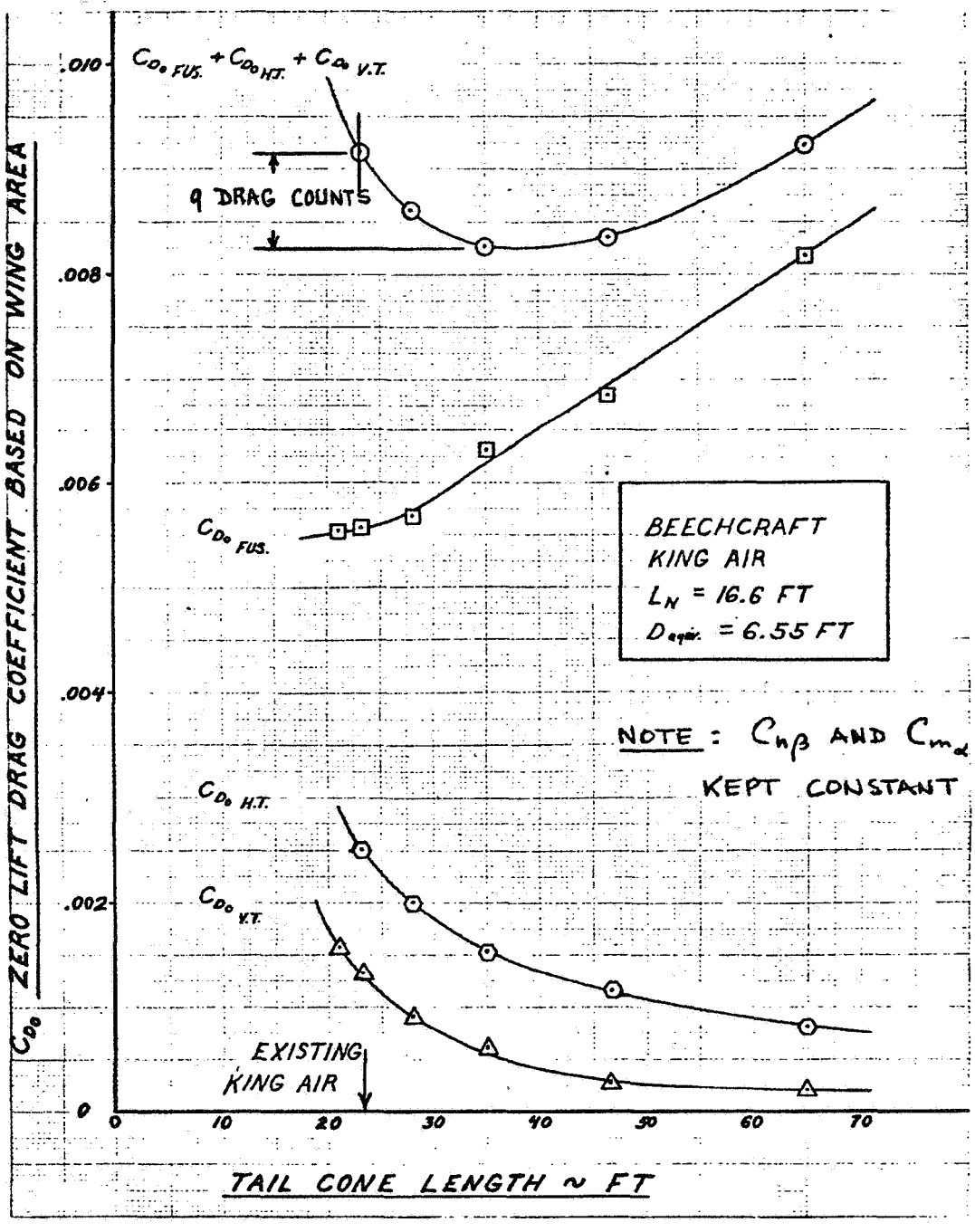

Figure 9A. Effect of Tailcone Length on Fuselage Plus Empennage Zero Lift Drag Under Constant Stability Constraints

C-2

Windshield Drag

Reference 4 presents a series of systematic data for windshield drag of small and transport type airplanes. It summarizes by stating that windshield drag can range from 20 to 1 percent of airplane drag depending on how well they are faired. This is a wide drag range!

Figures 10 and 11 illustrate the types of windshields investigated in reference 2.

Figure 12 illustrates a range of windshields found on current general aviation airplanes. It is seen that windshields of 1975 are quite different from those that prevailed in 1942. It would seem that some systematic research into this area would pay off for certain airplanes.

Surface Finish

The subject of skin waviness and surface finish has not been brought up, because of the strong interplay with production and tooling costs. However, as shown in Figure 13 there is probably considerable room for improvement. This could be attained by a more wide spread use of metal bonding in aircraft fabrication. This way, it is feasible to maintain large areas of laminar flow over the forward part of the fuselage and capitalize on the resulting lower friction drag.

Research Needs

The fuselage typically accounts for 30 to 50 percent of total airplane drag. It seems that improvements of at least 10-20 percent could be made by taking a good research look at:

1. fuselage fineness ratio;
2. windshield drag; and
3. low cost application of metal bonding to reduce skin friction drag.

It would seem that research in the area of windshield drag should be in the form of a series of systematic wind tunnel tests.

Optimization of fuselage fineness ratio could be achieved through the development of an appropriate computer program which would also account for the effect of weight.

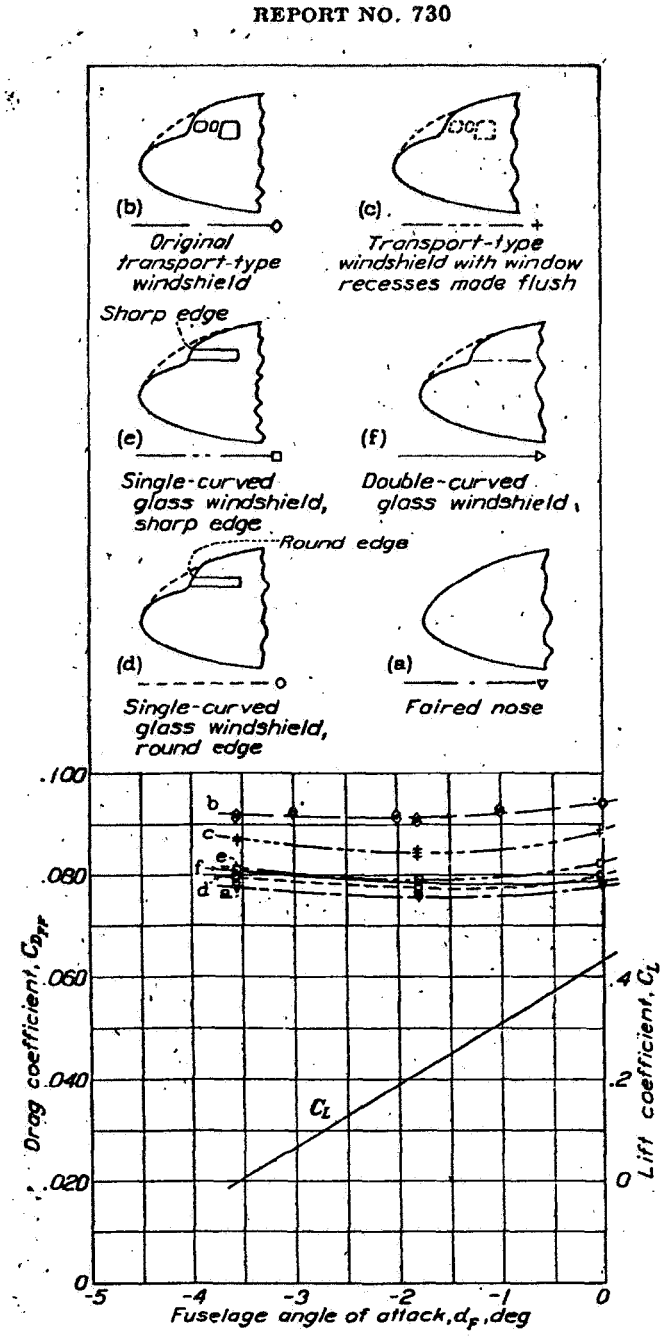

Figure 10. Drag of Fuselage with Transport-Type Windshields
M, 0.35; V, 265 mph

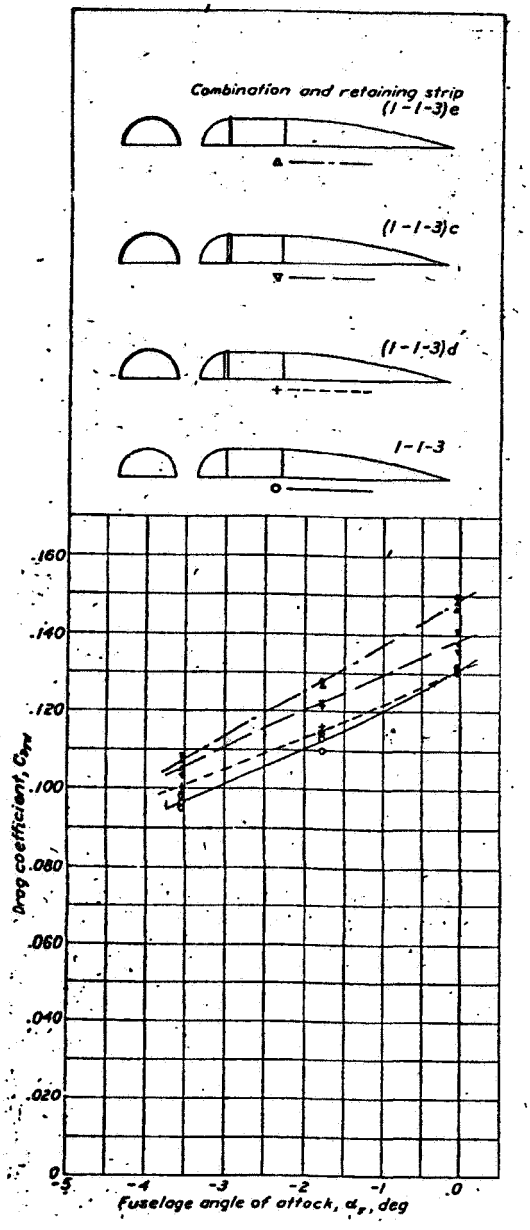

Figure 11a. Effect of Retaining Strips Combination 1-1-3, M, 0.34; V, 260 mph

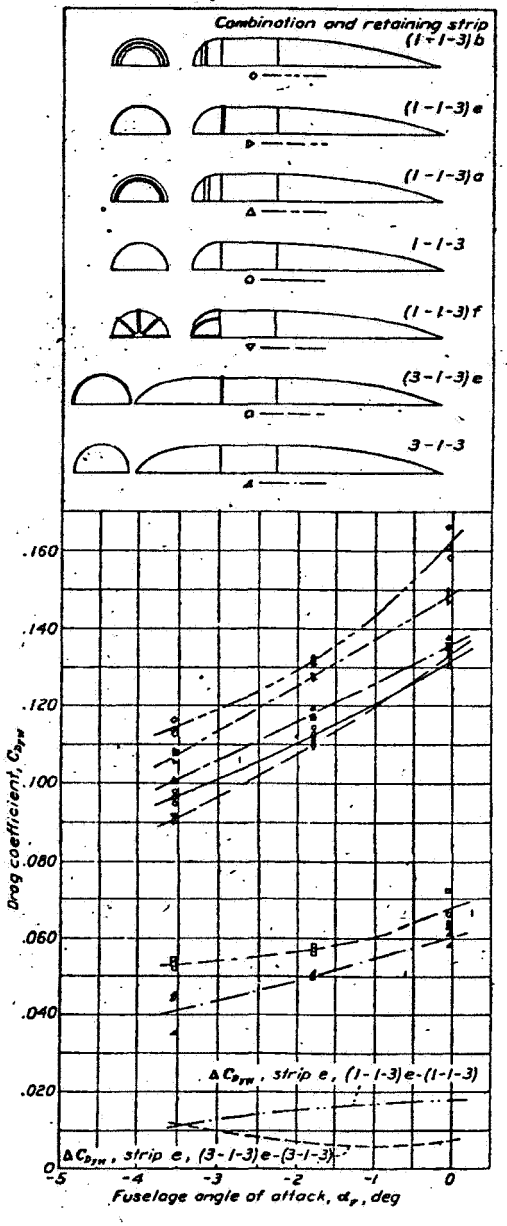

Figure 11b. Effect of Retaining Strips, Combinations 1-1-3 and 3-1-3, M, 0.34; V, 260 mph

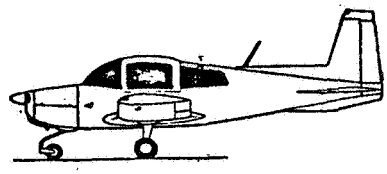

Grumman American AA-5 Traveler

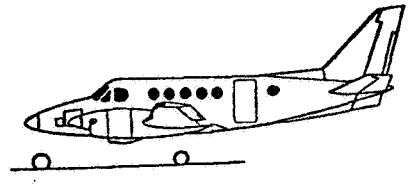

Beech King Air A100

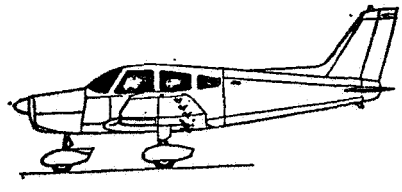

Piper Cherokee Warrior

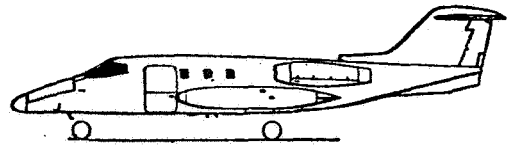

Gates Learjet 24D

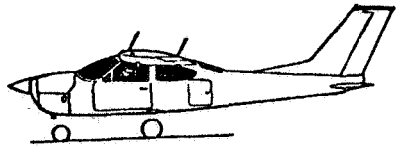

Cessna Cardinal RG

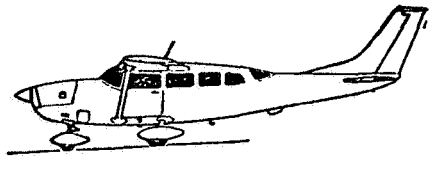

Cessna Skywagon 207

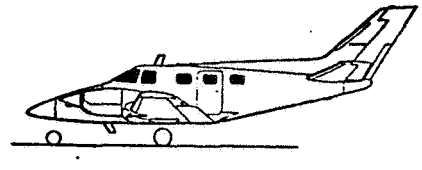

Beech Duke B60

Figure 12. Typical General Aviation Windshields for 1975

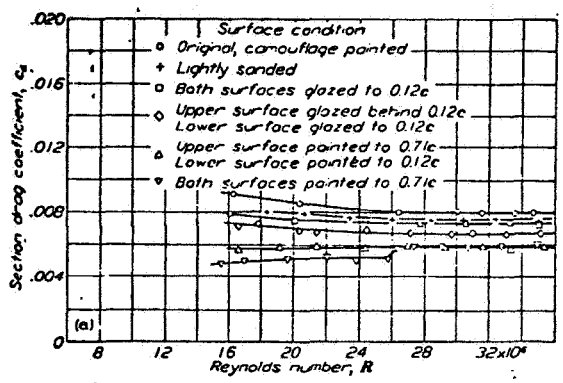

(a) Model 1, NACA 65(216)-3(16.5) (approx.) airfoil section. c_l=0.2.

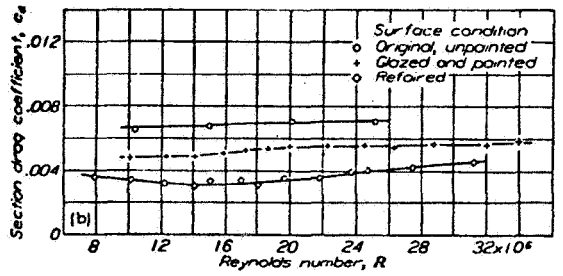

(b) Model 2, NACA 66(215)-214 (approx.) airfoil section. c_l=0.13.

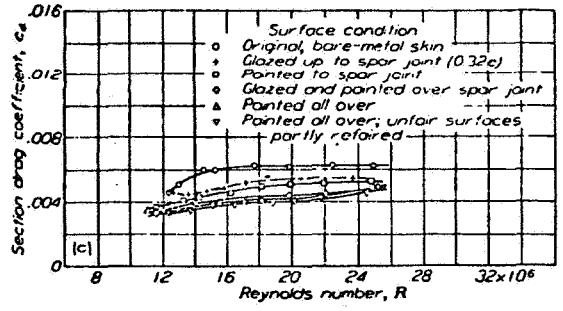

(c) Model 3, NACA 66(215)-116 airfoil section. c_l=0.18.

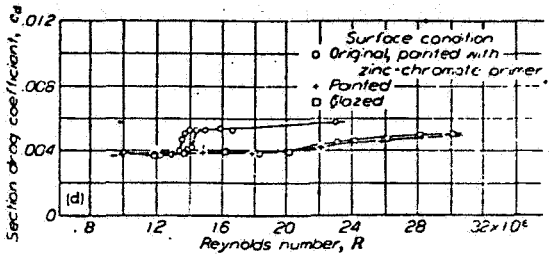

(d) Model 4, NACA 66(215)-116 $\begin{cases} a=1.0, c_{l_i}=0.2 \\ a=0.6, c_{l_i}=-0.1 \end{cases}$ airfoil section. c_l=0.1.

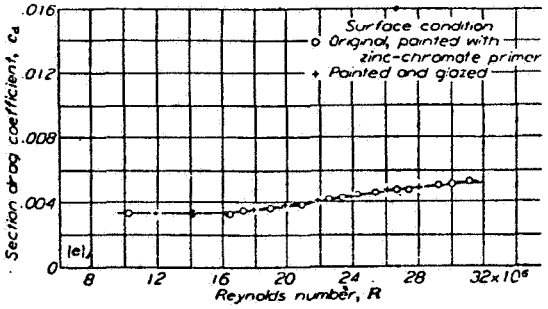

(e) Model 5, NACA 66(215)-116 $\begin{cases} a=1.0, c_{l_i}=0.2 \\ a=0.6, c_{l_i}=-0.1 \end{cases}$ airfoil section. c_l=0.1.

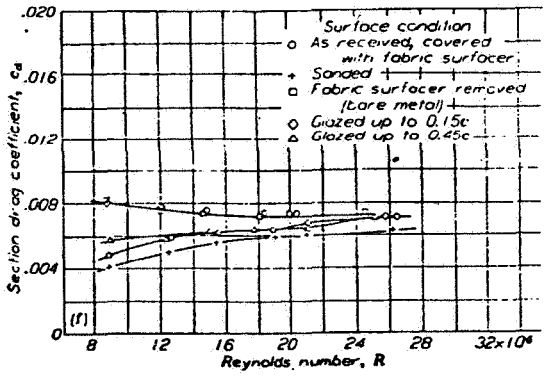

(f) Model 6, NACA 66(215)-116 practical-construction airfoil section. c_l=0.15 (appr

Figure 13. Effect of Surface Improvements on Drag Characteristics of Airfoil Sections

References

1. Roskam, J.; Methods for Estimating Drag Polars of Subsonic Airplanes; Published by Roskam Aviation and Engineering Corporation; 519 Boulder, Lawrence, Kansas 66044.

2. Roskam, J.; Methods for Establishing Stability and Control Derivatives of Conventional Subsonic Airplanes; Published by Roskam Aviation and Engineering Corporation; 519 Boulder, Lawrence, Kansas 66044.

3. Roskam, J.; Flight Dynamics of Rigid and Elastic Airplanes; Published by Roskam Aviation and Engineering Corporation; 519 Boulder, Lawrence, Kansas 66044.

4. Robinson, R.G. and Delano, J.B.; An Investigation of the Drag of Windshields in the 8-foot High Speed Wind Tunnel; NACA TR 730, 1942.

4.2 Propeller Blockage Research Needs

R. R. Tumlinson
Beech Aircraft Corp.

If the general aviation industry is to produce the most efficient airplanes, it is important that the best technical tools which can be economically used be employed. That is the business of this workshop. One of the technical tools that is needed and which is currently not available is a means to accurately determine propeller blockage.

Propeller blockage refers to the effect of mutual propeller-nacelle or fuselage interference on the propulsive efficiency. The interference of the body on the propeller arises from the retardation of the airflow through the propeller disk and the resulting change in advance ratios. The interference of the propeller on the body stems from additional drag on the body because of the slipstream effect on local pressure and boundary layer. This effect has been understood for many years, and there are many reports in the literature. In the interest of brevity, the present body of information will not be explored in this presentation except for the bibliography included and to note the important parameters of advance ratio, body shape, and the propeller-diameter-body-diameter ratio.

However, while the sources of the propeller body interference have been understood for some time, the experimental data available to allow accurate estimation is long out of date. Current configurations with horizontally opposed engines outdate the data available which was determined with radial engine and in-line engine configurations as well as RAF -6 and Clark -Y propeller blades.

Performance data provided by propeller manufacturers is either provided on the basis of an isolated propeller, or at best, with approximate correction factors based on experimental data on data of 20-year old configurations. The most recent propeller efficiency computer program compiled by Hamilton Standard under NASA contract (References 8 and 9) provide only isolated propeller information. This view is understandable for a propeller manufacturer; but for the airframe manufacturer, an important gap remains.

Current information is needed to provide a basis to determine accurate drag levels from flight-test data. The drag determined from flight can be only as accurate as the installed power basis. Improvement over the presently available data would also provide an improvement in accurately estimating installed thrust and drag and the resulting aircraft performance. Finally, improvement would provide a rational

basis to determine an accurate trade off between net propeller thrust and body drag in determining new configurations.

So, specifically, what is needed? First, a current body of empirical data is needed which covers the important parameters -- on current configurations with asymmetric shapes. Second, a mathematical model of this data with current computational fluid mechanism techniques is needed to provide a way to easily generalize data for specific cases.

Test programs could be conducted in a large-scale wind tunnel where thrust and drag can be accurately separated. As an alternate, flight test programs could also be used with special engine-propeller installations so that independent determination of installed thrust can be made. One such program has been proposed utilizing a separately driven propeller in the nose of a twin-engine airplane. With different nose body shapes and separately determined thrust, propeller-body interference effects could be determined. Perhaps a by-product of a flight test program would be a practical thrust-meter. This may be a little wishful thinking, but these recommendations for large-scale wind-tunnel tests and flight tests were proven practical by the testing performed many years ago on the obsolete configurations. So it is felt that these can be improved upon today, and I hope that such a program will be seriously considered.

References

1. McHugh, J.G., and Derring, E.H., "The Effects of Nacelle-Propeller Diameter Ratio on Body Interference and on Propeller and Cooling Characteristics," NACA TR 680, April 1939.
2. Glauert, H., "Airplane Propellers, Vol. IV of 'Aerodynamic Theory, div. L'," W.F. Durand, ed.
3. Anon., "Hamilton Standard Method of Propeller Performance Calculation," (Black Book), Hamilton Standard, 1941.
4. Anon., "Generalized Method of Propeller Performance Estimation" (Red Book), Hamilton Standard PDB 1601, Revision A, June 1963.
5. Anon., "S.B.A.C. Standard Method of Propeller Performance Estimation," Society of British Aircraft Constructors, Ltd.
6. Fage, A., Lock, C.N.N., Bateman, H., and Williams, D.H., "Experiments with a Family of Airscrews Including Effect of Tractor and Pusher Bodies; Part II Experiments on Airscrews with Tractor and Pusher Bodies," British A.R.C. R & M No. 830, November 1922.
7. Bateman, H., Townsend, H.C.H., and Kirkup, T.A., "Experiments with a Family of Airscrews, Including Effect of Tractor and Pusher Bodies; Part IV On the Effect of Placing an Airscrew in Various Positions within the Nose of a Streamline Body," British A.R.C. R & M No. 1030, February 1926.

8. Worobel, R., and Mayo, M.G., "Advanced General Aviation Propeller Study," NASA CR 114289, April 1971.

9. Worobel, R., and Mayo, M.G., "Advanced General Aviation Propeller Study," NASA CR 114399, December 1971.

4.3 Preservation of Wing Leading Edge Suction at the Plane of Symmetry as a Factor in Wing-Fuselage Design

E. Eugene Larrabee
Massachusetts Institute of Technology

Abstract

Most fuselage geometries cover a portion of the wing leading edge near the plane of symmetry, and it seems reasonable to expect that a large fraction of the leading edge suction which would be developed by the covered wing at high angles of attack is not developed on the fuselage. This is one of the reasons that the Oswald span efficiency factor for the wing body combination fails to approach the value predicted by lifting line theory for the isolated wing. Some traditional and recent literature on wing-body interference is discussed and high Reynolds number data on wing-body-nacelle drag are reviewed. An exposed central leading edge geometry has been developed for a sailplane configuration. Low Reynolds number tests have not validated the design concept.

Figure 1 illustrates the significance of leading edge suction in reducing wing drag at high angles of attack. The sketch on the upper left hand side of the figure gives the airload, normal to the chord, of a symmetrical airfoil at a moderate angle of attack. The sketch on the lower left hand side compares the experimental variation of drag that would be observed in the absence of leading edge suction -- the skin friction drag plus the load normal to the chord times the angle of attack in radians. It is seen that leading edge suction -- the chordwise component of the negative pressures acting on the wing leading edge -- reduces the variation of drag coefficient with lift coefficient to a very low level for $-1 < c_\ell + 1$; in particular, for $c_\ell = +0.4$, the leading edge suction is about 5 times the skin friction drag component.

The right side of Figure 1 raises the question, for the case of a finite span wing body combination, what happens to the leading edge suction that would have been developed by the wing now covered by the fuselage, the most intense leading edge load developed anywhere on the wing.

J. Lennertz[1] attempted to answer the related matter of lift carry-over for the case of a lifting line interrupted by a cylindrical fuselage having circular cross sections and aligned with the direction of flight in 1927. He showed that the circulation at the wing root is "mirrored" on the convex fuselage sides so that the

circulation is somewhat reduced (compared to the isolated wing) in the fuselage region. The lift carry over in the fuselage region is concentrated longitudinally near the lifting line, and nearly disappears in one fuselage diameter either in the up or downstream directions. The question of the leading edge suction in the chord direction (assuming symmetrical wing airfoil sections) is unresolved because the "infinitely" long fuselage is at zero angle of attack.

The problem of calculating the lift distribution for a wing body combination is now routinely solved with high speed digital computers, using any of several finite element - discrete singularity techniques for representing the flow field around a wing body combination in such a way as to align the flow with the body surface at many control points and to satisfy the Kutta-Joukowski condition at the wing trailing edge. Such a finite element calculation has been carried out by H. Korner[2] in a form which permits direct comparison with Lennertz's analytic result. Figure 2, taken from his paper, compares the lift distribution on wing body combinations with finite wing angle of attack, and fuselage angles of attack equal to wing angle of attack, or zero (the Lennertz case) with isolated wing lift.

It is seen that the zero fuselage angle of attack case agrees with Lennertz's result (Figure 1) and that the fuselage angle of attack equal to the wing angle of attack case is very similar. Unfortunately, finite element representations of the flow field near wing body combinations do not lend themselves to drag calculation, and so we do not know whether Lennertz's analytically derived relation for the reduction of Oswald's span efficiency factor

$$e = \frac{[(b/b_f)^2 - 1]^2}{(b/b_f)^4}$$

for the case of zero fuselage angle and varying wing angle holds approximately for the fuselage angle equal to the wing angle or not.

Next we examine, in Figure 3, some model build up data in which an unusually large portion of the wing was covered by the fuselage and two nacelles. The experimental drag coefficients (containing the usual corrections for attachment drag, alignment drag, and wall restraint) are plotted versus the square of the lift coefficient to aid in fitting parabolic polars to the data.

The resulting value of e, the Oswald span efficiency factor, are plotted on Figure 4 as a function of the fraction of the wing span covered, together with Lennertz's relation. It is seen that the addition of the fuselage to the wing, or to the wing nacelle combination, causes an appreciable drop in e about twice the size

expected from Lennertz's relation. Addition of the nacelles to the wing does not cause such a large charge, apparently because the wing leading edge suction was transferred to the leading edges of the relatively short nacelles (there was no flow through the nacelles, which were provided with well rounded, cylindrical leading edges), but that the suction developed by the portion of the wing covered by the fuselage was not transferred to the fuselage nose, which is more than one local chord upstream. It is also difficult to justify the low Oswald span efficiency factor of 0.804 for the isolated wing; it may be related to side edge vortex formation due to flow around the streamwise wing tip. Figure 4 also includes a point obtained in a full scale test of the Twin Commanche airplane, showing that the loss of Oswald span efficiency factor seen with XP-87 wind tunnel model is not unusual.

Figure 5 shows an innovative geometry for a sailplane, intended to preserve leading edge suction at the plane of symmetry by the simple expedient of exposing the leading edge from 20% chord on the lower surface to 20% chord on the upper surface. Additionally the tail assembly and the pilot's pod are attached to the wing by structures of minimum aerodynamic interference. The object is to obtain an Oswald span efficiency factor approaching 1 and to minimize stalling at the wing-tail boom junction so that $C_L^{3/2}/C_D$ can be maximized in circuling flight to improve rates of climb in weak thermals[3].

Figure 6 presents the results of an abortive wind tunnel program to verify this design feature. A wing body combination was tested as a mid wing (leading edge covered) and as a pylon wing arrangement at a low Reynolds number in a quiet tunnel where laminar separation might be expected to be an important aspect of the flow. The endplating of the wing was poor at the top of the tunnel, where air loads on the wing forced open the wing tip-ceiling gap by increasing amounts with increasing lift. The pylon arrangement had more skin friction (the pylon plus the exposed wing area) and it is uncertain whether the slight trend to lower drag at the highest values of C_L^2 is valid or not. A better test is contemplated in the near future.

---

(1) Lennertz, J., "Beitrag zur Theoretischen Behandlung des gegenseitigen Einflusses von Tragflache und Rumpf" (Contribution to the Treatment of the Opposing Effects of Wing and Body Abhandlungen aus der Technische Hochshule Aachen Heft. 8, 1928.

(2) Korner, H., "Theoretische Parameter Untersuchungen an Flugel-Rumpf-Kombinationen," (Theoretical Parameter Studies on Wing Body Combinations) Deutsche Forschungs-und Versuchsanstalt fur Luft-und Raumfahrt, Institute fur Aerodynamic Braunschweig FB 72-63.

(3) Larrabee, E.E., "Lateral Control and Saiplane Design Considerations to Optimize Altitude Gain While Thermalling," AIAA Paper 74-1004.

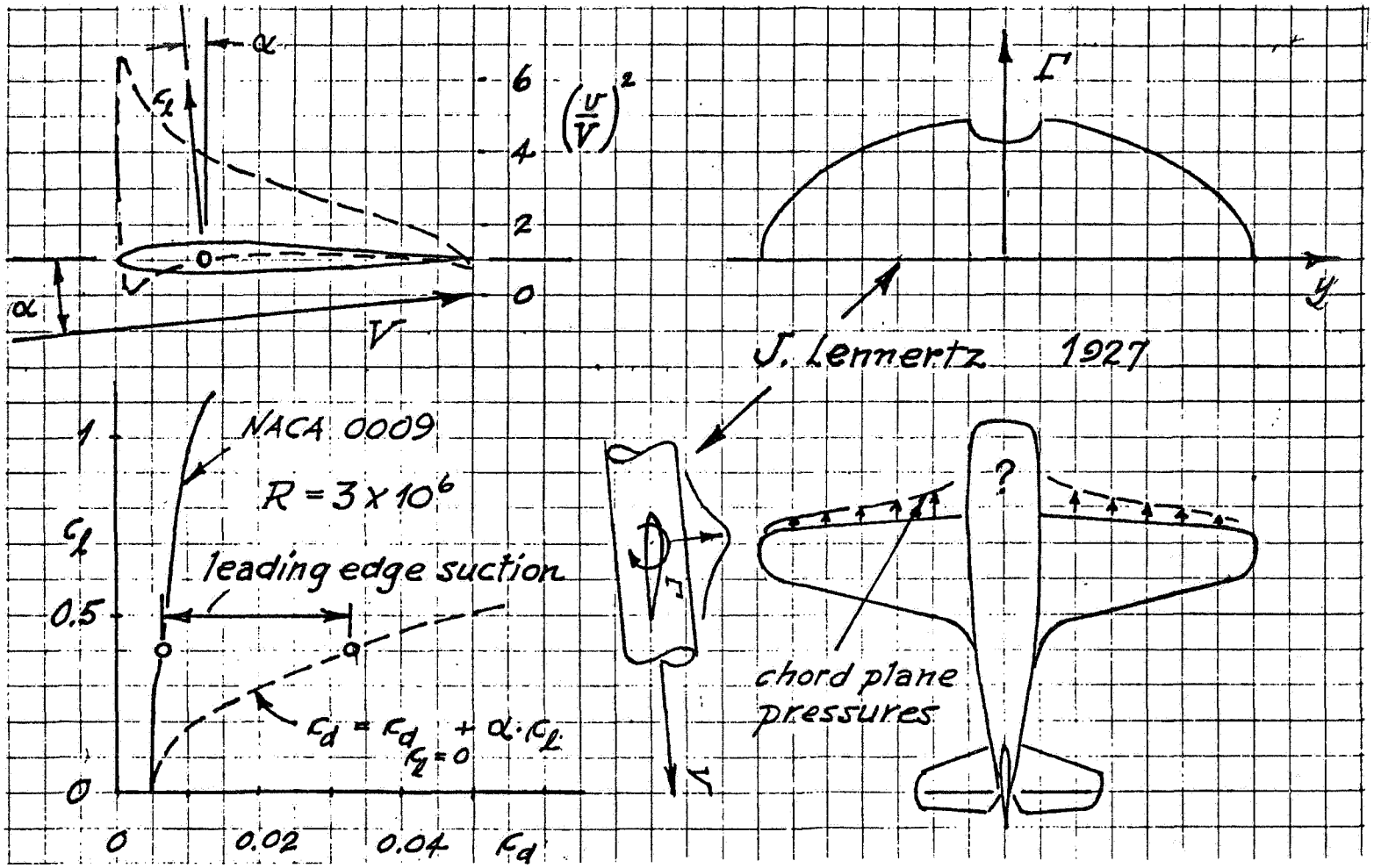

Figure 1. Drag Significance of Leading Edge Suction

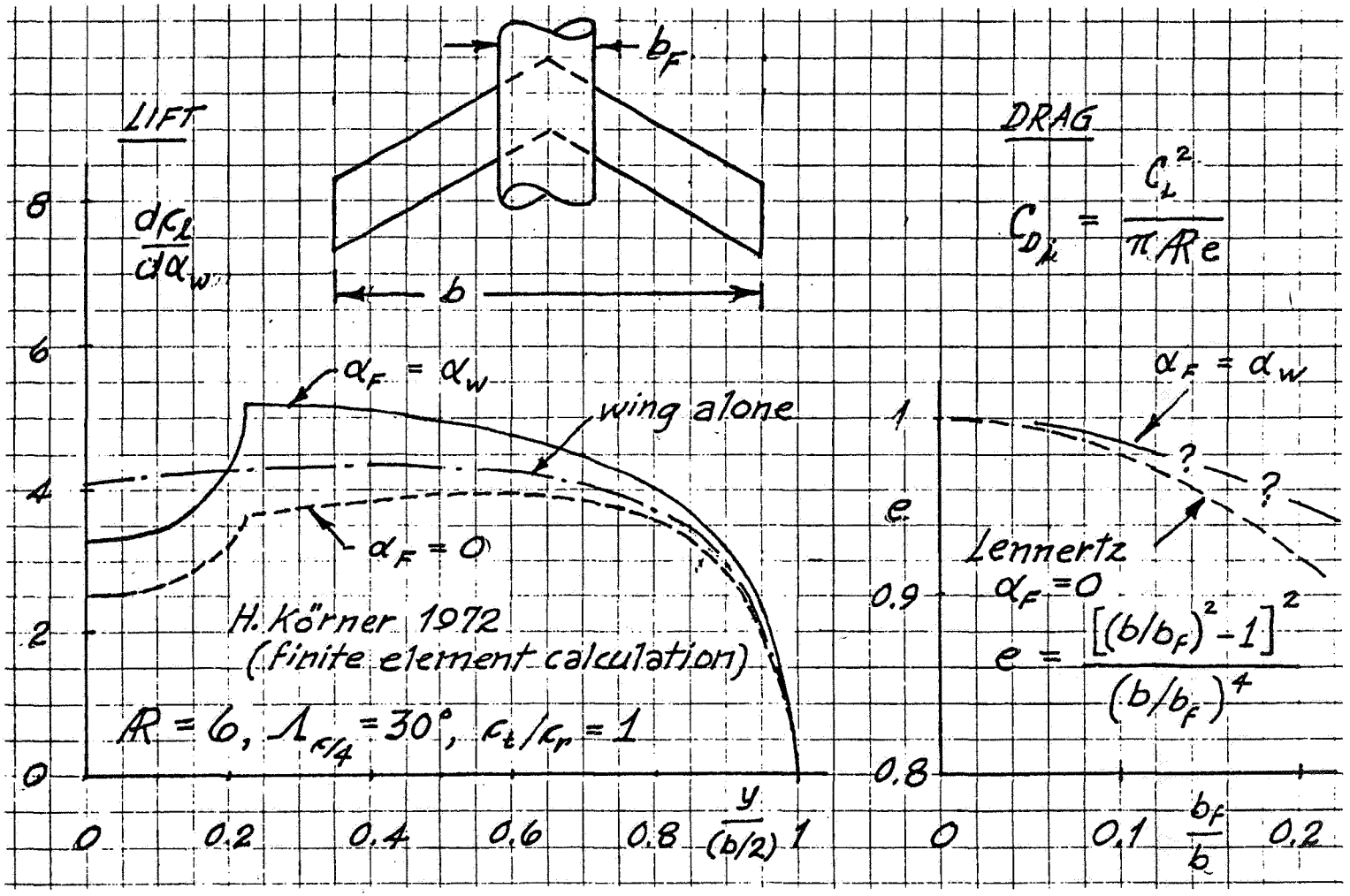

Figure 2. Fuselage Effects on Lift and Drag

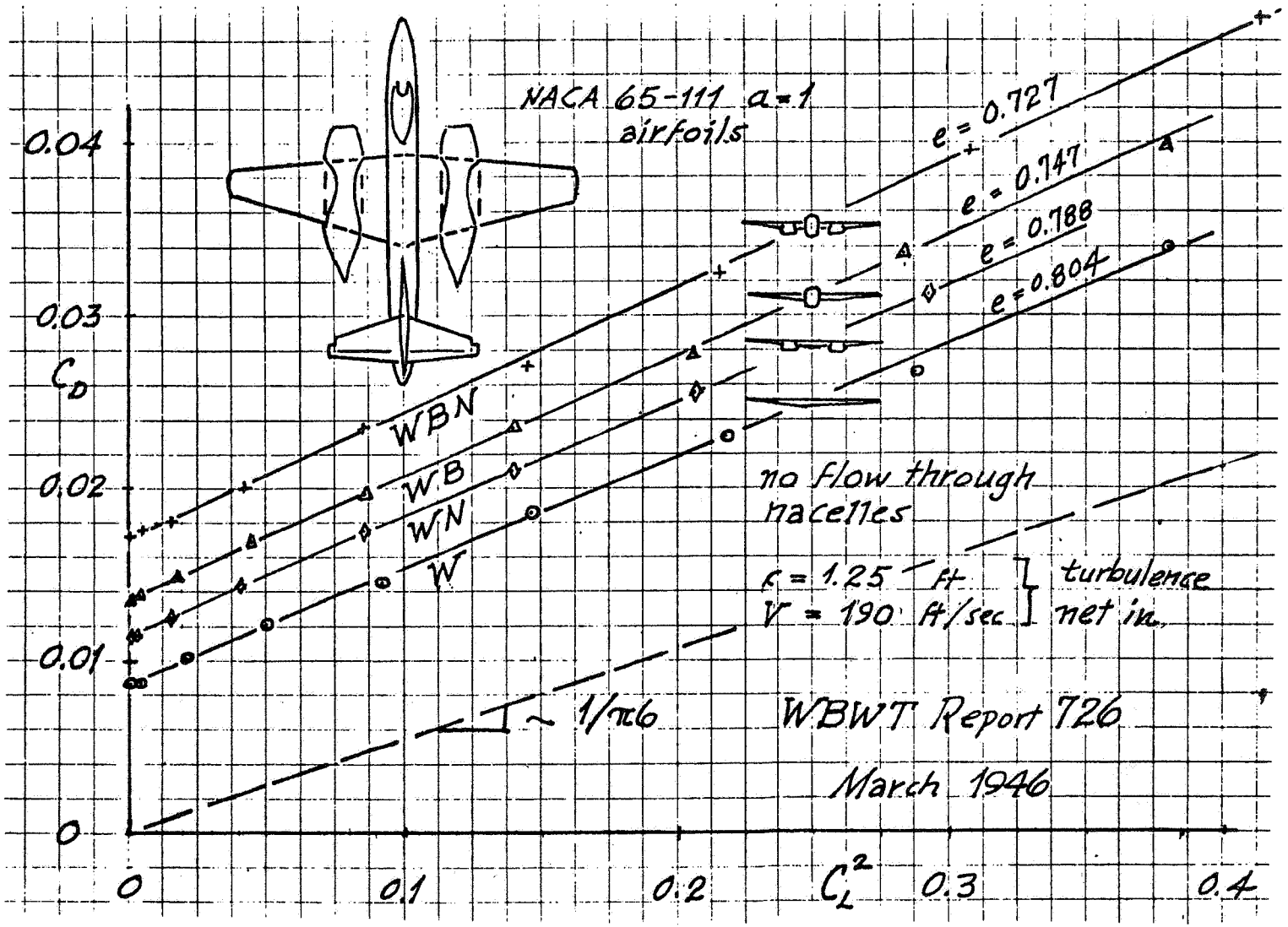

Figure 3. XP-87 Wind Tunnel Model Results

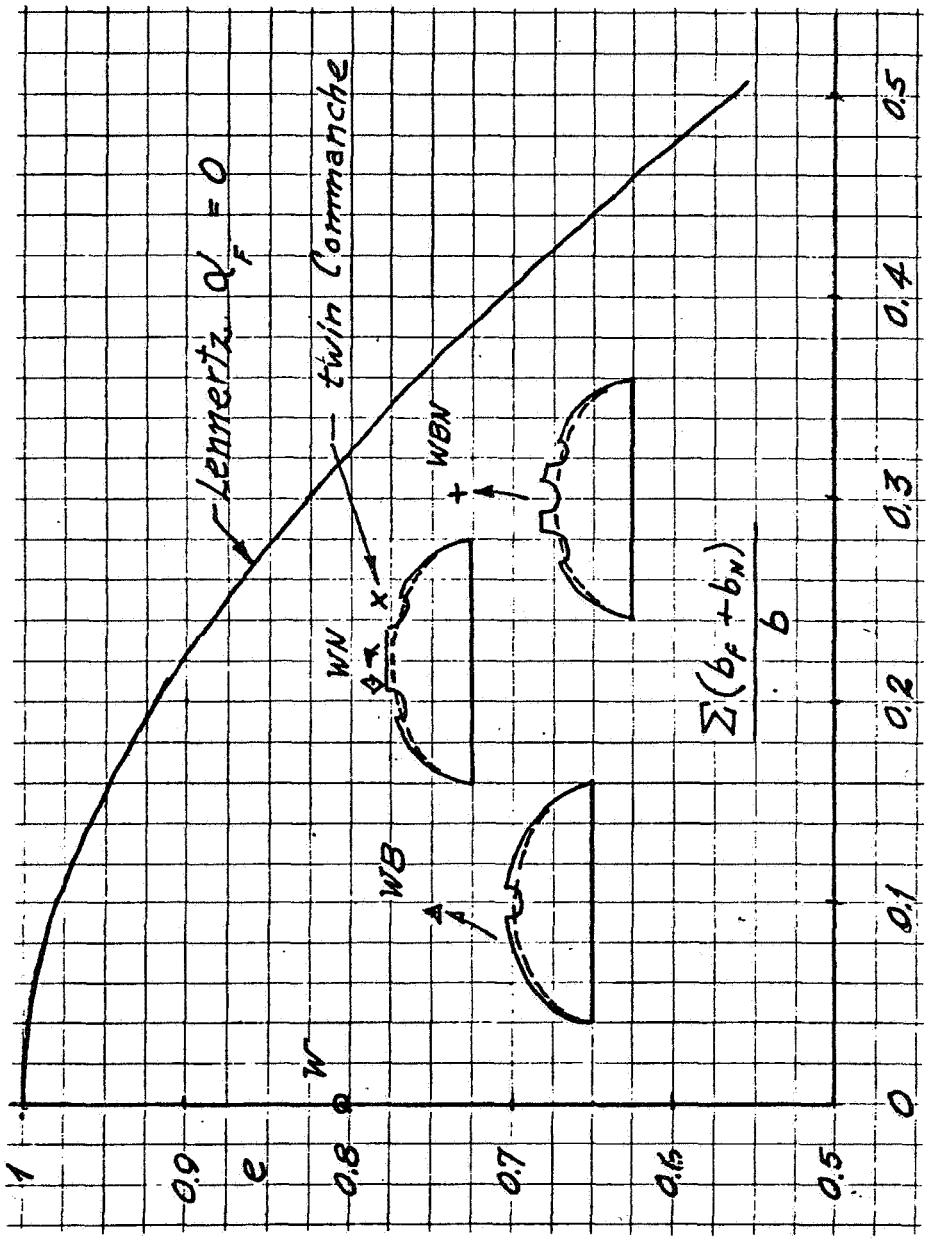

Figure 4. XP-87 Results vs. Lennertz's Theory

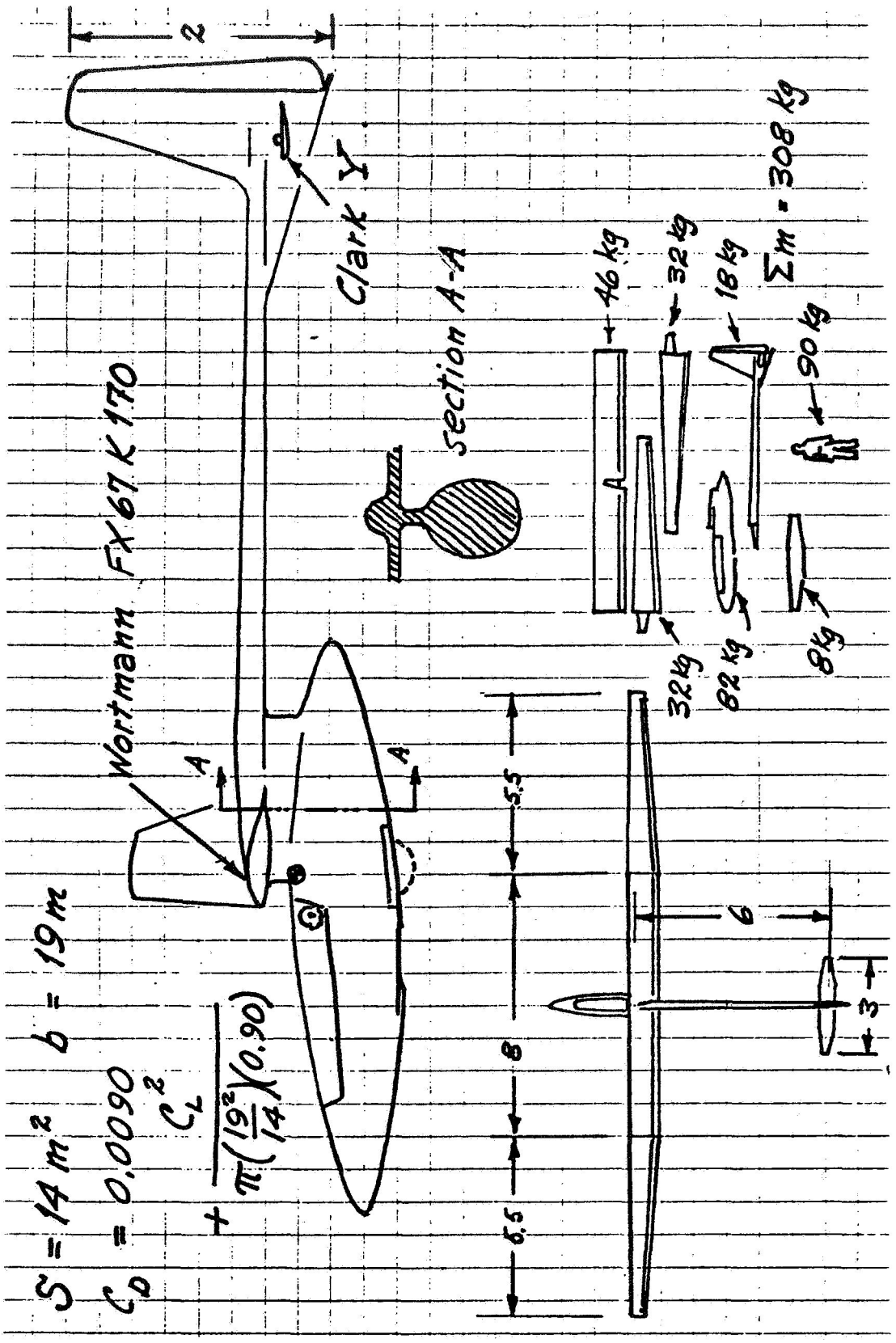

Figure 5. Example Sailplane

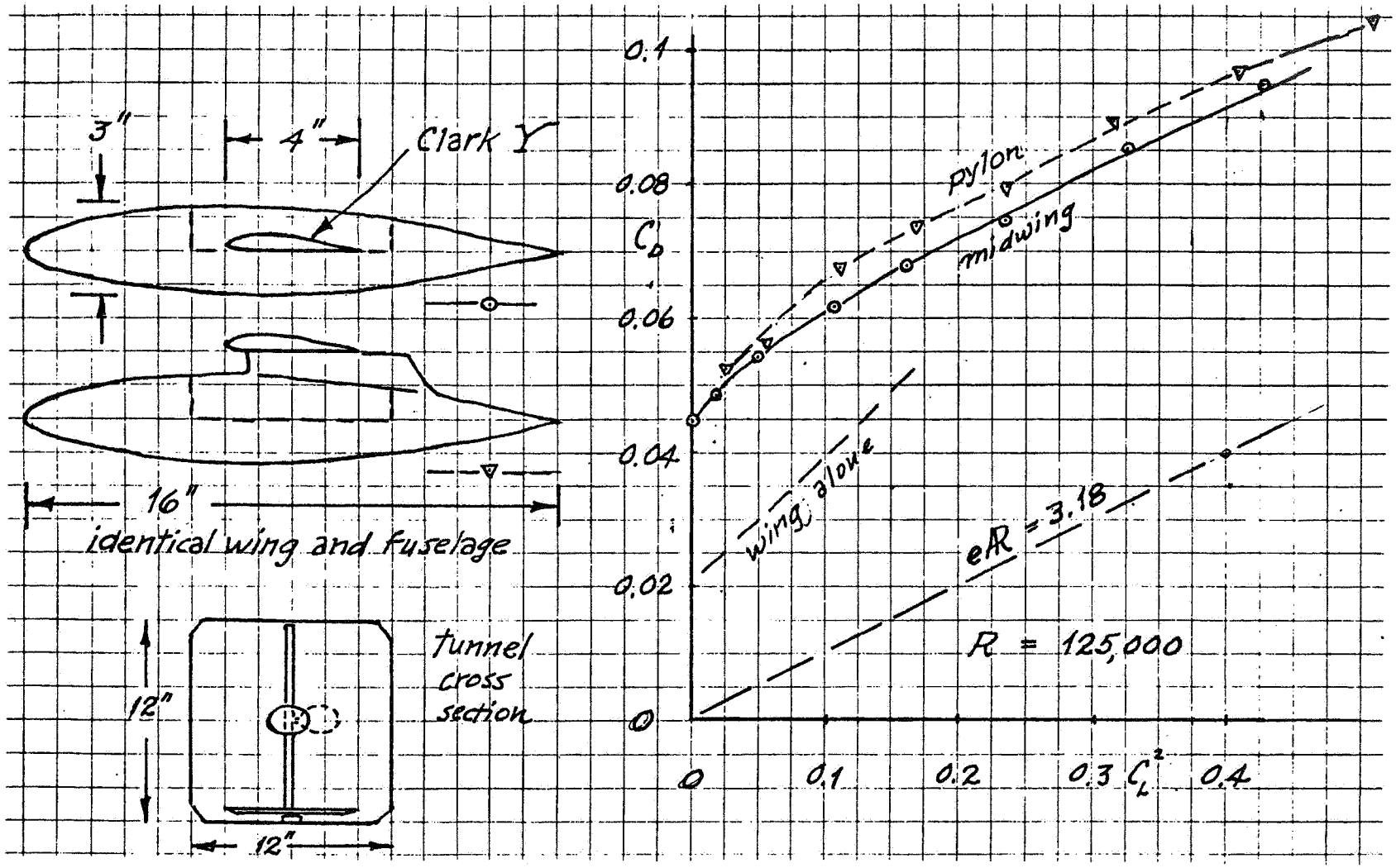

Figure 6. Exposed Central Leading Edge Experiment

4.4 Asymptotic Analytical Methods in Fluid Mechanics Related to Drag Prediction

G.R. Inger
Virginia Polytechnic Institute and State University

Introduction

As a counterpart to the numerical prediction methods we've heard about, I thought it would be useful to describe some recent theoretical work of a purely analytical nature which promises to provide engineering predictions for the important drag-related phenomena of flow in the stall regime. This analytical work deals with rigorous asymptotic studies of the complete Navier-Stokes equations that govern the viscous flow around any aerodynamic body under conditions where boundary layer separation takes place from the body surface (see for example the summary given in a recent NATO-AGARD conference proceedings[1]).

Asymptotic Analysis Approach

In a nutshell, asymptotic analysis (sometimes also called the "method of matched asymptotic expansions" after Van Dyke[2] or the "multiple-deck" approach after Stewartson[3]) consists of a detailed local study of the Navier-Stokes ("N-S") equations behavior in the limit of large Reynolds number which delineates the basic layered substructure of the flow in the presence of adverse pressure gradients leading to separation, including viscous-inviscid interaction effects. As such, this approach is the logical next step in Prandtl's original notion of the boundary layer theory as an asymptotic approximation for large Reynolds numbers. The results establish how the flow leading to separation and beyond can be decomposed into a set of matched multiple decks, each of which are governed by equations appreciably simpler than the full N-S equations and hence far easier (and cheaper) to solve.

Although these mathematical studies are still rather esoteric compared to the needs of the practicing general aircraft aerodynamicist, they yield valuable insight to the "fine grain" structure of the flow and its basic scaling parameters (which is very useful in numerical work), and also show how to eliminate the notorious separation point singularity of classical boundary layer theory by inclusion of viscous-inviscid interaction.[4] Moreover, the results of asymptotic analysis can be used to devise simplified but accurate approximate engineering solutions which are applicable over a wide range of practical flow conditions. An example of this for

laminar flow is given in Figure 1, where the approximate triple-deck viscous-inviscid flow model of separation proposed by Inger[5] is illustrated schematically. As outlined in Figures 2 - 4, the resulting analytical description of the flow is relatively simple and yields closed form results for the skin friction distribution along the surface including a very useful separation point - location criterion (Figure 4A). The turbulent flow counterpart of this layered approach can also be derived (assuming, of course, some appropriate turbulent eddy viscosity model), again resulting in a very simple engineering expression for the separation point (Figure 4B). It is gratifying indeed that these theoretical results have been found to be in a good agreement with experiment over a wide range of practical conditions.

The interaction effect on the pressure distribution due to the boundary layer displacement thickness growth $\delta^*(X)$ can also be accounted for in the context of this layered approach by means of a source-distribution simulation[5]; typical results showing the resultant smoothing out of the originally imposed non-interacting pressure are shown in Figure 5.

Concluding Remarks

With proper engineering adaptation, asymptotic analysis studies offer some valuable new methods for understanding and predicting the underlying fluid mechanics of drag (and lift) in the separation and stall regimes. Moreover, research is currently in progress on extending these methods to include suction or blowing through the surface (i.e., boundary layer control)[6] and the effects of Mach number (compressibility), including the presence of transonic shock - boundary layer interaction,[7] and finally to the case of three dimensional flows.

References

1. Flow Separation, NATO-AGARD Conference Proceedings CP-168, May 1975.
2. Van Dyke, M., Perturbation Theory in Fluid Mechanics, Academic Press, N. Y., 1964.
3. Stewartson, K., and P.G. Williams, "Self-Induced Separation," Proc. Royal Soc. A., 312, 1969, pp. 181-206.
4. Catherall, D. and K.W. Mangler, "The Integration of the Two-Dimensional Laminar Boundary Layer Egnations Past the Point of Vanishing Skin Friction," Journal of Fluid Mechanics, 26, 1966, pp. 163-182.
5. Inger, G.R., "Subsonic Laminar Boundary Layer Separation and Reattachment with Viscous-Inviscid Interaction," AIAA Paper 74-582, 7th Fluid and Plasma Dynamics Conf., Palo Alto, Calif., June 1974.

6. Bodonyi, R. and G.R. Inger, "Analytical Studies of Compressible Boundary Layer Flows in Adverse Pressure Gradients," VIP and SU Aerospace Engineering Report, Blacksburg, Virginia, May 1975.

7. Mason, W.H. and G.R. Inger, "Analytical Study of Transonic Normal Shock-Boundary Layer Interaction," AIAA Paper 75-853, 8th Fluid and Plasma Dynamics Conf., Hartford, Conn., June 1975.

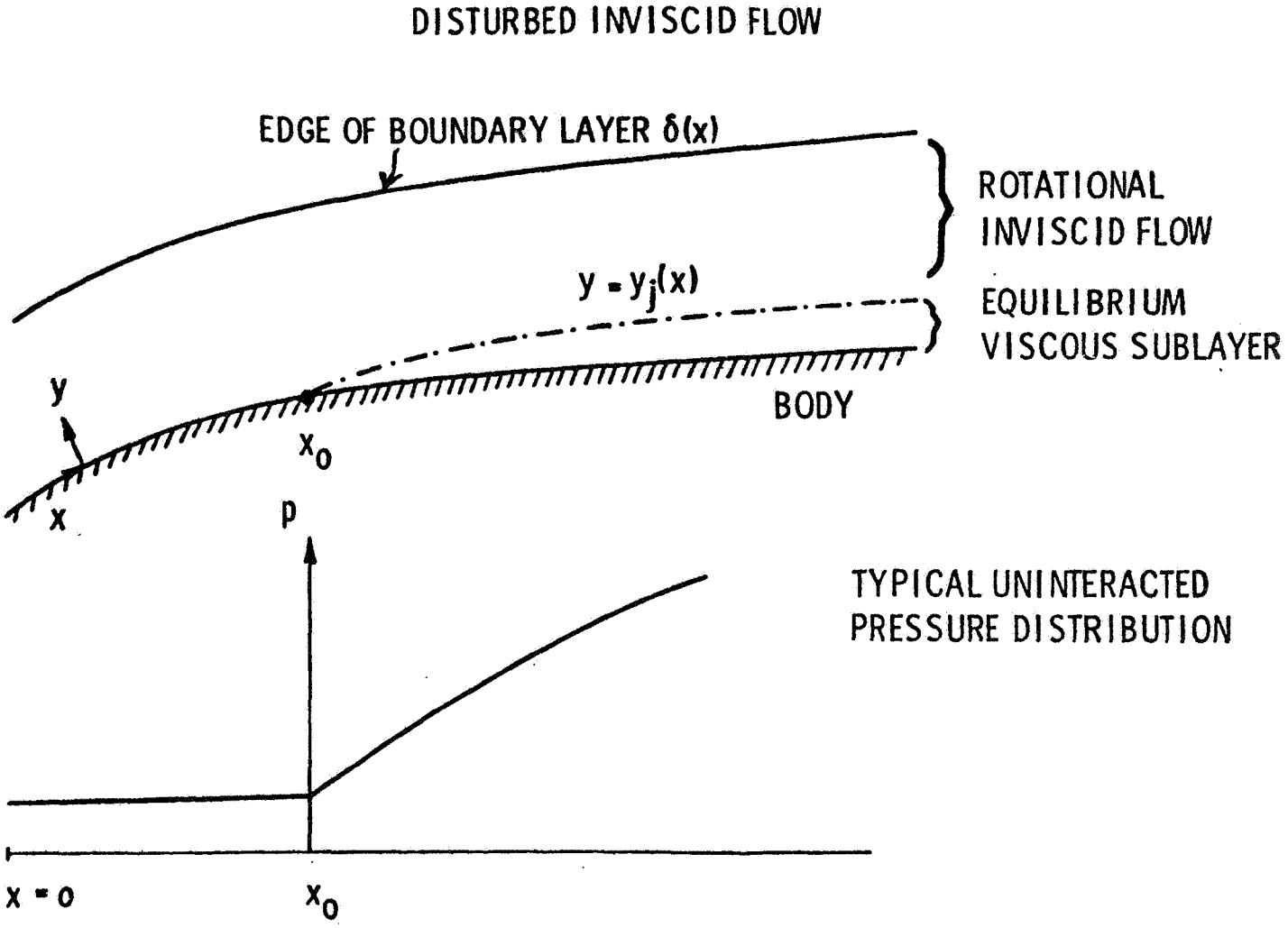

Figure 1. Schematic of Three Layered Flow Model

OUTER ($y_i \leq y \leq \delta$)

$$u \frac{du}{dx} + v \frac{du}{dy} + \frac{1}{\rho} \frac{dp}{dx} \simeq \nu \left(\frac{d^2 u}{dy^2} \right)_{REF}$$

GIVING

$$u^2(x,\psi) \simeq \underbrace{u^2_{REF}(x,\psi)}_{\text{KNOWN APPROX. FOR TOTAL HEAD LOSS}} - \frac{p - p_0}{\rho} \quad \bullet$$

INNER ($0 \leq y \leq y_i$)

$$\frac{dp}{dx} \simeq \frac{d\tau}{dy} = \mu \frac{d^2 u}{dy^2}$$

GIVING

$$\mu u \simeq \tau_w y + \frac{1}{2} \frac{dp}{dx} y^2 + a(x) y^N \quad \bullet$$

WITH $a(x)$ RELATED TO y_i

N GIVEN (≥ 3)

Figure 2. Analytical Relations

RESULTS OF MATCHING

ψ, u, du/dy & d^2u/dy^2 MATCHING AT $y = y_j$ YIELDS

$$\left(X \frac{dCp}{dX}\right)^2 Cp = K_1(N)(1-T)^3[1 + K_2(N)\cdot T] \quad \bullet$$

$$y_j = \left(\frac{N-1}{N-2}\right)(1-T)\frac{Cf_{REF}}{dCp/dX} \quad \bullet$$

$$a(X) = -(dp/dX)/N(N-1)\,y_j^{N-2} \quad \bullet$$

WHERE $T = \tau_w/\tau_{w_{REF}}$ = NON-DIMENSIONAL SKIN FRICTION

$$K_1(N) = \left[\left(X\ dCp/dX\right)^2 Cp\right]_{SEP} = \frac{.0041(N-1)^3(N^2+3)}{N^2(N+1)(N-2)^2}$$

$$K_2(N) = 3(N^2-1)/(N^2+3)$$

Figure 3. Results of Matching

a) LAMINAR FLOW

$$C_p \left(X \frac{dC_p}{dX} \right)^2_{sep} \simeq .0104$$

b) TURBULENT $(u \sim y^{1/N})$

$$C_p \sqrt[\frac{N-2}{4}]{X \frac{dC_p}{dX}_{sep}} \simeq 1.43 \left(\frac{N-2}{N+1} \right)^{\frac{N-3}{4}} \left(\frac{3}{N+1} \right)^{\frac{1}{4}} \frac{Re_{x,sep}^{1/10}}{\sqrt{(N+1)(N+2)}}$$

Figure 4. Separation Criteria

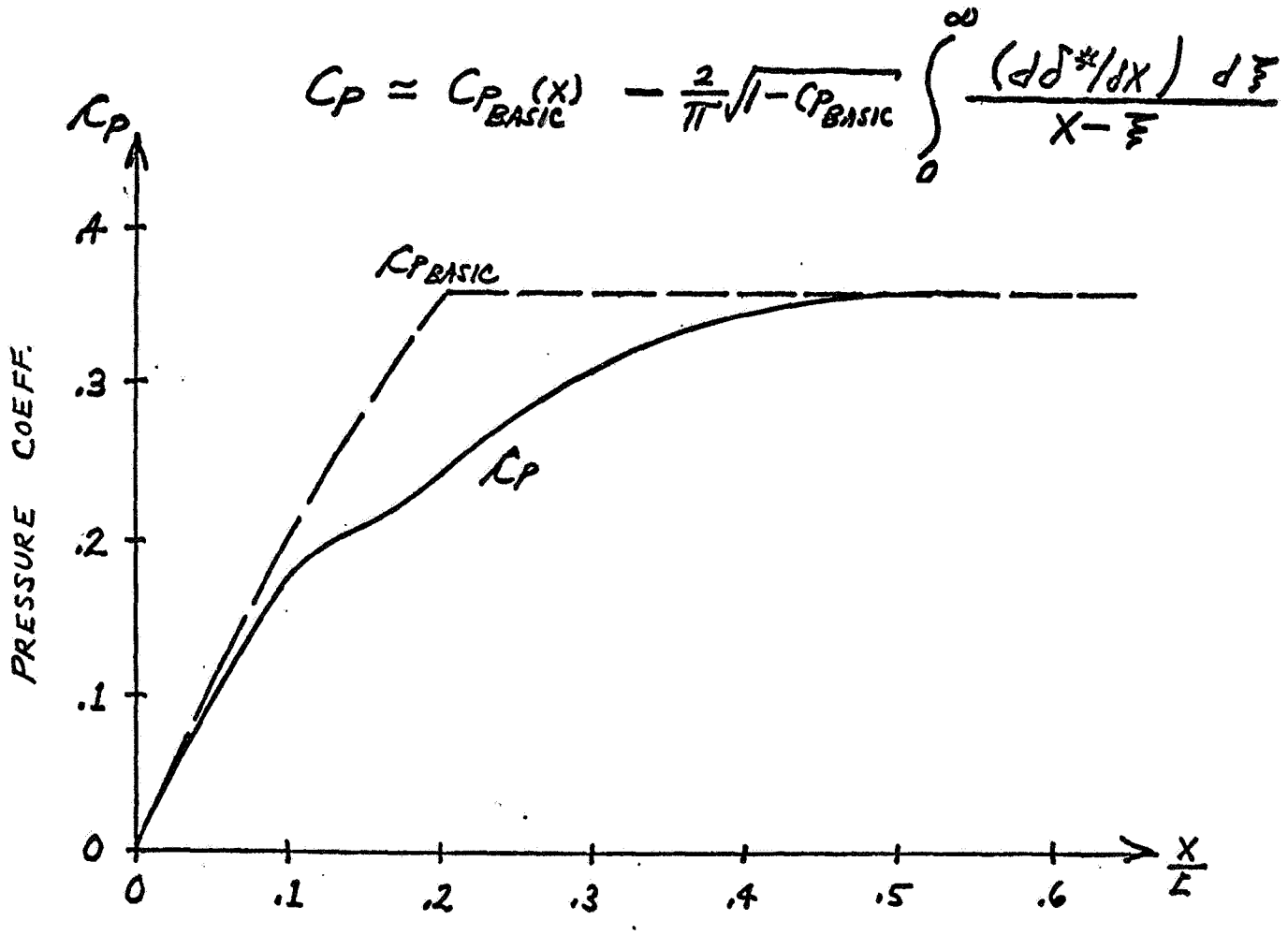

Figure 5. Typical Viscous-Inviscid Interaction

4.5 The Economic Impact of Drag In General Aviation

Ron D. Neal
Gates Learjet Corporation

Introduction

Historically, one of the major goals of the aircraft designer has been to provide improved performance and it has also been recognized that one of the most significant controlling factors for achieving this goal has been the basic drag of the vehicle. As a result of the energy crisis, there has been even more current emphasis placed on the potential fuel conservation that might be derived through the incorporation of various advanced technology concepts including improvements in aerodynamic drag.

An example of the aircraft fuel saving benefits being considered was recently given during testimony before the House Subcommittee on Aviation and Transporation when NASA officials indicated that aircraft fuel savings of up to 50% might be achievable beyond 1985, with 5% to 10% fuel savings possible in the next few years. NASA indicated that these fuel savings would come about through "technical modifications, advances in aerodynamics, structures and controls combined into a new highly efficient wing, and new materials to reduce aircraft weight." The projected 40% to 50% fuel savings would become available through development and integration of "optimum aircraft systems."

Additional comments by other NASA officials have indicated that they place fuel saving technologies into three time levels, namely,

* Near term - fuel consumption to be reduced 35% of that of current wide-body transports - to be achieved by 1985 - through incorporation of supercirtical aerodynamics, composite materials, advanced propulsion, advanced avionics, and active controls;
* Far term - fuel consumption to be reduced to 55% of that of current wide-body transports - beyond 1985 - through various boundary layer flow control concepts; and
* Unconventional design concepts - goals yet to be defined.

NASA is not alone in their pursuit of fuel savings for all of the major manufacturers are also evaluating the problem as it relates to their present and future aircraft development programs. McDonnell-Douglas studies of a stretch DC-10 have

shown that "drag reductions of 3.95% are attainable . . . . but there is a potential improvement of 11.2% if all the theoretical drag reduction could actually be gained in practice." The Boeing 727-300B airplane is reported to offer a 14% improvement in fuel burned per seat mile over the basis 727-200 version and for this the airlines would only pay about $2 million more per airplane. For an L-1011, Lockheed has estimated that in order to achieve a 20% improvement in direct operating costs it would require a combined 10% improvement in efficiency through aerodynamics, structures, and propulsion.

However, no matter how desirable improved fuel consumption may be, when one considers the question of "drag reduction" and its economic impact - be it for a transport or general avaiation airplane - it is necessary to evaluate two factors:

(1) the improvement in fuel flow (and thus lower direct operating costs) due to the drag reduction and

(2) the cost associated with the incorporation of the drag reduction technology.

Before undertaking a discussion on the economic impact of drag on general aviation airplanes, it seems that a necessary first step would be to define the types of aircraft to be included in such a study. A fairly standard definition of general aviation is that it includes all civil aircraft except those aircraft operated in the air carrier system. The activities of this segment of aviation then range from pleasure flying by an individual pilot to the professional corporate operation of a fleet of business aircraft. The type of aircraft found in general aviation can then include the amateur built airplane, the antique, a former WWII fighter, and a business jet. Thus it is that general aviation embraces a diverse range of equipment having a multitude of mission requirements.

Since the general aviation field includes an assortment and variety of aircraft, let us then determine what segment of general aviation aircraft most needs some thoughts and comments relating to the interdependence of drag and economics.

General Aviation Fuel Consumption

The general aviation population may be identified, and has been identified by the FAA, in the following manner: single engine (piston), multi-engine (piston), turbine, rotorcraft (piston and turbine).

These vehicles represent a fleet of some 151,000 flying machines. In terms of flying hours in 1974, general aviation airplanes flew a total of 30,400,000 hours. When turbine powered rotorcraft are included with the fixed wing turbine aircraft

the total estimated time flown by turbine powered vehicles becomes 2,640,000 hours. These turbine powered hours then represent about 8.7% of all general aviation flying.

In 1974, the total jet fuel and aviation gasoline consumed by the United States domestic civil aviation fleet (including general aviation) was 9,064,000,000 gallons, with the general aviation portion of this total amounting to 800,000,000 gallons.

From these data it is seen that general aviation consumes only 8.8% of the total domestic aviation fuel. If military aircraft operations are added to this picture, the general aviation fuel consumption drops to only 6%. When the fuel consumption of all forms of transportation are considered, the total fuel used by general aviation represents just seven-tenths of 1% of this total.

As a final result of evaluating these numbers, it is noted that one segment of general aviation, namely the turbine powered vehicles - which represent 3.4% of the general aviation fleet and flies about 8.7% of the general aviation hours - consumes some 44.6% of the general aviation fuel.

A further comparison of the fuel consumption of the piston powered versus the turbine powered airplane is offered by the example that in one hour, twenty-three single-engine Cessna Model 150 airplanes will consume the same amount of fuel as one twin-engined turbofan Cessna Citation. At the large end of the business jet scale, ninety-four Model 150 airplanes in one hour will consume the same amount of fuel as one Grumman Gulfstream II.

These numbers then clearly indicate that if a study of the effect of drag on the economics of general aviation is to be made, the most promising area for meaningful improvement and results is in the category of turboprop and turbojet/turbofan powered airplanes.

Operating Costs

When considering the operation costs of an airplane, there are many items of expense that must be evaluated. However, a fairly common and accepted measure of the economy of an airplane is given by its direct operating costs.

A recent review of the direct operating costs for existing turbojet/fan business aircraft shows that the fuel cost per hour accounts for 50% to 76% of the direct operating cost, with the average being 63%. A comparison of the turboprop airplanes shows similar trends with fuel cost averaging 54% of the direct operating costs for these airplanes.

The fuel cost per hour is directly related to the fuel consumption of the individual airplane - which in turn is a function of the airplane drag and efficiency of the engines - and to the price of the fuel. The fuel consumption of the airplane can be controlled by the aerodynamic design and by the selection of the engine. However, these engineering aspects of the problem have no direct bearing on the price of the fuel.

In the 1964 to 1970 time frame, the price for jet fuel rose from 27 cents per gallon to about 35 cents per gallon.

An added burden to fuel pricing occurred in July 1970, when the Airport/Airways Development Act went into effect. One impact of this new law was an addition of a 7 cent per gallon fuel tax for general aviation aircraft. A review of the cost analysis for a Learjet, prepared in October 1973, shows a fuel cost of 42 cents per gallon including the 7 cent tax. The same cost analysis prepared in September 1974, used a fuel cost of 59 cents per gallon (tax included). By November 1974, the national average for turbine fuel was being quoted at 63 cents per gallon. In the time frame of a year (1973-1974), the price of turbine fuel (excluding the 7 cent tax) increased about 60%. In terms of an out-of-pocket expense, this fuel price increase from 42 to 59 cents per gallon results in a $39 per hour increase in the direct operating cost of a Learjet. For the operator averaging 500 flight hours per year, this amounts to an increase in the cost of operation of $19,500.

Airplanes tend to fly in terms of gallons of fuel per hour or pounds of fuel per hour. However, in the petroleum industry fuel quantities are quoted in barrels rather than gallons. Airline calculations show that for every one dollar per barrel of oil cost increase, either as a result of a direct price increase or by added tax, the price for turbine fuel increases 2.4 cents per gallon.

One very simple method to reduce fuel consumption is to reduce speed and the 55 mile per hour speed limit for automobiles is a classic example of such a solution.

As one means of fuel conservation, the airlines are also using reduced cruise speeds. However, the impact of the reduced speeds on fuel consumption depends upon the specific airplane and its route structure. As an example, the Boeing 737 can reduce its fuel consumption by 7% on a 500 n.m. trip by decreasing the cruise Mach number from 0.78 to 0.74, while incurring only a 3 minute increase in block time. In the case of a Boeing 747, a cruise speed cut-back from Mach 0.86 to 0.84 results in a 4% fuel reduction and an increase in block time of 16 minutes

over a 4000 n.m. stage length. These same trends also hold true for the small business jet. In the case of a Learjet, a reduction in cruise speed from 0.81 to 0.77 will result in a total fuel reduction of about 3% over a 100 stage length with an increase in trip time of only 5 minutes. A reduction from 0.81 to 0.73 yields a fuel reduction of almost 5% and an increase in trip time of 11 minutes. Based on a Learjet fleet of 500 airplanes, with each airplane averaging 500 flying hours per year, a 5% reduction in fuel consumption translates into a fuel savings of about 6,500,000 gallons per year.

Drag Improvements

A speed cut-back offers an operational procedure for reducing fuel consumption. Yet, from a long term standpoint, it is desirable to obtain a fuel savings without imposing a speed reduction - even if that speed only results in a matter of a few minutes in flight time. Looking ahead to the future the real problem to be resolved is "What realistic improvements can be anticipated for the next generation of business aircraft?"

A recent magazine interview with Dr. Whitcomb posed the question, "What new designs do you see forthcoming in the near future for corporate and general aviation?" His answer was, "I do not think new designs of a radical nature are forthcoming in the near future, but all aircraft manufacturers are, of course, working on improvements to their current models."

This same basic viewpoint is being echoed for the large commercial air transports and this position has been summarized as follows: "Rising costs and reduced rate of technology advances indicate a long period of derivative commercial transport; large technological advances are required to justify an all-new aircraft."

From a historical standpoint, the general aviation market has not been noted for introducing major changes in the state-of-the-art technology. The changes occurring in general aviation airplanes have tended to be in the areas of improved systems and avionics, whereas the basic airframe and powerplant remain largely unchanged over a long period of time. This type of change does not indicate that general aviation lacks growth, for on the contrary, the general aviation industry provides a complete range of equipment designed to meet the flying needs of today.

This observation of conservative growth is not offered as a criticism of general aviation. If the general aviation industry were to embark on a program to incorporate high technology involving structures, aerodynamics or other advanced state-of-the-art concepts into this type of airplane they could certainly achieve this

goal. However, unless supported by military or other government funding, the development costs of such efforts would be passed on to the customer. A serious consideration to be faced is that the resulting "new technology airplane" might not offer a significant improvement over the more conventional and proven concept.

Critics of general aviation technology are all too ready to point out that while the airlines have grown in speed and capability through the years the general aviation airplane has remained stagnant. As proof for this premise they site the growth of the airlines that can be traced from the single-engine airlines of the 20's through the modern twin-engine DC-3, the introduction of the jet powered Comet, the four-engined Boeing 707, the new wide body transport and the supersonic transport.

However, when we examine the general aviation airplane, we also can find significant progress. The "small airplane" has developed all the way from the Wright airplane of 1903 to the high performance business jet of today. Thus, to claim that general aviation has not grown requires that one totally ignore and misunderstand the scope and magnitude of the general aviation market.

The real reason that the so-called "light aircraft" has not experienced a significant change in performance with the passage of time is simply due to the fact that the basic laws of aerodynamics are not time dependent. Thus, it is in the real world, that an airplane of a given size, weight, and horsepower, built in the 1970's or 80's, will have comparable performance to a similar airplane built in the 1930's.

An excellent example of the evolution of an aircraft is seen in the Beech Model 35, better known as the Bonanza. This airplane made its first flight in December 1945. In the thirty years since its introduction, the Model 35 has experienced a continued history of product improvement and yet the basic airframe design, fabrication techniques and powerplant remain unchanged.

"Exceptions to the rule" do occur in all fields and general aviation has seen its share of innovative ideas. Within recent history the Windecker "Eagle" offered the promise of increased aerodynamic efficiency plus the forecast of manufacturing economy which would result in lower selling prices. Advertisements for this fiber-glass airplane clearly stated that the Eagle represented "the greatest single advance in general aviation since the advent of the all-metal airframe." Yet in spite of these technical advantages, this airplane failed to achieve successful production and market status.

The twin-engine, two passenger "Derringer" also represented a step forward and advertisements of 1968 proclaimed: "The Derringer represents a completely advanced concept in light aircraft construction, with the same fine attention to details

as found in a million dollar jet. It's the only light twin made using chem-milled, stretch-formed, flush-riveted skins on wings and fuselage. All exterior surfaces are aerodynamically smooth and clean for optimum efficiency." As with the Eagle, the Derringer failed to develop into a commercial product.

The Learjet also offers an excellent example of the continued development of an airplane. The original Learjet Model 23 made its first flight in October 1963, and the delivery of the 500th airplane in April 1975 finds us with a five airplane product line. The latest addition to the Learjet family includes the Model 35/36.

The Model 35/36 is powered by turbofan engines which offer fuel savings of 30-35% over the turbojet powered Model 25 airplane. The development of this capability required design, development, certification and production effort covering five years. The development cost for the program was about $7 million and the airplane selling price is about $360,000 more than the Model 25.

In terms of general aviation airplanes the recent AIAA fuel workshop has provided some comments on the potential of fuel saving by means of a reduction in the drag of "protuberances." This workshop suggested that a full-scale drag clean-up study of several representative general aviation aircraft be undertaken as a means of assessing the magnitude of improvement possible.

While on the subject of "roughness drag," I would like to offer a comment. I find it difficult to think of a more useless effort than a study on the effects of a drag clean-up program for general aviation airplanes. It does not require a trained aerodynamics engineer to produce a list of items that, if removed or eliminated from a specific airplane, would result in some drag reduction. The real problem in a drag clean-up effort is not an aerodynamics problem, but rather the problem is one of how to design, manufacture and then sell at a realistic price the so-called aerodynamic improvements that have been conceived. If this area is to be investigated, our efforts should not be spent on detailed performance improvements that might result from drag clean-up, but rather our time and monies should be spent developing economical methods of fabrication that can accommodate some of these aerodynamic changes.

In terms of an aerodynamic clean-up program, one of the first items to be considered for removal from the airframe are the antennas. As an example, we can look at the business jet - an airplane that can fly at Mach 0.81 at altitudes of 45,000 feet - surely an airplane that would have no external protuberances to blemish its high speed contours. Yet, a review of the avionics installations for this airplane shows that for any individual airplane a total of some 13 different external antennas could be installed.

An antenna drag analysis on the Learjet has shown that if all of these 13 different antennas were to be flush mounted, the drag reduction would represent only about 1% of the total cruise drag. As a result of this study, it was concluded that any flush-mounting program should encompass all of the antennas because the individual drag contribution of any one antenna installation is so small as to be negligible. It should also be noted that the one percent reduction in drag, due to flush mounting all of the antennas, would be difficult to detect in engineering flight test since this level is within our $\pm$ 2% data scatter for cruise drag measurements. An added consideration, to this antenna drag question, is that for today's navigation and communication equipment it is doubtful that all of the antennas could be flush mounted. Thus, the actual antenna drag reduction to be realized would be somewhat less than the ideal one percent goal.

During one of the development programs on the Learjet, an attempt was made to flush mount one of the VHF antennas. The actual hardware installation of the antenna did not present a problem, however, the fact that the antenna failed to function for certain station/airplane orientations was found to be objectionable. The other factor of concern was that changing from an external antenna to a flush mount antenna involved a price change from $50.00 to about $1,000.00.

Antennas are, of course, only one source of drag in the category that may be identified as "roughness drag." Included in roughness drag calculations are such irregularities as manufacturing gaps, steps, surface waves, protuberances, various air inlets and outlets, pitot probes, angle-of-attack vanes, drain lines, vortex generators, and all other such items. Individually, these items usually do not produce enough drag to even be measurable from flight tests, yet taken as a sum, these items do constitute a portion of the total. Based on a drag analysis of the Learjet, it is estimated that the total roughness drag accounts for about 5% of the total cruise drag.

From an ideal standpoint it would appear to be desirable to eliminate the "roughness drag." However, consideration of the engineering manhours required for the task plus the fundamental question of how manufacturing would cope with these requirements may very well lead one to conclude that "roughness drag" will remain with us for the next several years.

The supercritical wing certainly offers the opportunity for improved performance in tomorrow's business jet aircraft. One possibility, of course, is to retrofit a supercritical wing onto an existing airplane. Yet the installation of a wing change only may not offer an economic profitable plan when the projected performance gains are weighted against the time schedule and development cost associated with this type of program.

As a specific example, in order to build two prototype airplanes with supercritical wings, conduct the normal development program and FAR 25 certification would require some three years and a total cost of about $8.5 million. In terms of airplane cost, this improvement would increase the price of the airplane about $150,000.

In actual fact, in order for a major change to be incorporated into a given airplane, it must offer a "significant" improvement over existing airplanes.

Conclusions

To then offer a summary, the turbine powered vehicles (fixed wing and rotorcraft) including turboprops, turbojets, and turbofans comprise a very small segment of the general aviation fleet, yet these vehicles consume almost 45% of the general aviation fuel. In terms of general aviation fuel savings, the turbine powered airplanes offer the greatest opportunity for productive gains.

It is possible to achieve small drag reductions through aerodynamic clean-up programs, but the improvements are usually minor relative to the engineering and development costs. The drag improvement from such programs is probably on the order of 1 to 5%.

Improvements in airplane drag are possible within the next 5 to 10 years, but these improvements will occur on "new" models and their effects will be in the 5 to 10% range.

Major improvements in fuel consumption over existing turbofan airplanes are realistic for 1985 and beyond, but these changes will be in the 15 to 25% range and will be the combined result of improved aerodynamics plus additional improvements from more advanced turbofan engines.

And I would hope that this workshop will serve as a springboard for the cooperation and research needed to achieve these goals in the years ahead.

5. PAPERS OF SESSION III - WING DRAG

5.1 Some Methods for Reducing Wing Drag and Wing-Nacelle Interference

Thomas C. Kelly
NASA Langley Research Center

Introduction

This paper summarizes the results of efforts directed toward drag reduction which are underway within the Transonic Aerodynamics Branch at NASA-LRC. Three areas of research which will be discussed are: (1) The development of both supercritical and subcritical families of airfoils (see, for example, references 1 to 3); (2) The development and application of vortex diffusers (or, more popularly, winglets) to reduce induced drag (reference 4); and (3) The application of supercritical wings to executive-type aircraft and the reduction of severe wing-pylon-nacelle interference problems which were identified during these investigations (reference 5).

It should be noted that this is not a summary of the total NASA-Langley effort devoted to drag reduction, but rather a discussion of several selected areas which would be of interest.

Work at Langley is continuing in several additional areas including the reduction of turbulent skin friction through the use of compliant surfaces, reductions in so-called "crud" drag through the application of various surface coverings, reductions in induced drag using over the wing blowing (see reference 6), tip-mounted engines (reference 7), favorable power interference effects, and the use of thick supercritical wings to achieve higher aspect ratios. Finally, the possibility of obtaining practical laminar flow control is also under consideration.

Airfoil Development

Supercritical airfoils - This new type transonic airfoil was developed by Dr. R.T. Whitcomb at NASA-Langley about 10 years ago. At that time, theoretical approaches for supercritical flows were non-existent and much of the early work in developing the airfoils was intuitive in nature.

Figure 1 presents two-dimensional wind tunnel results for several ten percent thick airfoils at a section lift coefficient of 0.7. The conventional airfoil results presented are for the NACA 64A-410. Comparison of the results for this airfoil with those for the supercritical airfoils illustrates the significant gain in drag-rise Mach number achieved by use of the supercritical section. The increase in drag-rise Mach

number is approximately 0.1. These results also indicate the presence of drag creep which was characteristic of all of the early supercritical airfoils. The drag creep, which results from increases in pressure drag associated with the onset of supercritical flows on the airfoil upper surface, was noted in the early flight test results for the F8 and T-2C research airplanes which employed supercritical wings having these early-type airfoils.

Much of the recent work at Langley has been devoted to the elimination of this undesirable drag creep, and the solid curve of Figure 1 shows the result of these efforts. Refinements to the airfoil were involved primarily with changes which resulted in a more favorable flow recompression over the forward upper surface and the elimination of a region of flow overexpansion near the three-quarter chord location also on the upper surface. A slight loss in force-break or drag-divergence Mach number is noted (about 0.01) as a result of slightly increased wave losses at the higher Mach numbers, but this compromise is felt to be of little consequence relative to the gains achieved in eliminating drag creep. It should be noted that, unlike the early work, the shaping changes used in the design of the recent airfoil, were guided by the use of the analytical program developed recently by Korn and others (reference 8) in achieving desired pressure distributions for the various cases.

Figure 2 indicates the status of the current supercritical airfoil development program. As is evident, the main effort is ambitious, and covers a broad range of design lift coefficients for airfoils ranging in thickness ratio from 6 percent to 22 percent. Solid symbols on the figure indicate airfoils which have been designed and tested. Open symbols represent airfoils which are currently under design using the analytical program noted earlier, and the crossed symbols indicate airfoils which are considered to have important applications and which are planned for design in the future.

Subcritical airfoils - The Langley work on supercritical airfoils led to a renewed interest on the part of NASA in developing airfoils designed for subcritical speeds. The first of these, designated the GA(W)-1, was a 17-percent airfoil designed specifically for the single-engine climb requirements for light twin-engine aircraft. Initial wind-tunnel results for this airfoil encouraged the design of several other airfoils for use at subcritical speeds.

Figure 3 presents a comparison of two-dimensional results obtained recently for the 13-percent thick GA(W)-2 airfoil and the older NACA 651-213 airfoil. Results for both airfoils were obtained in the Langley low turbulence pressure tunnel using the narrow fixed transition strip technique. Assuming section lift coefficients

of 0.4 and 1.0 for the cruise and climb cases, respectively, reductions in section drag coefficient on the order of 3 percent and 17 percent, respectively, are achieved for the newer airfoil. Significant gains at the higher lift coefficients are indicated.

Figure 4 corresponds to the earlier supercritical family figure and indicates the current status of the subcritical airfoil family development. All of the airfoils developed thus far have been designed for a lift coefficient of 0.4, having thickness ratios of 13, 17, and 21 percent. An additional airfoil in this group is being designed with a thickness ratio of 9 percent. Also in design are two 17-percent airfoils having design lift coefficients of 0.2 and 0.7. Planned for future development are two 13-percent airfoils with design lift coefficients of 0 and 1.2.

Vortex Diffusers

A sizeable effort is currently underway at NASA-LRC directed toward the reduction of induced drag. One phase of this effort, which has received wide notice, involves the use of vortex diffusers, or winglets as they are more popularly called, mounted at the wing tips. Unlike end plates, the vortex diffusers are designed with the same careful attention to local flow conditions as would be utilized in the design of the wing itself. The placement of the vortex diffuser within the rotational flow field of the wing tip results in forward inclinations of the lift (or side force) vectors for the vortex diffusers, producing a thrust component which increases with increasing lift. The action is analogous to the force which propels sailboats, of course.

Figure 5 shows the geometric characteristics of the semispan model used for the vortex diffuser development. The wing planform represents an early version of a wide-body transport configuration. The two tip configurations tested, shown in the right side of the figure, represent the basic tip configuration and the vortex diffuser configuration which was tested assuming the "soft tip" portion of the basic wing panel could be removed. This resulted in a reduction in the basic panel span of about 2.5 percent. The vortex diffuser geometry is shown on the left side of the figure. The upper vortex diffuser span is about equal to the basic wing tip chord; the leading edge sweep is equal to the wing leading edge sweep and the vortex diffuser root chord extends over the aft 60 percent of the wing tip chord. This particular arrangement was selected in order to avoid superimposing the high local velocities occurring on the wing upper surface and on the vortex diffuser upper surface, which faces inboard. This upper diffuser is canted outward about 18° from the vertical. The lower diffuser is reduced considerably in span to provide ground clearance, extends over the forward 40 percent of the wing tip chord, and is canted outboard about 36°. The upper and lower vortex diffusers were separated to avoid mutual interference effects.

Figure 6 presents incremental drag results associated with the vortex diffusers as a function of lift coefficient for three Mach numbers. Incremental drag is defined as the drag coefficient for diffusers on minus the drag coefficient for diffusers off so that negative values of this parameter represent gains or, thrust.

Near zero lift, a net penalty results as would be expected. At a lift coefficient of about 0.26 the diffusers are carried with no penalty, and above this lift coefficient, favorable effects are obtained which increase with increasing lift. For the case presented, the cruise lift coefficient is about 0.53 at a Mach number of 0.80, resulting in a gain of about 15 drag counts ($C_D = 0.0015$). In full-scale terms this would represent an increase in L/D of about 5 percent, which, of course, is significant.

Figure 7 indicates the effect of the vortex diffusers on the wing pitching-moment and root-bending-moment coefficients. These results are for the cruise Mach number of 0.80, and show relatively small effects of the diffusers, for example, a two percent increase in root bending moment at the highest lift coefficient tested. Also, early wind tunnel flutter tests have indicated relatively small reductions in flutter dynamic pressure resulting from addition of the diffusers. It was also concluded that these effects were associated with structural characteristics rather than any unsteady aerodynamic interaction.

Figure 8 illustrates one proposed application of vortex diffusers. NASA is currently involved in a joint program with the USAF to determine the possibility of adding vortex diffusers to both the C-141 and the KC-135. Tests of both configurations are scheduled for this fall in the 8-foot Transonic Pressure Tunnel. This model photograph depicts vortex diffusers installed on the C-141.

Wing-Nacelle Interference

In an effort to provide access to supercritical wing technology for the general aviation manufacturers, NASA has entered into several cooperative endeavor agreements with members of the industry whereby NASA provides expertise in the areas of aerodynamic design and application of supercritical wings to this class of aircraft and also provides limited wind tunnel testing for configurations which are under design. The remainder of this discussion will present some results obtained recently which relate to the problem of wing-nacelle interference which occurs at high subsonic speeds and which is characteristic of configurations where fuselage-mounted engines overhang the wing rearward upper surface. A representative configuration is shown in Figure 9. This is a photograph of a one-ninth scale model of an

executive-type aircraft under test in the Langley eight-foot transonic pressure tunnel. This particular investigation was conducted to determine the aerodynamic feasibility of replacing the original wing with one having supercritical sections of increased thickness, the thickness ratio being increased on the average from about .09 to .12. Because the wing was intended to be retrofitted, other configuration changes were to be kept to a minimum, therefore most of the tailoring or "tuning" changes were associated with the wing itself although some changes to the pylons were also made.

Figure 10 illustrates the severity of the interference problem which was found to exist between the wing and the engine-pylon arrangement for the modified configuration. These results are for a lift coefficient of 0.25 and are presented as an incremental drag coefficient versus Mach number, where $M = 0.60$ is used as a reference drag level for each configuration. It should be emphasized that all of the results presented are for the configuration with a supercritical wing. No comparisons are presented with the basic wing.

The data for the initial supercritical wing configuration, shown by the solid curve, indicate noticeable drag creep and an early drag rise. Reasons for these effects will be discussed later. Removal of the engines and pylons resulted in significant reductions in drag-creep, and the force-break or drag-rise Mach number was increased by about 0.02 to 0.03 as indicated by the dashed curve. Modifications to the wing root section, the addition of a wing glove and some reshaping of the pylon provided the results indicated by the long-short dashed curve. As can be seen, the drag creep was reduced considerably (about 75 percent at a Mach number of 0.80).

Figure 11 presents wing upper-surface oil flow photographs for a Mach number of 0.825 and a lift coefficient of about 0.35. The photograph on the left of the figure is for the initial configuration with nacelles and pylons and shows dramatically, the effect of the nacelle and pylon presence in forcing the uppers urface shock wave forward on the inboard wing region. The presence of a second wave which originates in the channel formed by the upper surface of the wing and the nacelle-pylon combination is also apparent. Examination of local pressure distributions for this case indicates the second wave and the adverse pressure gradients associated with it caused extensive separation in the "channel" region. The center photograph, for the case of the nacelles and pylons removed, shows what could be termed an expected supercritical wave location for this thickness ratio on the upper surface with little or no separated flow in evidence.

The final photograph of Figure 11 illustrates the upper surface condition for the tuned configuration. The main wave appears somewhat weaker compared to that for the initial configuration, and no evidence of the second wave is seen. Modifications to the configuration were accomplished through a number of steps. Figure 12 shows a comparison of the initial wing root and pylon lines with those for the final configuration tested. Most of the changes noted were made to eliminate what was essentially a converging-diverging channel formed by the wing-pylon-nacelle combination. Initially, material was removed from the aft region of the wing upper surface. Then, in order to reduce the upper surface velocities entering the channel, a glove was added and the forward portion of the resulting airfoil was increased in thickness. Finally, the lower surface of the pylon was thickened in order to provide for a relatively constant area in the channel. All of the noted changes represented an application of the area rule in a local sense, since the induced velocities approached and exceeded sonic values in the region.

The results just disaussed were obtained using an executive-type aircraft model which employed turbojet engines. It might be expected, therefore, that replacement of the turbojet engines with the newer and larger turbofan engines would serve to aggravate the interference problem which was noted and some recent wind tunnel results indicate this to be the case.

Figure 13 presents results for an executive-type aircraft very similar to the one previously discussed. Again, results are presented in the form of an incremental drag coefficient versus Mach number; however, the reference Mach number in this figure is 0.50. Because an interference problem was anticipated, provision was made on the model to allow translation of the engine-pylon combination to several longitudinal locations. The results given in Figure 13 are for the proposed initial location (identified in Figure 13 as the production location), the most rearward location possible, which corresponded to a full-scale rearward shift of 18 inches and for a final "tuned" configuration with the engines aft. For this span location, and neglecting the glove, the leading edge of the nacelle moved from about the 55-percent chord location to the 70-percent location. This relocation was made in three steps of 6 inches each, full scale, and the results indicate that further gains could be achieved by additional rearward movement of the nacelle. Obviously, however, airplane balance problems would impose some practical rearward limit to the nacelle relocation. As with the earlier results, noticeable additional gains were made through so-called "tuning" which, in this instance, involved primarily changes in the inboard airfoil shape.

Concluding Remarks

Efforts underway within the Transonic Aerodynamics Branch at NASA-LRC have been directed toward drag reduction in several areas. Primary efforts have been involved with the design of both supercritical and subcritical families of airfoils, the reduction of induced drag through the use of vortex diffusers, and the reduction of interference drag for executive-type aircraft.

The results of many of these efforts are felt to be applicable to the design of general aviation aircraft.

References

1. Whitcomb, R.T., "Review of NASA Supercritical Airfoils," ICAS Paper No. 74-10, The Ninth Congress of the International Council of the Aeronautical Sciences, August 1974.
2. McGhee, R.J., and Beasley, W.D., "Low-Speed Aerodynamic Characteristics of a 17-Percent-Thick Airfoil Section Designed for General Aviation Applications, NASA TN D-7428, 1973.
3. McGhee, R.J., Beasley, W.D., and Somers, D.M., "Low-Speed Aerodynamic Characteristics of a 13-Percent-Thick Airfoil Section Designed for General Aviation Applications, NASA TM X-72697.
4. Flechner, S.G., and Jacobs, P.F., "The Effects of Vortex Diffusers (Winglets) on a Semispan Model of a Representative Wide-Body Transport," Proposed NASA TN D.
5. Bartlett, D.W., "Application of a Supercritical Wing to an Executive-Type Jet Transport Configuration," Proposed NASA TM X. (L-9939).
6. Putnam, L.W., "Exploratory Investigation at Mach Numbers from 0.40 to 0.95 of the Effects of Jets Blown Over a Wing," NASA TN D07367, 1973.
7. Patterson, J.D., and Flechner, S.G., "An Exploratory Wind-Tunnel Investigation of the Wake Effect of a Panel Tip-Mounted Fan-Jet Engine on the Lift-Induced Vortex," NASA TN D-5729, 1970.
8. Bauer, F., Garabedian, P., Korn, D., and Jameson, A., "Supercritical Wing Sections II," Lecture Notes in Economics and Mathematical Systems, Springer-Verlag, c. 1975.

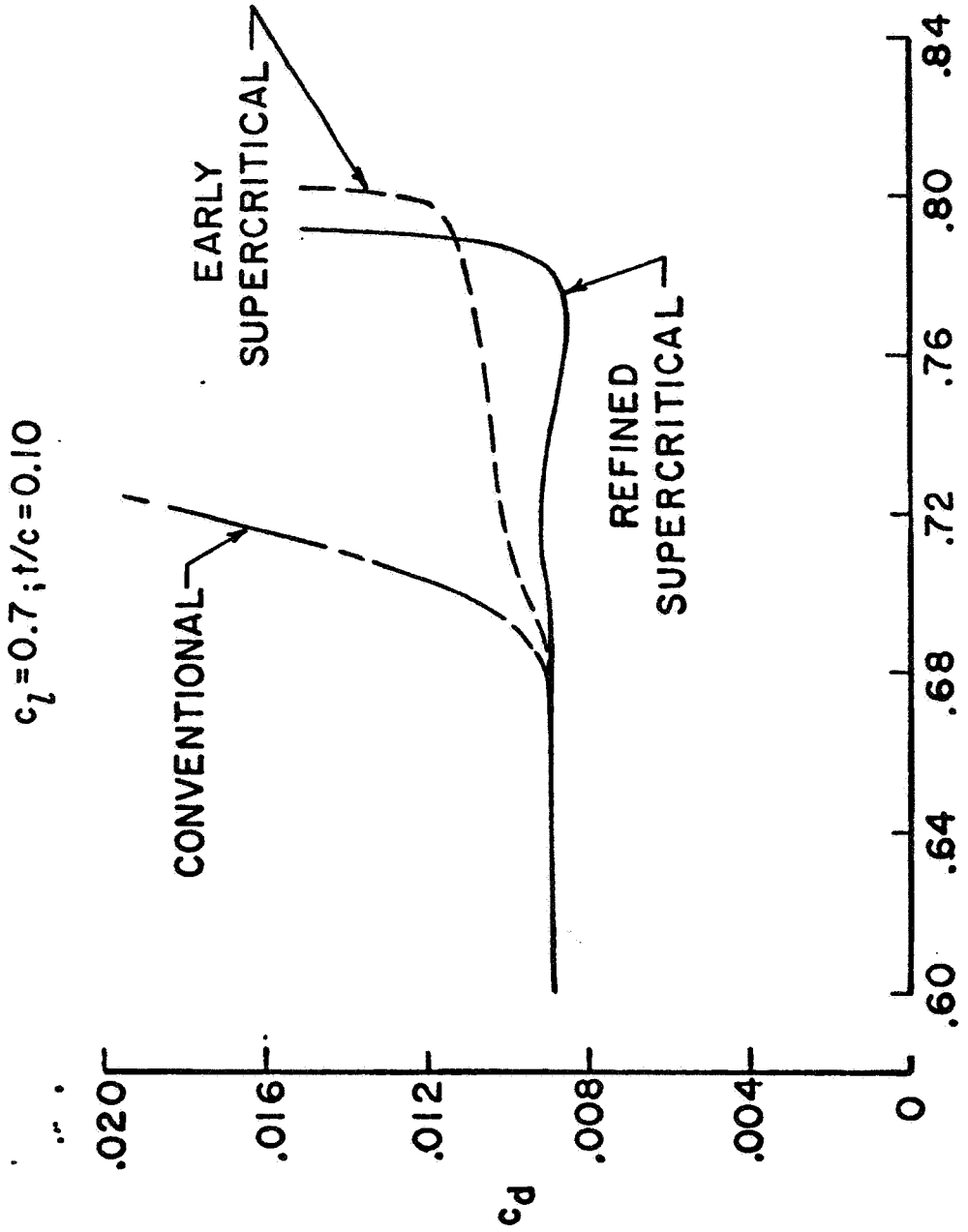

Figure 1. Supercritical Airfoil Improvements

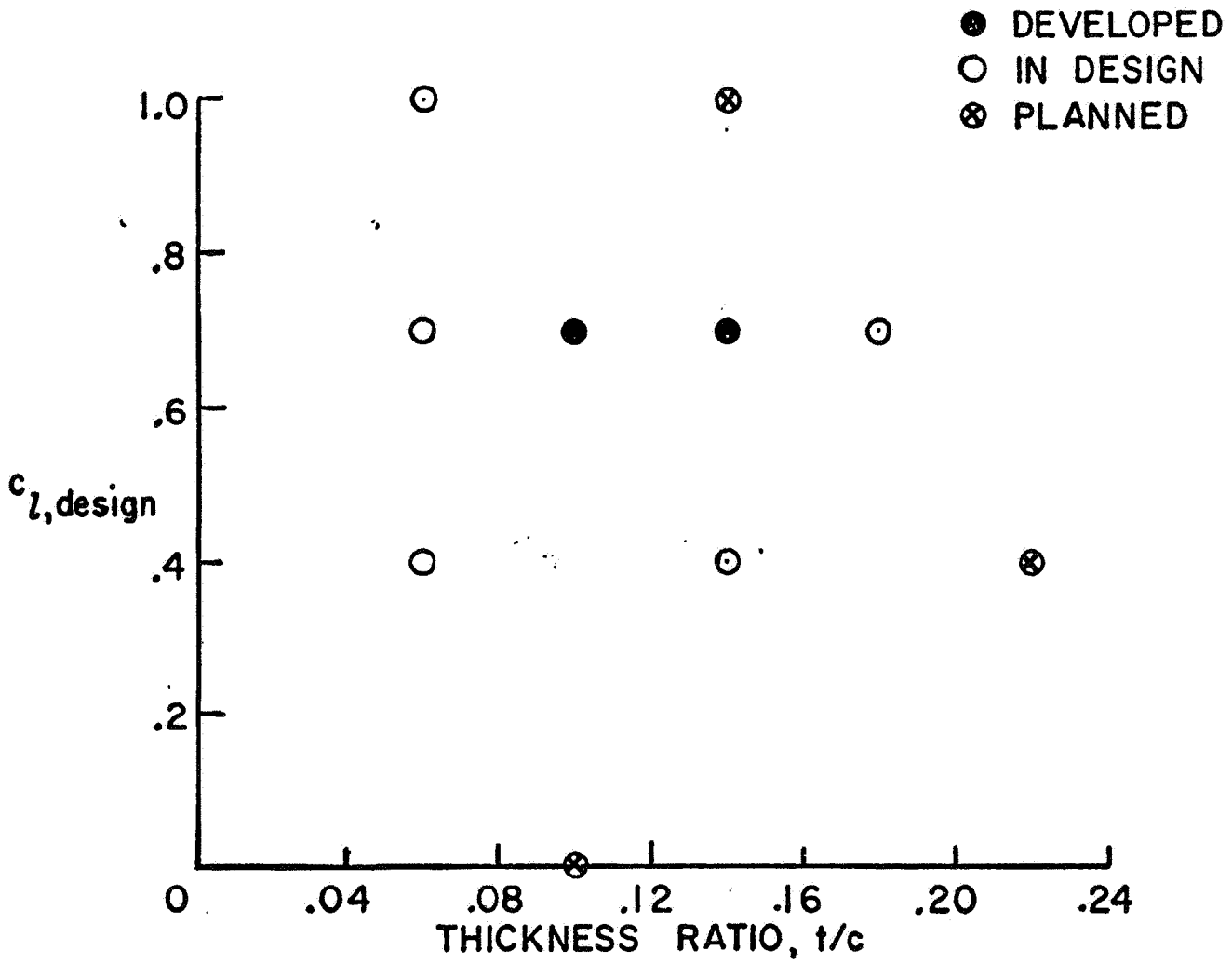

Figure 2. Supercritical Airfoil Family

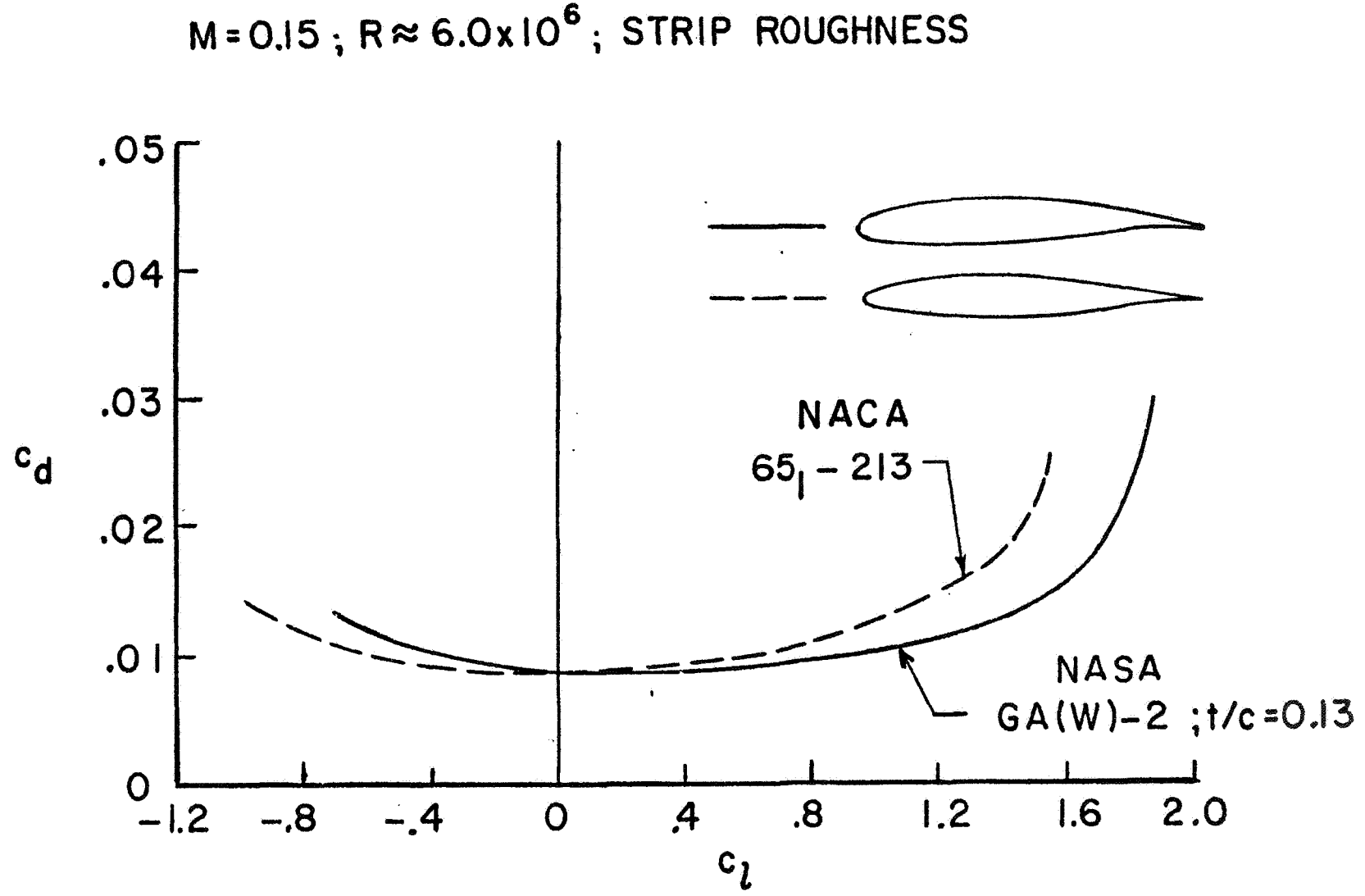

Figure 3. Subcritical Airfoil Improvements

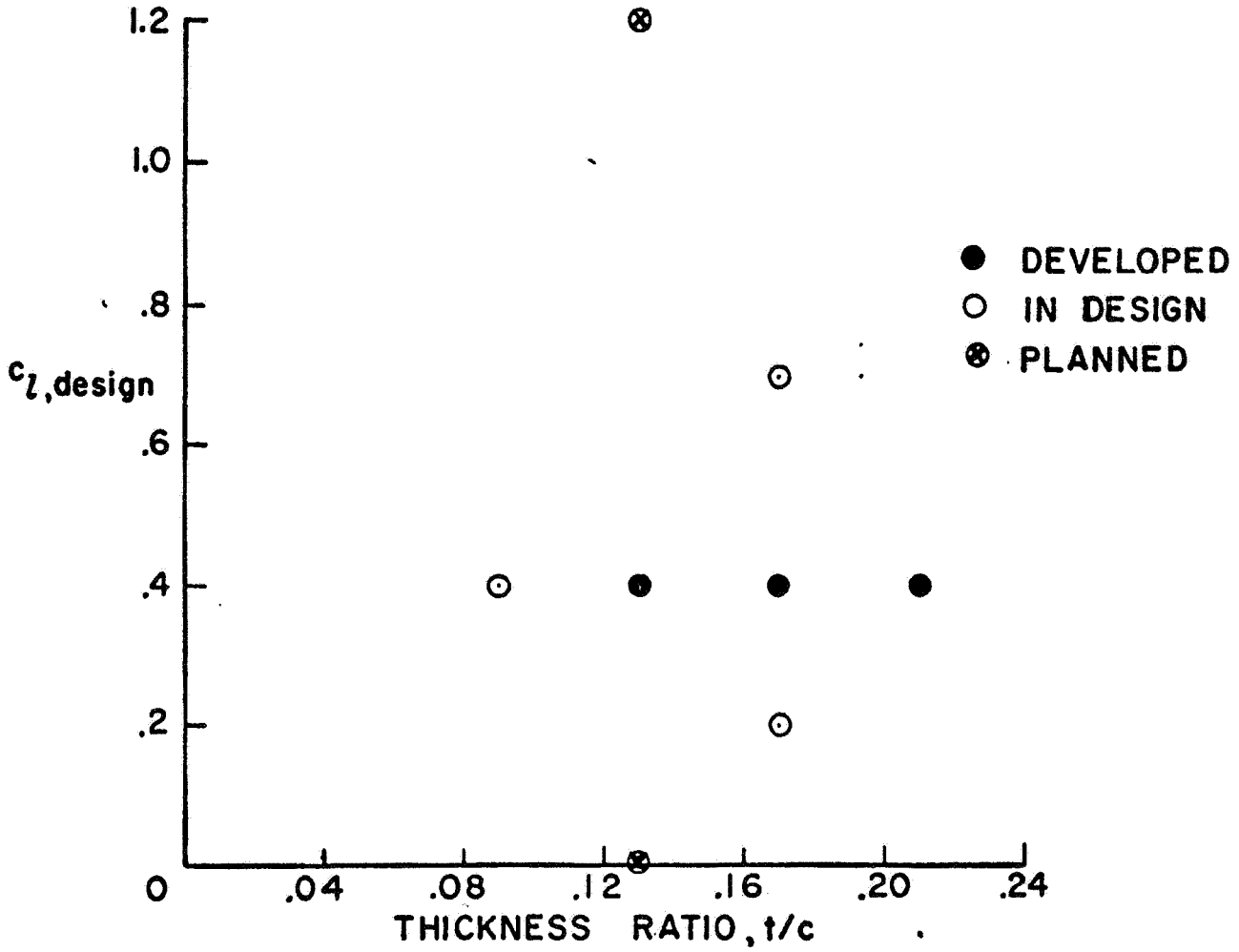

Figure 4. Subcritical Airfoil Family

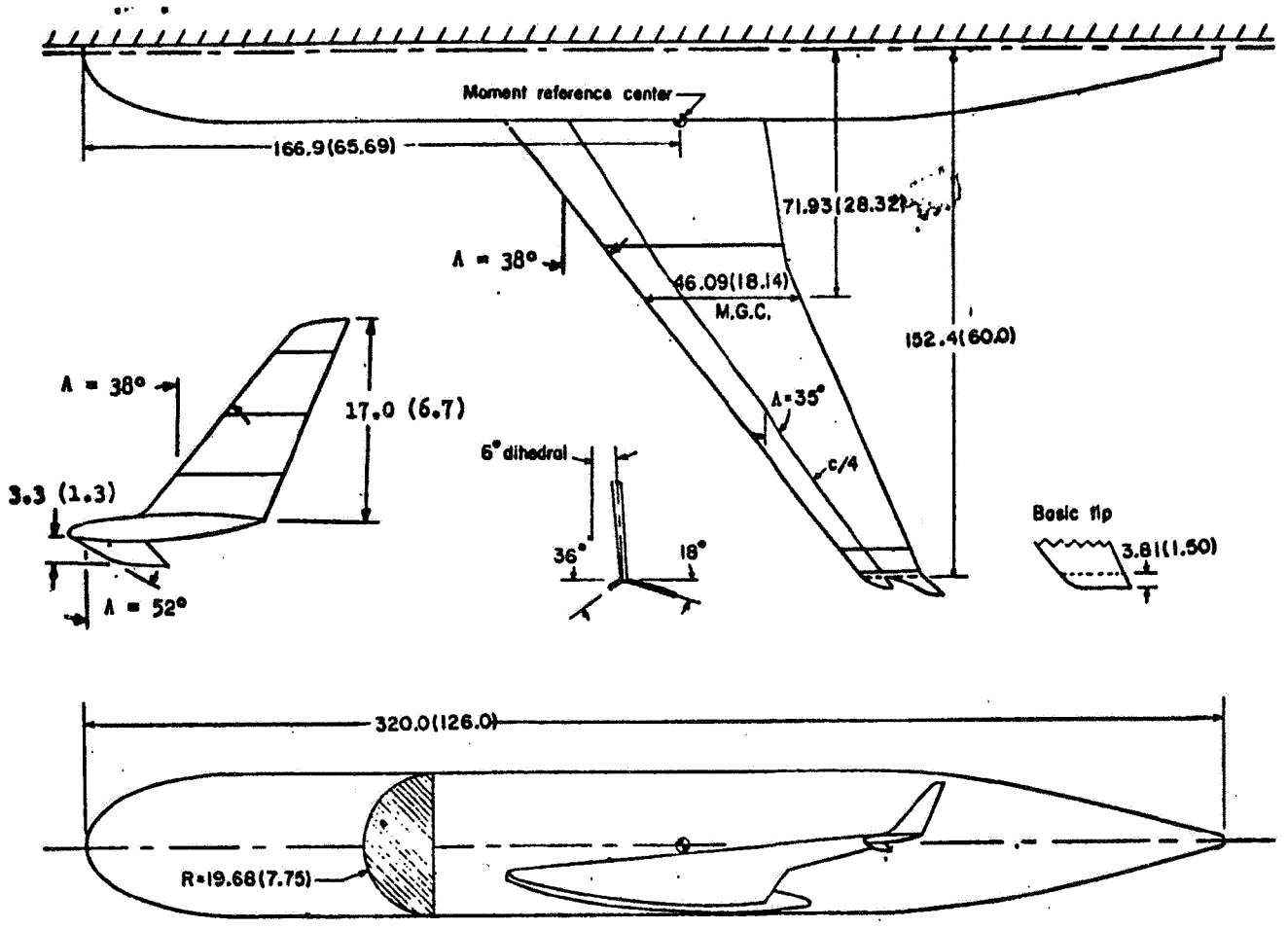

Dimensions in centimeters (inches).

Figure 5. Vortex Diffuser Model

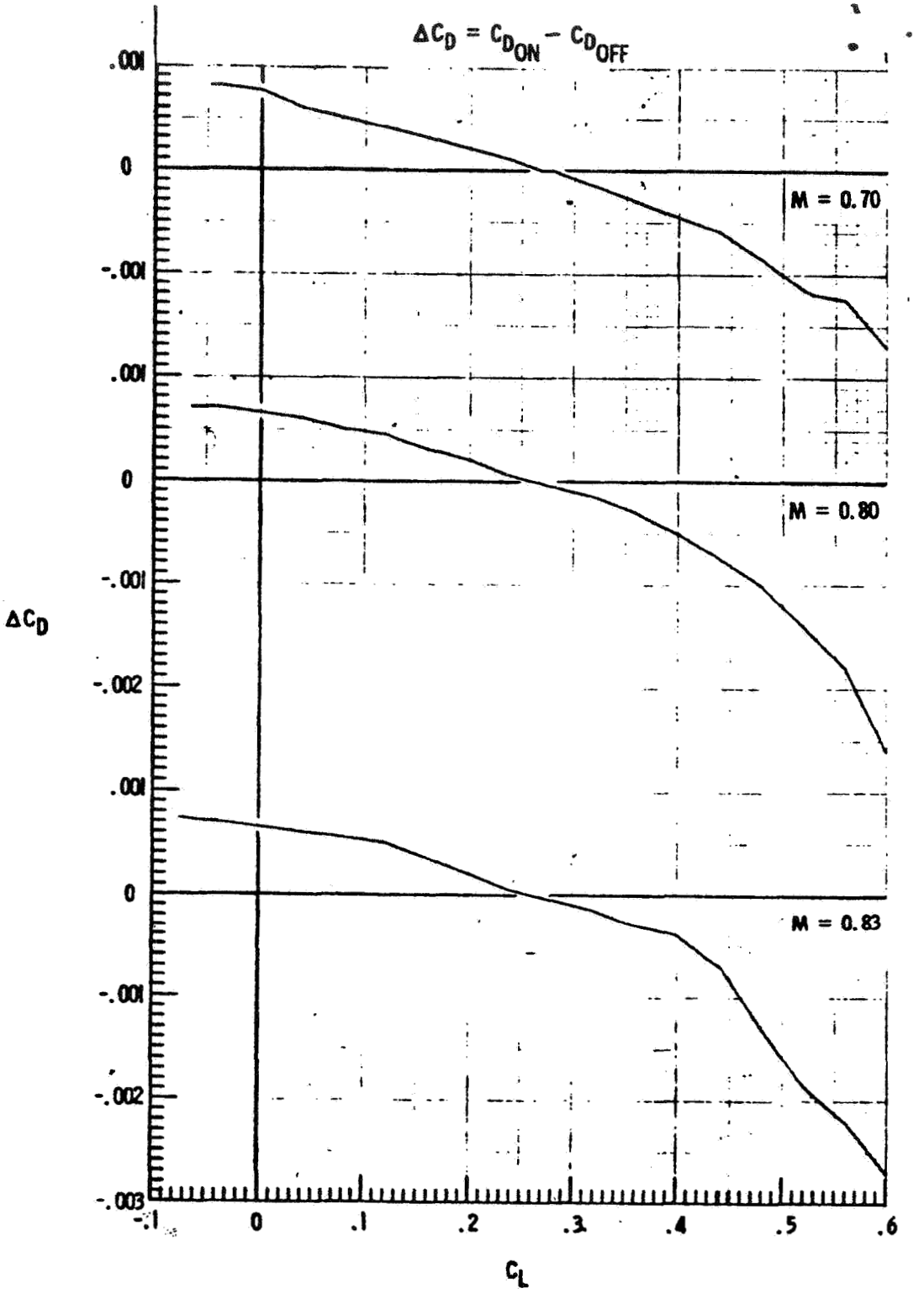

Figure 6. Vortex Diffuser Effects on Drag Coefficient

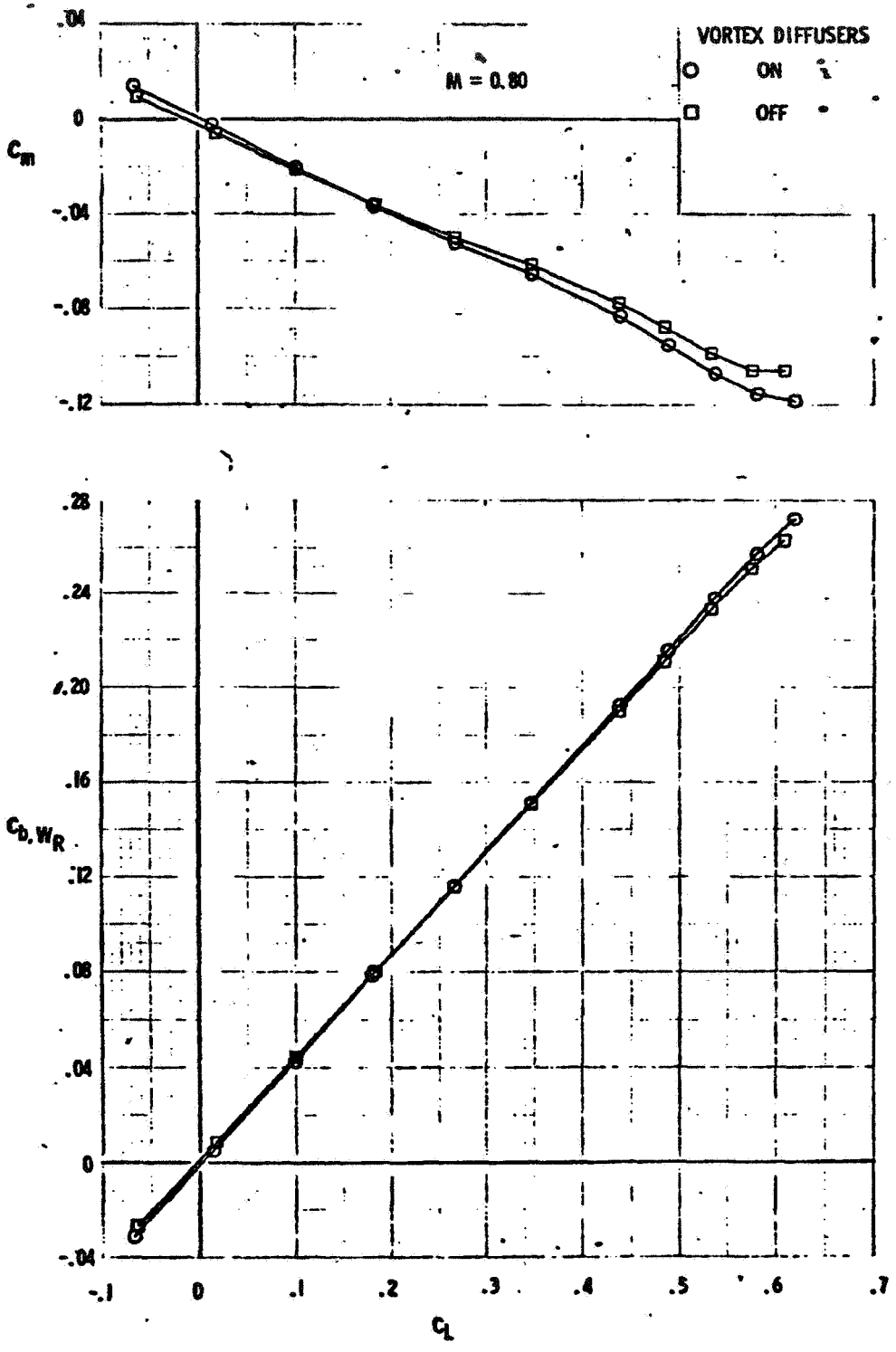

Figure 7. Vortex Diffuser Effects on Pitching-Moment Coefficient and Wing Root Bending-Moment Coefficient

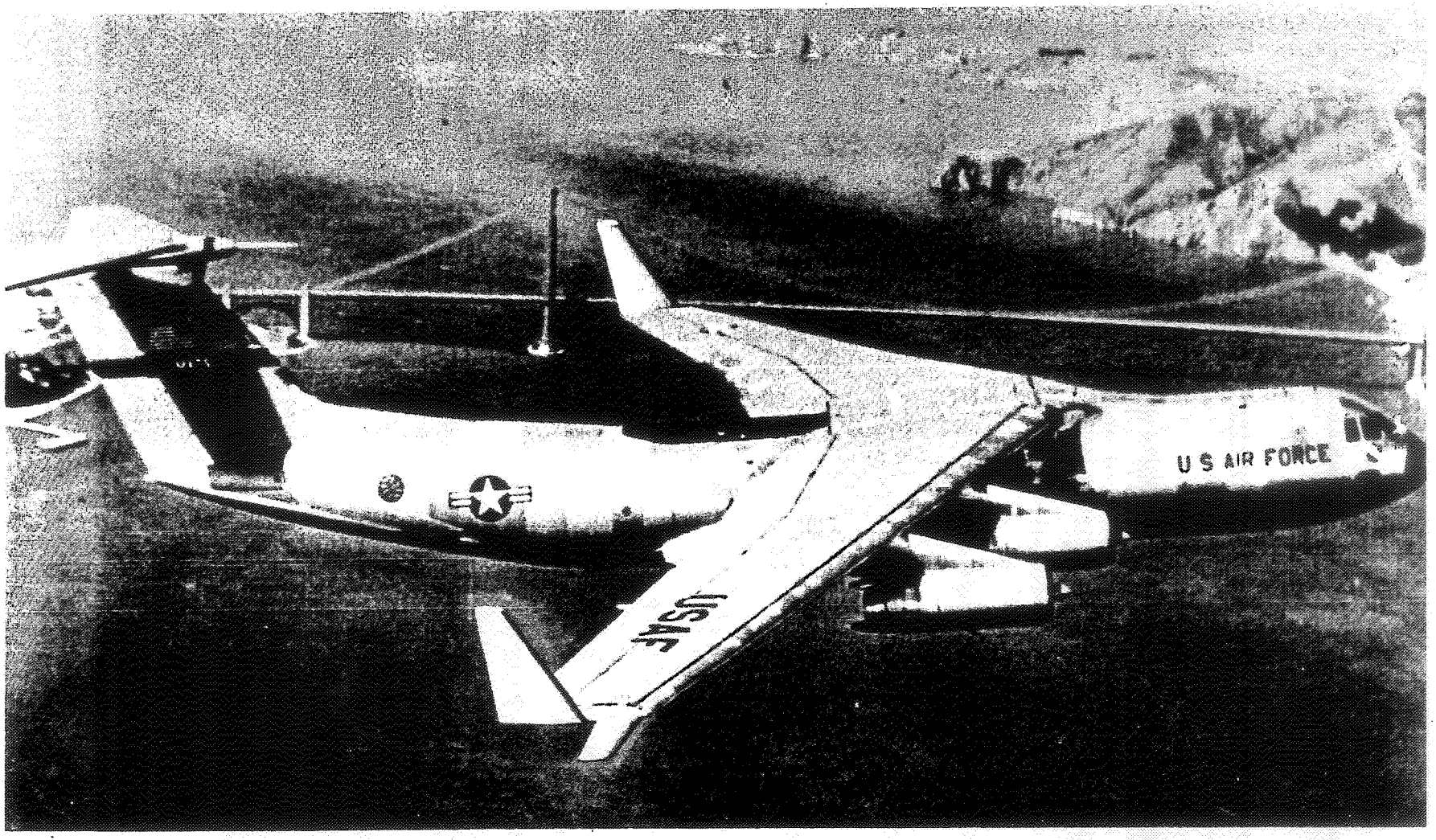

Figure 8. Lockheed C5A with Winglets

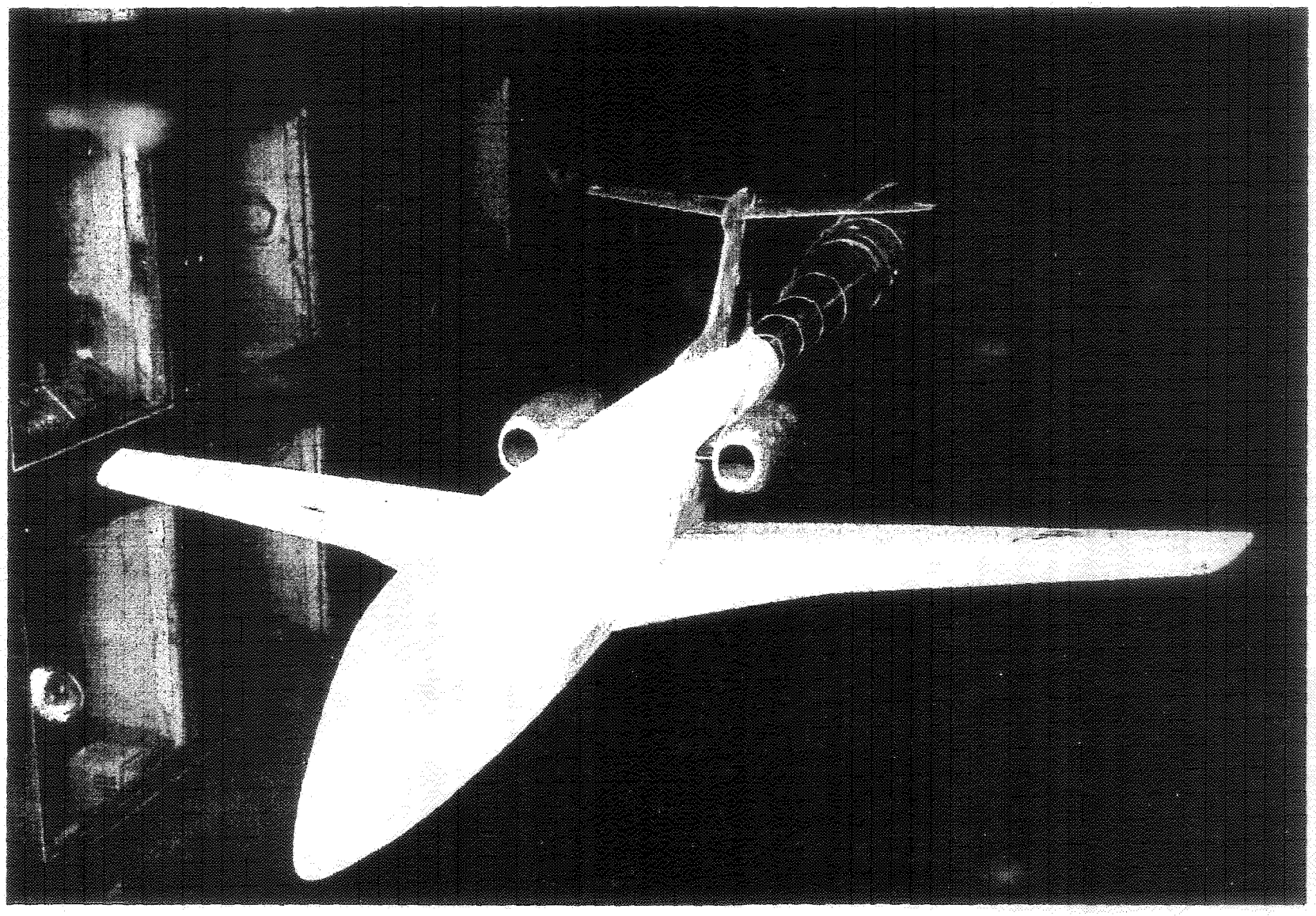

Figure 9. Typical Configuration Illustrating Wing-Nacelle-Fuselage Interference Problem

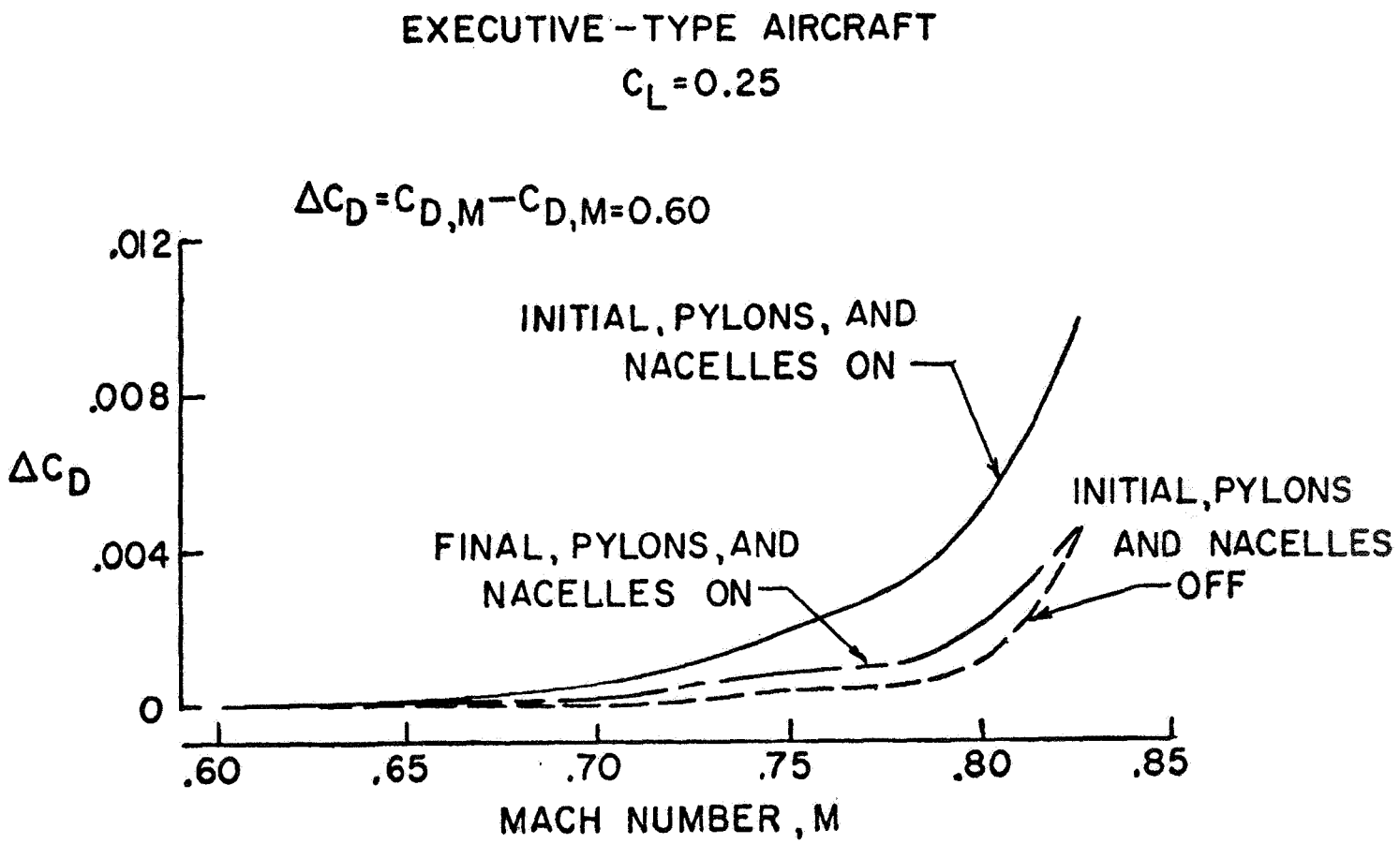

Figure 10. Effects of Wing-Root and Pylon Modifications

$M = 0.825$; $C_L \approx 0.35$

INITIAL CONFIGURATION

NACELLES & PYLONS ON

INITIAL CONFIGURATION

NACELLES & PYLONS OFF

FINAL CONFIGURATION

NACELLES & PYLONS ON

Figure 11. Wing Upper-Surface Oil Flows

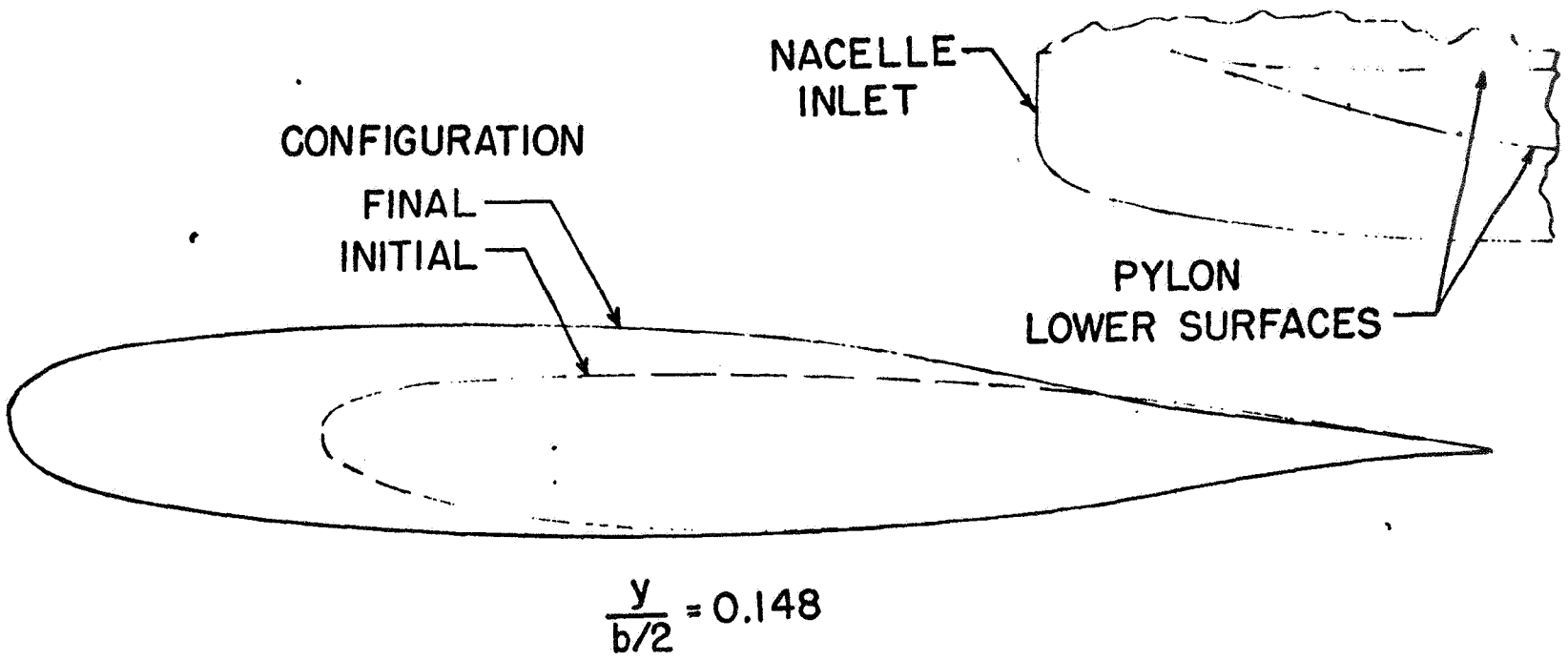

Figure 12. Wing-Root Airfoil and Pylon Modifications

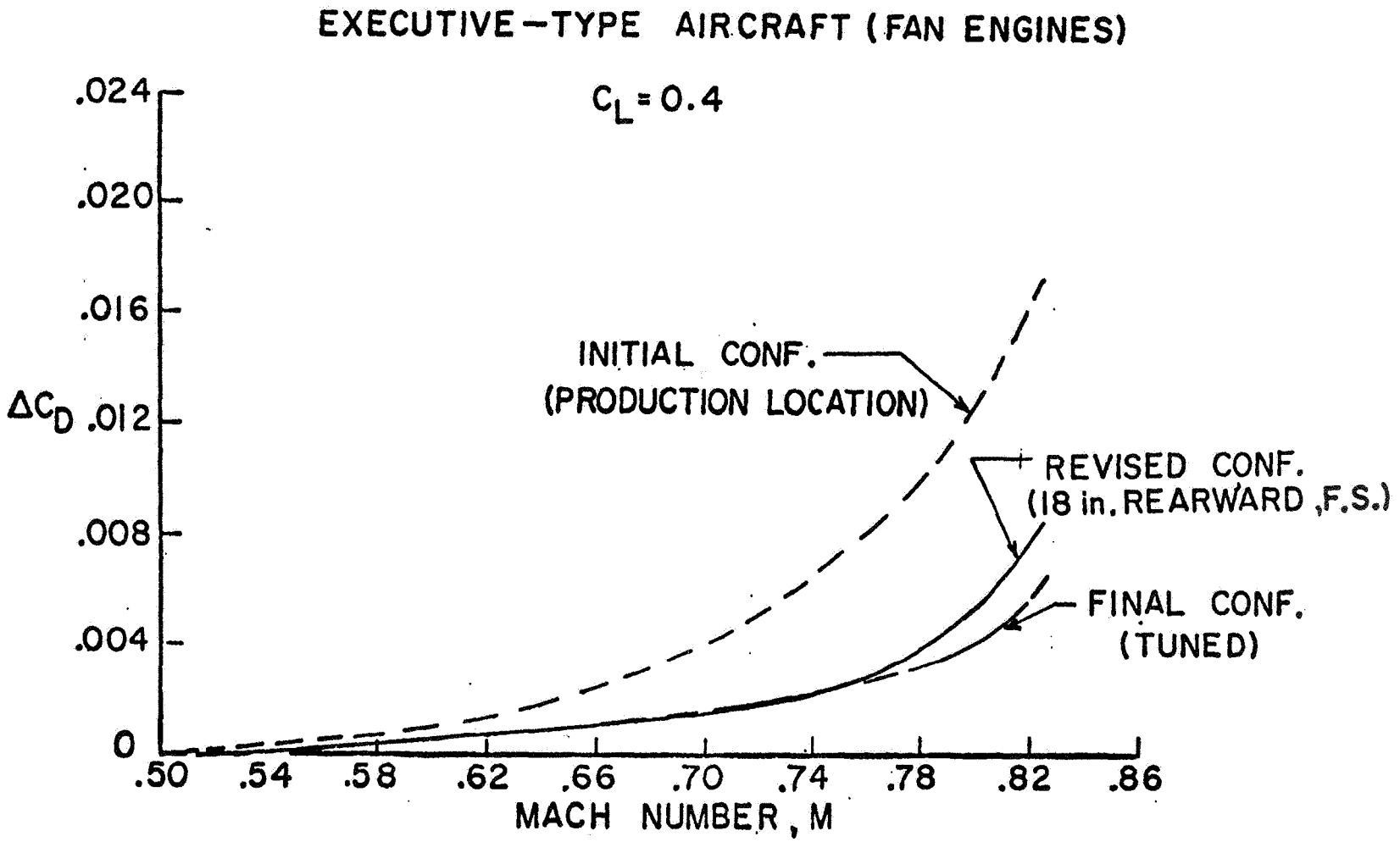

Figure 13. Effect of Engine Nacelle Translation

5.2 Drag Reduction Through Higher Wing Loading

David L. Kohlman
University of Kansas

Introduction

The wing typically accounts for almost half of the wetted area of today's production light airplanes and approximately one-third of the total zero-lift or parasite drag. Thus the wing should be a primary focal point of any attempts to reduce drag of light aircraft with the most obvious configuration change being a reduction in wing area. Other possibilities involve changes in thickness, planform, and airfoil section.

This paper will briefly discuss the effects of reducing wing area of typical light airplanes, constraints involved, and related configuration changes which may be necessary.

Constraints and Benefits

The wing area of current light airplanes is determined primarily by stall speed and/or climb performance requirements. Table I summarizes the resulting wing loading for a representative spectrum of single-engine airplanes. The maximum lift coefficient with full flaps, a constraint on wing size, is also listed. Note that wing loading (at maximum gross weight) ranges between about 10 and 20 psf, with most 4-place models averaging between 13 and 17. Maximum lift coefficient with full flaps ranges from 1.49 to 2.15.

Clearly if $C_{L_{max}}$ can be increased, a corresponding decrease in wing area can be permitted with no change in stall speed. If total drag is not increased at climb speed, the change in wing area will not adversely affect climb performance either and cruise drag will be reduced.

Though not related to drag, it is worthy of comment that the range of wing loading in Table I tends to produce a rather uncomfortable ride in turbulent air, as every light-plane pilot is well aware. The only way to reduce this gust sensitivity is to increase wing loading.

Typically, wing loading tends to increase as performance (cruise speed) increases. This is particularly evident in Table II which presents data for twin-engine aircraft. But gust response is proportional to the ratio of calibrated cruise speed to wing loading $(V_c/(W/S))$ and thus improvements in ride due to higher wing loading are partially, if not completely, offset by higher cruise speed.

It is also evident in Table II that even though wing loading is higher than for single-engine aircraft, it is translated directly into higher stall speeds. Twin-engine high lift systems produce virtually the same $C_{L_{max}}$ as shown in Table I for single-engine airplanes. Thus there appears to be an equal potential for reduction in wing area of single- and twin-engine aircraft by employing improved high lift systems. How to achieve higher $C_{L_{max}}$ for light aircraft is discussed later.

But assuming for a moment that improvements in $C_{L_{max}}$ are available, making higher wing loading possible for a given airplane or class of airplanes, it is important to consider how the wing area should be reduced. The easiest and most tempting way is by reducing span. Not only does this leave the inboard wing structure, mechanisms, and wing-body junction unchanged, but it reduces wing bending moments making possible a lighter wing. But reducing the span increases the span loading, thus reductions in parasite drag through a decrease in wing area are countered by an increase in induced drag.

On the other hand, reducing wing area by a decrease in wing chord decreases parasite drag almost in direct proportion to chord decrease, and if span remains constant there is virtually no change in induced drag. From an aerodynamic point of view this is most desirable, but it introduces possible structural and weight problems because aspect ratio increases while spar thickness and internal volume decrease if the same airfoil section is used.

To understand the potential and the constraints of drag reduction through wing area reduction, consider the following simplified analysis.

Assuming that the parasite drag coefficient and span efficiency factor remain unchanged, the parasite drag is directly proportional to wing area and induced drag is inversely proportional to the square of the span. Then the wing drag at any given flight condition may be written as

$$D_W = D_{P_R} \frac{b\,c}{b_R c_R} + (D_{W_R} - D_{P_R}) \frac{b_R^2}{b^2} \qquad (1)$$

where D_{P_R} is the reference wing profile drag; D_{W_R} is the total drag of the reference wing. The span and chord are denoted as b and c with a subscript R indicating reference values. For simplicity an untapered wing is assumed.
Normalizing equation (1) with respect to the original reference wing drag, D_{W_R}, gives

$$D = \frac{D_W}{D_{W_R}} = P \frac{bc}{b_R c_R} + (1 - P) \frac{b_R^2}{b^2} \qquad (2)$$

where $P = \frac{D_{P_R}}{D_{W_R}}$, the ratio of parasite drag to total drag.

If only the wing chord is reduced, then the change in total normalized wing drag is

$$dD = P \frac{dc}{c_R} \tag{3}$$

Thus the percent reduction in total wing drag is equal to the percent reduction in chord length times the original ratio of parasite to total wing drag. Clearly, the benefits of wing area reduction increase with air speed.

Consider a typical light airplane with the following characteristics:

Gross weight = 2800 pounds

Aspect ratio = 7.4

Wing area = 174 ft^2

Drag coefficient of body and empennage, $C_{D_{o_{BVH}}} = 0.017$

Wing parasite drag coefficient, $C_{D_{o_W}} = 0.009$

Airplane efficiency factor, e = 0.75

Cruise altitude = 8,000 ft

If only the chord is reduced, then, as shown in Reference 1, the resulting normalized total airplane drag, D_T, is shown in Figure 1. Although substantial drag reductions are possible, constraints are imposed by the requirement to cruise at a reasonably low lift coefficient and stall margin, and to keep stall speeds low enough for good takeoff and landing performance. Even with these constraints, however, significant reductions in wing area, cruise drag, and gust response are possible for today's general aviation fleet.

To analyze the effect of reducing span while holding chord constant, differentiate equation (2) with respect to span b. Then

$$dD = \frac{1}{b_R} \left[P - 2 (1 - P) \frac{b_R^3}{b^3} \right] db \tag{4}$$

For a decrease in span to result in a net decrease in drag the condition $\frac{dD}{db} > 0$ for $b = b_R$ must be satisfied.

This is true only if

$$P > \frac{2}{3} \tag{5}$$

In other words, a reduction in drag by reducing span can be achieved only if parasite drag is more than double the induced drag at the flight condition in question. While this may be satisfied during high speed cruise, it is rarely true during a climb. And when $P < 2/3$ a reduction in span increases induced drag more than it decreases parasite drag. For a tapered wing, P must be even larger than the value given in (5) to achieve drag reduction.

The limit to favorable span reduction is found by solving for the value of $\frac{b}{b_R}$ which yields $\frac{dD}{db} = 0$, assuming $P > 2/3$. Again from equation (4) it is easily shown that

$$\frac{dD}{db} = 0$$

when $$\left(\frac{b}{b_R}\right)^3 = \frac{2(1-P)}{P} \qquad (6)$$

Equation (6), plotted in Figure 2, establishes the boundary of favorable span reduction of a constant chord wing as a function of the reference wing parasite drag ratio, P.

Technical Developments

It is clear that wing area reduction can be achieved only if corresponding increases in $C_{L_{max}}$ can be designed into light airplanes in a practical manner. Several recent developments indicate that this is a very real possibility.

One promising development is a new family of general aviation airfoil sections. Two members of the family, the GA(W)-1 and GA(W)-2, have been defined at this time. As shown in Reference 2, the characteristics of these airfoils are:

- high $C_{L_{max}}$ compared to conventional airfoils (see Figure 3)
- gentle stall characteristics
- fairly thick section. The GA(W)-1 is 17% thick. This helps to maintain spar depth with reduced chord lengths.
- very little increase in C_{D_o} at climb lift coefficients (see Figure 4). This combined with decreased wing area offers the potential of significant increase in single-engine climb performance of twins.

Another interesting development is the recognition of the efficiency of spoilers for roll control on light airplanes. Among other features, spoilers permit the use of full-span, or at least increased span, flaps. This will increase $C_{L_{max}}$ with no change in airfoil or flap geometry. Several light airplanes are now using this concept: the advanced technology light twin (ATLIT), a modified Seneca; the Redhawk, a modified

Cessna Cardinal; the RSTOL Seneca, a modification kit developed by Robertson Aircraft Corporation; and the Mitsubishi MU-2 .

Another method of increasing $C_{L_{max}}$ is to increase the Fowler action of conventional single-slotted flaps. This can be done with very little increase in complexity or weight. Figure 5 shows the very large values of $C_{L_{max}}$ (2-D)which can be obtained with a GA(W)-1 airfoil using a 30% chord single-slotted Fowler flap.

Flight Test Results

Additional confirmation of the ability to increase $C_{L_{max}}$ through both airfoil design and flap design has been demonstrated in the Redhawk and ATLIT programs.

Table III, from Reference 3, shows maximum lift coefficients obtained on the Redhawk by using a 30% chord single-slotted Fowler flap. Note that the flap covers only 47% of the wing span.

The ATLIT, using full-span, 30% chord single-slotted flaps, and a GA(W)-1 basic airfoil, generated the high lift data shown in Table IV. Clearly, significant increases in $C_{L_{max}}$ are possible for this class of airplane.

Finally, Table V shows drag data generated during flight test of the Redhawk. The most significant result is that parasite drag was reduced 10.5% by reducing wing area, thickness, and span. This is a significant reduction, and it illustrates in flight that a reduction in wing area can be an effective and practical means of reducing drag.

References

1. Roskam, Jan, "Opportunities for Progress in General Aviation Technology," AIAA Paper No. 75-292, presented at AIAA 11th Annual Meeting and Technical Display, Washington, D. C., February 24-26, 1975.
2. McGhee, R. J., and Beasley, W. D., "Low Speed Aerodynamic Characteristics of a 17-Percent-Thick Airfoil Section Designed for General Aviation Applications," NASA TN D-7428, December 1973.
3. Kohlman, David L., "Flight Test Results for an Advanced Technology Light Airplane Wing," SAE Paper No. 740368, presented at Business Aircraft Meeting, Wichita, Kansas, April 2-5, 1974.

Table I. Wing Loading and $C_{L_{max}}$ for Typical Single-Engine Aircraft

Aircraft	W/S - PSF	$C_{L_{max}}$
Cessna 150	10.2	1.73
Cessna 172	13.2	2.15
Cessna 182	16.9	2.03
Cessna 210	21.7	2.01
Beech C23	16.8	1.89
Beech V35B	18.8	1.85
Grumman Tiger	17.1	1.92
Bellanca 300A	20.6	1.64
Mooney M20E	15.4	1.85
Piper PA-28-140	13.4	1.73
Piper PA-28-180	14.4	1.51
Piper PA-28-200R	15.6	1.49
Piper PA-32	19.5	1.92

Table II. Wing Loading and $C_{L_{max}}$ for Typical Twin-Engine Aircraft

Aircraft	W/S - PSF	$C_{L_{max}}$
Beech Baron	25.6	1.42
Beech Duke	31.8	1.64
Beech Queen Air	29.9	1.78
Cessna 310	30.7	2.02
Cessna 402	32.2	2.02
Cessna 421	35.2	1.86
Piper Seneca II	21.9	1.80
Piper Navaho PA-31-350	30.6	1.66
Piper Navaho PA-31P-425	34.1	1.93

Table III. Comparison of Stall Speeds and Maximum Lift Coefficients

Configuration	Redhawk		Cardinal	
	V_s, mph	$C_{L_{max}}$	V_s, mph	$C_{L_{max}}$
Cruise	79.6	1.40	64.7	1.35
Kruger flaps only	69.8	1.82	-	
Fowler flaps 10°	71.2	1.75	-	
Fowler flaps 10° and Kruger flaps	62.8	2.25	-	
Fowler flaps 40° (30° for Cardinal)	64.4	2.14	55.0	1.84
Fowler flaps 40° and Kruger flaps	56.0	2.83	-	

Notes:
1. Gross weight = 2500 lb
2. Redhawk c.g. location 7.2% m.a.c. (109 in.)
3. Cardinal c.g. location 19% m.a.c. (109.3 in.)

Table IV. ATLIT Preliminary Stall Data

f	V_{S_o} ~MPH	$C_{L_{max}}$
0	76	1.81
10°	66	2.40
20°	61.5	2.77
30°	59.3	2.98
40°	59.4	2.97

Gross weight = 4200 lb
Aft c.g. location

Table V. Comparison of Drag Characteristics Determined from Flight Test

		C_{D_p}	$C_{D_p} S_w$
Cardinal	Cruise	0.0267	4.67
	Full Flaps	0.0462	8.08
Redhawk	Cruise	0.0380	4.18
	Full Fowler and Kruger Flaps	0.0788	8.67

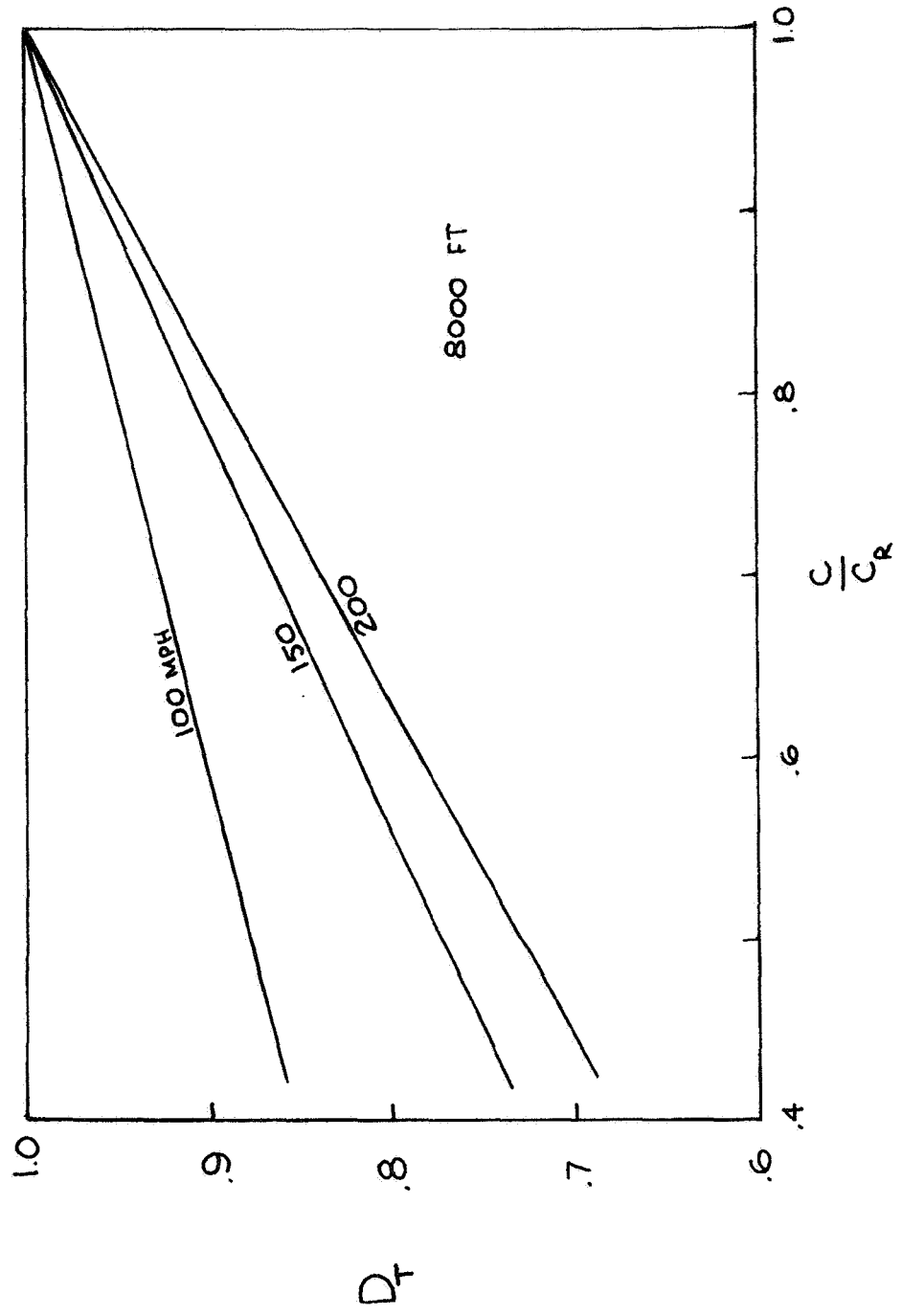

Figure 1. Effect of wing chord reduction on total drag of a typical single-engine light aircraft.

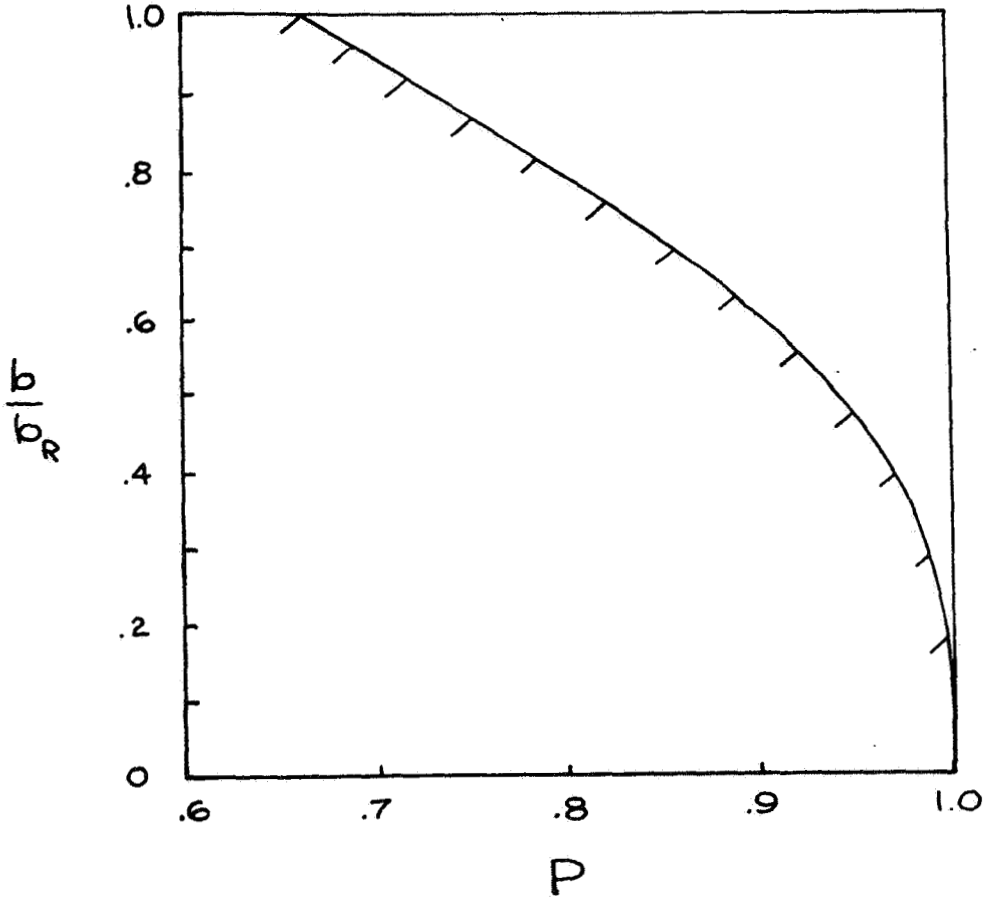

Figure 2. Limit of span reduction to decrease drag as a function of parasite drag ratio.

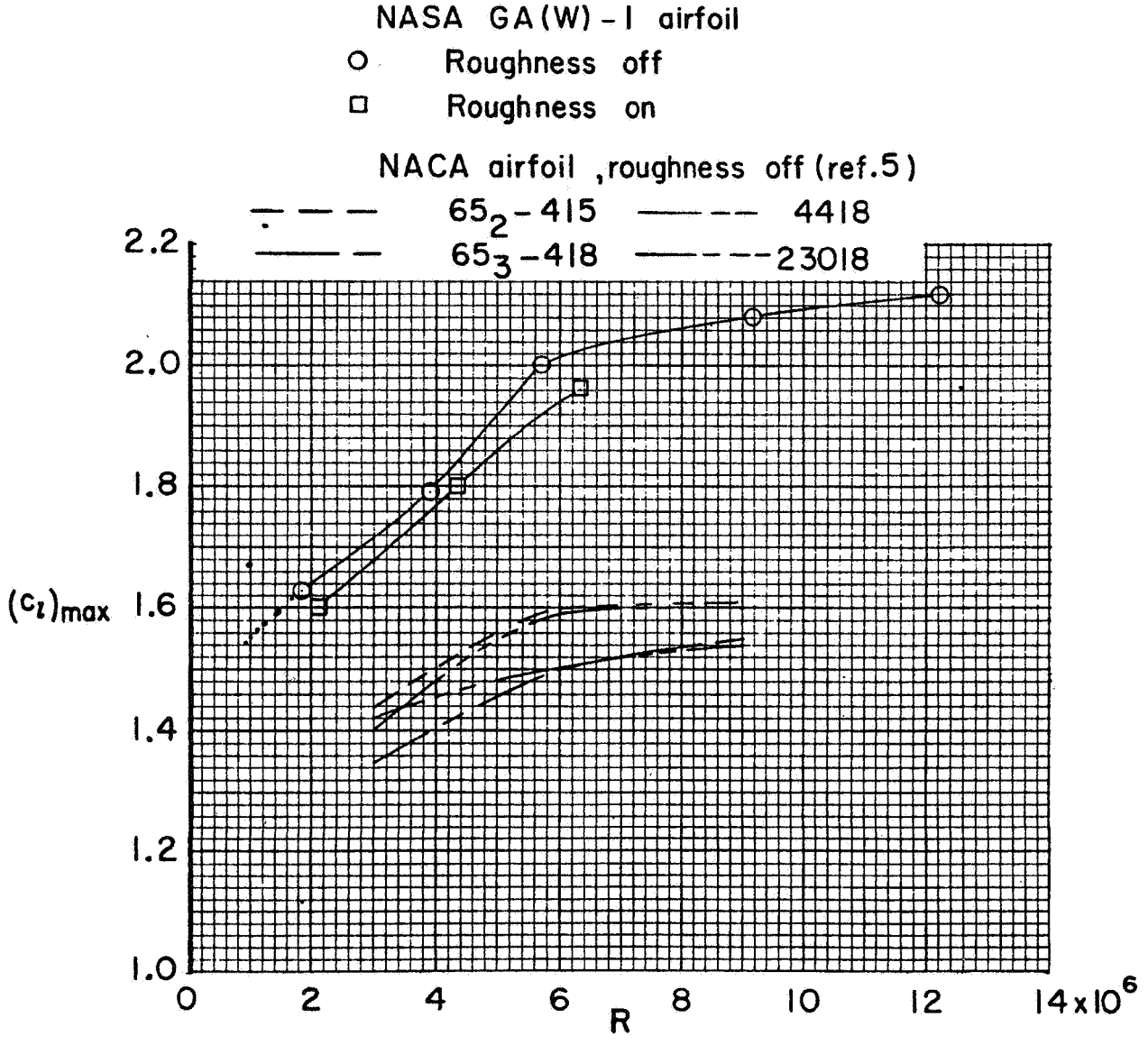

Figure 3. Variation of maximum section lift coefficeint with Reynolds number for various airfoils without flaps. M = 0.15.

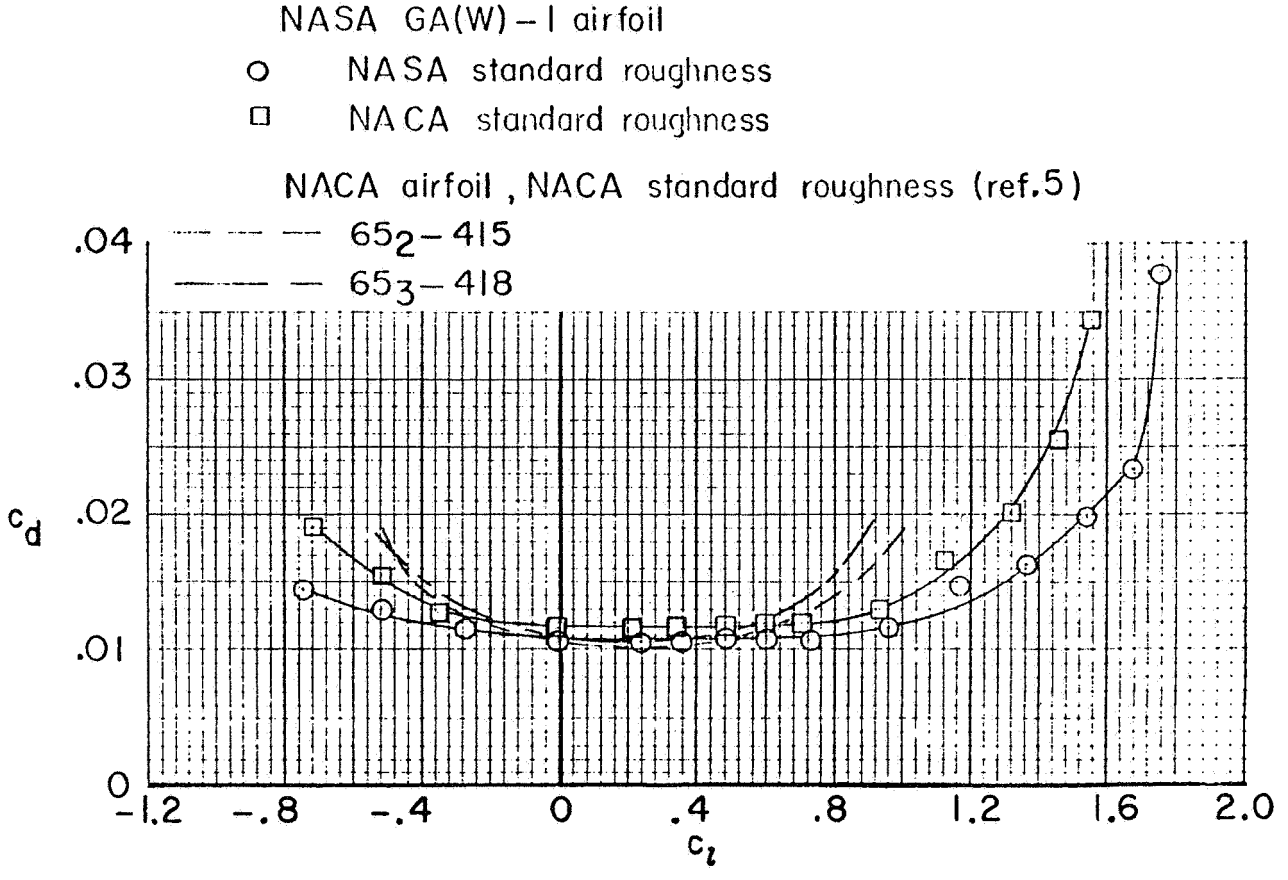

Figure 4. Comparison of section drag characteristics of NASA GA(W)-1 airfoil and NACA 65_2-415 and 65_3-418 airfoils. M = 0.20; R = 6×10^6.

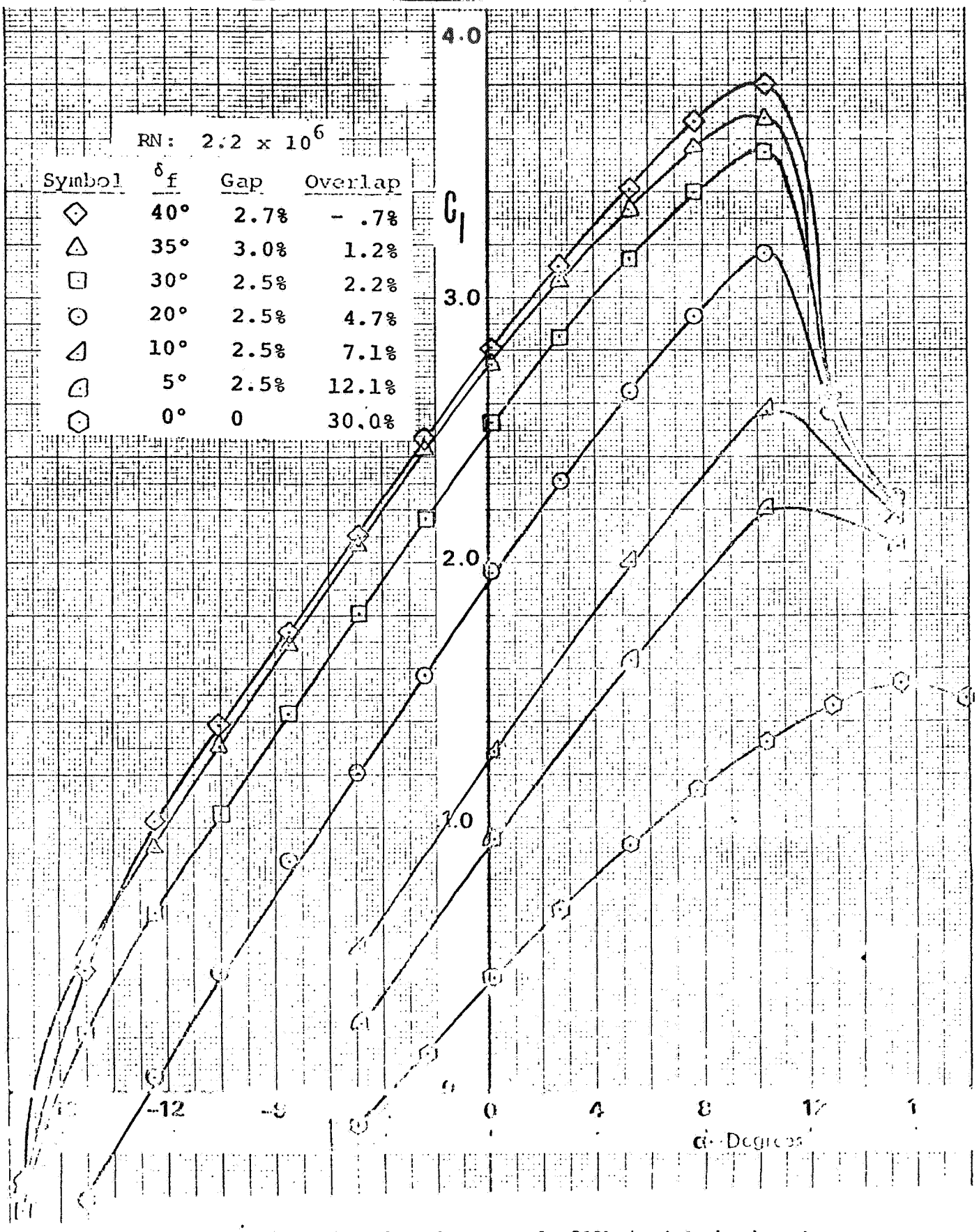

Figure 5. Lift performance of a 30% chord single-slotted Fowler flap on a GA(W)-1 airfoil.

5.3 Use of a Pitot Probe for Determining Wing Section Drag in Flight

Edwin J. Saltzman
NASA Flight Research Center

(A status report of development work of Lawrence C. Montoya and Paul F. Bikle)

Introduction

This paper presents the status of recently completed development work on the wake traverse method of obtaining section drag at low speeds. The method of B. M. Jones, Reference 1, has been applied to wake profile data obtained from the wing of a sailplane.

Though the sailplane provides a quiet and relatively vibration free environment, and a very clean and smooth high aspect ratio wing, it is limited to a dynamic pressure range from about 6 psf to somewhat above 20 psf. These low dynamic pressures are a severe challenge for the wake traverse method.

This paper is intended not only to rekindle interest in the wake traverse approach of defining profile drag, but it is also intended to demonstrate techniques for increasing reliability and minimizing certain bias errors when dealing with relatively low differential pressures. The thought which accompanies this paper is that if acceptable accuracy in section drag can be obtained at these low dynamic pressures, even better profile drag definition could perhaps be obtained for applications on general aviation aircraft where higher pressures would prevail.

Airplane and Test Conditions

The sailplane was a T-6 having a modified Wortmann FX-61-163 airfoil. The modification consisted of a straightening of the underside cusp region at the rear portion of the section. A sketch of the wing profile is shown in Figure 1.

The surface finish of the wing was very smooth and the maximum waviness was about 0.003 inches in a two-inch section of surface. At the semispan station of the wake traverse tests the waviness was less than this.

The wake measurements were made 9.6 inches behind the wing trailing edge which corresponds to about 32 percent of the 29.9 inch local chord. Data were obtained for speeds from about 40 knots to 125 knots which provided chord Reynolds numbers between 10^6 and 3×10^6.

Indicated airspeed was held constant during each data run and six "total-pressure" wake traverses were made during each run followed by three "static-pressure" wake traverses. This sequence of nine traverses took approximately one minute. Data been obtained for deflected flap conditions but the data to be shown herein are for zero flap deflection. The majority of the data were obtained for very smooth air conditions but some data were obtained for air that would be considered somewhat rough.

A photograph of the sailplane with the wake traverse probe installed is shown in Figure 2. A Kiel probe can be seen mounted ahead of the drive unit package on the right wing. The dark colored tape running parallel to the wing trailing edge covers and holds down the wiring harness which connects the drive unit package to the recording package inside the fuselage.

Instrumentation

Probe and Drive Unit: A closer view of the probe and drive unit, and some of the reference probes, is provided in Figure 3. The Kiel tube is used as the reference for the transversing total pressure probe and the trailing boom provides a static reference for the traversing static pressure probe. The trailing boom orifices are located about 5 feet behind the wing and are calibrated against the ships static system, which is in turn a system which has been calibrated for position error.

The traversing probe (with total and static heads) and drive unit are shown again in Figure 4(a) and in closer detail in Figure 4(b) where some of the parts have been labeled. The probe traversed to about 8 inches above and below the wing trailing edge. The probe travel rate was a little less than 3 inches per second. The hardware which is shown in Figure 4 weighed about 3 pounds.

A very important part of the unit was the switching valve which permitted the same pressure transducer to measure the wake station total pressure decrement, in one mode, and the difference between wake static and trailing boom static pressure, when in another mode. More detail will be provided about this feature in following figures.

Recorder Package: The recording package consisted of a tape recorder, battery and a component box which housed a pressure transducer and two amplifiers. This package was mounted on a shelf behind the pilot's head rest as can be seen in Figure 5. A closer view of this hardware is shown in Figure 6, after a covering hatch has been removed. The weight of this package is about 40 pounds. The switch shown in Figure 6 is also an important element in obtaining in-flight tare readings on the transducer which records "ships q."

Switching Features: Figure 7 will be used to show schematically how the switching feature mentioned in the previous section works. As sketched in Figure 7, the switch is in the "zeroing mode." When the pilot places the switch in this mode, freestream total pressure exists on each side of the pressure transducer element, thus providing an in-flight tare reading which minimizes the bias error of this transducer. When the switch is placed in the "q mode" (toggle to the left) there is freestream total pressure on one side of the transducer and ships static on the other side. This, of course, provides a record of "ships q." Because the ships static system has been calibrated for position error the appropriate corrections are applied and a true freestream dynamic pressure can be calculated as a function of time for correlation with the pressures recorded in the wake and the probe position in the wake. The airspeed indicator allows the pilot to hold "ships q" steady for a sufficient period of time to permit up to nine successive wake traverses to be made under quasi-steady state conditions.

Another switching feature involves the switching valve which was identified in Figure 4(b). In Figure 8, a slide valve is shown in schematic form to illustrate how this switching valve can be used to direct Kiel tube pressure (freestream total) to one side of the transducer and wake total pressure to the other side. Thus the transducer senses the total pressure defect, ΔP_T, in the wake. When the wake probe moves beyond the wake, the transducer experiences freestream total pressure on both sides of the sensing element which thereby provides inflight tare readings for the transducer. This feature minimizes the bias error for this transducer.

Another mode for this switching valve is illustrated in Figure 9. In this case the valve arrangement provides trailing boom static pressure to one side of the sensing element and wake station static pressure on the other side. As mentioned before, the trailing boom static pressure has been calibrated against the ships static system which in turn has been calibrated for position error. Therefore the true decrement between wake station static pressure and freestream static can be calculated. It is this corrected decrement, ΔP, which appears as an adjustment in the Jones expression for calculating section drag from wake measurements. The Jones equation follows:

$$C_d = \frac{2}{c} \int \sqrt{\frac{q \text{ wake}}{q}} \left(1 - \sqrt{\frac{q \text{ wake} + \Delta P}{q}} \right) dy$$

where

q, freestream dynamic pressure, from ships transducer plus position error correction

$\Delta P_{T_{wake}}$, total pressure decrement in wake, from probe transducer

ΔP , difference between freestream and wake static pressure, from probe transducer

dy, from probe position potentiometer

c, wing chord at wake survey location

$q_{wake} + \Delta P$, from $q - \Delta P_{T_{wake}}$

q_{wake} , from $(q_{wake} + \Delta P) - \Delta P$

or $(q - \Delta P_{T_{wake}}) - \Delta P$

It is important that the same transducer, through the switching valve feature just described, provides both $\Delta P_{T_{wake}}$, and ΔP because thereby the parameter ΔP has bias error minimization in the same way as has been described for the $\Delta P_{T_{wake}}$ measurement.

It is also important to note that six $\Delta P_{T_{wake}}$ traverses and three ΔP traverses are made in succession while indicated airspeed, and consequently q, is held constant. Section drag coefficients to be presented in a following section are the average of six such traverses for each Reynolds number condition.

Results

Profiles of $\Delta P_{T_{wake}}$ plotted as a function of distance above and below the wing trailing edge plane are presented in Figure 10. These are obtained from six consecutive traverses through the wake over a period of about 40 seconds. The airspeed was about 44 knots which resulted in a section lift coefficient of about 1.0. Note the low "delta pressures" with which the instrumentation must contend at these speeds. Some part of the apparent dispersion of the six profiles is random scatter; however, a part of it is caused by small changes in airspeed during the 40 seconds of run time. Therefore, a part of the apparent dispersion will be eliminated when each profile is normalized by the appropriate mean q for that traverse. As mentioned before, the six normalized profiles are then averaged when calculating section drag coefficients by Jones' equation.

Another set of profiles is shown in Figure 11 for an airspeed of about 42 knots which provided a lift coefficient near maximum. In this case only, four profiles are

shown. The profile with triangular symbols is the first of the sequence and is similar in appearance to those shown in Figure 10. The following profiles in their order of occurrence (diamonds and squares) progress toward local stall (circles) as speed was reduced ever so slightly. Earlier flying with flow visualization indicated that this region of the wing was indeed stalling at these speeds.

Section drag coefficients plotted as a function of chord Reynolds number are shown in Figure 12. Also shown are curves from Blasius and Schlichting representing fully laminar and turbulent flow over the upper and lower surfaces as if they were flat plates.

The circles represent three flights (each point is the average of 6 traverses) for natural transition. The wing surface was exceptionally smooth and clean for these runs.

The squares represent flight with the boundary layer tripped 5 percent behind the leading edge for both the upper and lower surfaces. The trip material was distributed grit of 0.035 inches mean height above the skin surface.

The results obtained to date have been encouraging and suggest several possibilities which may deserve to be included in follow-on flights. Some of these possibilities are listed below:

(a) 400 grit sanding of the local surfaces
(b) 200 grit sanding of the local surfaces
(c) add waves, up to 0.008" per 2 inches
(d) restore to best finish (fill, sand, rub)
(e) tape over flap gap
(f) insect roughness (bugs) on leading edges
(g) install wake traverse unit on several general aviation aircraft.

Closing Remarks

The experience reported has provided progressively improving accuracy in defining section drag for flight at low dynamic pressures. The accuracy is about 3 to 4 percent for the lower dynamic pressures and somewhat better than 3 percent at the higher dynamic pressures. It should be emphasized, however, that such accuracies were obtainable only by resorting to the detailed procedures described herein (especially the in-flight switching and tare evaluations) and by conducting all phases of the testing with the utmost care. Also of great importance was the precise position error calibration which had been accomplished on the ships airspeed-altitude system prior to the wake traverse work.

It is believed that with proper care and attention to detail, comparable or perhaps even more accurate section drag coefficients could be obtained on general aviation aircraft, considering the higher dynamic pressures encountered in general aviation.

References

Reference 1. Jones, B. M., Measurement of Profile Drag by the Pitot-Traverse Method, Cambridge University Aeronautics Laboratory, Rand M. No. 1688, 1936.

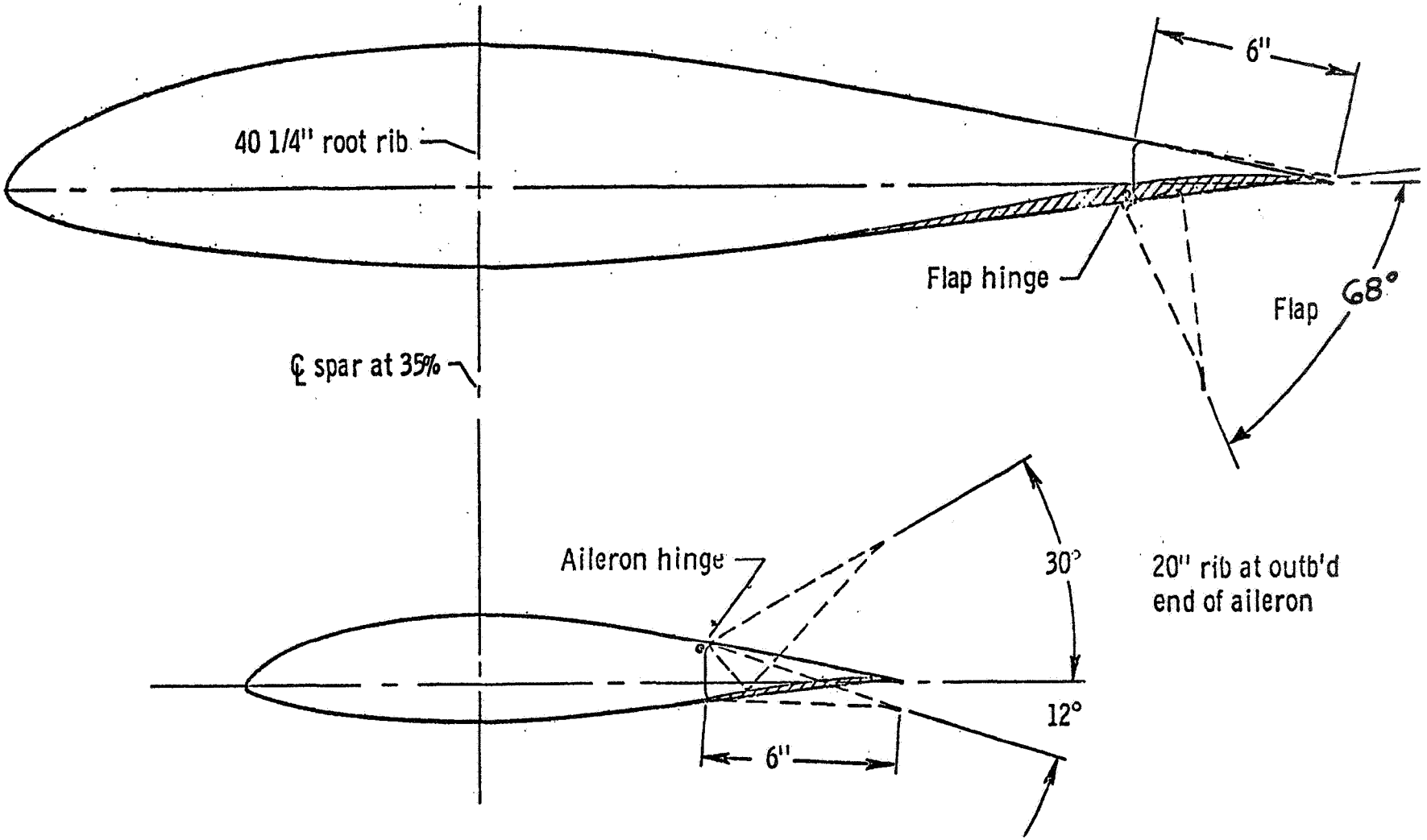

Figure 1. Example of Wortman FX-61-163 Airfoil

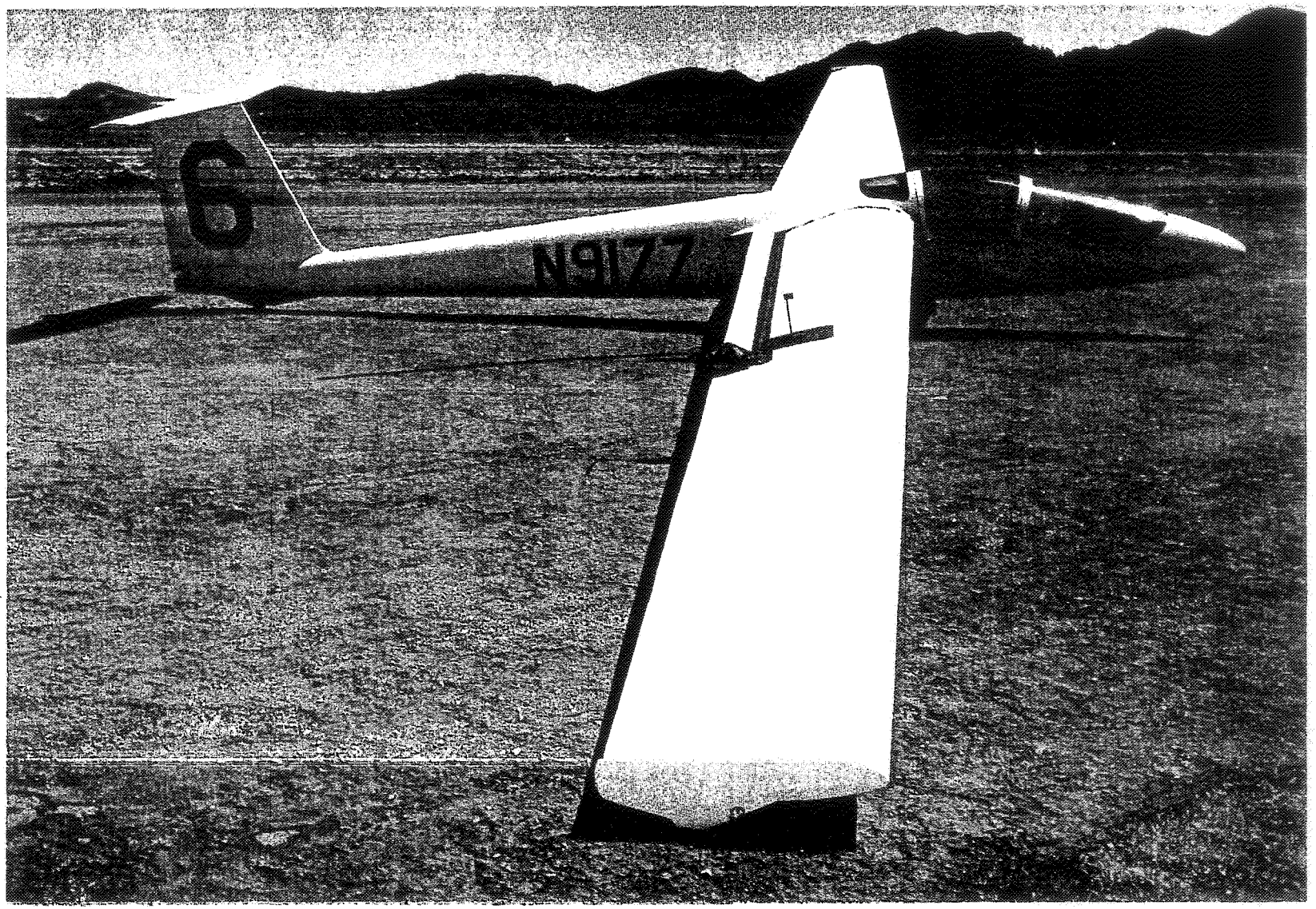

Figure 2. Example of Wake Traverse Probe Installation

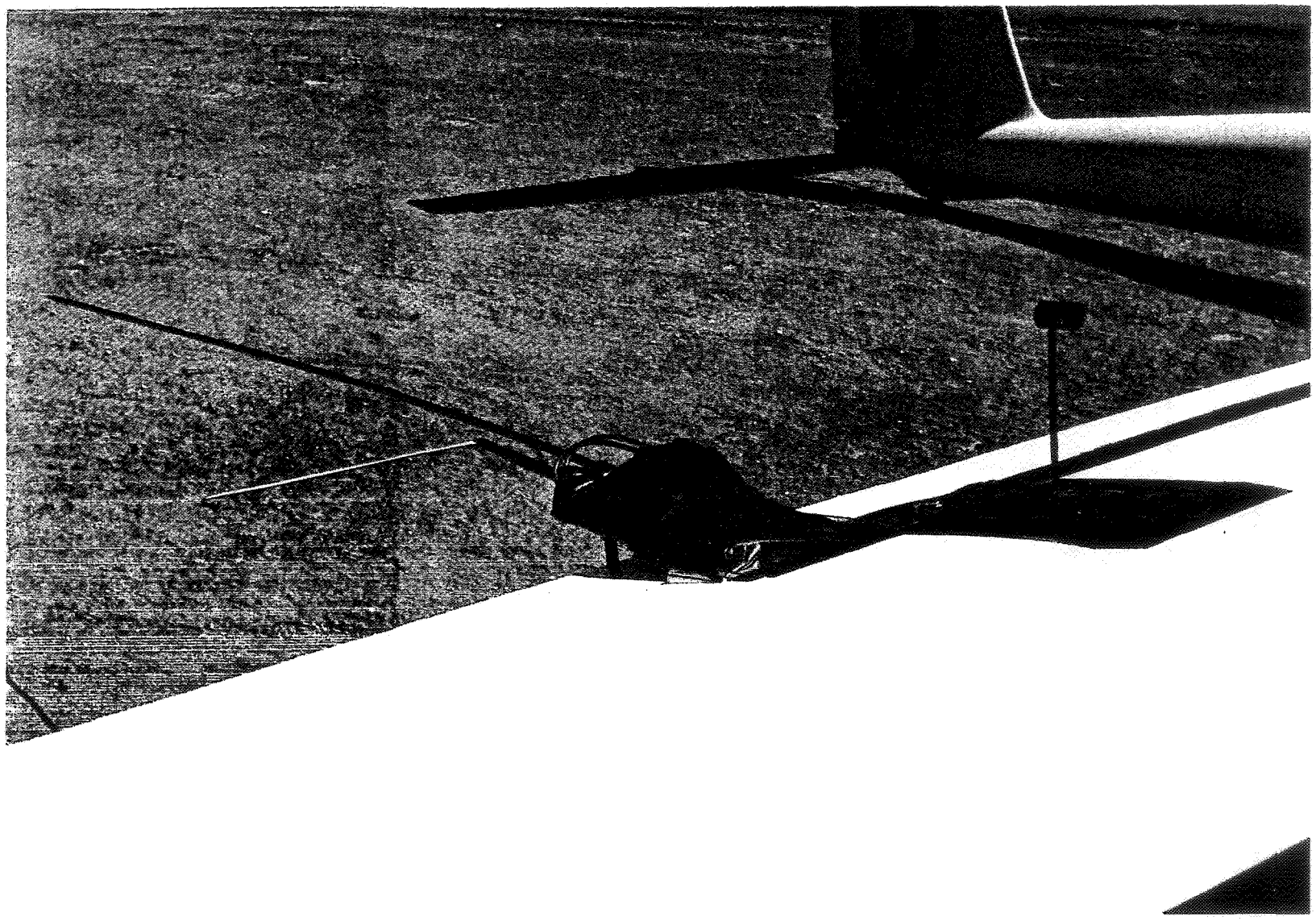

Figure 3. Close-up of Probe and Drive Unit and of Reference Probes

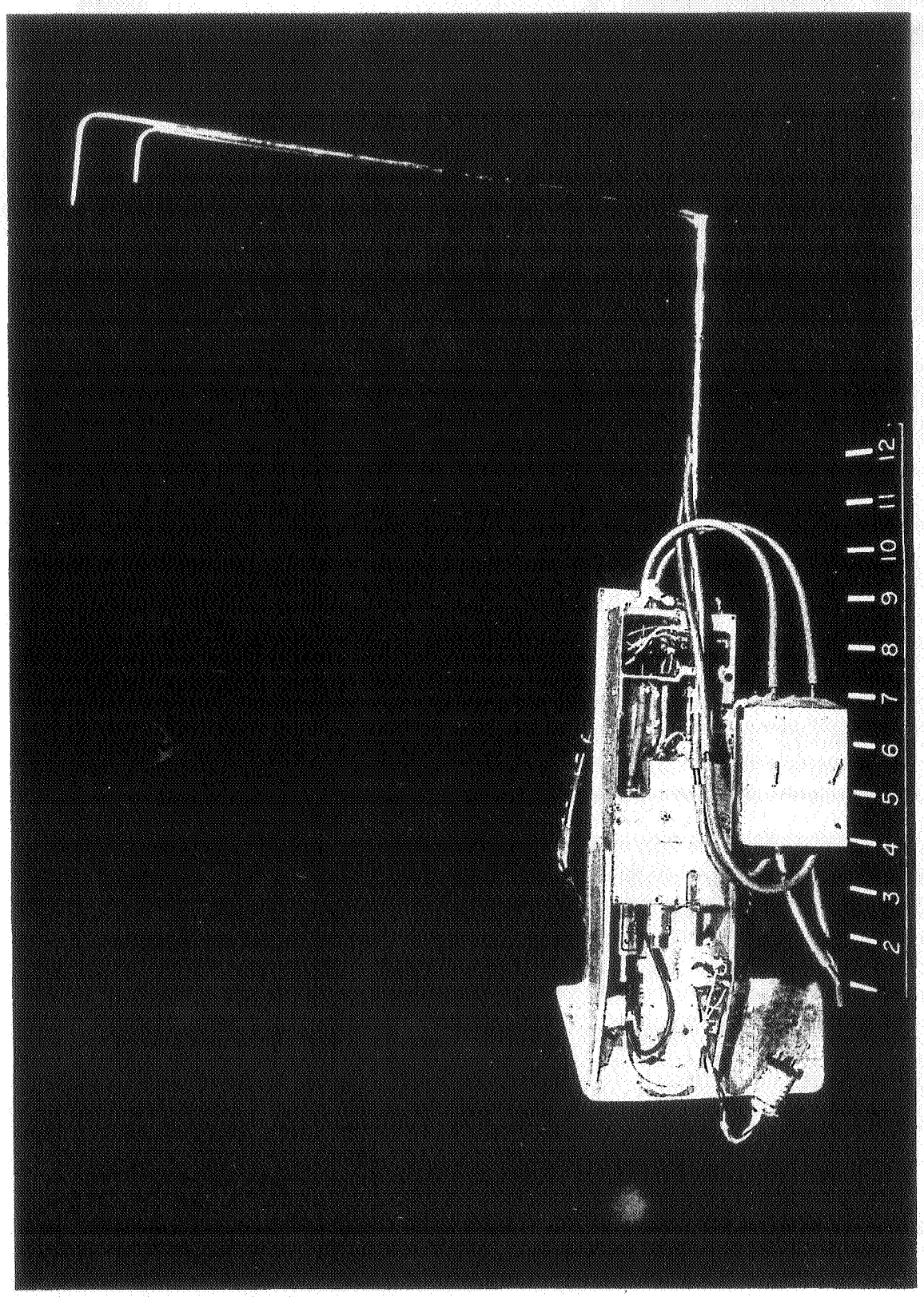

Figure 4(a). Traversing Probe in the Drive Unit

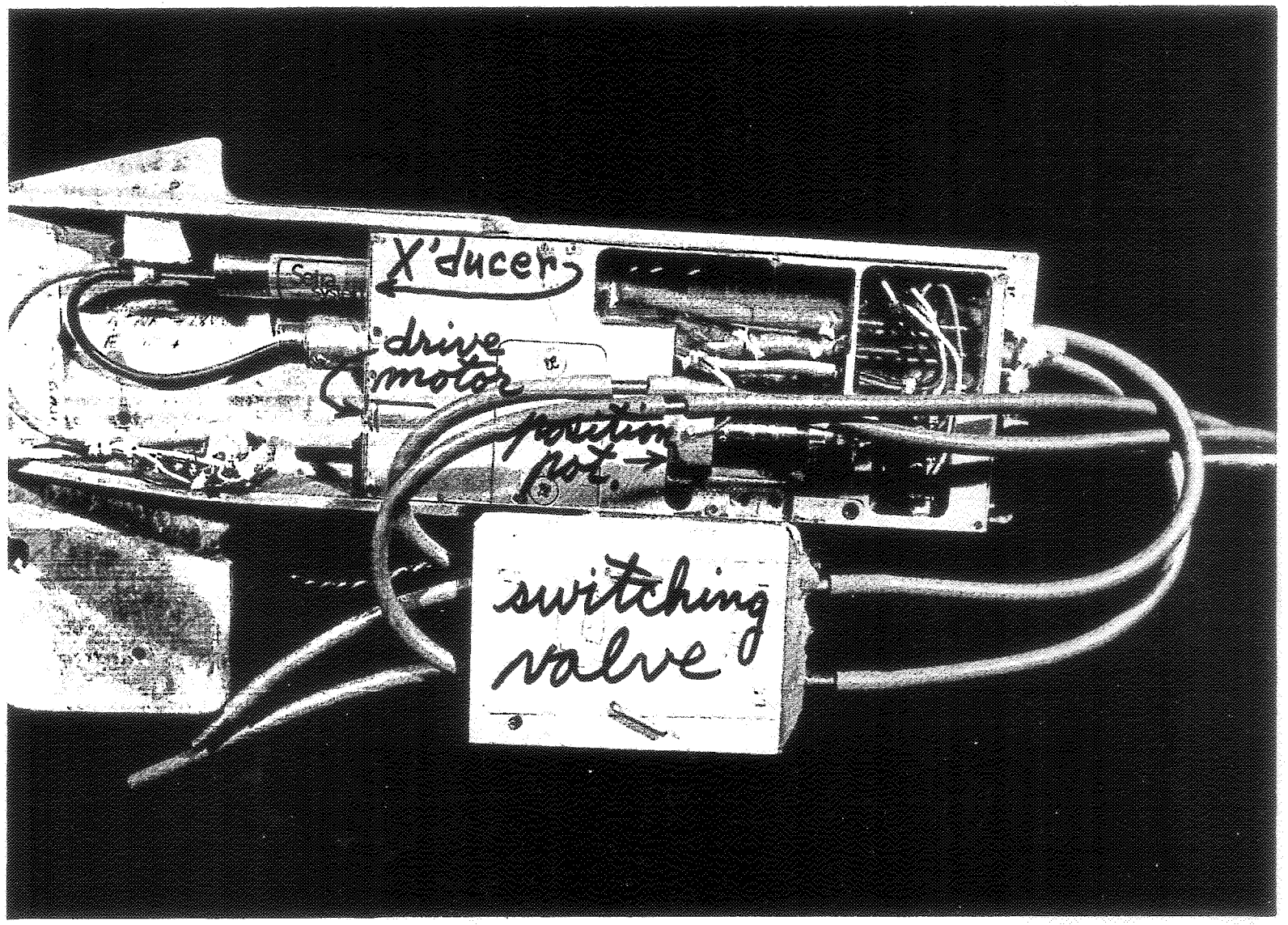

Figure 4(b). Transversing Probe and Drive Unit: Close-Up

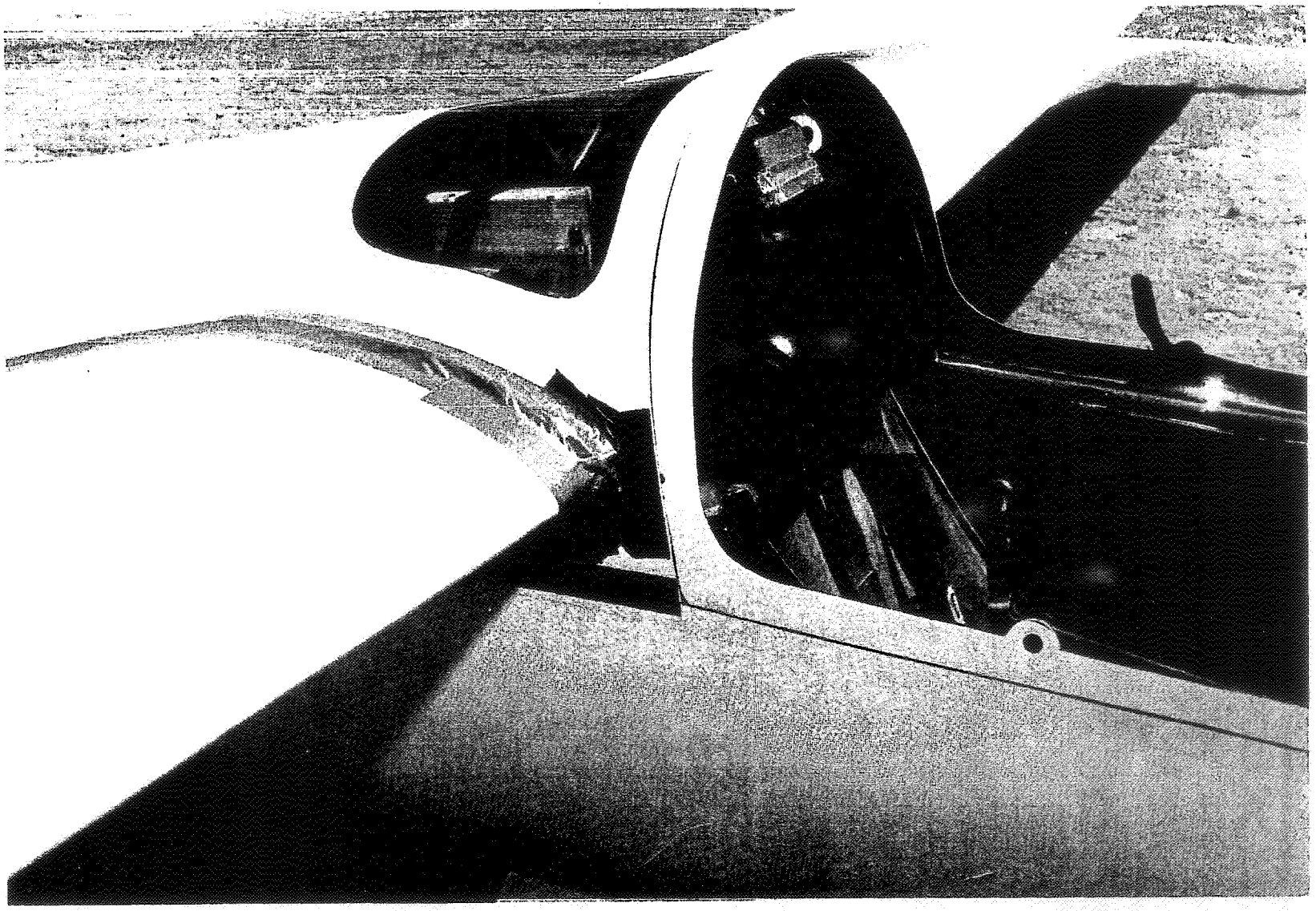

Figure 5. Recorder Package Installed behind Pilot's Headrest

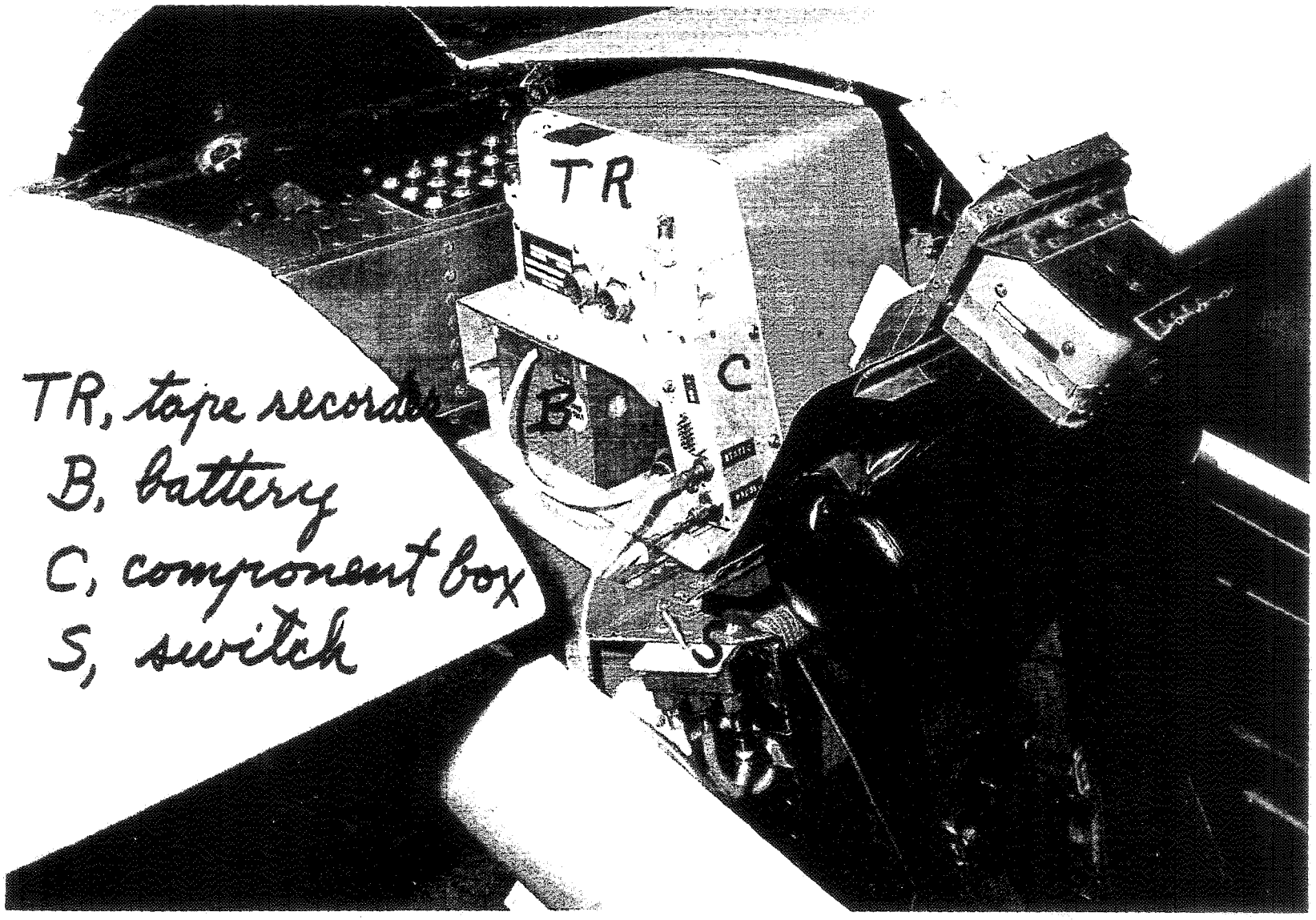

Figure 6. Recording Package: Close-Up

FREE STREAM "q" SCHEMATIC

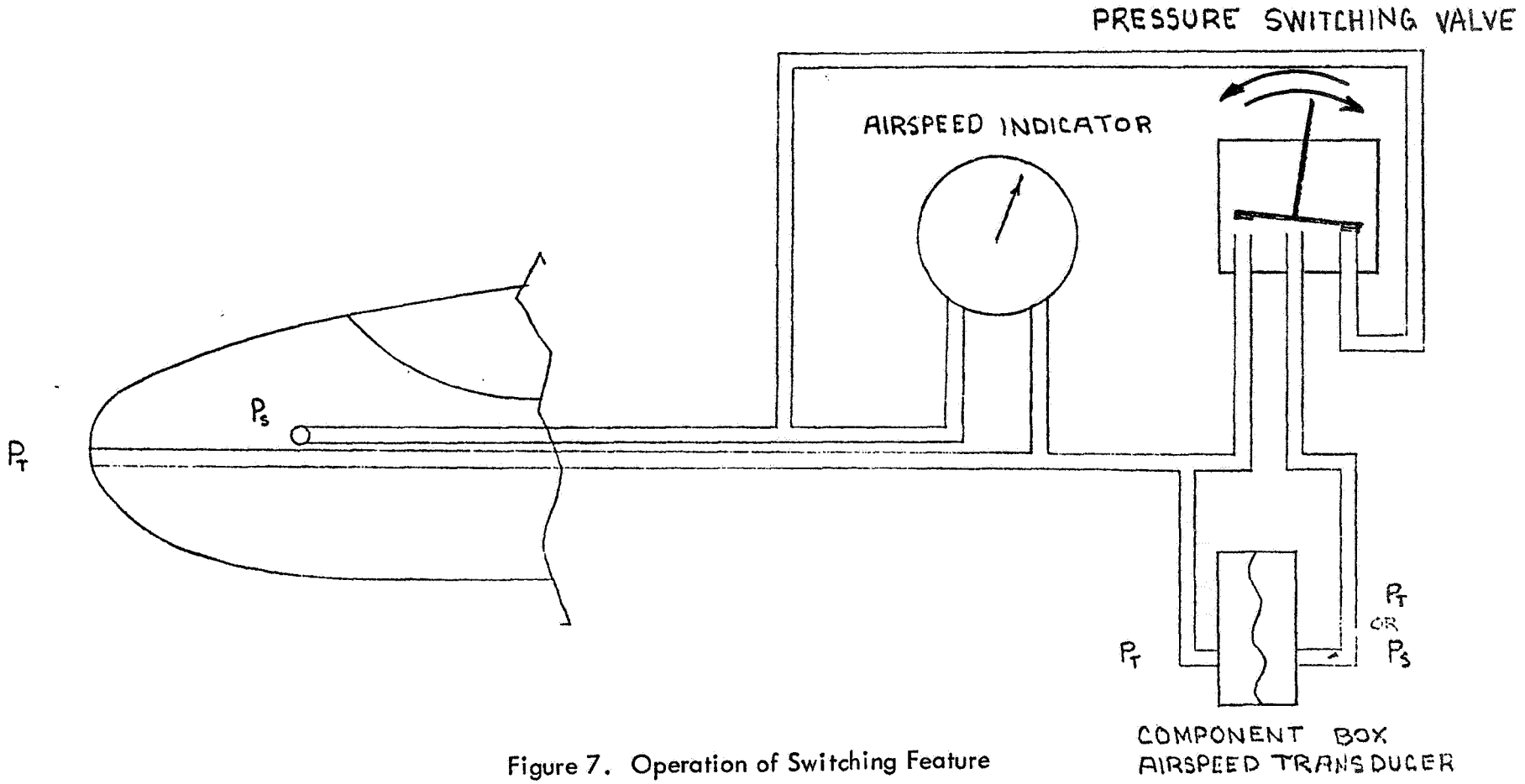

Figure 7. Operation of Switching Feature

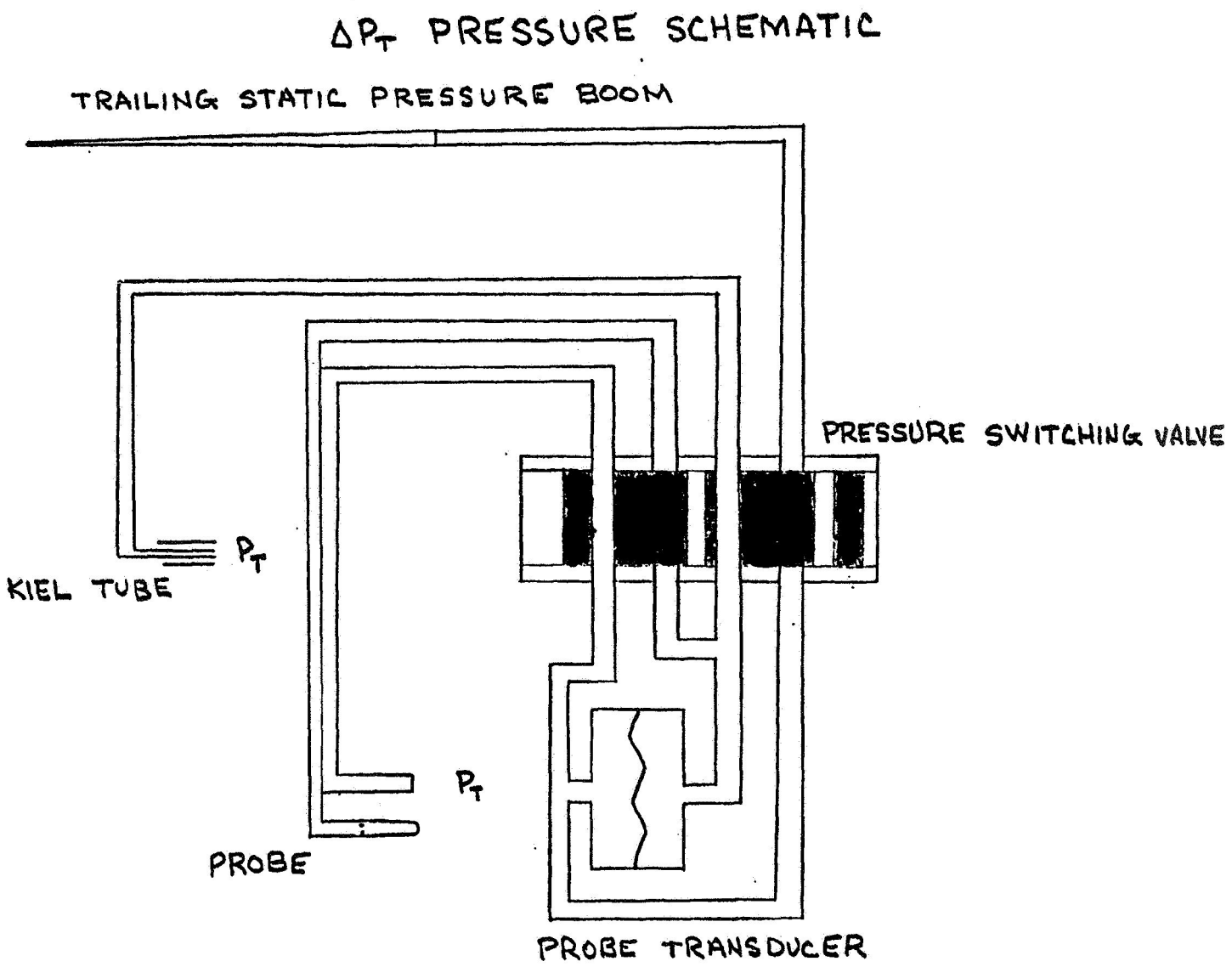

Figure 8. Slide Valve Used in Switching Feature (First Mode)

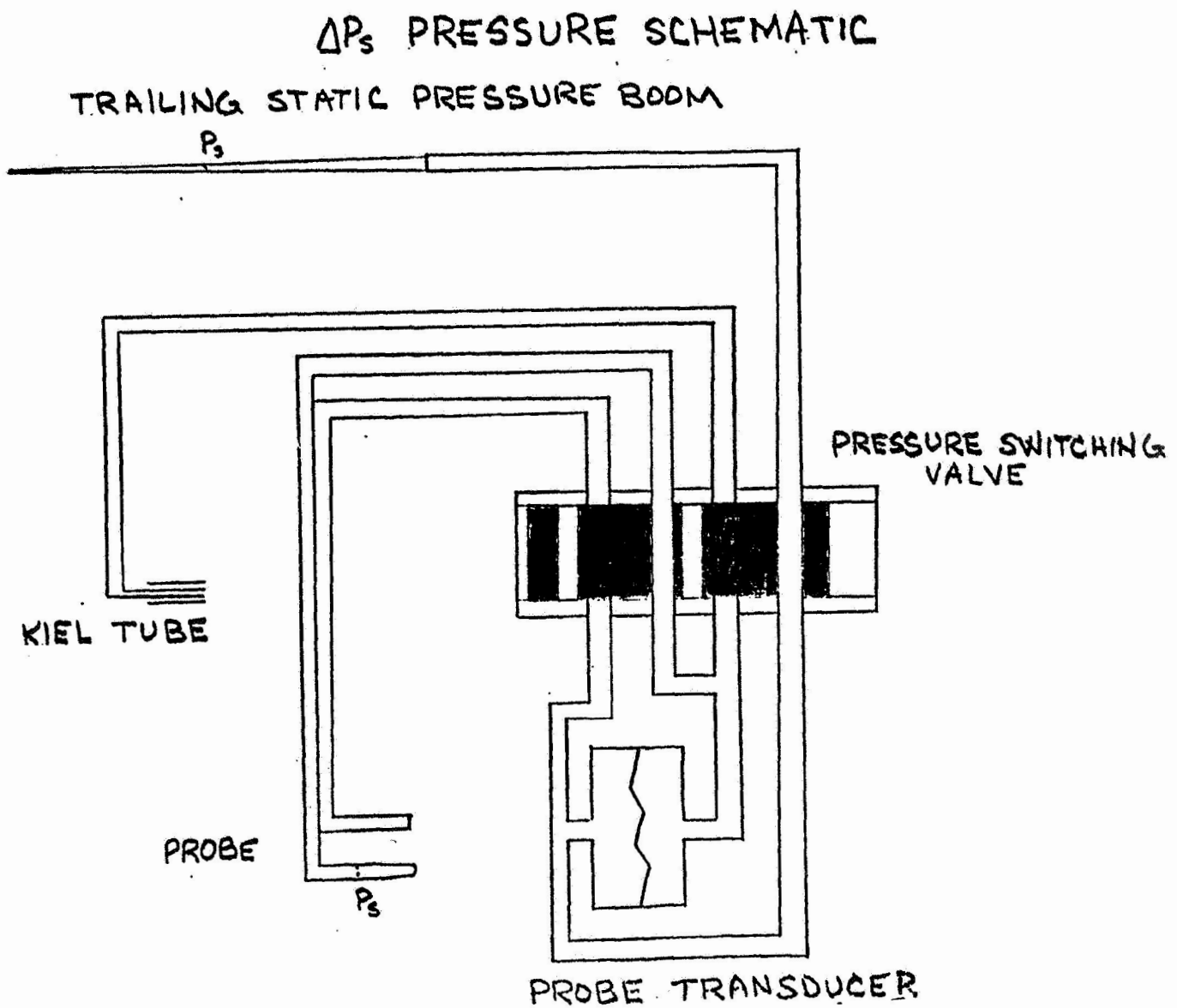

Figure 9. Slide Valve Used in Switching Feature (Second Mode)

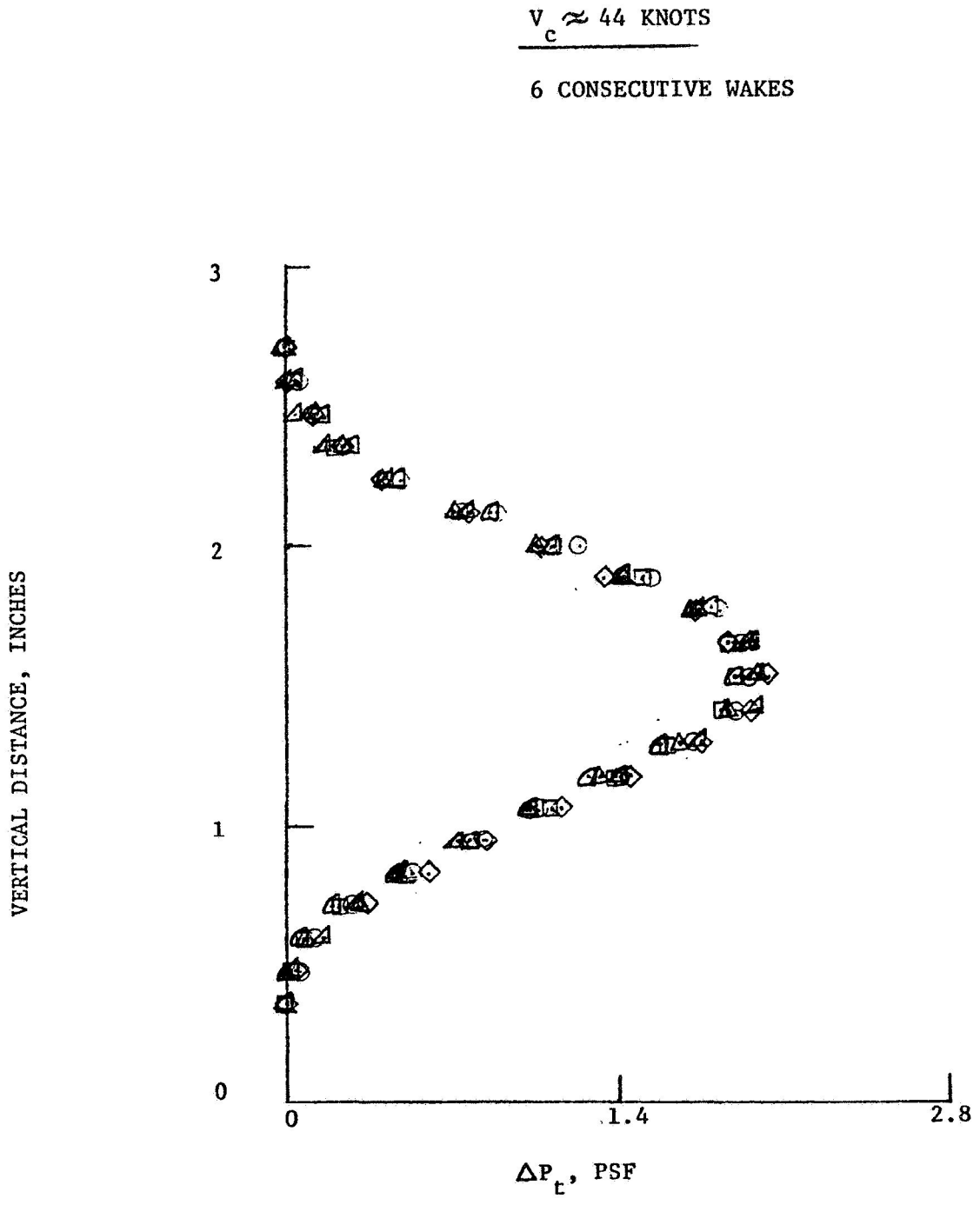

Figure 10. Example Wake Pressure Profiles (44 kts)

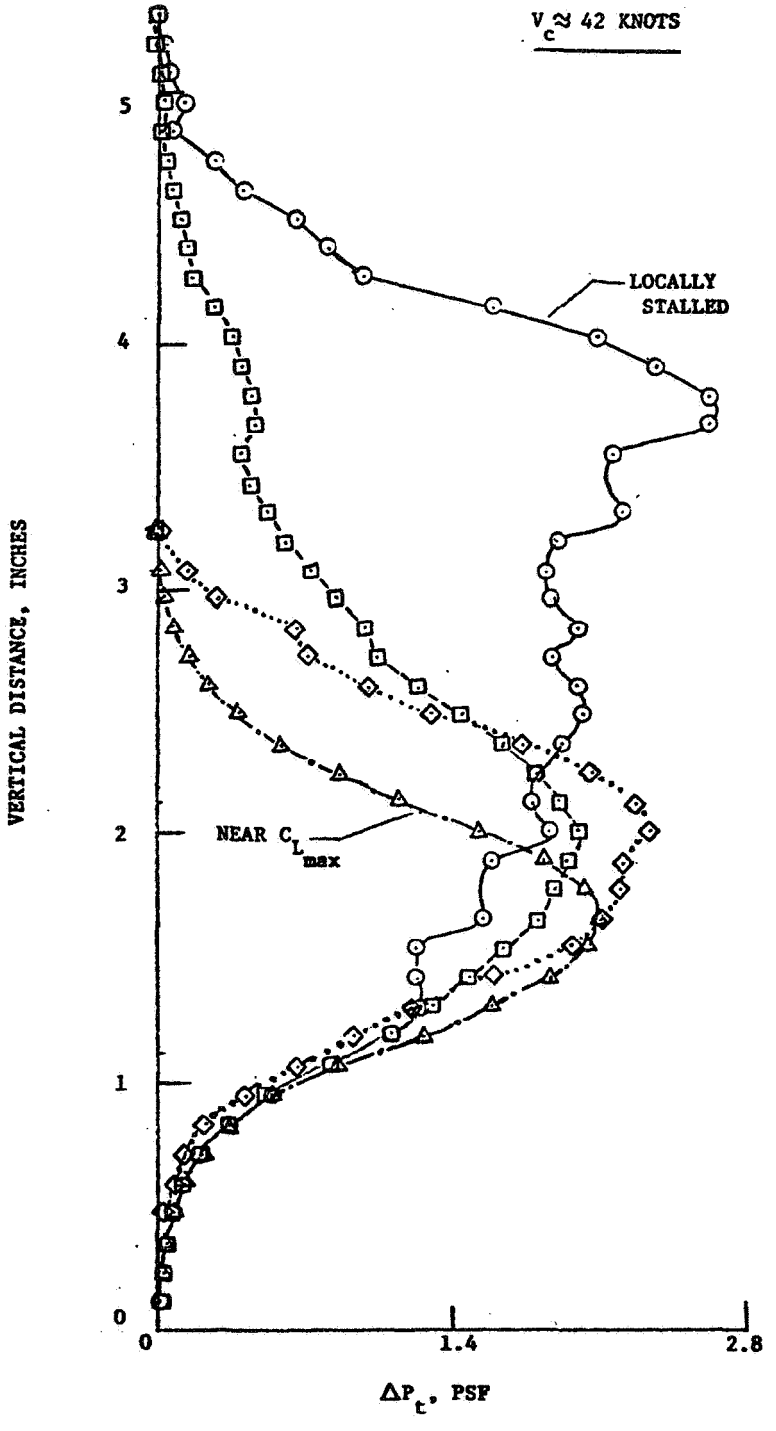

Figure 11. Example Wake Pressure Profiles (42 kts)

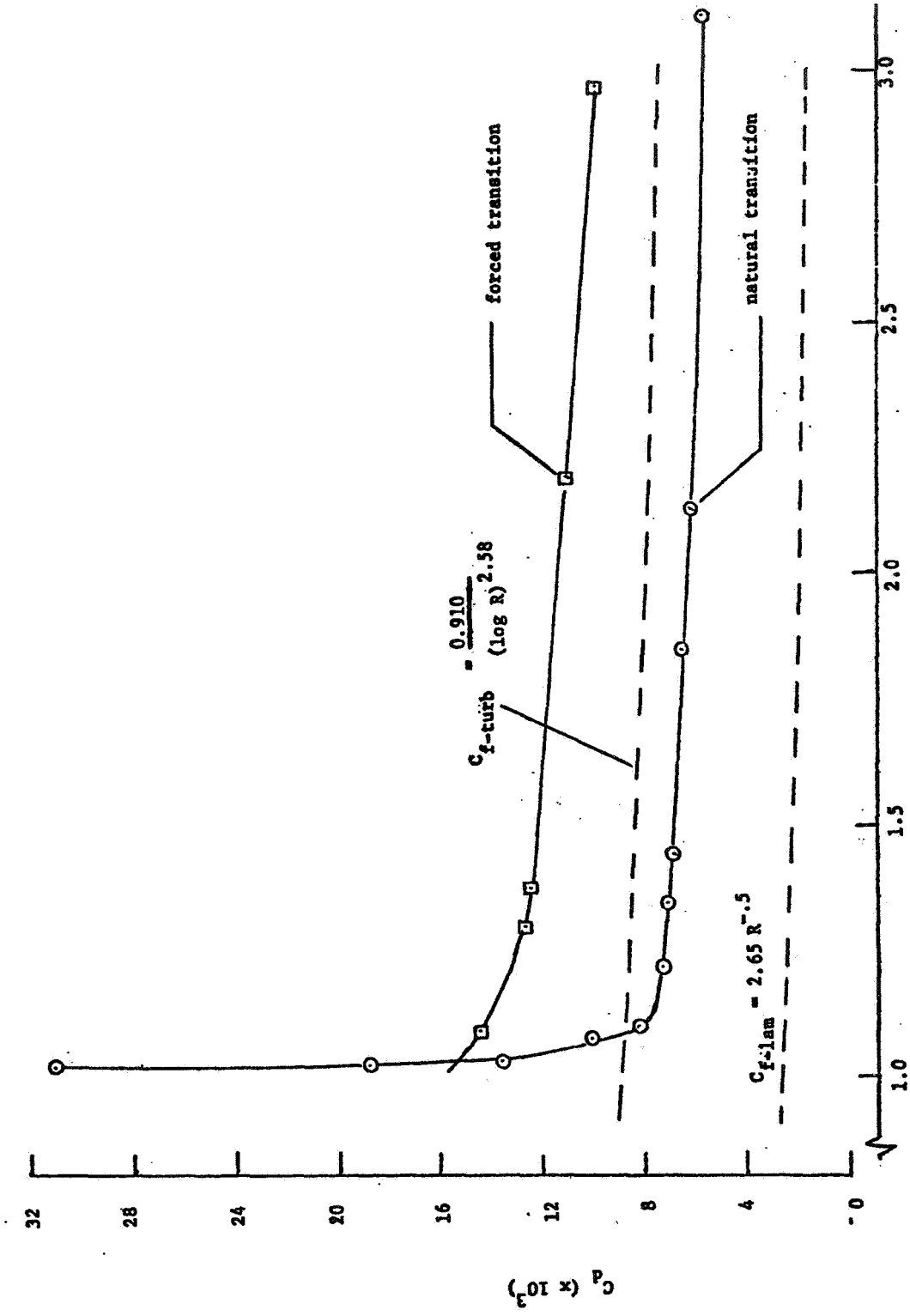

Figure 12. Section Drag: Measured Compared to Theoretical

5.4 An Application of the Ogee Tip

Jerald M. Vogel
Beech Aircraft Corp.

Introduction

Wind tunnel tests by NASA indicate that the aerodynamic performance of a rectangular 3-D wing can be increased by changing the tip to an ogee shape. Test data obtained during the tests show substantial gains in L/D throughout the angle of attack range of interest.

In order to investigate the potential gains in both cruise and climb performance, a Beech Baron was modified to include a pair of ogee tips on the configuration. Estimated gains in performance based on rectangular wing test data were somewhat optimistic. Increases in cruise speed and climb rate were predicted to be as much as 5 mph and 100 fpm, respectively. A series of quick tests were scheduled to see if the predicted gains could be realized in practice.

Ogee Tip Review

Ogee tip research during the past few years has been in conjunction with rotor blade study. One of the basic problems associated with rotor blade flows is the concentrated tip separation vortex generated with rectangular tips which degenerate the quality of the flow field encountered by the following blade. The ogee tip is designed to eliminate or diffuse the separation vortex. This is accomplished by cutting back the tip streamwise edge, starting at the leading edge as shown in Figure 1. Wind tunnel tests by NASA to indicate that the separation vortex can be diffused with the ogee tip. Figures 2, 3, and 4 show upper surface isobars for a rectangular wing and an ogee tip section with the same wing are. (Plots taken from reference 1.) As noted, the separation vortex is eliminated.

Balance data indicate that the decreased primary vortex activity leads to a substantial increase in wing L/D. Figure 5 shows the comparison between the rectangular wing and the equivalent ogee tip configuration.

The Modified Beech Baron

The Beech Baron was chosen as the test bed for two reasons. First, it has a detachable tip to easily accommodate the ogee tip; and second, the higher performance allows a chance for greater absolute changes in incremental performance, thus improving the flight-test accuracy.

Figures 6 and 7 show the baseline and modified Baron wing. As noted, the baseline tip is simply removed and the ogee tip is installed. The wing areas are the same. The ogee tip is a constant 23012 section along the tip span.

Flight Test Results

Flight tests included both speed-power and sawtooth climbs. Results, as noted in Figures 8, 9, and 10, indicate that incremental changes in performance due to the addition of the ogee tips are on the order of the data scatter associated with flight test techniques used. Climb data at density altitudes of 5500 feet and 9500 feet show a possible increase in climb at high C_L values and a decrease at low C_L values. The speed-power data indicate no substantial change in level-flight speeds.

References

1. "Effect of Sweep Angle on the Pressure Distributions and Effectiveness of the Ogee Tip in Diffusing A Line Vortex," J.C. Balcelak and R.F. Feller, NASA CR 32355
2. Rorke, J.B., Moffitt, R.C., and Ward, F.J., "Wind Tunnel Simulation of Full-Scale Vortices," Preprint #623, 28th Annual National Forum of the American Helicopter Society, Washington, D.C., May 1972.
3. Landgrebe, A.T., and Bellinger, E.D., "Experimental Investigation of Model Variable - Geometry and Ogee Tip Rotors," United Aircraft Research Laboratories, NASA Contract No. NAS - 10906, to be published, 1973.

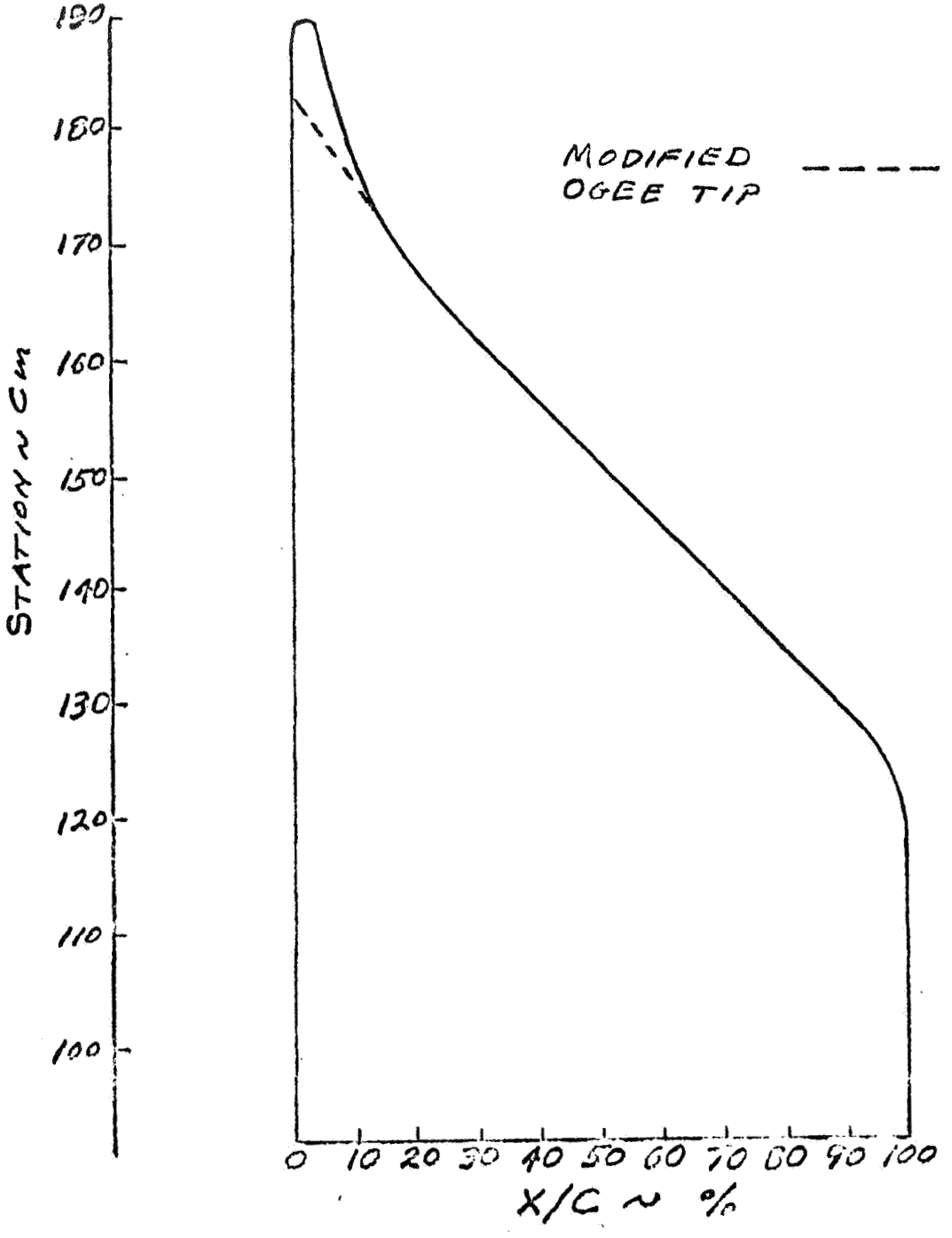

Figure 1. Ogee Tip Planform

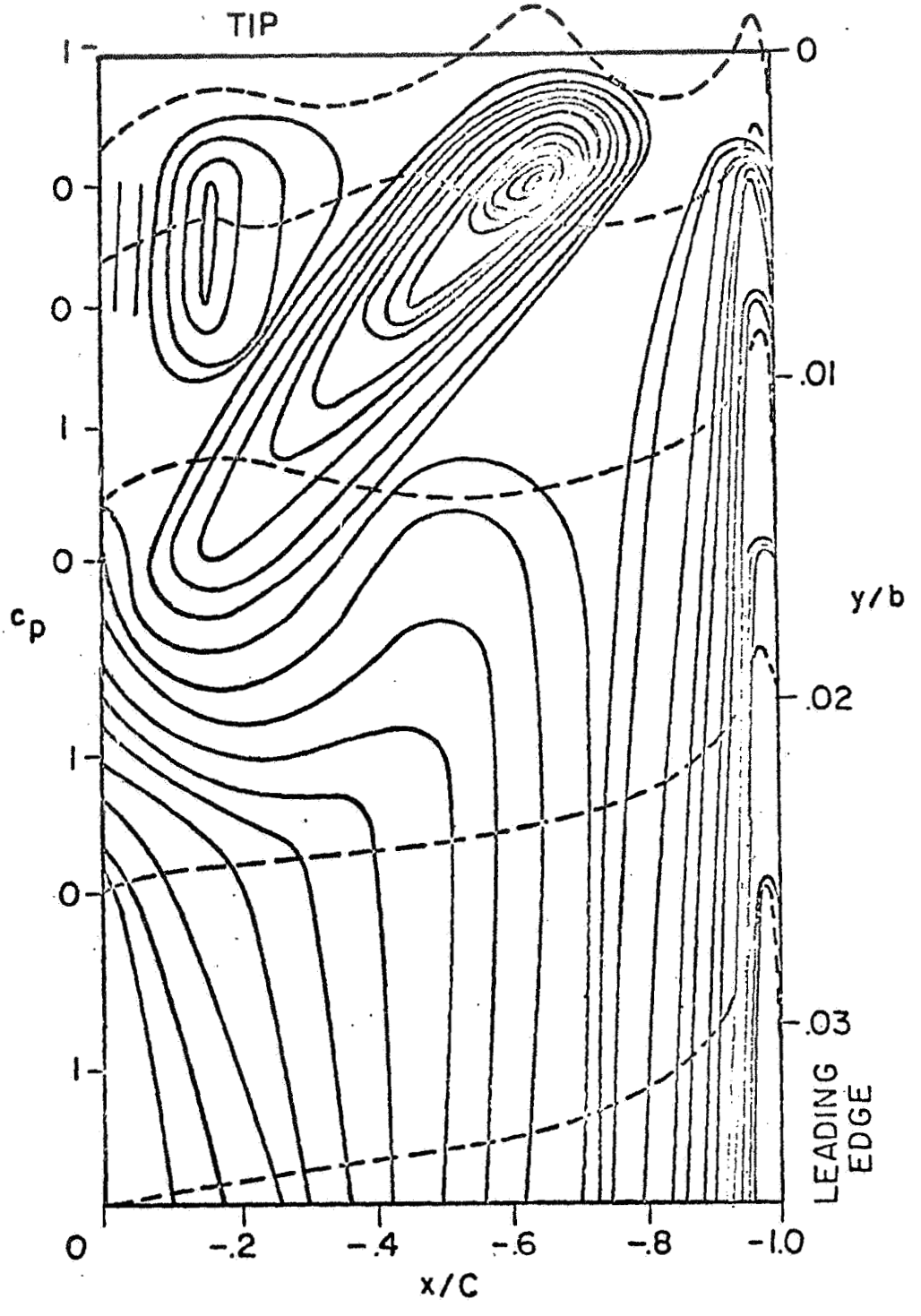

Figure 2. Isobars on top surface of wing (tip region)
$\lambda = 0$, $\alpha = 12^{\circ}$

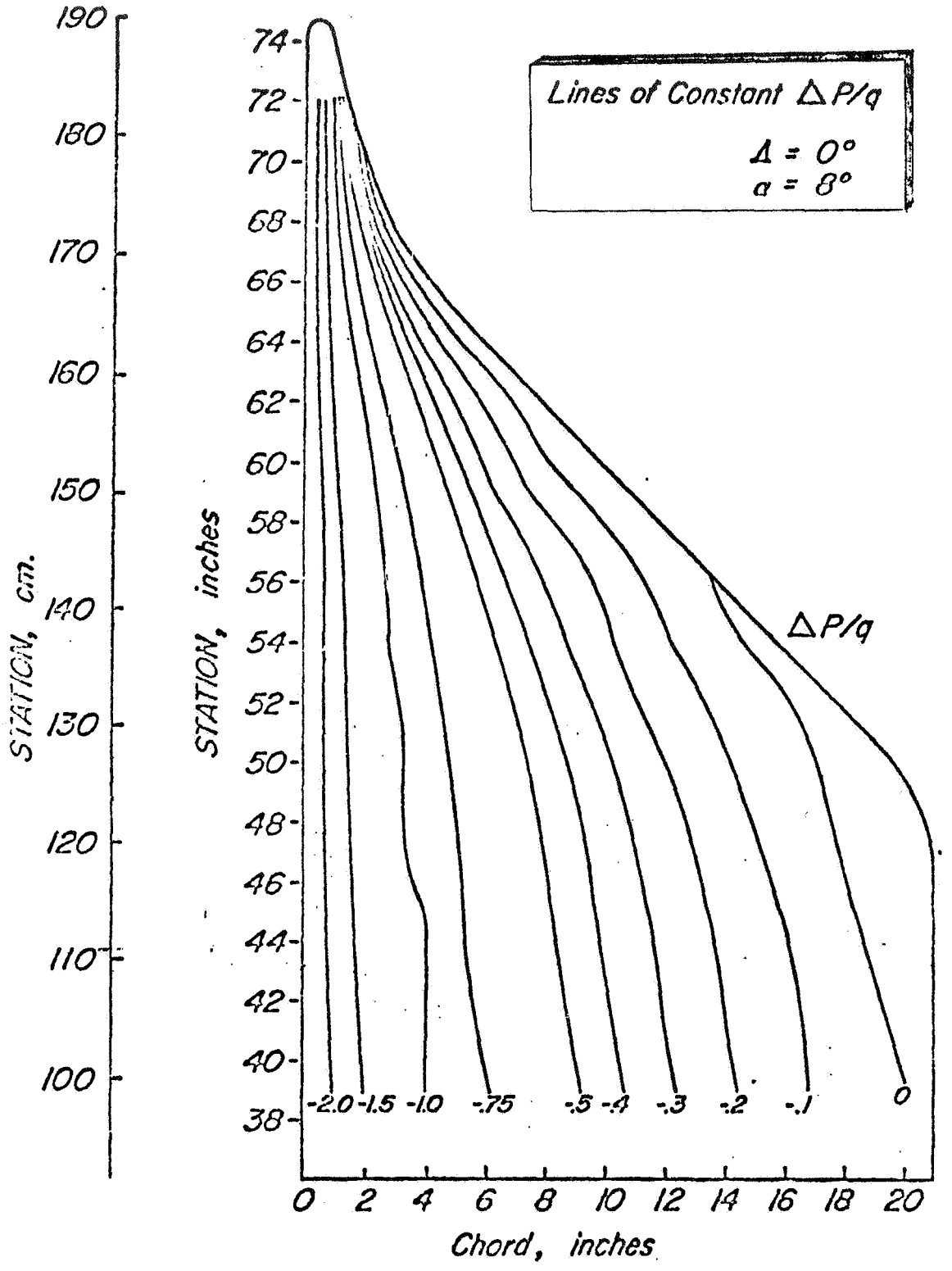

Figure 3. Contour pressure plot of the ogee-tip section at $\alpha = 8^{\circ}$ and $\Lambda = 0^{\circ}$

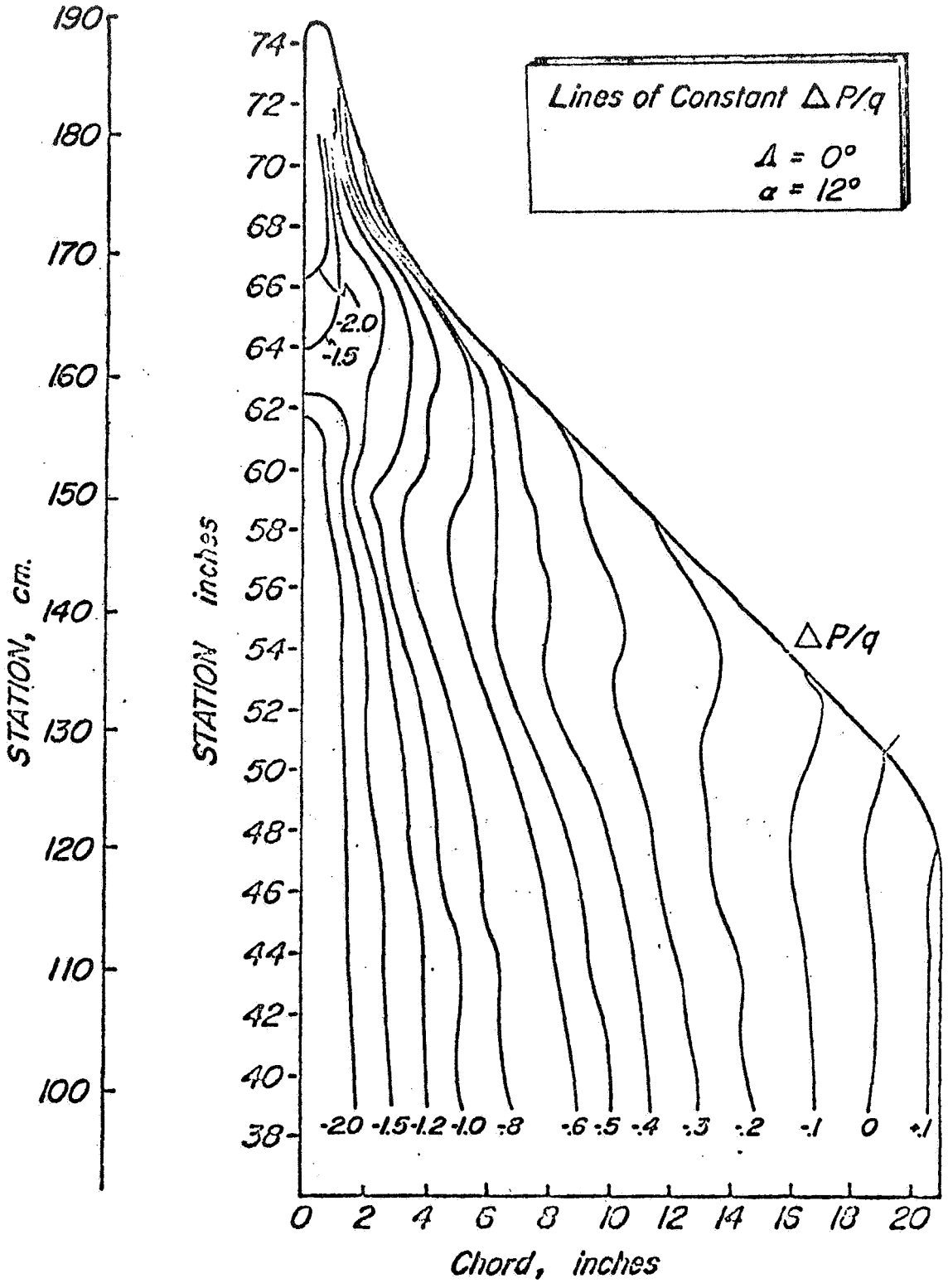

Figure 4. Contour pressure plot of the ogee-tip section at $\alpha = 12^{\circ}$ and $\Lambda = 0^{\circ}$

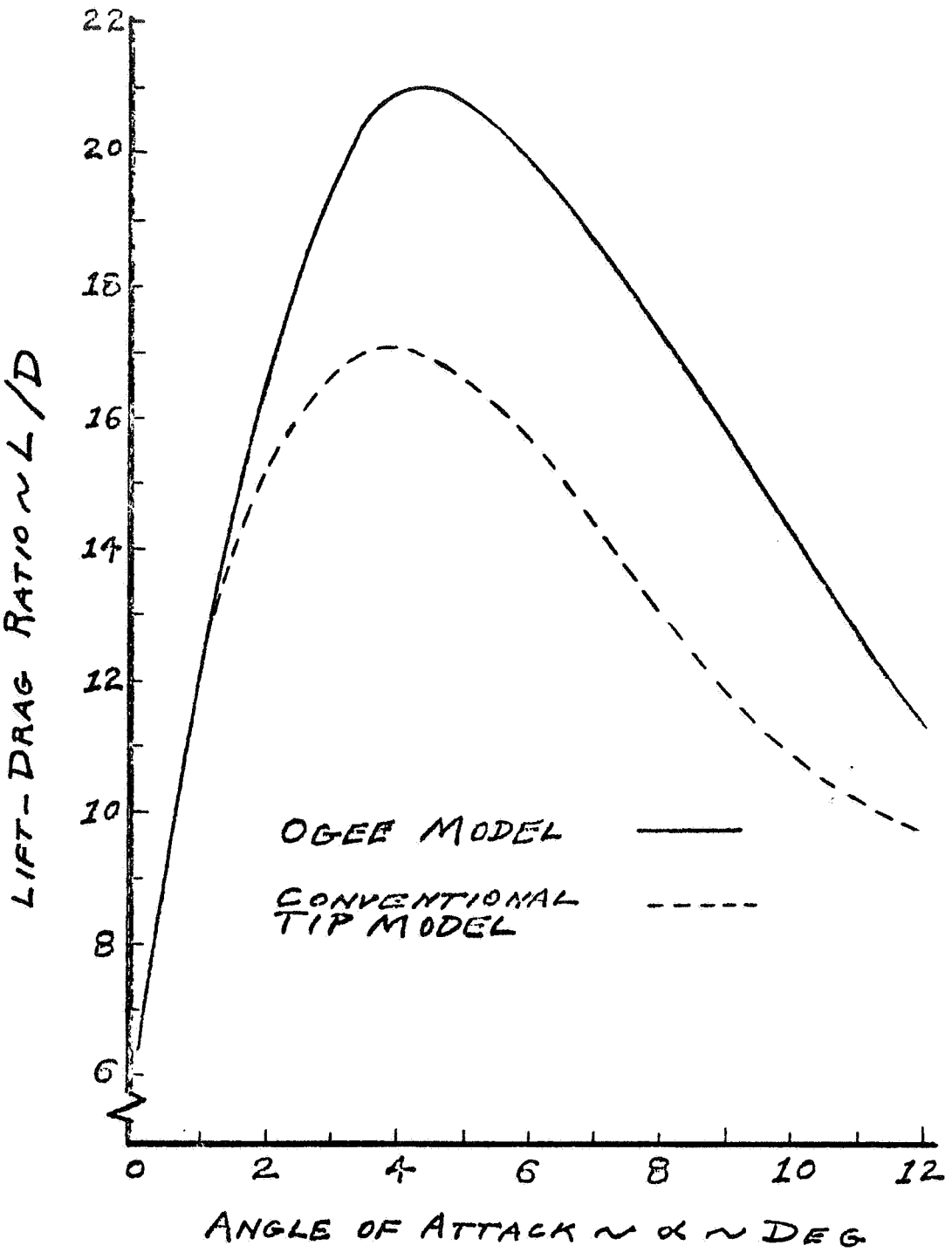

Figure 5. Lift-to-Drag Ratios vs. Angle of Attack

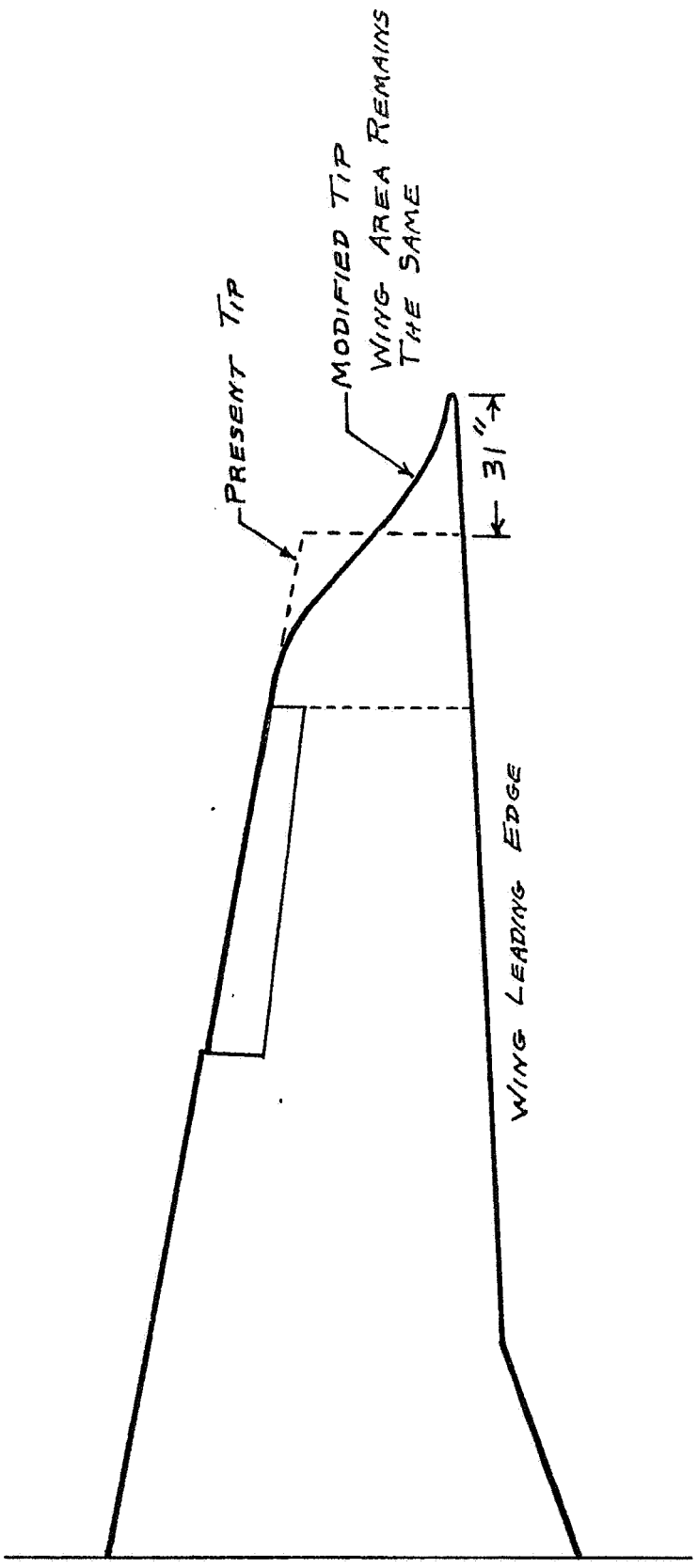

Figure 6. Ogee Wing Tip on Beech Baron

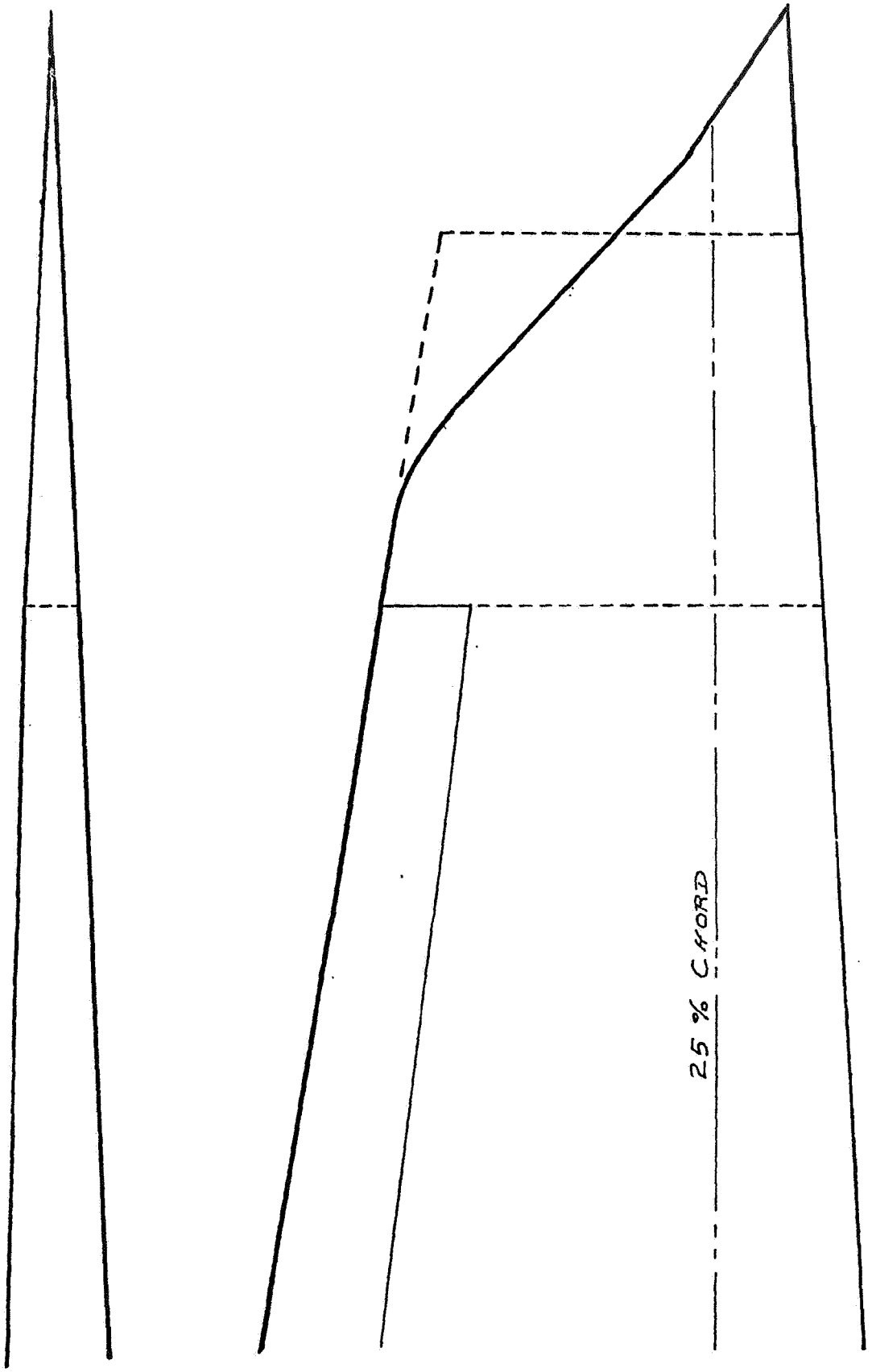

Figure 7. Wing Geometry for Ogee Tip Baron

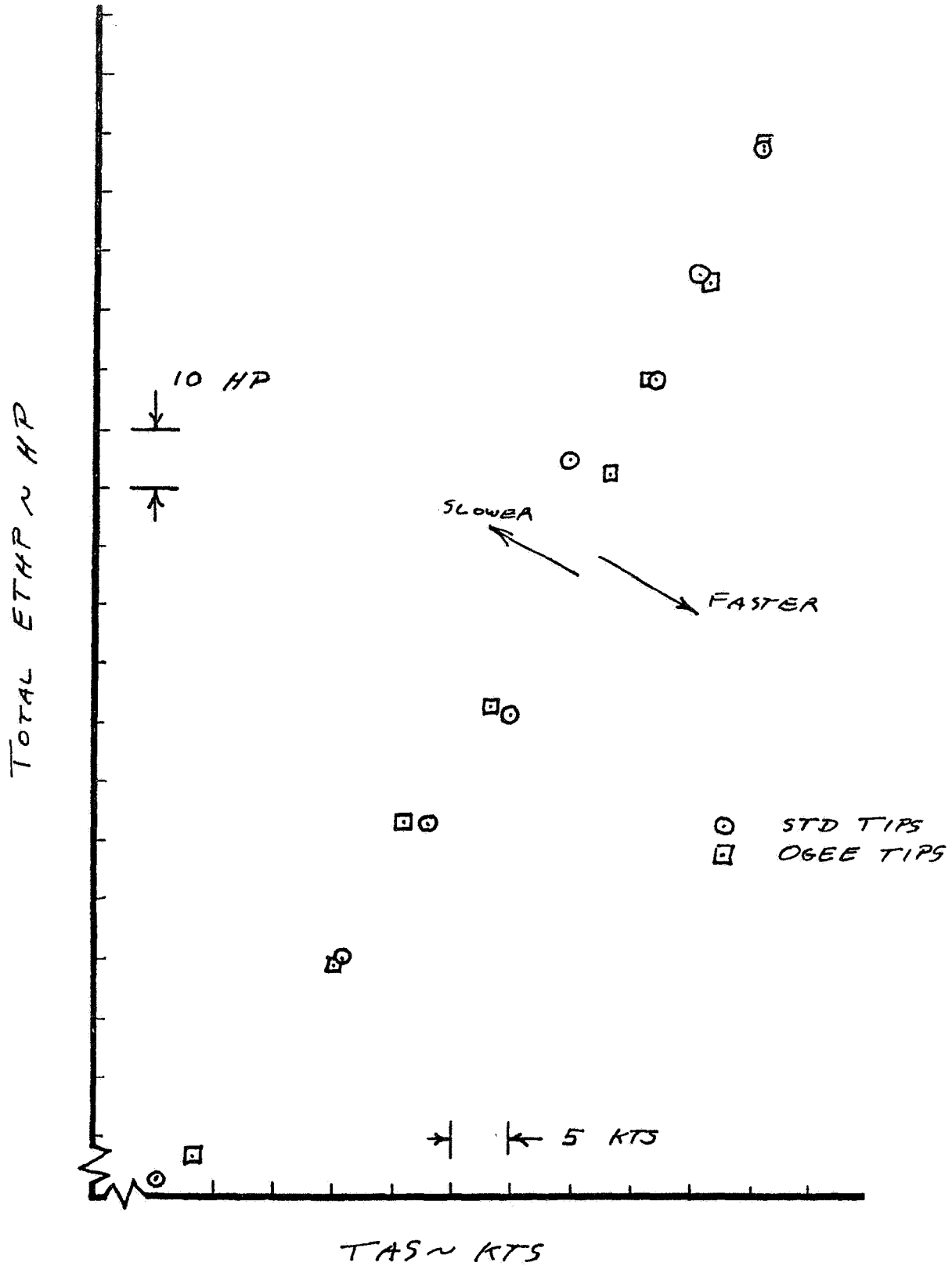

Figure 8. Speed-Power Std. Tips vs. Ogee Tips 16,000 Ft.

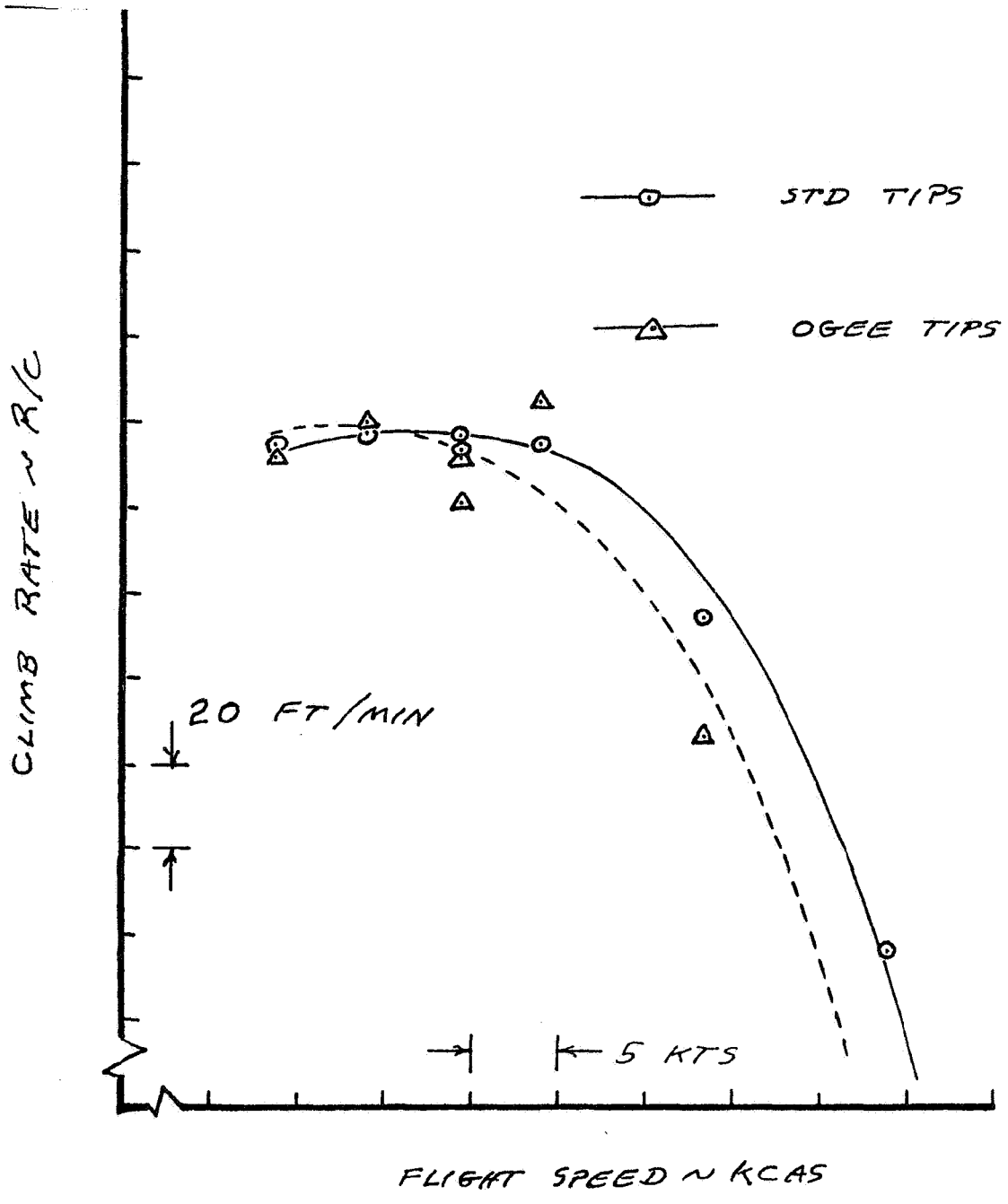

Figure 9. Ogee Tip Configuration R/C vs. KCAS
Density Alt. 5549 Ft.

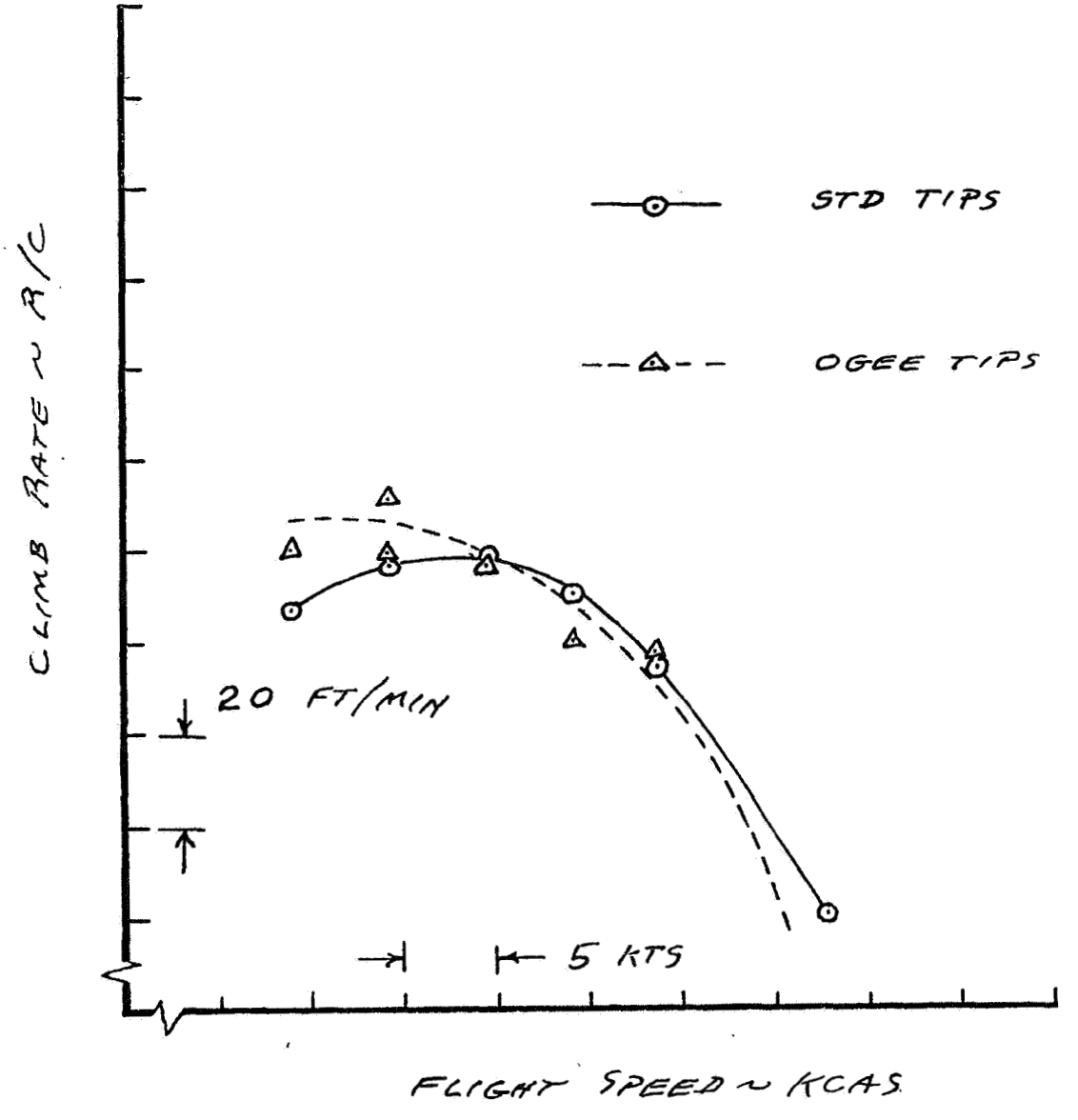

Figure 10. Ogee Tip Configuration R/C vs. KCAS
Density Alt. 9623 Ft.

5.5 Wing-Tip Vanes as Vortex Attenuation and Induced Drag Reduction Devices

W. H. Wentz, Jr. and M. G. Nagati
Wichita State University

Summary

Analytical studies have been conducted to examine the feasibility of utilizing wing tip turbines to remove swirl from the wing trailing vortex, and hence reduce the potential for upset of following aircraft. Energy recovery from the turbines is also analyzed. A computer routine has been developed to permit rapid parametric studies of various tip turbine designs.

The studies show that the optimum turbine is a non-rotating set of vanes which reduce swirl and recover energy in the form of reduced overall configuration induced drag. A specific case study indicates a 23% reduction in induced drag for a rectangular wing of aspect ratio 5.33, operated at a lift coefficient at 1.0.

Introduction

The problems associated with the operation of small aircraft in the vortex wake of a large aircraft are well documented (Figures 1 and 2 and reference 1). Many solutions to reducing vortex induced angles have been proposed and tested. Most of these however, are achieved at the expense of added drag and hence increased fuel consumption and noise. The present research was undertaken to study the feasibility of a rather novel scheme for diffusing wing tip vorticity, and at the same time recovering energy from the vortex wake.

At least two similar techniques have been tested. The flow straighteners designed by Uzel and Marchman (ref. 2) and the "winglets" developed by Whitcomb (ref. 3).

The present study is concerned with evaluation of a wind turbine mounted in the center of the wing tip vortex core (Figure 3). The turbine is designed to remove the swirl component of velocity from the tip vortex, and to provide rotating shaft torque for conversion to propulsive or stored energy.

Analytical Method

The vortex core is modeled as shown in Figure 4 based upon Reference 4. The turbine is analyzed using the blade element theory of Reference 5. Basic blade

element velocities and angles are shown in Figure 5. Since the function of the turbine is to reduce upset severity the blade is designed to remove the total swirl velocity at each radial station. This constrains the local induced angle to a value of one-half the local swirl angle, since half the downwash takes place downstream from the blade element.

It should be noted from the velocity vector diagram that not only is it possible to obtain a torque-producing force, but it is also possible to obtain a direct thrust force component which would appear as a reduced induced drag. The effect has been demonstrated by Whitcomb's winglets, but evidently the effectiveness of winglets in reducing vortex upset has not been evaluated. Uzel and Marchman evaluated fixed wingtip flow straighteners to reduce the vortex upset hazard, but their design evidently utilizes sharp-edged uncambered sections which cannot recover the leading section force which would produce thrust.

A computer program was developed to evaluate proposed designs in the present study. A simplified flow chart of the computational algorithm is shown in Figure 6. For simplicity, turbines utilizing constant chord blades were analyzed. The program was designed to adjust blade chord until the maximum angle of attack encountered along the span is between 14.5° and 15°. The effect of the constraint is to have a design near maximum unstalled lift coefficient condition, in order to minimize wetted area drag. Computer studies were made at a cost of less than $1 per configuration. Design conditions are given in Table 1.

Table 1. Design Conditions

Lift Coefficient	1.0
Aspect Ratio	5.33
Planform	Rectangular
Core radius	.01 (Span)
Maximum swirl velocity	.8 (Flight speed)
Vane section drag coefficient	0.010

Results

Results of the parametric studies of shaft power output as a function of rpm and diameter are shown in Figure 7. These data show that shaft power increases with diameter, and that rpm for maximum shaft power decreases as diameter is increased. Theoretical upper power limit occurs when shaft power equals wing induced power. Figure 8 presents net power, which is shaft power minus or plus the

drag or thrust power, including blade section drag effects. These data represent a realistic accounting since blade section drag effects are included. For the values chosen for this study, a maximum net return of 35% of induced power is achieved for turbine diameters of 32 and 64 vortex core diameters. Thus turbine diameter ratios greater than 32 provide no added benefit. The most intriguing result, however, is that the optimum rpm is zero!

From a practical point of view, these results show that for virtually any turbine diameter, the net power recovery is nearly optimum at zero rpm. Since the shaft power is zero under such conditions, it follows that the significant task of the tip-turbine blades is to recover thrust directly. While designs involving blade diameters ratios of 32 do not seem practical, designs with diameter ratios in the range of 2 to 8 may be quite feasible.

An additional computer run was made with zero rpm, turbine diameter ratio equal to 8, and vane section drag coefficient increased from 0.010 to 0.013. All other parameters were retained as given in Table 1. This run showed that an induced power recovery at 23% was possible. This is believed to be a very realistic set of design conditions.

Blade twist distributions for selected configurations are shown in Figure 9. These results indicate that twist requirements pose no extreme fabrication problems.

Concluding Remarks

The present analysis has many limitations. Some of these are described and discussed below:

1. Vortex core rollup is not complete one chord behind the trailing edge. Therefore the assumed vortex velocity model is only approximate.

2. The present analysis does not account for mutual aerodynamic interference between the vanes and the wing. The vane lift will certainly produce induced velocities which will influence the main wing lift and hence vortex distribution. A more sophisticated analysis would include mathematical modeling of main wing and tip-vane vortex.

3. The present analysis does not account for off-optimum performance. It is reasonable to expect that operation at lower wing lift coefficient will adversely influence performance, since blade twist will no longer be optimum. The design criteria should protect against stalling of the vanes under such conditions, however.

4. The effect of the tip vanes is to replace a single concentrated vortex with a series of vortices emanating from the vane tips. No analysis has been made

of the trajectory of this new vortex system. If the new vortices coalesce, it is possible that the upset hazard to following aircraft might not be reduced.

Conclusions

1. Feasibility studies indicate that tip mounted multi-vane turbines can recover energy from a wing vortex wake, while simultaneously reducing the vortex swirl and presumably the upset hazard to following aircraft.

2. The studies show that a non-rotating array of vanes properly twisted will provide maximum net energy recovery, in the form of vane thrust.

3. Practical designs from the present study should be evaluated by wind tunnel tests to determine actual performance gains, as well as penalties for off-design operation.

References

1. Roberts, L.: On Vortex Wake Alleviation. In "The Future of Aeronautics," Proceedings of NASA University Conference on Aeronautics, University of Kansas, Lawrence, Kansas, October 1974.

2. Bower, R.E.: Opportunities for Aerodynamic-Drag Reduction. In "The Future of Aeronautics," Proceedings of NASA University Conference on Aeronautics, University of Kansas, Lawrence, Kansas, October 1974.

3. Uzel, J.N. and Marchman, J.F. III: The Effect of Wing-Tip Modifications on Aircraft Wake Turbulence. Report No. VPI E-72-8, Virginia Polytechnic Institute and State University, July 1972.

4. Scheiman, and Shivers: Exploratory Investigation of the Structure of the Tip Vortex of a Semispan Wing for Several Wing Tip Modifications, NASA TND-6101.

5. Dommasch, D.O., Sherby, S.S. and Connolly, T.F., Airplane Aerodynamics, Pitman Publishing, 1967.

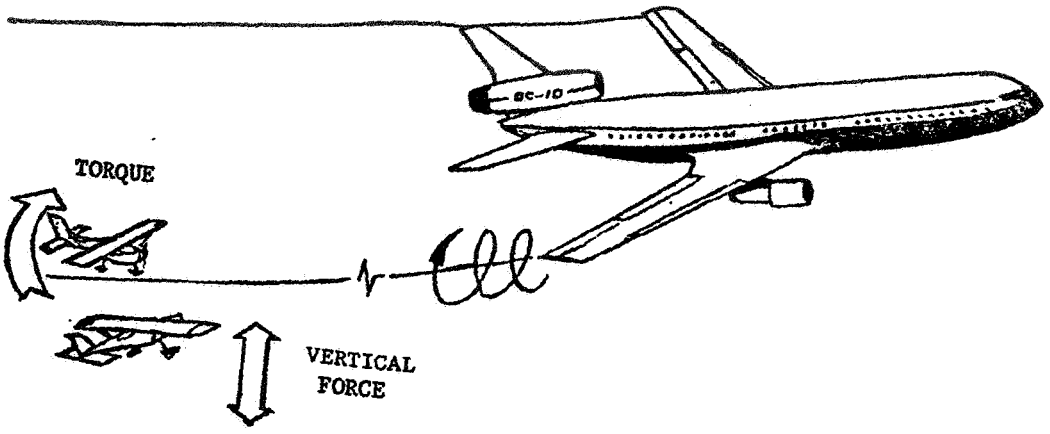

Figure 1. Vortex Upset Problem

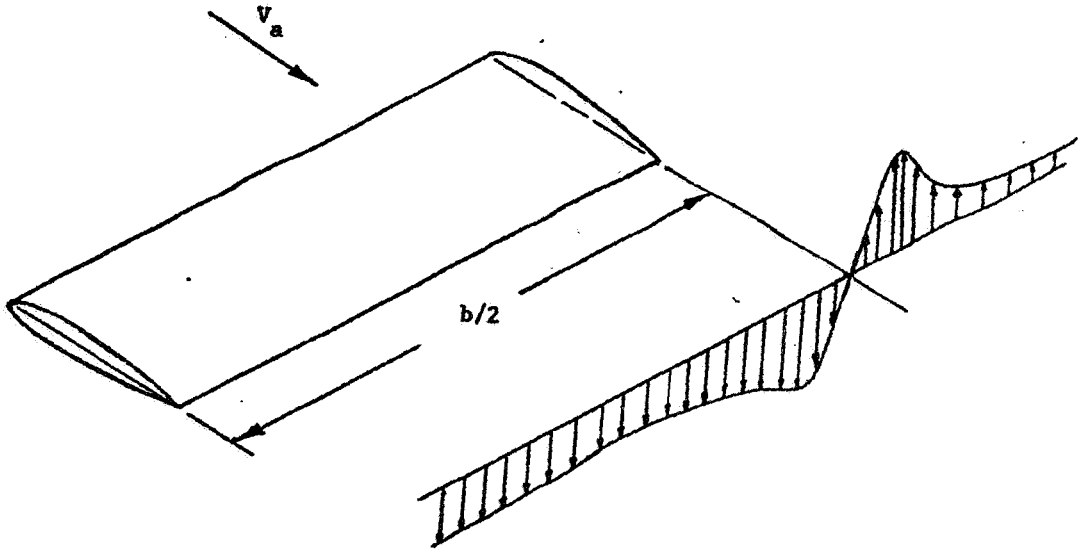

Figure 2. Wing Wake Velocities

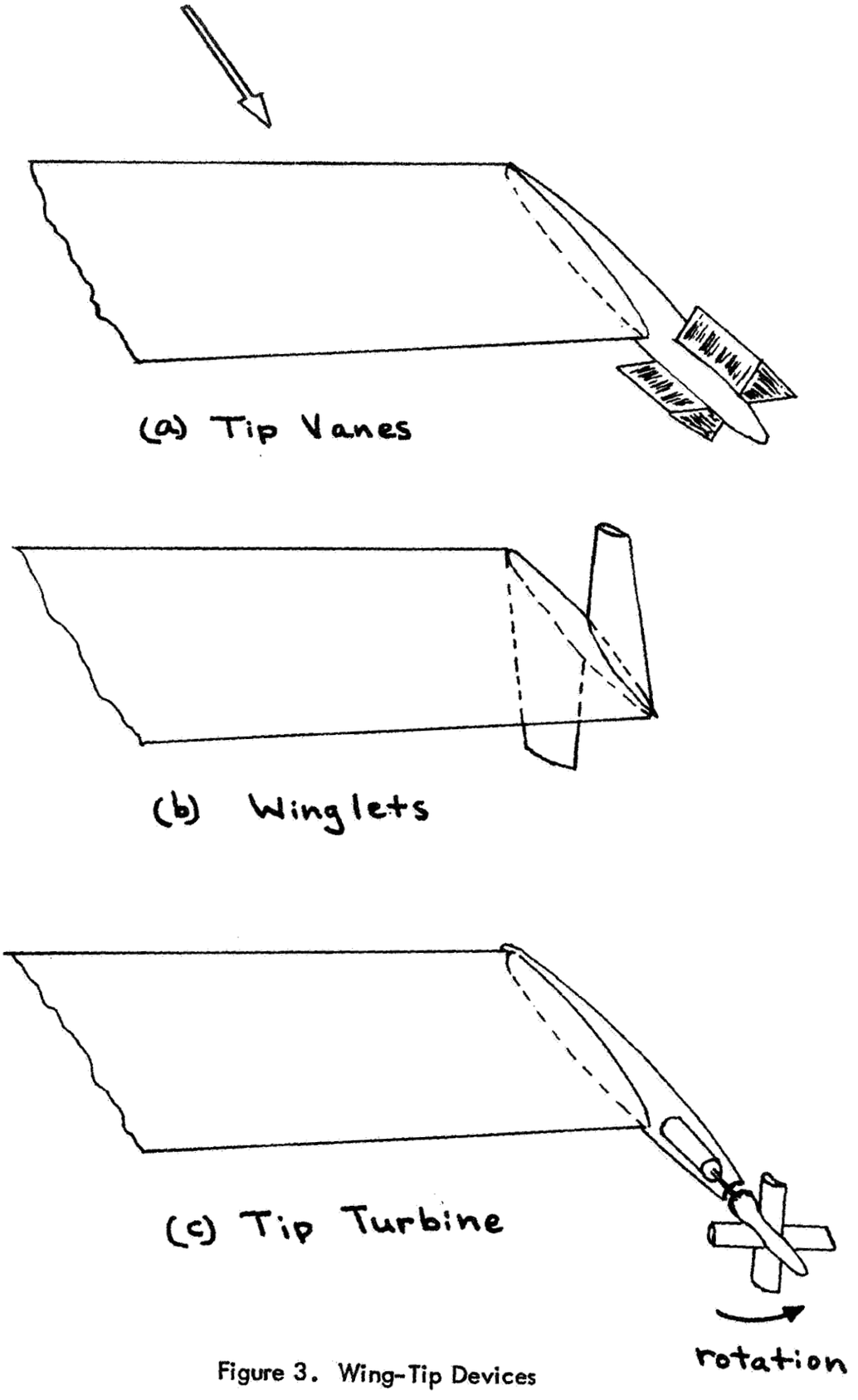

Figure 3. Wing-Tip Devices

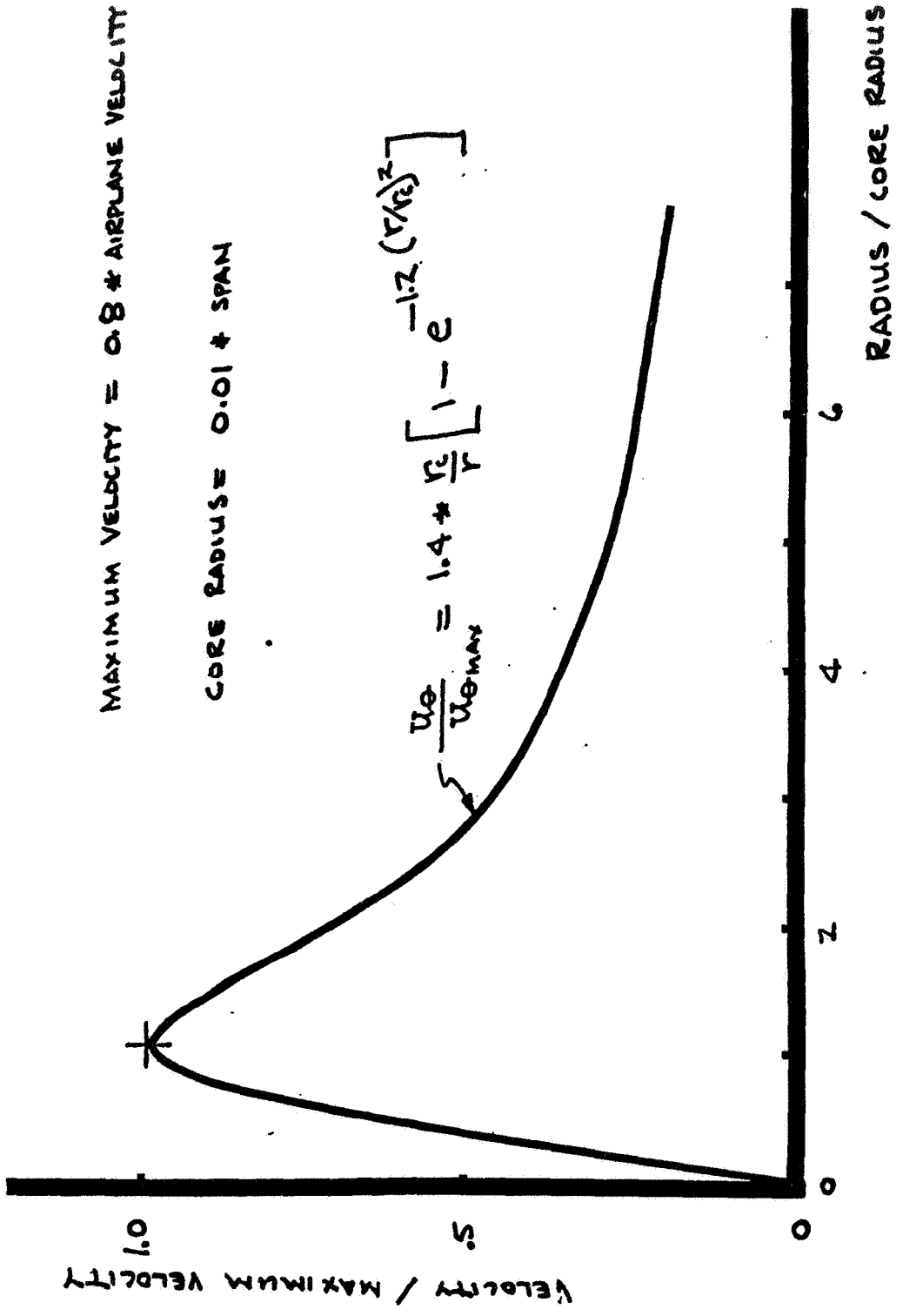

Figure 4. Vortex Velocity Distribution

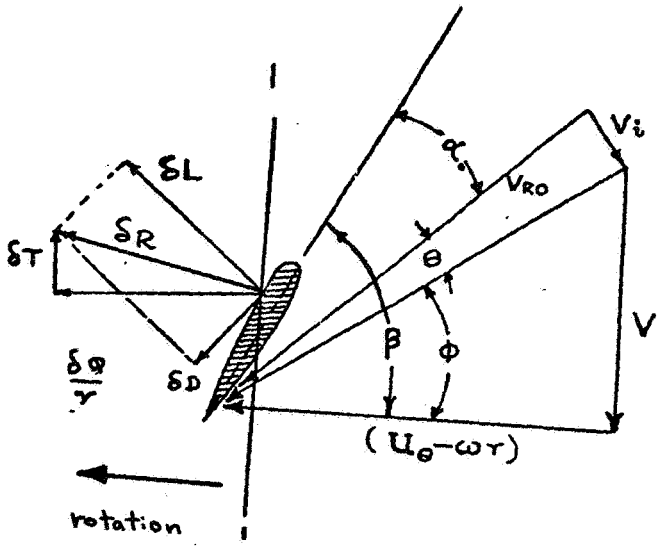

Definitions:

β = blade pitch

ϕ = effective pitch

θ = induced angle

α_o = effective angle of attack

δL = section lift

δD = section drag

δR = section resultant force

δT = section thrust

$\frac{\delta Q}{r}$ = section torque/radius

V = airplane velocity

V_i = induced velocity

V_{RO} = relative velocity

U_θ = swirl velocity

ωr = blade velocity

Figure 5. Blade Element Velocities and Forces

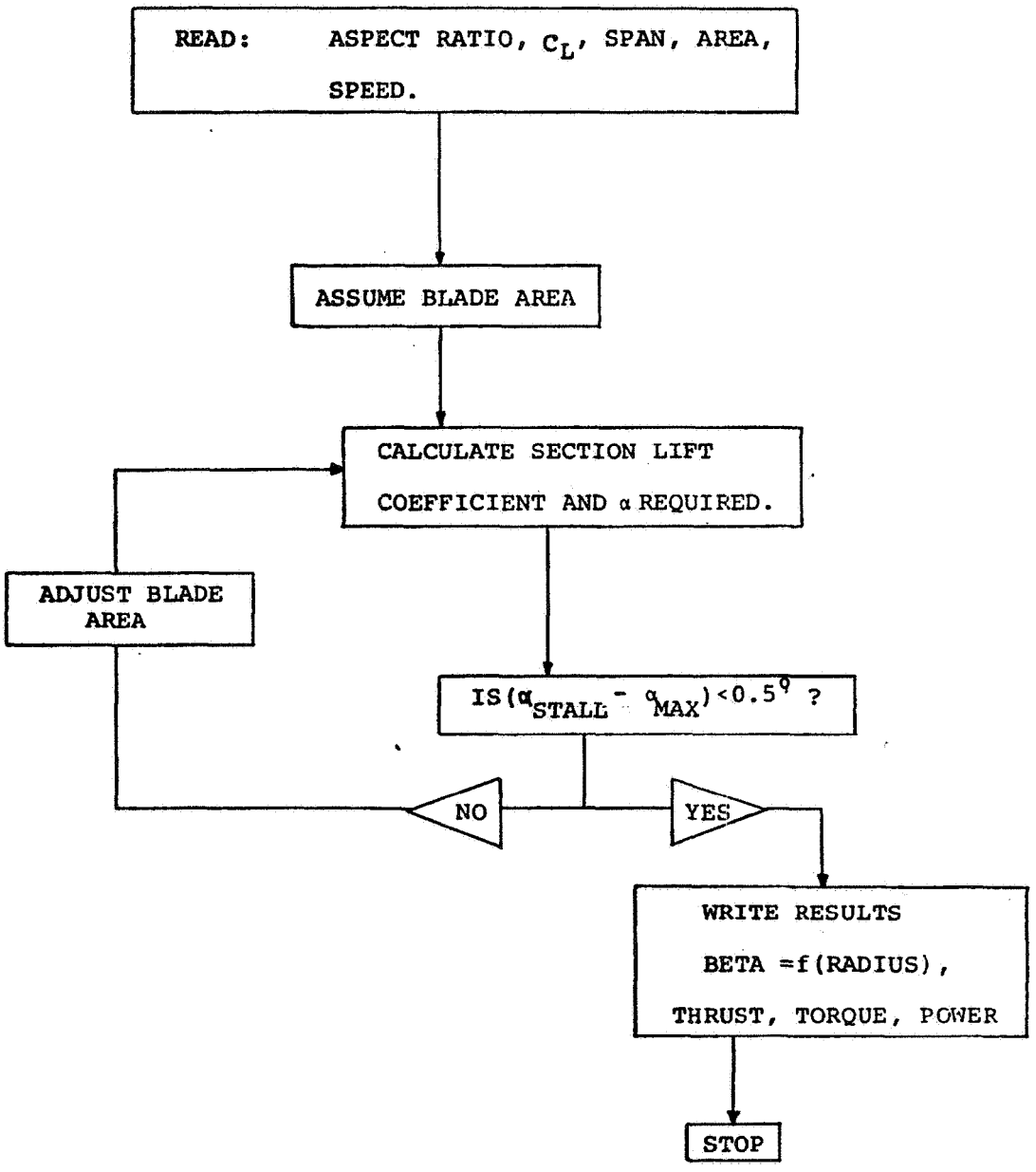

Figure 6. Tip Turbine Design Computer Program

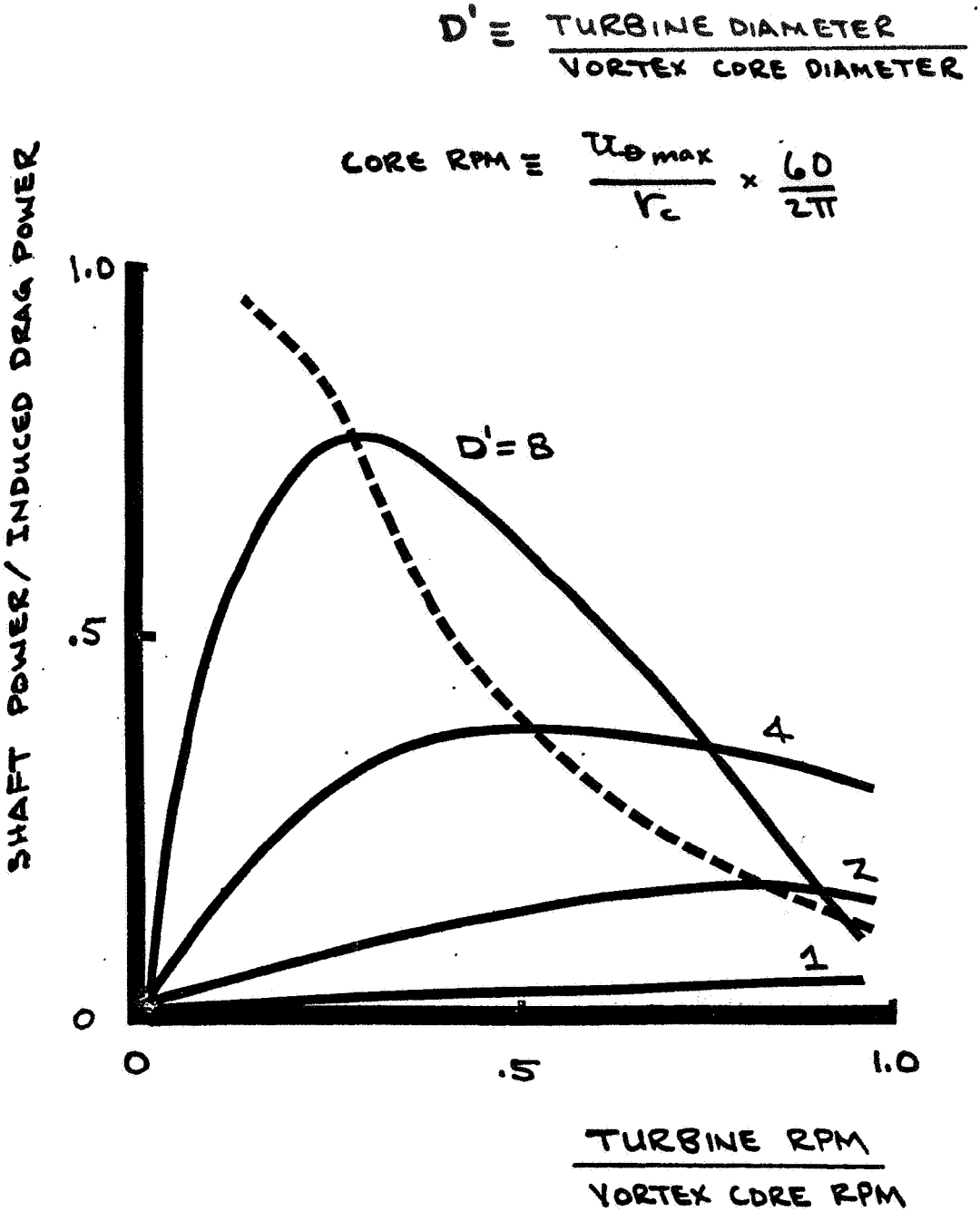

Figure 7. Shaft Power Ratio

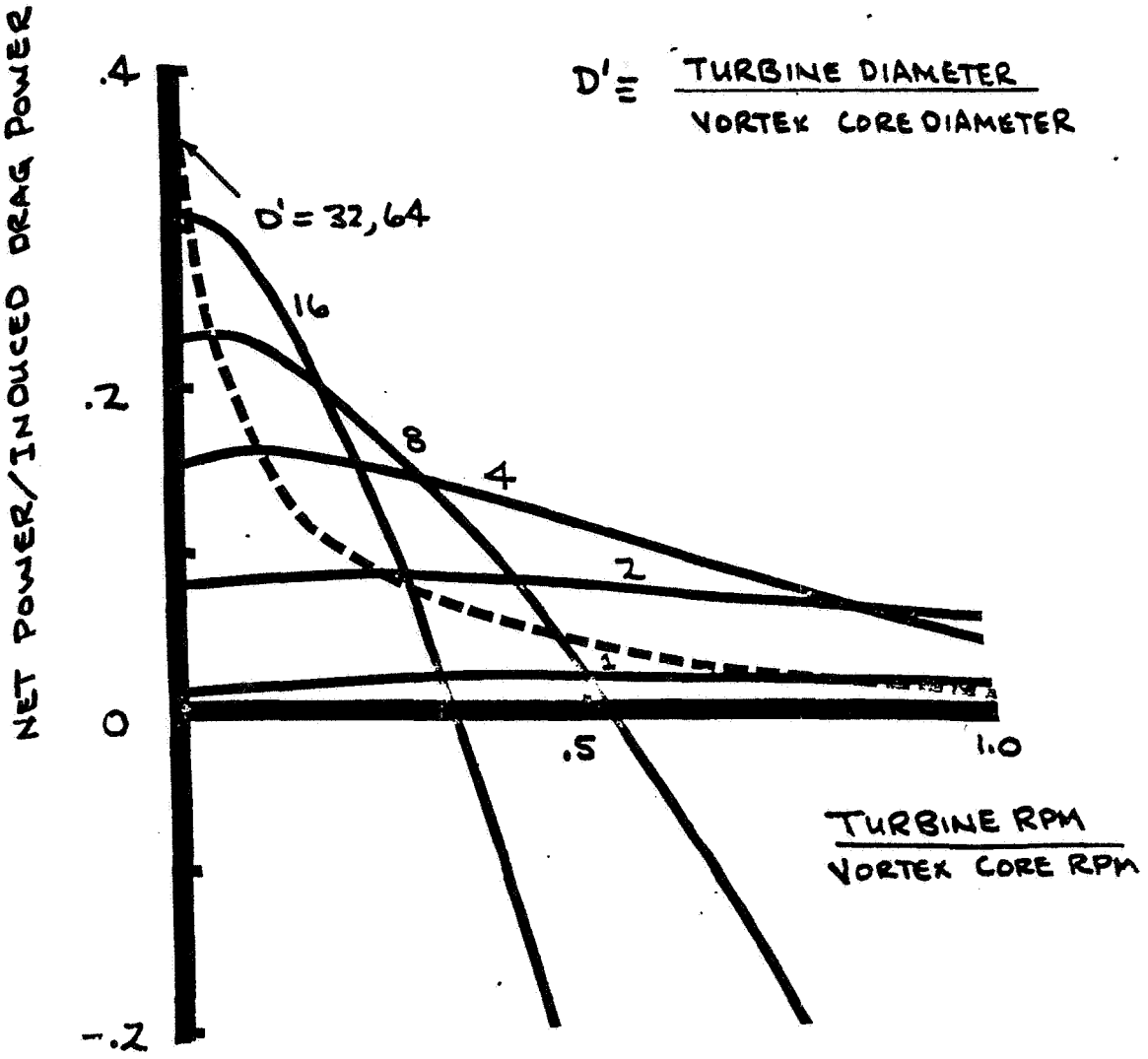

Figure 8. Net Power Ratio

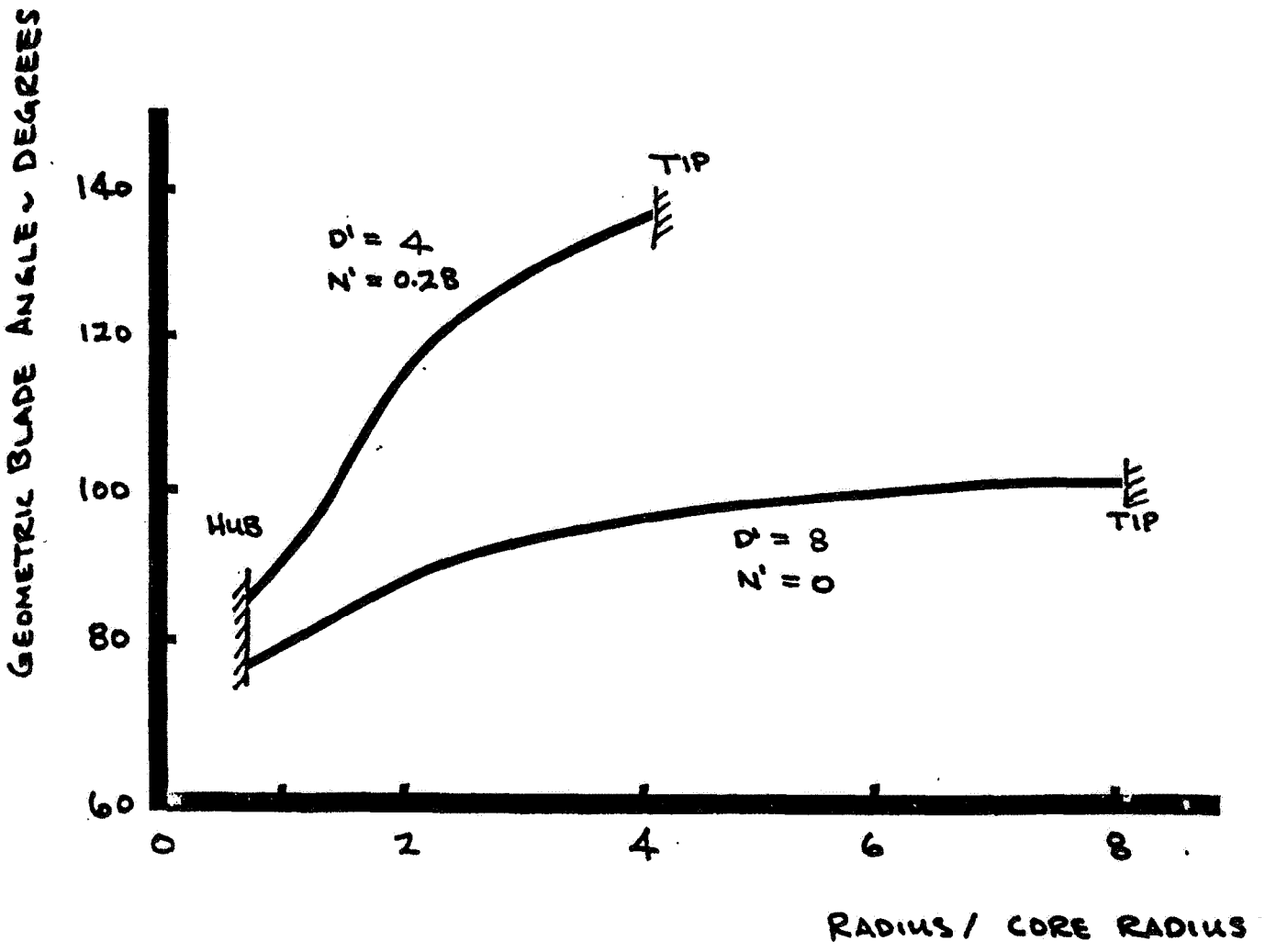

Figure 9. Blade Twist

5.6 Wing Tip Vortex Drag

Vincent U. Muirhead
University of Kansas

Introduction

The drag of a wing may be classified as composed of pressure drag, induced drag and skin friction drag. The induced drag which is the result of producing lift is induced by the vortex system set up around the finite three dimensional wing. By decreasing the strength of the trailing vortices, the induced drag may be reduced. The basic problem is to decrease the vortex without increasing the pressure and skin friction drag so that the total is decreased, or maximizing L/D.

The actual induced drag in pounds is:

$$D_i = \frac{W^2}{\pi b^2 qe}$$

By changing planform e may be varied up to the value for the ideal of the elliptical span loading. However, a two dimensional equivalent wing requires a maximum value of circulation of only $\pi/4$ that of the maximum for an elliptical wing loading. Thus, if the shed vortex could be reduced by this amount, the induced drag would be reduced 21 percent. Since induced drag accounts for 25 percent to 40 percent of the total aircraft drag, this would mean a total reduction of 5 percent to 8 percent over the elliptical loading. A number of methods such as wing tip end plates, tip tanks and winglets have been used or tested to provide an effective increase in aspect ratio and achieve a more two dimensional wing loading. In order to control the wing tip vortices the basic vortex characteristics need to be considered.

Basic Vortex Characteristics

The basic characteristics of the vortex are shown in the tornado[1], Figure 1. The core flow region and the free vortex region are clearly evident. Laboratory investigations[2] have shown that the strength of an unconfined vortex such as the wing tip vortex is a direct function of the vorticity present and the sink pressure and the area to create a core flow to organize the vorticity into a vortex. The circulation type vortex is shown in Figure 2, large diameter with little axial flow. Introducing an axial pressure differential, Figures 3, 4, and 5 show the development into a strong compresible flow vortex, Figure 6. Figure 7, the circulation is

continued with a large decrease in axial pressure differential. Vortex breakdown occurs. Figure 8 shows the continuation of the compressible flow vortex with pressure differential only. The rotation of the cage has been stopped. The basic vortex is unstable and wanders around. Figure 9 shows the pressure trace at a fixed point as the compressible core, Figure 6, moves over and around the point. Idealizing the compressible flow vortex the core flow, pressure and density are shown in Figure 10. Figure 11 shows the formation of two compressible flow vortices shown in Figure 12. Using neutrally buoyant helium bubbles the compressible core flow is evident in Figures 13 and 14. Continuing circulation and decreasing the axial pressure differential, the core flow breaks down, Figures 15 and 16.

The vorticity shed in producing lift and the sink provided by the negative pressure region on the upper surface must both be minimized and/or neutralized to decrease the induced drag. Laboratory tests have shown that the introduction of pressure in the core will stop the core flow and dissipate the vortex. An obstruction screen or splines can be introduced into the core flow to attenuate the vortex. Counter vorticity likewise is effective in reducing the vortex. In a number of tests the introduction of turbulence by various means has set up instabilities in a vortex which has hastened its decay. Thus, there are a number of avenues available for some measure of vortex control.

Wing

The basic object is to maximize the wing L/D for a particular operating condition for a given aircraft. Most of the research to date on the wing-tip vortex has been conducted for the purpose of attenuating the vortex downstream of the aircraft, Figure 17. A drogue device properly positioned downstream of the wing tip causes breakdown, Figure 18. A jet engine simulator at the tip with a high-energy jet blast produces the same results.

To increase L/D by decreasing the induced drag the two basic parameters of the vortex must be controlled:

1. The vorticity shed by the wing must be minimized.
2. The low pressure region on the top of the wing must be blocked from the shed vorticity. It is the wing-tip vortex core flow (or deficit flow) that is largely responsible for producing the induced drag.

The vorticity may be reduced by plates, tip-tanks, winglets and counter vortex flow which effectively increase the aspect ratio of the wing. The general effect of these on L/D are shown in Figures 19, 20, and 21. It will be noted that

there is a particular angle of attack at which the device offers the largest advantage. It would be expected that any one of these could be optimized further as to size, shape, angle and contour for a given angle of attack of the wing.

Efforts to use a jet have been directed at reducing vorticity downstream. Figure 22 shows the effectiveness of various jet strengths on the dissapation of vorticity. Obviously the upstream jet is not effective in reduction of L/D. The proper use of the downstream jet may be part of the answer. Again the size, location and strength must be optimized for maximum L/D.

The Method of Approach

The method of approach for optimization of L/D through minimizing induced drag should be through a detailed flow study together with force, pressure and vorticity measurements. Flow visualization with neutral helium bubbles, Figure 23 and 24, provides an excellent means of observing the effects of configuration changes. A systematic wind tunnel investigation of a large number of configuration changes should be made. The study should explore all avenues which appear promising as the study progresses even though it may lead to the rebirth of the biplane or triplane.

References

1. Muirhead, V.U., "Compressible Vortex Flow," AIAA Paper No. 73-106, 11th Aerospace Science Meeting, New York, New York, January 1973.
2. Eagleman, J.R.; Muirhead, V.U.,; Willems, N., Thunderstorms, Tornadoes, and Building Damage, Lexington Books, D.C. Heath and Company, Lexington, Mass., 1975.

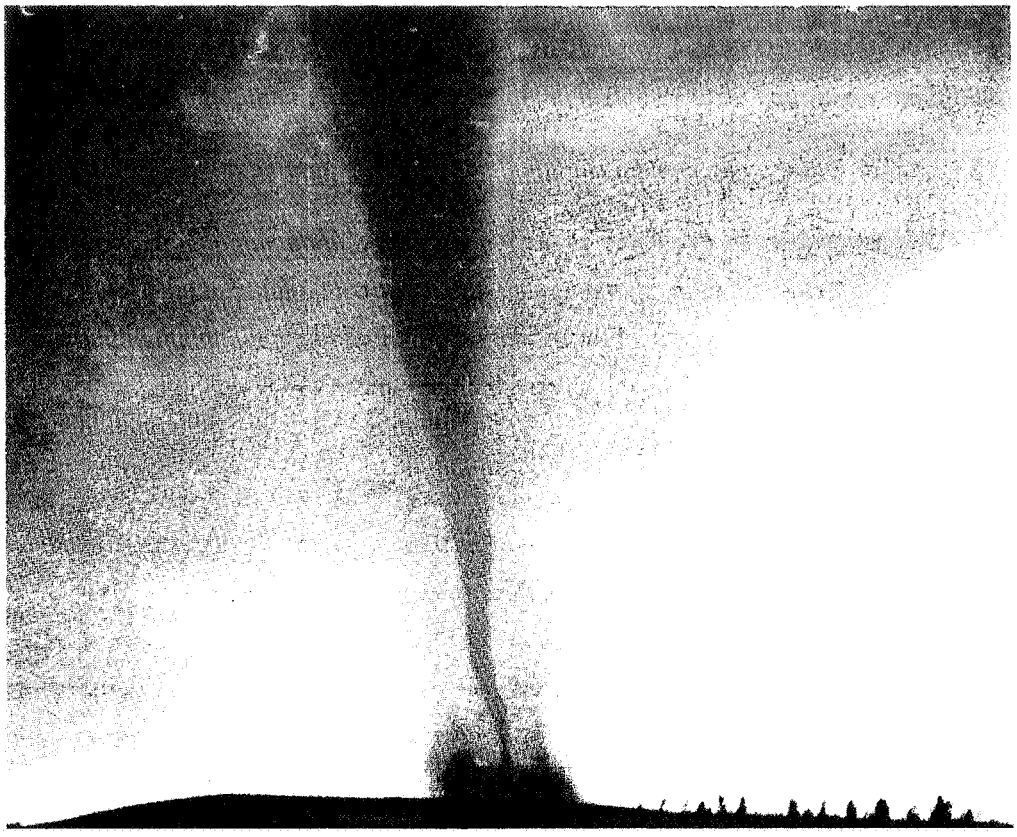

Figure 1. Tornado

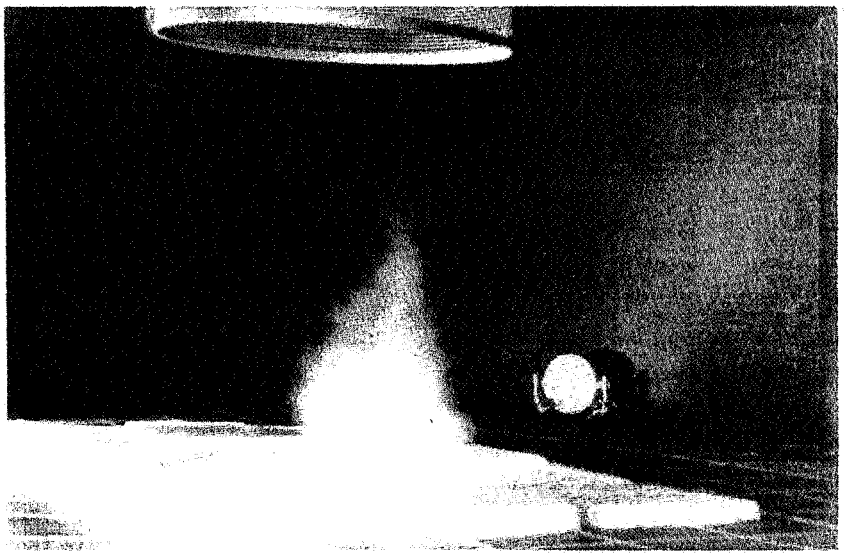

Figure 2. Circulation Vortex

Figure 3. Introduction of Axial Pressure Differential

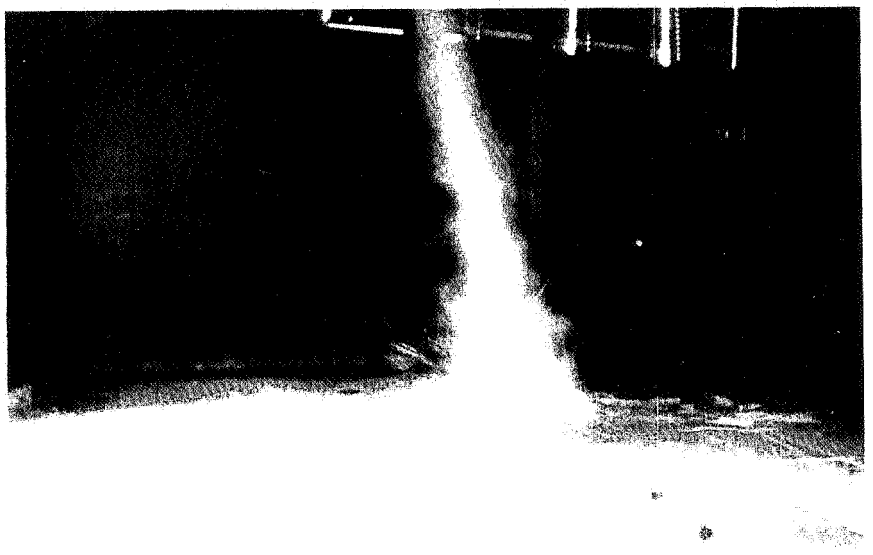

Figure 4. Early Vortex Development

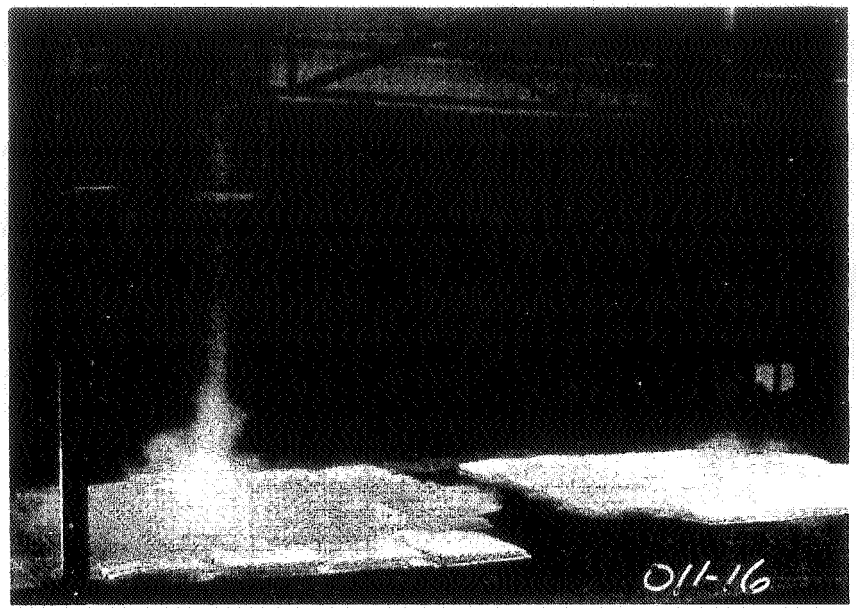

Figure 5. Vortex Development - Spiral Vortices

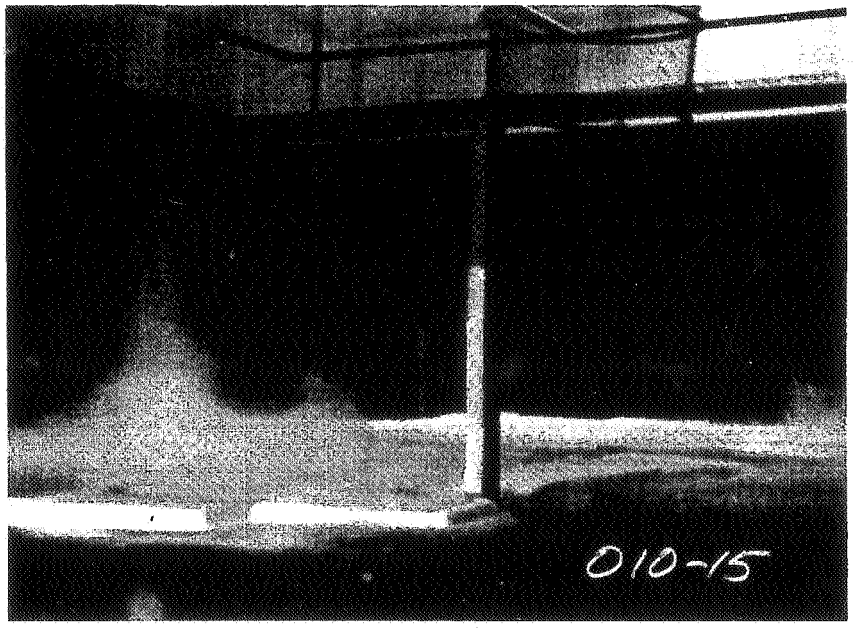

Figure 6. Compressible Vortex Flow

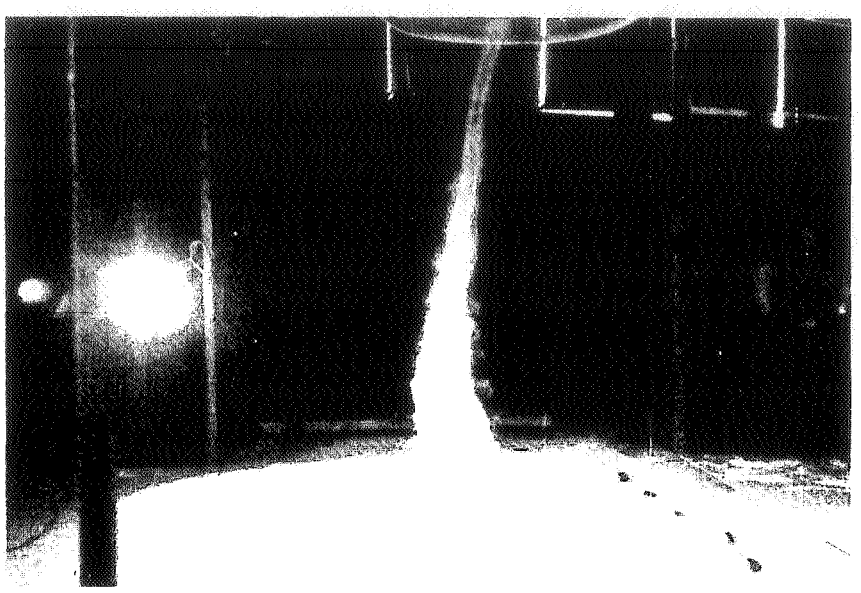

Figure 7. Vortex Breakdown - Circulation with Decreasing Axial Pressure Differential

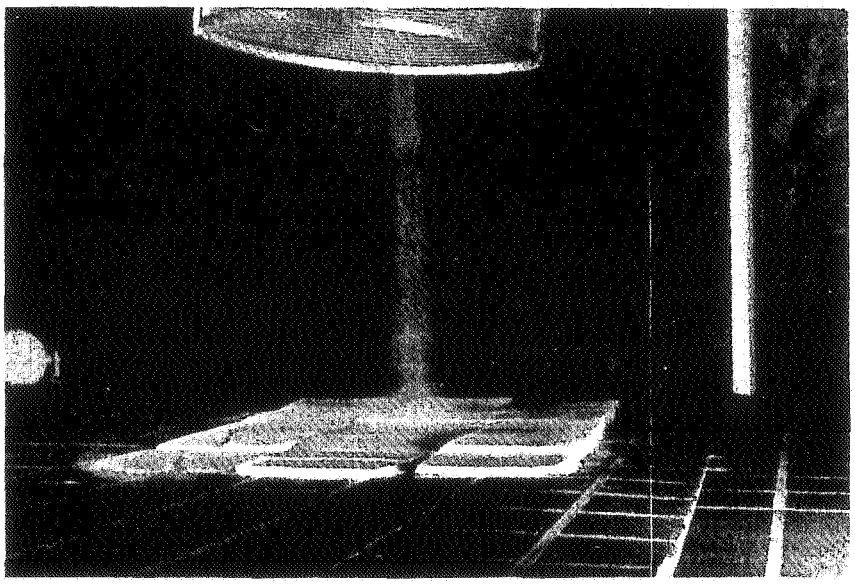

Figure 8. Vortex Sustained by Axial Pressure Differential

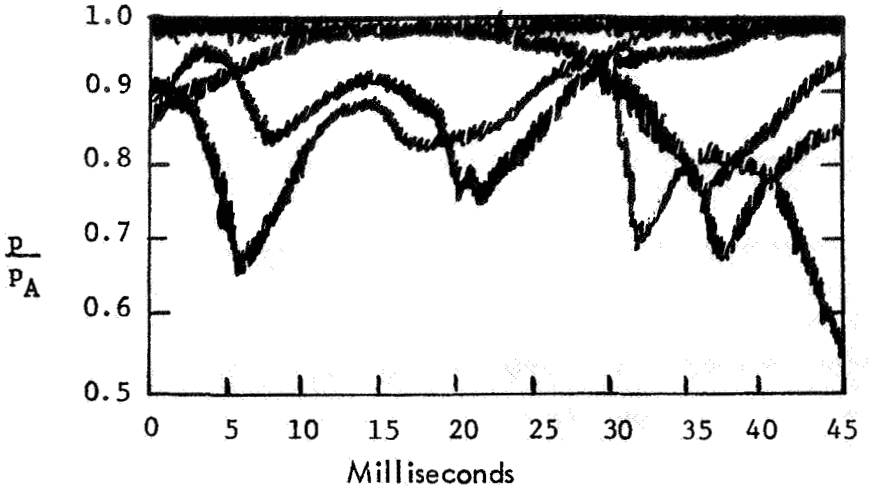

Figure 9. Pressure Traces

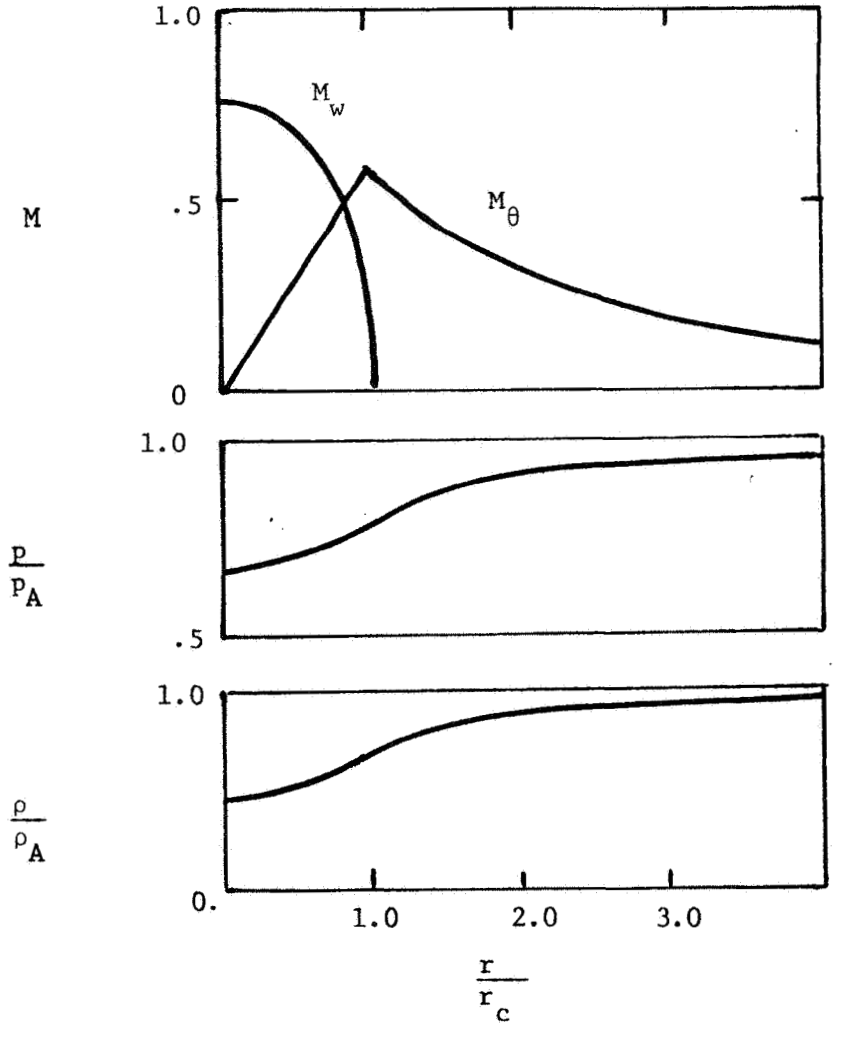

Figure 10. Compressible Vortex Core Conditions

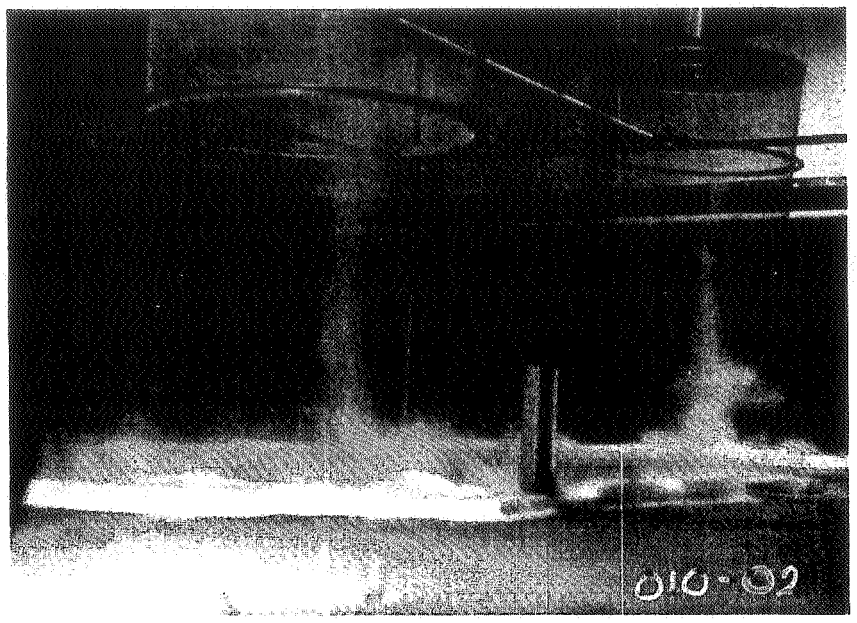

Figure 11. Two Vortices Forming

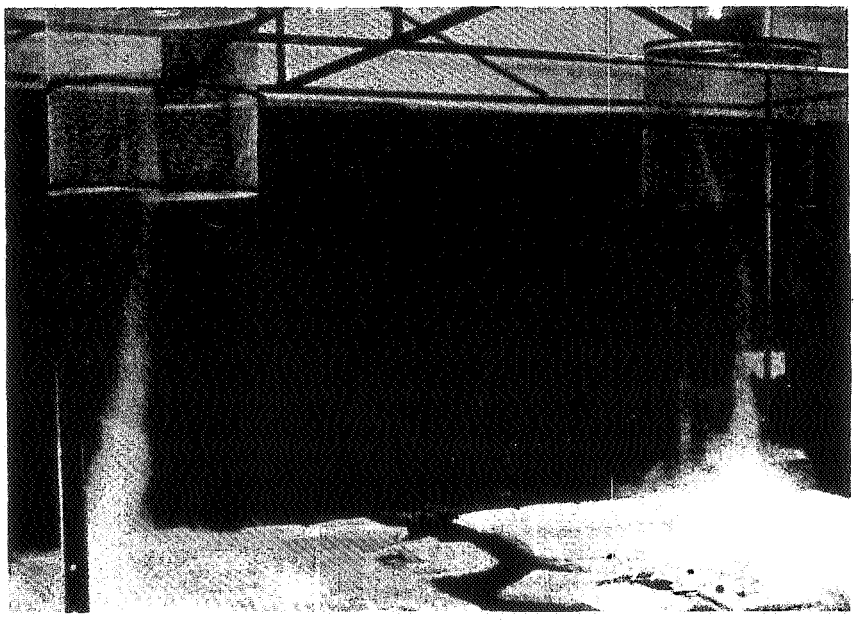

Figure 12. Two Strong Compressible Vortices

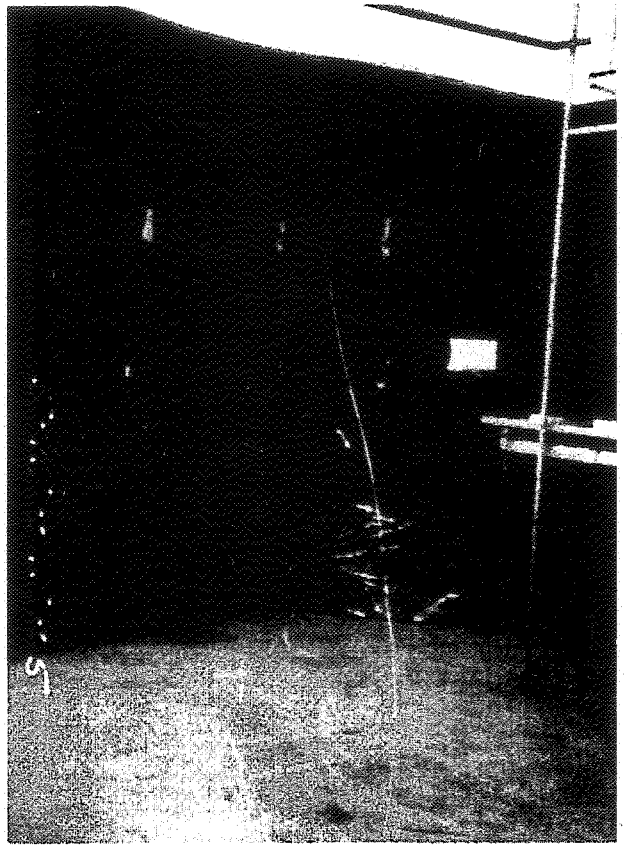

Figure 13

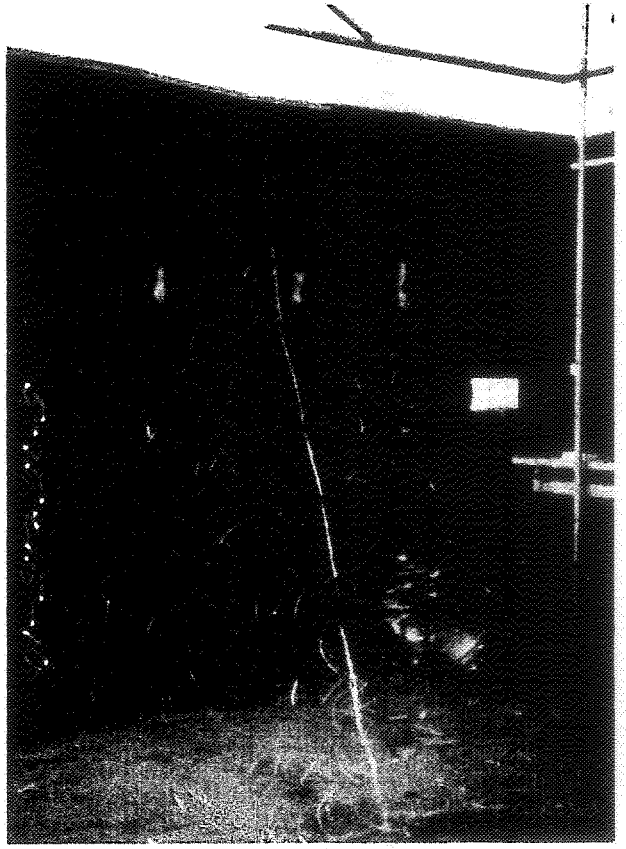

Figure 14

Visualization of Compressible Core - Helium Bubbles

Figure 16

Figure 15

Vortex Breakdown - Helium Bubbles

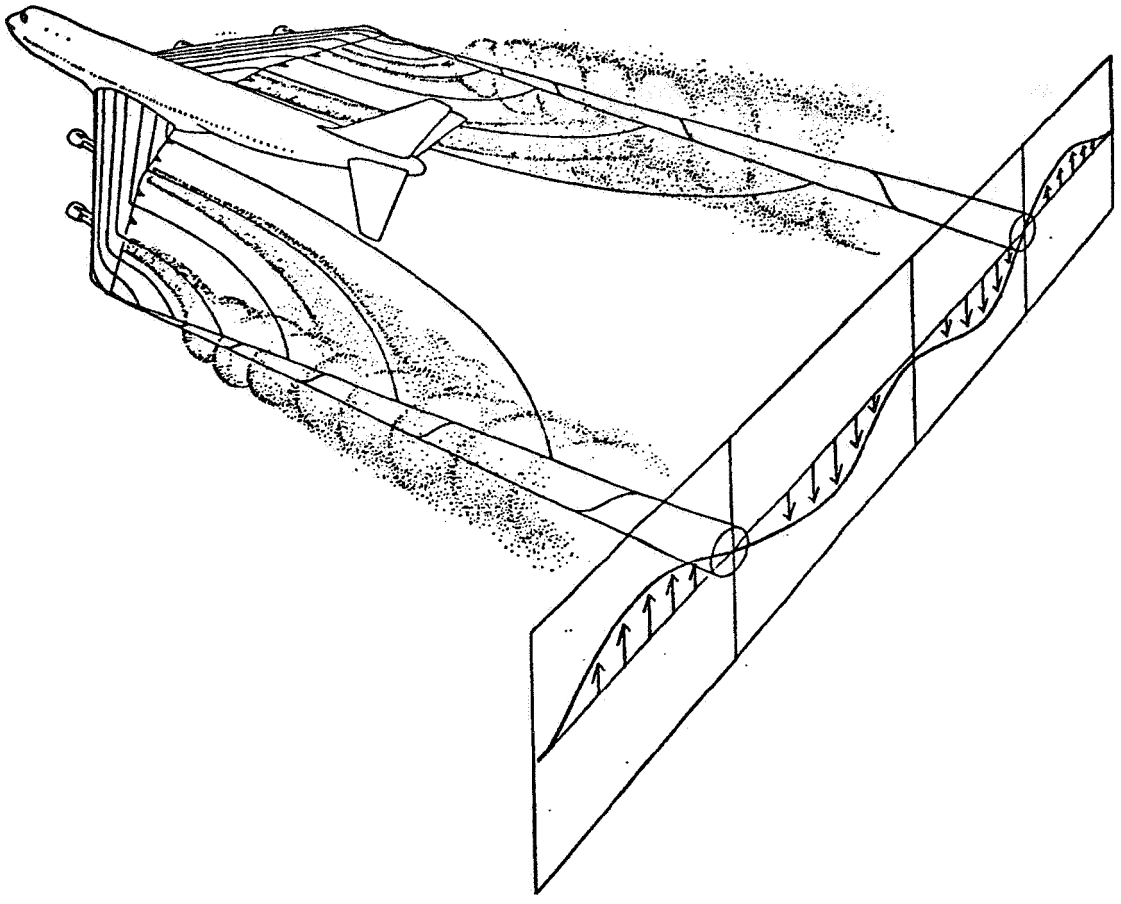

Figure 17. Vortex System

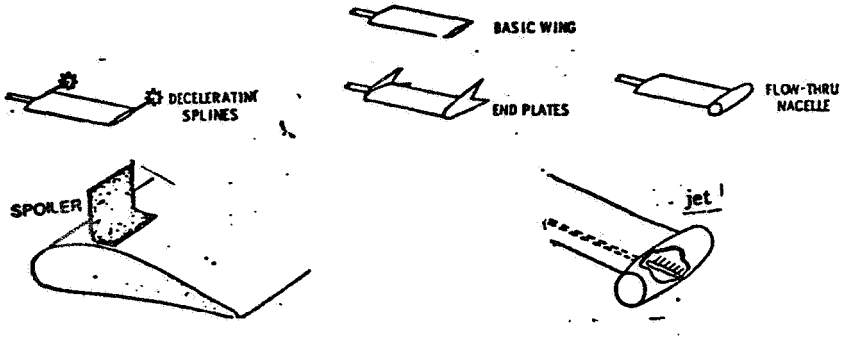

Figure 18. Attenuation Methods

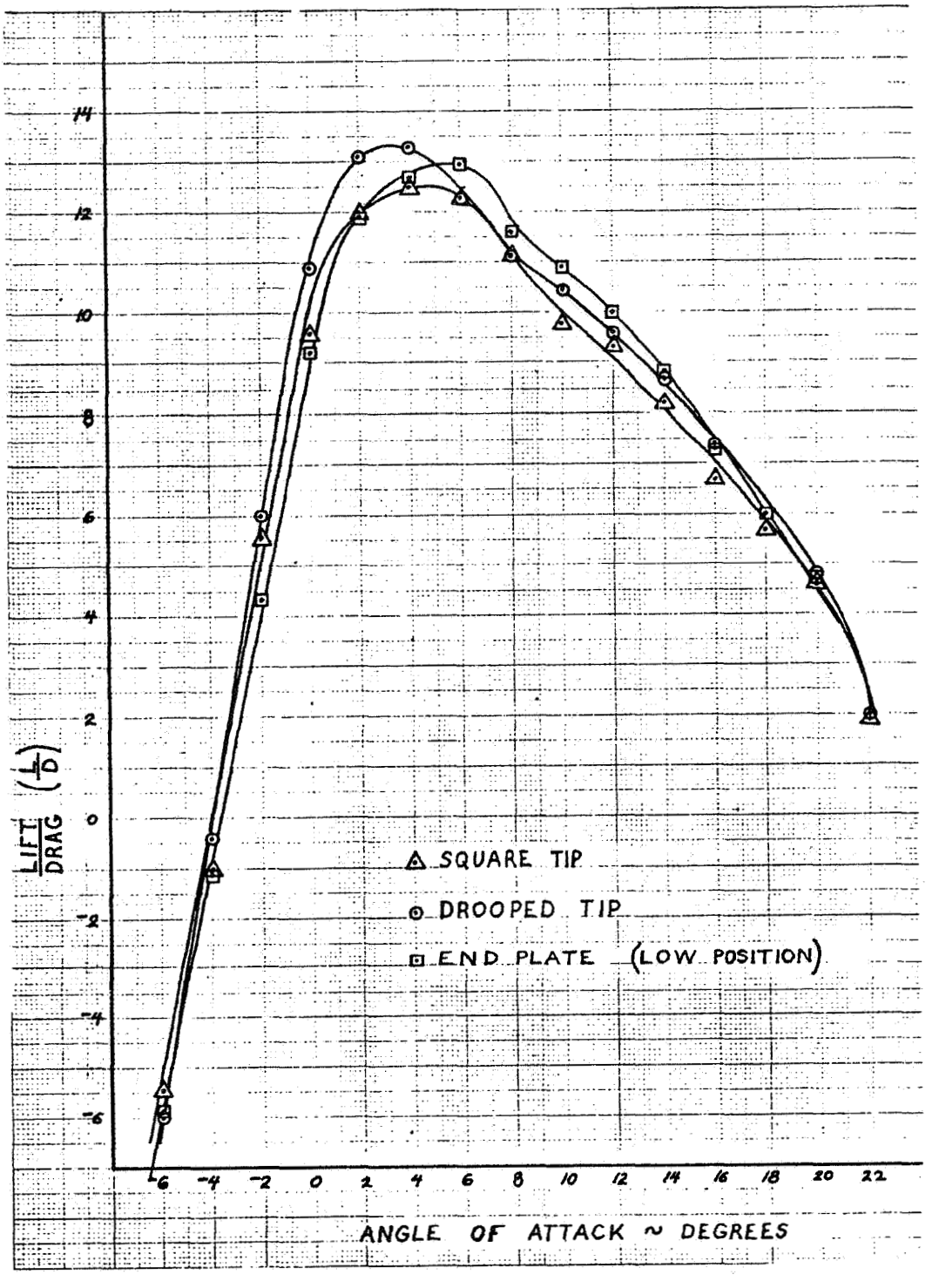

Figure 19. L/D of Wing Tip Configurations

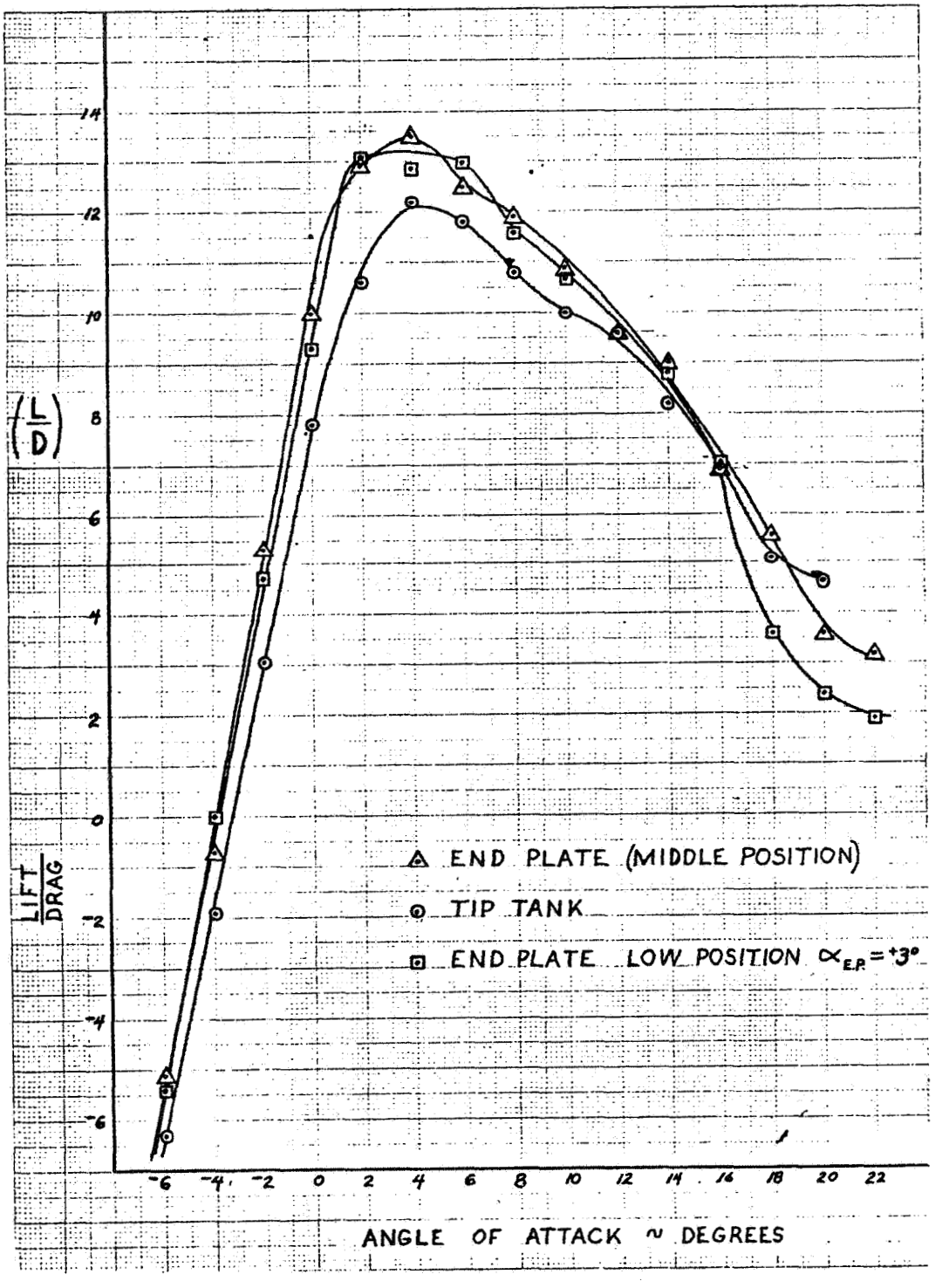

Figure 20. L/D of Wing Tip Configurations

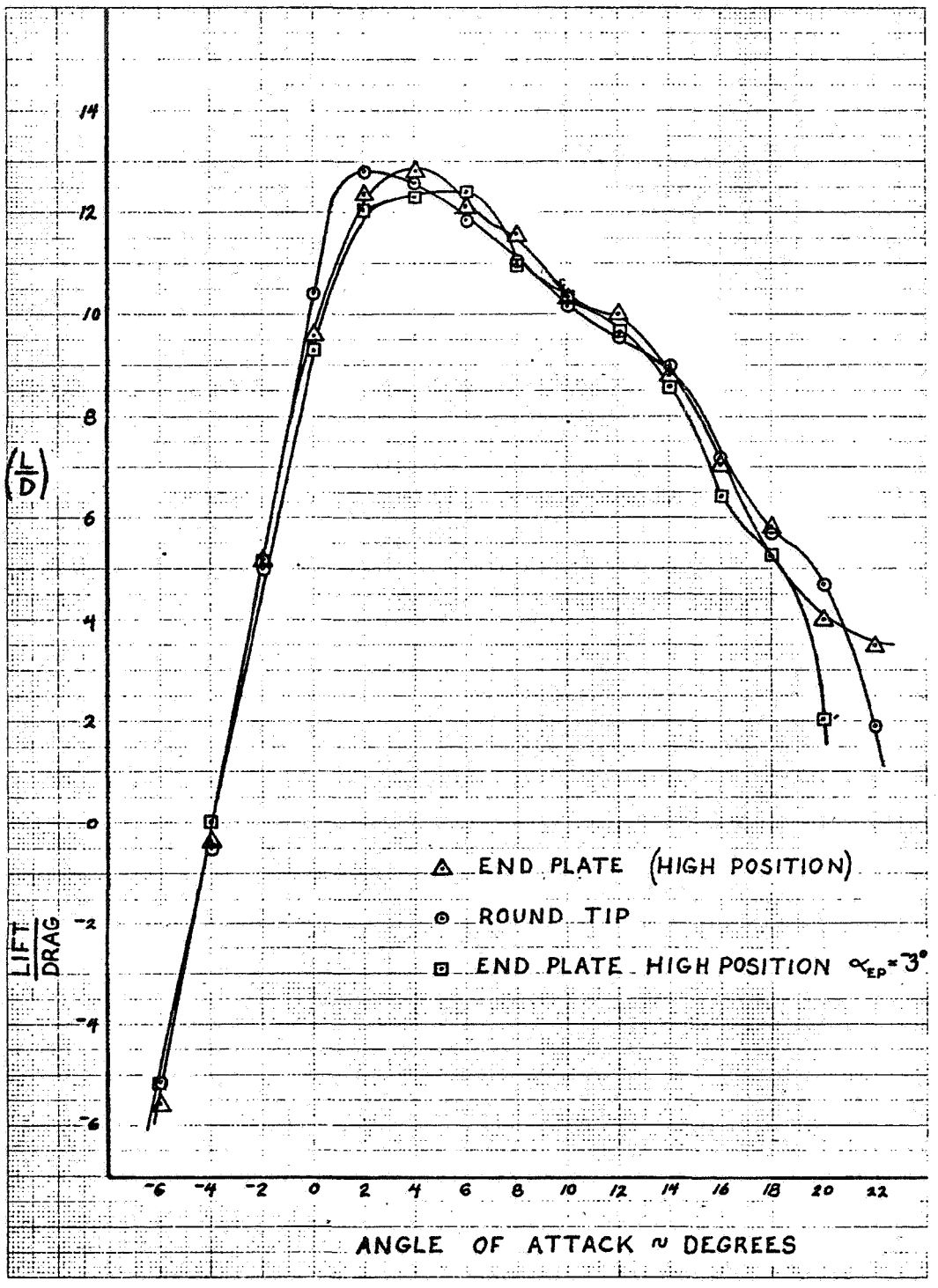

Figure 21. L/D of Wing Tip Configurations

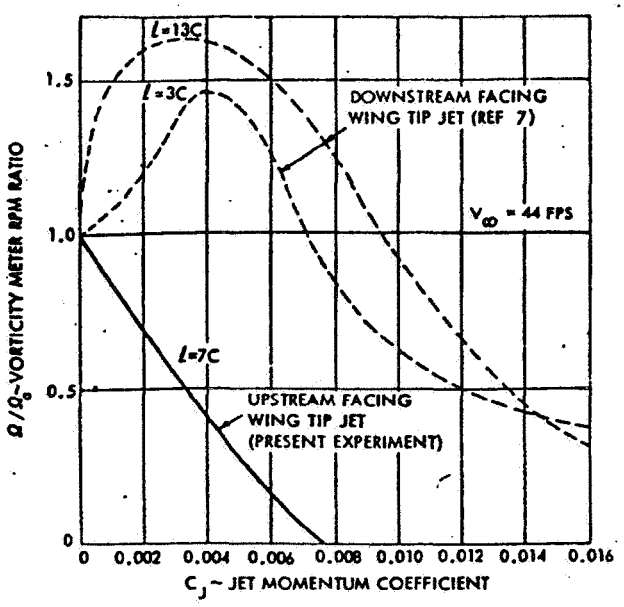

Figure 22. Jet Effect on Wing Tip Vortex

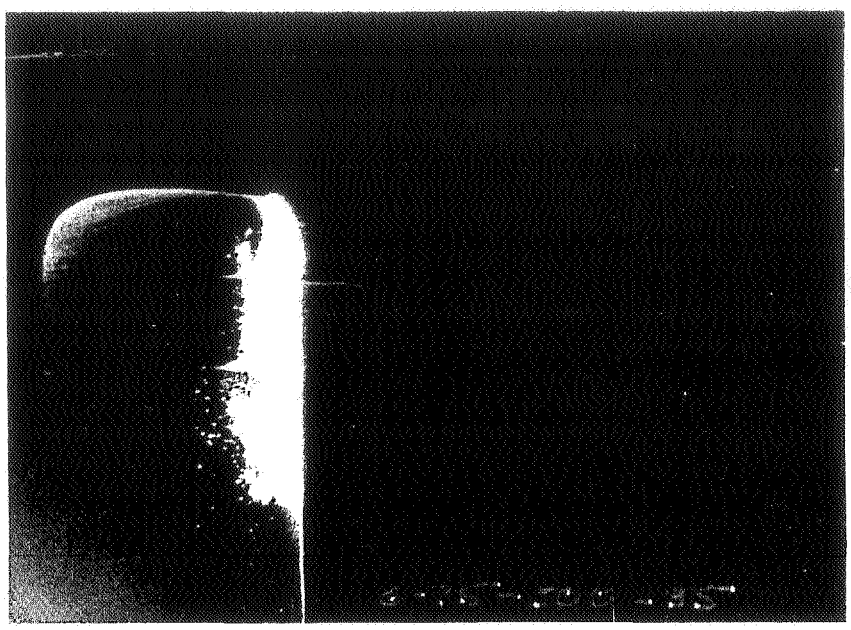

Figure 23. Rounded Wing Tip - Flow Visualization

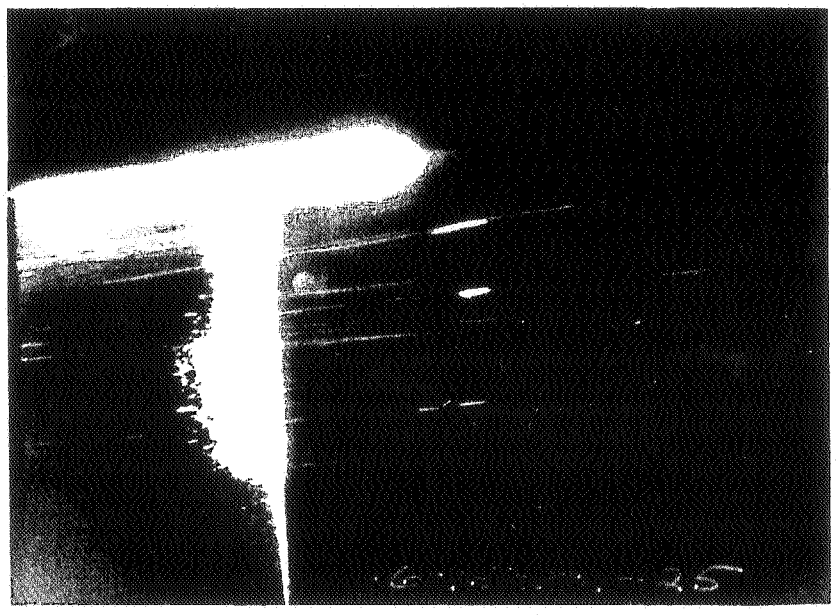

Figure 24. Wing Tip Plate - Flow Visualization

6. PAPERS OF SESSION IV - EXTERNAL DRAG AND INTERFERENCE DRAG

6.1 Overview of External Nacelle Drag and Interference Drag

Ronald D. Neal
Gates Learjet Corporation

Introduction

The purpose of this paper is to provide a written outline record of an oral presentation given at the General Aviation Drag Reduction Workshop.

Historical Review of Multi-Jet Engine Installations

Airplane performance is achieved thru a combination of aerodynamics and propulsion. In terms of the propulsion system, airplane configurations--be they powered by propellers or jets--are developed around the characteristics of a specific engine. For this reason, the integration of the powerplant and the airframe is truly the cornerstone of the aircraft design. The introduction and continued development of the turbine engine has only served to emphasize the importance of achieving a successful engine/airframe interface.

The beginning of the jet age took place on August 27, 1939, when the German Heinkel HE-178 research airplane made its first flight. This airplane was powered by a single gas turbine engine having a thrust of about 1,100 pounds.

The next jet airplane--and the first twin engine jet--was another Heinkel design, the He-280. Powered by two 1,320 pound thrust engines, this airplane made its initial flight in April 1941.

The next jet to fly was the Messerschmitt Me262, which was powered by two 1,850 pound thrust axial flow turbine engines, with the first flight occurring in July 1942. The Me262 certainly ranks as one of the most advanced aircraft designs to be developed during the Second World War and it also has the distinction of being the first jet aircraft to reach operational status.

By the end of the war, the German aviation industry had developed several jet aircraft designs. Examples of actual production flight hardware include the single-engine He-162 fighter and the twin-engine AR234 bomber.

The first allied jet to fly was the British Gloster E28/29. This airplane, powered by a single 860 pound thrust gas turbine engine, designed by Frank Whittle, made its initial flight in May 1941.

The United States entry into the jet era took place on October 1, 1942, when the twin-engine Bell XP-59A "Airacomet" took to the air.

The second American jet to fly was the single-engined Lockheed XP-80, with this flight taking place in June 1944. Neither the P-59 or the P-80 were to see combat in World War II, however, in November 1950, in the skies over Korea, an F-80 became the winner of the first all-jet aerial combat by downing a Russian built MIG-15.

The post-war years ushered in a whole new era in aircraft design. Examples of some of the multi-engine airplanes flown in this period include the twin-engine B-43, the three-engined B-51, the four-engined B-45 and B-46, the six-engined B-47 and B-48, and the eight-engined B-52.

In July 1949, the four-engined deHavilland Comet 1 made its first flight and the dawn of commercial jet transportation had begun. America's first jet transport was the Boeing 707 which made its maiden flight in July 1954, with the first 707 transatlantic service beginning in October 1958. The introduction of jet service on this transatlantic route reduced the flight time from twelve hours to seven hours.

In May 1955, the French entered the commercial transport field with the Sud-Aviation Caravelle. The Caravelle, with its two jet engines mounted on the aft fuselage, represented a design innovation that is still in vogue some twenty years later. The commercial aft-engine jet transports that have been developed thru the years include the following:

Sud-Aviation Caravelle
BAC-11
Douglas DC-9
Fokker F-28
TU-134
Yak-40(3-engine)
Yak-42 (3-engine)
Boeing 727
Hawker Siddeley Trident (3-engine)
TU-154 (3-engine)
Ilyushin Il-62 (4-engine)
BAC VC-10 (4-engine)

It is perhaps of historical interest to note that the original patent for the Caravelle design was filed in November 1951, and was entitled "Improvements in Aeroplanes Propelled by Several Jet Engines."

Development of Business Jet Aircraft

With the successful introduction and acceptance of commercial jet transports it was only a question of time until the performance potential of turbine power was applied to the general aviation airplane.

The origin of the business jet can be traced to the four-place, French built Morane-Saulnier MS760, which first flew in mid-1954. However, a 1955 attempt by Beech Aircraft to market this airplane in North America can best be described as unsuccessful.

The next airplane to enter the small jet transport arena was the Lockheed Jetstar, with the original twin-engined prototype flying in September 1957. The Jetstar was originally designed for the military market in response to the UCX program for a small jet transport with the eventual outcome of this effort being the four-engined C-140.

The next airplane to come along was the North American Sabreliner flying in September 1958, as an entry into the military UTX competition for a trainer category airplane.

The third small transport took to the air in February 1959, when the four-engined McDonnell Model 220 flew, with this airplane also competing for the UCX contract.

In the final analysis, the Jetstar won the UCX race, the Sabreliner took the UTX contract and McDonnell dropped the Model 220 program.

The next period of activity in this field took place in 1962, when the first deHavilland DH 125 flew. The following year, 1963, produced a bumper crop of airplanes with the first flights of the Jet Commander, the French designed Mystere 20, and the Lear Jet taking place. The swept-forward wing German Hansa Jet and the Italian PD808 made their first flights in 1964. A new era in big business jets began when the Grumman Gulfstream II made its initial flight in 1966. The latest business jets to join the field include the Cessna Citation, the Falcon 10, and the Corvette.

All of these business jets (with the exception of the MS760 and the McDonnell 220) are of the aft fuselage mounted engine configuration.

While the large commercial transports and the smaller business jets are similar in configuration, there is a difference between the two designs. Specifically the aft-engined transport aircraft tend to have the nacelles located well aft of the wing trailing edge, for example the DC-9 and 727. In the case of the smaller airplanes, the nacelles are located quite close to the wing and in several designs the nacelles overlap the wing. Because of the proximity of the nacelles to the wing, the business jet offers some challenging design problems in terms of achieving a minimum drag configuration.

Also, the trend in business aircraft design has been towards the incorporation of high bypass fan engines. These engines, with their larger physical size, make it

very difficult to arrive at a wing mounted engine arrangement that is compatible with a high performance business jet design. Thus, the aft-engined airplane appears to be a viable configuration in the years ahead.

A good example of the size impact of a turbofan engine is shown by the Learjet testbed airplane which incorporated the General Electric CJ610 turbojet engine on one side and the AiResearch TFE 731 turbofan engine on the other side.

Current Business Jet Engine Installations

Slides number 44 through 50 provide installation photos of various turbojet/turbofan aft fuselage mounted engine arrangements on current business jet designs.

Comments on some of the aerodynamic aspects of the installations were offered.

Aft-Engine Nacelle Drag Considerations

Viewgraph 1* presents sketches of a long fan duct and a short fan duct nacelle considered for the FTE 731 installation on the Learjet Model 35/36.

Viewgraph 2 presents a typical nacelle configuration trade-off that can be made for various design studies.

Viewgraph 3 presents wing pressure distribution as affected by nacelle position (data from Reference 9).

Viewgraph 4 presents typical nacelle drag characteristics for a turbojet engine installation and Viewgraph 5 shows the drag characteristics for a turbofan nacelle.

Viewgraphs 6 and 7 show some nacelle geometry configurations.

Viewgraphs 8 thru 12 present some nacelle drag results obtained with various nacelle locations.

Third-Engine Location

For a three-engined airplane there are two rather obvious locations for two of the engines, either on the aft fuselage or wing mounted. As for the third engine, there are also at least two options with examples being the S-duct (727, L-1011) or the straight-through duct (DC-10).

There appears to be little published information on comparisons between these two types of installations. Boeing has reported (Reference 18) that their studies have shown that the weight/performance trade between the S-duct and straight-duct is about even. Design studies conducted by Lockheed have shown that the S-duct offers better

*Viewgraphs not included in written version for proprietary reasons.

overall performance than a straight-duct. On the other hand, McDonnell-Douglas studies have identified the performance improvements of the straight-duct over the S-duct.

The final choice for the type of third engine installation is not completely clear, however, in terms of numerical numbers the S-duct is the winner. If the weight and drag are in fact an even trade between the two concepts, then other installation factors will dictate the final selection. In fact, as part of the Advanced Transport Technology (ATT) studies, United Airlines (Reference 20) preferred the S-duct from an engine maintenance viewpoint due to the lower engine position.

In the small transport category of aircraft, both the proposed Cessna 700 and the Falcon 50 have elected to utilize the S-duct arrangement.

In terms of an historical viewpoint the Martin XB-51, which flew in October 1951, had its third engine located in the rear fuselage with inlet air being provided via an S-duct configuration.

From the civil aviation standpoint, Sud-Aviation applied in December 1951, for a patent covering "Improvements in Aircraft Equipped with a Propelling Motor at the Rear" with this patent covering various S-duct configurations.

Slides number 62-67 provide illustrations of various third-engine installations. Viewgraphs 13 thru 15 provide additional information of S-duct configurations.

R & D Study Recommendations

a) There appears to be a need and requirement to investigate the interference drag of nacelle configurations mounted on the aft fuselage with specific emphasis on configurations having the nacelle in close proximity to the wing.

b) For high bypass ratio turbofan engines the drag interference problem of the short cowl nacelle on the aft fuselage should be examined.

c) There appears to be a need for published research information on the aerodynamics of S-ducts and other third-engine installation aerodynamics.

Reference Material

The following reference material presents some sources containing information relating to the overall subject of aft-engine installations and basic nacelle design considerations.

T-Tail/Aft-Engine Configurations

1. Taylor, Robert T., and Ray, Edward J., "Deep-Stall Aerodynamic Characteristics of T-Tail Aircraft." Conference on Aircraft Operating Problems, May 10-12, 1965, NASA SP-83, pages 113-121.

2. Ray, Edward J., and Taylor, Robert T., "Effect of Configuration Variables on the Subsonic Longitudinal Stability Characteristics of a High-Tail Transport Configuration." NASA TM-X-1165, October 1965.

3. Taylor, Robert T., and Ray, Edward J., "Factors Affecting the Stability of T-Tail Tranports." Journal of Aircraft, July-August 1966, pages 359-364.

4. Taylor, Robert T., and Ray, Edward J., "A Systematic Study of the Factors Contributing to Post-Stall Longitudinal Stability of T-Tail Transport Configurations." NASA TM-X-56882, November 1965.

5. Thomas, H.H.B.M., "A Study of the Longitudinal Behavior of an Aircraft at Near-Stall and Post-Stall Conditions." AGARD Conference Proceedings No. 17, September 20-23, 1966, pages 729-769.

6. Kettle, D. J., and Kerby, D. A., "Low-Speed Wing Tunnel Tests on the Effects of Tailplane and Nacelle Position on the Superstall Characteristics of Transport Aircraft." R.A.E. R&M 3571, August 1967.

7. Shevell, Richard S., and Schanfele, Roger D., "Aerodynamic Design Features of the DC-9." AIAA Paper 65-738, November 1965.

8. Waaland, I. T., and Curtis, E. J., "Gulfstream II Aerodynamic Design." SAE Paper 670242, April 1967.

9. Lobert, G., and Thomas J., "Engine Airframe Ingegration Problems Peculiar to Aircraft Configurations with Nacelles Mounted Above the Wing." Paper presented at 31st meeting of the AGARD Flight Mechanics Panel, Gottingen, Germany, September 13-15, 1967.

10. Putman, Lawrence E., and Trescot, Charles D., Jr., "Effects of Aft-Fuselage-Mounted Nacelles on the Subsonic Longitudinal Aerodyanmic Characteristics of a Twin-Turbojet Airplane." NASA TND-3781, December 1966.

11. Aoyagi, Kiyoshi, and Tolhurst, William H., Jr., "Large-Scale Wing-Tunnel Tests of a Subsonic Transport with Aft Engine Nacelles and High Tail." NASA TND-3797, January 1967.

12. Neal, Ronald D., "Correlation of Small-Scale and Full-Scale Wing Tunnel Data with Flight Test Data on the Lear Jet Model 23." SAE Paper 700237.

13. Williams, P. R. G., and Steward, D. J., "The Complex Aerodynamic Interference Pattern Due to Rear Fuselage Mounted Power Plants." AGARD Conference Proceedings No. 71, Aerodynamic Interference, September 1970.

14. Callaghan, J. T., Donelson, J. E., and Morelli, J. P., "The Effects on Cruise Drag of Installing Re-Fan-Engine Nacelles on the McDonnell Douglas DC-9." NASA CR-121219, May 1973.

15. Blaha, Bernard J., "Integration of Aft-Fuselage-Mounted Flow-Through Engine Nacelles on an Advanced Trasnport Configuration at Mach Numbers from 0.6 to 1.0." NASA TM-X-3178, March 1975.

16. Swan, Walter C., and Sigalla, Armand, "The Problem of Installing a Modern High Bypass Engine on a Twin Jet Transport Aircraft." AGARD Conference Proceedings No. 124 on Aerodynamic Drag, April 1973.

17. Williams, P. R. G., and Steward, D. J., "An Aircraft Designer's Review of Some Airframe and Engine Ingegration Concepts." Paper presented at 1st International Symposium on Air Breathing Engines, June 19-23, 1972.

18. Goodmanson, Lloyd T., and Schulta, William H., "Installation and Integration of Transonic Transport Propulsion Systems." SAE Paper 710762.

19. Hawkes, J. E., "Development Status of the L-1011 TriStar." SAE Paper 710755.

20. "Assessment of the Application of Advanced Technologies to Subsonic CTOL Transport Aircraft." NASA CR-112242, April 1973.

Nacelle Design

21. Saylor, James M. and Smith, Robert E., "Internal and External Aerodynamics of the C-141 Nacelle." AIAA Paper 65-604.

22. Allison, H. B., and Leslie, H. R., "Installation Considerations for High Bypass Ratio Turbofan Engines." AIAA Paper 67-390.

23. Viall, W. S., "Aerodynamic Considerations for Enginer Inlet Design for Subsonic High-Bypass Fan Engines." SAE Paper 660733.

24. Frazier, G. T., "Aerodynamic Considerations for Engine Exhaust Design for Subsonic High-Bypass Fan Engines." SAE Paper 660734.

25. Viall, W. S., "The Enginer Inlet on the 747." ASME Paper 69-GT-41.

26. Saylor, J. M., and Hancock, J. P., "C-5 Engine Inlet Development." ASME Paper 69-GT-52.

27. Hancock, J. P., and Hinson, B. L., "Inlet Development for the L-500." AIAA Paper 69-448.

28. Rohling, Walter J., "The Influence of Nacelle Afterbody Shape on Airplane Drag."

29. Leynaert, Jr., "Engine Installation Aerodynamics," paper given at AGARD Lecture, Series No. 67, Prediction Methods for Aircraft Aerodynamic Characteristics. AGARD-LS-67, May 1974.

Wing Mounted Nacelles

30. Patterson, James C., Jr., "A Wind-Tunnel Investigation of Jet-Wake Effect of a High-Bypass Engine on Wing-Nacelle Interference Drag of a Subsonic Transport." NASA TN D 4693, August 1968.

31. Patterson, James C., Jr., and Flechner, Stuart G., "Jet-Wake Effect of a High-Bypass Engine on Wing-Nacelle Interference Drag of a Subsonic Transport Airplane." NASA TND-6067, November 1970.

32. Raney, D. J., Kurn, A. G., and Bagley, J. A., "Wind Tunnel Investigation of Jet Interference for Underwing Installation of High Bypass Ratio Engines." ARC C.P. No. 1044, March 1968.

33. Kurn, A. G., "A Further Wind Tunnel Investigation of Underwing Jet Interference." ARC C. P. No. 1156, April 1969.

Powered Nacelle Testing

34. Fasano, A., Erlandsen P., and Barrett, D., "The Powered Nacelle as an Experimental Tool." AIAA Paper 70-636, June 1970.

35. Welge, H. R., and Ongaroto, J. R., "Powered Engine Simulator Porcedures and Experience for the DC-10 Wing Engine at High Subsonic Speeds." AIAA Paper 70-590, May 1970.

36. Grunnet, James L., "Designing Jet Aircraft Wing-Tunnel Test Programs with Propulsion System Simulation." J. Aircraft, Vol. 8, No. 6, June 1971.

List of Slides

1. He-178 Single-Engine Jet Airplane
2. He-280 Twin-Engine Jet Airplane
3. Me161 Twin-Engine Jet Airplane
4. He-162 Single-Engine Jet Airplane
5. AR 234 Twin-Engine Jet Bomber
6. Gloster E28/39
7. Bell XP-59
8. Lockheed XP-80
9. Douglas B-43
10. North American B-45
11. Convair B-46
12. Boeing B-47
13. Martin B-48
14. Martin B-51
15. Boeing B-52
16. Boeing 707
17. Caravelle
18. DC-9
19. Fokker F-28
20. BAC-111
21. Yak 40

22. 727
23. 11-62
24. VC-10
25. MS760
26. Jetstar
27. Sabreliner
28. McDonnell 220
29. DH-125
30. Jet Commander
31. Falcon 20
32. Learjet
33. Hansa Jet
34. PD808
35. Gulfstream II
36. Citation
37. SN600
38. Falcon
39. DC-9
40. 727
41. Learjet 35/36
42. Learjet Test Bed Airplane
43. Blank Slide
44. Front view of JT15D Citation
45. Front view of TFE 731 on Falcon 10
46. Front view of TFE 731 on Learjet
47. Front view of CJ610 on Jet Commander
48. Aft view of TFE on Falcon 10
49. Aft view of TFE 731 on Learjet
50. Aft view of Larzac on Falcon 10
51. Side view of JT15D on Citation
52. Side view of JT15D on SN600
53. Side view of Larzac on Falcon 10
54. Side view of DJ610 on Learjet
55. Side view of JT12 on Sabreliner
56. Side view of CF700 on Sabreliner
57. Side view of CF700 on Falcon 20
58. Aft view of CF700 on Falcon 20
59. Side view of TFE 731 on Learjet
60. Side view of TFE 731 on Falcon 10
61. Black Slide
62. Boeing 727
63. Lockheed L -1011
64. Yak 40
65. Falcon 50
66. DC-10
67. Martin B-51
68. Blank Slide

List of Viewgraphs

1. Nacelle Configurations
2. Short-Duct vs. Long Duct TradeOoff
3. Effect of Nacelle Position on Wing Pressure Distribution
4. Turbojet Nacelle Drag Characteristics
5. Turbofan Nacelle Drag Characteristics
6. Nacelle Location
7. Nacelle Location
8. Effect of Nacelle Incidence
9. Effect of Nacelle Rotation
10. Effect of Nacelle Position
11. Effect of Nacelle Rotation
12. Effect of Nacelle Incidence
13. Design Comparison of the L-1011 and DC-10 Third-Engine Installations
14. Comparison of Boeing 727 and Lockheed L-1011 Duct Contours
15. Sud-Aviation 1951 S-Duct Patent

6.2 Installation Drag Considerations as Related to Turboprop and Turbofan Engines

G. A. Burnett
Garrett AiResearch Manufacturing Company of Arizona

Introduction

Considerable effort is presently being expended by NASA, various universities, and industry to improve and develop technology in many areas directly applicable to general aviation aircraft design. One of these major areas is directed toward new airfoil designs for improved lift-to-drag-ratio characteristics for improved climb and cruise performance. Another is directed toward high-lift-device improvements that could open the door for increased wing loading design criteria, thus reducing wing area and cruise drag. The results of these programs will undoubtedly provide some significant aerodynamic improvements when the research and development work has been completed; however, the testing, proving, and optimization of most of these concepts are still in the early-to-moderate stage with respect to being introduced into production general aviation aircraft.

With this in mind, it would appear advantageous to approach the problem of improved aircraft performance and/or drag reduction along at least two parallel paths which consist of new technology development and identification of areas where potential improvement with existing technology could be attained. The latter would also tend to complement advanced technology.

One such area is the drag penalties associated with propulsion system installation. Typically, at representative cruise operating conditions, the total installed drag of a turbofan engine installation can effectively amount to between 10 and 15 percent of the total aircraft drag. Similarly, a turboprop engine installation can amount to between 20 and 40 percent of the total aircraft drag. As a starting point, some of the specific areas associated with straight jet and turboprop engine installations have been outlined where drag reductions and, thus, improved aircraft system performance can be obtained.

Discussion

Before the subject of drag reduction can be addressed, an accounting procedure for evaluating the propulsive effort must be defined. For the straight jet engine installation, this is a relatively simple procedure, as shown in Figure 1.

$$F_{N_e} = F_{N_{SPEC}} - \Sigma\ (\Delta F_N) - D_N - D_{ADD} - D_{MISC}$$

WHERE:

F_{N_e} = NET INSTALLED THRUST FOR PROPULSIVE EFFORT

$F_{N_{SPEC}}$ = SPECIFICATION NET THRUST (NO LOSSES, REFERENCE NOZZLES)

$\Sigma(\Delta F_N)$ = NET THRUST CORRECTION FOR RAM RECOVERY, BLEED, ACCESSORY LOAD, EXHAUST NOZZLE DEVIATION FROM REFERENCE

D_N = NACELLE DRAG (FRICTION AND PRESSURE)

D_{ADD} = ADDITIVE DRAG DUE TO FLOW PREDIFFUSION CORRECTED FOR LIP SUCTION

D_{MISC} = NET RAM DRAG OF SECONDARY FLOW SYSTEMS CORRECTED FOR EXITING MOMENTUM (COMPARTMENT VENTILATION, LEAKAGES, ETC.)

Figure 1. Propulsive Effort for Jet Installations

With the use of accounting procedures that have been accepted where drag is defined as the summation of forces acting on the outside of the stream tube bounding the flow that passes through the complete engine and thrust is defined as the summation of forces on the inside of the stream tube, the complexity of thrust and drag accounting becomes relatively simple.

Obviously, this same exact procedure cannot be applied to a propeller powered installation, since the stream tube or slip stream now has moved from the inside of the engine to the outside. However for a turboprop engine installation, an extension of the basic straight jet accounting procedure may be established as shown in Figure 2.

The purpose of defining an accounting procedure is twofold. First, it provides the means of completing a preliminary performance assessment of one engine installation with respect to another, which is an obvious requirement for aircraft performance analysis and trade-off studies; and secondly, it provides a method to identify areas of potential improvement. This procedure has apparently not been as fully utilized on propeller installations as straight jet installations. This is indicated by the lack of design guidelines and installation aerodynamic trade-off data. This may be attributed in part to the fact that propeller-powered aircraft engine installations come in many variations, whereas straight jet engine installations are fairly standard in terms of comparing one installation to another, independent of thrust or application.

Air-Intake Design Considerations

All turboprop and straight jet aircraft propulsion system installations have primary air intakes for directing airflow from the free stream into the engine. Most installations utilize secondary air intakes for providing cooling and ventilation airflows to various components and hot sections of the engine. The design considerations in terms of sizing, design-point selection, location, and shape can significantly affect the propulsive effort of the propulsion installation (net thrust, nacelle drag, and additive drag).

The design objective for most business jet intake systems is minimum length for weight and surface area considerations while maintaining a high drag-rise Mach number, low spillage drag characteristics, and high total pressure recovery with low flow distortion to the engine. With the advent of modern high-bypass-ratio turbofan engines (high flow per unit frontal area and increasing maximum diameters), this objective has become quite a challenge to the aerodynamicist. If the intake sizing is too large for the required engine airflow (low mass-flow ratio), flow spillage

$$THP_e = \eta_p \left[SHP_{SPEC} - \Sigma (\Delta SHP)\right] + \left[F_{N_{SPEC}} - \Sigma (\Delta F_N) - D_N - D_{ADD} - D_{COOL} - D_{MISC}\right] K$$

WHERE:

- THP_e = NET THRUST HORSEPOWER FOR PROPULSIVE EFFORT
- η_p = PROPELLER EFFICIENCY ADJUSTED FOR BLOCKAGE
- SHP_{SPEC} = SPECIFICATION SHAFT HORSEPOWER
- $\Sigma (\Delta SHP)$ = SHAFT HORSEPOWER CORRECTION FOR BLEED, ACCESSORIES, EXHAUST NOZZLE DEVIATION FROM REFERENCE, AND INLET/EXHAUST DUCT LOSSES
- $F_{N_{SPEC}}$ = SPECIFICATION NET THRUST WITH REFERENCE NOZZLE
- $\Sigma (\Delta F_N)$ = NET THRUST CORRECTION FOR EXHAUST DEVIATION FROM REFERENCE (AREA, DISCHARGE ANGLE), BLEED, ACCESSORIES, AND INLET/EXHAUST DUCT LOSSES
- D_N = TOTAL DRAG ON NACELLE TO INCLUDE INFLUENCE OF PROPELLER SLIP STREAMS
- D_{ADD} = ADDITIVE DRAG OF PRIMARY AND SECONDARY AIR INTAKES (CORRECTED FOR LIP SUCTION)
- D_{COOL} = NET RAM DRAG OF SECONDARY AIR FLOWS (OIL COOLING, COMPARTMENT VENTILATION, ETC). FULL RAM DRAG OF EACH SYSTEM ADJUSTED FOR THRUST OF EXISTING MOMENTUM
- D_{MISC} = PARASITIC DRAG DUE TO PRIMARY AND SECONDARY AIR INTAKES AND EXHAUST NOZZLES, INTERFERENCE, LEAKAGE, ETC.
- K = CONVERSION FACTOR

NOTE: ALL DRAG COMPONENTS MUST BE CORRECTED FOR SLIPSTREAM EFFECTS.

Figure 2. Propulsive Effort for Turboprop Installations

results which can lead to flow separation. If the forebody shape (fineness ratio) is not adequate, supersonic expansion can occur which may result in flow separation. If the inlet lip (from the highlight to the throat) and internal diffuser characteristics are not considered, excessive additive drag can result.

Up to now the NACA Series I profile has been used for most forebody air-intake designs; but at low mass flow ratios, excessive spillage drag can result due to the high local flow angle at the inlet lip or highlight. This is especially true of modern high-bypass-ratio turbofans used on general aviation aircraft where fixed-geometry air intakes are used predominantly. The air-intake throat is sized for good cruise diffuser performance, but the static takeoff conditions require generous highlight-to-throat-area-contraction ratios to preclude flow separation during static ground and crosswind operation. As a result, during some operating conditions (speed and engine power setting), extremely low mass flow ratios can result. While operating in these conditions the stagnation streamline can be located well within the air intake to the inside of the highlight, which will require the flow on the outside of the streamtube (spillage flow) to rapidly accelerate and expand around the highlight within the forward region of the cowl. If the flow separates, the effect of the suction pressure loss reduces the lip suction force and , thus, increases the additive drag in addition to the basic pressure drag of the nacelle. Some recent studies have suggested that the problems associated with low-mass-flow air-intake operation may be alleviated by incorporating forebody profile shapes similar to those being investigated for supercritical airfoils--the principle being that the suction pressure on the modified forebody shapes is retained well beyond the point where suction pressure collapse occurs on a Series 1 profile.

As shown in Figure 3, the reduction in additive drag from a NACA Series 1 forebody and a modified supercritical forebody is indicated as:

Mass Flow Ratio	C_D Spillage, Based on Frontal Area
0.6	-43%
0.4	-77%

With turboprop engine installations, the problems associated with air-intake design can become more of a challenge than that of straight jets. This can be attributed to propeller slipstream interaction effects, which complicate accurate local flow field definition. As a consequence, the air intakes on most propeller-powered aircraft are oversized to offset the uncertainties, thus resulting in high additive drags, increased surface areas, and propeller blockages. In addition to the basic

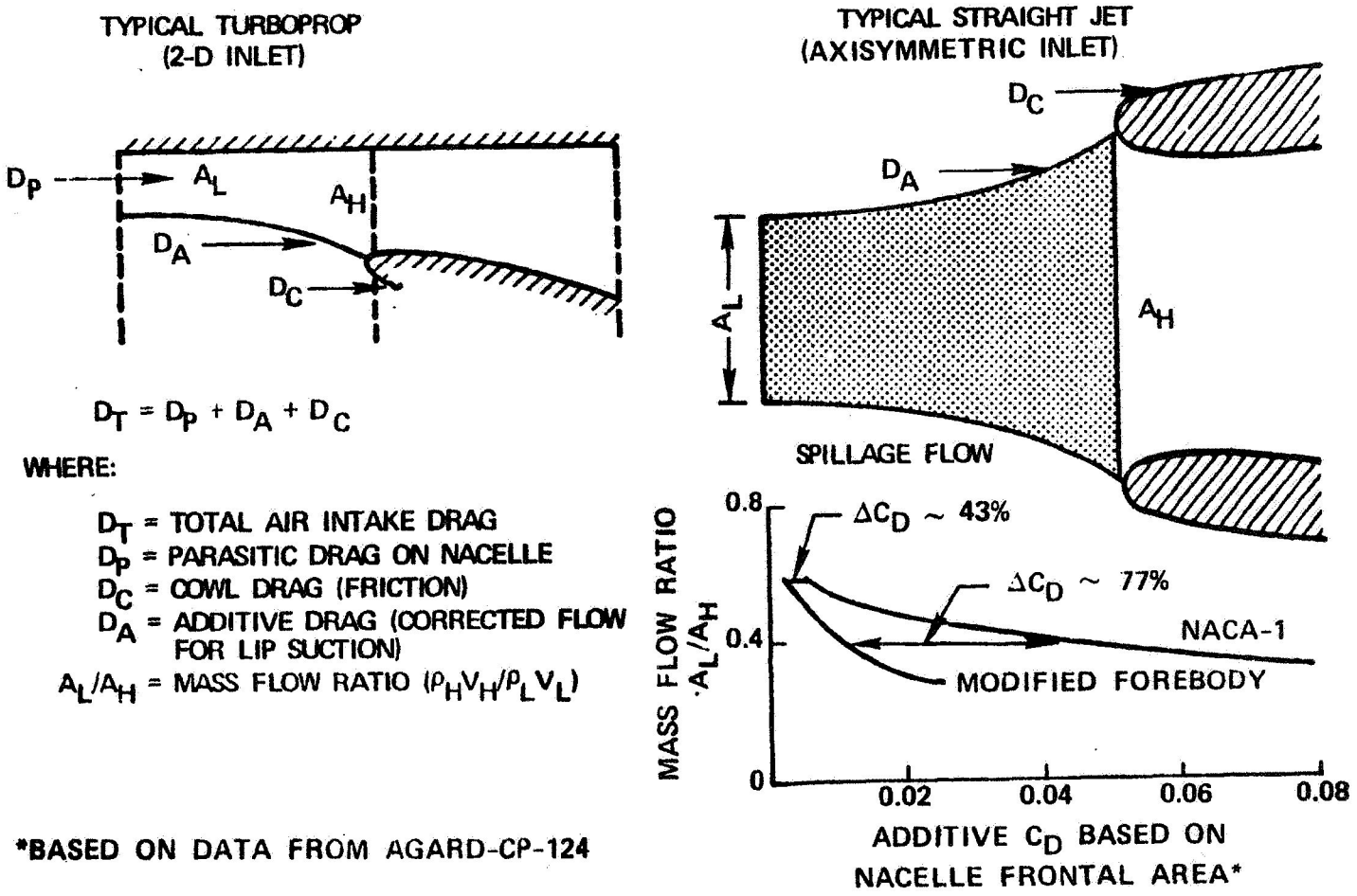

Figure 3. Air Intake Design Considerations

- SELECTION OF EXHAUST DUCT GEOMETRY IS BASED ON AIRCRAFT CONSTRAINTS, COST, AND PERFORMANCE

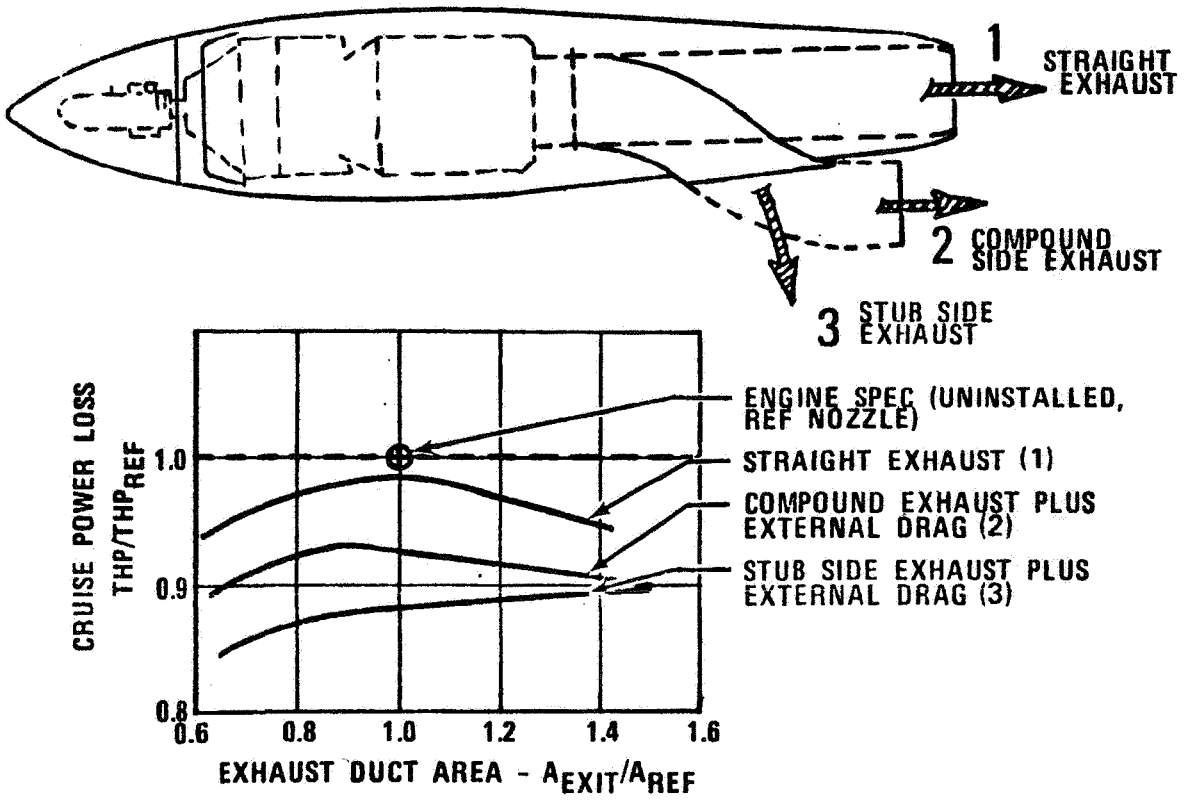

Figure 4. Turboprop Exhaust Arrangements

drags associated with the air intakes, the parasitic drag resulting from local flow separations on the nacelle due to prediffusion can be significant.

Turboprop Exhaust-Duct Arrangement

Some turboprop engine installations offer options in the approach to designing the required exhaust duct and cooling systems. When these options exist, trade off studies in terms of aircraft constraints, cost, weight, and performance should be completed to assess the best configuration for the engine installation and, thus, the total aircraft system.

Figure 4 shows three possible exhaust-duct configurations that may be considered for a typical turboprop aircraft installation. As shown, the three configurations consist of a straight duct that has been designed to minimize internal pressure losses (no bends, minimum length), to provide maximum use of the jet thrust, and to minimize frontal area or blockage.

The second duct is a typical compromise that could be encountered on some installations. Like the straight exhaust, it has been designed to utilize the available jet thrust, but at the expense of additional internal pressure loss and external drag.

The third duct illustrates a configuration where the designer may consider minimizing external drag and frontal blockage at the expense of utilizing the engine exhaust jet energy.

To provide insight as to impact on propulsive effort of the three exhaust-duct configurations considered a simple performance assessment is shown that considers the relative effect of each configuration with respect to the power attainable with an uninstalled specification engine. The result obtained from this parametric analysis is unique for each exhaust-duct area considered with respect to internal pressure loss and external drag.

As expected, the straight duct configuration results in the smallest power loss (approximately 1.5 percent). The difference between the compound side exhaust (optimum area) and the straight duct (optimum area) is approximately 5.0 percent, which is attributable directly to external drag and internal pressure-loss effects on the engine. The optimum area stub side exhaust performance was estimated to be approximately 8 percent lower than the straight exhaust duct.

In terms of airplane drag, the difference between the optimum straight duct design and the stub side exhaust design represent 30 to 35 lbs drag differential at a typical cruise operating condition.

Turboprop Cooling Systems

As previously indicated for exhaust-duct trade-offs, turboprop engine cooling requirements (compartment ventilation and oil cooling) provide some design alternatives. Most systems use either full ram systems, which are dependent upon recovering kinetic energy from the propeller slipstream or free-stream velocity, or augmented systems using the kinetic energy of exhaust velocity to provide an eductor. Both systems have advantages and disadvantages.

At static or low-speed operating conditions, where the free-stream kinetic energy is low, eductor systems can provide the augmentation necessary to obtain the required cooling flows; however, the optimization of an eductor system requires a complete parametric analysis at the design point and off-design operating conditions to fully assess the interaction of the interrelated flows and the effect on propulsive effort. In comparison , full ram systems are simpler to analyze due to the elimination of the interacting flow fields. Improperly sized eductor systems can result in significant engine power loss and ram drag at normal cruise operating conditions.

As indicated previously, full ram systems are less risk to design than flow-augmentation systems. Proper designs can be obtained that result in minimum performance loss to the aircraft if proper design criteria are followed for air-intake sizing, internal diffuser design, and flow control employed for cruise operation where the cooling flow requirements are low.

Figure 5 shows the cruise power loss as a function of flow control area ratio for a full eductor cooling system and an isolated ram cooling system design. The points at 100 percent area ratio show the power loss if no flow control is used. As indicated, the power loss of the full ram system amounts to approximately 6 percent (oil cooler plus compartment ventilation), whereas the eductor system cruise power loss is only 2 to 2.5 percent. If the full ram-system flow control is implemented, the resulting power loss of the ram system can be reduced to approximately the same level as the eductor system. This is in direct contrast to the requirements for the flow-augmented eductor system. As shown on the figure, if flow control is imposed on the eductor system through a variable-area air intake or some internal device, the cruise power loss increases as the eductor flow is decreased. This is attributed to interacting effects of off-design eductor operation (higher pressure loss, incomplete mixing) being more pronounced on engine performance than the reduction in ram drag. These performance effects do not include the additional drags that may be encountered with each of the systems, such as additional wetted area, blockage, and nacelle interference drags with the full ram system.

- TURBOPROP INSTALLATIONS OFFER ALTERNATIVES FOR COOLING FLOW REQUIREMENTS SUCH AS FLOW CONTROLLED ISOLATED SYSTEMS VERSUS NO FLOW CONTROL VERSUS FULL EDUCTOR SYSTEMS FOR FLOW AUGMENTATION.

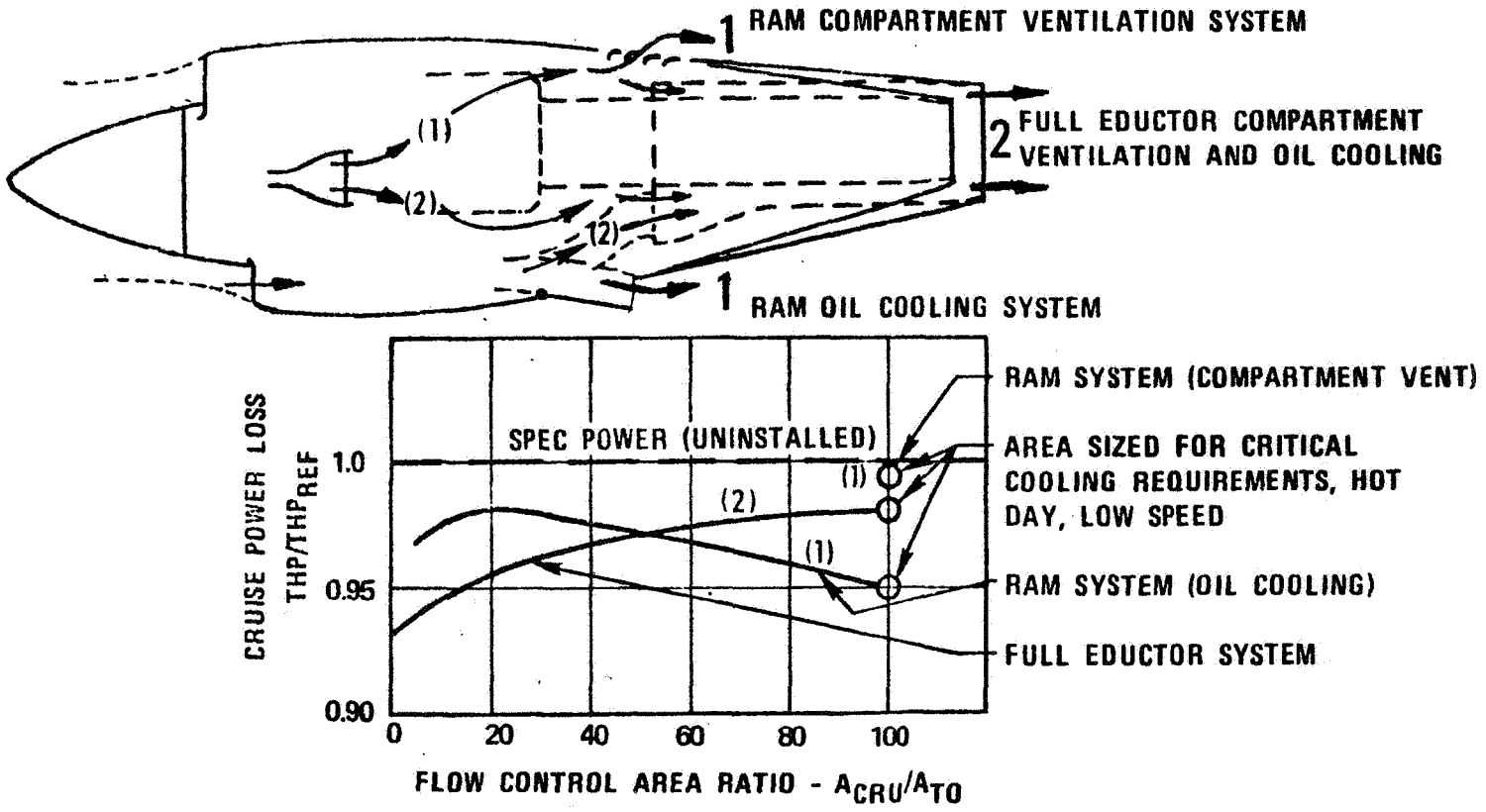

Figure 5. Turboprop Cooling System Arrangements

Proposed Programs for Drag Reduction

The performance penalties associated with the propulsion system installation can result in a significant percentage of the total effective aircraft drag. The specific areas associated with the engine installation where the major performance penalties are encountered should be identified and evaluated for potential improvements through improved design criteria.

Fundamental to improving design criteria is the definition of a propulsive effort thrust and drag accounting method that clearly identifies the interaction of the propulsion system and airframe. These procedures must be defined early in the preliminary phases of an aircraft program and maintained through flight test.

Through this approach of identification and accounting, a technical data base applicable to each component considered in assessing the effectiveness of the propulsive effort would be accumulated for defining improved design procedures. In addition, it would tend to reduce the uncertainties associated with evaluating preliminary aircraft performance.

Specific areas that suggest potential performance improvements on current and future general aviation aircraft are the design considerations used for air-intake sizing on all general aviation aircraft, and exhaust duct geometries and cooling system arrangements for propeller-powered aircraft. Studies have indicated that the power loss at typical turboprop aircraft cruise conditions can range from 16 percent (for a stub side exhaust duct, with no flow control installation) to between 2 and 3 percent (for a straight exhaust, full flow control system), thus suggesting a 13- to 14- percent improvement in system performance.

The key to arriving at a minimum drag, maximum propulsive effort engine installation on any aircraft system is the interface between the airframe and engine manufacturers. The concept of "teaming" has been an accepted practice, to a limited degree, among the larger airframe and engine manufacturers for some time. However, within the last few years, the realization of the true significance of the concept in terms of achieving the best performing aircraft system (airframe/engine intergration) with minimum cost and program delays has been acknowledged.

From the general aviation point of view, the concept of teaming should be even more significant, since a large percentage of general aviation aircraft evolve through engine retrofits for performance improvements. In order to obtain the full aircraft performance potential, the general aviation airframe and engine manufacturer must understand each others sytems in terms of constraints, performance, penalties, and trade-offs.

The proposed programs for drag reduction are summarized on Figure 6.

- IDENTIFY AREAS ON CURRENT AIRCRAFT DESIGNS WHERE POTENTIAL PERFORMANCE IMPROVEMENTS CAN BE OBTAINED
- ESTABLISH DETAIL THRUST AND DRAG ACCOUNTING PROCEDURES FOR ASSESSING AIRCRAFT PERFORMANCE
- DEVELOP A DATA BASE FOR ESTABLISHING DESIGN CRITERIA RELEVANT TO GENERAL AVIATION AIRCRAFT
- INVESTIGATE MODIFIED PROFILES FOR AIR INTAKE NACELLE DESIGNS TO REDUCE ADDITIVE DRAG ASSOCIATED WITH INLET/ENGINE MATCHING
- REVIEW AND UTILIZE CORRECT AIR INTAKE SIZING CRITERIA ON TURBO-PROP APPLICATIONS TO REDUCE PROPELLER BLOCKAGE, WETTED AREA, AND NACELLE INTERFERENCE DRAGS
- REVIEW EXHAUST DUCT AND COOLING SYSTEM DESIGNS AND DEVELOP VALID ANALYTICAL/PRELIMINARY DESIGN TOOLS FOR TOTAL SYSTEM ASSESSMENTS
- IMPLEMENT AN INTEGRATED PROPULSION SYSTEM APPROACH TO GENERAL AVIATION AIRCRAFT DESIGN (TEAM EFFORT OF ENGINE AND AIR FRAME COMPANIES)

Figure 6. Proposed Programs for Drag Reduction

6.3 Nacelle Drag Reduction: An Analytically-Guided Experimental Program

Frederick O. Smetana
North Carolina State University

Standard estimation procedures as well as the NCSU "Body" Computer program (Ref. 1) predict that the drag of the two nacelles on the NASA ATLIT airplane will equal the drag of the fuselage. These estimates are based on computations of the drag of isolated nacelle-shaped bodies in uniform streams with no internal flow. Losses due to air motion through the cooling fins, to helical components in the flow over the nacelle, or to unusually high levels of streamwise turbulence are not accounted for in the analysis, nor are interference effects arising from the presence of the wing or fuselage. The analysis must therefore be regarded as qualitative at best.

Within these limitations, however, one finds that the high drag of the nacelles is due to their high form drag, this being about three times as large as their skin friction drag. Normally, for a streamlined body the skin friction drag is three times as large as the form drag! When one considers this result and the nacelle shape it seems apparent that the nose of the nacelle is too blunt. Thus the indicated course is to increase the dimensions of the nacelle forebody so that the nose (cooling intake) is relatively less blunt. A preliminary computer analysis following such an approach (using NCSU "Body") indicates that the reduction in form drag is much greater than the increase in skin friction drag which accompanies the increase in surface area. However, to validate this approach it would be necessary to conduct flight tests with modified nacelles during which the total aircraft drag could be determined. Comparison of the drag of the new configuration with that of the original would then yield the increment (plus or minus) due to the change in nacelle geometry.

What is needed, then, is a simple procedure, similar to what is done in the wind tunnel with clay and wax which permits one to make minor alterations in the nacelle surface contours quickly and inexpensively. A configuration which, on the basis of computer calculations, seem propitious can then be tested easily. The results of the tests can then be fed back to correct the estimation procedure. With such an iterative scheme it seems reasonable that one should not have to test more than three or four nacelle shapes before finding a practical optimum.

It seems reasonable to suppose that these nacelle modifications can be effected through the use of sprayed on polyurethane foam perhaps with bolts into the nacelle structure to provide additional wind shear resistance. This foam is easily shaped and smoothed after application. Or, it is conceivable, that fiberglass shells of appropriate contour could be appended to the normal nacelle for the duration of the test. Since the required recontouring of the nacelles is not expected to be very extensive so far as lift and moment characteristics of the airplane are concerned, it should not be necessary to investigate changes in handling qualities in a substantive fashion for each modification.

One would probably wish to do so, however, for the configuration finally selected for production, particularly its effect on handling qualities at high angles of attack.

The two figures below show the original nacelle as analyzed by the NCSU "Body" program and an alternate also analyzed by "Body". These results are the basis for believing that there is significant improvement to be gained by recontouring the nacelles. If the question of fuel economy becomes critical enough, it is to be expected that efforts will also be directed toward treating analytically the internal cooling flow, the propwash components, and the wing and fuselage interference effects.

A completely analytical treatment of the loss in total head experienced by the flow which is ingested at the front of the nacelle, proceeds over the cooling fins, and then leaves near the rear of the nacelle is difficult virtually to the point of impossibility. In addition to the three-dimensional nature of the multiplicity of tortuous flow passages, one has variable heat fluxes and temperatures at each of these boundaries. The indicated approach therefore is an integral analysis with the magnitudes of the various contributions to be determined experimentally. By placing a pitot rake and total temperature probe at the cooling air intake as well as at the cooling air exhaust and measuring the flow areas at these points one can determine the cooling mass flow, its total head loss (which appears as aircraft drag) and its heat gain. Comparison of the head loss with that for equal heat addition for flow between parallel plates will then give an indication of how efficient the cooling path is. A significant difference will indicate the need for redesign.

Proper analytical treatment of the propwash components and the interference effects must await both the development of accurate, three-dimensional turbulent boundary layer calculation routines and a computer of sufficient size and speed to perform the combined inviscid-viscous problem in a relatively short time, say 30 minutes.

This is probably some five years in the future. In the meantime, a very crude analytical model treating the situation on the basis of equivalent flat plate area, supplemented by flight measurements using tufts and/or skin friction gauges seems to be the approach most likely to yield tangible near-term results.

References

Smetana, F.O.; Summey, D.C.; Smith, N.S.; and Carden, R.K. "Light Aircraft Lift, Drag, and Moment Prediction - A Review and Analysis" NASA CR-2523, May 1975, 492 pp.

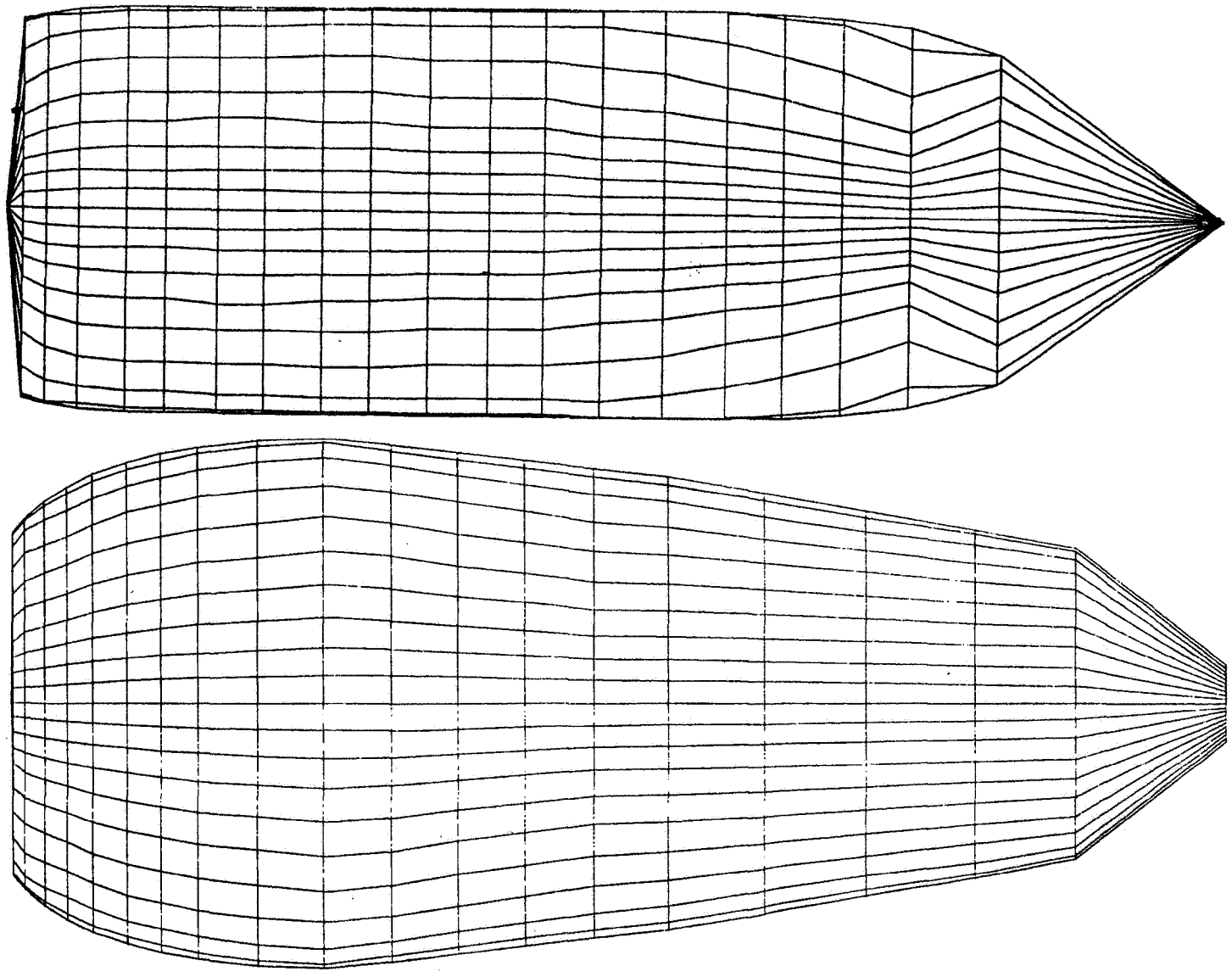

ORTHOGRAPHIC PROJECTION OF THE ORIGINAL ATLIT NACELLE AND THE MODIFIED LOW-DRAG NACELLE.

PLANFORM VIEW OF THE ORIGINAL ATLIT NACELLE AND THE MODIFIED LOW-DRAG NACELLE.

6.4 An Exploratory Investigation of the Cooling Drag Associated with General Aviation Propulsive Systems

NASA Grant Number NSG 1083

E. J. Cross
Mississippi State University

An exploratory effort has been undertaken to systematically investigate the drag associated with the cooling-air flow of contemporary general aviation engine installations. The purpose of this research is to develop a clear specification of cooling drag, provide design data and information, and to develop experimental methods and techniques for determining the value of the cooling drag. It should be noted that this program represents the initial phase of an extensive study of this subject which will be required in order to develop a full understanding of the physical processes involved. The specific objectives of the program (Figure 1a) are as follows: determine the state-of-the-art which is manifest by available data and design methods, establish appropriate instrumentation and experimental techniques for determining cooling drag by flight test, and determine the relative magnitude and define the significant components of cooling drag. The approach, taken to reach the objectives, is shown in Figure 1b.

The flight test vehicle is a Beechcraft T-34, Mentor, on loan from the Department of the Navy. The T-34, although a relatively old design, is representative of contemporary, high-performance, single-engine aircraft. The cooling drag will be experimentally determined by two independent methods which will provide a cross-check and the opportunity to correlate techniques.

A complete bibliography of source material has been compiled that covers the mid-1920 period to early 1975. Synopses of the available technical papers and reports are being prepared and will be assembled as a compendium of design information for installation of aircraft piston engines. The state-of-the-art of design factors which are relevant to the general aviation propulsive system installation is not well represented by publications in the open literature. Much of the pertinent data and some of the design methods are proprietary and cannot be obtained for publication. The most highly developed design procedure available in the open literature is the Lycoming installation manual which is essentially an adaptation of design methods developed by Pratt and Whitney circa 1945, and specifications of cooling air requirements peculiar to each of the Lycoming engines. Although

this manual is inconclusive, it is a noteworthy addition to the literature and Lycoming is to be commended for their exceptional efforts. A work task has been undertaken to develop a design manual that will include inputs from the engine installation engineers and airframe propulsive system designers. This manual will incorporate current design practice to the extent that company proprietary policies will permit release and publication of data and procedures.

A general purpose instrumentation system has been designed and fabricated for the measurement of pressures and temperatures in and around the engine cowl/nacelle. The system is modularized and is easily portable and can be moved intact to other test vehicles. It is completely self-contained and does not rely on the host aircraft for power or support. The measurement system is composed of three synchronized 48 channel scannivalves which provides for 144 pressure data-points, 20 thermocouples for the measurement of engine internal cowl temperatures, an air-speed transducer and an altitude transducer. All of the data are synchronized to a crystal controlled clock. This system is shown schematically in Figure 2.

Installation of two flight test booms incorporating total and static pressure probes, and pitch and yaw servos has been completed. Calibration flights have been completed and demonstrated satisfactory performance of each of these. These are self-aligning probes and have virtually no position error from 70 knots through 150 knots. In addition, an outside air temperature probe, and a shielded thermister, have been installed on the lower left wing. These probes are the primary source of aircraft performance data, altitude, airspeed, etc.

An array of total pressure and static pressure probes and thermocouples has been installed in each of the inlets and augmentor tubes as shown in Figures 3 and 4 respectively. The engine baffle is instrumented similarly to standard Lycoming test cell practice (Figure 5). In addition, total and static pressure probes and thermocouples are located at several position in the upper and lower cowl to provide flow data throughout the cowl. Surface pressures are being measured at points extending along lines from the inlet lip to the firewall. The cowl is adequately instrumented to allow calculation of all the pertinent characteristics of the internal flow.

The data are recorded on board the aircraft in analog form on a seven channel FM/FM analog tape recorder (Lockheed Model 417). The data recorded are: 3 channels of scannivalve measured pressures, 1 channel of airspeed data, 1 channel of altitude data, 1 channel of multiplexed temperature data, and a channel of master clock data. The master clock data are used to time synchronize

the analog to digital converter that is used to convert the recorded data into digital form for storage on digital magnetic tape. The ditigal magnetic tape interfaces directly with the University mainframe computer, a UNIVAC 1106, which is used for data analysis and manipulation. The data are converted to engineering units and plotted at the computing center. A secondary instrumentation system has been installed on a photo panel to provide a redundant source of aircraft performance data. The panel has a calibrated airspeed indicator, calibrated altimeter, clock, outside air temperature read-out and a binary counter. Data are recorded on a 16 mm film at a rate of 1-frame per second.

The flight test program consists of six schedules which involve calibration of the pitot-static system, calibration of the primary instrumentation system, gliding flight drag polars for three cowl configurations, and cowl performance with engine power. All calibration flights and approximately 80% of the gliding flight schedules have been completed. The flight test procedure for developing drag polars consists essentially of a series of saw tooth climbs and power-off glides at constant calibrated airspeed. A drag polar is generated for each of the aircraft test configurations as illustrated in Figure 6. In addition, cowl internal flow data is accumulated for each flight condition so that momentum changes of the cooling-air flow through the cowl can be compared with changes in total airplane drag indicated by drag polar shifts. All glides are with the engine off and propeller feathered. The propeller was obtained on loan from Hartzell Propeller and the governor and unfeathering accumulator from Woodward Governors. This system provides increased safety and flexibility during the power-off gliding flight tests.

The three cowl configurations are: the standard T-34 arrangement, inlets blocked so there is no internal flow, and the augmentor tubes fixed with butterfly valves in each to throttle the cowl flow. Changes in total airplane drag, changes in the momentum of the internal flow, and changes in the external cowl pressure field are determined as a function of flight condition and air mass flow rate through the cowl. The drag associated with the engine installation and the internal flow of cooling air is determined by comparing the airplane total drag for each cowl configuration to the case of no cooling air flow with the cowl closed. Airplane drag increments due to changes in airframe parasite drag caused by perturbations to the external flow induced by inlet spillage are also attributed to cooling drag.

A steering committee has been established to provide a working interface between potential industry users and the University research team. Industry members are from each of the following companies: Avco-Lycoming, Teledyne-Continental,

Beech Aircraft, Cessna Aircraft, and Piper Aircraft. Formal meetings are scheduled twice each year at the University and frequent visits are planned at the individual company facilities. The purpose is to establish a mechanism for the exchange of ideas between the research group and the industry design group to insure the validity of program objectives and increase the probability of useful results and the direct transfer of technology developments to application.

The NASA Technical Officer is Mr. Albert W. Hall

Mail Stop 247, RAFD
NASA-Langley Research Center
Hampton, Virginia 23365.

OBJECTIVES

- Determine State-of-the-Art
  - Data
  - Design Practice
- Define Significant Components
- Establish Flight Test Procedures
  - Instrumentation
  - Methods
- Identify Additional Research Requirements

Figure 1(a). Objectives

APPROACH

- Flight Test of Beechcraft T-34 Mentor
  - Gliding Flight
  - Momentum Loss of Internal Flow
- Steering Committee
  - Industry/University

PRODUCT

- Design Information
  - Data
  - Criteria
- Experimental Methods

Figure 1(b). Approach

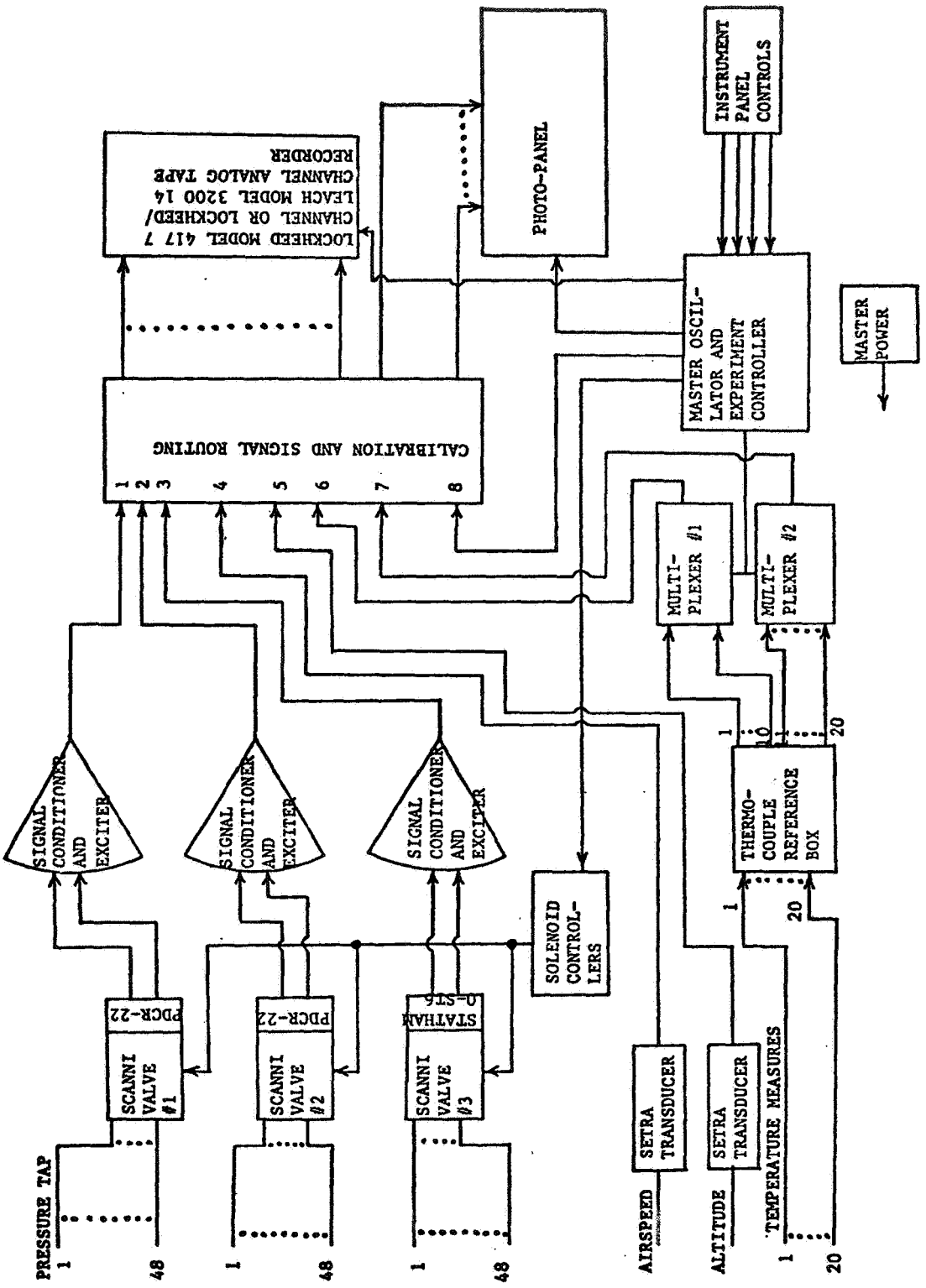

Figure 2. Cooling Drag Instrumentation

● Inlet Instrumentation

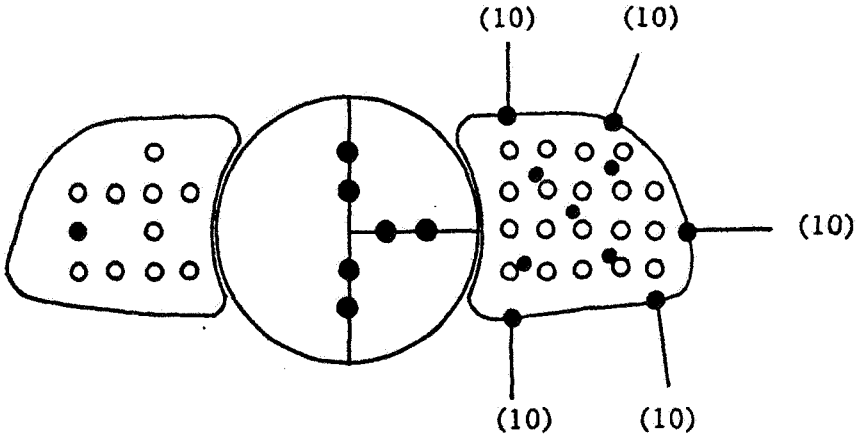

Right	Left	
10	20	Total Pressure Probes
1	5	Static Pressure Probes
0	50	Surface Static Pressure

Spinner - 6 Surface Static Pressure Taps

Total - 86

Figure 3. Location of Inlet Instrumentation

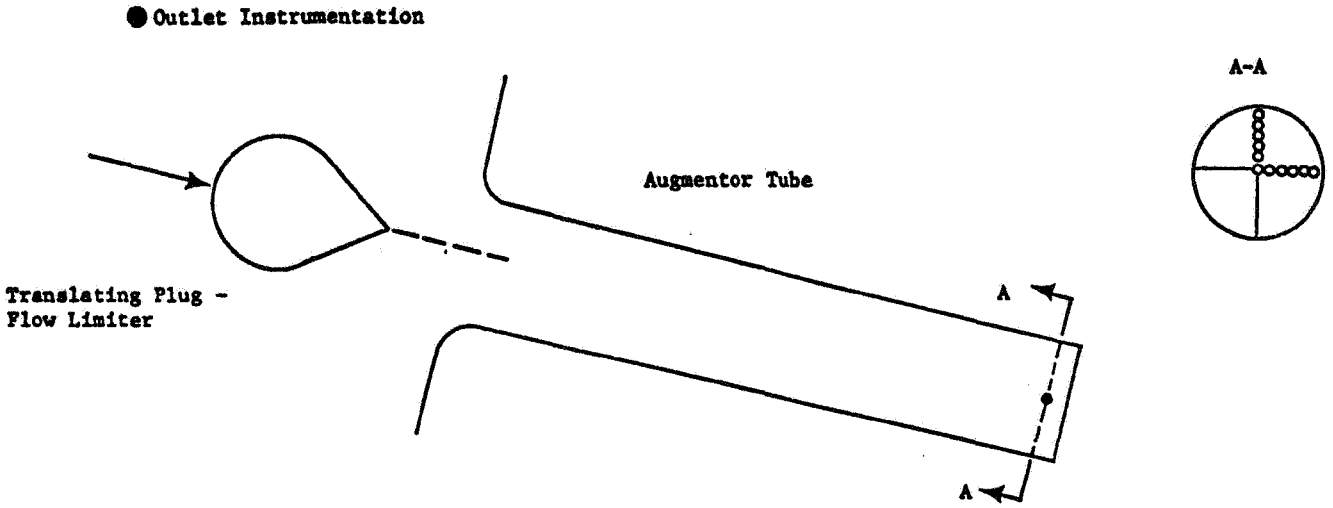

Right	Left	
10	20	Total Pressure Probes
1	1	Static Pressure Probes
1(4)	1(4)	Surface Pressure Tap (Manifolded)

Total - 34

Figure 4. Location of Outlet Instrumentation

1, 2, ..., 10	Total tube, located located above intercylinder baffles
11, 12, 13, 14	Static tube located below intercylinder baffles

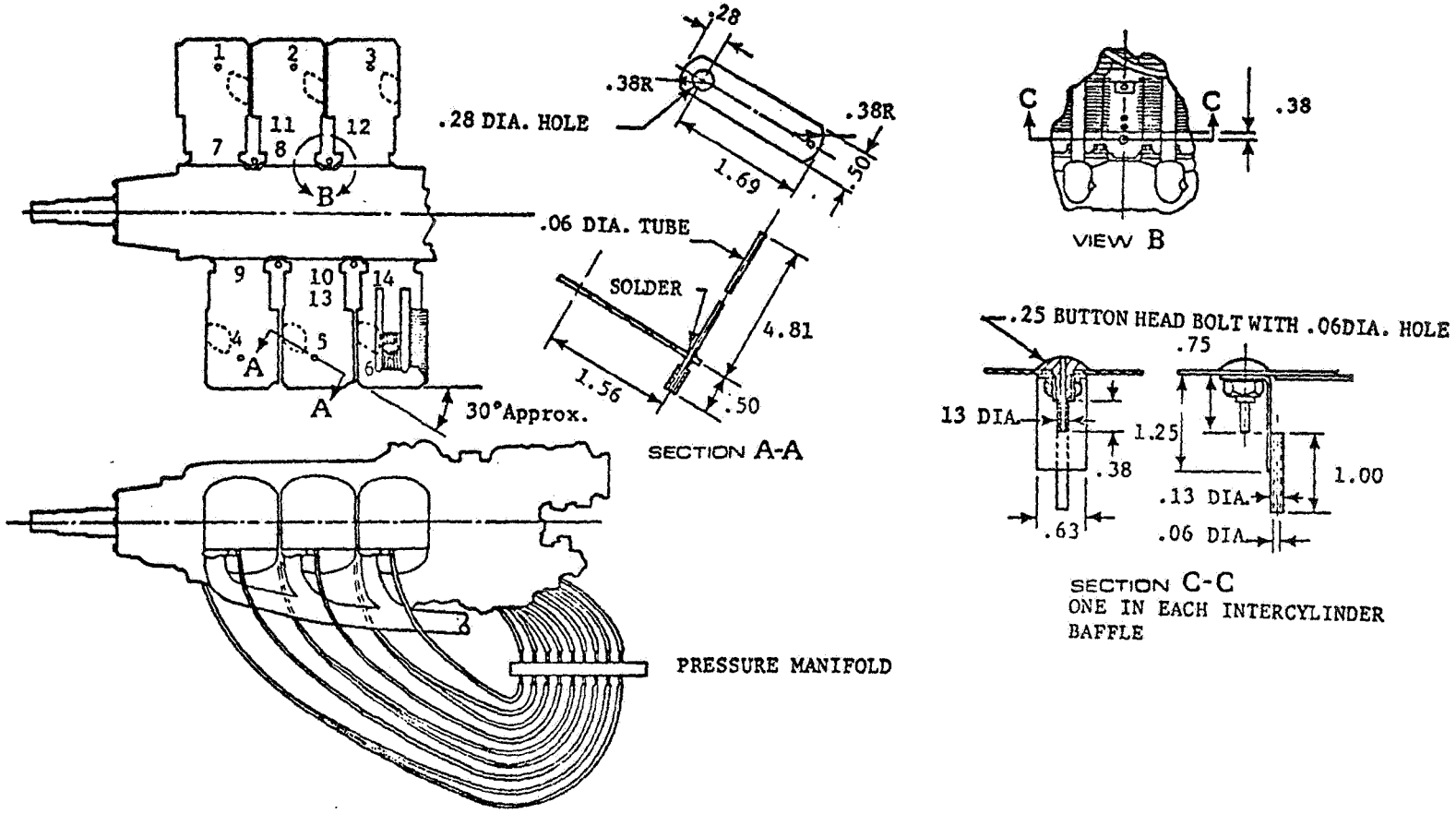

Figure 5. Engine Baffle Pressure-Probe Arrangement
(ref. Lycoming Aircraft Enginer Installation Manual)

Flight Polars Obtained in Glide
(Gross Wt 1735 Lbs)

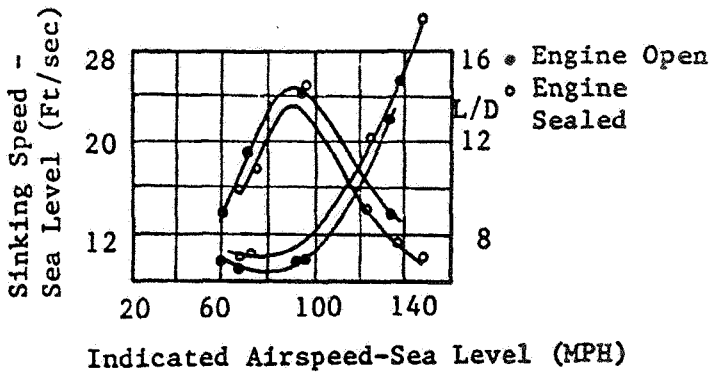

● Gliding Flight Tests

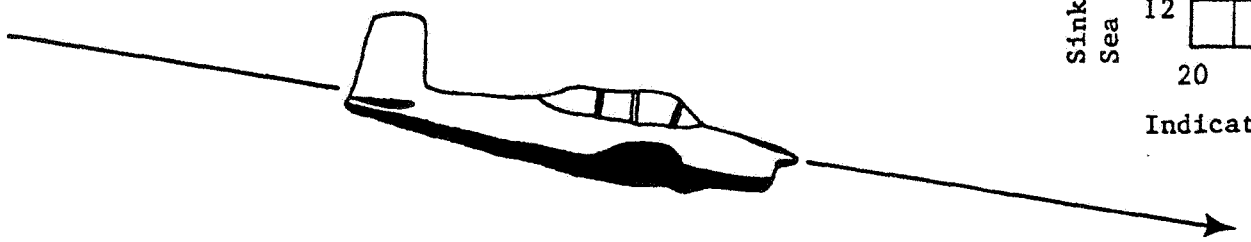

Drag Data Flights

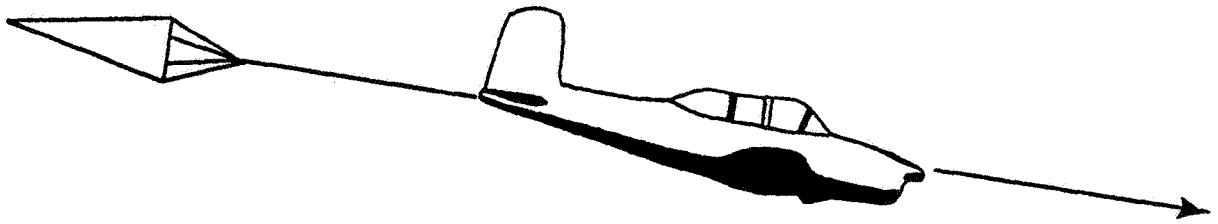

Calibration Flights

Figure 6. Flight Polars Obtained in Glide

6.5 Propellers of Minimum Induced Loss, and Water Tunnel Tests of Such a Propeller

E. E. Larrabee
Massachusetts Institute of Technology

Abstract

The fundamental vortex theory for a single rotation propeller with a finite number of blades is reviewed. The theory leads to the specification of a radial distribution of bound circulation on each blade for minimum induced loss, analogous to the elliptic spanwise distribution of bound circulation on a wing for minimum induced drag. A propeller designed in accord with this theory has been tested in the water tunnel at M.I.T.'s Marine Hydrodynamics Laboratory where it exhibited high efficiency in spite of localized cavitating flow. A knowledge of the flow field for an optimum propeller is of value to the airframe designer seeking to maximize the performance of the airplane-propeller combination.

Figure 1 presents the geometry of the force and velocity components associated with the operation of a representative blade element. The fluid velocity W at the blade element is made up of the flight, or advance velocity, V, the rotational velocity, Ωr, and the induced, or "inflow" velocity w_i. The induced velocity is customarily resolved into an axial component aV and a rotational component $a'\Omega r$. The elementary force dF is resolved into lift and drag components dL and dD where the angle ϵ, defined as $\tan^{-1}(c_d/c_\ell)$, is an angle determined by blade profile characteristics in two dimensional flow at the appropriate Reynolds number, as in lifting line theory.

The blade element efficiency is given by

$$\eta_{element} = \frac{VdT}{\Omega dQ} = \frac{V}{\Omega r}\,\frac{dF\cos(\phi_i+\epsilon)}{dF\sin(\phi_i+\epsilon)} \qquad 1$$

and since

$$\tan\phi_i = \frac{V(1+a)}{\Omega r(1-a')} \qquad 2$$

while

$$\tan(\phi_i+\varepsilon) = \frac{\sin(\phi_i+\varepsilon)}{\cos(\phi_i+\varepsilon)} \qquad 3$$

it follows that

$$\eta_{element} = \frac{\tan\phi_i}{\tan(\phi_i+\varepsilon)} \times \frac{1-a'}{1+a} = \eta_{profile} \times \eta_{induced} \qquad 4$$

In this discussion I will be mainly concerned with the "induced" efficiency $(1-a')/(1+a)$.

Figure 2 presents the geometry of the velocity field in the propeller slipstream. An elementary helical vortex filament is convected normal to itself with velocity w by the induced velocities of all the vortex filaments lying in the approximately helicoidal vortex sheets trailed by each of the propeller blades. The vortex velocity w, which is the same as the local slipstream velocity, may be resolved into axial and rotational (or "tangential") velocity components w_a and w_t, respectively.

If the filament helix angle is ϕ, the filament will appear to move with an axial velocity v', which might be due either to real axial velocity w_a or to real rotational velocity w_t (like the rotating stripes on a barber pole); but since it is a vortex filament, and can only move normal to itself,

$$w_a = v' \cos^2\phi, \text{ and} \qquad 5$$

$$w_t = v' \cos\phi \sin\phi \qquad 6$$

Figure 3 presents the so called "lightly loaded" propeller relations between velocities w_a and w_t in the slipstream at radius r and the corresponding inflow velocity components aV and $a'\Omega r$ at the propeller disc. Since the propeller is lightly loaded, the trailing vortex helix angle ϕ in the slipstream at radius r is indistinguishable from the angle $\tan^{-1}(V/\Omega r)$ at the propeller blade element at the same radius. Following momentum theory the inflow velocities are taken as half their values in the developed slipstream:

$$a = \frac{1}{2}\frac{w_a}{V} = \frac{1}{2}\left(\frac{v'}{V}\right)\frac{\Omega^2r^2}{\Omega^2r^2+V^2} \qquad 7$$

$$a' = \frac{1}{2}\frac{w_t}{\Omega r} = \frac{1}{2}\left(\frac{v'}{V}\right)\left(\frac{V^2}{\Omega^2r^2+V^2}\right) \qquad 8$$

The induced efficiency of a blade element

$$\eta_{induced} = \frac{1-a'}{1+a} \cong \frac{1}{1+a'+a} = \frac{1}{1+\frac{1}{2}(\frac{v'}{V})} \qquad 9$$

may thus be expressed in terms of the apparent axial velocity of the slipstream, v', which up to now has been considered to be an arbitrary function of r. Betz showed in 1919 that $\eta_{induced}$ for the propeller as a whole is maximized if $\eta_{element}$ is the same for all blade elements, that is, if v'/V is independent of r. If v' is independent of r, all vortex filaments in a helicoidal vortex sheet <u>appear</u> to move axially as a rigid surface, although this is not actually the case, since w_a and w_t are given by eqs. 5 and 6.

Since circulation cannot be added to the flow in the slipstream, it follows that the circulation within a slipstream tube of radius r

$$\Gamma = 2\pi r w_t \qquad 10$$

must comprise the total circulation of the helical vortex filaments trailed by each of the B blades of the propeller, an amount equal to the total bound vorticity at the radius r. The bound vorticity on each blade at radius r is then

$$\Gamma(r) = \frac{2\pi r w_t}{B} = \frac{2\pi}{B}\,\frac{Vv'}{\Omega}\,\frac{\Omega^2 r^2/V^2}{(\Omega^2 r^2/V^2)+1} \qquad 11$$

or

$$\frac{B\Omega\Gamma(r)}{2\pi V v'} = \frac{x^2}{x^2+1} \qquad 11a$$

where $x \equiv \Omega r/v$.

Since, B, Ω, 2π, V, and v' are all constants for a minimum induced loss propeller, $B\Omega\Gamma(r)/2\pi Vv' = x^2/(x^2+1)$, can be regarded as a normalized form for the bound circulation, $\Gamma(r)$, expressed as a function of the normalized radial coordinate, $x = \Omega r/V$. Alternatively, the quantity $x^2/(x^2+1)$, which is also equal to $\cos^2\phi$, may be regarded as the ratio of the axial velocity in the slipstream to the apparent velocity, w_a/v'. Figure 4 presents the normalized radial circulation distribution (or the w_a/v' ratio) as a function of the normalized radial coordinate, x. The ratio of the rotational velocity in the slipstream to the apparent velocity w_t/v', equal to $x/(x^2+1)$, is given for comparison. It is seen that single rotation propellers of minimum induced loss inevitably have appreciable slipstream swirl near

the center of the slipstream where ϕ is large; the swirl angle in airplane coordinates being given approximately by $\tan^{-1}[w_t/(V+w_a)]$.

Strictly speaking, eqns. 7-11a apply to a propeller with so many blades that the spacing between the individual vortex sheets in the slipstream is small compared to r, called the $B\to\infty$ case. Since actual propellers have a small number of blades and may operate at large helix angles, which also tends to increase the spacing between vortex sheets (note that $\eta_{profile} = \tan\phi_i/\tan(\phi_i+\epsilon)$ is maximized when $\phi_i = \pi/4 - \epsilon/2$), it is necessary to account for the reduction in the average rotational velocity between vortex sheets in the developed slipstream (compared to the $v' \cos\phi \sin\phi$ value at the sheets themselves) when calculating the circulation.

Figure 5 shows Prandtl's approximate solution to this problem. He assumed that the flow near the edges of the helicoidal vortex sheets in the slipstream is like the two dimensional flow near the edges of a semi-infinite array of flat plates moving with velocity v. The average velocity of the fluid between the plates is given by the fraction $F = (2/\pi)\cos^{-1} e^{-f}$ times v, where $f = \pi(\xi/s)$ is a dimensionless measure of the distance ξ from the edge of the plates spaced a distance s apart. The corresponding edge distance function for the helicoidal vortex sheets is

$$f = \frac{B(1-\lambda x)\sqrt{1+\lambda^2}}{2\lambda} \qquad 12$$

where $\lambda = V/\Omega R$ is an advance ratio based on the flight velocity V and the rotational tip speed ΩR. The quantity F is interpreted as the ratio of the average rotational velocity in the slipstream at radius r to the rotational velocity near the sheets, $v'\sin\phi\cos\phi$, or, what is the same thing, the ratio of the bound circulation at radius r for a propeller with a finite number of blades to the corresponding circulation for $B\to\infty$.

Figure 6 presents representative examples of the radial distribution of bound circulation for a minimum induced loss three blade propeller operating at two advance ratios, $\lambda = 1/5$ and $\lambda = 2/3$, corresponding to climbing and cruising flight conditions, respectively, where F has been calculated according to Prandtl's rule. These optimum radial circulation distributions for propeller blades loaded so as to produce constant apparent velocity of the helicoidal vortex sheets in the slipstream, independent of the radius, correspond to the elliptic spanwise distribution of circulation for a wing, loaded so as to produce constant downwash velocity at the trailing vortex sheet in the wing wake, independent of a spanwise coordinate.

Although an untwisted wing of elliptic planform gives an elliptic spanwise

circulation distribution for all angles of attack within the linear range of section lift coefficient versus angle of attack, there is no corresponding propeller blade planform that gives the optimum radial circulation distribution for all advance ratios. Figure 8 presents plots of $(\Omega/\pi v')cc_\ell$ versus $\lambda x = r/R$ for three bladed propellers of minimum induced loss operating at the two advance ratios given on Figure 7. If the section lift coefficient, c_ℓ, is considered constant for all values of r/R, the curves may be interpreted as plots of the optimum radial chord distribution. It is seen that a propeller optimized for a low advance ratio needs blades with a wide chord inboard where the airspeed is low, and a narrow chord outboard where the airspeed is high. A propeller optimized for large advance ratios, on the other hand, will require a more elliptic distribution of chord since the blade element airspeeds are not so strongly dependent on the radial coordinate. In any event, it is seen that a propeller can only be optimized at one advance ratio and that a general theory of non-optimum propellers will be required to calculate propeller performance away from the design point.

A traditional method for doing this was developed by Glauert. In his scheme the differential increases in axial and rotational momentum in an annular element of slipstream of radius r and width dr are set equal separately to the thrust and torque components of the airload acting on each of the B blade elements, thus:

$$\frac{dT}{dr} = 2\pi\rho rV(1+a)2aV = \frac{1}{2}\rho W^2 BcC_y \qquad 13$$

and

$$\frac{1}{r}\frac{dQ}{dr} = 2\pi\rho rV(1+a)2a'r\Omega = \frac{1}{2}\rho W^2 BcC_x \qquad 14$$

where

$$C_y = c_\ell \cos\phi_i - c_d \sin\phi_i \qquad 15$$

$$C_x = c_\ell \sin\phi_i + c_d \cos\phi_i \qquad 16$$

Equations 13 and 14 are adapted for calculation by solving 13 for a and 14 for a', where σ is the local solidity, $Bc/2\pi r$:

$$\frac{a}{a+1} = \frac{\sigma C_y}{4 \sin^2\phi_i} \qquad 13a$$

$$\frac{a'}{1-a'} = \frac{\sigma C_x}{4 \sin\phi_i \cos\phi_i} \qquad 14a$$

An iterative procedure is employed at each of several blade radial stations whereby blade element angles of attack are assumed giving c_ℓ and c_d (airfoil properties),

$\phi_i = \beta - \alpha$ (β is the blade angle),

C_y and C_x (eqs. 15 and 16),

a and a' (eqs. 13a and 14a),

and finally

$$\phi_i = \tan^{-1}\left(\frac{V}{\Omega r}\right)\left(\frac{1+a}{1-a'}\right)$$

for each assumed value of α. The iteration is terminated when $\phi_i = \beta - \alpha = \tan^{-1}\left(\frac{V}{\Omega r}\right)\left(\frac{1+a}{1-a'}\right)$ and the converged values of C_y and C_x are then suitably integrated radially to yield the propeller thrust and torque (or power).

Equations 13 and 14 depend on the absence of radial flow in the slipstream, the very thing that Prandtl's vortex sheet spacing correction was intended to account for in the case of a propeller operating with minimum induced loss. Glauert in his article in Durand's "Aerodynamic Theory" (1934) suggested modifying Eqs. 13a and 14a to read

$$\frac{a}{1+a} = \frac{\sigma C_y}{4 \sin^2\phi_i F} \qquad 13b$$

$$\frac{a'}{1-a'} = \frac{\sigma C_x}{4 \sin\phi_i \cos\phi_i F} \qquad 14b$$

(there is a misprint in the book whereby the quantity F appears in the numerator of the right hand side of eqns. 13b and 14b instead of the denominator). Goldstein, in his doctor's thesis (published as "On the Vortex Theory of Screw Propellers" in the Proceedings of the Royal Society (A) 123, 440 1929) refined Prandtl's value for F by considering the flow about moving helicoidal surfaces of B sheets per turn rather than an array of moving flat plates. F. N. Lock proposed an alternative scheme based on Goldstein's values for F (Lock calls them $\mathcal{L}$, sometimes read "kappa") in which the momentum balance of eqns 13 and 14 is abandoned and the inflow velocity, w_i, (Fig. 1) is considered to be normal to the resultant velocity at the blade element, W. The inflow velocity, in turn, is considered to be half the developed slipstream velocity increment, w, given by a form of eq. 10:

$$B\Gamma(r) = 2\pi r(w \sin\phi)F \qquad 10b$$

Lock's procedure would be identical to Glauert's modified scheme if the blade elements had no drag. Theodorsen introduced a correction to Lock's procedure to allow for slipstream contraction; he also verified Goldstein's F values by rheo-electric analog computation, and extended them to the case of intersecting helicoidal vortex sheets, as would be trailed by a counterrotating propeller. Lock's method has recently been reviewed by Pauling ("The Effects of Uncertainties on Predicting Rotor and Propeller Performance", Pennsylvania State University report PSU AERSP 75-3) who wrote a digital computer program to carry out a version of Lock's procedure with several optional features, including a slipstream contraction effect. I personally am bothered by the fact that all of these non-optimum propeller theories depend on Prandtl or Goldstein F values, which are calculated on the assumption of trailing vortex sheet geometry appropriate to a propeller of minimum induced loss. The procedures are analogous to an approximate lifting line wing theory in which the two dimensional lift on a chordwise element is corrected by $[1-(2y/b)^2]^{1/2}$ to account for three dimensional flow effects.

Figure 9 presents a marvelous smoke flow visualization photograph of the operation of a two bladed propeller obtained by Prof. F. N. Brown at Notre Dame. The helicoidal vortex sheets are seen to roll up rather rapidly as they are left behind in the slipstream by the propeller blades, exactly in the way that the trailing vortex sheet left behind a wing does. The picture suggests that the propeller is not optimally loaded because there is perhaps not enough axial motion of the inboard portions of the trailing vortex sheets--although this is difficult to judge, because the sheet is marked by smoke particles which have <u>both</u> rotational as well as axial velocities, while the "apparent" v' of the theory specifies the motion of the helicoidal <u>surfaces</u> past a fixed point; for example, the "apparent" axial velocity v' component due to "barber pole" helix rotation, $v'_{bp} = w_t \tan\phi$, does not show in the picture.

I will conclude this presentation of propeller theory with the observation that the propeller equivalent of lifting line theory does not exist, and that all propeller computation procedures contain some element of empiricism. Helicopter aerodynamicists have had some success in the application of machine based discrete vortex models to the prediction of rotor characteristics; see for example Landgrebe's "The Wake Geometry of a Hovering Helicopter Rotor and its Influence on Rotor Performance" (Journal of the American Helicopter Society, Vol 17, no. 4, October 1972), but in my opinion work still needs to be done.

Figure 10 shows a research propeller constructed at M.I.T. for testing in the water tunnel of the Marine Hydrodynamic Laboratory. The propeller was designed to have two blades of a minimum induced loss geometry appropriate in an application to a direct drive 1700cc Volkswagen engine installation which develops 47 hp at 3800 rpm at sea level. The full scale propeller would have a diameter of 50 inches and be optimized at 120 mph, giving an advance ratio $J = V/nD = 0.667$ ($\lambda = 0.212$). The model propeller had a diameter of 12 inches and was constructed so it could be tested either in a four blade or a two blade version, since additional blades could be readily made once the milling machine cam had been constructed to make one blade.

Figure 11 shows the propeller operating near its design advance ratio in the water tunnel at a pressure low enough to cause appreciable cavitation over the outer quarter of the blades. Note that the propeller is tested in a pusher configuration with the shaft extending upstream into the tunnel stilling section, and with a spinner fitted downstream to preserve good flow at the inboard blade stations. The compound helical character of the cavitation marked tip vortex core is noteworthy.

Figure 12, finally, presents the measured characteristics of this propeller as tested in the water tunnel at a loading high enough to produce light cavitation. The effects of cavitation are seen in the upward bulge and the downward dip of the torque and thrust curves, respectively. The peak efficiency of 85%, obtained at an advance ratio, $J = 0.8$, is the highest ever measured in this tunnel.

It is hoped that this paper will encourage general aviation aerodynamicists to seek propeller geometries better suited to the operation of their own airplanes than the compromise production propellers available as off-the-shelf items. It should be borne in mind that the interference flows produced at the propeller by a large fuselage downstream need to be taken into account in the design of an actual propeller, and that efficient propellers inevitably create large slipstream swirl components on the fuselage nose and flanks which should be considered in the design of engine air inlets, carburetor air scoops, exhaust stacks, landing gear struts, and even door handles.

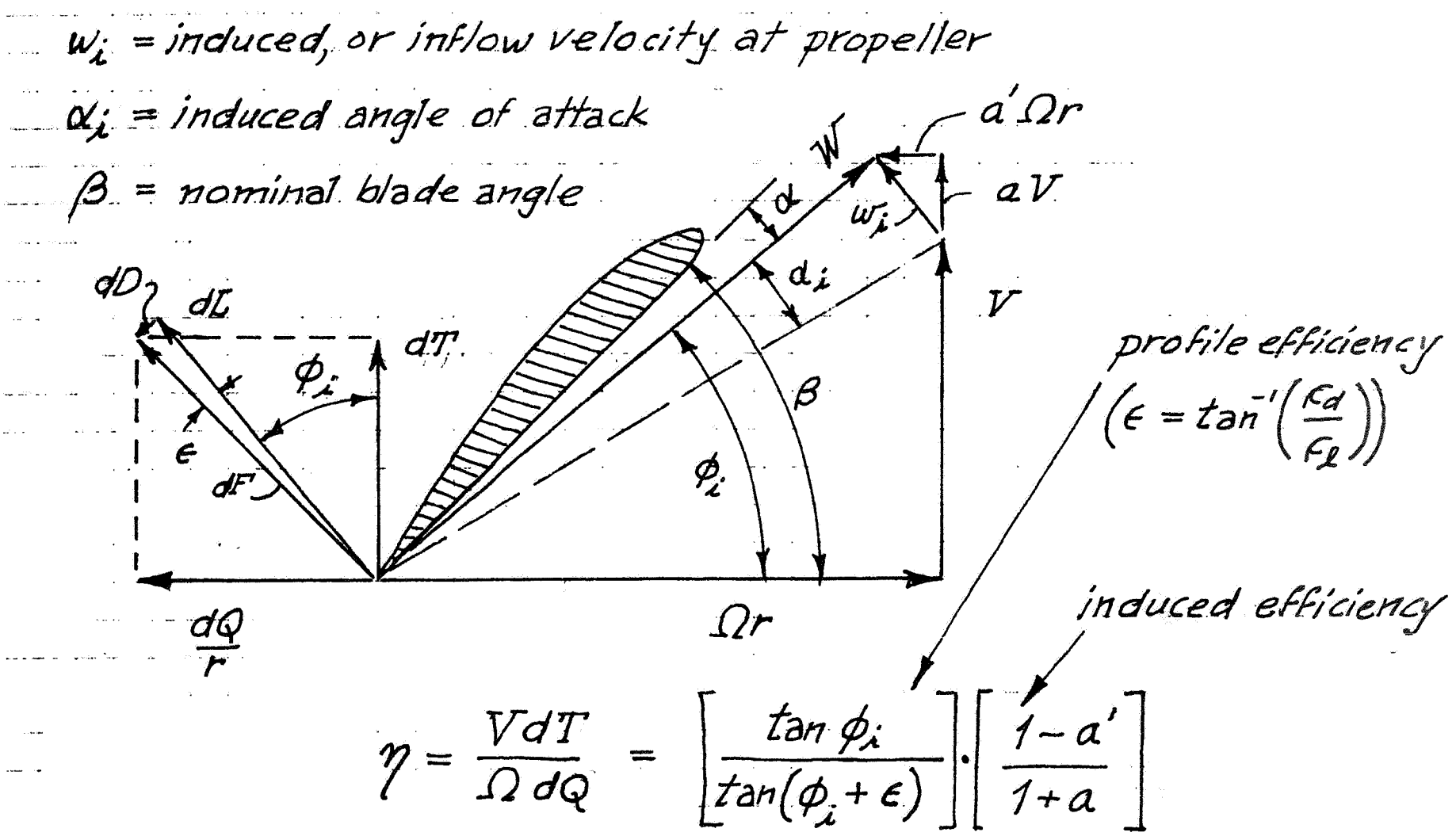

Figure 1. Blade Element Geometry

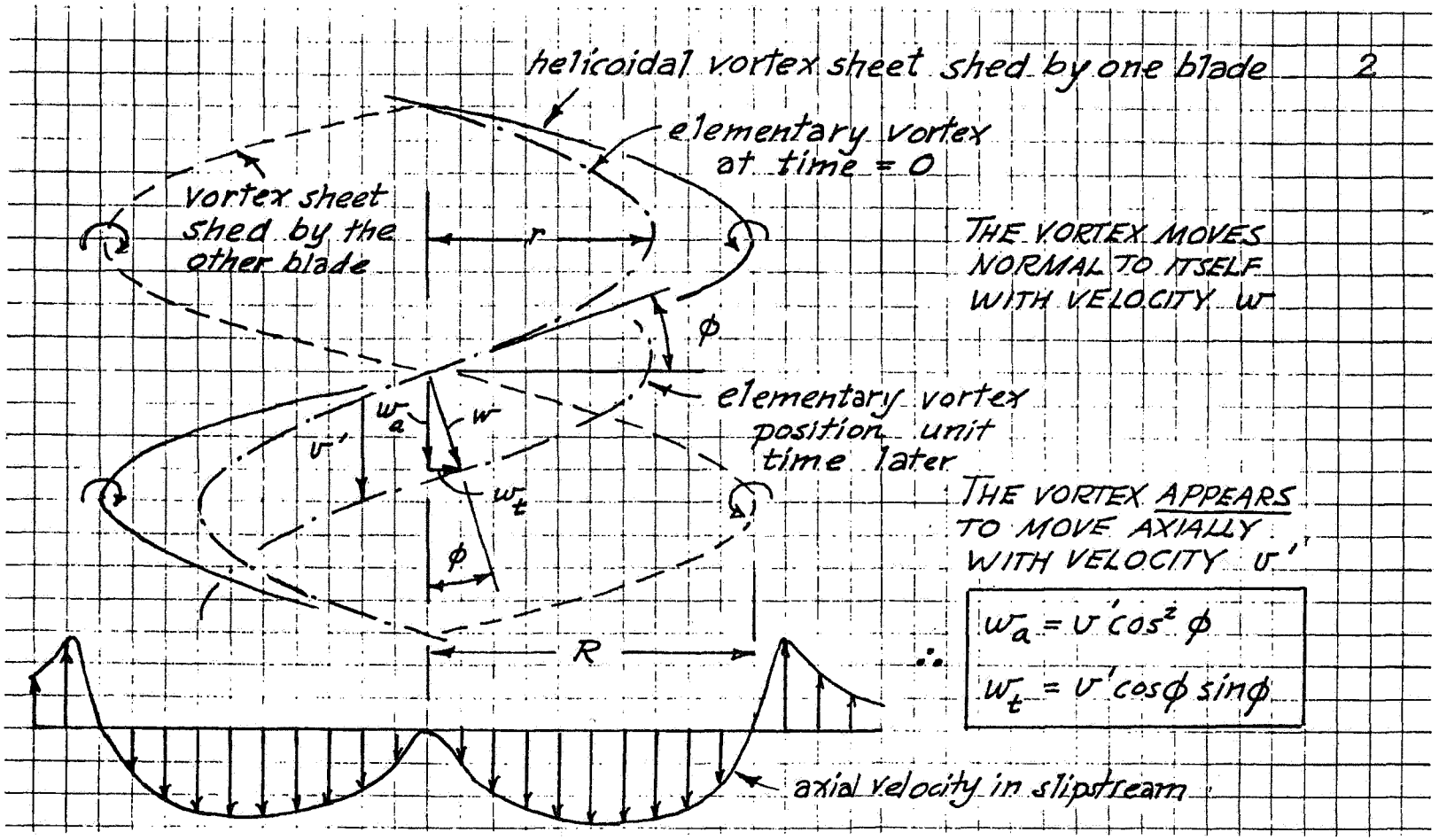

Figure 2. Propeller Slipstream Vortex Geometry

$$\tan\phi \cong \tan\phi_i \cong \frac{V}{\Omega r} \quad \begin{cases} \sin\phi = \dfrac{V}{\sqrt{V^2+\Omega^2 r^2}} \\ \cos\phi = \dfrac{\Omega r}{\sqrt{V^2+\Omega^2 r^2}} \end{cases}$$

in the slipstream

$$w_a = v'\cos^2\phi = v'\left(\frac{\Omega^2 r^2}{V^2+\Omega^2 r^2}\right)$$

$$w_t = v'\cos\phi\sin\phi = v'\left(\frac{V\Omega r}{V^2+\Omega^2 r^2}\right)$$

at the propeller

$$a = \frac{w_a}{2V} = \frac{1}{2}\left(\frac{v'}{V}\right)\left(\frac{\Omega^2 r^2}{V^2+\Omega^2 r^2}\right)$$

$$a' = \frac{w_r}{2\Omega r} = \frac{1}{2}\left(\frac{v'}{V}\right)\left(\frac{V^2}{V^2+\Omega^2 r^2}\right)$$

Figure 3. "Lightly Loaded" Propeller Relations

$$\eta_{induced} \equiv \frac{1-a'}{1+a} \cong \frac{1}{1+a+a'} = \frac{1}{1+\frac{1}{2}\left(\frac{v'}{V}\right)}$$

THE INDUCED EFFICIENCY FOR THE PROPELLER AS A WHOLE IS MAXIMIZED IF v'/V IS INDEPENDENT OF r

For a slipstream with "closely spaced" vortex sheets the circulation at radius r is

$$\Gamma_{total} = 2\pi r w_t$$

This is equal to the bound circulation on each of B blades at radius r (neglecting wake contraction) so that, for any blade

$$\Gamma(r) = \frac{2\pi r w_t}{B} = \left(\frac{2\pi v'}{B}\right) \frac{V\Omega r^2}{V^2+\Omega^2 r^2}$$

which may be written as

$$\left(\frac{B\Gamma\Omega}{2\pi V v'}\right) = \frac{\Omega^2 r^2}{V^2+\Omega^2 r^2} = \frac{x^2}{1+x^2}$$

where $x = \Omega r/V$

Figure 4. Betz's Minimum Induced Loss Condition (1919)

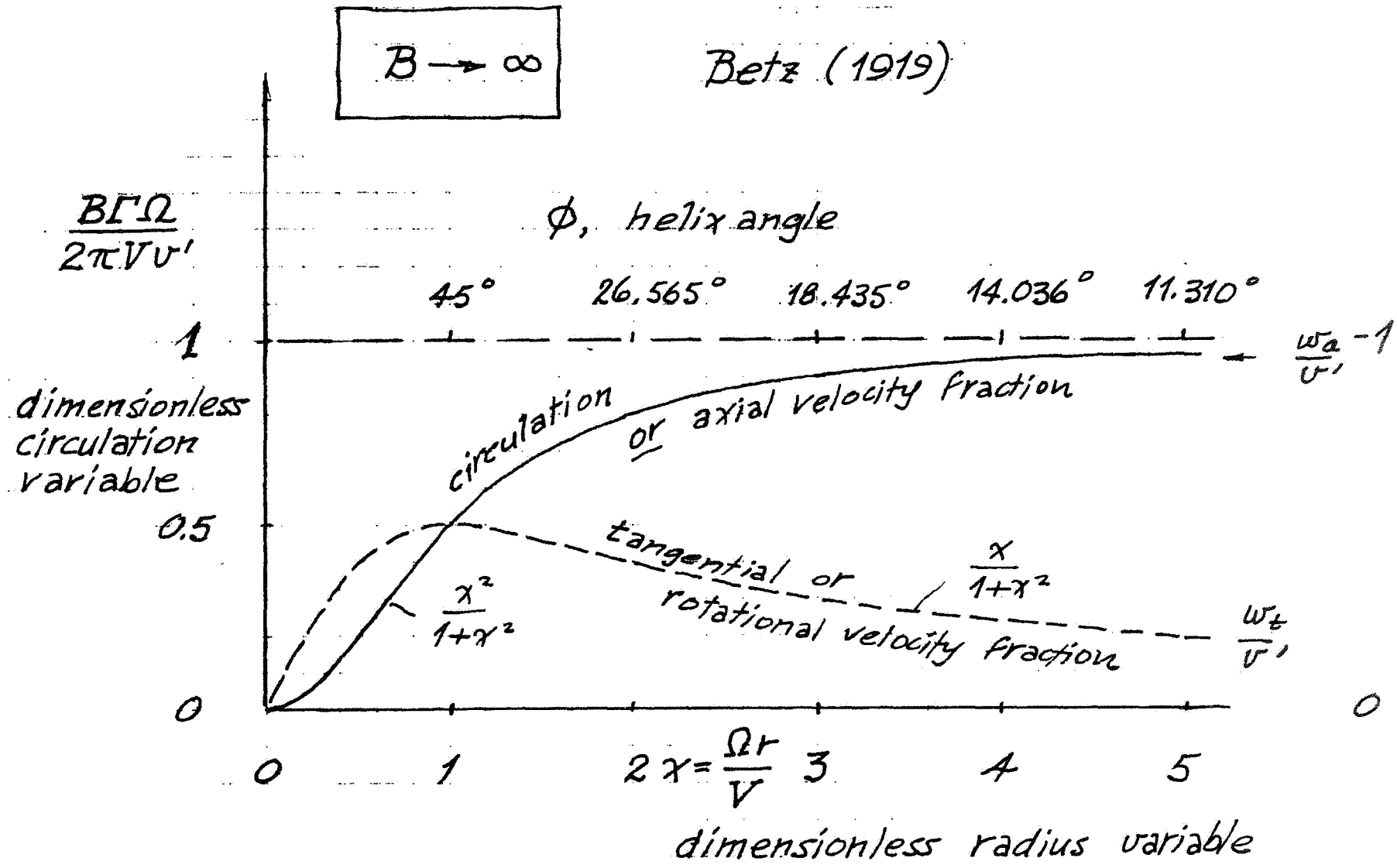

Figure 5. Radial Circulation Distribution for Minimum Loss

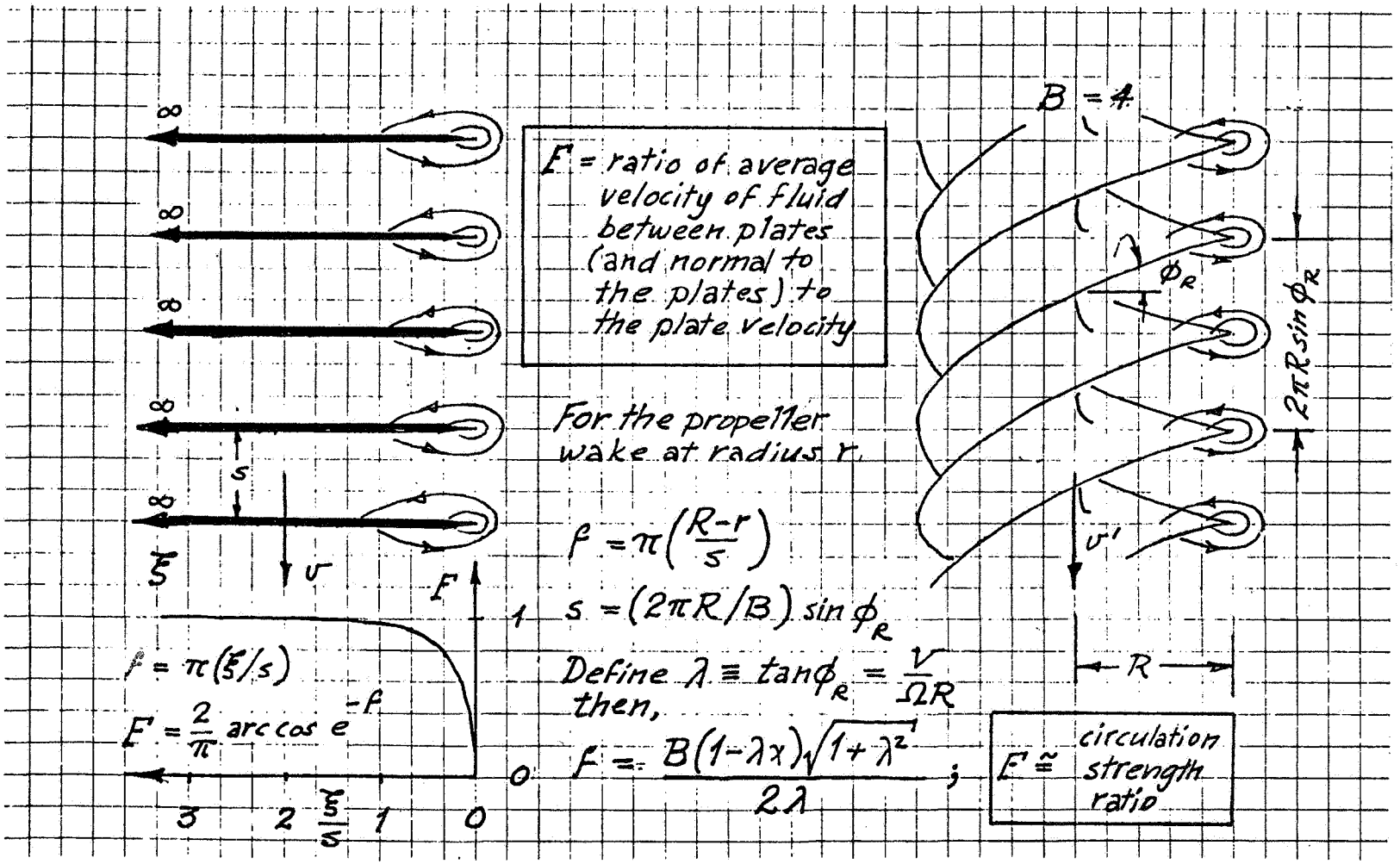

Figure 6. Prandtl's Vortex Sheet Spacing Correction (1919)

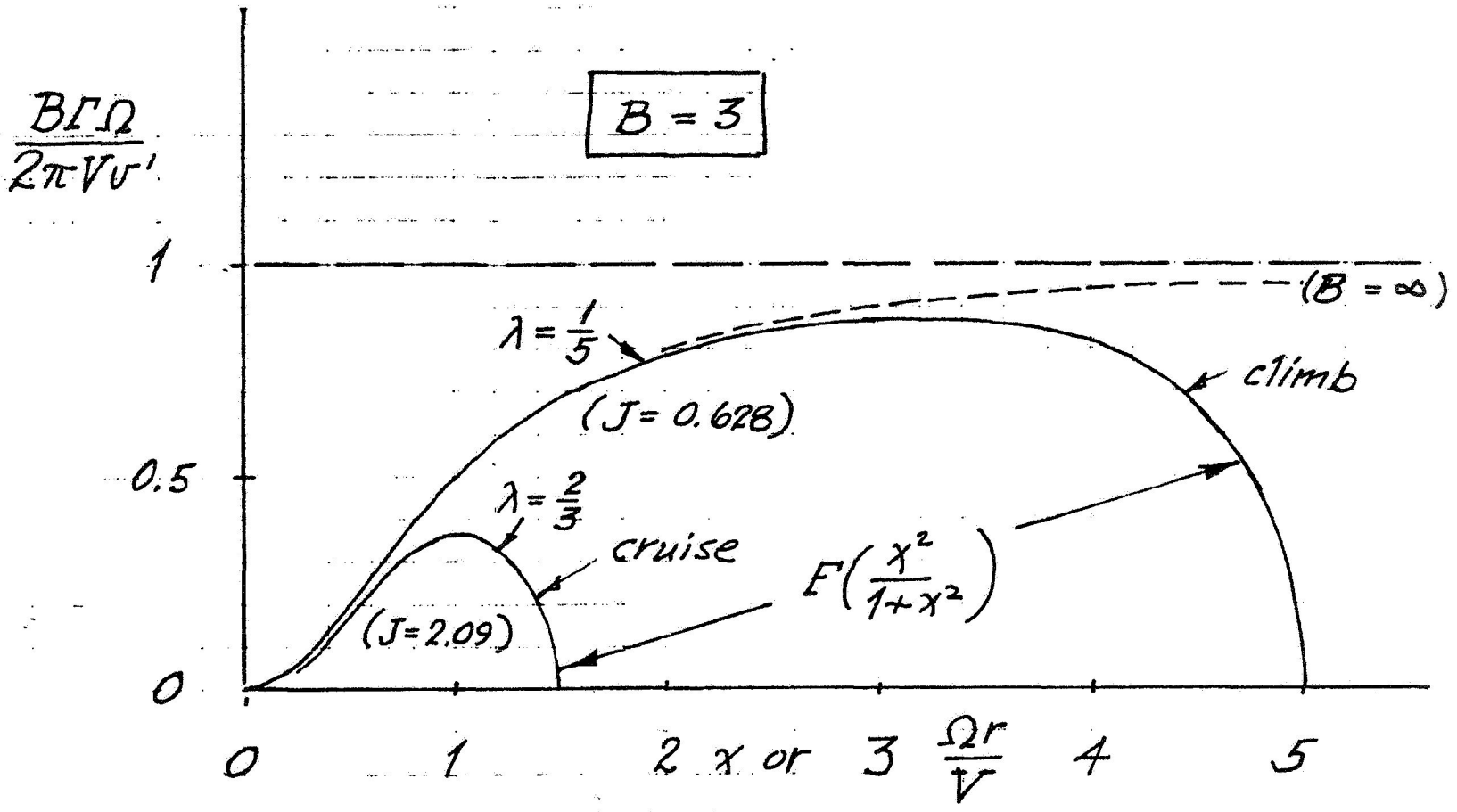

Figure 7. Typical Circulation Distributions for Minimum Induced Loss

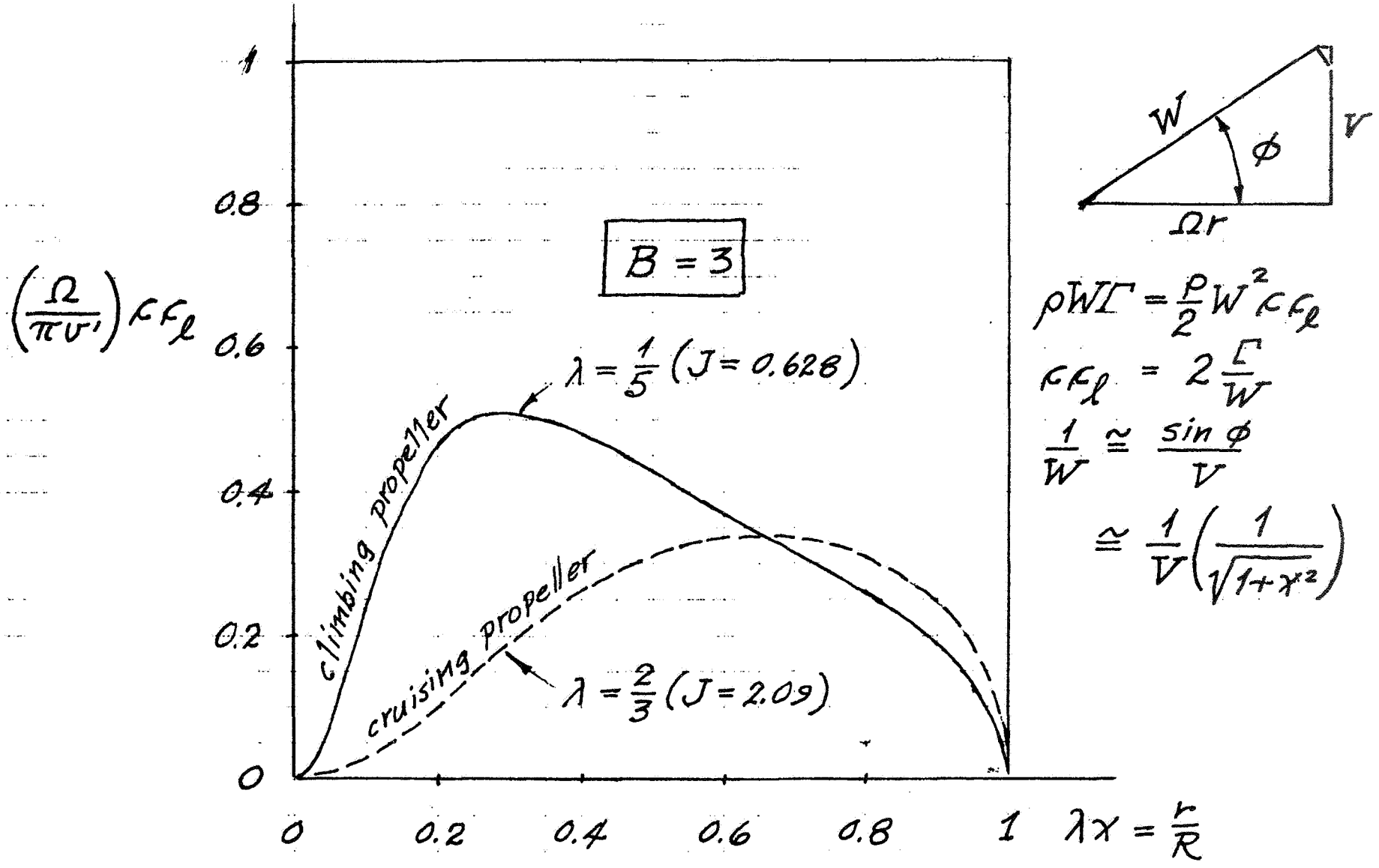

Figure 8. Typical Blade Chord Distributions for Minimum Induced Loss

Figure 9. Flow Visualization of a Two-Bladed Propeller
(Professor F.N.M. Brown's Propeller Smoke Picture - 1950)

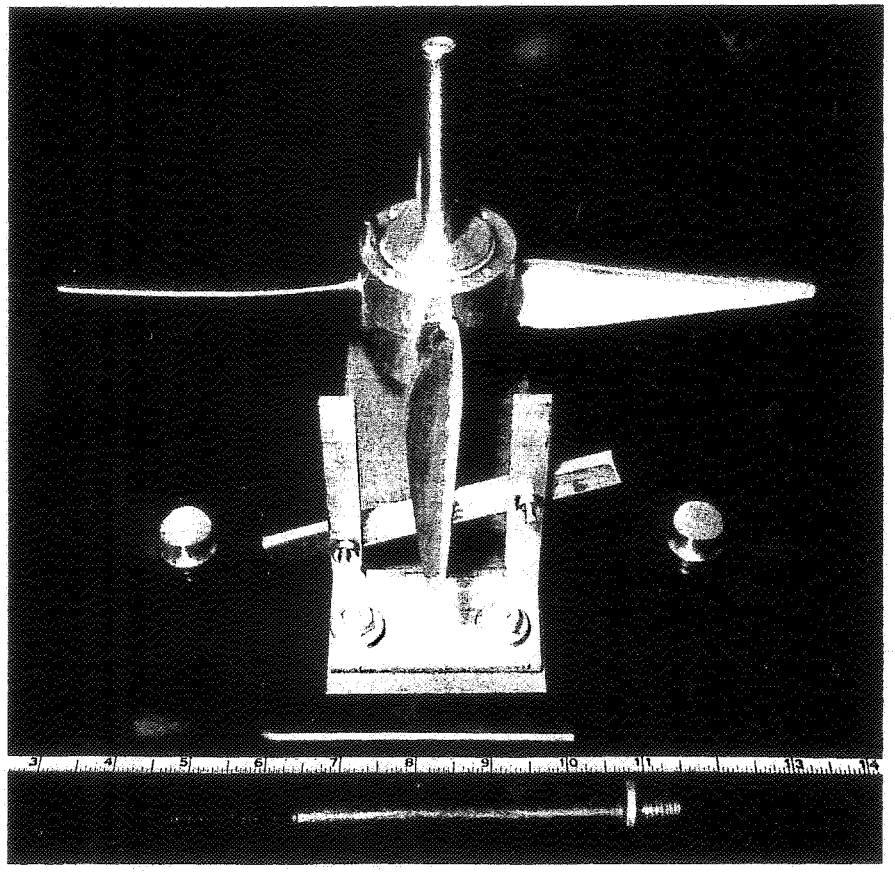

Figure 10. M.I.T. Research Propeller for Water Tunnel Tests

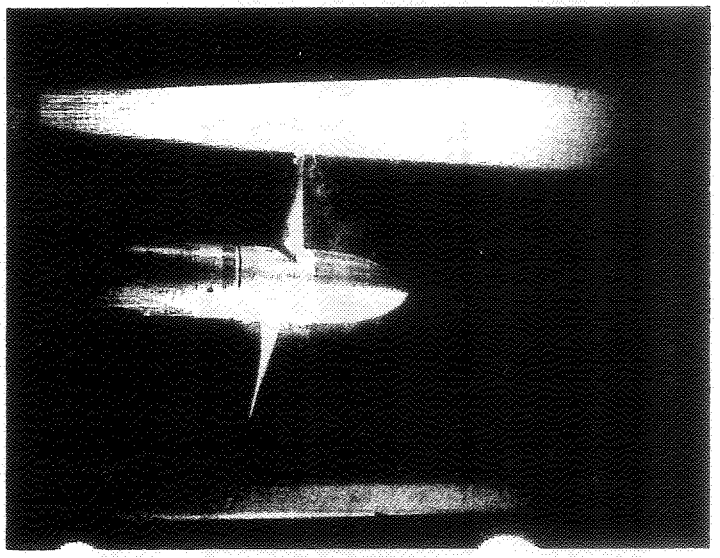

Figure 11. M.I.T. Research Propeller Operating Near Design Advance Ratio in Water Tunnel

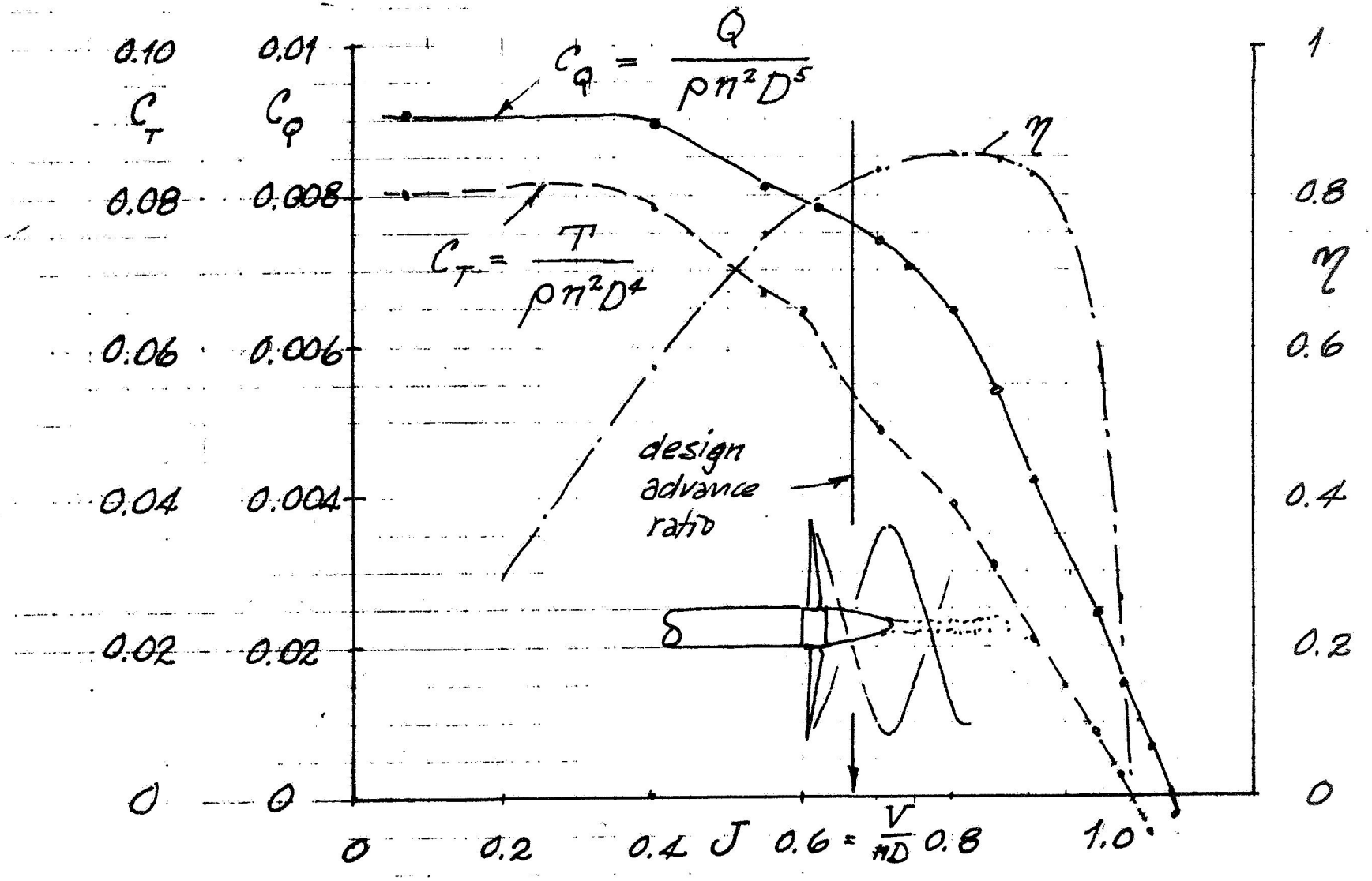

Figure 12. Water Tunnel Tests of a Minimum Induced Loss Propeller

7. PAPERS OF SESSION V - TRIM DRAG

7.1 Some Comments on Trim Drag

Jan Roskam
University of Kansas

Introduction

This paper presents a discussion of data of and methods for predicting trim drag. Specifically the following subjects are discussed:

- Economic impact of trim drag.
- The trim drag problem in propeller driven airplanes and the effect of propeller and nacelle location.
- Theoretical procedures for predicting trim drag.
- Research needs in the area of trim drag.

An Example of the Economic Importance of Trim Drag

Trim drag is here defined as the horizontal tail induced drag caused by the need to trim the airplane for $C_m = 0$. Tail profile drag is included in overall airplane zero lift drag.

Trim drag typically varies from .5 percent to five percent of total airplane drag in cruise, depending on airplane type and on center of gravity location.

For a typical business jet, Figure 1 shows the variation of $\Delta C_{D_{trim}}$ with center of gravity location. Using this example, assuming a cruise L/D = 10.8, a cruise thrust required of 1092 lbs. at M = .72 and 45,000 ft., Table 1 shows the fuel flow caused by this drag for three c.g. locations.

Table 2 summarizes what this means for an operation using one airplane 1000 hours per year. Table 2 also shows what the fuel expenditures due to trim drag are for a fleet of 500 airplanes in one year.

Although trim drag by itself seems so small as to be negligible, integrating it over time and fleets indicates that more careful attention should be paid to trim drag.

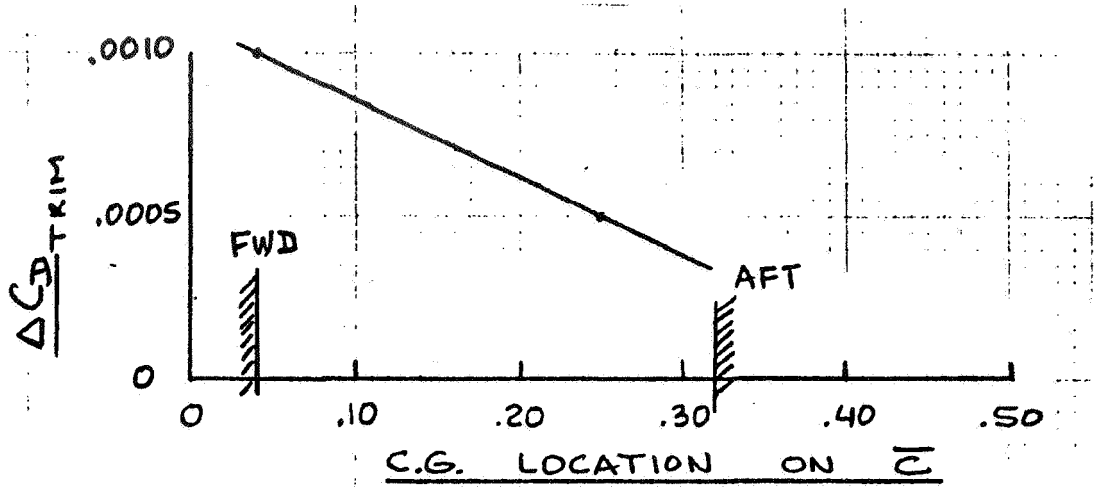

Figure 1. Example of Trim Drag Variation with Center of Gravity Location

Table 1. Fuel Flow due to Trim Drag as Function of Center of Gravity Location

Center of Gravity (See Fig. 1)	Fuel Flow due to Trim Drag (lbs./hr.)
FORWARD LIMIT	39
MID	19.5
AFT LIMIT	12

Table 2. Economic Importance of Trim Drag

	Aft C.G. extra gallons burned due to trim drag	Fwd C.G. extra gallons burned due to trim drag
1 airplane 1000 hours	1832	5954
500 airplanes 1000 hours each	916,000	2,977,000

The Trim Drag Problem in Propeller Driven Airplanes

Illustration of the Problem - It would seem that the designer, when trying to minimize drag, including trim drag is confronted with many unsolved problems. To illustrate the complexity of the design problem when including trim drag, consider Figure 2 and the following equations which need to be satisfied:

$$C_M = C_{m_o} + \frac{\partial C_{m_o}}{\partial T_c} T_c + C_{m_\alpha}\alpha + \frac{\partial C_{m_\alpha}}{\partial T_c} T_c \alpha + C_{m_{\delta_E}}\delta_E + \frac{\partial C_{m_{\delta_E}}}{\partial T_c} \delta_E T_c \delta_E + C_{m_{i_H}} i_H + \frac{\partial C_{m_{i_H}}}{\partial T_c} i_H T_c i_H \qquad (1)$$

$$C_L = C_{L_o} + \frac{\partial C_{L_o}}{\partial T_c} T_c + C_{L_\alpha}\alpha + \frac{\partial C_{L_\alpha}}{\partial T_c} T_c \alpha + C_{L_{\delta_E}}\delta_E + \frac{\partial C_{L_{\delta_E}}}{\partial T_c} \delta_E T_c \delta_E + C_{L_{i_H}} i_H + \frac{\partial C_{L_{i_H}}}{\partial T_c} i_H T_c i_H \qquad (2)$$

$$C_D = C_{D_o} + \frac{C_{L_{WBV}}^2}{\pi A e|_W} + \frac{C_{L_H}^2}{\pi A e|_H} \frac{q_H}{q} \frac{S_H}{S_W} \qquad (3)$$

$$C_{L_H} = a_H \left(\alpha + i_H + \alpha_{\delta}\delta_E - \varepsilon - \frac{\partial \varepsilon}{\partial T_c} T_c\right) \qquad (4)$$

$$C_L = C_{L_{WBV}} + C_{L_H} \frac{q_H}{q} \frac{S_H}{S_W} \qquad (5)$$

It is noted that all coefficients and derivatives in equations 1 through 5 are functions of the shape of the configuration (including fuselage camber) and the location an angular orientation of the thrustline. The question which needs to be answered is how to optimize L/D. In view of potential importance of trim drag and the interaction of associated design decisions with the handling qualities of the airplane, some theoretical (methodological) research into this area seems needed. Certainly no solution to this problem is readily available today, except perhaps in the case of pure jet airplanes.

In nearly all current propeller driven general aviation airplanes, trim drag is ignored, so that the entire problem of trying to minimize it as part of the overall drag does not come up.

Illustrations of the Effect of Nacelle and Propeller Location on Trim Drag - Reference 1 shows the importance of thrust coefficient on C_{M_o} of different airplane configurations. Figure 3 illustrates the favorable effect increasing thrust coefficient can have on C_{M_o}. At the same time, Figure 4 shows how decreasing wing height

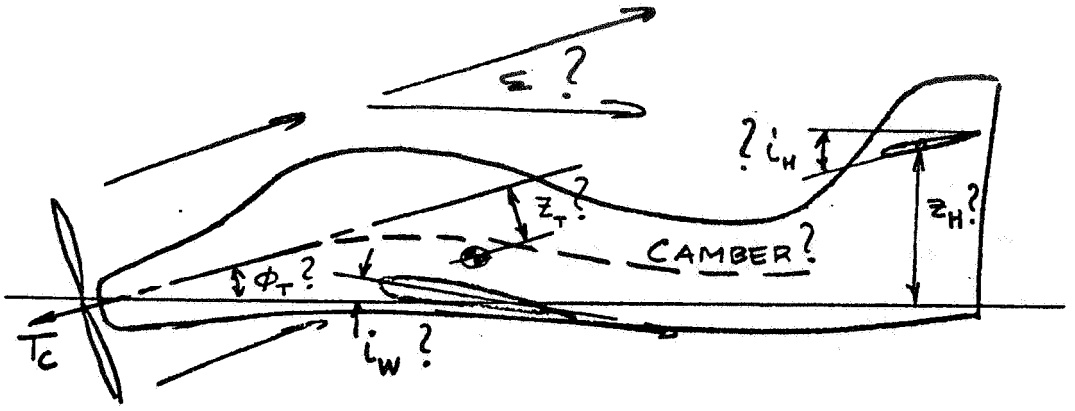

Figure 2. Illustration of Design Choices Affecting Trim Drag

can have an unfavorable effect on C_{M_o}. (A change in C_{M_o} of $|.10|$, using $C_{M_{\delta E}} = -.02$ means a 5 degree change in elevator required for trim.)

Reference 2 shows that a downward tilt of 5^o of the propeller axis of a typical WWII fighter configuration can cause an aft shift in a.c. of 5 to 10 percent, while also causing very large changes in C_{M_o}. Even though the aft shift in a.c. may be desirable to attain satisfactory longitudinal stability on high horsepower configurations the effect on trim drag is unfavorable.

These illustrations are meant to show the importance of considering the complicated interactions of these factors. No simple, reasonably accurate preliminary design procedures exist to account for them. Evidently there is a need to develop them.

A Method for Predicting Trim Drag of Jet Airplanes

Figure 5 illustrates the relation between WBV-lift and H-lift vectors. Note that it is not immediately clear from Figure 5 whether overall lift-to-drag ratio improves or deteriorates with c.g. movement. This depends to a large extent on the L/D of WBV in its untrimmed state relative to the value of $L/D|_{max}$ of WBV. It evidently also depends on whether the tail is uplifting or downlifting to achieve pitching moment balance. (These comments also apply to propeller driven airplanes.) Figure 6 illustrates the possibilities and Figure 7 shows the potential outcome.

Reference 3 shows that the trimmed drag coefficient of a tail-aft configuration can be estimated from:

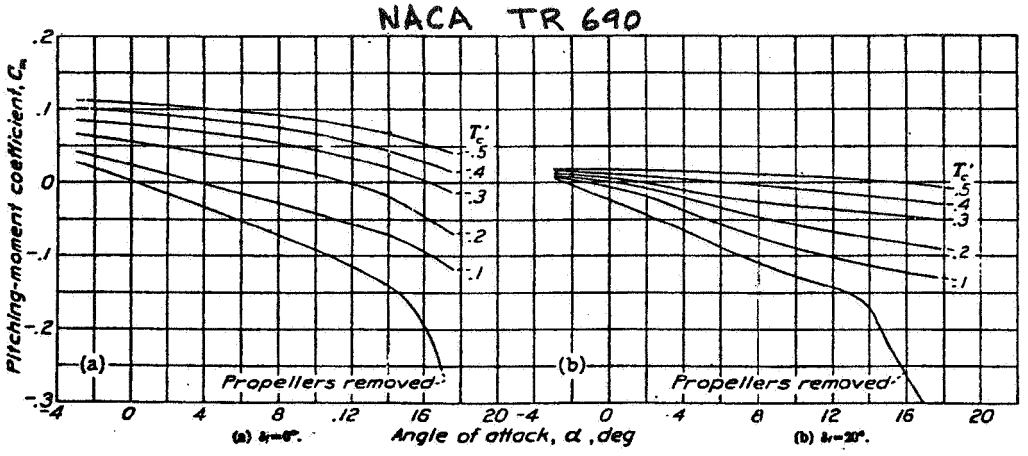

Figure 3. Effect of Propeller Operation on the Pitching-Moment Coefficient

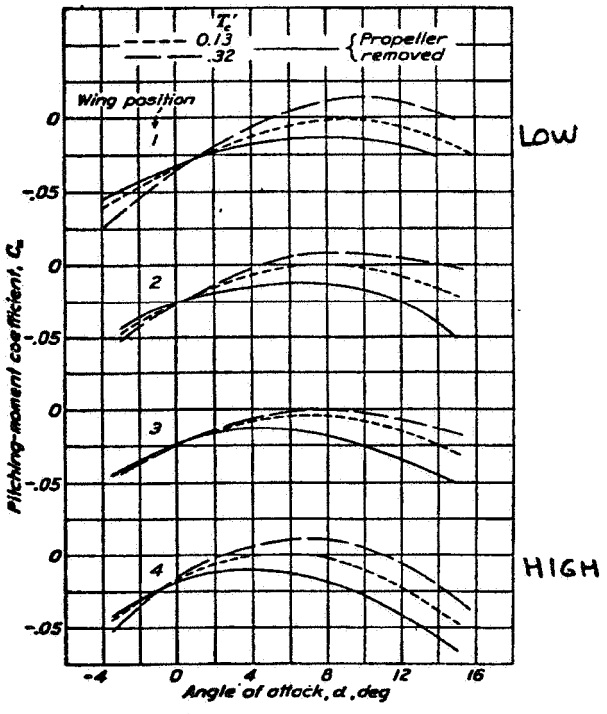

Figure 4. Effect of Propeller Operation on the Pitching-Moment Coefficient

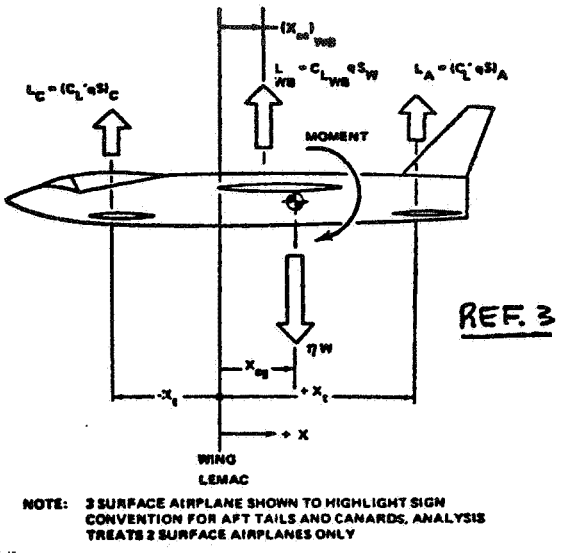

Figure 5. Coordinate System and Sign Convention

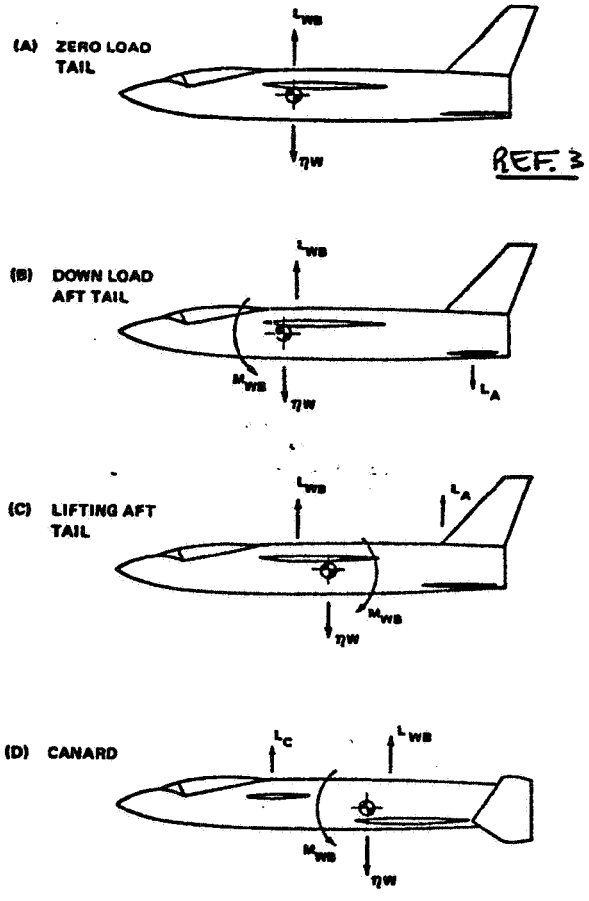

Figure 6. Effect of Center of Gravity and Wing-Body Aerodynamic Center Location on Lift Sharing $C_{M_o} = 0$.

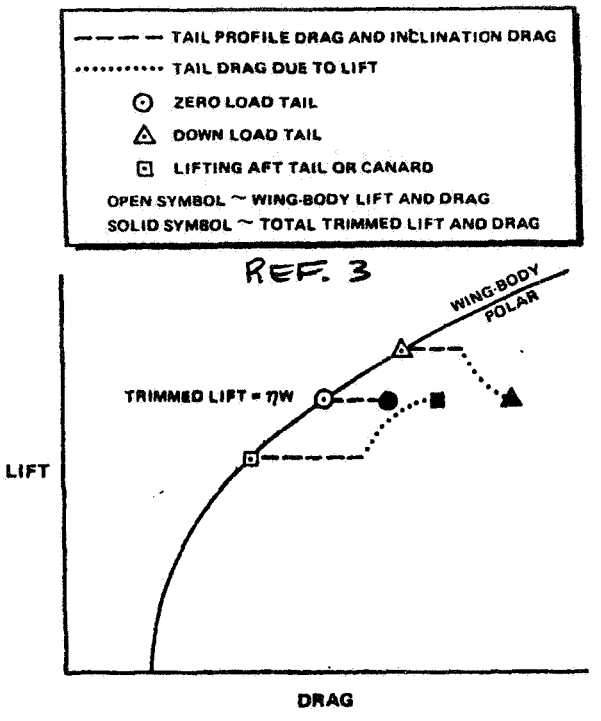

Figure 7. Trim Drag Elements

$$C_{D_{TRIM}} = C_{D_{o_{WBV}}} + C_{D_{o_H}} \frac{S_H}{S_W} \frac{q_H}{q} + \frac{(C_L - C_{L_o})^2_{WBV}}{\pi A e|_{WBV}} + \frac{C_{L_H}^2}{\pi A e|_H} \frac{S_H}{S_W} \frac{q_H}{q} \qquad (6)$$

Note the absence of thrust effect terms.

Expressions for $C_{L_{WBV}}/C_{L_{trim}}$ and $C_{L_H}/C_{L_{trim}}$ can be found by imposing the conditions that total lift equals airplane weight (level flight) and that the total pitching moment is zero:

$$C_m = C_{m_{o_{WBV}}} + C_{m_{\alpha_{WBV}}} \alpha + C_{m_H} \qquad (7)$$

where

$$C_{m_H} = - C_{L_H} \frac{\ell_H}{\bar{c}_w} \frac{q_H}{q} \qquad (8)$$

and

$$C_{m_{\alpha_{WBV}}} = (\bar{X}_{cg} - \bar{X}_{ac_{WBV}}) C_{L_{\alpha_{WBV}}} \qquad (9)$$

Reference 3 shows for fighter type configurations that this method gives accurate results. Results indicate that trim drag can affect the trimmed L/D of such configurations by $\pm$ 7 percent depending on overall arrangement and c.g. location.

From equation (7) it is evident that C_{M_o} can play a role in reducing adverse (i.e., down load on tail) trim requirements. It would be desirable to give the airplane a positive value of $C_{M_o} > 0$ by fuselage camber. What is not known today, is how the general aviation fuselage can be shaped in such a way that:

1. C_{M_o} is as close as possible to being positive
2. fwd visibility and windshield shape are compatible with $C_{M_o} > 0$ and low windshield drag
3. contour lines are not expensive to produce
4. aft fuselage shape does not violate take-off rotation requirements.

Some systematic research into this area may very well pay off. Perhaps a theoretical trade-off study of a wide range of fuselage camber shapes should precede a systematic windtunnel investigation.

The effect of wing mounted nacelles on C_{M_o} and C_{D_o} should also be investigated in a systematic manner. The latter in view of the fact that general aviation twins use widely varying wing-nacelle shapes not all of which can be particularly good. (See Reference 4.)

Summary of Research Needs in the Trim Drag Area

In view of the fact that trim drag can affect the cruise lift-to-drag drag ratio by up to seven percent, it would seem desirable to have procedures available to accurately account for it. For propeller driven airplanes these procedures do not seem to exist.

Because of the potentially large effect of C_{M_o} on trim drag, this quantity should be accurately predictable. It is not today.

The following research is therefore needed:

1. Development of a theoretical procedure to predict C_{M_o} including propeller thrust interactions;
2. Development of a preliminary design method for predicting trim drag of propeller configurations; and
3. Configuration research to see if perhaps other than conventional tail-aft configurations are capable of yielding better cruise lift-to-drag ratios.

References

1. Katzoff, S.; Longitudinal Stability and Control with Special Reference to Slipstream Effects; NACA TR 690, 1940.
2. Goett, H.J. and Delany, N.K.; Effect of Tilt of the Propeller Axis on the Longitudinal Stability Characteristics of Single-Engine Airplanes; NACA TR 774, 1944.
3. Goldstein, S.E. and Combs, C.P.; Trimmed Drag and Maximum Flight Efficiency of Aft Tail and Canard Configurations; AIAA Paper 74-69 presented at the AIAA 12th Aerospace Sciences Meeting, Jan. 30 - Feb. 1, 1974, Washington, D.C.
4. Roskam, J.; Drag of the Complete Configuration, Part II, Aerodynamic Considerations; Paper presented at the NASA/Industry/University General Aviation Drag Reduction Workshop; July 14, 15, 16, 1975, The University of Kansas.

7.2 Trim Drag Research Results

H. Chevalier
Texas A & M University

This paper was not submitted for inclusion in these proceedings.

Preceding Page Blank

7.3 Reduction of Trimmed Drag

F. H. Lutze, Jr.
Virginia Polytechnic Institute and State University

It is important at the outset to distinguish between "trim drag" and "trimmed drag." According to the USAF Stability and Control Handbook,[1] the trim drag coefficient is "the drag coefficient increment between the drag coefficient of the complete vehicle in pitch equilibrium and the drag coefficient of the wing-body-vertical tail configuration." The trimmed drag coefficient, on the otherhand, is the drag coefficient of the complete vehicle in pitch equilibrium. It is clear that our interest should be focused on reducing the trimmed drag and not on the nebulous problem of reducing the trim drag penalty. Consequently, emphasis will be placed on the complete configuration and the associated trimmed lift and drag with particular attention paid to the load distribution between the wing-body and the tail surfaces.

Aircraft Equations for Equilibrium, Balance, and Drag

The equations for the total aircraft lift and pitching moment coefficient are given by (for small downwash, ϵ)[2], [6]

$$C_L = a_{wb} (\alpha - \alpha_{owb}) + C_{L_t} n_t S_t/S \tag{1}$$

and

$$C_m = C_{m_{owb}} + C_{m_{\alpha wb}} (\alpha - \alpha_{owb}) - C_{L_t} n_t S_t/S \; l_t/\bar{c} \tag{2}$$

For balance in equilibrium flight, $C_m = 0$, allowing equations (1) and (2) to be solved for the tail lift coefficient and the aircraft angle of attack:

$$C_{L_t} = \frac{C_{m_{\alpha wb}} C_L + a_{wb} C_{M_{owb}}}{n_t S_t/S \left(a_{wb} \frac{l_t}{\bar{c}} + C_{m_{\alpha wb}}\right)} \tag{3}$$

$$\alpha - \alpha_{owb} = \frac{\frac{l_t}{\bar{c}} C_L - C_{m_{owb}}}{a_{wb} \frac{l_t}{\bar{c}} + C_{m_{\alpha wb}}} \tag{4}$$

Equations (3) and (4) govern the distribution of the required lift force between the wing and the tail and insure a zero pitching moment. Several observations can be made concerning these equations:

(i) The tail contribution to the aircraft lift coefficient, $(C_L)_t = C_{L_t} \eta_t S_t/S$, is a function of wing-body properties, c.g. position, and lift coefficient. Consequently for a given speed and weight, $(C_L)_t$, the tail load can be adjusted by shifting the c.g. position or by changing the wing-body aerodynamic characteristics.

(ii) The expression in the denominator common to both equations is independent of the c.g. position.

(iii) The magnitude of C_{L_t} determined by equation (3) must be less than $C_{L_{tmax}}$.

The key to the selection of wing-body parameters and c.g. position is the introduction of the aircraft drag coefficient. We would like to select these parameters to reduce or minimize the drag coefficient for a given lift coefficient. The drag coefficient for the aircraft is given by (for small downwash ϵ):[6]

$$C_D = C_{D_{owb}} + K_{wb} C_{L_{wb}}^2 + [(C_{D_{ot}} + K_t C_{L_t}^2 + C_{L_t} \varepsilon) \eta_t S_t/S] \tag{5}$$

where

$$C_{L_{wb}} = a_{wb} (\alpha - \alpha_{owb})$$

$$\varepsilon = \varepsilon_o + \frac{\partial \varepsilon}{\partial \alpha} \alpha \equiv \frac{\partial \varepsilon}{\partial \alpha} (\alpha - \alpha_{owb}) + \bar{\varepsilon}_o \tag{6}$$

The bracketed term in equation (5) is the trim drag coefficients as indicated by the definition at the beginning of the paper.

The problem of the aircraft designer then is to select the wing-body aerodynamic parameters and c.g. position such that the trimmed drag coefficient given

by equation (5) is minimized in some sense, subjected to the equilibrium lift and zero pitching moment constraints given by equations (3) and (4). Conventional design practices also require that certain inherent stability specifications be satisfied. Consequently in current design practices the stability and performance characteristics of an aircraft are virtually determined independent of each other in the sense that one aspect (stability) is considered and then the other (performance).[3]

The continuous improvement of digital computational equipment with respect to size, speed and reliability has led to the consideration of utilizing digital control systems to maintain stability, reducing the number of constraints on the selection of c.g. position and wing-body aerodynamic parameters to reduce the aircraft drag coefficient.[4], [5] These increased degrees of freedom present a considerable challenge to the aircraft designer leading to some of the new concepts of design associated with controlled configured vehicles. Although it is anticipated that such sophisticated control systems will not be available for general aircraft for a considerable period of time the advantages of such systems should not be completely ignored.

In what follows the concept of reducing the aircraft drag coefficient by appropriate selection of the wing-body aerodynamic parameters and c.g. position, will be examined. This approach is equivalent to finding the minimum drag for a given speed as opposed to maximum L/D for the aircraft.

C.G. Position for Minimum Drag

If we ignore stability requirements it is possible to determine the c.g. position which minimizes the drag coefficient for a given lift coefficient. In order to accomplish this, the appropriate terms in (5) are replaced by the expressions given in (3), (4) and (6). Furthermore the c.g. position can be introduced by noting the following relations:

$$\frac{l_t}{\bar{c}} = h_t - h_o \qquad (7)$$

$$C_{m_{awb}} = a_{wb} (h_o - h_{nwb})$$

where h_x is position of x in chord lengths behind the leading edge of wing and

x = 0 c.g. position

= t tail aerodynamic center

= nwb wing-body aerodynamic center

The derivative of the drag coefficient with respect to c.g. location can be evaluated and set equal to zero. The resulting expression can then be solved for the c.g. position, h_o, which provides minimum drag coefficients. The result is

$$h_o = \frac{[(2k_{wb}a_{wb} - \frac{\partial\varepsilon}{\partial\alpha})h_t + (2k_t'a_{wb} - \frac{\partial\varepsilon}{\partial\alpha})h_{n_{wb}}]C_L + 2[\frac{\partial\varepsilon}{\partial\alpha} - a_{wb}(k_{wb}+k_t')]C_{m_{owb}} + \bar{\varepsilon}_o a_{wb}(h_{nwb}-h_t)}{2[a_{wb}(k_{wb}+k_t') - \frac{\partial\varepsilon}{\partial\alpha}]\,C_L} \qquad (8)$$

where $k_t' = k_t/(n_t S_t/S)$

Equation (8) gives the c.g. position for given lift coefficient for minimum drag coefficient in terms of wing-body aerodynamic parameters, tail parameters and geometry.

Several observations concerning equation (8) can be made:

(i) The c.g. position for minimum drag coefficient changes with lift coefficient (speed)

(ii) The c.g. position dictated by (8) is not restricted by stability constraints allowing the possibility of inherent static stability

(iii) The c.g. location given by (8) is a function of wing-body and tail aerodynamic parameters and geometry. Consequently the c.g. location for minimum drag coefficient can be changed by judicious selection of these parameters.

Design Characteristics

As indicated earlier it is undesirable to have an inherently unstable (or overly stable) aircraft when sophisticated control systems are not available for compensation purposes. Consequently it would be desirable to take advantage of observation (iii) and adjust the aerodynamic and geometric parameters in such a manner so that the c.g. position for minimum drag provides the desired static margin. It is possible to approach this problem several ways, two of which will be outlined below.

One method of approach is to treat the drag coefficient as a function of several aerodynamic and geometric parameters, including c.g. position and attempt to find a minimum with respect to all these parameters subject to certain specified constraints (static margin, etc.). The drawback with such a method is that a large

number of constraints may have to be applied to obtain "optimal" parameters which are realistic.

Another approach takes advantage of equation (8) and the related observation (iii). Here the optimal c.g. position as a function the aerodynamic and geometric parameters is determined by (8). Furthermore, the drag coefficient and the neutral point position can be determined in terms of the same set of parameters. For small changes in the parameters we can approximate the changes in drag coefficient, c.g. position for minimum drag coefficient, and neutral point by:

$$\Delta h_o \doteq \frac{\partial h_o}{\partial p_1} \Delta p_1 + \frac{\partial h_o}{\partial p_2} \Delta p_2 + \ldots \quad \text{from (8)}$$

$$\Delta C_D \doteq \frac{\partial C_D}{\partial p_1} \Delta p_1 + \frac{\partial C_D}{\partial p_2} \Delta p_2 + \ldots \quad \text{from (5)} \qquad (9)$$

$$\Delta h_n \doteq \frac{\partial h_n}{\partial p_1} \Delta p_1 + \frac{\partial h_n}{\partial p_2} \Delta p_2 + \ldots$$

Consequently for a given aircraft, the "optimal" c.g. position can be selected from equation (8). Then equations (9) can be used to find the changes in the parameters p_i required to move the c.g. and neutral point to satisfy static margin requirements and at the same time keep $\Delta C_D \leq 0$. In other words Δh_o, Δh_n and ΔC_D are specified and (9) solved for p_i. If there are more or less than three parameters the solution is either nonunique or not possible. In such a case a minimum norm. type solution is proposed.

The changes in the parameters can be incorporated by appropriate changes in the wing-body and tail geometry, another area which needs development. Again several observations can be made:

(i) Clearly a necessary assumption is that the parameters can be changed independently. This assumption is better for small changes in parameters and decreases in its validity as the magnitude of the changes increases.

(ii) The calculation of sensitivities in the above method allows an evaluation of the importance of each parameter in achieving a desired goal.

Concluding Remarks

The above remarks were aimed at examining methods for reducing the aircraft drag coefficient for a given aircraft lift coefficient, or speed. The emphasis was placed in determining the load distribution between the wing-body combination and the tail which would reduce the overall drag coefficient. Furthermore a technique was presented which would allow the determination of various aerodynamic and geometric parameters which would permit the 'best' c.g. location to satisfy inherent stability requirements. Included in the method was the calculation of sensitivity coefficients which indicates the importance of various parameters in achieving specified goals ie. c.g. movement, drag coefficient change, etc.

Preliminary results indicate that such an approach is feasible. For given aircraft parameters c.g. movement alone yields drag coefficient reduction of the order of 1% over the nominal case for a conventionally designed aircraft. Tentative results indicate that if the downwash angle at the tail is large enough (at zero lift) then a down load on the tail at the expense of the same additional load on the wing is desireable in reducing the overall drag coefficient. The reason is that the tail lift vector is tilted rearward by the downwash angle. If the tail lift is negative the contribution to the aircraft drag is negative. Under these circumstances the optimum c.g. is forward of the nominal. The amount and direction of movement is sensitive to this downwash parameter.

Although the drag reduction due to c.g. movement alone is small, the inclusion of other parameter changes can improve this drag reduction significantly. How these desired parameters changes can be obtained through wing-body and tail geometry changes still needs to be investigated. Clearly all drag reduction methods should be examined together.[7]

References

1. Hoak, D.E. (Project Engineer), USAF Stability and Control DATCOM, October 1960, revised 1974. Section 4.5.3.2.
2. Etkin, B., Dynamics of Atmosphere Flight, John Wiley and Sons, Inc. New York, 1972.
3. Goldstein, S. E. and Combs, C. P., "Trimmed Drag and Maximum Flight Efficiency of Aft Tail and Canard Configurations," AIAA Paper 74-69, 12th Aerospace Sciences Meeting, Washington, D. C. 1974.
4. Lutze, F. H. and Cliff, E. M., "Control-Configured General Aviation Aircraft," SAE paper 730303, Business Aircraft Meeting, Wichita, Kans. April 1973.
5. Hood, R.V., "Active Controls Changing the Rules of Structural Design," Astronautics and Aeronautics, August 1972, pp. 50-55.
6. Hofmann, L. G. and Clement, W.F., "Vehicle Design Considerations for Active Control Application to Subsonic Transport Aircraft," NASA CR-2408, August 1974.
7. Rediess, H.A. (Editor) "Advanced Control Technology and its Potential for Future Transport Aircraft," Preprint from NASA Symposium of same name, July, 1974.

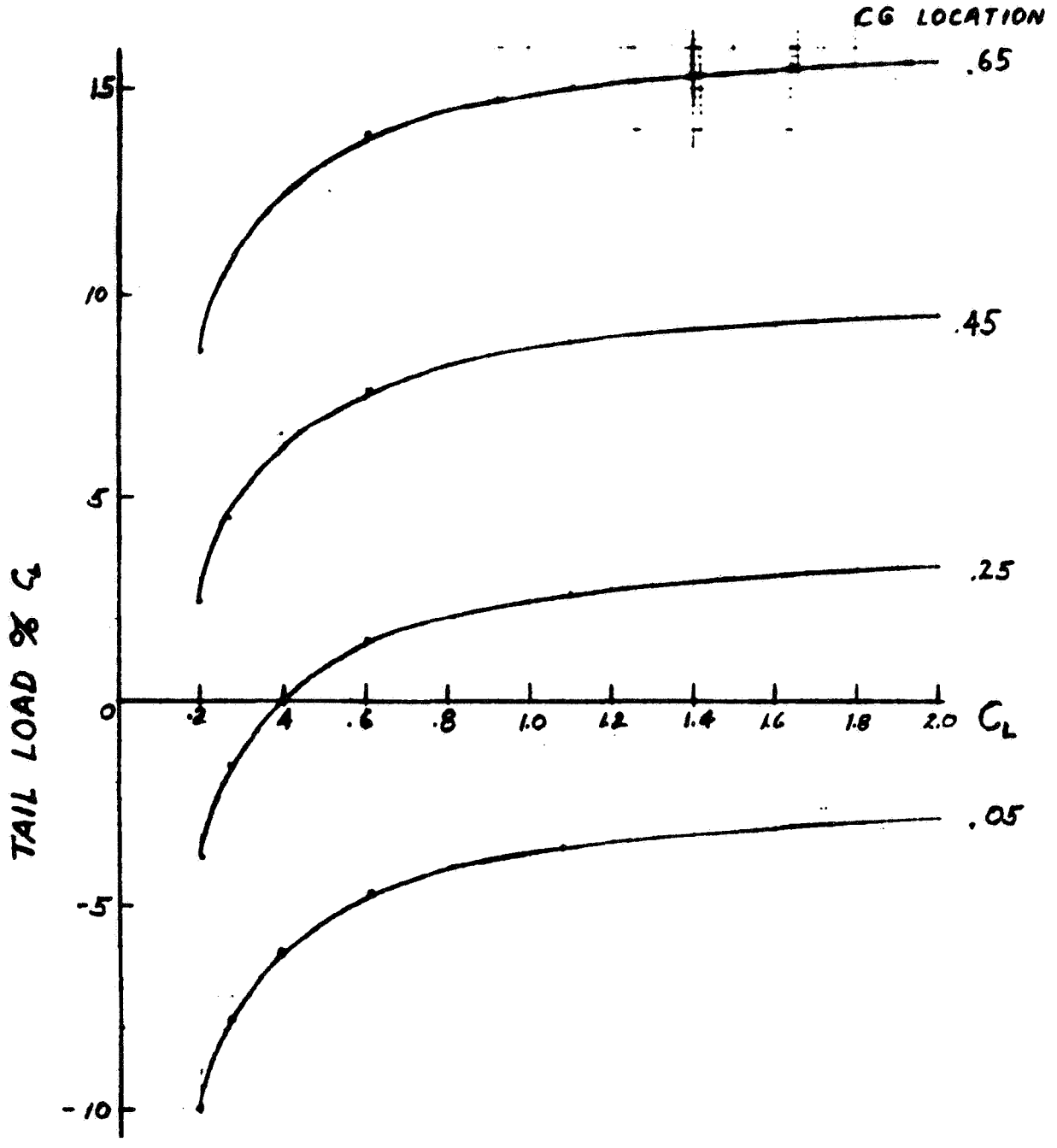

Load Distribution for Various CG Positions
(Speed Changing)

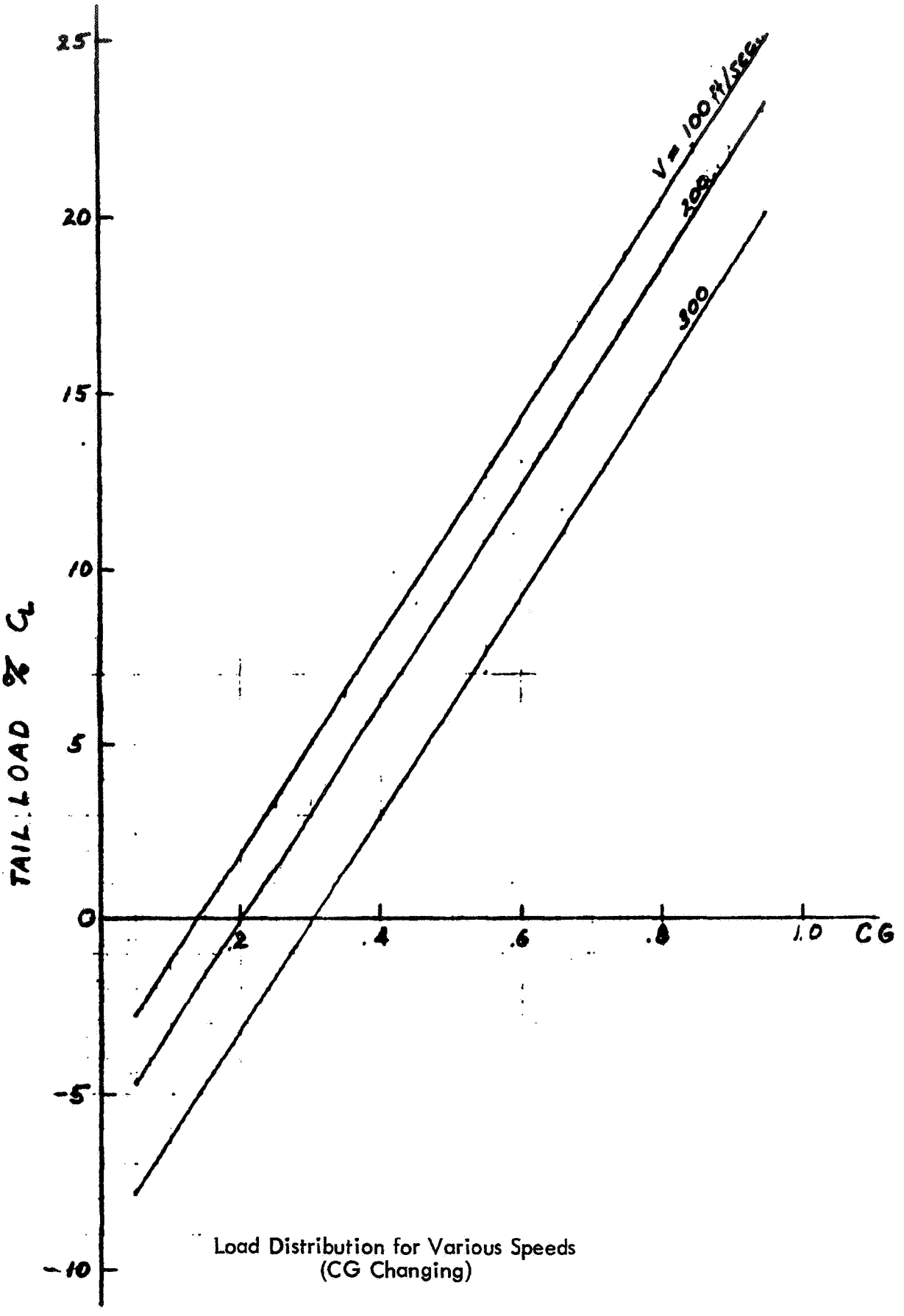

Load Distribution for Various Speeds
(CG Changing)

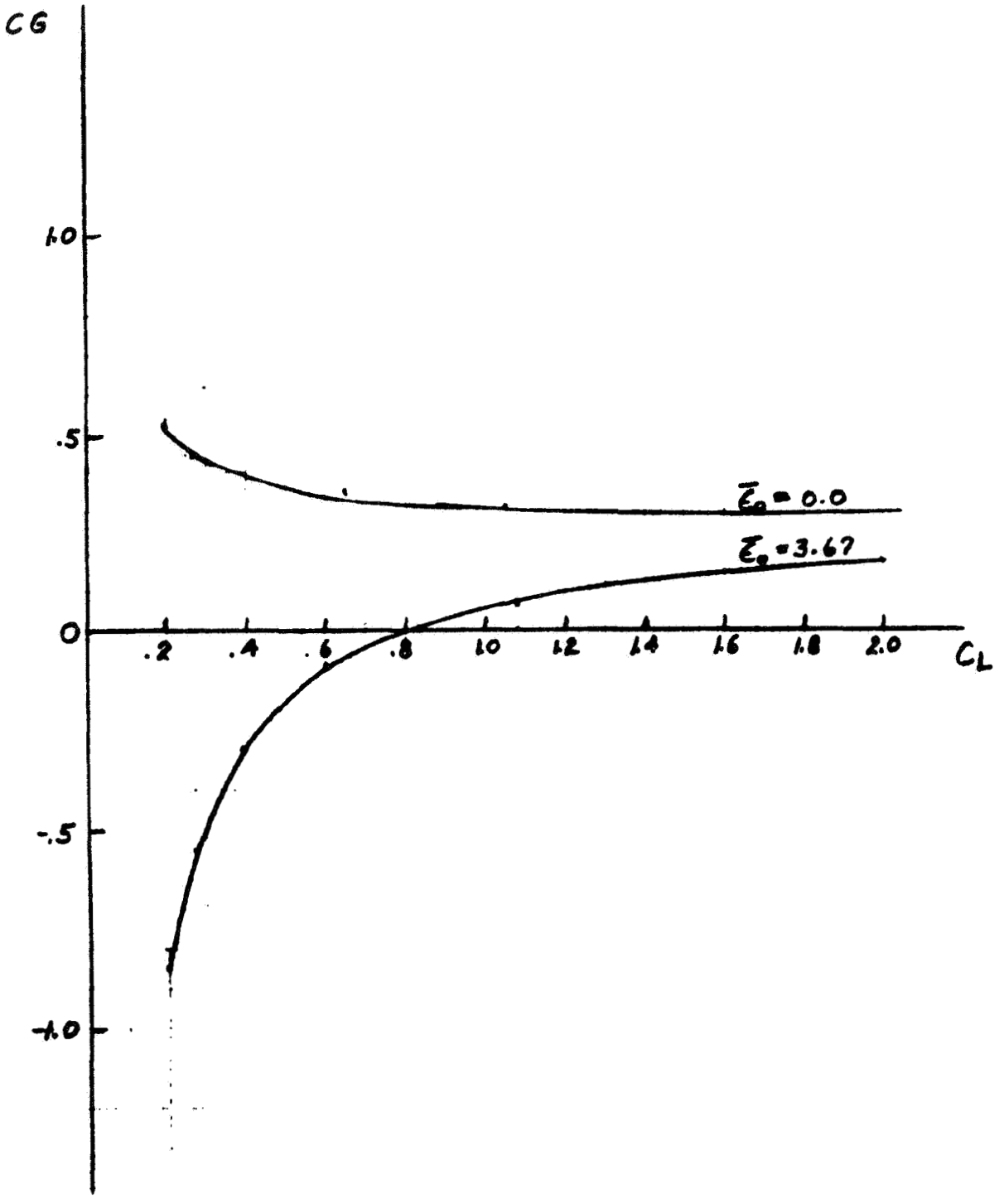

CG Position for Minimum Drag Coefficient

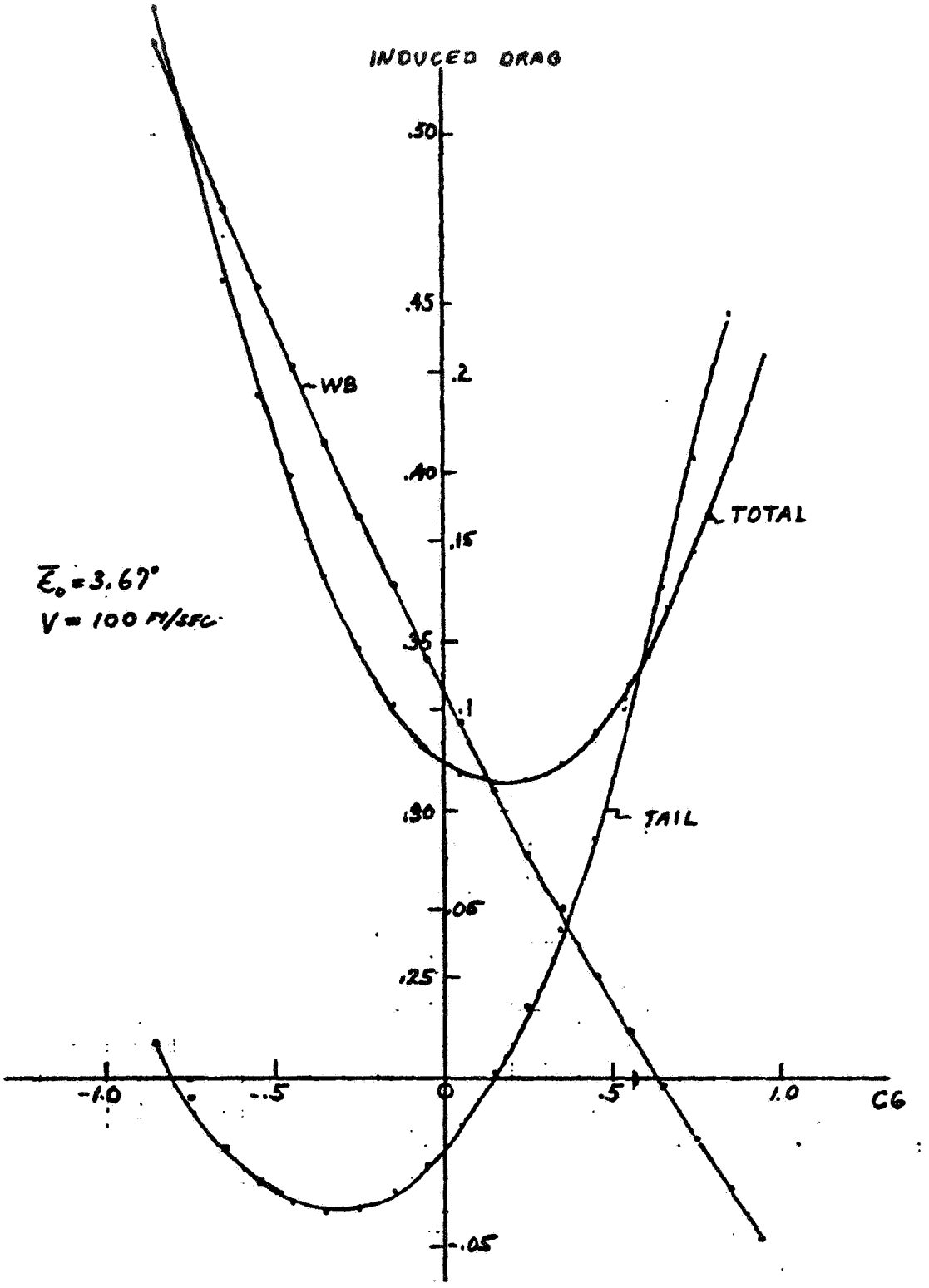

Induced Drag vs CG Position

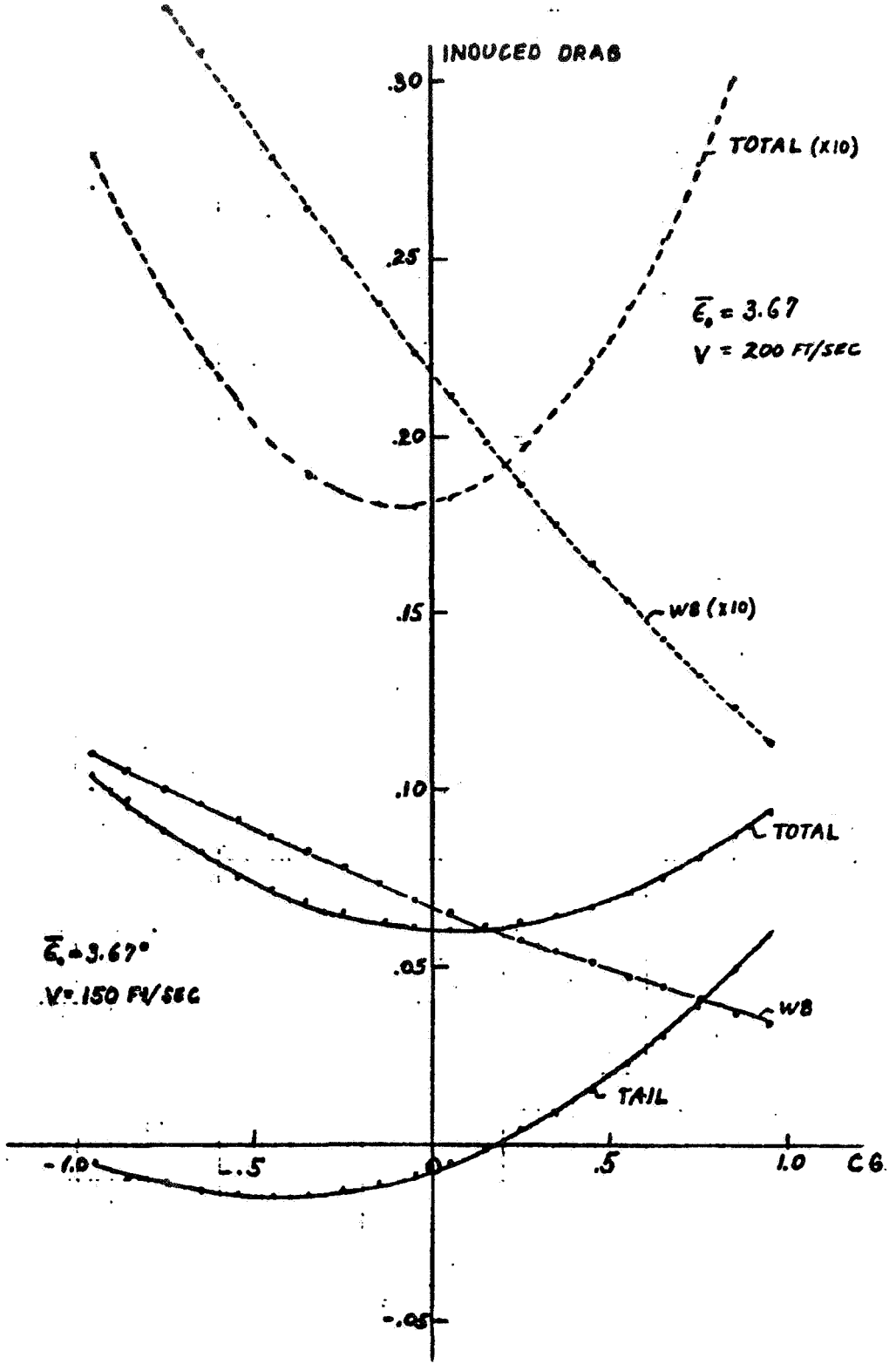

Induced Drag vs CG Position

7.4 Trim Drag in the Light of Munk's Stagger Theorem

E. E. Larrabee
Massachusetts Institute of Technology

Abstract

Munk's stagger theorem holds that the induced drag of a multiplane is independent of the streamwise position (the stagger) of its lifting elements so long as the gap/span ratios and the element/element lift ratios are specified. In particular, a monoplane-tailplane or a monoplane-foreplane (canard) arrangement can be regarded as a biplane of zero gap and the trim drag due to tailplane download or foreplane upload can be readily calculated. The trim drag penalty is the same for both configurations. Relations are given for trim drag estimates for various practical arrangements.

Max Munk was one of the first generation of Goettingen aerodynamicists. Later he worked for the old NACA, and was largely responsible for the concept of, and the first test programs carried out in, the Variable Density wind tunnel. He contributed greatly to our present understanding of aerodynamic drag. While still at Goettingen he discovered some general laws about the induced drag of multiplanes, one of which is set forth in Figure 1.

Prandtl used this law as one of the cornerstones of a monograph on the "Induced Drag of Multiplanes", which appears in German in the Technical Reports (Technische Berichte) Vol. III, No. 7, pp. 309-315 of the aerodynamics research establishment at Goettingen. This report was immediately translated into English and published by the NACA as Technical Note No. 182 in 1924. Its contents also appear in Glauert's "Elements of Aerofoil and Airscrew Theory".

Figure 2 gives Prandtl's formula for the induced drag of a biplane. It is written as the sum of the self-induced drag of the elements of the biplane, plus twice the induced drag of one element due to the flow about the other for the case of an unstaggered array. Munk showed that the cross induced drags of the two elements were equal for an unstaggered biplane, but that also, by virtue of his stagger theorem, the sum of the cross induced drags was unchanged by stagger so long as the lift distribution between the elements is preserved. Thus the cross induced drag of the forward element of a biplane is reduced by the upwash about it

due to the aft element; conversely, the cross induced drag of the aft element is increased by the downwash about it due to the forward element.

The magnitude of the cross induced drag is specified by the biplane interference factor, σ, defined by the relation on Figure 2. Its numerical value was calculated by Pohlhausen, who graphically evaluated an integral which gave the cross induced drag of one element of an unstaggered biplane carrying an elliptic span loading in the presence of the other element, also assumed to be elliptically loaded, and creating the downwash field appropriate to an elliptic span loading at the arbitrary location of the first element. The values of σ were evaluated for three discrete element span ratios and several gap to average span ratios. The results are presented in Figure 3. It might be worthwhile to refine Pohlhausen's calculations with a modern calculating machine. For our purposes it will suffice to note that σ approaches the span ratio in the limit as the gap/span ratio approaches zero.

Professor Ober of M.I.T., now emeritus, always taught his students (and I teach mine) that the induced drag of a monoplane-tailplane combination can be closely estimated by treating it as a staggered biplane of zero gap. Figure 4 presents some results of such a calculation. It is seen that the induced drag penalty for carrying a download of 10% of the total lift on the tailplane of a conventional airplane is slightly more than 10% of the minimum induced drag of the wing alone for a tailplane to wing span ratio of 0.3; surprisingly, the trim drag penalty for carrying an upload of 10% of the total lift on a canard foreplane of the same span ratio is identical. The trim penalty disappears for tailplane (or foreplane) span equal to the wing span, as one might expect.

Figure 5 compares the induced trim drag penalties for two representative wing-body-tailplane combinations in which the tail off pitching moment of the two wing body combinations differ only in the magnitude of the pitching moment about the wing aerodynamic center, the first example corresponding to a conventional NACA 4 digit airfoil, and the other corresponding to a heavily cambered airfoil of the Whitcomb supercritical, or general aviation type. It is seen that the drag penalties at the rather high total lift coefficient of 0.6 amount to about 0.2 counts and 2.2 counts, respectively; amounts which would be difficult to establish by wind tunnel testing.

Figure 6 presents an experimental verification of this technique for calculating the additional induced drag due to tail load by comparison with experimental drag data obtained on an 1/8 scale model of the XP-87 airplane during

the course of wind tunnel tests conducted to determine the average downwash angle at the tailplane as a function of airplane angle of attack with deflected flaps. The experimental tail loads were large and the additional tail drag could be measured accurately.

The minimum induced drag of a wing (W) tail (H) configuration may be written as:

$$C_{D_{\substack{\text{induced}\\ \text{minumum}}}} = \frac{C_{L_W}^2}{\pi \mathcal{R}_W} + \frac{S_H}{S_W} \quad \frac{2\sigma}{\pi} \frac{C_{L_W} C_{L_H}}{(b_W b_H / S_W)} + \frac{C_{L_H}^2}{\pi \mathcal{R}_H}$$

where

$$\mathcal{R}_W = b^2_W / S_W$$
$$\mathcal{R}_H = b^2_H / S_H$$

In this particular case the drag of the complete airplane was computed from the relation

$$C_D = C_{D_{P_{wBNF}}} + \frac{C_{L_W}^2}{\pi \mathcal{R}_W e_{wBNF}} + \frac{S_V}{S_W} c_{d_V} + \frac{S_H}{S_W} c_{d_H}$$
$$+ \frac{S_H}{S_W} \quad \frac{2\sigma}{\pi} \frac{C_{L_W} C_{L_H}}{(b_W / b_H / S_W)} + \frac{C_{L_H}^2}{\pi \mathcal{R}_H e_H}$$

where

$$C_{L_W} = C_L - \frac{S_H}{S_W} C_{L_H}$$

$$C_{D_{P_{wBNF}}} = 0.0660 \qquad e_{wBNF} = 0.877$$

$$\mathcal{R}_W = 6$$

$$S_V / S_W = 0.146 \qquad c_{dv} = 0.01$$

$$S_H / S_W = 0.219 \qquad c_{dH} = 0.01$$

$$b_H / b_W = 0.373$$

$$2\ gap / (b_W + b_H) = 0.0995 \rightarrow \sigma = 0.325$$

$$\mathcal{R}_H = 3.81,\ e_H = 0.85,\ b_W b_H / S_W = 2.236$$

The experimental tail loads corresponding to the various tailplane incidences are given by

$$C_{L_H} = \frac{c\,S_W}{\ell_H S_H}\left(C_{m_{\text{tail off}}} - C_{m_{\text{tail on}}}\right) \qquad \alpha = \text{constant}$$

A comparison of the computed tail on drag for the complete airplane with the experimental drag shows that the cross induced drag term

$$\frac{S_H}{S}\,\frac{2\sigma}{\pi}\,\frac{C_{L_H} C_{L_W}}{(b_H b_W/S)}$$

is very important when the tail is carrying a download; its calculated value overcomes the skin friction drag of the tail assembly and the self induced drag of the horizontal tail itself at $C_{LH} = -0.4$. The experimental data do not quite confirm this result: The experimental skin friction of the tail assembly and the self induced drag of the horizontal tail were underestimated; but note that the general shape of the complete airplane drag with tail plane lift curve is correctly predicted.

It is concluded that biplane theory presents a simple method for calculating tail drag, and that the trim drag penalties are generally small, for foreplanes or tailplanes of reasonable span and loading.

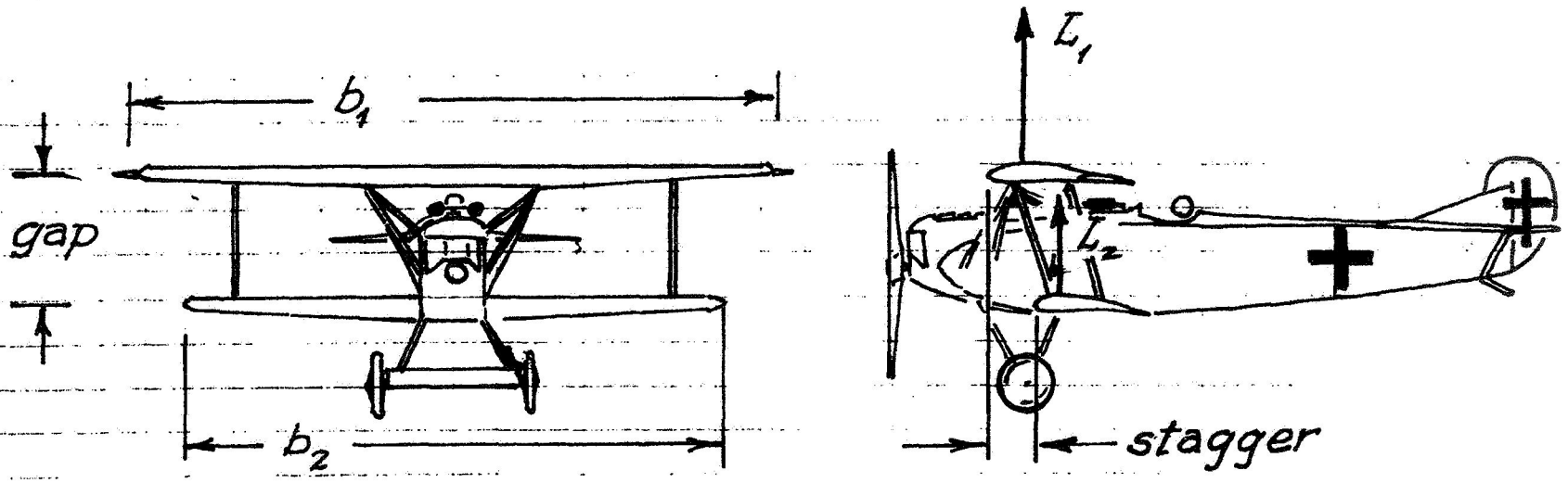

The induced drag of a multiplane is independent of the streamwise location of its lifting elements (the stagger) so long as its front view is unchanged (the gap/span ratios), and so long as the lift distribution between the elements (L_2/L_1) is preserved. (1918)

Figure 1. Munk's Stagger Theorem

$$D_{induced} = \frac{1}{\pi q}\left[\frac{L_1^2}{b_1^2} + 2\sigma\frac{L_1 L_2}{b_1 b_2} + \frac{L_2^2}{b_2^2}\right]$$ (L. Prandtl 1923)

self-induced drag of wing 1

induced drag of wing 1 due to wing 2 plus induced drag of wing 2 due to wing 1.

self-induced drag of wing 2

$q = \frac{1}{2}\rho V^2$, flight dynamic pressure

σ = biplane interference factor

Figure 2. Induced Drag of Biplanes

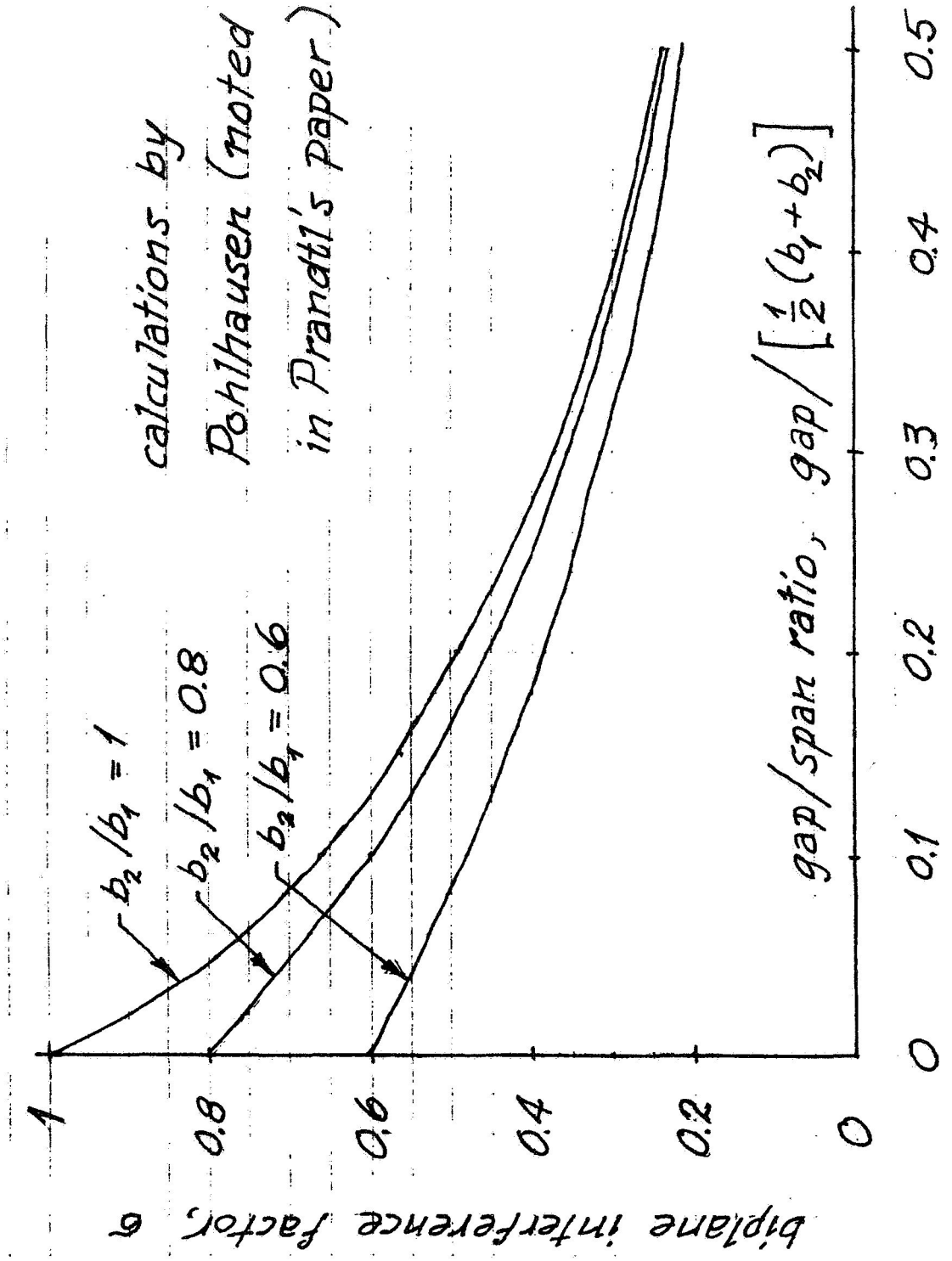

Figure 3. Biplane Interference Factor

DOWNLOAD FOR TRIM

UPLOAD FOR TRIM

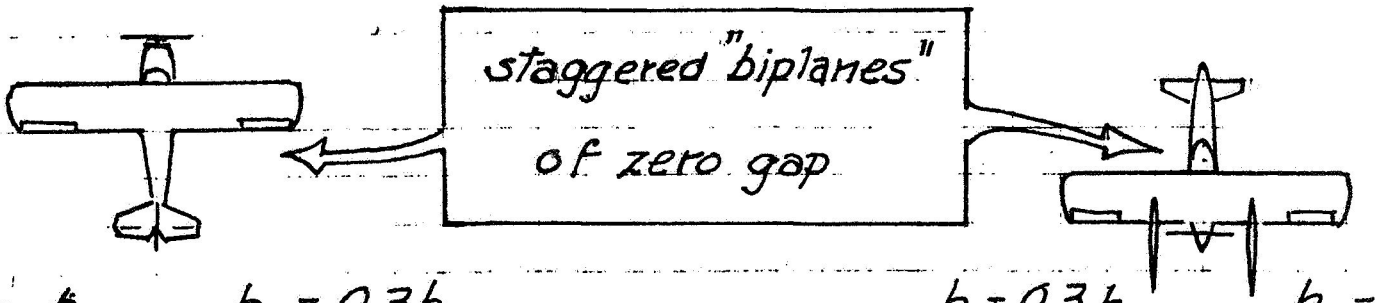

$b_1 = b \qquad b_2 = 0.3b$

$L_1 = 1.1L \qquad L_2 = -0.1L$

$\sigma \cong b_2/b_1 = 0.3$

$$D_{ind} = \frac{L^2}{\pi q b^2}\left[1.21 - 0.22 + 0.1111\cdots\right]$$

$$= 1.1011\cdots\left(\frac{L^2}{\pi q b^2}\right)$$

$$= \frac{L^2}{\pi q b^2}\left[1 + \left(\frac{\delta}{r}\right)^2 - \delta^2\right]$$

δ = download fraction, r = span ratio

$b_1 = 0.3b \qquad b_2 = b$

$L_1 = +0.1L \qquad L_2 = 0.9L$

$\sigma \cong b_1/b_2 = 0.3$

$$D_{ind} = \frac{L^2}{\pi q b^2}\left[0.1111\cdots + 0.18 + 0.81\right]$$

$$= 1.1011\left(\frac{L^2}{\pi q b^2}\right)$$

$$= \frac{L^2}{\pi q b^2}\left[1 + \left(\frac{\epsilon}{r}\right)^2 - \epsilon^2\right]$$

ϵ = upload fraction r = span ratio

Figure 4. Trim Drag of Conventional vs Canard Monoplane

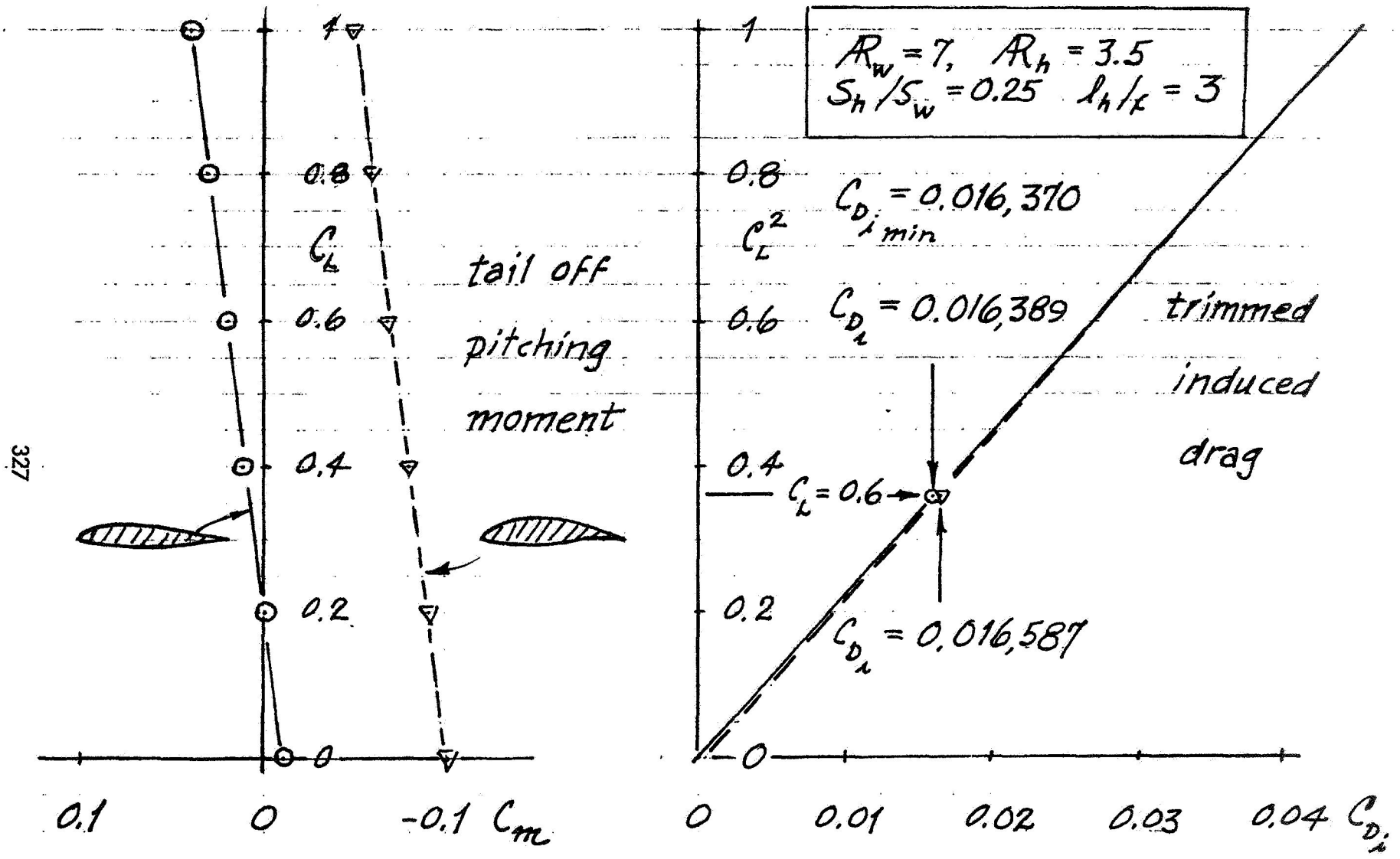

Figure 5. Trim Drag Penalty for Large Wing $C_{m_{ac}}$

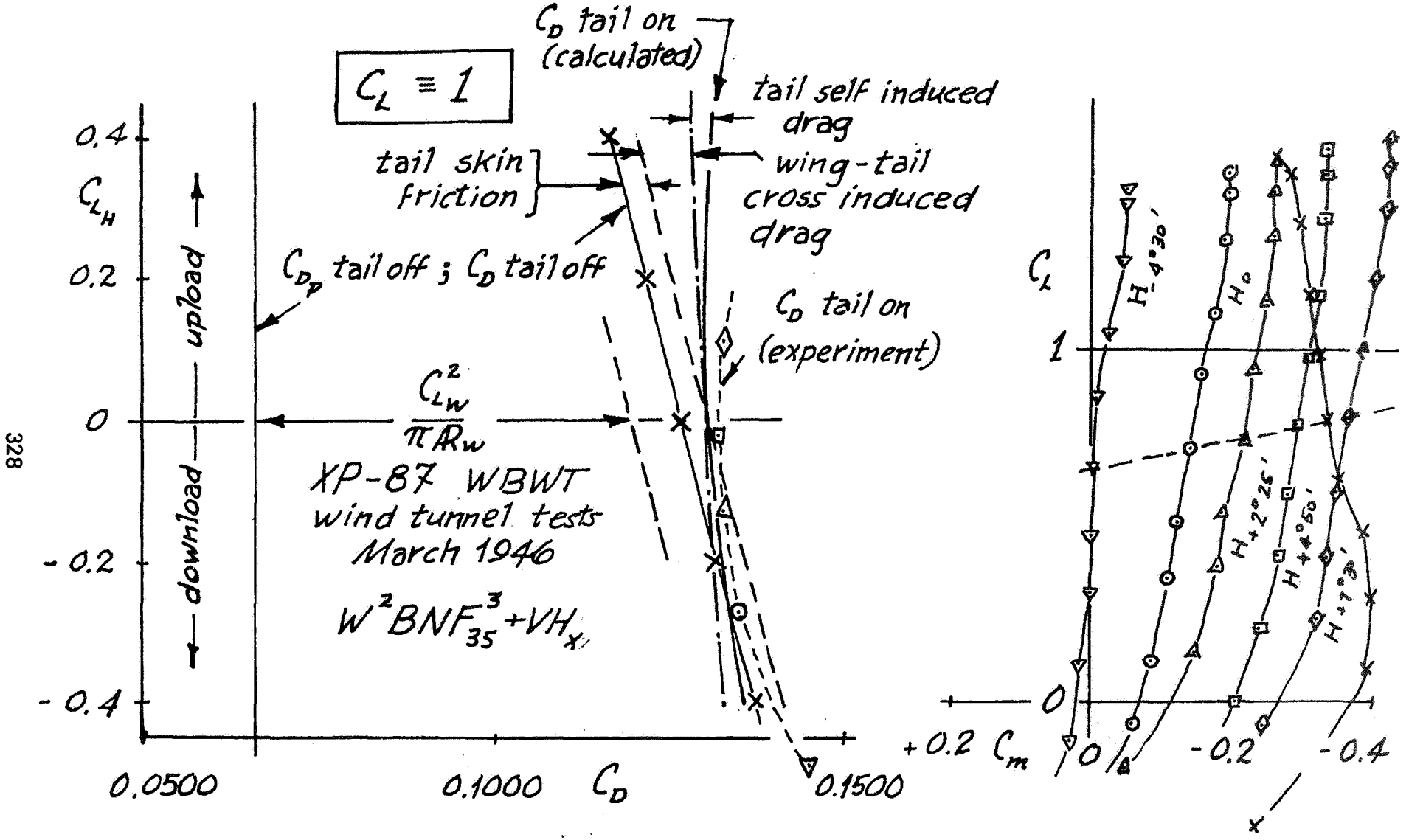

Figure 6. Calculated vs. Experimental Tail Drag

8. PAPERS OF SESSION VI - DRAG OF THE COMPLETE CONFIGURATION

8.1 (I) Cost Consideration For Aircraft Configuration Changes

R. R. Tumlinson
Beech Aircraft Corporation

Drag reduction, in our industry, is a principle that ranks with Motherhood. There are about as many aircraft engineers who would demean ways to reduce drag as there probably are politicians who would attack apple pie. Most of the people here have spent a great deal of time searching for ways of reducing drag and of trying to convince others of the merits of the efforts required to do so. I am sure that I have a lot of company in the frustration that goes with that search and effort.

We are all members, or supporters, of an industry which is fueled by profit. And that profit is directly dependent upon delivery of aircraft which provide good value for our customers. Or, simply said, the costs of changes and evolutionary improvements must be at least balanced by the benefits.

I'm not an expert by any means on costs, but I have had a lot of experience in trying to overcome the obstacles provided by the cost considerations of proposed changes. So, today, let me take the role of the Devil's Advocate on aircraft costs and cite some of the considerations which must be made and which may outweigh potential performance improvements.

As a means of illustrating both costs and benefits, I'd like to present a very arbitrary example which will touch on many of the important cost considerations which must be made to arrive at a production decision.

Let's say that we have arrived at a modification which will reduce the drag of our airplane so as to provide an increase in cruising speed of 4 mph. In the course of this workshop, we have considered many possibilities for achieving this, so I'm not going to specify how this was achieved. But, as an arbitrary assumption, let's say that we can, in fact, increase our cruising speed by 4 mph; and also, just as arbitrarily let us assume that the resulting changes would net an increase in airframe weight of 5 pounds. This represents a loss of payload of 5 pounds. And, in addition, this will typically require design and production changes to another 10 pounds of the existing airframe weight, although this would depend in a particular case on the nature of the configuration change. For the purpose of this example, we will apply this to a hypothetical turboprop with a cruising speed of 250 mph.

Let me emphasize at this point that the figures I am using have been chosen to be representative for the industry, and I believe they are suitable for this example.

First, let's consider the cost increase for direct labor. The 5 pounds of new and increased weight will be a net increase to the airplane, and an appropriate slope and man-hour/pound figure must be selected for the new effort. The 80% learning curve is found to be fairly typical for the general aircraft industry, and I believe they are suitable for this example. The 5 pounds will be projected from Unit 1000 at 1.0 man-hour/pound to obtain Unit No. 1. This is shown to be an increase of 46 hours at Unit 1 with a cumulative increase of 15 hours for 100 units.

A somewhat different consideration must be made for the "changed" weight of 10 pounds, where there is not the same potential for "learning" improvements. Something less than the 80% slope typical for "new" production would be more appropriate. If we assume a 90% learning-curve slope, using the same factors as before (1.0 man-hours/pound at Unit 1000 for 10 pounds, this time), the cumulative man-hours over 100 units is 16.6 man-hours.

As the changed effort has replaced an existing task at 1.0 man-hours/pound, this 10 hours can be subtracted from the 16.6, leaving 6.6 hours for new learning. Our total direct labor increase now becomes 15 hours + 6.6 hours, or a total of 21.6 hours each for the 100 units.

Next, these man-hours must be converted to dollar costs. The latest figures published by the Bureau of Labor Statistics show that direct labor rate applicable for the aircraft industry as a whole is $5.78 per man-hour. With inflation and differences within the industry, this rate can become obsolete quickly. Overhead and direct expenses plus general and administrative expenses can add a so-called "burden" of 200 to 300 percent to this rate.

TABLE I

Overhead and Direct Expenses Include

Indirect salaries and wages; support labor such as planning, scheduling personnel, etc.; holidays, vacations, sick leave, etc.

Insurance, payroll taxes, social security, group life-insurance, workmen compensation, retirement plan, sales taxes, personal property taxes, and depreciation.

Maintenance and repair on shop equipment and on buildings.

Shop supplies such as perishable tools, office supplies, etc.

Travel, telephone, freight, etc.

Overtime premiums, product liability, etc.

General and Administrative Expenses Include

Executive and management salaries; accounting; procurement; office supplies; and other costs which cannot be directly associated with labor cost - either manufacturing or engineering.

There are two other contributions to the costs: the materials and the development costs. Material costs for an airplane in this category vary with the size and complexity. Development costs also vary with the class of airplane and the accompanying complexity of the development effort and the FAA certification program required. A range of $3000 to $4000 per pound is the general ballpark figure when everything is added up, and in this example 100 units was selected to amortize these costs.

When the pieces are all assembled, a price change can be determined for the improved airplane which adds up to approximately $1600.

The cost to the customer must be weighed against the additional value to the customer. Let's look at it this way: our hypothetical airplane cruises at 250 mph. To keep it simple, I'll use this cruising speed, although it would be more accurate to determine an average block speed based on a customer's particular routes. For a customer's usage, we will assume 600 hours per year. Appropriate operating costs are quoted on Table II. And, as noted on the table, the costs of the modification can be recovered by the savings in operating costs in 1.87 years. After that time, the savings would represent a net gain to the customer which would continue.

TABLE II

Operating Cost Comparison

Before Modification

Direct Operating Costs/Hour		$ 77.50
Indirect Operating Costs/Hour		13.18
Total Operating Costs/Hour		$ 90.68
Cruising Speed	250 MPH	
Total Operating Costs/Mile =	$\frac{\$90.68/HR}{250\ MPH}$	$ 00.3627

After Modification

Total Operating Costs/Mile =	$\frac{\$90.68/HR}{254\ MPH}$	$ 00.3570
Savings Per Mile		0.0057

Savings Per Year = $.0057 x 250 MPH x 600 Hours = $855.00

$$\frac{\$1600.00}{\$\ 855/YR} = 1.87 \text{ years}$$

I am not going to exercise judgment on the 1.87 years, because of some of the arbitrary assumptions that could drastically affect the results. In estimating costs for a particular project, appropriate values must be used which would not be the same as those used in the examples. The actual special improvement, the weights affected, the cost factors that are current for a particular project, the number of units used to amortize the development costs could each produce significant differences. I believe the figures here are representative, but primarily, I hope they illustrate the key factors which can affect a production decision considering the costs involved.

And, even after this type of analysis, there are other factors which may strongly influence both the costs and/or the decision to proceed. For example, the FAA recertification considerations. If this can be avoided, perhaps by timing the modification with a complete model change, these cost figures would look much more favorable.

In the last analysis, a decision to proceed may depend on the philosophy of the company management. Beauty is in the eye of the beholder, the saying goes. There are many changes made in the name of progress, or to satisfy a dedication for a clean-looking

airplane, which might be difficult to justify solely on the basis of this type of comparison. I would not suggest that this would not be desirable. But--- sometimes the stroke of intuition is not enough to convince a cost-minded management --- and that's where this analysis would help.

Thank you.

8.2(II) Drag of the Complete Configuration
Aerodynamic Considerations

Jan Roskam
University of Kansas

Introduction

The purpose of this part of the paper is to focus on a number of drag items and relate them to the performance of the complete configuration.

First, the effect of fuselage camber, wing and nacelle incidence are discussed from a viewpoint of design decision making.

Second, the effect of overall cruise drag on the design gross and empty weight of the airplane is discussed. Examples show that cruise drag can have a very important influence on total airplane weight.

Third, the effects of usable cruise lift-to-drag ratio and wing-loading are shown to be important.

Finally several research needs relating to design of the complete configuration are reviewed.

Effect of Fuselage Camber, Wing and Nacelle Incidence

In putting together a new airplane, a number of fundamental geometric choices must be made. Typical examples of such choices are:

- extent of fuselage camber;
- wing incidence on fuselage; and
- nacelle incidence and position relative to the wing.

In determining the extent of wind tunnel testing required to "optimize" the configuration, the aerodynamicist is confronted with a large number of variables. For example, if it is assumed, that two camber shapes, two wing-fuselage incidence angles and two wing-nacelle incidence angles are to be investigated, this alone leads to eight combinations to be tested. Under the economic constraints of the general aviation industry it is usually not feasible to do this much testing.

Major aircraft manufacturers, on fighter, bomber and even on some transport programs, obtain significant inputs from NASA in terms of systematic wind tunnel configuration testing.

How does the general aviation designer choose the best configuration? Well, very often he ends up guessing or, the shaping decision (for lack of definitive aerodynamic input) is made for him by engineers or managers outside of aerodynamics.

Inputs such as tooling costs and marketing opinions outweigh the aerodynamicist in the decision making process, primarily because the aerodynamicist does not have convincing arguments one way or the other.

To illustrate these points and to point once more to the need for systematic tunnel testing of general aviation research models, the following examples are given.

Note from Figure 1 that three different vertical nacelle installations are being used for turbopropeller airplanes. Note also, that all three use rather differing aft fairing shapes. The question arises: can they all be right?

Observe from Figure 2 that one manufacturer employs two quite different piston engine nacelle configurations. Figure 3 illustrates two more and again different nacelle shapes. The questions arises again: can they all be right?

Possible pay-offs of such research are illustrated in Figure 4 taken from Reference 1 (1942). Figure 4 shows a range of wing-body-nacelle drag coefficients of .1250 to .1050, (.0078 to .0066 based on wing area!) depending on vertical nacelle location alone. In other words, there are 12 drag counts to be gained by selecting the vertical nacelle location.

It would seem that the industry could derive significant benefits from a series of systematic wind tunnel test to determine the best (lowest drag) shape of such wing-nacelle installations. Such research should also account for the effect of thrustline location and orientation, as well as for the possible beneficial effect of forward propeller shaft extensions, such as used on the Navajo.

Drag Effect on Airplane Weight and Airplane Market Price

Aerodynamic drag is not generally thought of in general aviation airplane design as an important factor affecting airplane weight. The reason may be the fact that usually new airplane "designs" consist of adaptations of components which are already in production, to a new airplane. The term "tinker toying", although not a kind description probably applies to much of general aviation airplane design.

However, every now and then a truly new design evolves and then the effect of drag on weight can be important as will be illustrated in the following simplified analysis.

Assume that total airplane weight is broken down as follows:

$$W = W_{PL} + W_F + W_E \qquad (1)$$

where:

W_{PL} = payload weight
W_F = fuel weight (including reserves)
W_E = empty weight

Fuel weight and empty weight are assumed to be broken down as follows:

$$W_F = \overline{A} + T \times SFC \times \frac{V}{R} \quad \text{and:} \tag{2}$$

$$W_E = \overline{B} + \overline{C}T + \overline{D}W_F \tag{3}$$

where:

$\overline{A}$ = weight of reserve fuel
T = cruise thrust
SFC = cruise fuel consumption lbs/lbs/hr
V = cruise speed
R = cruise range
$\overline{B}$ = empty weight without power plant and fuel system
$\overline{C}$ = weight of power plant per lbs of cruise thrust
$\overline{D}$ = weight of fuel system per lbs of cruise fuel

In cruise flight:

$$T = W \text{ and } L = D \tag{4}$$
$$\text{lift} \quad \text{drag}$$

so that

$$T = W\left(\frac{D}{L}\right) \tag{5}$$

Substituting equations (2) through (5) into equation (1) yields:

$$W = W_{PL} + \left(\overline{A} + W\frac{D}{L}(SFC)\frac{V}{R}\right) + \left(\overline{B} + \overline{C}W\frac{D}{L}\right) + \\ + \overline{D}\left(\overline{A} + W\frac{D}{L}(SFC)\frac{V}{R}\right) \tag{6}$$

Upon solving for W it is found that:

$$W = \frac{W_{PL} + \overline{A} + \overline{B} + \overline{D}\overline{A}}{1 - \frac{D}{L}\left\{(SFC)\frac{V}{R} + \overline{C} + \overline{D}(SFC)\frac{V}{R}\right\}} \tag{7}$$

or

$$W = \frac{W_{PL} + \overline{A}(1+\overline{D}) + \overline{B}}{1 - \frac{D}{L}\left\{(SFC)\frac{V}{R}(1+\overline{D}) + \overline{C}\right\}} \tag{7}$$

By introducing:

$$a = W_{PL} + \bar{A}(1+\bar{D}) + \bar{B} \qquad (8)$$

$$b = (SFC)\frac{V}{R}(1+\bar{D}) + \bar{C} \qquad (9)$$

it is possible to rewrite equation (7) as:

$$W = \frac{a}{1 - b/L/D}$$

To determine the effect of drag on airplane weight, the differential $\partial W/\partial(L/D)$ can be found from equation (10) as:

$$\frac{\partial W}{\partial(L/D)} = \frac{-ab}{(L/D - b)^2} \qquad (11)$$

Table 1 presents data from which $\partial W/\partial(L/D)$ can be calculated for a typical general aviation piston engine driven twin.

So using equation (11):

$$\frac{\partial W}{\partial L/D} = \frac{-4326 \times 2.15}{(11 - 2.15)^2} = -119 \text{ lbs}/(L/D)$$

This means that per unit L/D, the airplane gross weight can be lowered by about 120 lbs, a significant saving when compared to the empty weight, W_E.

Figures 5 and 6 illustrate similar results obtained in Reference 2 on small two-place turbofan (1200 lbs max thrust) airplanes.

Table 1 and Figure 5 and 6 all show the importance of designing to the maximum possible cruise lift-to-drag ratio, if the lowest possible airplane weight is to be achieved.

It should be noted, that lower empty weight, achieved by better aerodynamic design has a very significant effect on the marketing price of an airplane. Table 2 shows typical market prices related to gross and empty weights for general aviation twins.

For the example twin of Table 1 the typical market price per pound of empty weight would be about 34 $/lbs. Attaining a 120 lbs saving would cut the market price by $4,080, a rather significant competitive advantage!

Table 1. Data for Calculation of $\partial W/\partial(L/D)$ for a Typical Twin.

W_E = 3700 lbs — Engines 2 x 300 hp. at 450 lbs each

W_F = 1000 lbs

W_{PL} = 1600 lbs — SFC_{hp} = .45 lbs/hp/hrs

W = 6300 lbs — Assume propeller and engine weight =1100 lbs
Assume fuel system weight = 100 lbs

Assuming a cruise L/D = 11 and W_{ave} = 5,800 lbs
$_{cruise}$

T_{cruise} = 527 lbs

Assume V_{cruise} = 216 mph, then HP_{cruise} = 303

Fuel flow in cruise then is 136 lbs/hr. This yields a range of

$\left(\frac{1000-200 \text{ (reserves)}}{136}\right)$ 216 = 1270 miles. The value of SFC is

$\frac{136}{527}$ = .26 lbs/lbs/hr

So, $\overline{A}$ = 200 lbs $\quad \overline{B}$ = 3700-1200 = 2500 lbs

$$\overline{C} = \frac{1100}{527} = 2.1 \qquad \overline{D} = \frac{100}{1{,}000-200} = .13$$

From equations (8) and (9):

$$a = 1600 + 200\ (1 + .13) + 2500 = 4326 \text{ lbs}$$

$$b = .26 \times \frac{216}{1270}\ (1 + .13) + 2.1 = .05 + 2.1 = 2.15$$

Lift-to-Drag Ratio and Wing Loading Effects Revisited

Light airplanes, such as the Cessna 172 typically cruise at lift coefficients in the range of:

$$C_L \approx .3 \text{ to } .5$$

Figure 7 shows that the corresponding L/D value varies from 10.0 to 13.2. This compares with a maximum L/D value of 13.8 indicating that significant improvements must be attainable by increasing wing loading. Increasing wing loading not only will bring the cruise C_L closer to L/D/max on the polar but it will also shift the polar to

Table 2. Typical General Aviation Light Twin Airframe Prices, (1975 Flying Annual Data)

Type	Gross Weight W (lbs)	Empty Weight W_E (lbs)	Price $	Price / W $/lbs	Price / W_E $/lbs
Cessna Skymaster	4,630	2,710	63,300	13.7	23.4
Piper Seneca	4,570	2,770	63,995	14.0	23.1
Piper Aztec E	5,200	3,042	88,200	17.0	29.0
Beech Baron B55	5,100	3,155	89,000	17.5	28.2
Cessna 310	5,500	3,251	89,950	16.4	27.7
Averages	5,000	2,986	78,889	15.7	26.3
Rockwell Shrike Commander	6,750	4,608	128,150	19.0	27.8
Cessna 402 B	6,300	3,741	138,500	22.0	37.0
Piper Navajo B	6,500	3,930	139,100	21.4	35.4
Cessna 414	6,350	4,042	174,950	27.6	43.3
Beech Duke	6,775	4,265	219,450	32.4	51.5
Averages	6,535	4,117	160,030	24.5	39.0

the left in the higher C_L range (note that C_{D_o} actually will increase because it is based on a smaller wing area!). This fact has been previously demonstrated also in such papers as References 3, 4, and 5.

Figure 8 illustrates some typical results. Cutting wing area in the chordwise direction by 30 percent results in a 10 percent reduction in thrust required and therefore in fuel flow. Figure 9, shows the relative aerodynamic "cleanness" of 1975 general aviation single engine airplanes compared to what is felt feasible in the future. To achieve this however, will require the introduction of new designs and new manufacturing technology.

Research Needs

It appears that research into the following areas would have significant potential for paying off in imporved general aviation airplanes:

- Nacelle shape and nacelle location on wings (for horizontally opposed piston engines and for turbo propeller installation);
- Improved methods for predicting the effect of drag on weight (Adaptation of NASA/Ames GASP?); and
- Expansion and specialization of GASP to single engine and twin engine propeller driven airplanes with detailed accounting for weight, stability and control and propulsion interference factors.

References

1. Becker, G.V. and Leonard, L.H.; High Speed Tests of a Model Twin-Engine Low-Wing Transport Airplane; NACA TR 750, 1942.
2. Heldenbrand, R.W.; Merrill, G.L. and Burnett, G.A.; Study of Small Civil Turbofan Engines Applicable to Military Trainer Airplanes: Final Report; NASA CR 137575; Garrett Airesearch 74-210987-A; April 1975.
3. Roskam, J.; Opportunities for Progress in General Aviation Technology; AIAA Paper 75-292, Presented at the AIAA 11th Annual Meeting and Technical Display, Washington, D.C. February 24-26, 1975.
4. Roskam, J.; New Airfoils and Higher Wing Loadings: A New Look at General Aviation Airplane Design; Paper presented at the Technological University of Delft, The Netherlands, May 20, 1974.
5. Roskam, J. and Kohlman, D.L.; An Assessment of Performancy, Stability and Control Improvements for General Aviation Aircraft; SAE Paper 700240 presented at the SAE Business Aircraft Meeting, Wichita, Kansas, April 1970.

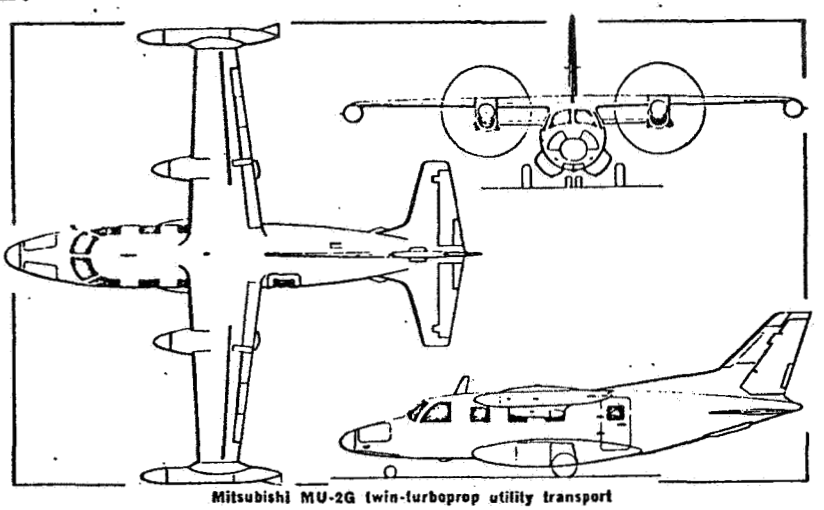

Mitsubishi MU-2G twin-turboprop utility transport

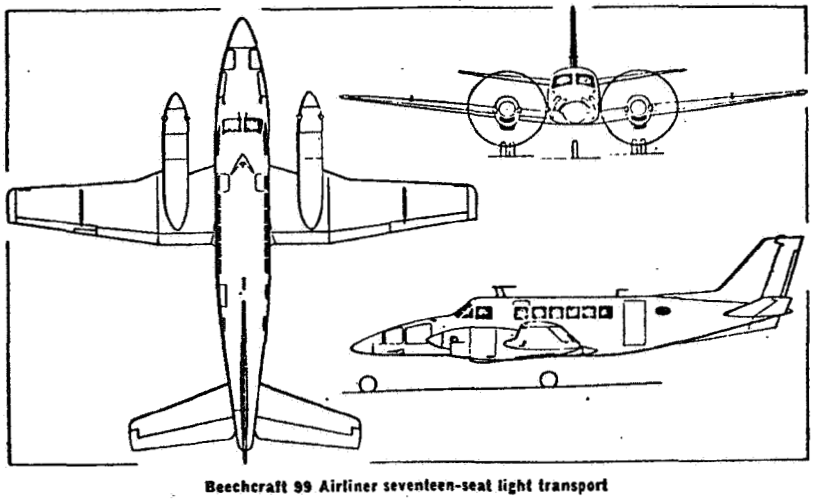

Beechcraft 99 Airliner seventeen-seat light transport

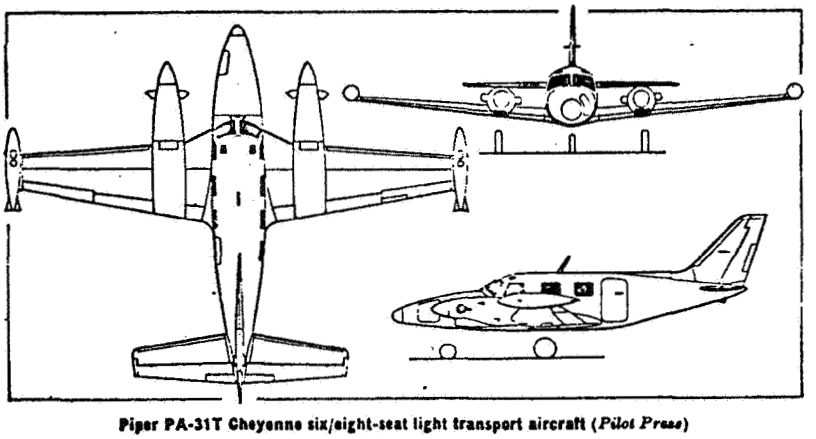

Piper PA-31T Cheyenne six/eight-seat light transport aircraft (*Pilot Press*)

Figure 1. Examples of General Aviation Turbopropeller Installations

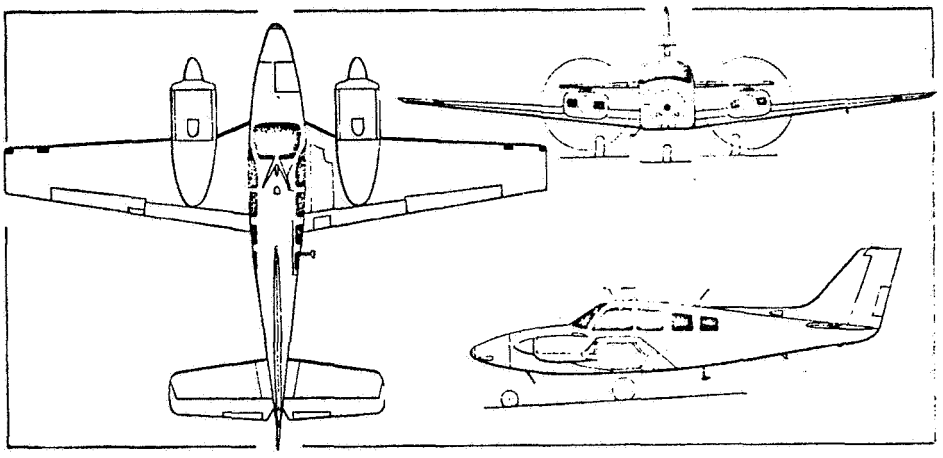

Three-view drawing of the Beechcraft Baron 58 four/six-seat cabin monoplane

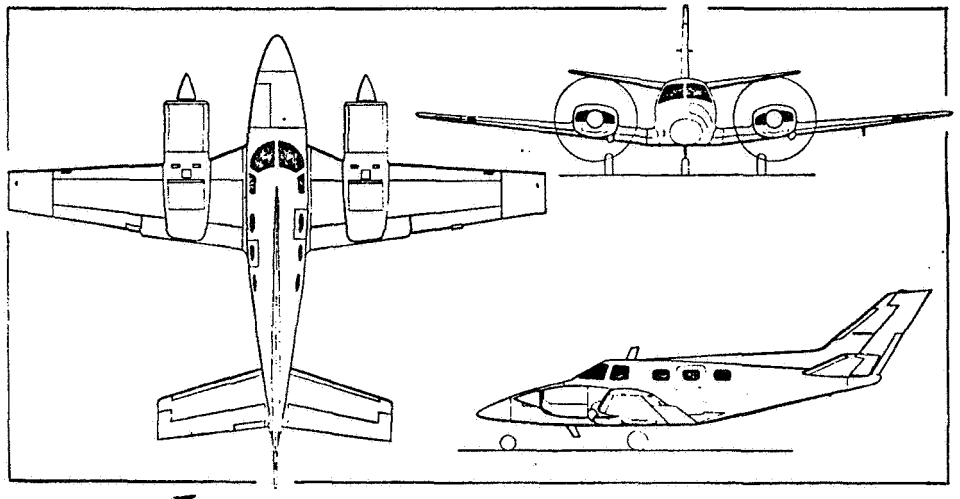

Three-view drawing of the Beechcraft Duke B60 4/6-seat pressurised transport (two 380 hp Lycoming TIO-541-E1C4 engines)

Figure 2. Different Piston Engine Nacelle Shapes Used by One Manufacturer

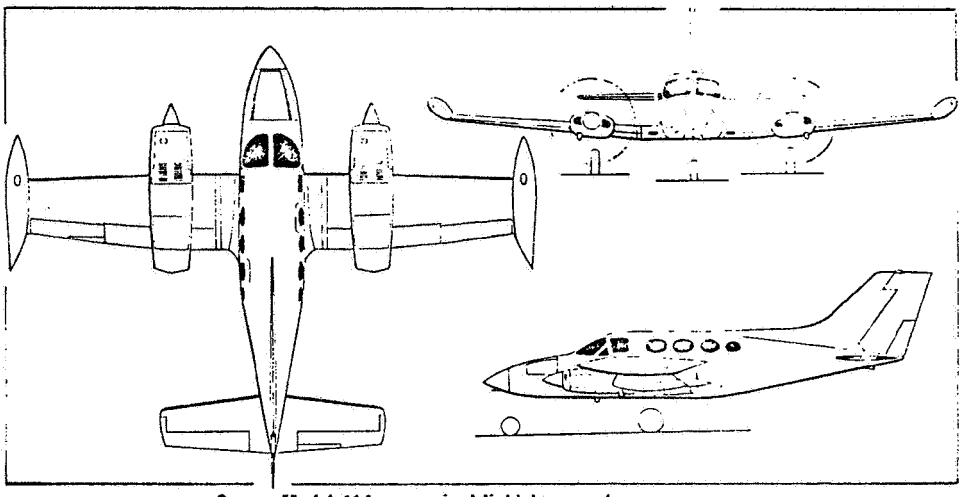

Cessna Model 414 pressurised light transport

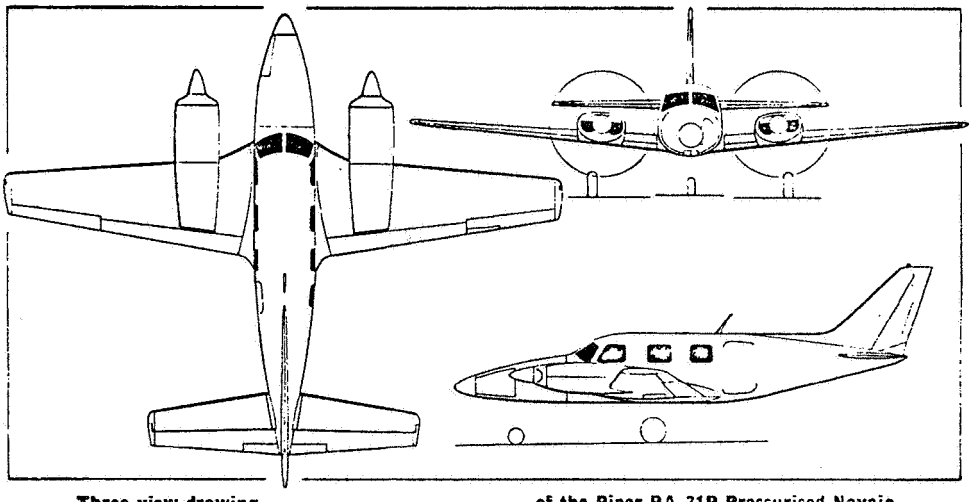

Three-view drawing of the Piper PA-31P Pressurised Navajo (two 425 hp Lycoming TIGO-541-E1A engines)

Figure 3. Further Examples of Piston Engine Nacelle Shapes

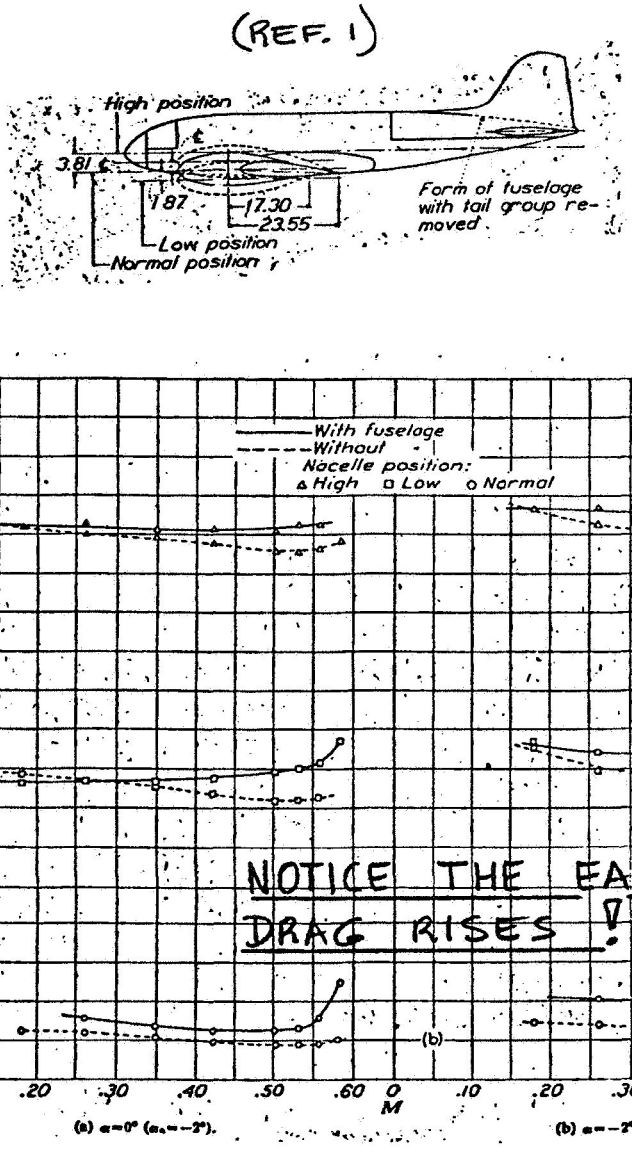

Figure 4. Example of the Effect of Vertical Nacelle Location on Drag

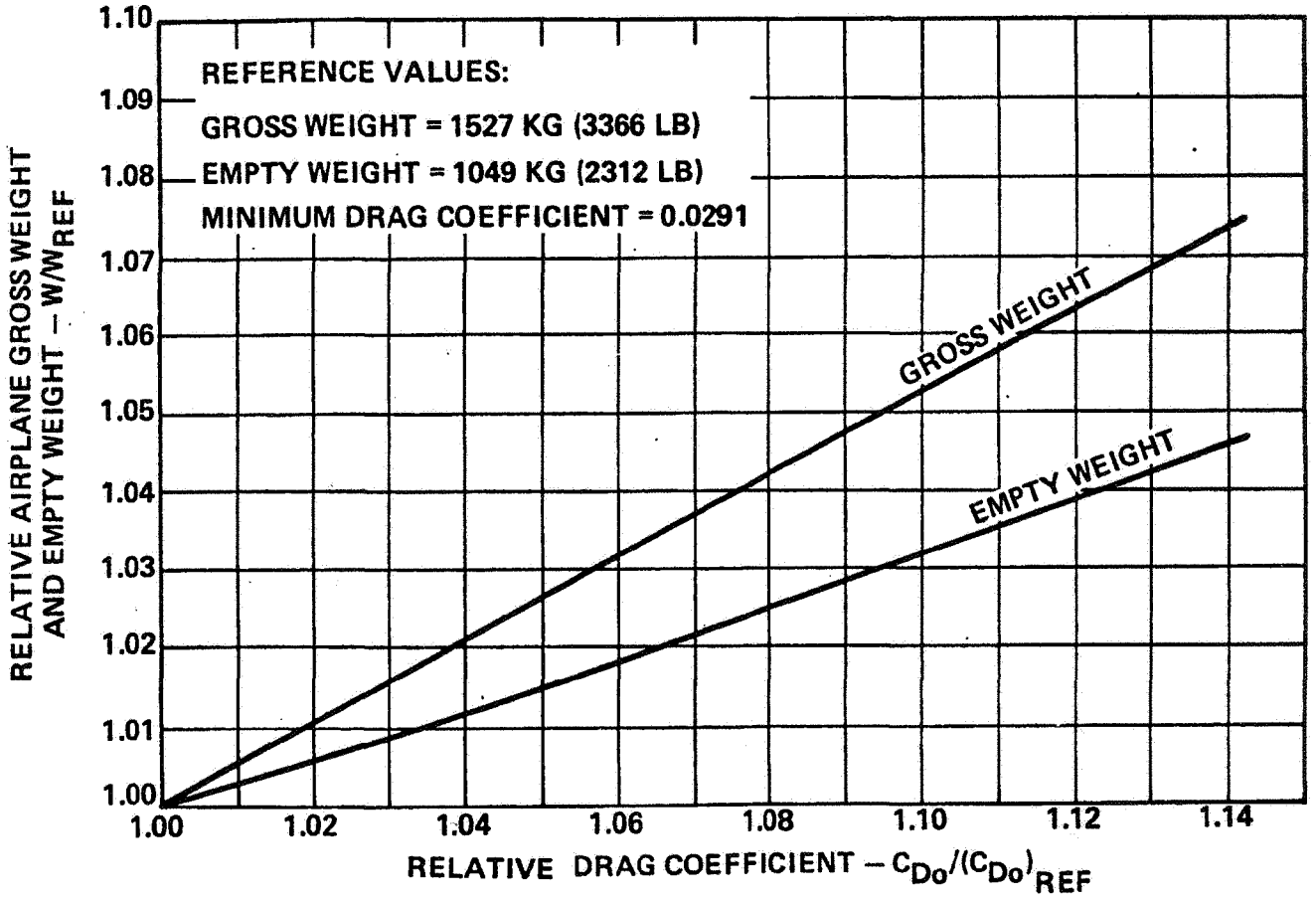

Figure 5. Gross and Empty Weight Sensitivity to Zero-Lift Drag Coefficient

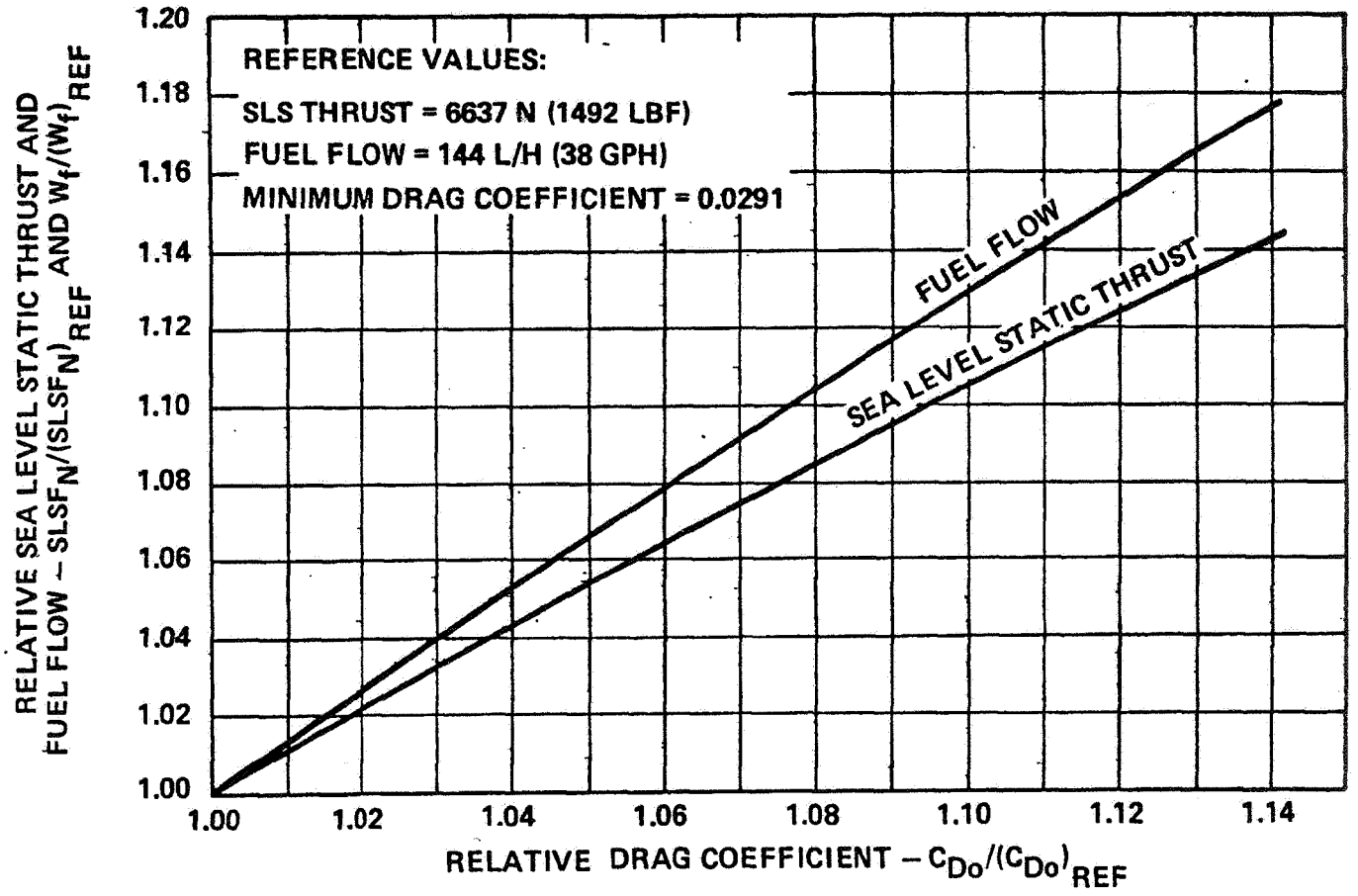

Figure 6. Engine Size and Cruise Fuel Consumption Sensitivity to Zero-Lift Drag Coefficient

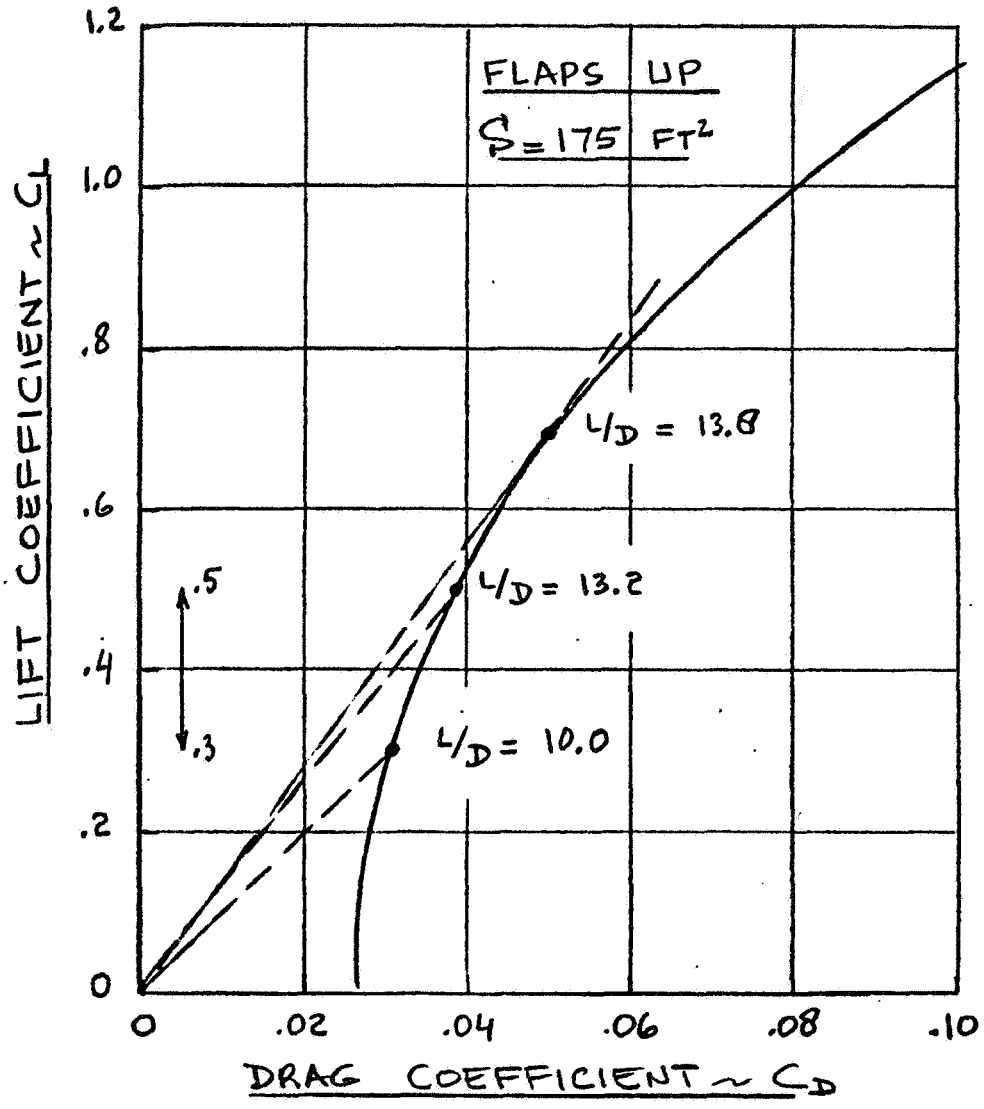

Figure 7. Typical Single Engine Airplane Drag Polar

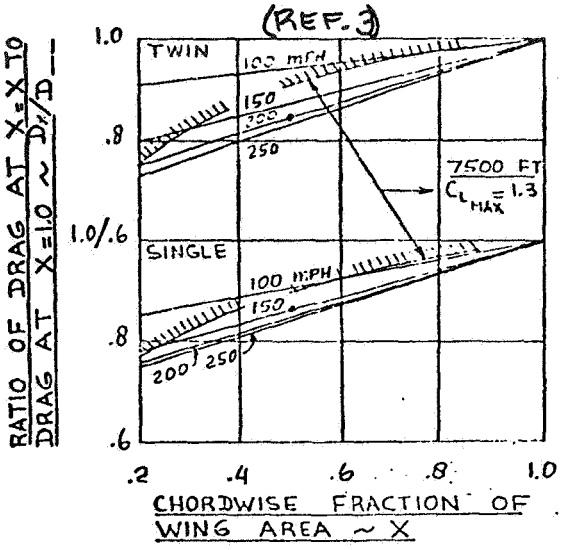

Figure 8. Effect of Chordwise Area Reductions on Thrust Required

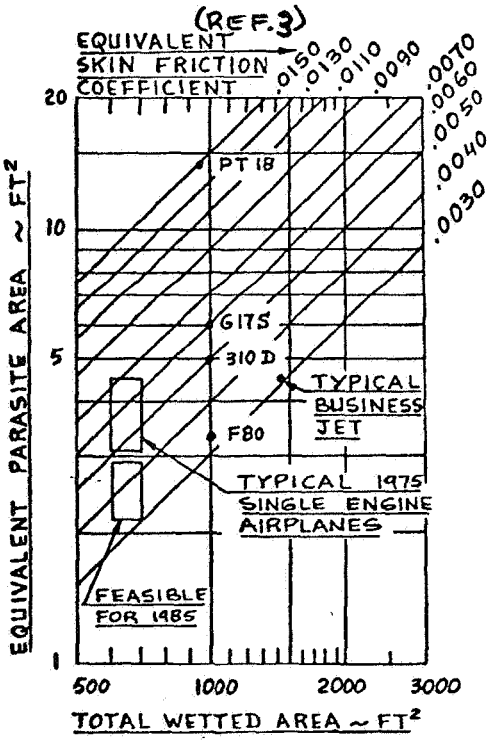

Figure 9. Typical Range of Wetted Areas and Equivalent Parasite Drag for General Aviation Airplanes

8.2 Learjet Model 25
Drag Analysis

Richard Ross
and
Ronald D. Neal
Gates Learjet Corporation

Drag Analysis

The procedures and data for estimating drag at Gates Learjet are contained in the Learjet Aerodynamics Handbook and were used to calculate the drag characteristics of the Model 25 airplane. Based on cruise flight test data obtained on the Model 25, these methods generally predicted the total drag characteristics within current acceptable and reasonable engineering accuracy.

The use of wind tunnel model results will not guarantee absolute accuracy because of the many corrections and interpretations that must be applied to the data. However, small scale tunnel tests can provide the technique for minimizing configuration drag as well as identifying the aerodynamic contributions of each individual component.

Flight testing, when carefully executed, will provide the complete trimmed drag of the airplane. Such a program requires extensive testing since it is necessary to define the characteristics throughout the operating envelope of the airplane. What a flight program does not do and cannot do (within practical limitations) is to isolate and identify drag characteristics for each of the major components of the total vehicle. Without knowing the drag build-up for the airplane it is difficult and costly, from flight test data alone, to identify drag problems and then through the continued use of flight tests to arrive at a solution to the problem.

Only by integration of the results of all the available techniques can confidence in drag prediction and eventual control of drag levels be developed.

The total airplane drag is produced by several separate contributions that are identified as:

- profile drag (skin friction)
- interference drag
- roughness and gap drag
- induced drag
- compressibility drag
- profile drag variation with lift
- trim drag

Estimated data, flight test data and small scale and full-scale wind tunnel tests are available for the Learjet. It is then reasoned that from these sources an assessment of the individual magnitudes can be determined. The following comments provide the reasoning and analysis for using these data to determine the drag for the Model 25. For purposes of evaluation and comparison a mid-cruise weight of 12,000 pounds, an altitude of 40,000 feet and a cruise Mach number of 0.75 will be used.

Figure 1 presents the trimmed, level flight drag characteristics for the Model 25 at cruise Mach numbers of 0.60, 0.70, 0.75 and 0.80. For a weight of 12,000 pounds and a cruise Mach number of 0.75 the lift coefficient is 0.336 and the corresponding total drag coefficient is 0.0338.

Profile, Interference, and Roughness Drag

The estimated skin friction drag is 0.0186, interference drag is 0.0032, and roughness and gap drag is 0.0016. The total zero lift drag is then estimated to be 0.0234 or 69.23 percent of the flight test cruise drag. Therefore, if the zero lift drag estimate is correct, the balance of the drag, 0.0104 may be attributed to:

- induced drag
- compressibility drag
- profile drag variation with lift
- trim drag

Induced Drag

One accounting technique that can be used in evaluating the drag contribution due to induced drag is to evaluate the induced drag term with the span efficiency factor equal to 1.0. By using this procedure all of the losses due to non-elliptical spanwise loading and wing-tip tank effects will be included in the profile drag variation with lift. Using this technique the induced drag at the cruise condition is 0.0072 or 21.30 percent of the total cruise drag. For reference purposes, Figure 2 presents a plot of induced drag based on e = 1.0.

At this point the contribution due to zero lift drag and induced drag is 0.0306. The remainder of the cruise drag 0.0032 or 9.47 percent should be accounted for by

- compressibility drag
- profile drag variation with lift
- trim drag

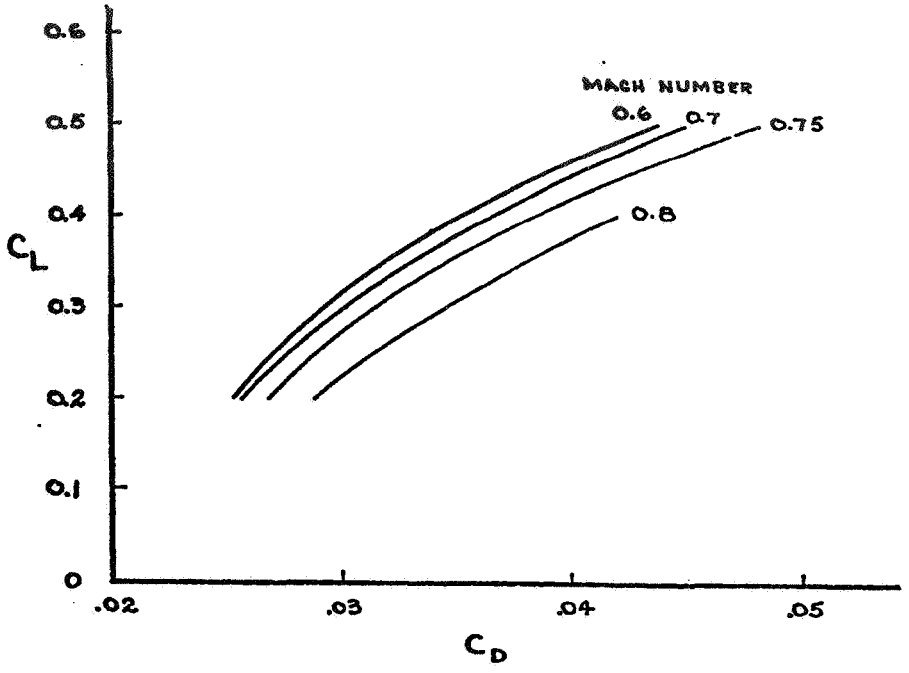

Figure 1. Learjet Model 25 Drag

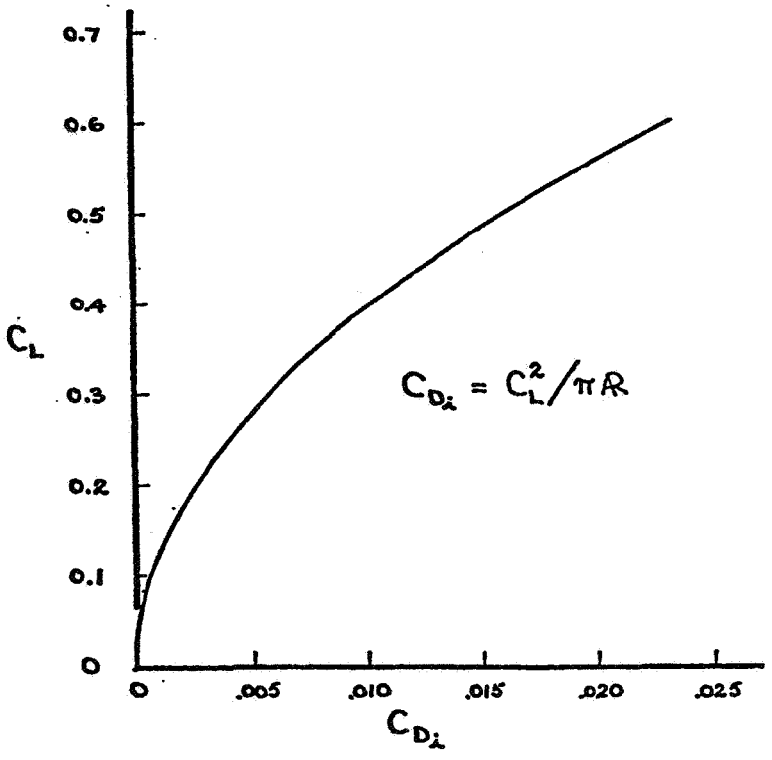

Figure 2. Learjet Model 25 Induced Drag

Compressibility Drag

Based on flight test data, Figure 3 presents the compressibility drag increments for the Model 25. Using these data the compressibility drag coefficient for a Mach number of 0.75 and a lift coefficient of 0.336, is determined to be 0.0028. The remaining drag increment of 0.0004 should be the sum of the

- profile drag variation with lift
- trim drag

In comparing the actual flight test compressibility drag increments to the original estimated curves it was noted that the flight values were higher than the predicted values. The difference between the actual and the estimated increases with Mach number and lift coefficient which is not unexpected. The reason for this difference may be better rationalized if the prediction procedures are reviewed.

As previously noted the total drag of the airplane may be attributed to profile drag (skin friction), profile drag variation with lift, interference drag, roughness and gap drag, induced drag, compressibility drag and trim drag. At zero lift the induced drag contribution is zero and the remainder of the zero lift drag should be accounted for by the other contributions.

Considering the data presented in Figure 4 and similar data for $M = 0.6$, the increment between the zero lift drag coefficient values for $M = 0.6$ and $M = 0.75$ should then be equal to the compressibility drag and the trim drag contributions. The difference between trim drag at zero lift for these two Mach numbers will be considered as being insignificant. The reason for this assumption is that between these speeds the stability values that determine trim drag should not be significantly different. Therefore, the increment between the zero lift drag coefficients should represent compressibility drag alone.

At zero lift for $M = 0.6$, $C_D = 0.0210$ and for $M = 0.75$, $C_D = 0.0226$ with $\Delta C_D = 0.0016$. From the data of Figure 3, the compressibility drag increment at $C_L = 0.2$ is determined to be 0.0015 which is in good agreement with the sixteen count increment at zero lift. This correlation would then indicate that from $M = 0.6$ to 0.75 the compressibility drag increment is the same for all lift coefficients in the range from 0.0 to 0.2. Such results are not unexpected with similar trends being shown in available literature. At Mach numbers greater than 0.75 the compressibility drag increments for lift coefficients of 0.0 and 0.2 should deviate as shown.

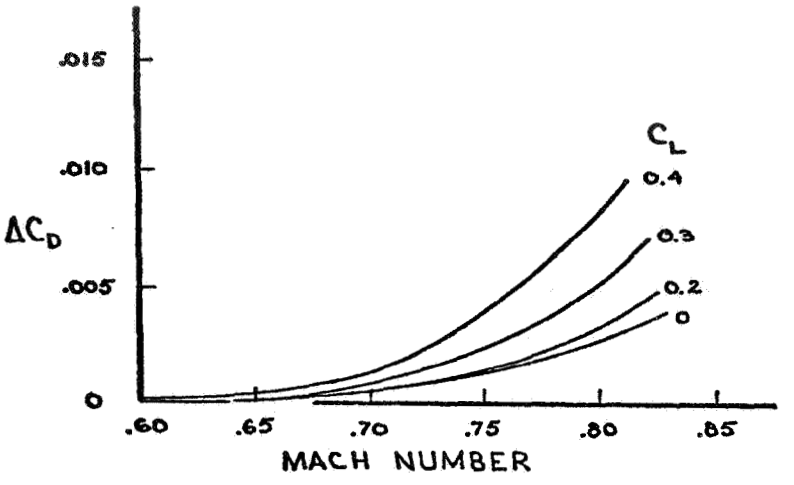

Figure 3. Learjet Model 25 Compressibility Drag

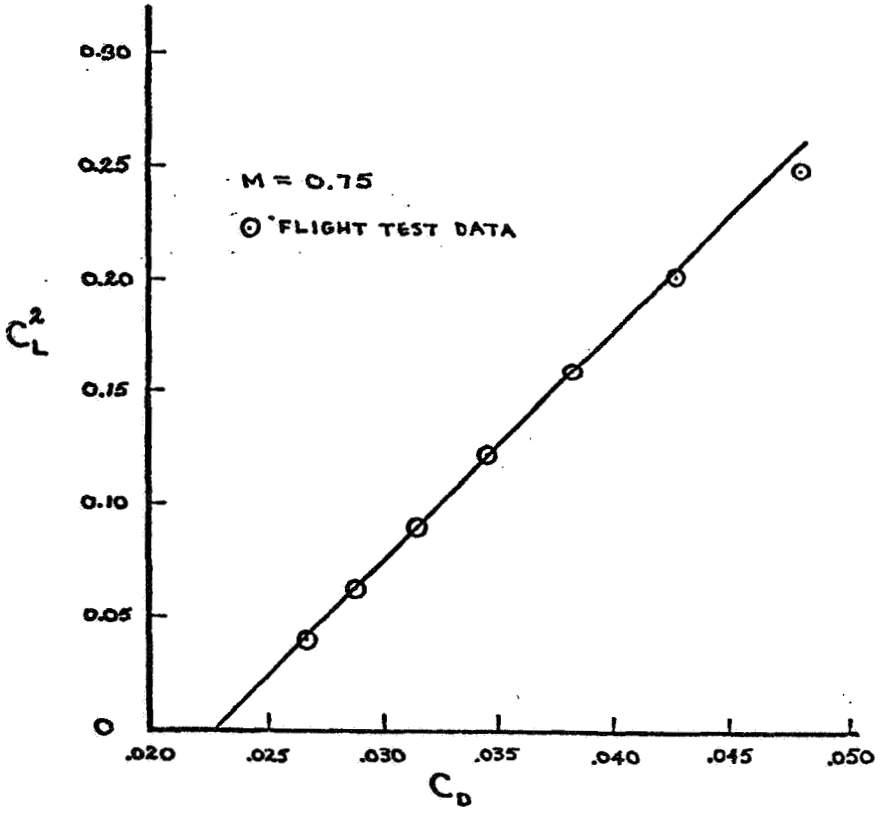

Figure 4. Learjet Model 25 Drag

Profile Drag Variation With Lift

Using the full scale wind tunnel test results and letting e = 1.0 for evaluating induced drag the profile drag variation with lift is determined from $C_{D_P} = C_D - C_{D_i}$ with the results being presented in Figure 5.

Using the data of Figure 5 the profile drag increment due to lift for a $C_L = 0.336$ is $\Delta C_{D_P} = 0.0007$ or 2.07 percent of the total cruise drag. However, this value is 0.0003 more than the total drag increment allowed for both profile drag variation with lift and trim drag.

Trim Drag

In considering the trim drag increment it is noted that the basic skin friction drag of the horizontal tail has already been included in the basic profile drag of the airplane. A profile drag variation with lift will exist for the horizontal stabilizer. However, this contribution is probably so small as to be negligible. Thus, the horizontal stabilizer trim drag increment will be considered to consist only of the induced drag contribution of the tail.

Low speed wind tunnel test data are used to show that the tail induced drag or trim drag increment is 0.0005. Compared to the total cruise drag of 0.0338 the trim drag amounts to 1.48 percent.

It is noted the sum of the estimated profile drag due to lift, 0.0007, and the trim drag, 0.0005, is 0.0008 more than the total drag increment allowed for them.

Discussion of Drag Analysis

By using the reasoning and procedures given in the preceding analysis, all of the drag, except for a drag increment of 0.0008 can be accounted for in the analysis. Balance of the total drag picture can be obtained by slight revisions in the estimates of any of the individual sources. However, the more likely and suspect areas for reassessment are the contributions due to profile drag (skin friction), interference drag, and roughness and gap drag. These items are open to question because they represent the estimated portion of the previous analysis, whereas all of the other items have a firmer basis for conviction. The eight drag count increment represents 2.37 percent of the cruise drag. In order for the individual drag contributions to balance it is reasoned that this drag reduction may be distributed between profile, interference and roughness so that the total for these three sources is 0.226 instead of the original estimate of 0.0234.

If the zero lift drag is 0.0226 it should then be possible to take the flight test drag polar at M = 0.75 (Figure 1), plot these data as C_L^2 versus C_D and extrapolate this curve to zero lift and verify the 0.0226 value. Figure 4 presents a plot of C_L^2 versus C_D with the symboled points being taken directly from Figure 1. The zero lift drag, as determined from this plot is 0.0226 which then substantiates this zero lift drag value as determined from the previous analysis.

Distributing the eight drag count reduction between the three sources so that the total zero lift is 0.0226, the breakdown of total airplane cruise drag is then given in Figure 6.

Based on a total profile drag of 0.0180 and on the original estimated profile drag contribution of each individual component the profile drag (skin friction) may be summarized as shown in Figure 7.

The total profile drag accounts for 53.25 percent of the total cruise drag of the airplane.

Drag Distribution

Figure 8 presents the drag distribution for the airplane as a function of Mach number with the data being extended to Mach 0.85. This plot provides a summary presentation of the drag contributions of the various drag sources discussed in this report. Throughout the flight range the drag contribution due to profile drag continues to be the major source of drag representing 61 to 66 percent of the total cruise drag. With increasing cruise speed the induced drag decreases, varying from 24 to 11 percent of the total. The compressibility drag increases with increasing Mach number, varying from 4 to 24 percent. The contribution due to trim drag and profile variation with lift represents the smallest source for a range of 8 to 2 percent of the total cruise drag.

A comparison of high Mach number estimated drag with flight test determined drag is presented in Figure 9.

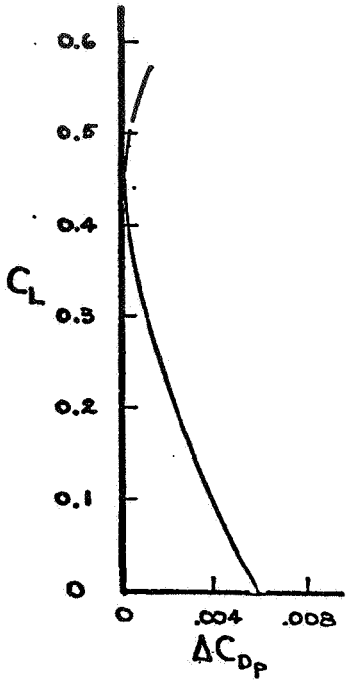

Figure 5. Learjet Model 25 Profile Drag Variation with Lift

M = 0.75 C_L = 0.336 C_D = 0.0338

Source	ΔC_D	% of Total
Profile drag (skin friction)	.0180	53.25
Profile drag variation with lift	.0007	2.07
Interference drag	.0031	9.17
Roughness and gap drag	.0015	4.44
Induced drag	.0072	21.30
Compressibility drag	.0028	8.28
Trim drag	.0005	1.48
TOTAL	0.0338	100.00

Figure 6. Cruise Drag Breakdown

C_{Dp}, Profile Drag = 0.0180

Item	% of ΔC_{Dp}	ΔC_{Dp}
Wing	29.57	.0053
Fuselage	34.95	.0063
Tip Tanks	11.83	.0021
Tip Tank Fins	0.54	.0001
Nacelles	6.45	.0012
Pylons	1.61	.0003
Horizontal	9.14	.0016
Vertical	5.91	.0011
TOTAL	100.00%	0.0180

Figure 7. Profile Drag (Skin Friction) Breakdown

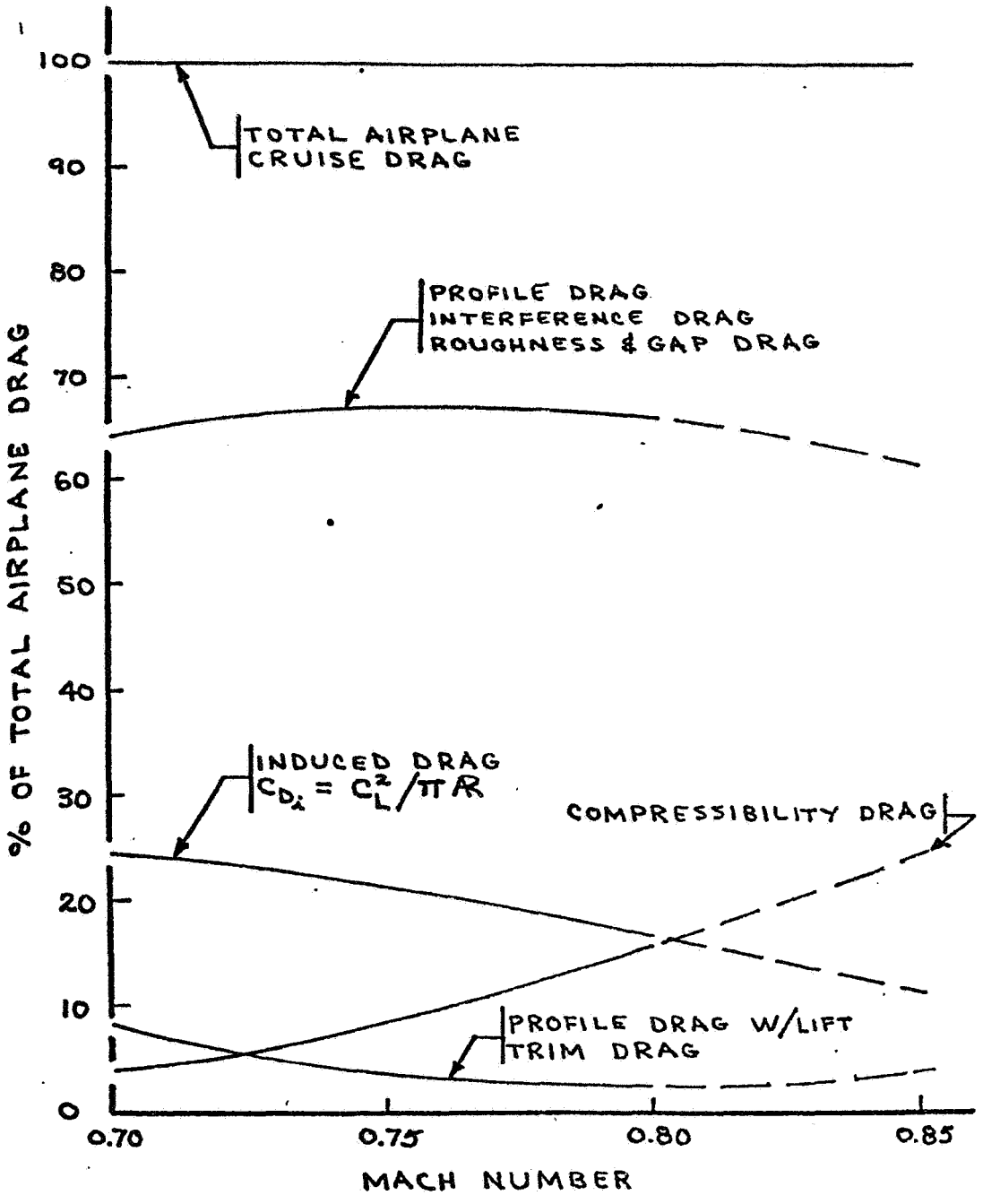

Figure 8. Learjet Model 25 Drag Distribution

EXAMPLE @ MID-CRUISE WT.
40,000 FT.

M	C_L	C_D (Actual)	C_D (Estimated)	ΔC_D	% DIFF.
.70	.385	.0353	.0353	0	0
.75	.336	.0338	.0335	.0003	0.9
.77	.318	.0338	.0331	.0007	2.1
.80	.295	.0341	.0326	.0015	4.6

Figure 9. Comparison of Flight Test Drag and Estimated Drag

8.3 Problems in Propulsion System Integration

W. Henderson and J. Runckel
NASA Langley Research Center

Problems in Propulsion System Integration

The problems associated with propulsion system integration are related to the placement of the engine on the airframe. The complexity of the problem, and the associated drag, depends on the area where the power plant is located--as indicated on Figure 1.

Wing installations can consist of nacelles located under or over the wing or propulsive wing concepts. The exhaust stream can produce either favorable or unfavorable induced effects on lift and drag.

The fuselage could contain lift engines or adjacent nacelles which produce interference drag and the hot exhaust can have detrimental effects on the structure.

The afterbody with buried engines is a particular problem with military aircraft since a large portion of the drag occurs in this region.

Reverse thrust on rear mounted engines can pose plume impingement problems on stabilizing surfaces.

I will touch briefly on several of the areas indicated on Figure 1.

The main problems with jet-engined aircraft are with the induction system and the exhaust system and the effects on configuration performance consisting of mutual interferences between the propulsion system and the airframe.

Interference effects are usually evaluated first by looking at the isolated components of the propulsion system and then with the system integrated into the airframe. I would like to present some recent NASA work on jet engine components which can influence the related aircraft drag areas.

FOREBODY

PROPELLER/ENGINE, INLETS

WING

FLOW FIELD/NACELLE INTERFERENCE

INDUCED EFFECT - LIFT AND DRAG

FUSELAGE

INTERFERENCE DRAG

EXHAUST EFFECTS

- INDUCED PRESSURES - STATIC/DYNAMIC-ACOUSTIC
- INDUCED TEMPERATURES

AFTERBODY

POWER EFFECTS ON DRAG

NOZZLE/AIRCRAFT CLOSURE

REVERSE THRUST

EMPENNAGE

PLUME EFFECTS ON STABILITY

VERTICAL TAIL ENGINE INSTALLATION

Figure 1. Influence of Propulsion System on Airframe Aerodynamics

Nose Inlets

The early work on NACA inlets has recently been extended to higher Mach numbers and updated for geometries corresponding to the mass flow requirements of high bypass rotor fan engines. Figure 2 shows the experimental results of the investigation. The variables were fineness ratio, inlet highlight to maximum diameter ratio mass flow and angle of attack. The upper left chart in Figure 2 shows the effect of fineness ratio at a constant mass flow ratio of 0.8. The short inlets are best at lower speed but drag rise Mach number increases with fineness ratio. Figure 2 shows the effect of diameter ratio-drag increases as the inlet is opened up but the critical Mach number is extended. The right side of the figure shows the effect of mass flow ratio variation where reductions in drag and increases in the knee of the drag curve increase with increased inlet mass flow ratio. These data were obtained from force balance measurements and the drag coefficient is based on the maximum cross-sectional area.

Reference

An Investigation of Sever NACA 1-Series Axisymmetric Inlets at Mach Numbers from 0.4 to 1.29. Richard, J. Re. NASA TM X-2917, March 1974.

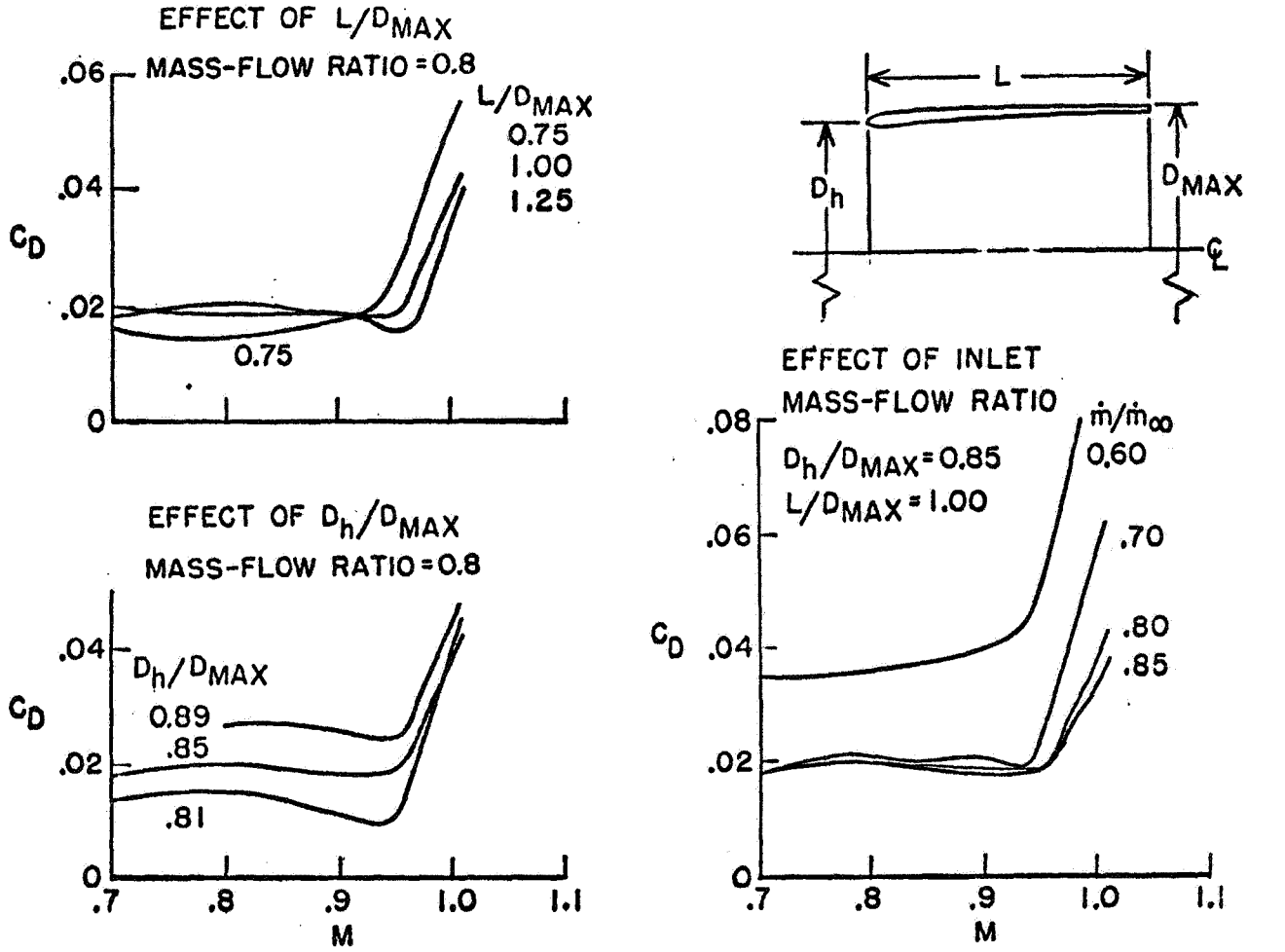

Figure 2. Nose Inlets at Transonic Speeds

Inlet Instrumentation Prediction

Pressure destribution measurements were also obtained during the inlet investigation. Figure 3 shows a comparison of a theoretical prediction with an experimental pressure distribution. The measured pressure coefficients are indicated by the circular symbols for both the outer cowl and on the inside of the inlet. Data are for an inlet with highlight to maximum diameter ratio of 0.85 and fineness ratio of 1.0 at 0.7 Mach number and a mass-flow ratio of 0.87. The calculated pressure distribution using a stream tube curvature theory developed for NASA is shown by the line. This theory accounts for both the internal and external flow field at the inlet and can also be used to calculate the pressure distribution on afterbodies with a jet exhaust. The agreement is very good with only a slight miss on the lip peak suction pressure.

Reference

Analystical Method for Predicting the Pressure Distribution about a Nacelle at Transonic Speeds. J. S. Keith, D. R. Ferguson, C. L. Merkle, P. H. Heck and D. J. Lahti. NASA CR-2217, July 1973.

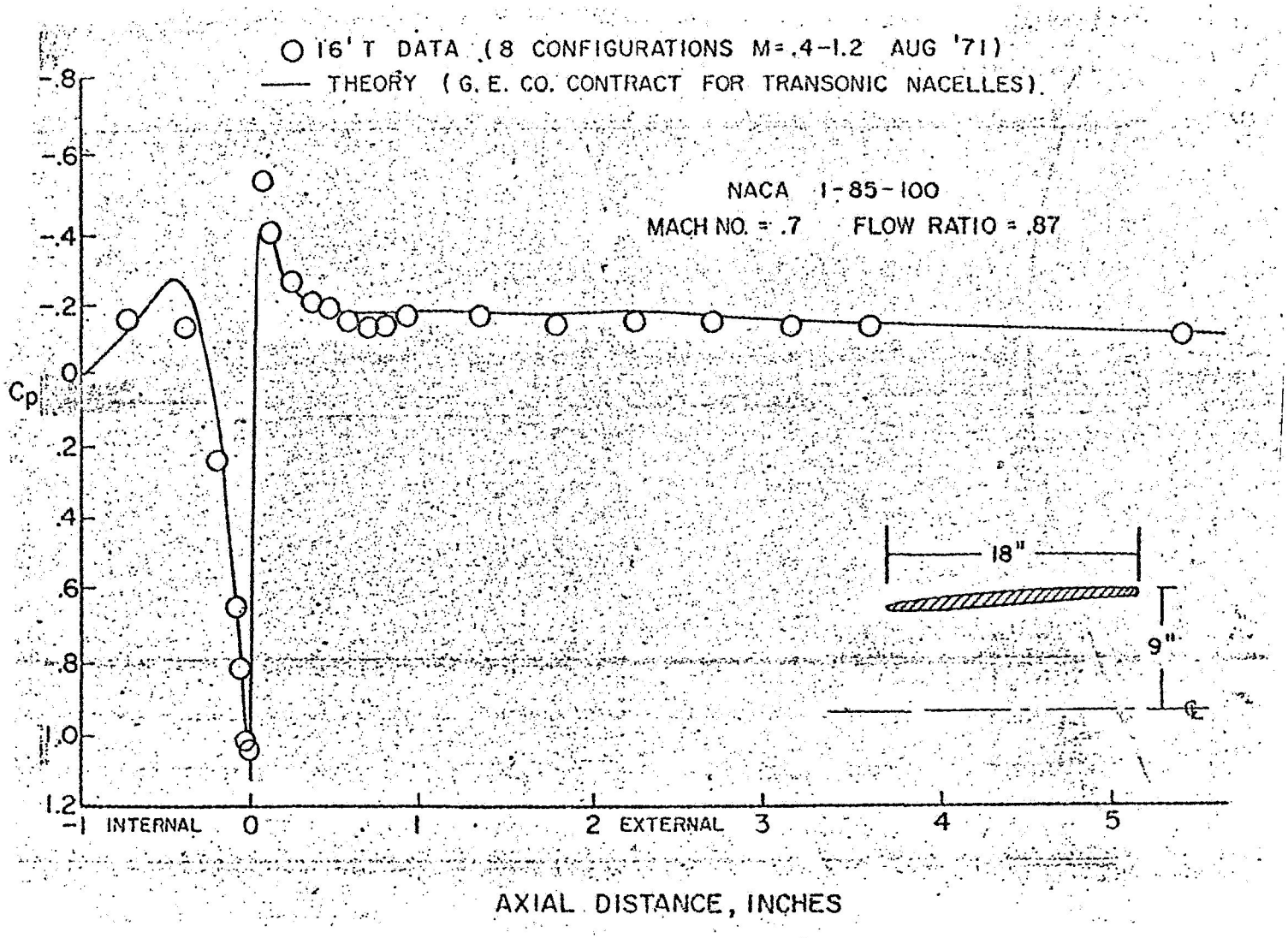

Figure 3. Transonic Inlet Results

Nozzle Boattail Drag

(We have also developed an extensive data base on the drag characteristics of boattailed afterbodies.)

A series of nozzle boattail configurations has been investigated at subsonic and transonic speeds to determine the pressure drag for various shapes, fineness ratios and closure ratios which should be applicable to several types of jet and fan engines. Shown in Figure 4 are samples of data for circular arc boattails from a program where fineness ratio varied from 0.8 to 2.0 and closure ratio from 0.5 to 0.7. The variation of drag with Mach number is shown for a short steep boattail on which the flow separated and a higher fineness ratio boattail with attached flow. Experimental data is indicated by the symbols and theoretical predictions by the lines. For attached flow the prediction is reasonable until supercritical velocities are approached. For the separated flow case, however, existing theory is inadequate and further work is being done to improve the situation. The limitations to existing theory include transonic flow and imbedded shocks, separated flow regions and inadequate modeling of the jet exhaust to include entrainment effects.

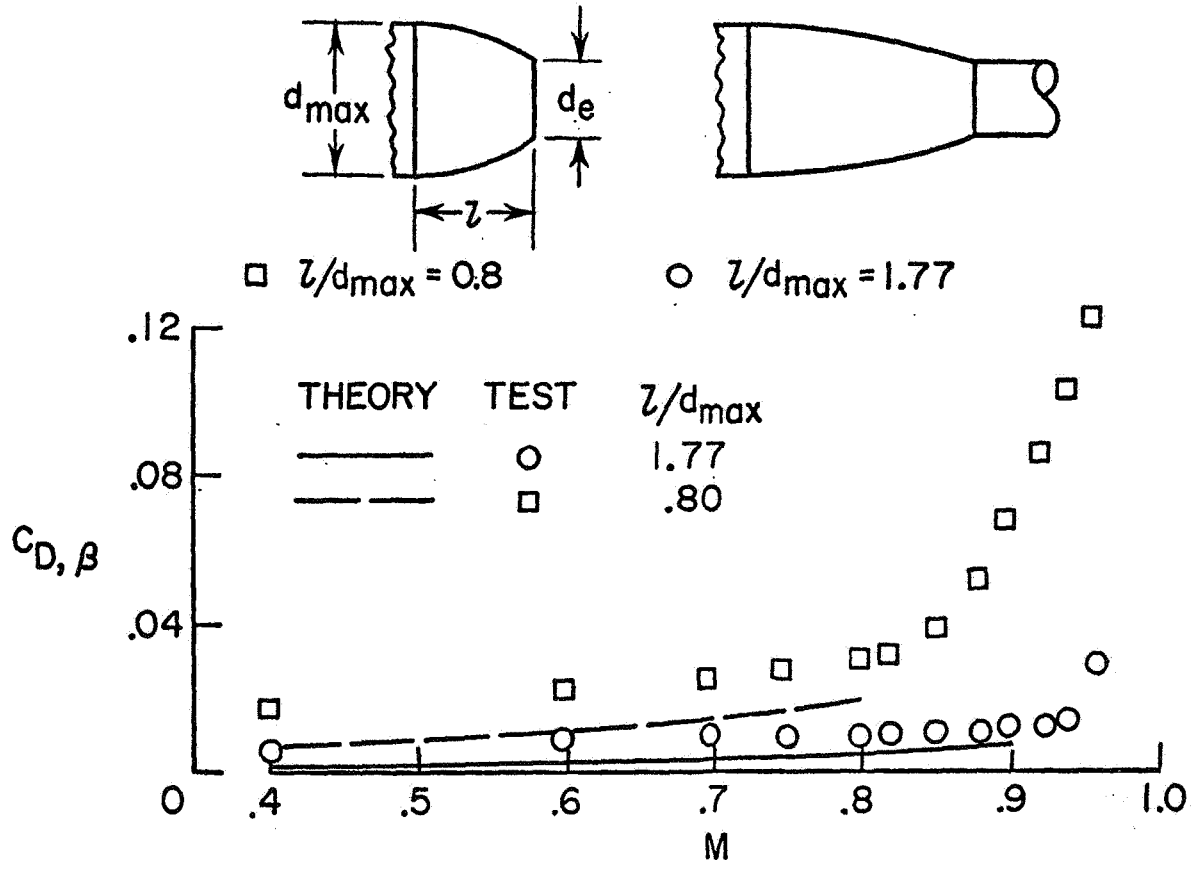

Figure 4. Nozzle Boattail Drag Shape, Fineness Ratio, Closure Ratio = 0.5

Propulsive Wing Installation

Figure 5 shows an example of a propulsion system completely integrated into the wing. The configuration is a propulsive wing utilizing four tip-turbine driven fans. The wing fans, oriented in the axial direction, induce air into the leading edge of the wing and exhaust it at the trailing edge. Either lift and/or axial thrust are obtained by means of a slipstream deflection and modulation system. In the cruise mode, variable angle flaps aid in the control of fan flow direction as well as provide expansion surfaces for the two-dimensional turbine exhaust flow from the gas generator--similar to a jet flap concept. Although the wing was geometrically thick (thickness to chord ratio of 25 percent), aerodynamically it was relatively thin as indicated by the drag rise which occurred at a Mach number of 0.85.

Reference

Longitudinal Aerodynamic and Propulsion Characteristics of a Propulsive-Wing V/STOL Model at High Subsonic Speeds. Leland B. Salters, Jr., and James W. Schmeer. NASA TMX-2693. January 1973.

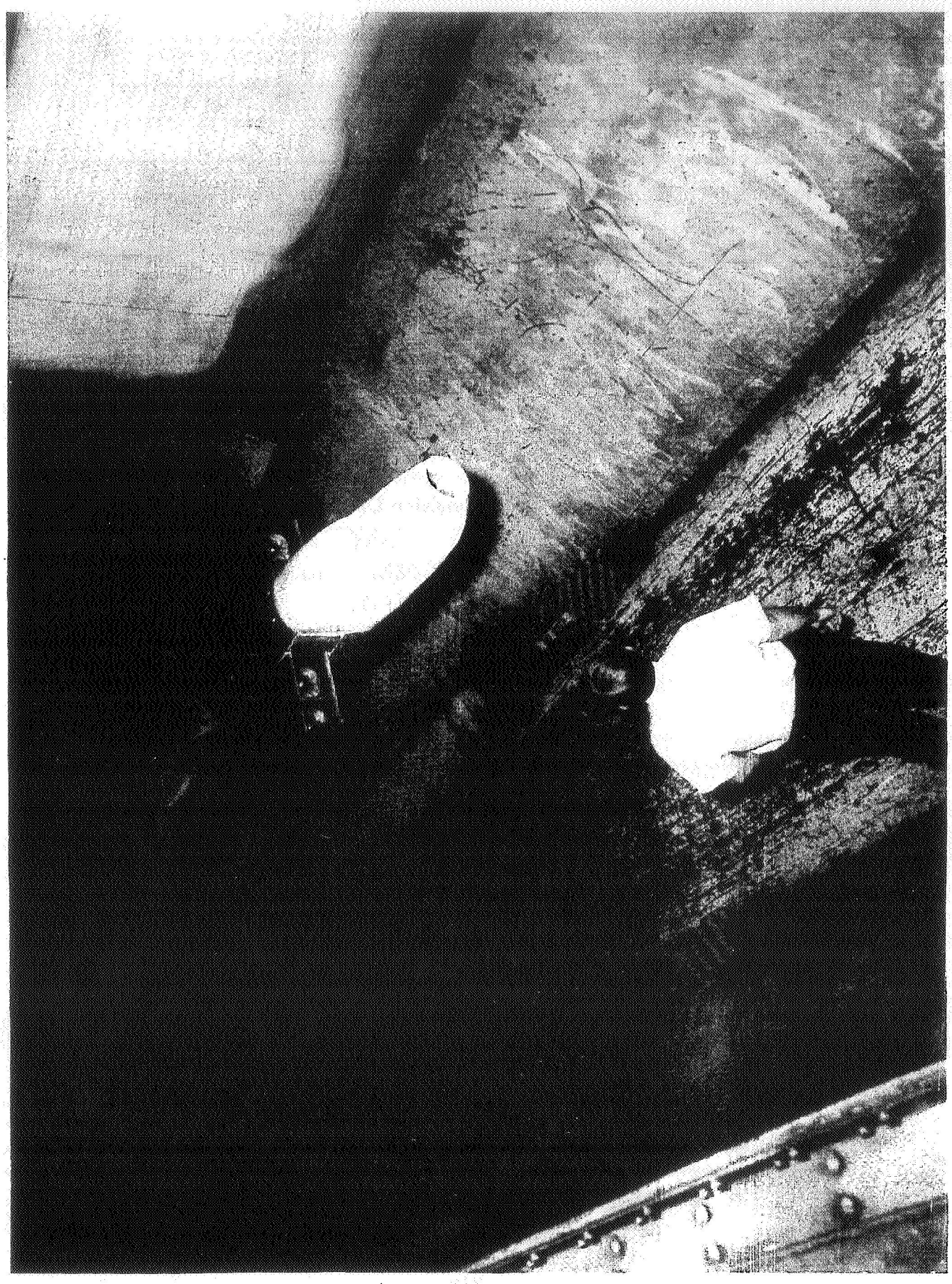

Figure 5. Example Propulsive W Installation

Blowing Over the Wing

Upper-surface blowing propulsive lift concepts have shown a potential for attaining good low-speed high-lift performance with lower noise levels because of the shielding afforded by the wings between the jet related noise and the ground. Only preliminary work has been done on the effects of propulsive lift cruise performance. Shown on Figure 6 are results from an experimental and analytical investigation to determine the effects of forward mounted jets blowing over a wing. The model had a low aspect ratio wing and forces were measured on the wing-afterbody portion. The nacelles were located forward and above the wing. The analytical method represented the wing lifting surface with a lattice of horseshow vortices and simulated the effects of the exhaust plume with a line sink-source distribution located on the axis of the jet. The theory accurately predicted the variation in interference lift due to the jet flow for Mach numbers of 0.4 to 0.7. The theory also predicted the reduction in induced drag indicated by the data. The favorable increment in induced drag increases with both the ratio of jet velocity to free stream velocity and wing lift coefficient. The plots on the right side of Figure 6 show that the theory correctly predicts both the increase in lift and the reduction in induced drag coefficient.

References

1. Exploratory Investigation at Mach Numbers from 0.40 to 0.95 of the Effects of Jets Blown Over a Wing. Lawrence E. Putnam. NASA TND-7367, November 1973.
2. An Analytical Study of the Effects of Jets Located More than One Diameter Above a Wing at Subsonic Speeds. Lawrence E. Putnam. NASA TND-7754, August 1974.

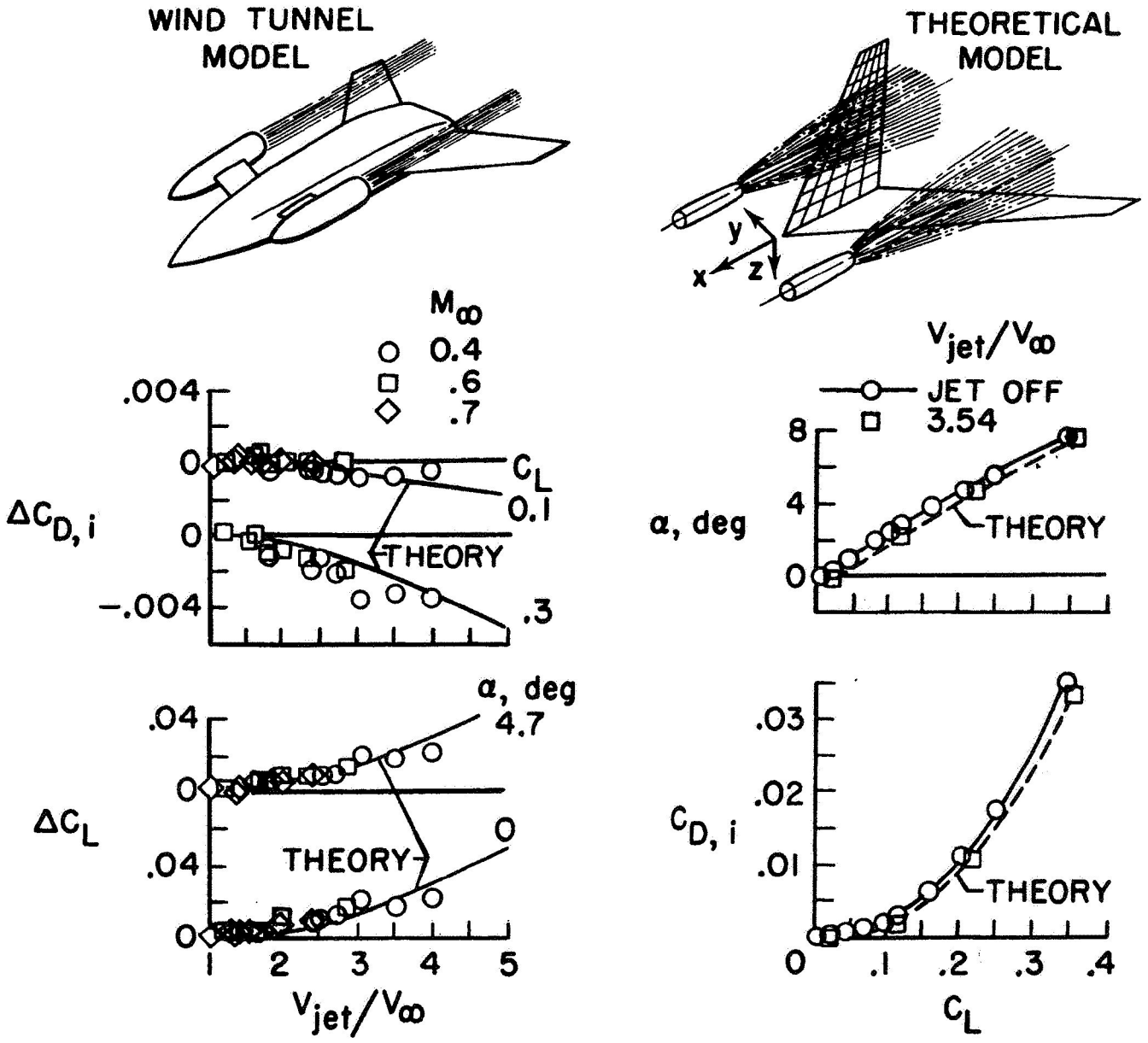

Figure 6. Jets Blowing Over Wing

Induced Drag Reduction By Over-the-Wing Blowing

The theoretical method we developed was also used to correlate some existing data on blowing over the wing. Fokker VFW research results presented at a 1974 AGARD meeting are shown in Figure 7. The engine-nacelle configuration is shown in the upper right hand corner and was located above and forward of the wing. The plot shows the change in induced drag coefficient for jet off and a jet to free stream velocity ratio of about 7.5 by the data points; circles for cruise, squares for climb values of left coefficeint. The theory calculations are indicated by the broken lines, and again, the predictions agree well with the data. The actual values of velocity ratio required for climb and cruise are indicated by the broken bars. The reductions in induced drag at climb are still substantial and some benefits still occur at cruise.

Reference

Airframe-Engine Interaction for Engine Configurations Mounted Above the Wing. Part 1: Interference Between Wing and Intake/Jet, by G. Kreng. In: AGARD Conference Proceedings No/SD on Airframe/Propulsion Interference AGARD-CP-150, September 1974.

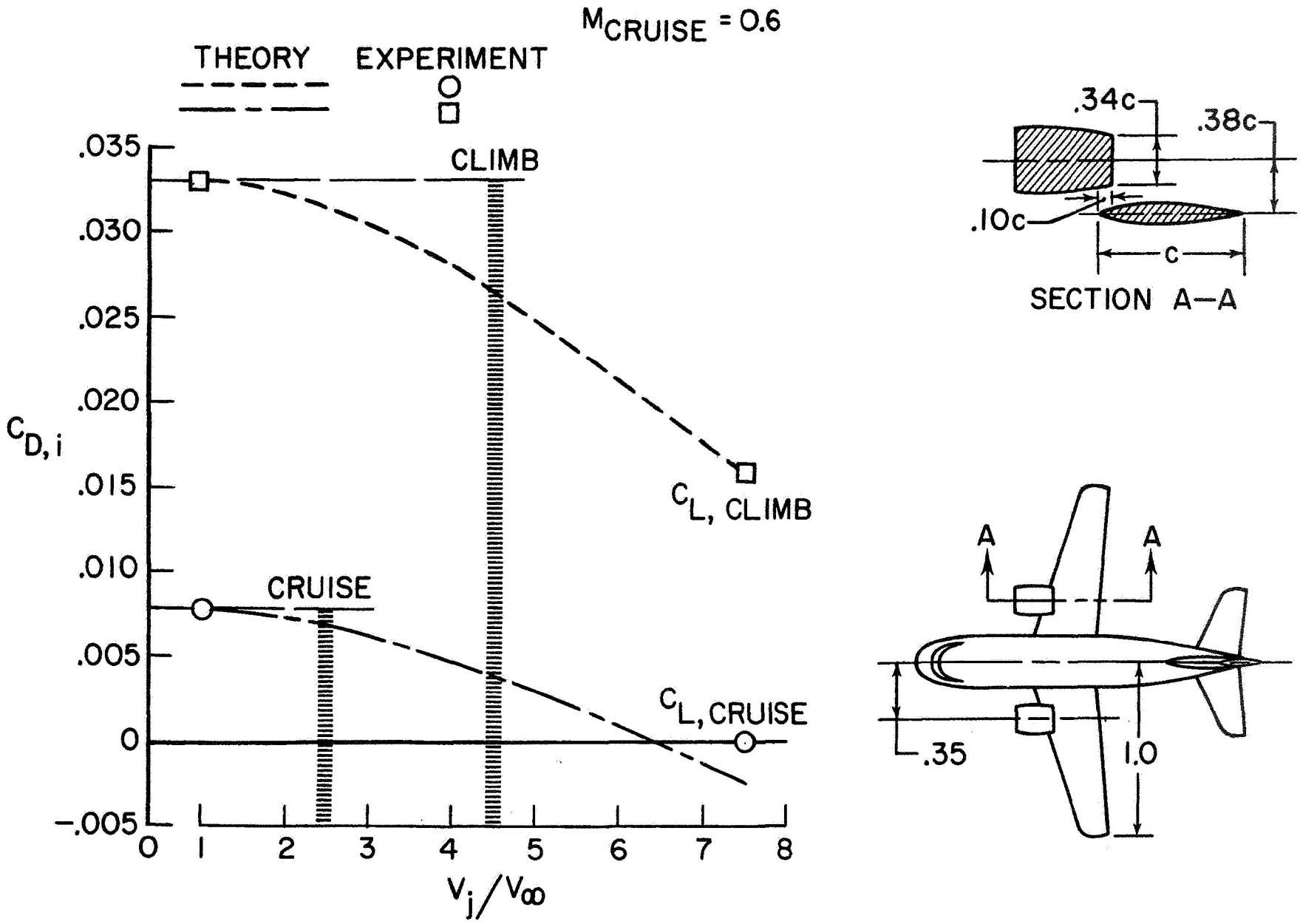

Figure 7. Induced Drag Reduction by Over-the-Wing Blowing

Propulsion/Aero Effects on Cruise Efficiency

These exploratory results have encouraged us to look at the performance benefits that may be possible with transport configurations during cruise flight.

Figure 8 illustrates a current program aimed at determining the cruise efficiency of highly integrated propulsion systems. A powered model of a basic transport configuration is under construction which will allow various types of engine locations on the wing to be studied and performance comparisons to be determined. Three types of engine installations will be considered: conventional under the wing pylon mounted nacelles; over the wing nacelles; and a blended upper surface blowing configuration. An internal balance system will measure all forces on the model including the thrust. The types of propulsion systems are shown on the right and consist of flow through nacelles, blown nacelles with air jets and turbofan simulators. These simulation systems will provide aerodynamics model data comparisons, the jet induced lift and drag increments and the contribution of the inlet flow simulation on the flow field.

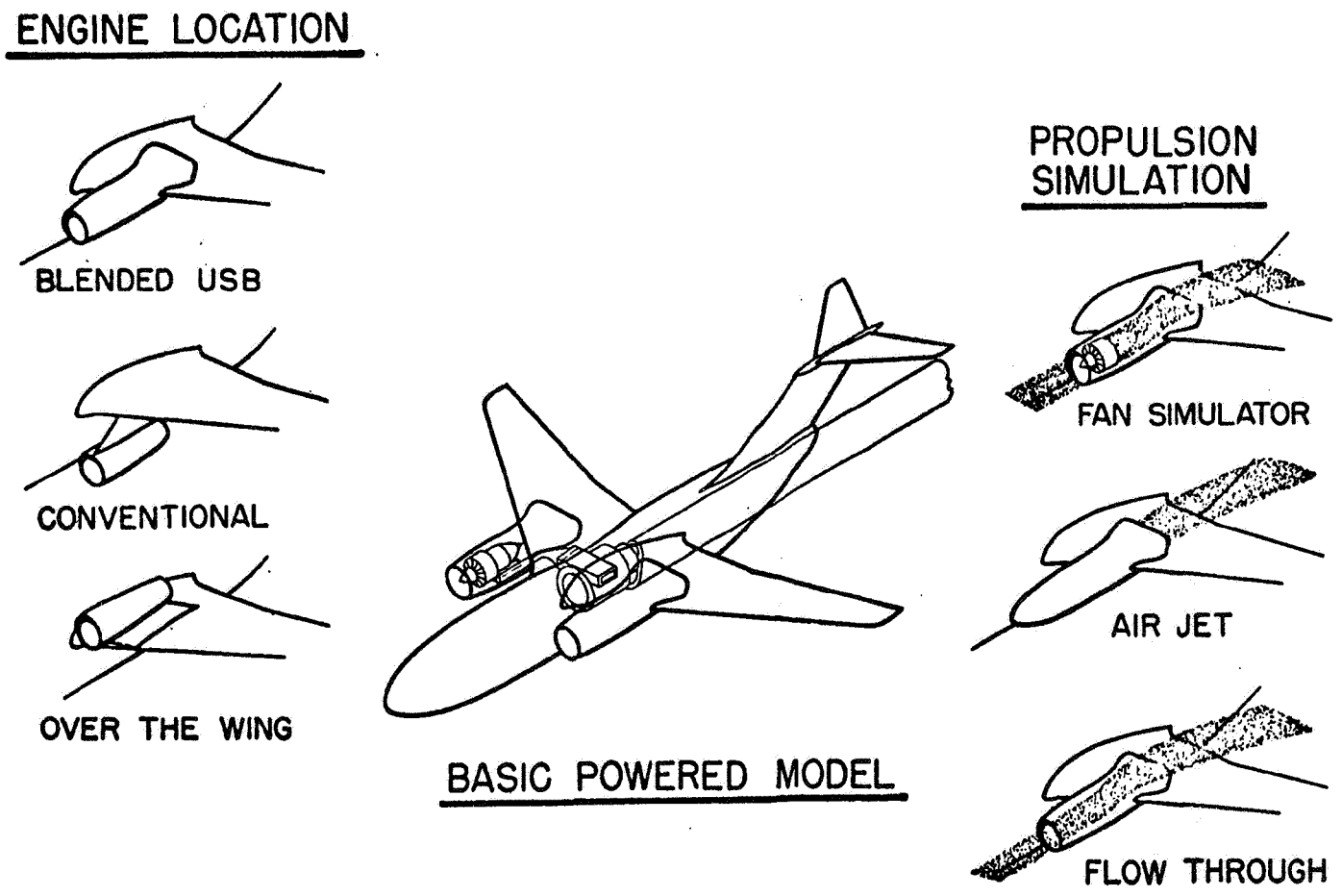

Figure 8. Propulsion/Aero Effects on Cruise Efficiency

Fuselage Mounted Nacelles

The information presented on Figure 9 shows the drag increments that can be expected with an aft fuselage mounted nacelle configuration. The model represented a small twin-jet business transport and was investigated with various nacelle arrangements. The circular symbols show the variation of drag coefficient with Mach number for the basic wing-fuselage-empennage. Addition of the fuselage mounted pylons and nacelles increase the drag to the level shown for the square symbols. The calculated skin friction of the pylon nacelle combination when added to the baseline configuration would give a drag variation as indicated by the top line of the cross hatching. The installation penalty for the propulsion system package is small in this case and there is some beneficial interference at the highest speeds. Even lower values of the complete aircraft drag can be obtained by the alterations to the nacelle installation as indicated on the right side, where decreases in drag due to changing longitudinal location, increasing incidence angle and cant angle and changes in the effective area distribution in the fuselage nacelle region are shown.

References

Effects of Aft-Fuselage-Mounted Nacelles on the Subsonic Longitudinal Aerodynamic Characteristics of a Twin-Turbojet Airplane. Lawrence E. Putnam and Charles E. Trescot, Jr. NASA TND-3781, December 1966.

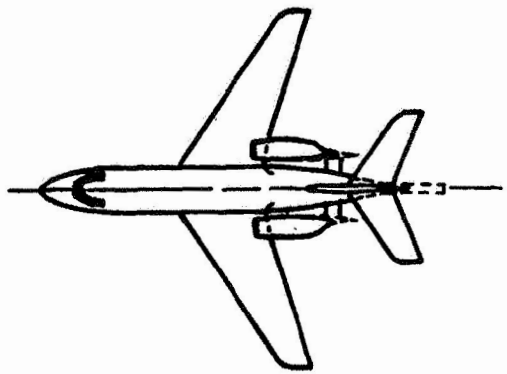

INTERFERENCE DRAG REDUCTIONS

	DRAG COUNTS
LONGITUDINAL LOCATION	2–5
INCIDENCE ANGLE	3–10
CANT ANGLE	3–4
NACELLE AND PYLON EXTENSION	3–8

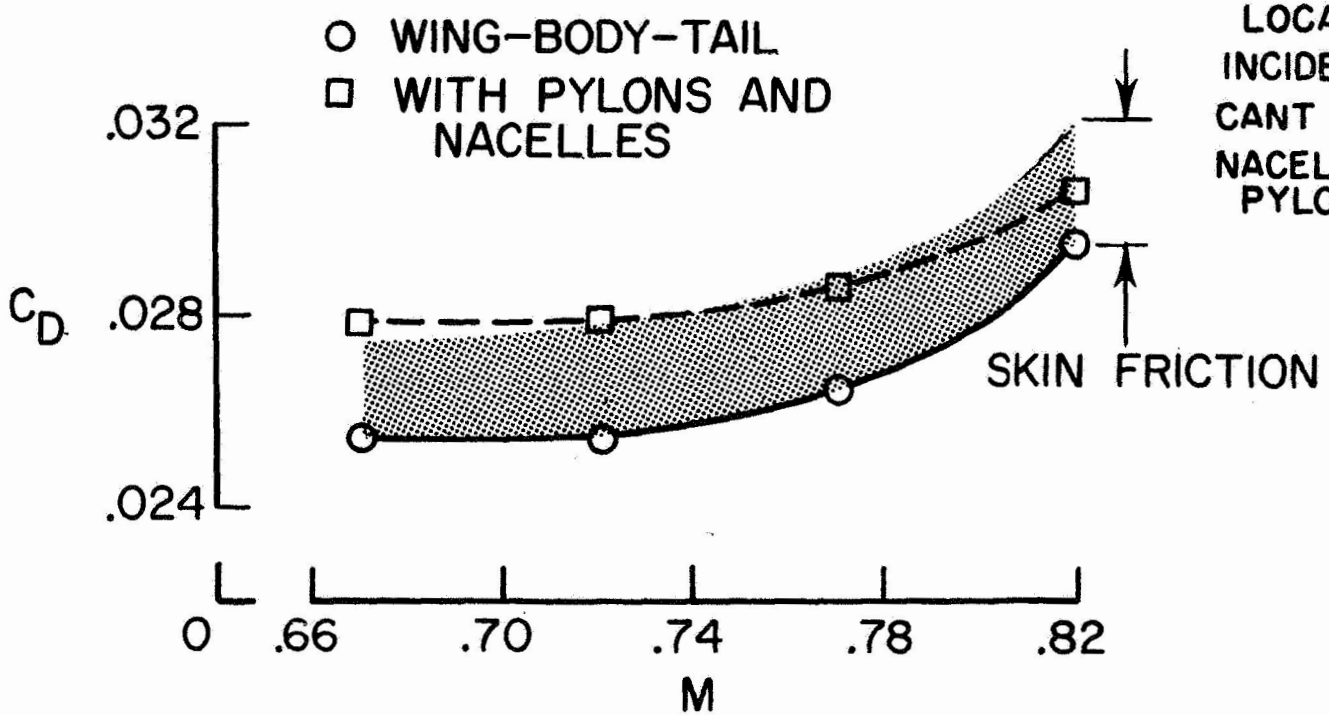

Figure 9. Aft Fuselage-Mounted Nacelle Configuration - $C_L = 0.25$

In-Flight Thrust Reversal

Shown in Figure 10 is a 1/15-scale model of the Gulfstream II mounted in the Langley 16-foot transonic tunnel. The model was modified for powered model testing by splitting the fuselage aft of the wings and measuring forces on the rear end. The objective of this investigation was to increase the drag to make the vehicle suitable for a Shuttle Training Aircraft. This was accomplished by use of both speed brakes and in-flight cascade type thrust reversers. Figure 10 shows flow through nacelles which were faired over for the reverse jet thrust simulation. In-flight thrust reversal was enhanced by both the reverse thrust vector and drag produced by low pressures on the aircraft behind the reverser. As reverse thrust power level increased and speed decreased, the exhaust plume got progressively closer and in some cases enveloped the horizontal tail. This resulted in a decrease in tail contribution to stability and control effectiveness as well as increased trim changes and horizontal tail dynamics. Reverse thrust plume visualization was obtained by injecting water into the exhaust and verified the force data. Exhaust plume impingement can be a problem with conventional aircraft at high angles of attack.

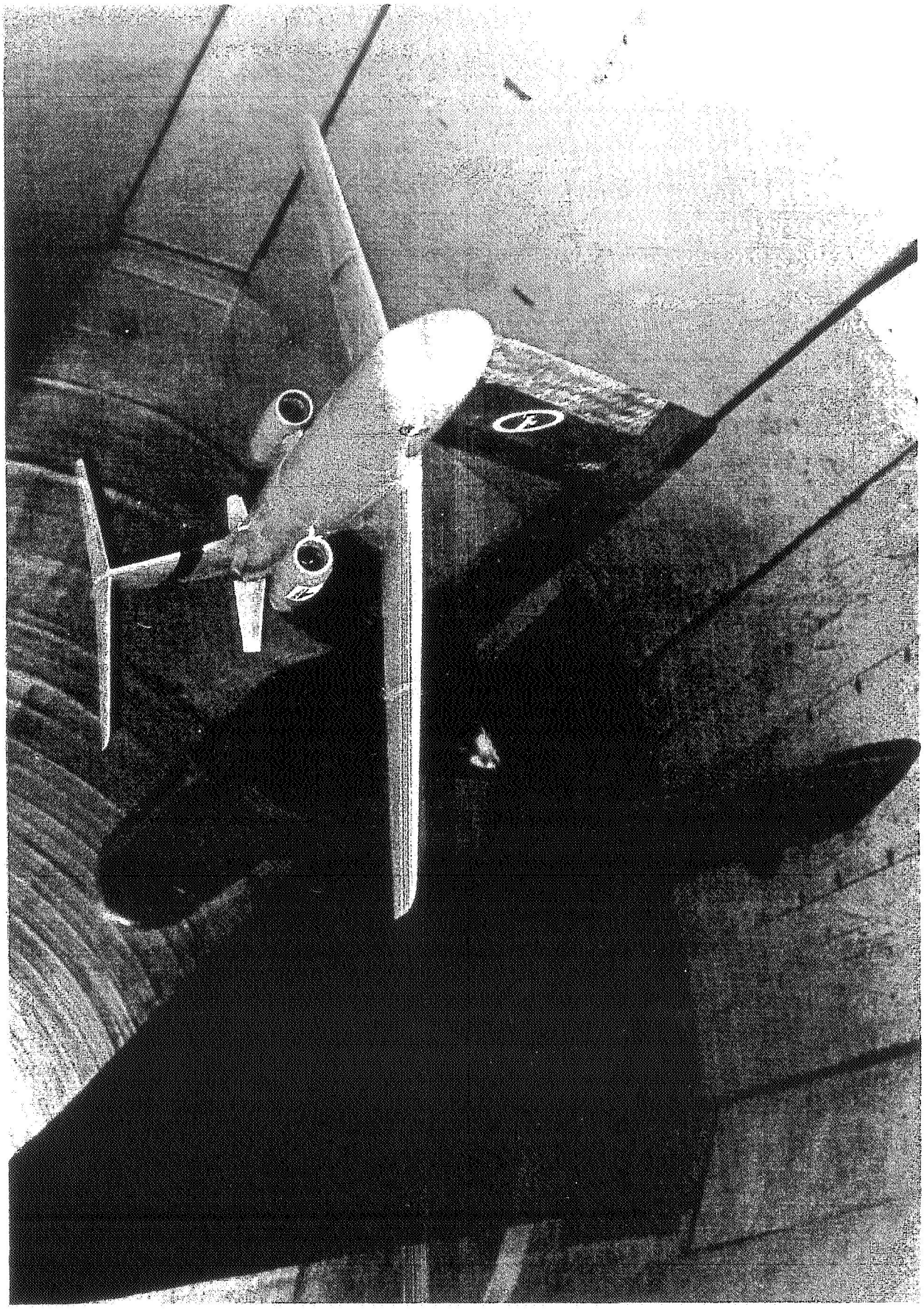

Figure 10. In-Flight Thrust Reversing System

Jet Effects on Aero Characteristics

An example of jet interference effects on complete aircraft aerodynamics is shown in Figure 11. (The testing techniques for complete powered models are usually more difficult because of support system and inlet simulation problems.) This single-engine four-jet V/STOL type aircraft was tested with an injection propulsion system. The exhaust nozzles, two on each side are located close beneath the wing. The data represent the change in aerodynamic coefficients caused by a change from power-off to power-on flight. Results are shown as a function of angle of attack for $M = 0.8$ and horizontal tail deflections of 0° and 5°. In this case, jet effects are not large. Jet operation decreased lift and drag and increased pitching moment. When referred to the absolute values of the coefficients required in flight, these increments represent a reduction in lift and drag respectively, of about 5 and 10 percent. Although the magnitude of pitching moment coefficient increased due to simulated jet operation, only slight changes in model longitudinal stability were found.

I have attempted to illustrate some problems that may be associated with the integration of the power plant into the airframe. The examples illustrated are probably much more severe than those occurring with general aviation aircraft.

NASA has the experimental facilities and is developing the analytical tools which will aid in the reduction of interference drag and provide guides for the best ways to incorporate the power plant into the aircraft.

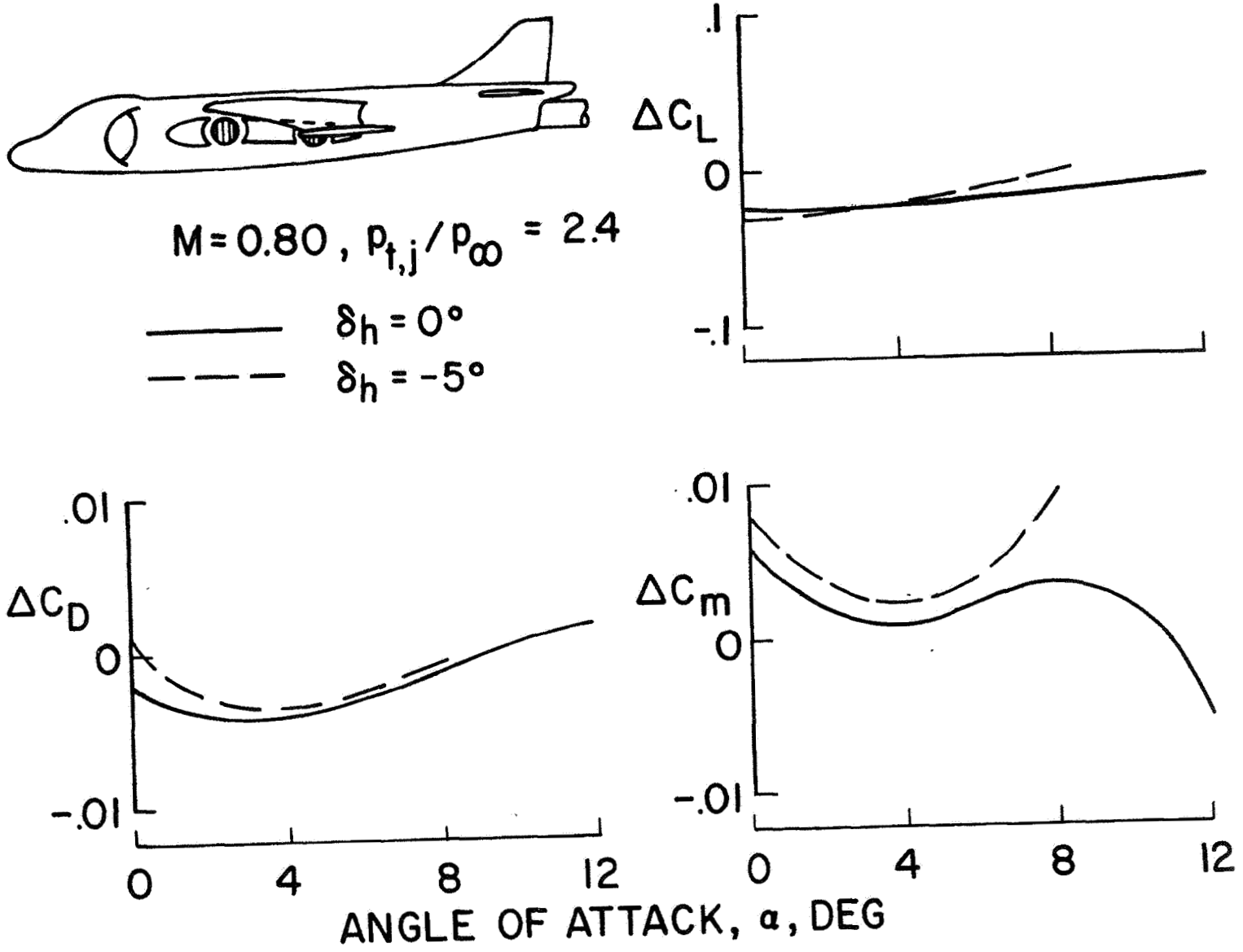

Figure 11. Jet Effects on Aero. Characteristics
(Jet On - Jet Off)

8.4 Propulsion Airframe Integration

D. Mikkelson
NASA Lewis Research Center

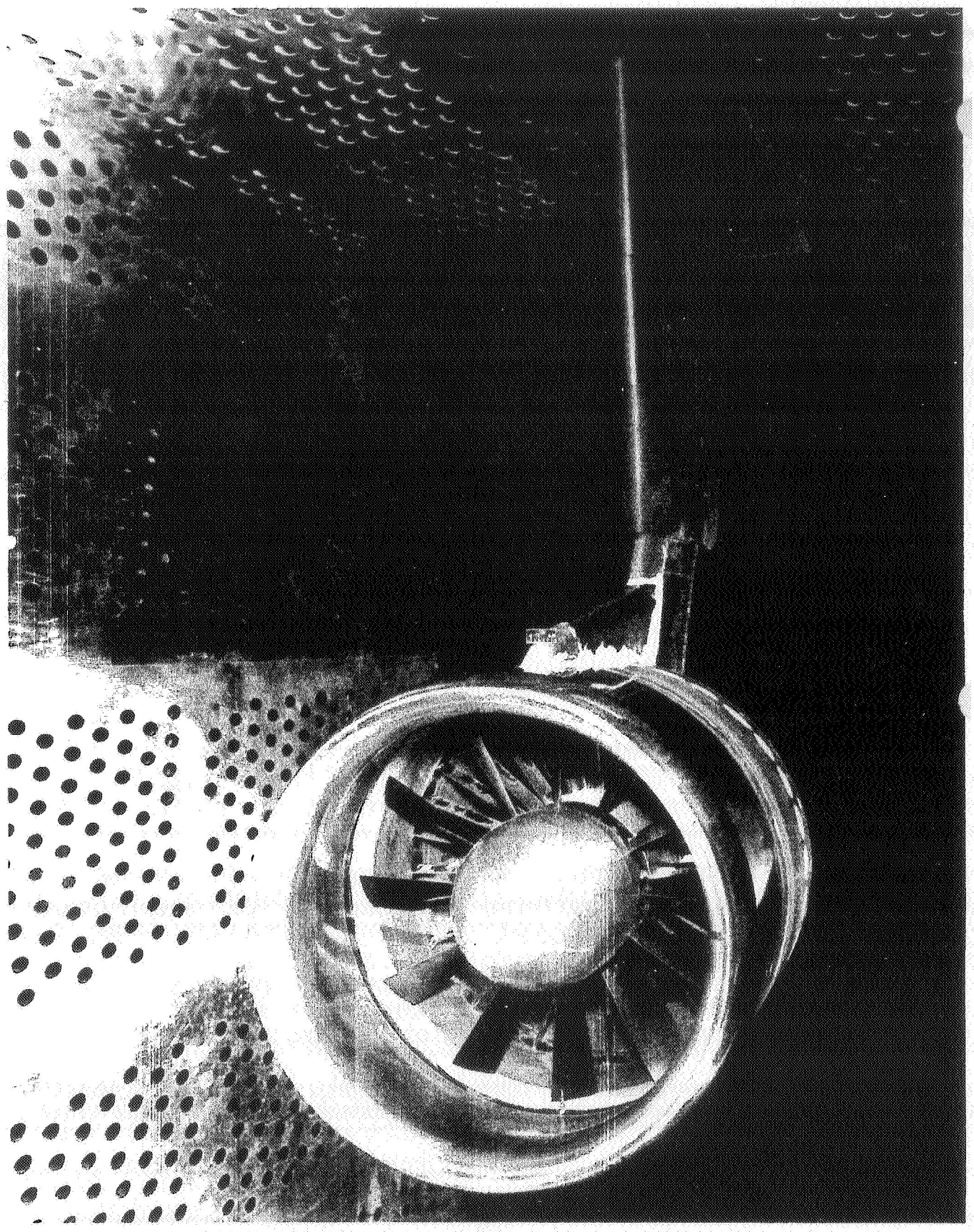

Figure 1. 20" Turbofan Simulator. Proper simulation of the propulsion system can be quite important for both isolated propulsion system work and propulsion/airframe integration work. We found this out in an isolated simulator test using a 20" powered nacelle (shown in this figure). This simulator had a fan pressure ratio of 1.15 and was tested in the Lewis 8-by-6-foot Supersonic Wind Tunnel. (Reference: NASA TMX-3064.)

20" FPR 1.15 NACELLE

$D_m/D_f = 1.08$ $\quad X_i/D_m = .175$

$L_c/D_m = 1.51$ $\quad D_n/D_m = .884$

$D_{h\ell}/D_m = .935$

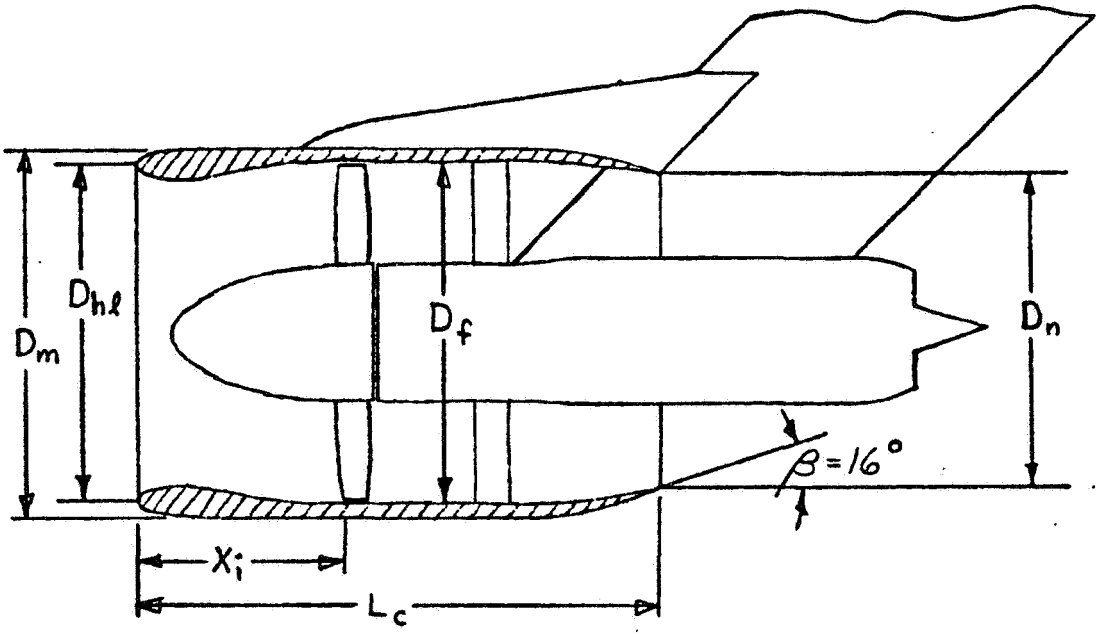

Figure 2. 20" Fan Pressure Ratio 1.15 Nacelle .
Design drag divergence Mach number: 0.8
Tightly cowled: $D_m/D_f = 1.08$
Inlet: $D_{h\ell}/D_m = .935$
Inlet capture mass flow ratio: $A_o/A_{max.})_{des.}$ $_{M=.75} = 0.66$
Inlet cowl length: $X_i/D_m = .175$
Fan Boattail angle: 16°

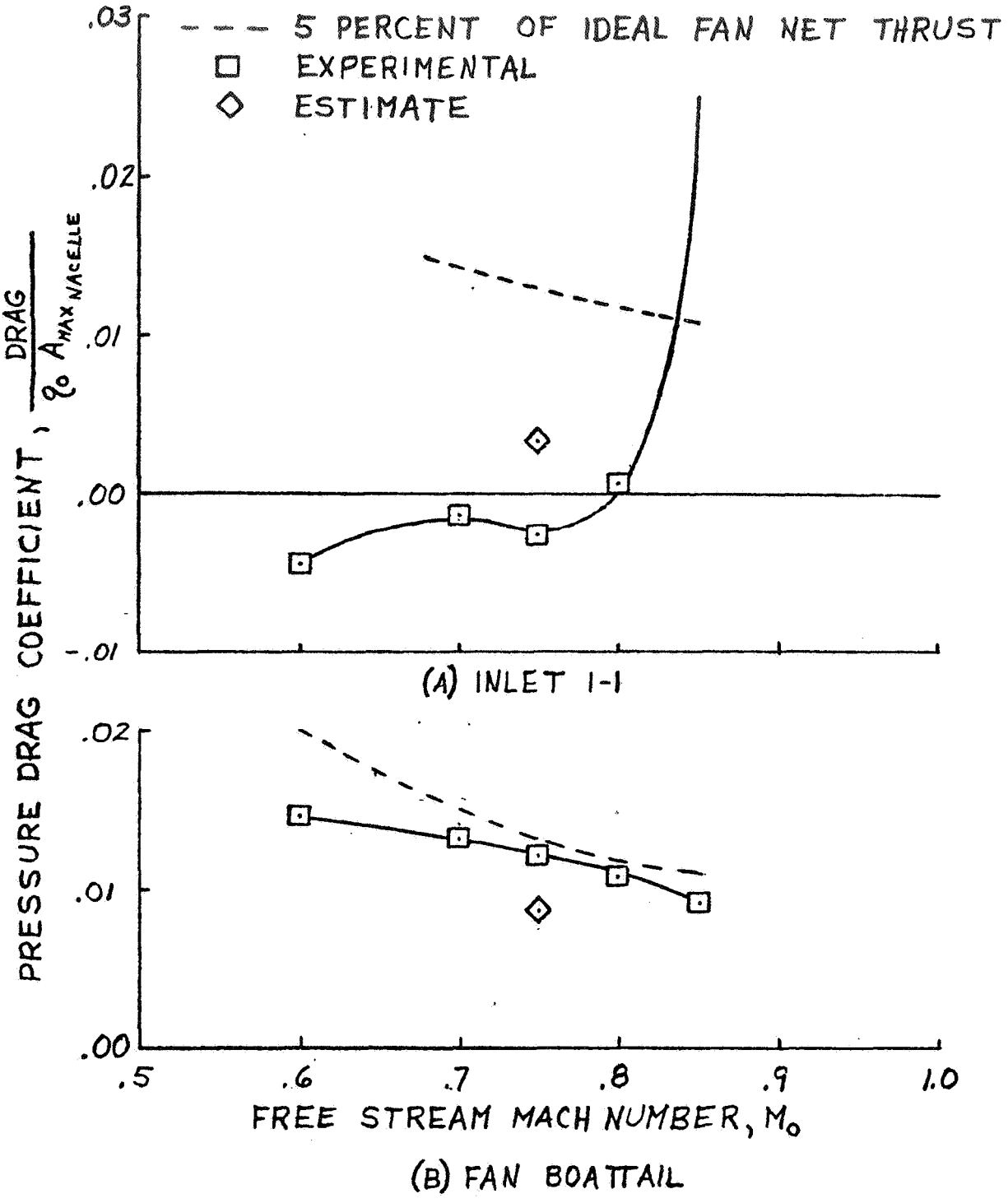

Figure 3. Variation of Inlet and Fan Boattail Pressure Drag with Mach Number

1. Below drag rise the inlet pressure drag was less than the estimated value. However, in the same speed range boattail drag was higher than the value estimated from model boattail tests.
2. In addition, as the inlet went into drag rise (above M=0.8) the boattail drag decreased somewhat.
3. Both of the above trends indicate the possibility of an interaction between the inlet and aft end flow fields for close coupled propulsion systems like this one.

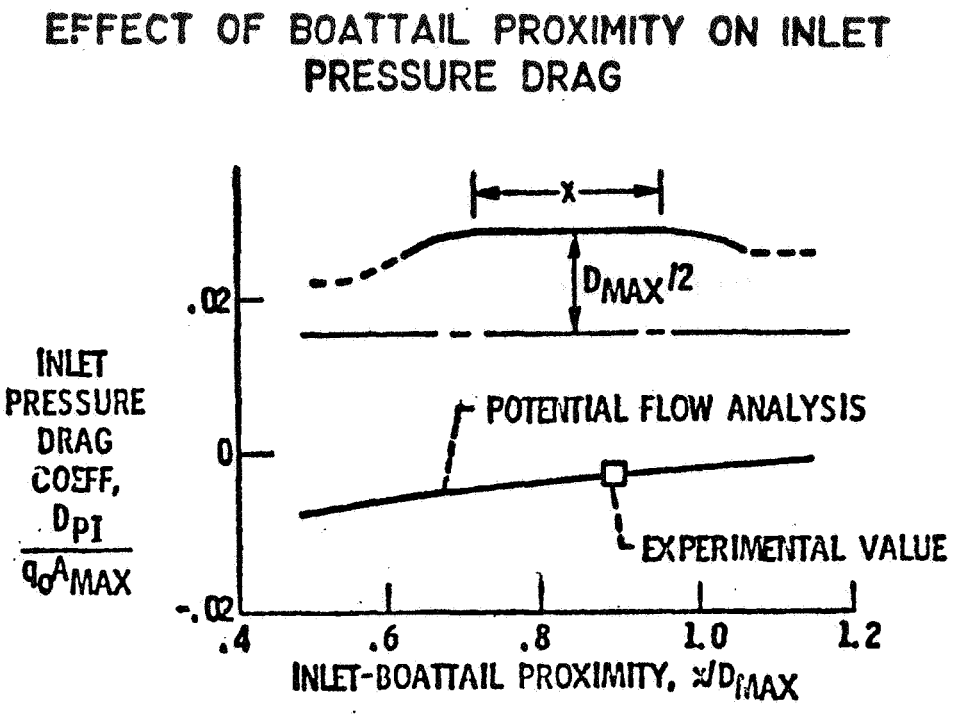

Figure 4. Effect of Boattail Proximity on Inlet Pressure Drag.

To verify the interaction between inlet and exit flow fields, we analyzed the effect of the proximity between the inlet and nozzle on the inlet pressure drag using a 2D potential flow program. This was done by varying the distance between the inlet and boattail. The calculated pressure force was adjusted to pass through the experimental value shown at $X/D_{max} = .9$. As the boattail was moved closer to the inlet (decreasing X/D_{max}), it resulted in a reduction of the inlet drag; thus indicating that there is an interaction between these two flow fields.

In light of this interaction between the inlet and aft end flow fields, it may be quite important to simulate the proper flow fields of both components simultaneously when doing isolated propulsion system and propulsion system/ integration work. Three propulsion simulation techniques that are commonly used are:

1. Flow thru nacelle--which is normally used to properly model the inlet flow field.
2. The blown nacelle --for proper simulation of nozzle flow only (correct NPR).
3. Powered turbofan simulator--close simulation of both inlet and nozzle flow fields.

At NASA Lewis we have a program underway to evaluate and compare these three simulation techniques (both isolated and installed with the airframe) in terms of their degree of simulation and their relative accuracy. This program will be conducted for both conventional and unconventional types of airframe installation.

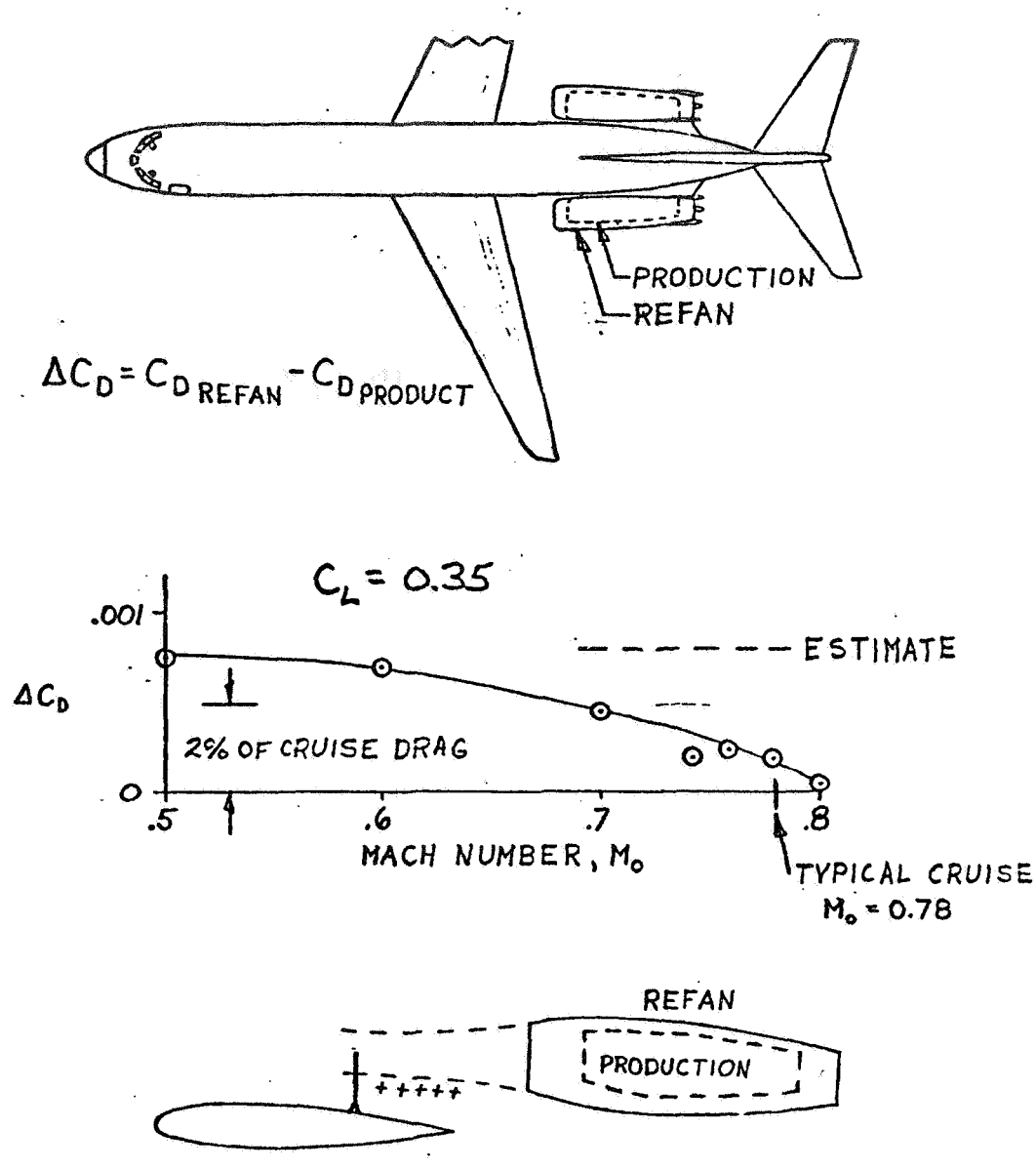

Figure 5. Effect of Nacelle Size on DC-9-30 Cruise Drag.

Flow-thru nacelles are normally adequate when concerned about the interaction between the inlet and wing flow fields like aft fuselage installations. Some of the results from the DC-9 refan program are shown above. Shown is the drag penalty associated with the larger refan nacelle poltted as a function of free-stream Mach number, M_o(at $C_L = 0.35$). An estimate was made of the drag penalty and is shown as a dashed line. Based on these wind tunnel results, the drag increment decreased as M_o was increased.

At the cruise Mach number of 0.78, most of the estimated drag increment was cancelled out due to a favorable interference effect. This favorable effect was associated with the larger refan inlet and its closer proximity to the wing. This effect most likely occurs because the positive pressures on the stream tube suppress the wing upper surface velocities, thereby moving the wing shock forward and reducing the Mach number at the shock with subsequent reduction in wing compressibility drag. This trend was observed from wing pressure data. (Reference: NASA CR-121219.)

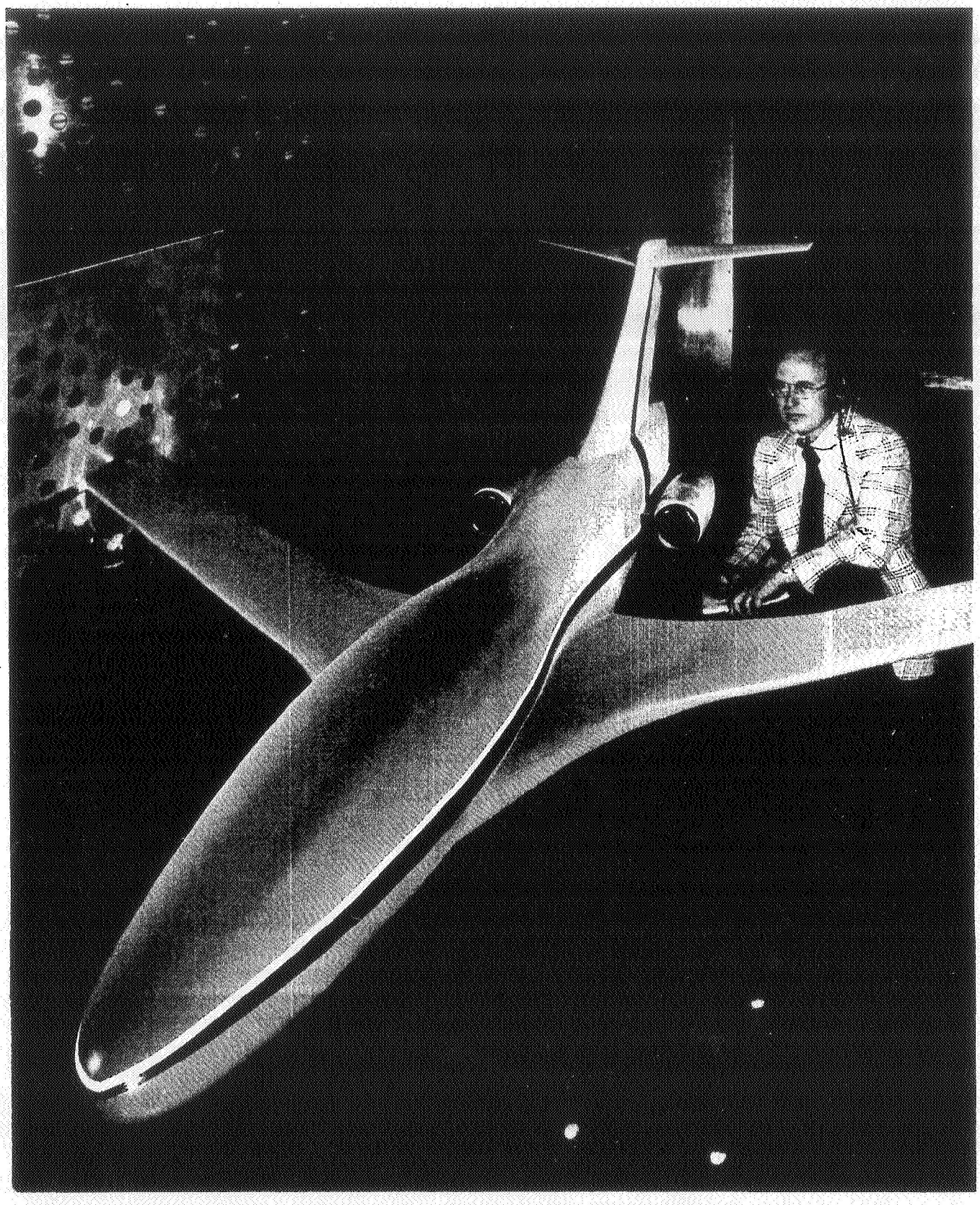

Figure 6. CTOL Full Span Model. At higher Mach numbers it may also be possible to achieve a favorable interference effect. Shown here is a full span CTOL model which was tested in the Lewis 8 x 6 SWT to investigate propulsion system/airframe integration at cruise speeds above M = 0.9 for the same type of aft fuselage nacelle installation. This model was also tested with flow thru nacelles and incorporated local area ruling in the nacelle vicinity. The part of the model aft of the wing trailing edge was on a balance. (Reference: NASA TMX-3178)

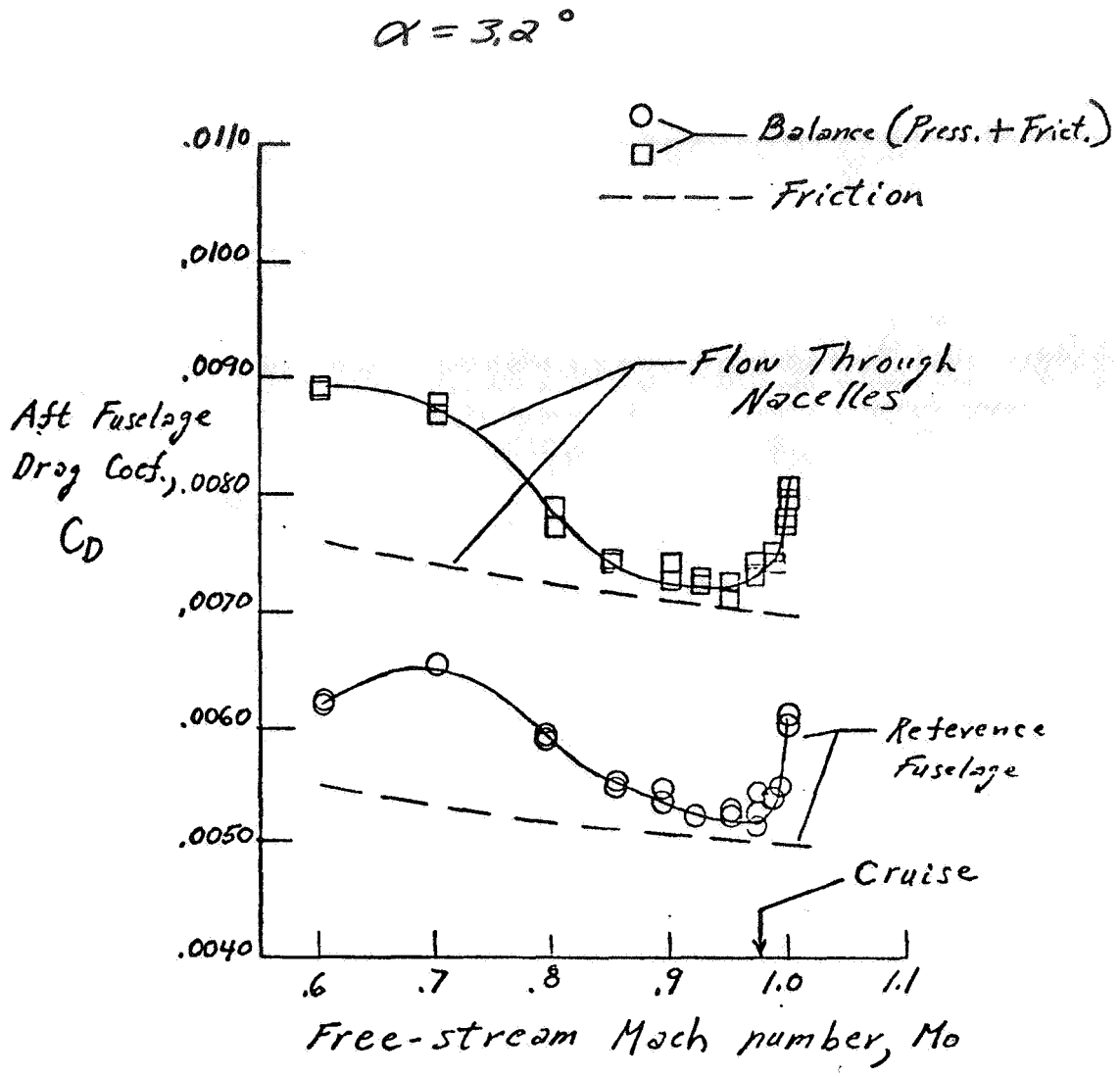

Figure 7. Full Span CTOL Aft Fuselage Drag

Shown above is the total aft fuselage drag with and without nacelles installed. The nacelles had NACA-1 inlet cowl contours and relatively low boattail angles (8 to 10°). The estimated friction drag (flat plate type calculation) is shown as a dashed line. The reference fuselage did not have nacelles; however, it had the same total area distribution as the fuselage with nacelles installed.

For the reference fuselage, the measured drag was quite close to the calculated skin friction level. With the nacelles installed, the incremental increase in the drag at Mach numbers from 0.7 to 0.97 was approximately equal to the increase in skin friction drag associated with the larger wetted area nacelles installed case. This comparison indicates that the pressure drag of the isolated nacelles was essentially cancelled out when the nacelles were installed with the airframe. We found that this favorable effect was quite sensitive to inlet cowl geometry. When a cowl with a more blunt contour than the NACA-1 was tested, a relatively large adverse effect occurred at these speeds.

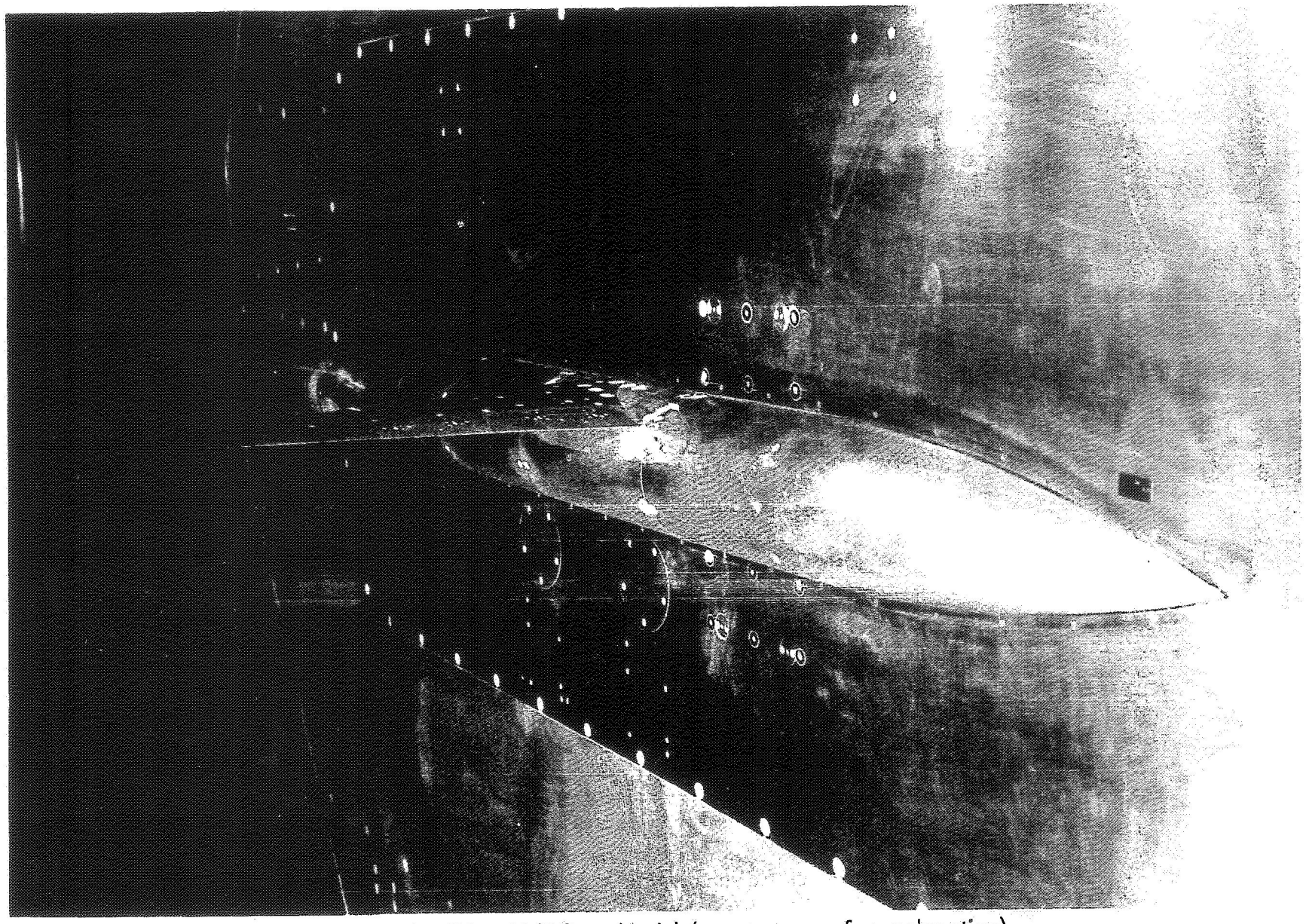

Figure 8. Over-the-Wing Half Span Model (see next page for explanation)

Figure 8. Over-the-Wing Half Span Model

An example of an unconventional propulsion system installation is shown in Figure 8. This model is presently being tested in the Lewis 8 x 6 SWT to investigate integration of over-the-wing (OTW) type of nacelle installation. This test is a joint NASA-Douglas Aircraft test to support the QCSEE engine program. The cruise Mach number for this particular installation is 0.72. Both flow thru and powered simulator nacelles will be tested. Some of the important features of this model are:

1. One and two nacelles with variation in the inboard nacelle spanwise position.
2. Four different nozzle designs.
3. Variations in local wing geometry in the region where the exhaust flow passes over the wing.
4. Supercritical wing.

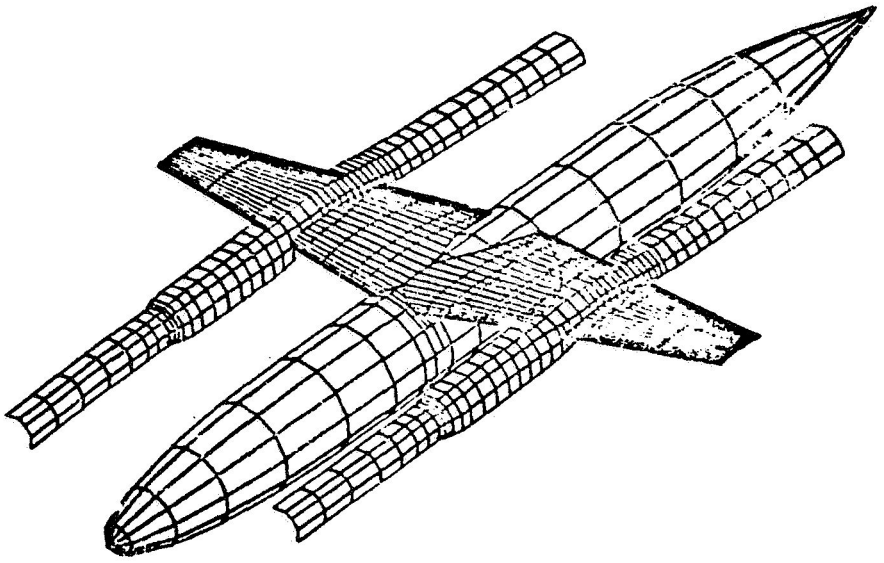

Figure 9. 3-D Newmann Representation of OTW Model

An extensive aerodynamic design effort was done on this model. The main analytical tool used in this design was the 3-D Neumann Lifting Potential flow program. Shown here is a graphical representation of how the model was paneled up for this program.

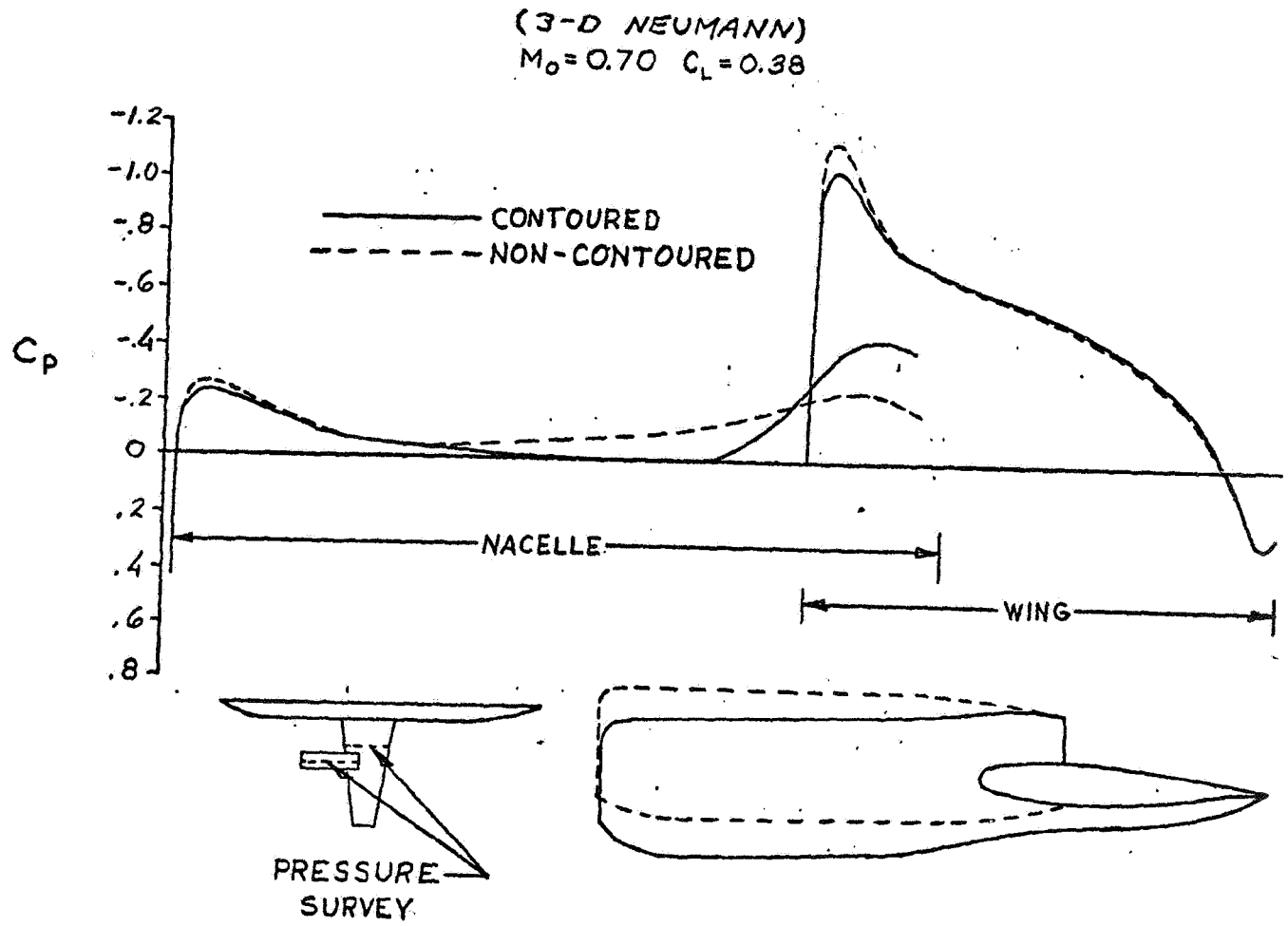

Figure 10. Effect of Nacelle Streamline Contouring on Nacelle and Wing Pressure Distributions

Some of the results from the 3-D Neumann are shown above. Computed pressure distributions on a straight nacelle are compared with those for a nacelle that was contoured to follow the stream sheets that pass over and under the wing at the cruise condition. The streamline contouring resulted in an improvement in the flow quality in the vicinity of the nozzle and wing region. The minimum pressure on the wing was increased (reduced Mach number). The pressures on the nozzle were more closely matched to wing surface pressures.

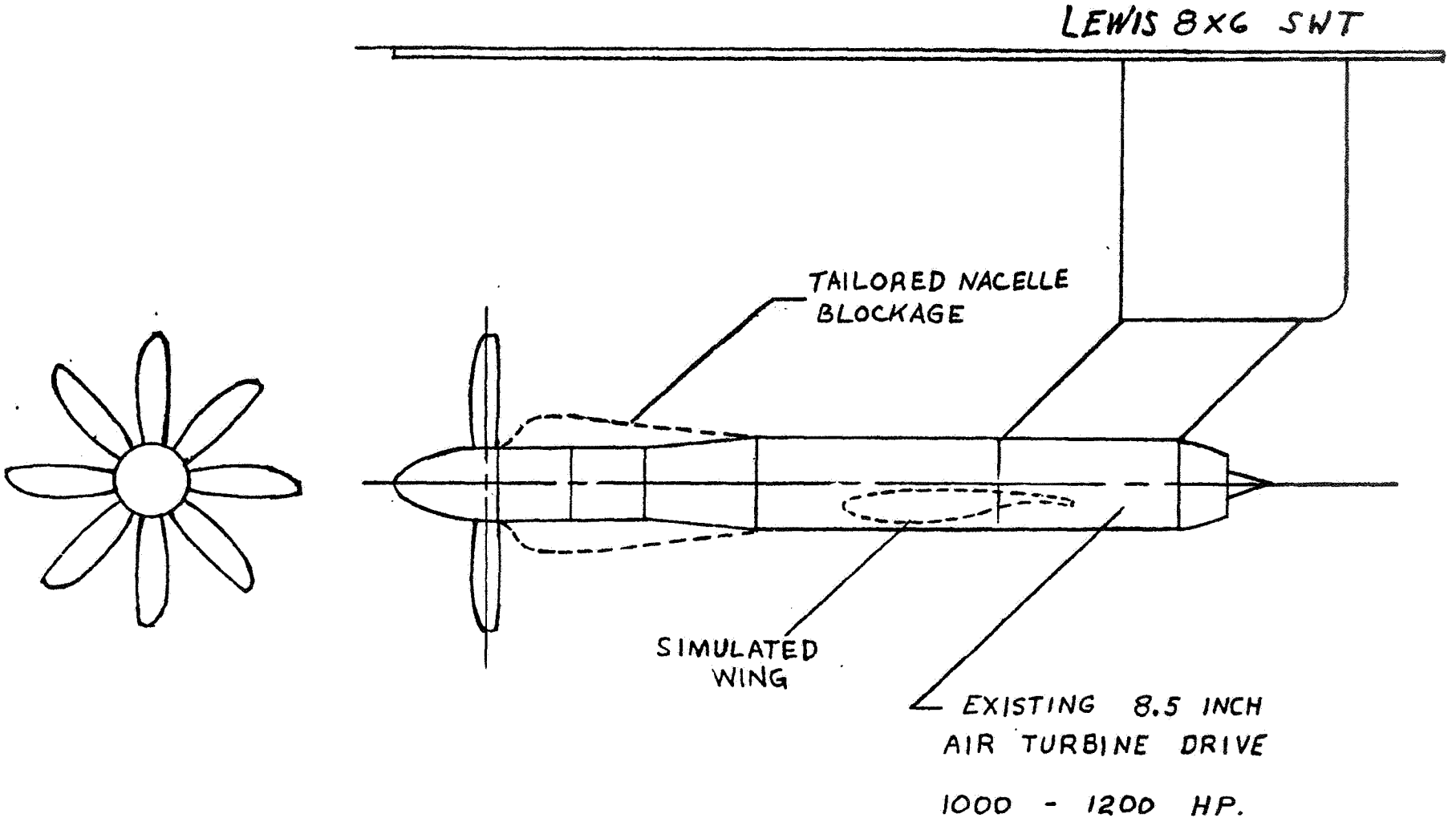

Figure 11. Isolated Turboprop Tests - $M_{cr} = 0.75 - 0.9$ (see explanation next page)

Figure 11. Isolated Turboprop Tests - $M_{cr} = 0.75 - 0.9$

Because of the energy shortage and high fuel prices it is highly desirable to reduce aircraft drag and improve propulsion system efficiency. Two new propulsion system concepts we have come up with at the LeRC are the high speed turboprop and the ducted fan. These concepts show a large potential for reducing energy consumption (10 to 25%) compared to the conventional high BPR turbofan. These potential improvements would be obtained through increased propulsive efficiency.

NASA Lewis has recently initiated a high speed ($M_{cr} = 0.8$) turboprop aerodynamic technology program. The model shown in the figure will be used to do part of this work. An $8\frac{1}{2}$" air drive turbine will be used to drive 30" diameter highly loaded propellers. This turbine is capable of producing over 1000 hp. The propellers will have eight blades and be designed for M = 0.8 cruise at 35,000 feet. They will be tested in the Lewis 8 x 6 SWT. Increased propeller efficiencies may be achieved if tailored nacelle blockage shapes behind the propellers can be designed to suppress the Mach number in the propeller plane (and reduce propeller compressibility losses) without incurring high drag themselves. These blockage shapes will be investigated on this model.

These very high power loading propellers ($SHP/D^2_{prop} = 70$ at take off) have significant swirl thrust losses (6 to 8%) at cruise. It may be possible to recover part of these losses using a second counter rotating propeller, fixed stators, or even the wing. These areas will also be investigated in this program. A simulated wing is shown mounted on the model. The integration of the high speed turboprop with the airframe will be further investigated on a small half-span aircraft model.

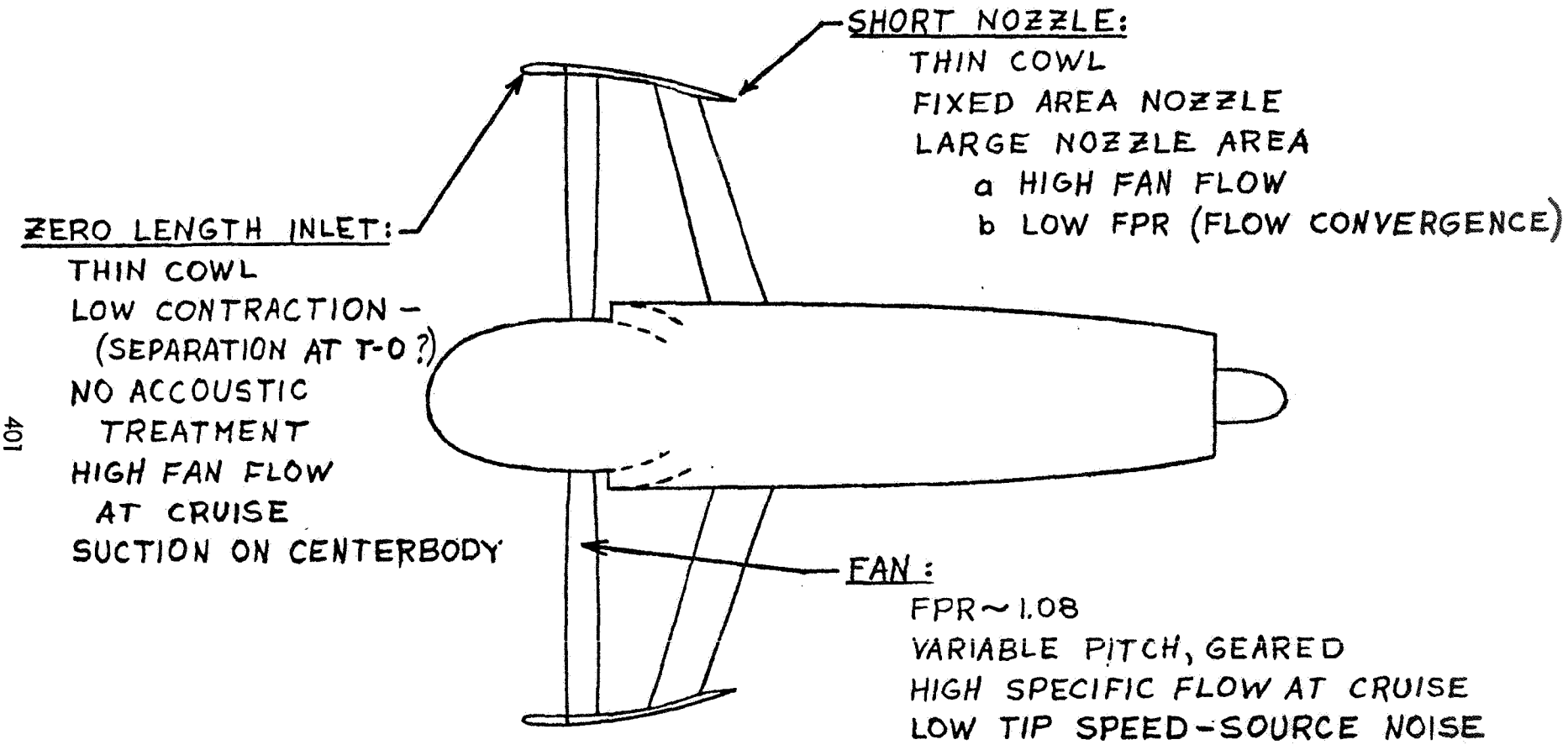

Figure 12. Ducted Fan (see explanation next page)

Figure 12. Ducted Fan

The unconventional ducted fan concept shown in Figure 12 may offer some advantages compared to the high speed turboprop. Some of these advantages are: smaller fan diameter, and reduction in swirl and tip losses. In order to make this concept viable, it must have a minimum size fan cowling as shown. Conventional size cowlings (relative to fan diameter) that are utilized with existing high BPR engines would have very high cruise drags. This drag would cancel any thrust improvement obtained by going to this very high bypass ratio concept. A short cowl requires a fixed area nozzle and a thin inlet. The fixed nozzle with a large exit area results in a high fan flow at cruise where ram effects increase the nozzle pressure ratio, and low fan flow at takeoff where there is little ram recovery. This wide weight flow range requires a variable pitch fan. Also, the thin cowl requires small flow spillage and therefore high fan flow to avoid drag problems at cruise. In addition to the high cruise flow, the low fan pressure ratio (FPR~1.08) would minimize the amount of internal flow convergence at the nozzle exit and would result in a large exit stream tube size and short boattail length. At takeoff, the low fan flow dictated by the fixed nozzle minimize the sharp lip inlet losses, but some separated flow would occur during static operation.

Another concern that would have to be evaluated is the aeroelastic stability of the fan blades and cowling during operation with separated flow. This separated region would diminish as forward speed increased. No appreciable amount of acoustic treatment can be utilized with this fan cowling due to its small size. Therefore, a relatively low tip speed fan with low inherent noise would have to be incorporated. This concept is currently being analyzed for NASA by Pratt and Whitney and General Electric under two study contracts (NAS3-19121 and NAS3-19201).

8.5 Determination of the Level Flight Performance of Propeller-Driven Aircraft

E. J. Cross
Mississippi State University

A flight test method to determine the level flight performance of propeller-driven aircraft is currently being investigated at Mississippi State University. By measuring the amount of power it takes to overcome a known increment of added drag to maintain steady state flight conditions, it may be possible to determine the overall drag and the propeller efficiency of a general aviation-type aircraft.

Propeller efficiency, η_p, is defined as the ratio of thrust horsepower to brake horsepower, or

$$\eta_p = \frac{TV}{550BHP} \tag{1}$$

Equating thrust to drag by the thrust inclination angle γ gives

$$\eta_p^* = \frac{DV}{550BHP} \tag{2}$$

where $\eta_p^* = \eta_p \cos\gamma$.

If an increment of drag ΔD is added and power is increased such that the airspeed remains constant, then

$$\eta_p^* + \Delta\eta_p^* = \frac{(D + \Delta D)V}{550(BHP + \Delta BHP)} \tag{3}$$

Using a propulsive efficiency factor

$$E_p = \frac{\eta_p^* + \Delta\eta_p^*}{\eta_p^*} = 1 + \frac{\Delta\eta_p^*}{\eta_p^*} \tag{4}$$

and eliminating drag gives

$$\eta_p^* = \frac{\Delta DV}{550[(BHP + \Delta BHP)E_p - BHP]} \tag{5}$$

Expressing BHP as the product of torque, Q, and propeller rpm, n, and substituting for η_p^* in (2) gives the basic incremental drag equation

$$D = \frac{\Delta D}{(1 + \frac{\Delta Q}{Q})E_p - 1} \tag{6}$$

If there is little or no change in propeller efficiency, $E_p \approx 1$ and

$$D = Q \frac{\Delta D}{\Delta Q} \tag{7}$$

Thus we have expressed the total drag of the aircraft as a function of three easily measured parameters. A standard propeller torquemeter will be used to measured Q and ΔQ, while a load cell attached to a drag chute will measure ΔD. By also measuring γ, the propeller efficiency η_p can be computed directly from (2).

Equations (6) and (7), however, neglect changes in induced drag and profile drag. It is expected that the profile drag will remain constant, but it may be necessary to consider ΔD_i, the change in lift-dependent drag. By using a parabolic polar for the aircraft and including an amount of lift ΔL, it is possible to express the drag as

$$D = \frac{2a_0 \Delta\alpha W + \pi\ AR\ e\ \Delta D_D}{\pi\ AR\ e\ [(1+ \frac{\Delta Q}{Q})E_p - 1]} \tag{8}$$

where a_0 is the slope of the lift curve, $\Delta\alpha$ is the change in angle of attack, W is the aircraft weight and ΔD_D is the incremental drag of the parachute. Further, e is the Oswald efficiency factor and AR is the aspect ratio.

Note that this equation requires measurement of flight test variables and aircraft parameters that are not included in the simpler forms. If the added drag is small, it is expected that equations (6) and (7) will be sufficient. However, the final form of the drag equation which will be most suitable remains to be determined.

The incremental drag method of determining aircraft performance appears to offer an excellent alternative to current flight test practice. The aircraft lift, drag and thrust values and propulsive efficiency are readily determined from a simple flight test procedure. It seems reasonable to expect that sophisticated data acquisition and processing systems will be unnecessary since the flight test is conducted under steady state conditions. The current practice of determining aircraft drag by the gliding flight method is tedious and provides no information concerning

propulsive system performance. The incremental drag method appears to provide the potential for significantly greater flexibility and utility at reduced cost and complexity with increased safety.

9. ADDITIONAL PAPERS RECEIVED AFTER THE CONFERENCE

9.1 Possible Applications of Soaring Technology to Drag Reduction in Powered General Aviation Aircraft
J. H. McMasters and G. M. Palmer, Purdue University

9.2 Minimum Vertical Tail Drag
E. E. Larrabee, Massachusetts Institute of Technology

Preceding Page Blank

9.1 Possible Applications Of Soaring Technology To Drag Reduction In Powered General Aviation Aircraft

John H. McMasters
and
George M. Palmer
Purdue University

Introduction

The term "General Aviation" usually brings to mind the range of powered aircraft encompassing the Piper Cub through executive jet transport aircraft. Depending on one's definitions and biases, however, a case can be made for inclusion of other types of aerodynamically supported vehicles such as the sailplane and their powered derivatives (self-launched sailplanes or motor gliders) and perhaps even the lowly hang glider. While participation in soaring in this country is rather limited and the economic impact of sailplane manufacture is miniscule, the current level of technology in this branch of light aviation is extraordinary - particularly in the areas of aerodynamic efficiency and utilization of advanced materials and fabrication techniques. The purpose of this brief discussion is to outline the present state-of-the-art in soaring performance and review some of the techniques (particularly in the area of drag reduction) used to achieve this performance. It can legitimately be objected that the performance requirements of sailplanes and light powered aircraft are quite different and that sailplane manufactures are not bound by the same economic constraints as their counter parts in powered flight. However, to ignore the aerodynamic lessons learned in sailplane development would be, in our view, a serious oversight. In view of the fact that sailplane technical literature is infrequently consulted by many aeronautical engineers, particularly those at universities, this brief review is considered appropriate.

State-of-the-Art

Most modern soaring aircraft are pure sporting devices, the most elegant and advanced of which are optimized for competition - which today implies racing. The classic design problem is one of optimizing an aircraft for two design points: (1) low speed (minimum sink rate) flight in a rectilinear or banked turning attitude to maximize rate of climb and (2) minimum glide angle (or maximum lift-drag ratio) in high speed rectilinear cruise. In racing performance, however, absolute maximum L/D

is less important than maintaining a "low" sink rate (e.g. 2m/sec) at the highest possible speed.*

At present two major types of competition sailplanes are in wide spread use: Standard Class, with spans limited to 15m (49.2 ft) with water balast (to increase wing loading in strong lift conditions) and only simple hinged flaps not connected to the ailerons permitted, and Open Class where anything is permitted. Under pressure mainly from European designers, the Standard Class will be divided into two classes for international competition after 1976, with one branch becoming an "unlimited" class keeping only the 15m span limit and the other basically retaining the present Standard Class rules.

The other category of soaring device of interest in this discussion, the "motor glider", is slowly becoming more popular in Europe and the United States. It is basically a moderate performance sailplane fitted with an engine providing it with a self-launch and out-landing retrieval capability.

Some typical modern sailplanes and motor gliders are shown in Figure 1. Performance and geometric data for several typical types are listed in Table 1. Performance capabilities are further clarified in Figure 2. Also shown for comparison in Figure 2 are glide polars for several other types of low speed flying device from (1). There are few standard handbook type references available on sailplanes and soaring technology. Probably the best sources of information are Soaring magazine, Technical Soaring (12) and the publications of the Organization Scientifique et Technique Internationale du Vol-a-Voile (OSTIV) available from the Soaring Society of America (SSA). Important recent material is available in (5.6).

The basic configuration of the high performance sailplane was well established prior to WWII. Performance increases since that time have been very large, however, due mainly to three factors:

1. A greater appreciation of the importance of the quality of the aerodynamic surfaces and the necessity of sealing gaps and flow leakage in reducing drag.

2. Advanced airfoil designs with greatly improved (compared with Göttingen and NACA 4 and 5 digit airfoils) characteristic in the Reynolds number range characteristic of sailplane operation.

* The ideal sailplane glide polar would be as "flat" as possible over the widest possible speed range. Sailplanes, as in the case of most other aircraft types, seldom "cruise" at the speed for L/D_{max}.

3. The introduction of fiberglass construction.

These factors will be discussed in more detail later. Some comparison, based on data from Table 1, for typical sailplanes of good pre-war technical vintage and modern technology are presented in Table 2.

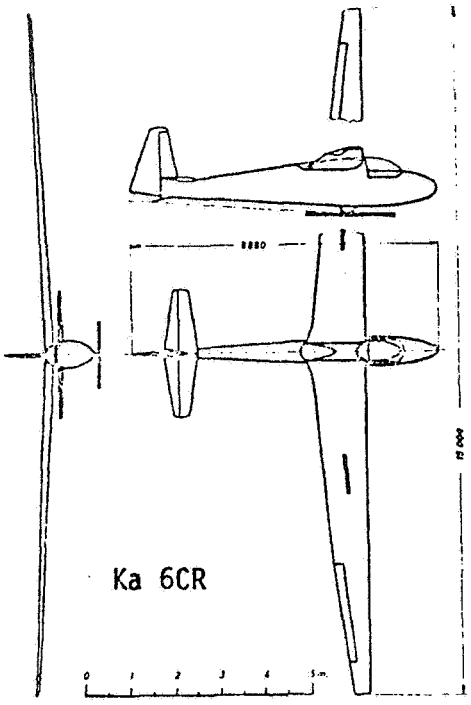

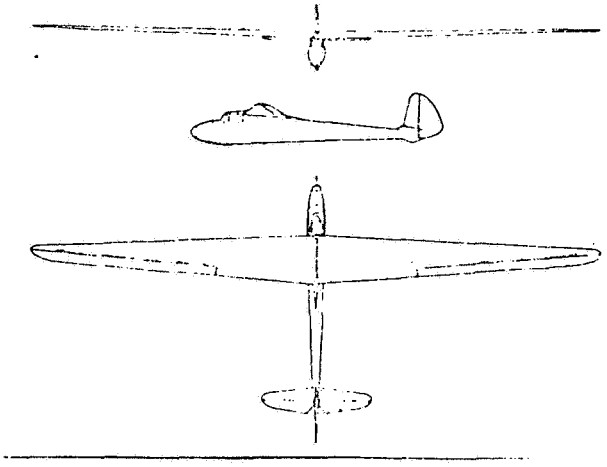

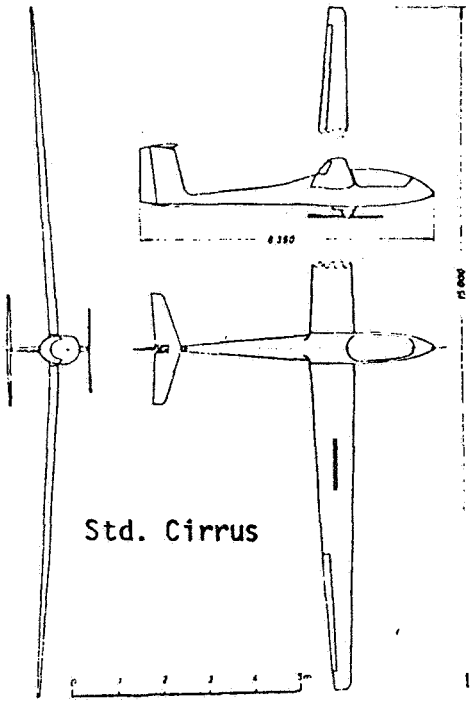

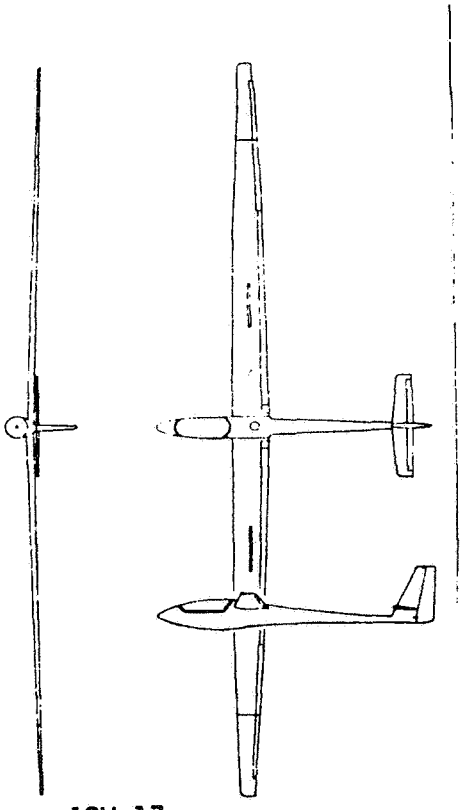

Figure 1. Sailplanes and Motor Gliders

GLASFLUGEL KESTREL

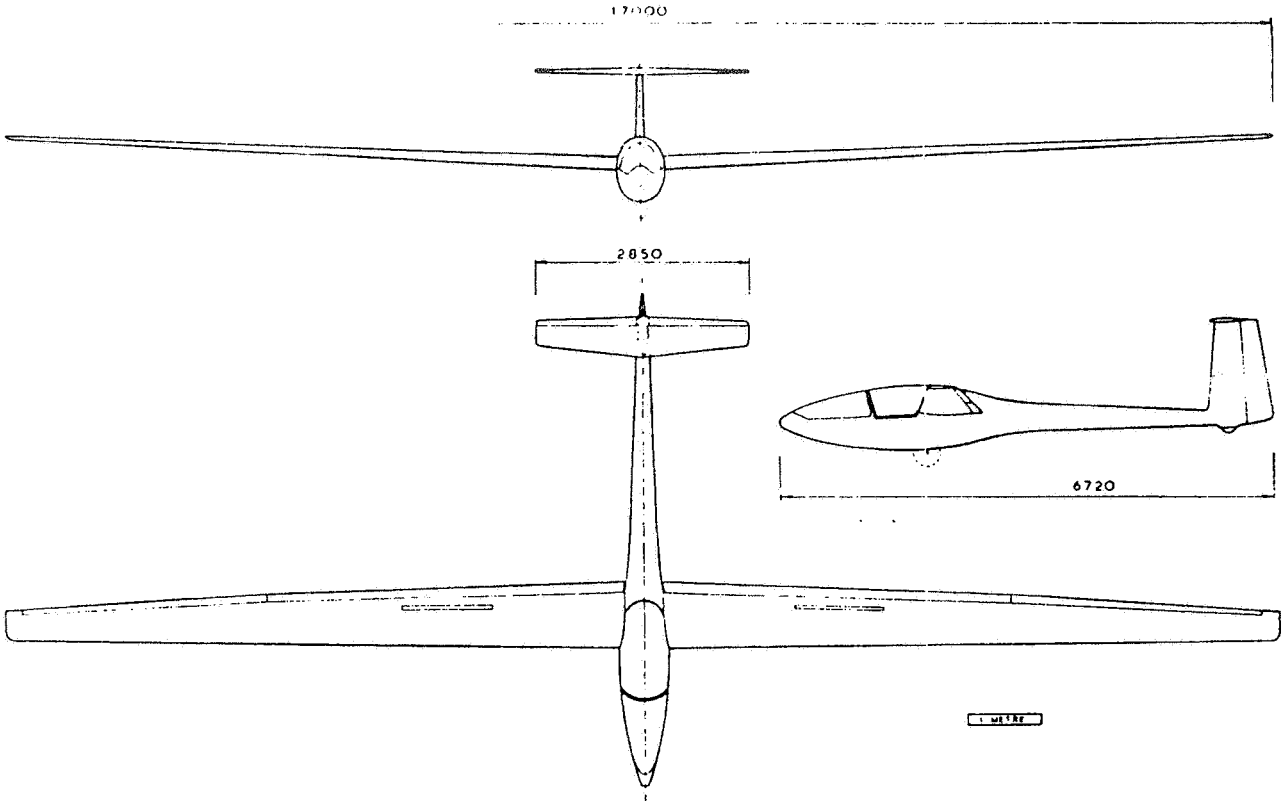

SIGMA.

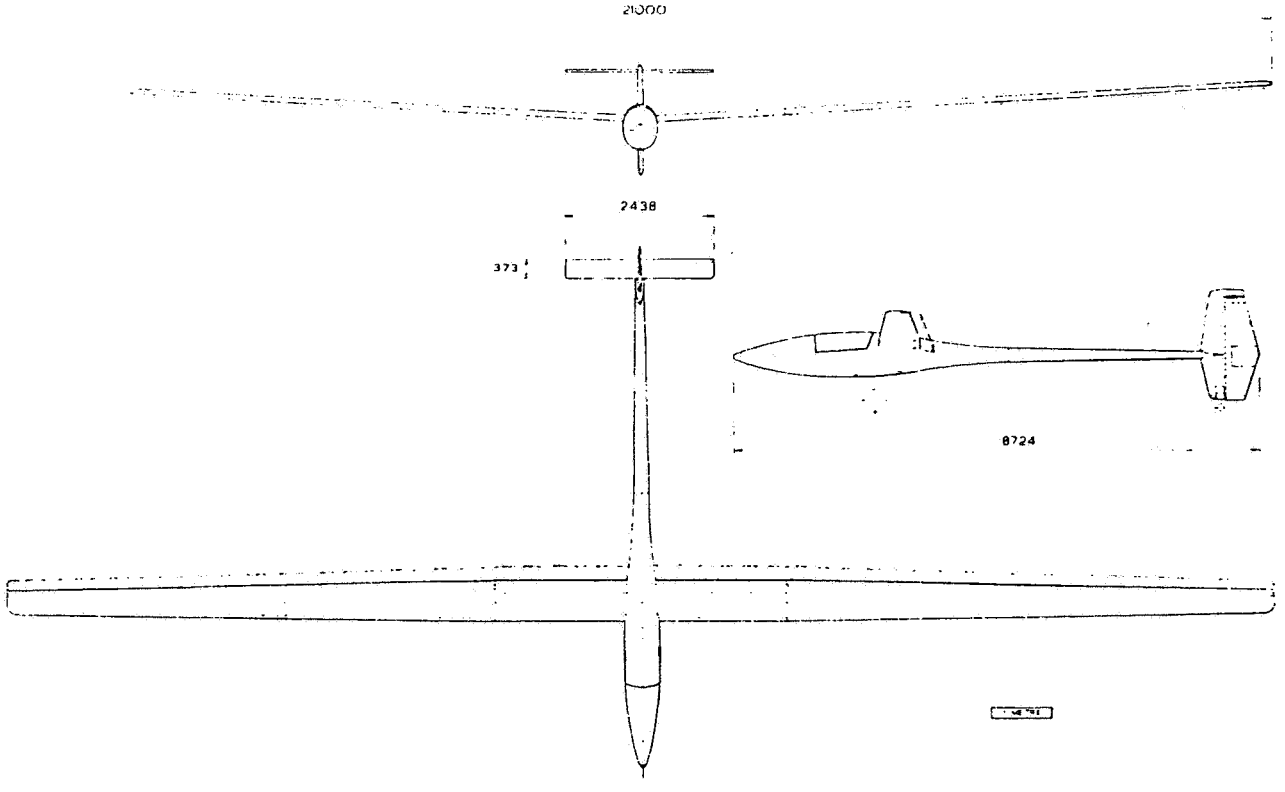

Figure 1. (continued) Sailplanes and Motor Gliders

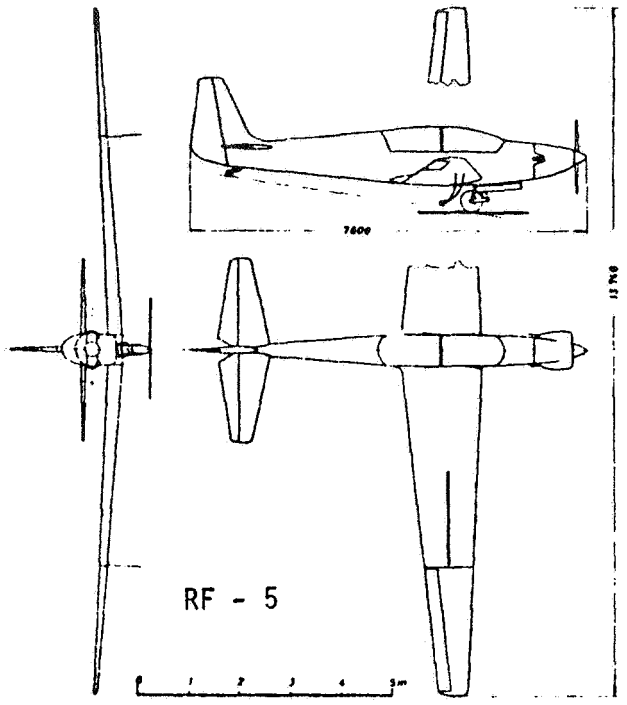

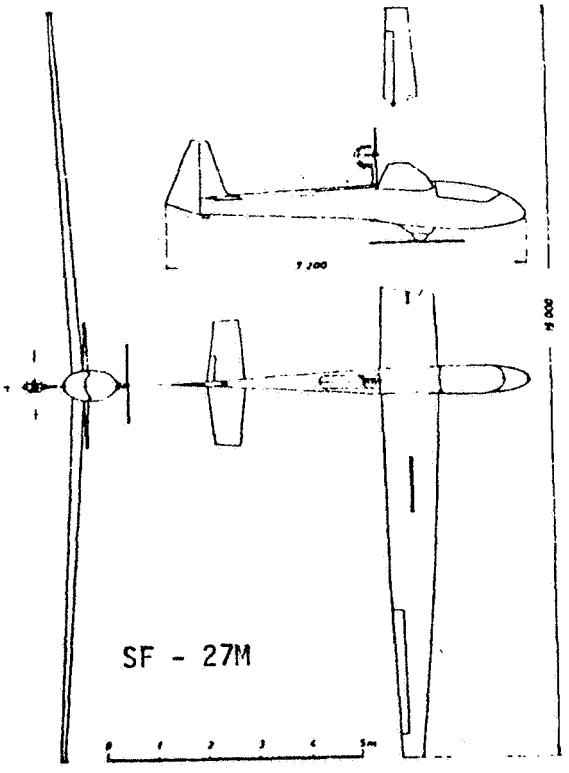

Figure 1. (continued) Sailplanes and Motor Gliders

Table 1. Sailplane & Motor Glider Characteristics

Type	First Flt.	Wing Span (ft)	Wing Area (ft^2)	Aspect Ratio	Weights (lb) Empty	Weights (lb) Loaded	Wing Load (lb/ft^2)	Airfoil	$\dot{Z}$ (fpm) at (V - kt)	L/D_{max} at (V - kt)	y (kt) at Z = 2 m/s	Power (BHP)	Ref.
Schleicher													
Ka 6 CR	1955	49.2	134	18.1	408	610	4.55	NACA63-618	134 (36)	29 (42)	70		3
ASW 12	1964	60	140	26	680	909	6.5	FX62-K-131	109 (43)	43.3 (48)	91		2
ASW 17	1972	65.6	159.7	27	893	1257	6.7 - 7.9	FX62-K-131$_{mod.}$	97	48 (54)			4
Schempp-Hirth													
Std. Cirrus	1969	49.2	107.5	22.5	466	734	6.82	FX66-S-196	134 (42.5)	35.2 (51)	85.5		2
Nimbus 2	1971	66.6	154.9	28.6	760	954	6.16	FX67-K-150	102 (43)	46 (51)	92		3
Glassflügel													
Libelle H-201	1964	49.2	102.3	23.6	397	633	6.18	Hütter	134 (43)	34.5 (50)	82.5		2
Kestrel H-401	1968	55.7	123.7	25.1	638	803	6.5	FX 67-K-170	124 (45)	38 (52)	92		2
Laister													
Nugget	1973	49.2	109	22.2	425	900	5.7 - 8.25	FX67-K-170	128 (42.5)	36 (50.5)	~88		4
Sigma	1973	68.9	131.2 (177.2)	36.2 (26.8)	1000	1300	9.9 (7.33)	FX67-VC-170/136	108 (37.5)	~50 (55.5)			
Jacobs "Weihe"	1938	59.1	198	17.6	508	738	3.7	Gö 549	120 (35)	31.5 (41)	~60		4
Schweizer 1-26	1954	40	160	10	433	593	3.7	NACA 43012A	165 (32.5)	21.5 (42)	64		2
Fornier RF-5	1968	45.0	162	12.5	1035	1430	8.85	NACA 23015	300 (51.5)	18 (57)	67.5	68	
Scheibe SF27M	1968	49.2	130	18.6	617	815	6.25	FX 61-184	152 (45)	31 (51.5)	82.5	26	
Schleicher ASK-14	1967	46.8	137.6	16.2	507	793	5.85	NACA 63-618	148 (39)	28 (45)		26	

C/H

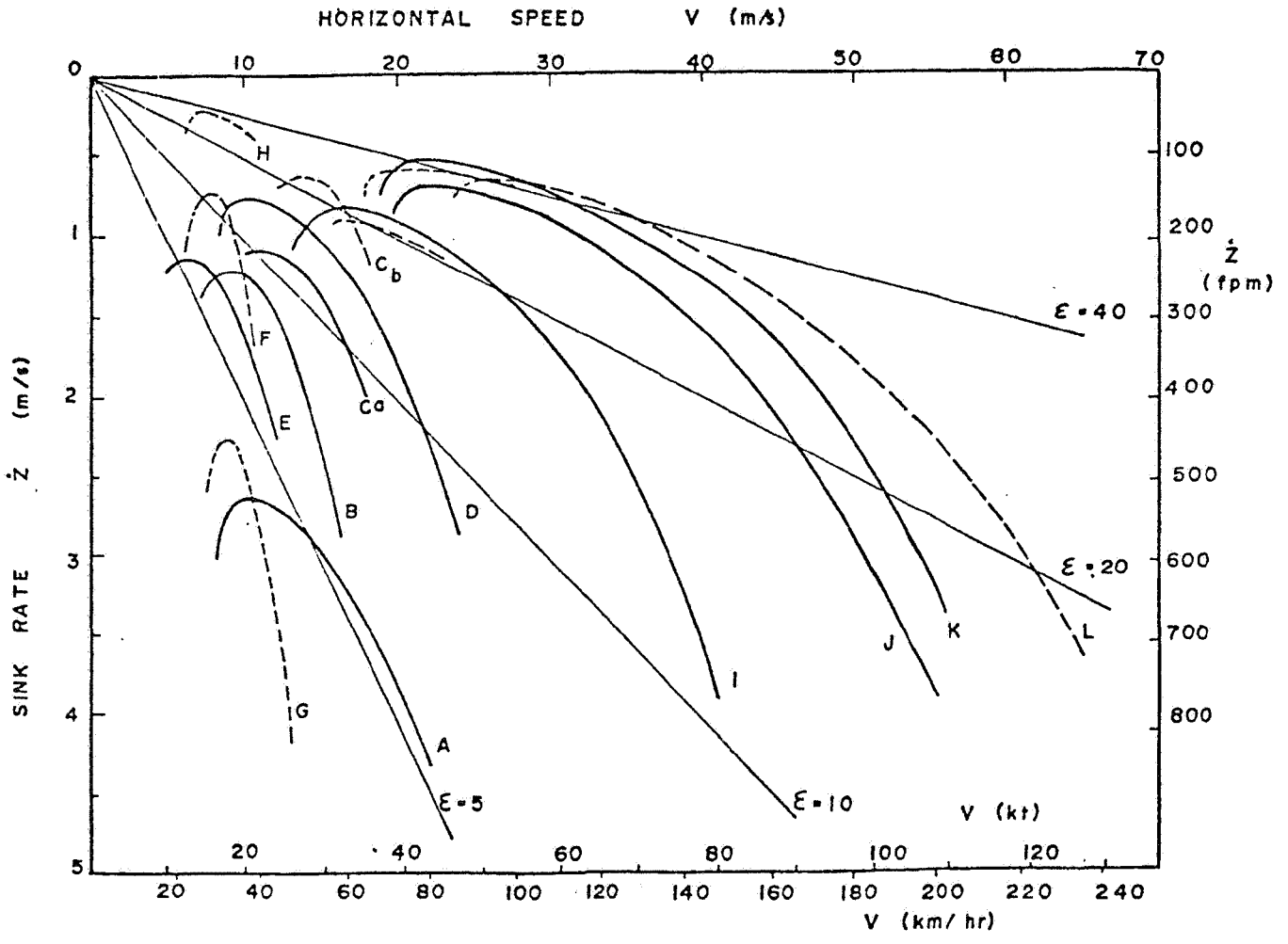

A. PIGEON (5)
B. FULMAR (6)
C. BLACK VULTURE (7)
(a. Parrot, b. Raspet)
D. WHITE-BACKED VULT. (8)
E. DOG-FACED BAT (11)
F. PTERANODON (12 b)
G. ROGALLO HANG GLD. (14)
H. PUFFIN II MPA (18)
(outside grd. effect)
I. I-26 SAILPLANE (22)
J. STD. CIRRUS (23)
K. ASW-12 SAILPLANE (24)
L. VVG SAILPLANE (25)

Numbers in ( ) refer to entries in Table I, Ref. 1

Dashed curves are estimated.

$\varepsilon = L/D$,

Figure 2. Still Air Sea Level Glide Polars For Several Natural And Man-Made Flying Devices

COMPARISON OF FLIGHT TEST RESULTS WITH THEORY

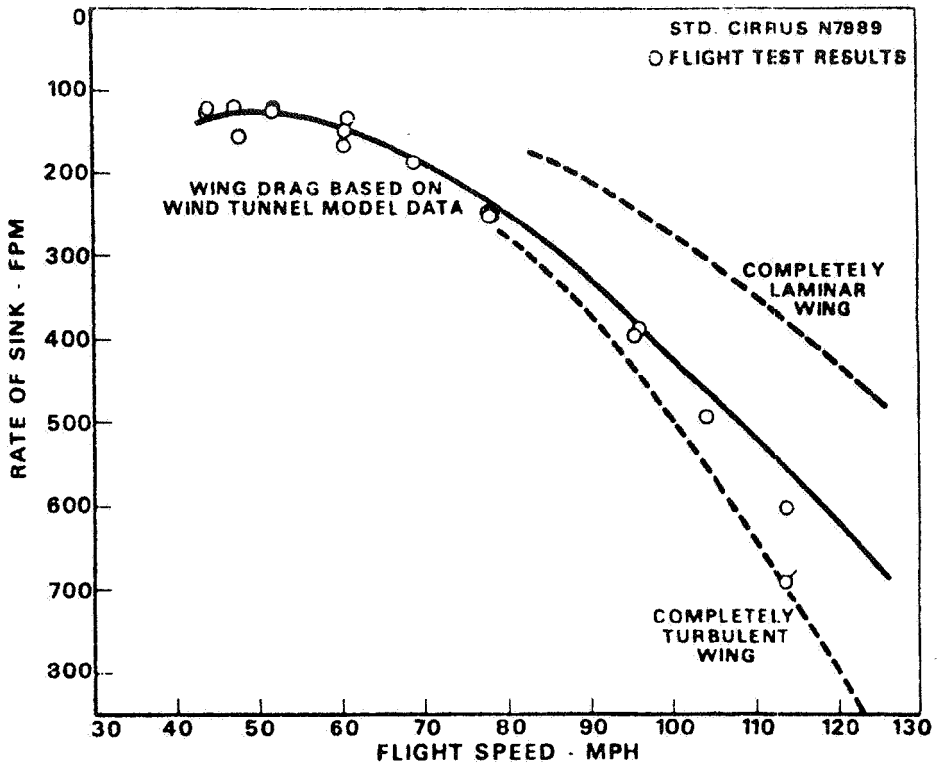

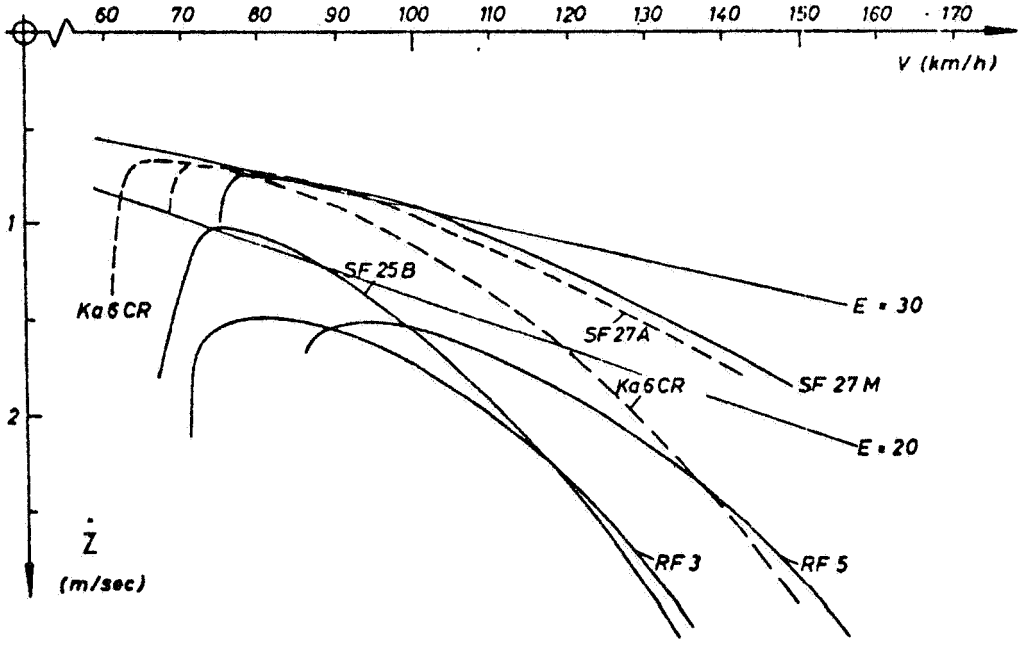

Figure 2. (continued) Still Air Sea Level Glide Polars for Several Natural And Man-Made Flying Devices

Table 2. Performance Improvement Comparison

	Weihe (1938)	ASW-12 (1964)	% Improv.
Min. $\dot{Z}$	120 fpm	109 fpm	+ 9%
V at $\dot{Z}_{min}$	35 kt	43 kt	-23%
L/D_{max}	31.5	43.3	+38%
V at L/D_{max}	41 kt	48 kt	+17%
V at $\dot{Z}$ = 6 fps	62.5 kt	88 kt	+41%
L/D at $\dot{Z}$ = 6 fps	17.6	24.7	

	Ka 6 CR (1955)	Std. Cirrus (1969)	% Improve.
Min. $\dot{Z}$	134 fpm	134 fpm	0%
V at $\dot{Z}_{min}$	36 kt	42.5 kt	-18%
L/D_{max}	29	35.2	+21%
V at L/D_{max}	42 kt	51 kt	+21%
V at $\dot{Z}$ = 2m/s	70 kt	85.5 kt	+22%
L/D at $\dot{Z}$ = 2m/s	18	21.9	

It should be noted that these gains in aerodynamic efficiency have not been accompanied by serious deterioration in stability, control or safety.

Technical Considerations

A number of practical factors make the sailplane design problem difficult, not all of which are directly related to the absence of an engine. For good climb performance (low sink rate) a low wing loading, low weight and excellent aerodynamic efficiency are desired. Further, if climbing is to be done predominantly in thermals, trim drag in moderately steep turns must be low and the speed for minimum sink rate (maximum climb rate) should be low to minimize turn radius (which, for a given bank angle, varies directly with speed squared). On the other hand, for high speed cruise the main concern is aerodynamic efficiency (high L/D). In a first order analysis (i.e. neglecting Reynolds number effects), L/D is independent of weight and thus for a given wing area, a "high" wing loading is desired. The obvious solution of use of variable geometry (e.g. Fowler flaps) to ameliorate the wing loading conflict is limited by several factors (e.g. class

rules, economic and/or drag considerations, manufacturing difficulties) some of which will be discussed later. The demands of high aerodynamic efficiency in both climb and cruise require that great care be taken to minimize both parasite and induced drag. The latter is "easily" accomplished by use of high aspect ratio wings of near ideal planform. Given presently achievable values of parasite drag coefficient (about 0.010 based on wing area), the optimum compromise aspect ratios for Standard Class (span limited) sailplanes are between 18 and 22. Corresponding values for Open Class machines are between 25 and 30. *

The use of high aspect ratio wings of moderate area at typical sailplane speeds, means that the wing operates in a Reynolds number range well below that of conventional GA aircraft. For example, assuming a machine with an aspect ratio of 22 and wing area of 110 ft^2, with a useful speed range of 40 to 100 kt, the corresponding Reynolds number range (based on average wing chord) is 1.0 to 2.4 x 10^6 at sea level. If the machine weighed 700 lbs. loaded, the corresponding lift coefficient range at sea level would be C_L = 1.18 to 0.19. The general speed/Rn ranges for several types of low speed flying machines are shown in Figure 3. Sailplane experience indicates that with a little care, GA aircraft designers need not be overly concerned about the adverse influence of lowered Reynolds numbers on wing drag when large reductions in wing chord are contemplated.

Parasite Drag Reduction

Post-war advances in sailplane performance began when Raspet (7) demonstrated the startling performance gains achievable by systematically cleaning up a machine of initially good aerodynamic layout. The machine used was Dick Johnson's one-of-a-kind RJ-5 Open Class sailplane which was of conventional layout and construction (largely wood) employing an NACA 6-series laminar flow airfoil. The results of the successive improvements resulting from careful sealing of gaps and leaks, and reduction of wing waviness and roughness are shown in the now classic Figure 4. The total cleanup resulted

* The "optimum" in this case is not really clear, although practice indicates that machines with span greater than about 22 meters encounter serious flight and ground handling problems. Required wing area depends on the extent to which variable geometry can be achieved and desired wing loading. Thus overall operational consideration defining span and area limit optimum aspect ratios based on achievement of pure maximum L/D in both Standard and Open Class machines.

in a 25% reduction in parasite drag at L/D_{max}, about 40% of which was achieved by simple sealing and smoothing. A slightly more modern discussion of these effects has been presented by Wortmann (8). The impressive results obtained by Wil Schuemann in a general cleanup of an H-301 Libelle are discussed in (9).

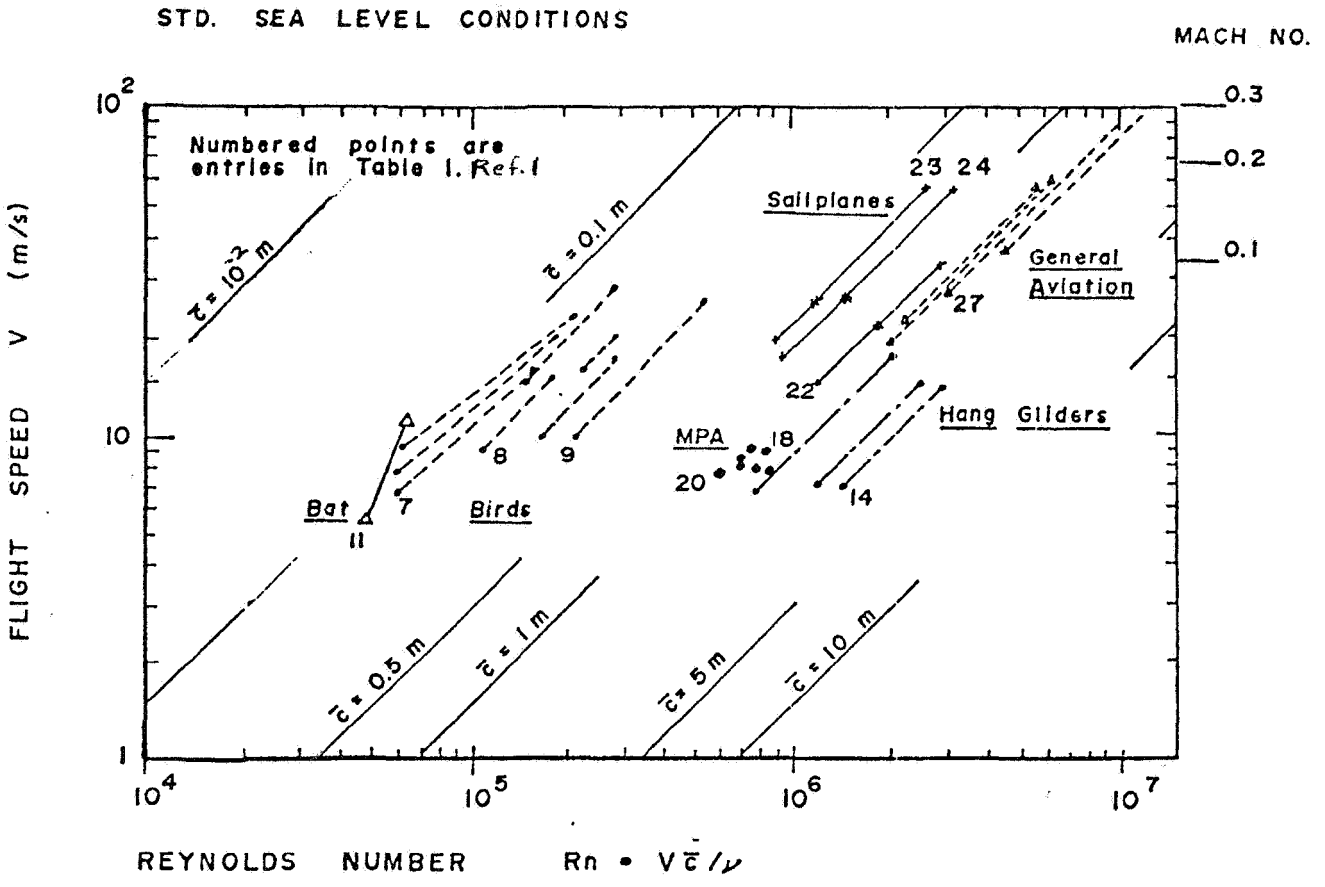

Note: Reynolds number based on average wing chord

Figure 3. Flight Speed/Reynolds Number Range for Various Low-Speed Flying Devices

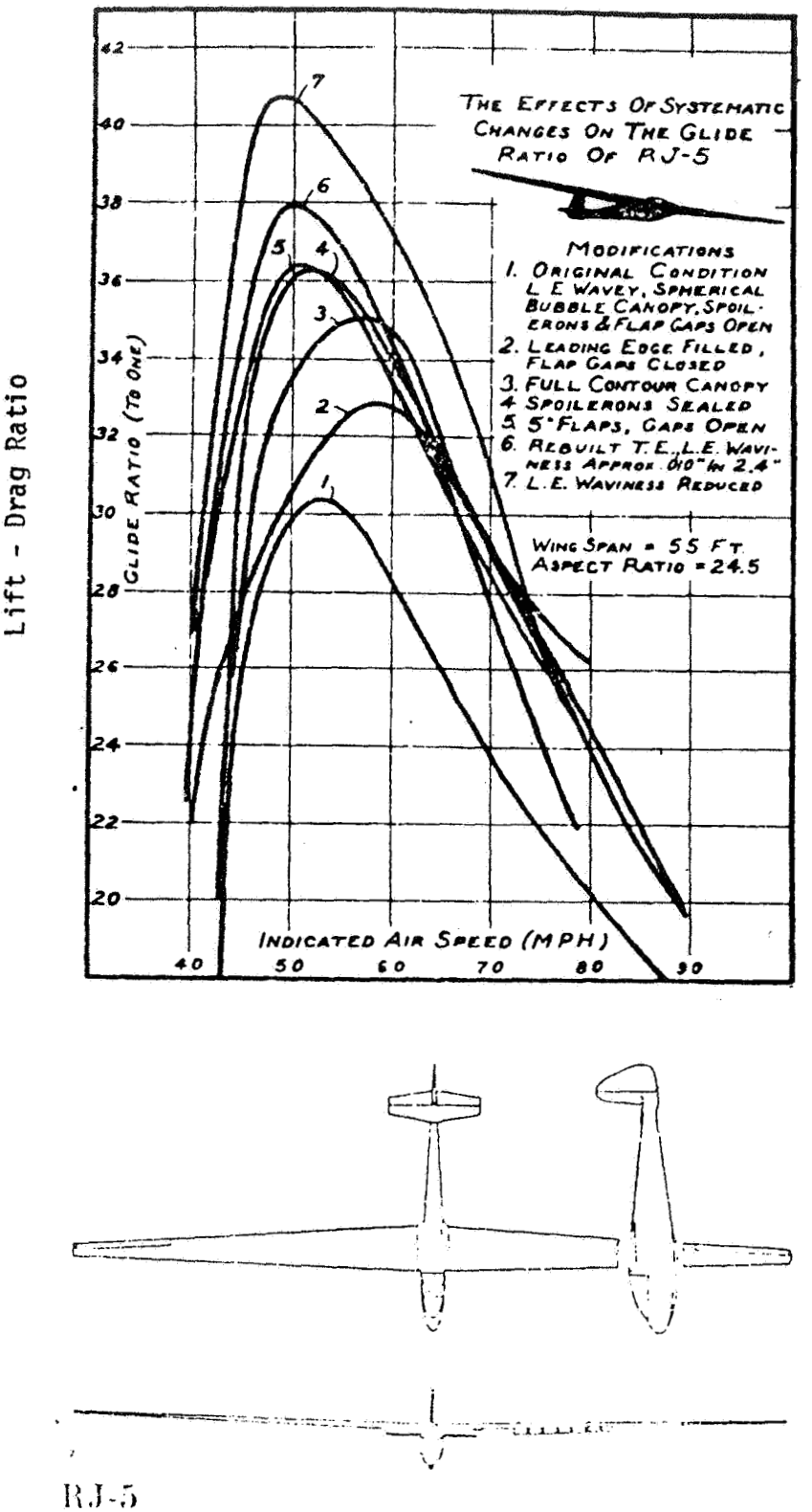

Figure 4. Results of Drag Clean-up on the RJ-5 Sailplane

Low-Speed Airfoils

The requirements of low drag over a reasonably wide lift coefficient range and the generally low values of operating Reynolds number make airfoil selection for sailplanes somewhat difficult. Pre-war sailplane designers relied primarily on Göttingen and NACA 4 and 5 digit airfoil, some of the former type (e.g. Gö 549) being specifically tested for sailplane applications. The advent of the NACA 6-series airfoils held promise of substantial drag reduction over at least the C_L range of the "laminar bucket" and, provided care was taken in manufacture, there appeared hope of obtaining the "bucket" in practice. A number of very successful designs were thus produced in the late 1940's and 1950's using various NACA 6x - 4xx and 6x - 6xx airfoils; the moderate camber of these sections representing a reasonable compromise for centering the "bucket" between the high and low speed extremes in required C_L.

The theoretical work of R. Eppler and F.X. Wortmann in Germany, beginning in the 1950's, showed that by careful contouring of the airfoil envelope and camber line, the transition point on low-to-moderate speed laminar airfoils could be controlled with some precision. This work lead to a family of Wortmann airfoils (the FX or Franz Xavier series) which have been almost universally adopted in sailplanes designed during the last decade. Wortmann's work is well summarized in his paper in (5) and his airfoils have produced something of a revolution in modern sailplane performance.

Wortmann has shown that by carefully contouring the upper surface of a fairly highly cambered airfoil, the upper end of the laminar flow range can be extended to section C_L values required for low sink rate.

When a highly cambered airfoil is operated at low C_L values, however, the airfoil is frequently flying at a negative geometric angle of attack, and thus the lower surface of the airfoil is the one on which transition (and/or separation) is of primary concern in maintaining low profile drag. Thus, by careful contouring of both the upper and lower surfaces, the low drag "bucket" can be significantly extended (in operating C_L range) compared to NACA 6-series sections of similar thickness and minimum drag. The extent of the bucket can often be further increased by adjusting the camber line with a small chord (10 - 20%) simple hinged flap at the trailing edge. Examples of the possible improvement are shown in Figure 5. Several typical sailplane and related airfoils are shown in Figure 6, and the general trend in maximum section lift-drag ratio with Reynolds number for several Wortmann and NACA Sections are shown in Figure 7.

While Wortmann's results are impressive the limited data available on the new Liebeck (10) sections appears spectacular. Whether such airfoils, which appear to

approach some sort of theoretical limit in single element airfoil lift-drag ratio, can perform in practice when built into a practical wing remains at present an open question. Wortmann's investigations of the same type airfoils is reported in his paper in (6).

High Lift Devices

In the modern gospel of sailplanes airfoil design according to Dr. Wortmann the wing contour must be absolutely smooth and unbroken as far aft as possible. Thus, leading edge high lift devices, wide chord flaps or ailerons and particularly conventional Fowler flaps of significant chord are out of the question in sailplane design. Thus the designers choice of high lift devices is severely limited. As one example of a way to circumvent this problem, and provide the performance benefits theoretically available from use of area changing flaps *, Wortmann tailored a unique airfoil/flap system specifically for the very advanced British "Sigma" sailplane project (see Figure 1) . The FX 67-VC-170/136 section for "Sigma" is fully described in (11) and the combined polar at $Rn=3x10^6$ is shown in Figure 5. The flap of this airfoil is "hidden" inside the basic FX 67-VC-170 airfoil when retracted, thus avoiding flow disruption at high speed. When extended, it produces a 36% increase in chord. An even more exotic scheme has been proposed and tested by Wortmann (11) which involves deploying a large sheet of sailcloth (e.g. dacron) allowing chord extensions of greater than 50% in the high C_L range.

Structures

The third component in the post-war revolution in sailplane performance has been the introduction of fiberglass as the main construction material; as pioneered by Nägele, Eppler, Stender and Hänle in Germany. The use of fiberglass wing skins allows fabrication of relatively wave free surfaces of unexcelled smoothness. A further consequence of the use of relatively low modulus of elasticity fiberglass is that in order to maintain desired levels of torsional and bending stiffness, wing skins must be quite thick and correspondingly stronger than required by existing sailplane airworthiness standards. One thus finds fiberglass sailplanes with load factors approaching those of modern fighter aircraft with little weight penalty (due to the low specific gravity of the fiberglass). Considerable room for further improvements in structures exists by use of advanced composites and materials such as DuPont Kevlar (PRD-49) with nearly three times the modulus of elasticity of existing E-glass systems.

* Partial span Fowler flap systems have been extensively tested on the South African BJ-series of sailplanes with generally poor results.

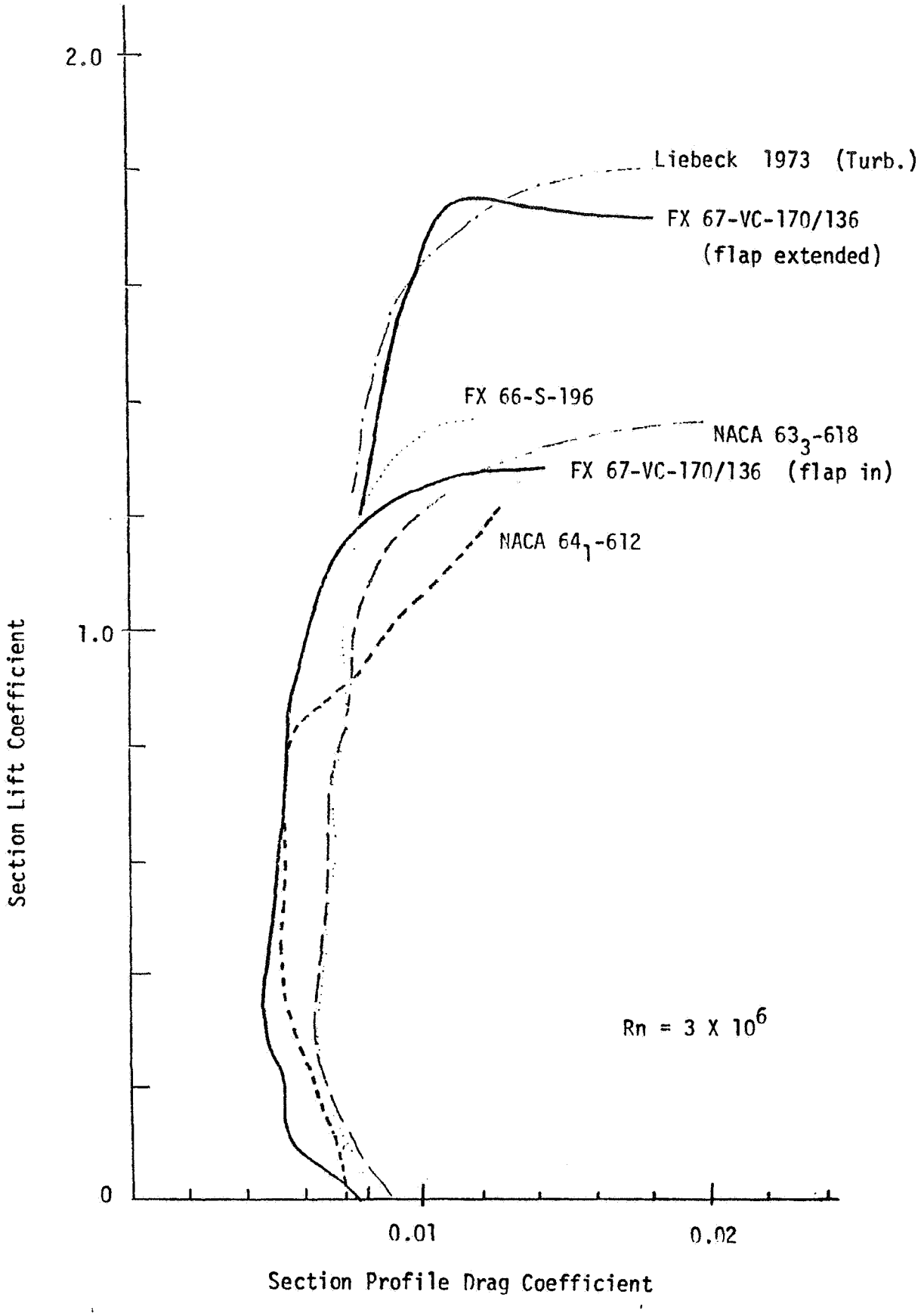

Figure 5. Several Airfoil Drag Polars at a Reynolds Number of 3 X 10^6

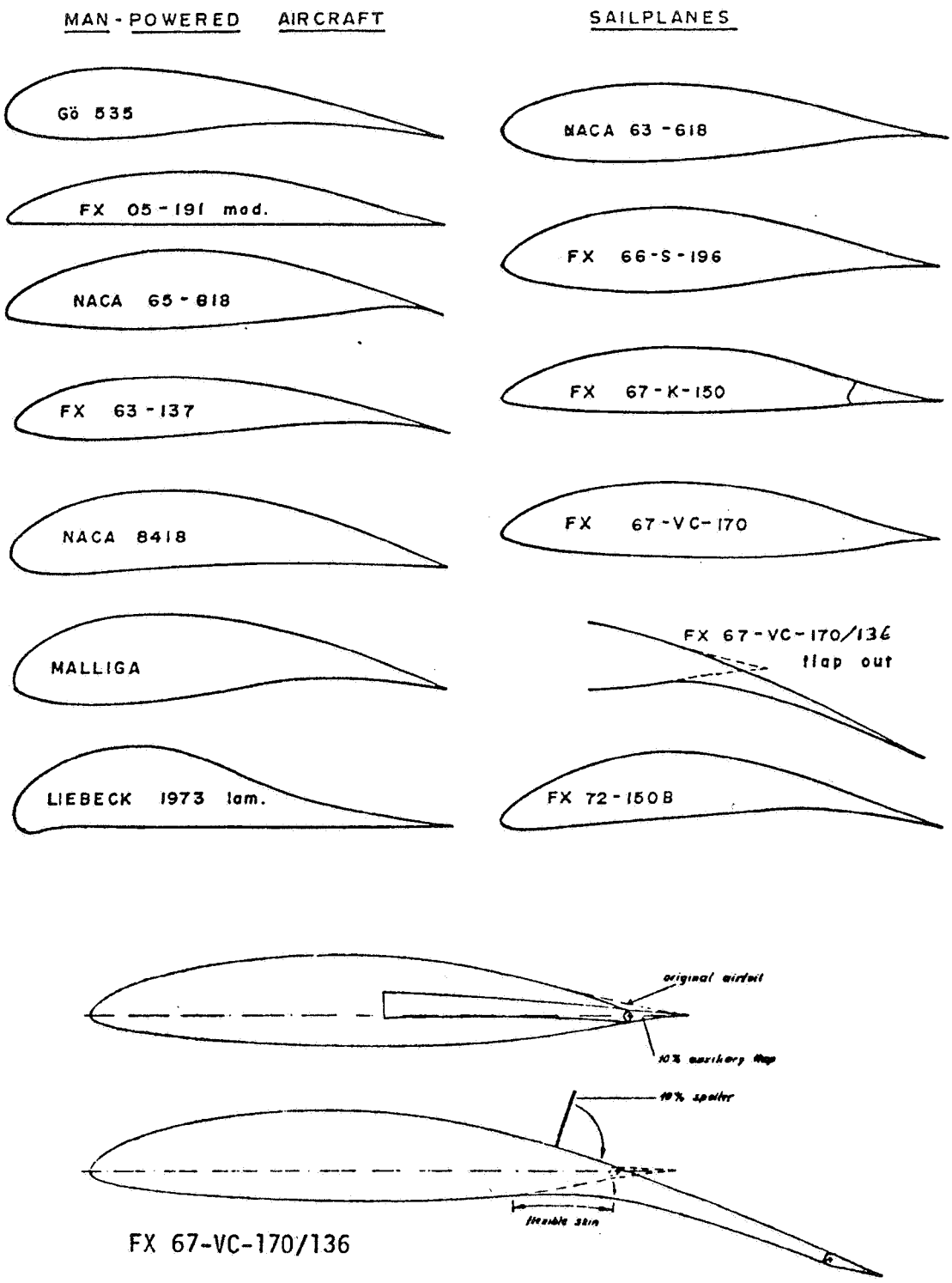

Figure 6. Typical Sailplane and Related Airfoils

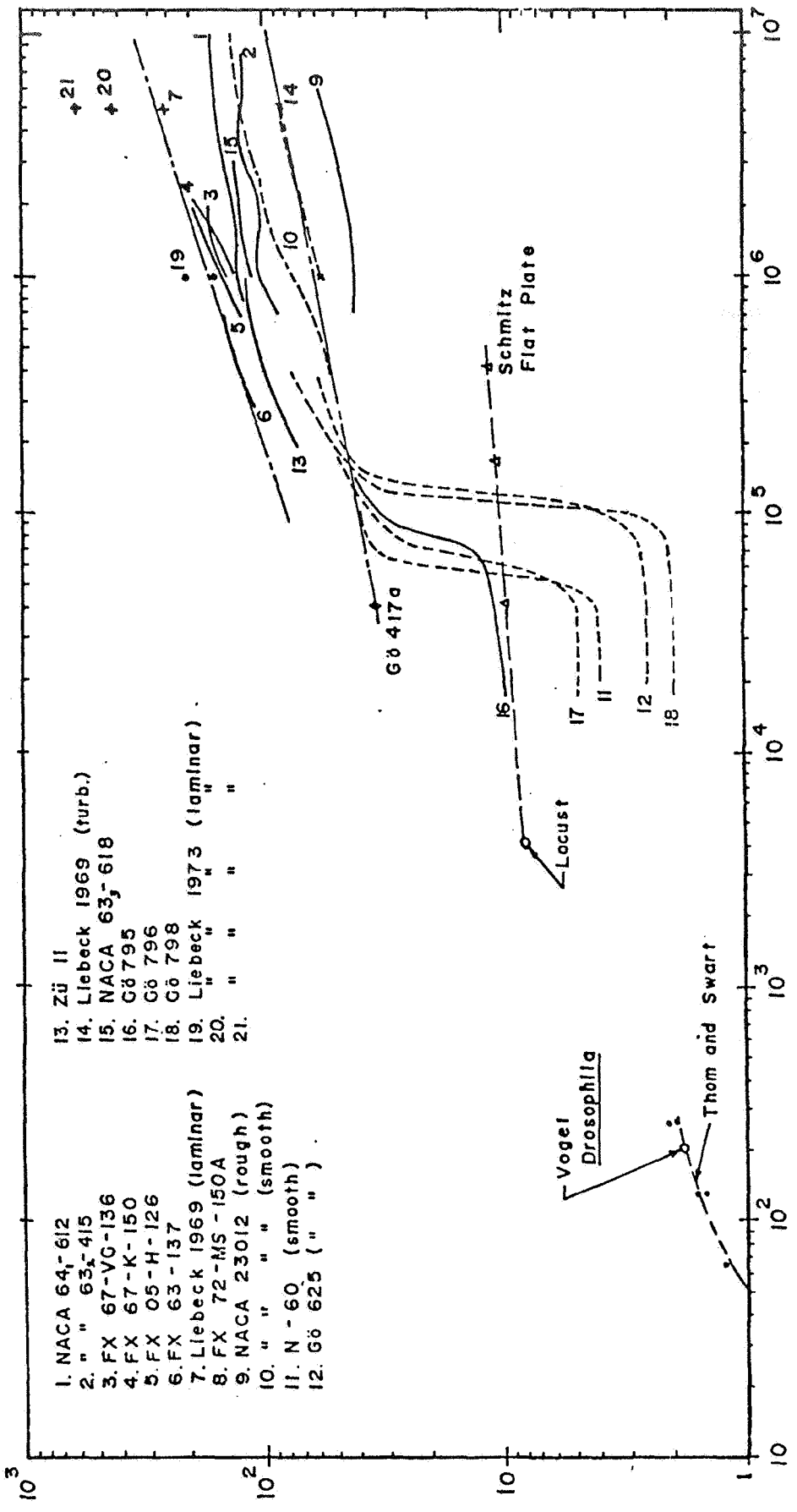

Figure 7. Variation in Maximum Airfoil Section Lift-Drag Ratio with Reynolds Number

Existing fiberglass systems have several disadvantages, however. Since most high performance sailplanes are produced in limited quantities, most fabrication is done by hand lay-up resulting in high cost and major quality control problems. Inspection for structural integrity remains a major difficulty. Questions also remain about the aging characteristics of existing fiberglass systems, and the problem of ultra-violet degradation of the structure carries the commerical disadvantage of offering the customer a choice of the basic color scheme of his aircraft. Thus, alternative fabrication schemes to preserve the beneficial aerodynamic qualities of fiberglass construction, while reducing cost, etc. continue to be explored. Notable among these schemes are the use of bonding (e.g. the Liaster "Nugget") (4), the use of "plastic" coatings over conventional aluminum structure (e.g. Schweizer 1-35) (4) and the extrusion of major structural assemblies as described by Morelli (5).

Concluding Comments

The design of modern high performance sailplanes is an enormously challenging task. The absence of an engine means that the designer cannot indulge in the "luxury" of simply fitting the machine with a larger powerplant to obscure deficiencies in aerodynamic design, weight overruns or to provide the basic design with "growth potential". Further, the machine must have very low drag values over a relatively wide lift coefficient range and these values must be achieved in a relatively low Reynolds number range. It is for these reasons that a careful study of the remarkably successful methods sailplane builders have used to achieve these goals may well repay the designers of powered General Aviation aircraft. It has not been the intention of the authors of this brief discussion to advocate or imply that all sailplane technology is applicable to General Aviation aircraft in general or that the operational and economic constraints faced by the GA designer make incorporation of applicable features feasible. However, even a brief examination of the performance figures achieved by modern soaring machines and a little reflection as the often huge disparity in L/D values between sailplanes and GA aircraft indicates that careful attention to the lessons learned in sailplane design and manufacture hold realistic promise for substantial gains in the aerodynamic efficiency of several GA types. The fuel crisis, whether transient or permanent, may force a redirection in GA design with greatly increased emphasis on operation "economy", perhaps even at the expense of speed (or productivity) and initial vehicle cost. Modern soaring technology indicates one path along which future development might progress.

Research Needs

1. Performance of Wortmann type sail plane airfoils in wings with roughness, waviness and Reynolds numbers typical of light powered general aviation aircraft need to be further investigated.

2. Simple, economical methods of construction need to be found which lead to improved surface finish and manufacturing tolerance to approach the performance of sailplane types for powered general aviation aircraft. Possible examples are:
   - "Plastic" coatings over conventional structures. (e.g. Schweizer I-35 sailplane)
   - Metal bonding techniques (e.g. the Laister "Nugget")
   - Major assembly extrusions from metal and plastic

3. The optimum configuration design implications of the use of sailplane technology in powered general aviation aircraft needs to be investigated. Specifically:
   - optimum wing geometry
   - engine/thrust producing device location
   - requirements for high lift devices
   - wing/body integration (i.e. wing position and body shape) to minimize adverse interference

4. The economic and configuration implications, in light of the fuel crisis and sailplane technology, of optimizing the design of a given general aviation aircraft toward maximum "transport economy" even at the possible expense of "productivity" needs to be evaluated.

References

1. McMasters, J.H., "An Analytic Survey of Low-Speed Flying Devices - Natural and Man-Made", AIAA Paper No. 74-1019, Sept.1974. (Also contained in Ref. 6 below). An expanded version of this paper will be published in Tech. Soaring, Vol. 3, 1975.

2. Bikle, P., "Polars of Eight - 1971", Soaring, June 1971.

3. Zacher, H., "Some Flight Tests on Self-Launching Sailplanes", NASA CR-2315, Nov. 1973. "Flug messung mit 52 Segelflugzeugen", Aero Revue, Oct., Nov., Dec. 1973.

4. Soaring, August 1974 (Journal of the Soaring Society of America, P.O. Box 66071, Los Angeles, California 90066).

5. Nash-Webber, J.L., "Motorless Flight Research - 1972", NASA CR 2315, Nov. 1973.

6. Proc. of the Second Inter. Symp. on the Tech. and Sci. of Low-Speed and Motorless Flight, MIT, Sept. 1974. (Available from SSA, P.O. Box 66071 Los, Angeles, California 90066 for $10.)

7. Raspet, A. "Systematic Improvement of the Drag Polar of the Sailplane RJ-5", Soaring, Sept., Oct. 1951.

8. Wortmann, F.X., "Drag Reduction in Sailplanes", Soaring, June and July 1966.

9. Scheumann, W., 1972 Symposium on Competitive Soaring. (Available from SSA).

10. Liebeck, R. H., "A Class of Airfoils Designed for High Lift in Incompressible Flow", AIAA Paper No. 73-86, Jan. 1973.

11. Wortmann, F. X., "Airfoils of the Variable Geometry Concept", OSTIV Pub. XI, 1974. (available from SSA).

12. Technical Soaring, Vol. I and II (4 issues each), available from SSA or Dr. Bernard Paiewonsky, 9309 Burning Tree Rd., Bethesda, Maryland 20034.

9.2 Minimum Vertical Tail Drag

E. E. Larrabee
Massachusetts Institute of Technology

For an airplane with no asymmetric power problem (a glider or a cross-shafted twin) and with no directional stability constraint (a control configured vehicle, or a skillful pilot) there still exists a requirement for a vertical tail large enough to perform a coordinated turn reversal, that is to maintain nearly zero sideslip when banking from a coordinated turn in one direction to a coordinated turn in the other direction. Presumably this vertical tail maneuver load requirement establishes a minimum tail size and a corresponding minimum tail drag.

This is explained by the aid of Figure 1. In a coordinated turn the angular velocity about the aircraft Z axis, R, is proportional to the sine of the roll angle ϕ times the ratio of the acceleration of gravity g to the flight speed V. Differentiation of the expression for R shows that the angular acceleration during a turn reversal is proportional to the roll rate $P = d\phi/dt$, and is a maximum as the aircraft rolls through wings level where $\cos\phi = 1$.

When the lateral control is deflected to produce the roll rate P, it invariably produces an adverse yaw due to rolling

$$\Delta N = \frac{\rho}{2}V^2 SbC_{n_p}\frac{b}{2V}(P)$$

where C_{n_p} is a dimensionless stability derivative depending primarily on wing characteristics. For an elliptically loaded wing of moderate to high aspect ratio the local lift vectors are rotated nearly through the local helix angle (2y/b) $(\frac{Pb}{2V})$ giving rise to a value of C_{n_p} approaching $-C_L/8$, the negative sign indicating a negative (adverse) yawing moment to be overcome by the vertical tail in phase with a positive rolling velocity. The adverse yaw due to ailerons themselves ($C_{n_{\delta A}}$) may actually make

$$\Delta C_n = C_{n_{\delta_A}}\,\delta_A + C_{n_p}\,(\frac{Pb}{2V})$$

larger than $(-C_L/8)(Pb/2V)$ for a given value of P, but I retain the $-C_L/8$ result for simplicity.

When the vertical tail load is multiplied by the tail arm to provide the yawing moment necessary to overcome the inertial resistance of the aircraft to yawing $I_Z(dR/dt)$, and the adverse aerodynamic yawing moment due to rolling, it

is found that the tail load may be expressed as

$$\text{Tail load} = mg\left(\frac{b}{\ell_V}\right)\left[\frac{1}{8} + 2\left(\frac{k_z}{b}\right)^2\right]\left(\frac{Pb}{2V}\right)$$

which is a convenient form since most lateral controls will produce a maximum value of the tip helix angle (Pb/2V) independent of speed if the control can be fully deflected.

For example, let full aileron deflection produce a helix angle of 0.1 radian, let the vertical tail arm be 0.4 of the wing span, and let the radius of gyration in yaw be 0.25 of the wing span. The vertical tail load in a turn reversal is then

$$= mg\left(\frac{1}{0.4}\right)\left[\frac{1}{8} + 2\left(\frac{1}{4}\right)^2\right](0.1)$$

$$= 0.0625\ mg$$

independent of the flight speed.

If the maximum lift coefficient of the vertical tail is the same as the wing, a tail area of 0.0625 times the wing area is then required to perform a coordinated turn reversal at minimum flying speed. It is seen that an "STOL" conversion, which would double $C_{L_{max}}$ for the wing relative to the vertical tail, requires doubling the tail area. Short tail arm to wing span ratios ("tailless airplanes") are seen to require very large vertical tails for satisfactory lateral control. The desirability of increasing fuselage length in the interest of reducing vertical tail size is clearly seen.

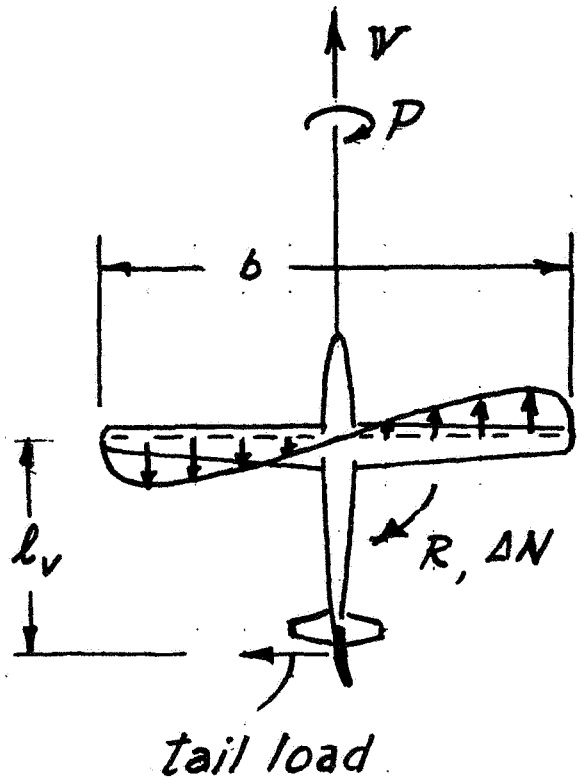

a) Turn coördination:

$$R = \Omega \cos\phi = \frac{g}{V}\sin\phi$$

$$\frac{dR}{dt} = \frac{g}{V}\cos\phi\,(P)$$

b) Adverse yaw due to rolling:

$$\Delta N = \frac{\rho}{2}V^2 S b C_{n_p}\frac{b}{2V}(P)$$

$$C_{n_p} \cong -C_L/8$$

$$\text{Tail Load} = mg\left(\frac{b}{l_v}\right)\left[\frac{1}{8} + 2\left(\frac{k_z}{b}\right)^2\right]\left(\frac{Pb}{2V}\right)$$

where $I_z = \int (x^2+y^2)\,dm = mk_z^2$

Figure 1. Tail Load Required for Turn Coordination

10. SUMMARY OF DISCUSSIONS ON RESEARCH RECOMMENDATIONS

10. SUMMARY OF DISCUSSIONS ON RESEARCH RECOMMENDATIONS

10.1 Discussion - Session I - Status of Drag Prediction Methods

Roskam reiterated the purpose of the conference: to formulate research and development needs in all drag areas associated with general aviation airplanes. Because of lack of discussion time after Session I, Roskam appointed a six-man committee headed by Ruhmel of Cessna Aircraft Co. to formulate the research needs coming out of this session. During Session II, Ruhmel presented the views of his committee. Ruhmel indicated that there was a need for the following types of wind-tunnel tests:

I) Full Scale

- a. Tests on one or two full scale airplanes (low and high wing) to determine their drag characteristics accurately.
- b. Drag clean-up tests on these airplanes in a manner analogous to tests conducted by M. McKinney on fighter airplanes during WWII.
- c. Wake survey and thrust measurements on these airplanes.

II) Component/Build-up Drag Tests

- a. Component/build-up drag tests on about three general aviation type airplanes: a twin, a high wing single and a low wing single. The idea is to generate sound baseline drag data on individual components and on their interference.
- b. A systematic series of drag tests on general aviation windshield shapes and fuselages of different length-to-diameter ratios.

III) A study of empirical and theoretical drag prediction methods in use today

- a. Make a study of which empirical and theoretical drag prediction methods appear to predict drag reasonably well.
- b. Determine if it is possible to mesh some of these methods into computer programs (for example, Smetana's finite element program).
- c. Apply the results of a. and b. to a number of existing general aviation configurations (preferably the ones tested under I and II) and see how well these analytical and/or empirical methods perform.
- d. Use the theoretical models (i.e., computer programs) to predict some "optimum" shape for a typical general aviation airplane and then verify this in the windtunnel. These computer programs should not be so complex that it takes a sub-branch of IBM to handle them. General aviation needs simple but accurate drag prediction methods.
- e. The end result should be methods and/or computer programs that have

been verified for accuracy and which can be used in design. That means they should again be simple and suitable for parametric studies.

10.2 Discussions - Session II - Fuselage Drag

There seemed to be a strong consensus that there is a need for wind-tunnel testing a number of different general aviation fuselage shapes (and length-to-diameter ratios) as well as different windshield shapes. The point was made by Larrabee that if these tests are indeed run they should be carried out also to high angles of attack and sideslip. Tumlinson indicated such fuselage tests should be run both in and out of the presence of appropriate wings. Smetana made the point that these data should then be correlated against computer program predictions. Loftin pointed out that although testing a limited number of shapes would be all right, we should be careful not to generate large amounts of experimental data such as was done in the past (remember the 209 wing-fuselage combinations tested by NACA).

Smetana stated that it was essential to have good full scale fuselage and fuselage plus wing drag data on a high and a low wing airplane. He said that was the only way to check the theoretical models (computer programs) and build confidence in them. Smetana also felt that it would be important to get good pressure distribution data, for the same reason. McKinney agreed but wanted to emphasize the need for small scale model data when it comes to doing detail configuration build-up drag tests.

A lengthy discussion evolved on the subject of propeller/fuselage interference. It was agreed that there appears to be a lack of accurate ways of predicting propeller performance in the presence of fuselages and nacelles. Particularly propeller interference effects on the total configuration are a mystery. An experimental and analytical look at existing and new fuselage propeller arrangements was felt to be needed.

Windecker indicated that they had evaluated five different propellers from five different manufacturers. He said that the performance of all five deviated considerably from the predictions. He supported the need for this type research.

McCormick felt that propeller performance predictions were well inside the state-of-the-art. Ruhmel disagreed. He said that if you take something like a Cessna Skymaster, that there was no way to accurately predict the propulsion-drag sum-total of front-propeller + fuselage + aft-propeller.

10.3 Discussions - Session III - Wing Drag

Several attendees expressed the need for tunnel research in the area of leakage through flap and control surface gaps. Wentz said that some work is being done in this regard on the GA(W) airfoils at W.S.U. There was a feeling that more work on this was needed with these aft-cambered airfoils, since they have more potential for "pumping" air through gaps.

Kohlman mentioned that by merely sealing the flap and spoiler flaps on the ATLIT airplane a 4 mph cruise speed increase was registered. One practical problem that needs manufacturing attention was brought out by Neal. Manufacturing tolerances can play a very important role here. There may be a need to define the sensitivity of the new airfoils to flap, spoiler and aileron gap and/or seal tolerances.

Larrabee made a pitch for airfoil computer optimization using different geometric constraints (for example, from a manufacturing viewpoint). Anderson indicated that Ames (R. Hicks) has the capability to do just that with their existing airfoil optimization program. Ecklund and Tumlinson both agreed that manufacturing constraints on airfoil shapes should be closely watched. Kohlman said that a good look is needed into the Reynolds number sensitivity of the new airfoils. If the trend is toward higher wing loadings through smaller chords, then maybe someone ought to look at optimizing the new airfoils at lower Reynolds numbers.

McKinney made a pitch for more work in the area of spoiler control and high lift control on the new airfoils. He cautioned against too much parametric airfoil work at the expense of much needed control and high lift work. There seemed to be a consensus about the need for NASA's ongoing programs in airfoil theoretical development and continued airfoil wind tunnel testing.

10.4 Discussions - Session IV - External Nacelle Drag and Interference Drag

Neal made a pitch for both windtunnel tests and improved math modeling of wing-fuselage-nacelle combinations for business jets. He said that no reliable methods exist for predicting the correct arrangement of wing, nacelle and fuselage or fan-powered business jets. Particularly the fuselage-nacelle, wing-nacelle and nacelle-wing-overlap problems are not tractable in the current state-of-the-art. Another area that needs researching is the design of S-ducts in the case of business tri-jets.

A discussion between Anderson, Kohlman, Tumlinson and Ecklund brought out again the need for an updated propeller theory accounting for fuselage and

nacelle interference (blockage) and for noise. Particularly the effect of the new airfoils on propeller development needs attention. Crupper also emphasized the need for accurate methods for predicting propeller performance in the presence of nacelles and/or fuselages.

McCormick and to some extent McKinney felt that propeller theory was reasonably well established, even in presence of symmetrical bodies. Ruhmel pointed out that current propeller theories were not sophisticated enough to allow the prediction of pressure and velocity distributions over associated bodies. He again cited the Cessna Skymaster as a typical configuration which cannot be handled satisfactorily by current propeller theories. Industry and research people seemed to disagree on this point.

In the area of cooling drag it was agreed that no good methodology exists to predict the drag nor the cooling effect of the internal handling of airflow around today's horizontally opposed reciprocating engines. Research needs in this area were also identified during the Cooling Drag Workshop held at the University of Michigan earlier this year.

Tulinius mentioned that he has a computer program that has been used with good results to handle the over the wing type of nacelle installation as found on the VFW-Fokker 614.

Nicks pointed out that Langley is working on a jet-nacelle study which may help provide some answers. Kalberer said that one of industry's problems is to decide on long or short nacelles in the case of front-fan engines. There is no consistent methodology to solve the complex interference problem between what is drag and what is thrust, in such instances.

Riddell cautioned against just looking at finding the best nacelle-propeller shaping. He said that the structural integrity problem of the propeller shaft and the propeller blade is always a problem particularly in new and different installations.

McCormick said that he has a computer program (developed for the Army Research Office) which predicts static thrust and thrust versus speed of free propellers. This program is documented and contains also a lot of experimental data. However, interference effects with nacelles and fuselages are not included.

10.5 Discussions - Session V - Trim Drag

Larrabee indicated that he had a fundamental disagreement with the trim drag procedures as presented in the session. Several people expressed opposing

views regarding the need for research into the trim drag area. It did seem obvious from the discussion that there is a need for a well defined bookkeeping system to account for trim drag. Without that, it is hard to keep track of this drag item with any degree of accuracy. One item that came through loud and clear is the need to study fuselage plus wing shapes for producing positive C_{m_o}.

10.6 Discussions - Session VI - Drag of the Complete Configuration

There was time for only a very brief discussion after this session. No new ideas were brought out. Most attendees seemed to agree on the need for a detail component build-up drag test on three or four typical general aviation airplanes:

- high wing single engine
- low wing, single engine
- reciprocating twin
- jet twin

11. SUMMARY OF RESEARCH RECOMMENDATIONS

Preceding Page Blank

11. SUMMARY OF RESEARCH RECOMMENDATIONS

The research recommendations listed below were perceived to be the most important ones by the editor of this document.

1. Full Scale Drag Tests

It is recommended that NASA run comprehensive full scale drag tests on the following airplanes:

a) A typical single engine high wing airplane (propeller driven)

b) A typical single engine low wing airplane (propeller driven)

c) A typical twin engine, propeller driven airplane

d) A typical twin engine, aft fuselage nacelle mounted business jet airplane.

The idea is to first establish accurate baseline data and second to perform drag clean-up tests on these airplanes. Wake surveys and thrust measurements should be included, so that the effects of thrust and drag can be separated. A clearly defined bookkeeping system should be used to accomplish this.

2. Model Component Build-up Drag Tests

It is recommended that NASA conduct a series of systematic model component build-up drag tests. These tests should utilize models of two or more airplanes tested under 1. These tests should be carried out to high angles of attack and sideslip.

3. Correlation with Theoretical Models

It is recommended that NASA perform a number of studies aimed at determining which drag prediction methods are best suited for drag prediction of: wing drag, fuselage drag, wing plus fuselage plus nacelle drag. It is recommended that the results of 1. and 2. be used to correlate theoretical results with experimental data.

4. Windtunnel Tests of Fuselage and Windshield Shapes

It is recommended that a series of windtunnel tests be run to determine the drag and pitching moment characteristics of fuselages of varying camber, slenderness and typical general aviation windshield shapes.

5. Propeller Interference

It is recommended that NASA conduct studies and tests aimed at defining the problem of predicting propeller performance in the presence of nacelles, wings, and fuselages.

6. Nacelle Interference

6.1 Props

It is recommended that NASA conduct studies and tests to determine minimum drag shapes and locations for reciprocating engine nacelle-wing installations.

6.2 Jets

It is recommended that NASA conduct studies and tests to determine: a) flow characteristics through S-ducts (as on tri-jets), b) drag of aft-nacelle installations, with particular attention paid to nacelle-wing overlap and interference and nacelle-fuselage interference.

7. Gaps

It is recommended that NASA perform studies and (or) tests to determine the drag sensitivity of aft-loaded airfoils to gaps and to seal tolerances.

12. ACKNOWLEDGMENTS

12. ACKNOWLEDGMENTS

The editor would like to acknowledge the work done by Mrs. Pat Nicholas, Ms. Nancy Montgomery, Miss Melinda Henderson and Mr. Greg Fillman, in organizing the workshop, and in typing and proofreading this document.

Preceding Page Blank

ADDENDUM

(This paper was received after the proceedings document had gone to the printer.)

7.2 Effect of Tail Location on Airplane Trim Drag

Howard Chevalier
Texas A & M University

The Flight Mechanics Laboratory at Texas A & M University has been actively engaged in the study of methods and devices for preventing airplane stall spin accidents. The results of these studies clearly showed that in many cases the airplane's handling characteristics at high angles of attack could be greatly improved by changing the location of the horizontal tail surface. Relocating the horizontal tail surface would improve the flight characteristics of the airplane at high angles of attack and thus for many situations reduce the potential hazards of a stall spin accident. However, relocating the tail surface could also change the trim drag of the airplane.

Figures 1 and 2 illustrate the difficulty in control characteristics due to tail location. Figure 1 shows an example of elevator deflection angle required for a given angle of attack. For this case, the airplane could increase angle of attack without any appreciable change in horizontal tail deflection angle at high angles of attack. This characteristic was primarily due to the tail location relative to the wing downwash and the wake from the propeller.

Another example of control difficulty is shown in Figure 2. For this airplane the stick-force curve had a very distinct shift near 64 mph. This shift in the curve and almost adrupt change in stick-force was caused by both wing wake and flow separation along the sides of the fuselage. This effect was even more noticeable in yawed flight conditions.

As a result of these findings, several different tail locations were investigated. I will discuss a few of these locations and resulting effect on trim drag. Figure 3 shows equations which were used to determine the trim drag. The first set of terms within the bracket of the first equation is the change in airplane drag due to the additional lift or reduction of lift on the wing resulting from the addition of the airplane tail lift. The next equation was used to determine the drag of the trimmed airplane. The next two equations were used to determine the tail drag and tail lift. The tail incidence

angle was determined by the last equation. One of the obvious effects that can be seen from this equation is that if the cg of the airplane is moved aft, the trim drag will decrease.

Figure 4 shows some of the results that we have obtained for a twin-engine airplane. The curve at the top is the variation in trim drag with the tail in the original location. As the cg moved aft toward the aerodynamic center, the moment about the cg becomes less so that you do get a reduction in trim drag with angle of attack. As shown, the amount of reduction is small, less than .0002. The curves at the bottom of Figure 4 show the effect of changing the tail location. For this configuration, we could obtain more tail effectiveness at high angles of attack by moving the tail aft or putting on a T-tail configuration. Moving the tail aft results in a reduction in trim drag; however, it is not very large. It should be noted that we did not reduce the tail surface area for the aft tail locations. Retaining the same tail volume would have resulted in a smaller tail area and drag. As shown, the trim drag reduces very rapidly with angles attack. This is due to the fact that the tail is out of the downwash area and an additional tail deflection angle is required to obtain the same download on the elevator or stabilizer; however, at small angles of attack near cruise where we are concerned with the drag, the difference is very small.

Figure 5 shows results obtained from the single engine airplane. For this airplane, the center of gravity was near the aerodynamic center of the airplane and a reduction in trim drag occurs with an increasing angle of attack. The trend for moving the tail aft and for the T-tail configuration are similar to those obtained for the twin engine airplane. In general, the change or the additional trim drag was not very large. In concluding, I would have to say that our work was not very detailed and not too extensive; however, from these preliminary results, the tail location alone is not a major factor in determining trim drag for given airplane configurations. In my opinion, it would improve control by relocating the tail and the results show that there would not be any appreciable drag penalty.

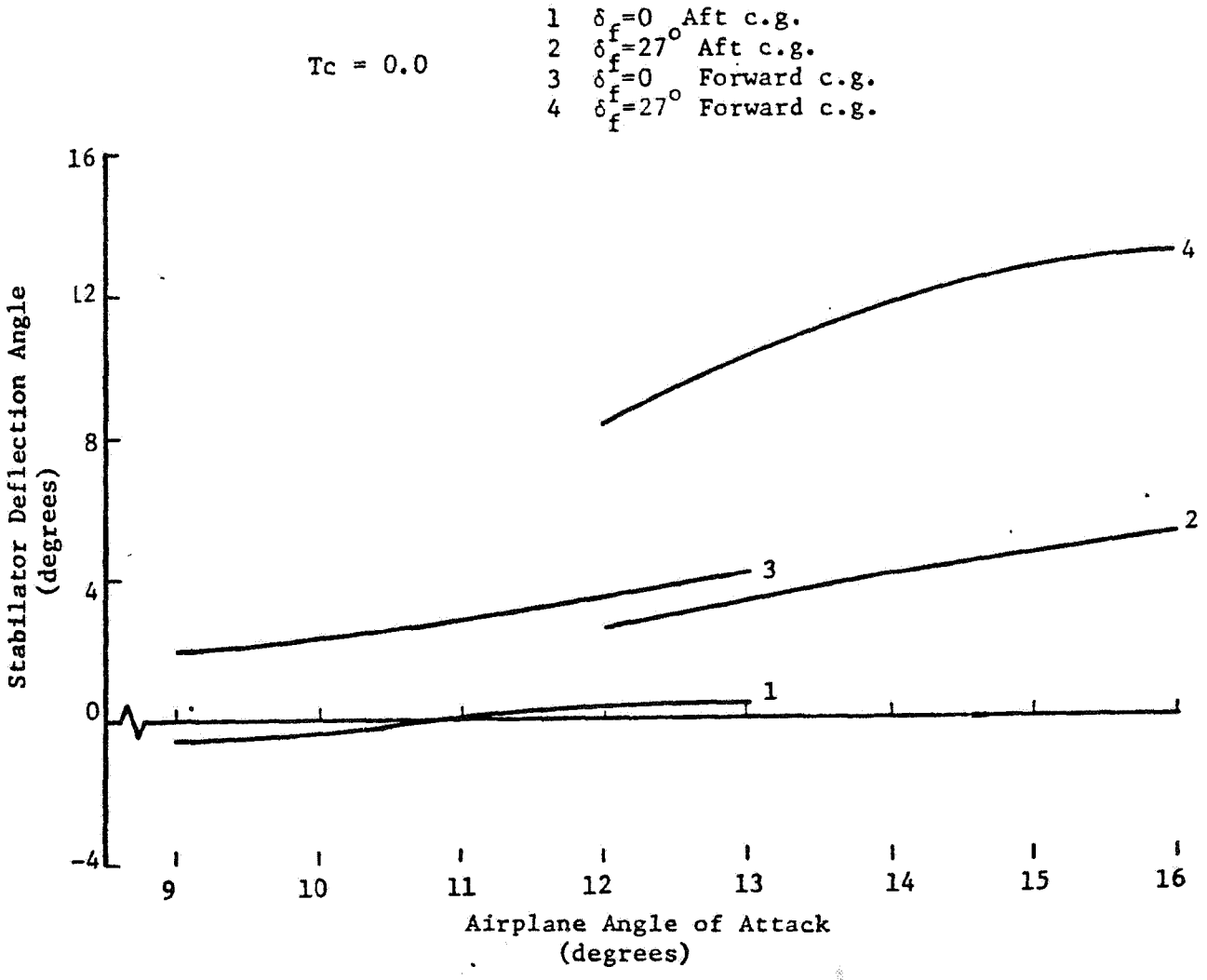

Figure 1. Stabilator Deflection of the Twin-engine Airplane

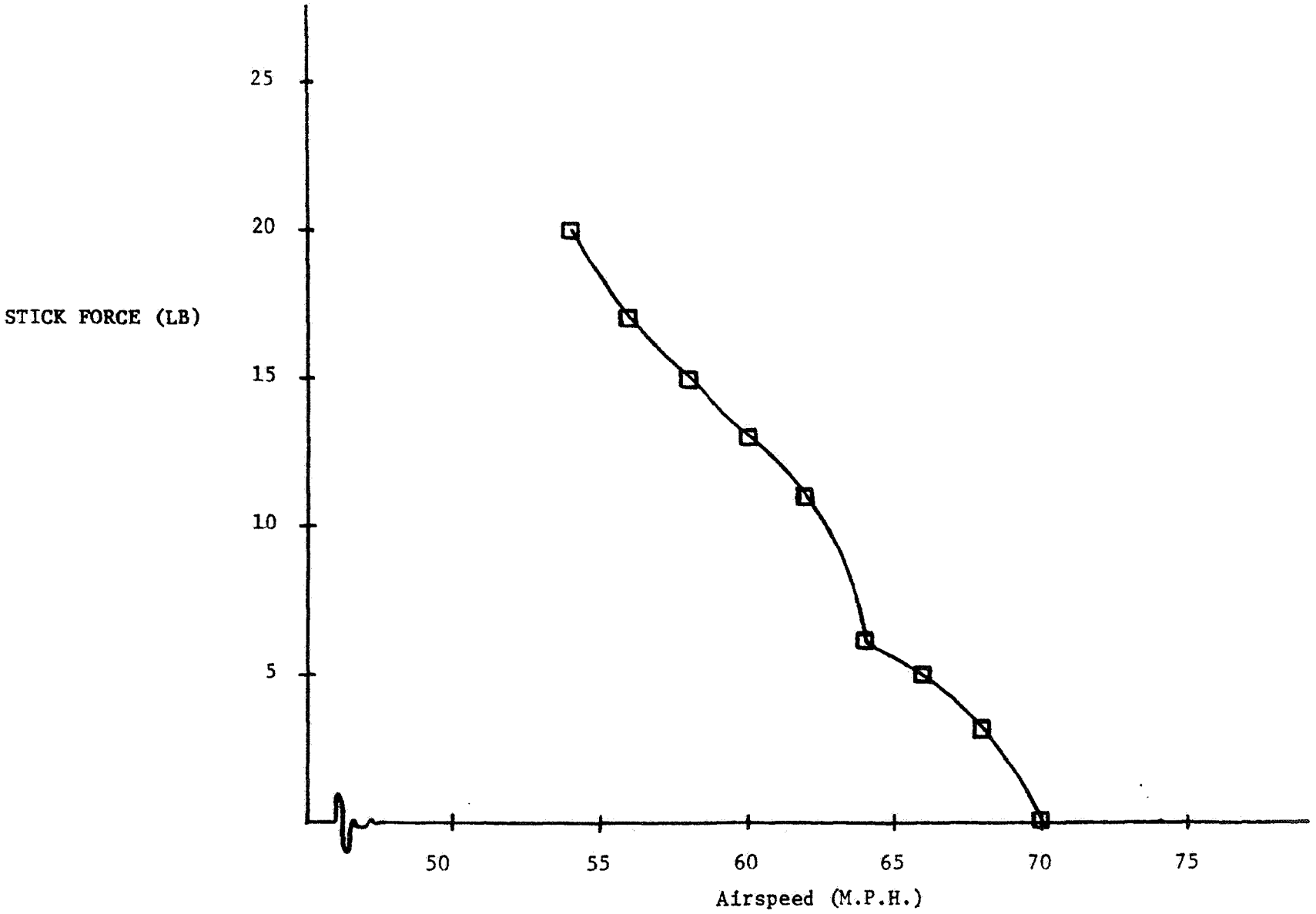

Figure 2. Stick Force as a Function of Indicated Airspeed Power-Off

$$\Delta C_{D_{trim}} = C_{D_{trimmed}} - \left[C_{D_{o_W}} + \left(\frac{\partial C_D}{\partial C_L^2}\right)_W \left(C_{L_{o_W}} + C_{L_{\alpha_W}} \alpha\right)^2 -\right.$$

$$C_{D_{trimmed}} = C_{D_{o_W}} + \left(\frac{\partial C_D}{\partial C_L^2}\right)_W \left(C_{L_{o_W}} + C_{L_{\alpha_W}} \alpha_{trim}\right)^2$$

$$+ C_{D_t} \cos \epsilon + C_{L_t} \sin \epsilon$$

$$C_{D_t} = \left(\frac{\partial C_D}{\partial C_L^2}\right)_t \left\{C_{L_{i_t}} i_t + C_{L_{\alpha_t}} \left[-\epsilon_o + \left(1 - \frac{\partial \epsilon}{\partial \alpha}\right)\alpha\right]\right.$$

$$\left. + C_{L_{o_t}}\right\}^2 \frac{S_t}{S_W} \frac{q_t}{q_W} + C_{D_{o_t}} \frac{S_t}{S_W} \frac{q_t}{q_W}$$

$$C_{L_t} = \frac{C_{m_{o_W}} + C_{m_{\alpha_W}} \alpha + C_{L_W} \frac{X}{c} + \Delta C_{L_W} \frac{X}{c}}{\frac{l_t}{c}}$$

$$i_t = \frac{C_{m_{o_W}} + C_{m_{\alpha_W}} \alpha + C_{L_W} \frac{X}{c}}{C_{L_{i_t}} \frac{S_t}{S_W} \frac{q_t}{q_W} \frac{l_t}{c}} -$$

$$\frac{C_{L_{\alpha_t}} \left[-\epsilon_o + \left(1 - \frac{\partial \epsilon}{\partial \alpha}\right)\alpha\right] + C_{L_{o_t}}}{C_{L_{i_t}}}$$

Figure 3. Equations Used to Determine Trim Drag

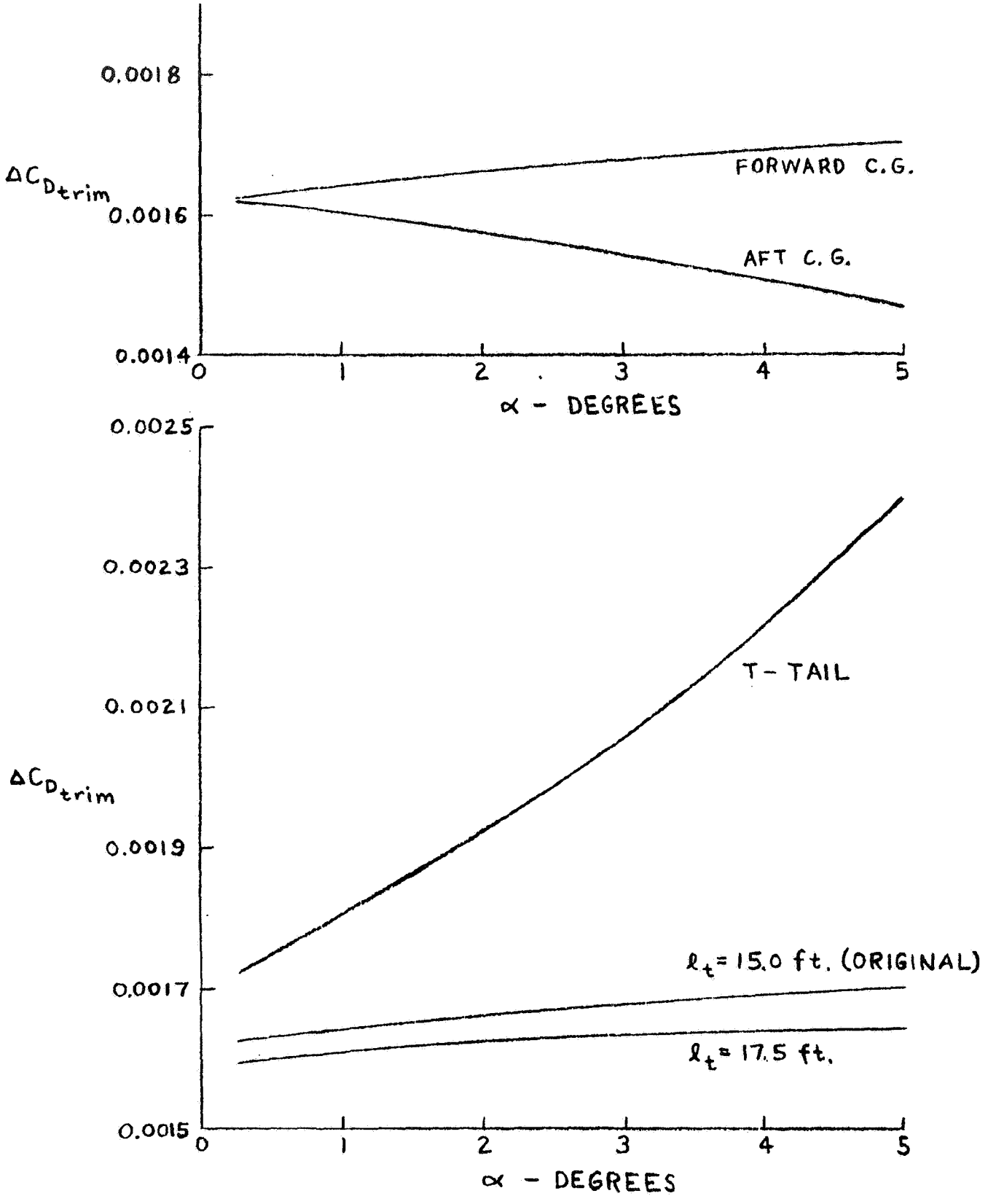

Figure 4. Twin Engine Airplane

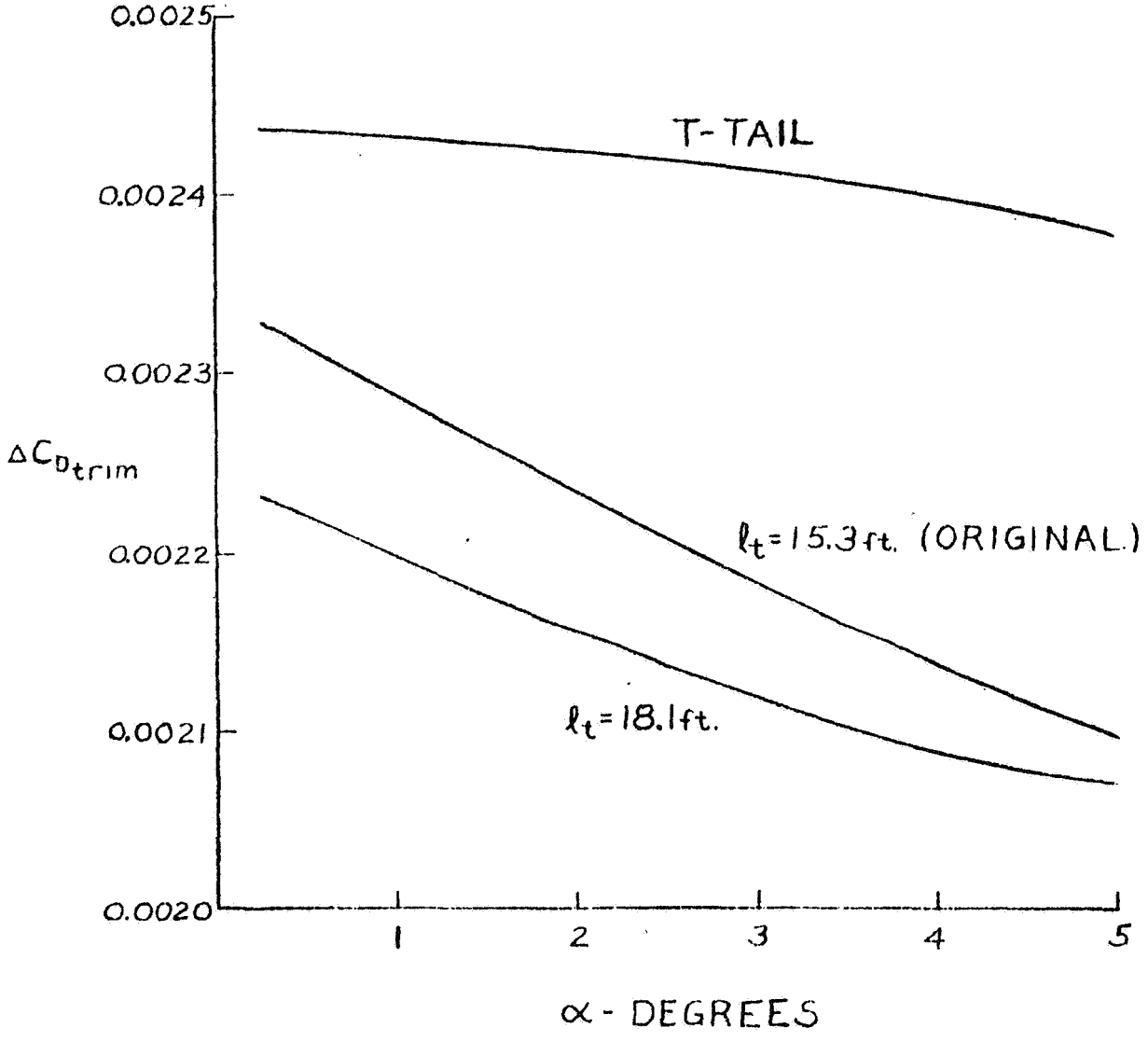

Figure 5. Single Engine Airplane